

**C–H Activation *via* Iridium and Rhodium  
Electrocatalysis and Undirected Electrochemical  
Fluorination**

**Dissertation**

for the award of the degree

“Doctor rerum naturalium”

of the Georg-August-Universität Göttingen



within the doctoral program of chemistry  
of the Georg-August-University School of Science (GAUSS)

submitted by

**Maximilian Daniel Stangier**

from Kirchen (Sieg)

Göttingen, 2022



## **Thesis Committee**

*Prof. Dr. Lutz Ackermann*

Institut für Organische und Biomolekulare Chemie  
Georg-August-Universität Göttingen

*Prof. Konrad Koszinowski*

Institut für Organische und Biomolekulare Chemie  
Georg-August-Universität Göttingen

## **Members of the Examination Board**

1<sup>st</sup> Reviewer: *Prof. Dr. Lutz Ackermann*

Institut für Organische und Biomolekulare Chemie  
Georg-August-Universität Göttingen

2<sup>nd</sup> Reviewer: *Prof. Dr. Konrad Koszinowski*

Institut für Organische und Biomolekulare Chemie  
Georg-August-Universität Göttingen

## **Further Members of the Examination Board**

*Prof. Dr. Dietmar Stalke*

Institut für Anorganische Chemie, Georg-August-Universität Göttingen

*Jun.-Prof. Dr. Johannes Walker*

Institut für Organische und Biomolekulare Chemie, Georg-August-Universität Göttingen

*Dr. Daniel Janßen-Müller*

Institut für Organische und Biomolekulare Chemie, Georg-August-Universität Göttingen

*Dr. Michael John*

Institut für Organische und Biomolekulare Chemie, Georg-August-Universität Göttingen

**Date of the Oral Examination:** May 24, 2022



**TABLE OF CONTENTS**

1	Introduction .....	1
1.1	Transition Metal-Catalyzed C–H Activation .....	2
1.2	Iridium Complexes for C–H Activation.....	8
1.2.1	Iridium-Catalyzed C–H Activation .....	9
1.3	Rhodium-Catalyzed C–H Activation .....	15
1.4	Undirected C–H Functionalization.....	21
1.4.1	Benzylic C–H Fluorination .....	21
1.4.2	Metal-Free Arylation of Benzylic Fluorides .....	25
1.5	Electrochemical C–H Functionalizations.....	27
1.5.1	Electrochemical C–H Fluorination.....	29
1.6	Electro-Catalyzed C–H Activation.....	33
1.6.1	Ruthenium Electro-Catalyzed C–H Activation.....	40
1.6.2	Rhodium Electro-Catalyzed C–H Activation.....	41
2	Objectives .....	48
3	Results and Discussion .....	51
3.1	Iridaelectro-Catalyzed C–H Alkenylation by Redox Catalyst Cooperation .....	51
3.1.1	Optimization Studies for the Iridaelectro-Catalyzed C–H Alkenylation .....	52
3.1.2	Substrate Scope for the Iridaelectro-Catalyzed C–H Alkenylation .....	57
3.1.3	Mechanistic Studies on the Iridaelectro-Catalyzed C–H Alkenylation .....	62
3.1.4	Proposed Catalytic Scenario for the Cooperative Iridaelectrocatalysis .....	67
3.2	Rhodaelectro-Catalyzed Assembly of Chromones <i>via</i> formyl C–H Activation ...	68
3.2.1	Optimization of the Electrochemical Rhodium-Catalyzed formyl C–H Activation of 2-Hydroxybenzaldehydes.....	69
3.2.2	Electrosynthesis <i>versus</i> Chemical Oxidants for the Rhodium Catalysis.....	72
3.2.3	Scope of the Rhodaelectro-Catalyzed formyl C–H Annulation.....	73

3.2.4	Application of Electrocatalytic formyl C–H Activation to the Functionalization of Peptides .....	80
3.2.5	Mechanistic Insights for the Rhodaelectro-Catalyzed Alkyne Annulation of Salicylic Aldehydes.....	87
3.2.6	Proposed Catalytic Cycle for the Rhodaelectro-Catalyzed Annulation of Salicylic Aldehydes.....	96
3.3	Rhodaelectro-Catalyzed C–H Activation of Alkenes .....	97
3.3.1	Optimization Studies for the Rhodaelectro-Catalyzed Synthesis of Pyrroles.....	97
3.4	Electrochemical C(sp <sup>3</sup> )–H Fluorination.....	103
3.4.1	Optimization for the Electrochemical Metal-free C(sp <sup>3</sup> )–H Fluorination ....	104
3.4.2	Scope of the Undirected C(sp <sup>3</sup> )–H Fluorination.....	106
3.4.3	Development of an Electrochemical C–H Fluorination/Arylation Sequence .....	111
3.4.4	Mechanistic Insights by Cyclic Voltammetry.....	112
3.4.5	Proposed Reaction Mechanism.....	115
4	Summary and Outlook .....	116
5	Experimental Part.....	120
5.1	General Remarks.....	120
5.1.1	Solvents and Reagents .....	120
5.1.2	Analytical and Experimental Methods.....	121
5.1.3	Electrochemical Methods.....	125
5.2	General Procedures .....	127
5.2.1	General Procedure A: Iridaelectro-Catalyzed C–H Alkenylation by Redox Catalyst Cooperation.....	127
5.2.2	General Procedure B: Rhodaelectro-Catalyzed Assembly of Chromones <i>via</i> formyl C–H Activation.....	127
5.2.3	General Procedure C: Rhodaelectro-Catalyzed Assembly of Chromones <i>via</i> formyl C–H Activation under Water-free Conditions.....	128

---

5.2.4	General Procedure D: Rhodium-Catalyzed Synthesis of Chromones using Cu(OAc) <sub>2</sub> as the Terminal Oxidant .....	128
5.2.5	General Procedure E: Photoelectrochemical Annulation of 2,3-Aryl-Substituted Chromones.....	128
5.2.6	General Procedure F: Rhodaelectro-Catalyzed Annulation of Alkenes.....	129
5.2.7	General Procedure G: Electrochemical Fluorination of C(sp <sup>3</sup> )-H bonds ....	129
5.2.8	General Procedure H: Benzylation of Electron-Rich Arenes.....	130
5.3	Iridaelectro-Catalyzed C-H Alkenylation by Redox Catalyst Cooperation .....	131
5.3.1	Characterization Data .....	131
5.3.2	Gram Scale Synthesis of <b>41bb</b> .....	143
5.3.3	Cyclic Voltammetry .....	144
5.3.4	Racemization Studies for Phthalide <b>160bd</b> .....	148
5.3.5	H/D Exchange Experiment.....	149
5.3.6	Crystallographic Data of Phthalide <b>41be</b> .....	151
5.4	Rhodaelectro-Catalyzed Assembly of Chromones <i>via</i> formyl C-H Activation .	152
5.4.1	Characterization Data .....	152
5.4.2	Multi-gram Scale Synthesis of <b>48aa</b> .....	200
5.4.3	KIE Studies .....	201
5.4.4	Competition Experiment .....	203
5.4.5	On-line NMR Monitoring in Flow .....	205
5.4.6	Detection of Intermediates by HR-MS.....	207
5.4.7	Crystallographic Data of Chromones .....	209
5.4.8	Studies on Potential Racemization .....	212
5.5	Rhodium-Catalyzed Electrochemical C-H Activation of Alkenes.....	213
5.5.1	Characterization Data .....	213
5.6	Electrochemical C(sp <sup>3</sup> )-H Fluorination .....	215
5.6.1	Quantitative <sup>1</sup> H and <sup>19</sup> F{H}-NMR Analyses for Benzyl Fluorides.....	215

## TABLE OF CONTENTS

---

5.6.2	Fluoride Displacement for the Benzylation of Electron-rich Arenes .....	242
5.6.3	Comparison with Previously Reported Conditions.....	245
5.6.4	Solar Energy Enabled Fluorination.....	248
6	References .....	250
7	Appendix .....	264
7.1	NMR Spectra.....	268



**LIST OF ABBREVIATIONS**

A	ampere
Å	Angstrom
Ac	acetyl
acac	acetylacetonate
Ad	adamantyl
alk	alkyl
Am	amyl
AMLA	ambiphilic metal ligand activation
API	active pharmaceutical ingredients
aq.	aqueous
Ar	aryl
atm	atmospheric pressure
ATR	attenuated total reflection
BDE	bond dissociation energy
BIES	base-assisted internal electrophilic-type substitution
Bn	benzyl
Boc	<i>tert</i> -butyloxycarbonyl
BPhen	bathophenanthroline
BQ	1,4-benzoquinone
br	broad (spectral)
Bu	butyl
C	Celsius
calcd.	calculated
cat.	catalytic
CCDC	Cambridge Crystallographic Data Centre
CCE	constant currency electrolysis
CFL	compact fluorescent lamp
CMD	concerted metalation-deprotonation
cod	1,5-cyclooctadiene
Cp*	pentamethylcyclopentadienyl
CPE	constant potential electrolysis

## LIST OF ABBREVIATIONS

---

C <sub>q</sub>	quaternary carbon
CV	cyclic voltammetry
$\delta$	chemical shift
d	doublet (spectral)
DAST	(diethylamino)sulfur trifluoride
DBA	dibenzylideneacetone
DBU	diazabicycloundecene
DCE	1,2-dichloroethane
DCM	dichloromethane
DDQ	2,3-dichlor-5,6-dicyano-1,4-benzoquinone
DFT	density functional theory
DG	directing Group
Di- <i>t</i> Bu-BQ	2,6-di- <i>tert</i> -butyl-1,4-benzoquinone
DMA	dimethylacetamide
DME	dimethoxyethane
DMF	dimethylformamide
DMSO	dimethylsulfoxide
dppe	1,2-bis(diphenylphosphino)ethane
<i>E</i>	potential
e <sup>-</sup>	electron
<i>E</i> <sub>1/2</sub>	half-peak potential
ECF	electrochemical fluorination
EDG	electron-donating group
<i>ee</i>	enantiomeric excess
EI	electron ionization
<i>E</i> <sub>p</sub>	peak potential
equiv	equivalent(s)
ESI	electrospray ionization
Et	ethyl
EWG	electron-withdrawing group
F	<i>Faraday</i> constant
F <sub>4</sub> -BQ	tetrafluoro-1,4-benzoquinone

Fc	Ferrocene
FE	faradaic efficiency
FG	functional group
g	gram
GC	gas chromatography; glassy carbon
GF	graphite felt
GVL	$\gamma$ -valerolactone
h	hour(s)
Hal	halogen
HAT	hydrogen atom transfer
HBPIn	pinacolborane
HER	hydrogen evolution reaction
Het	heteroatom
Hex	hexyl
HFIP	1,1,1,3,3,3-hexafluor-2-propanol
HMBC	heteronuclear multiple bond correlation
HPLC	high performance liquid chromatography
HR-MS	high-resolution mass spectrometry
HSQC	heteronuclear single quantum coherence
HTE	High throughput experimentation
Hz	hertz
<i>I</i>	current
<i>i</i>	<i>iso</i>
IES	internal electrophilic substitution
IR	infrared
<i>J</i>	coupling constant
KIE	kinetic isotope effect
L	ligand
LED	light-emitting diode
LG	leaving group
LSD	late-stage diversification
$\mu$	micro

## LIST OF ABBREVIATIONS

---

$\mu\text{A}$	microampere
<i>m</i>	<i>meta</i>
M	molar
m	multiplet (spectral)
M.p.	melting point
<i>m/z</i>	mass-to-charge ratio
$\text{M}^+$	parent molecular ion
mA	milliampere
Me	methyl
MeCN	acetonitrile
Med	mediator
MeHQ	4-methoxyphenol
MeTHF	2-methyltetrahydrofuran
mg	milligram
MHz	megahertz
min	minute(s)
mL	milliliter
mmol	millimole
MS	molecular sieve
mV	millivolt
NFSI	<i>N</i> -fluorobenzenesulfonimide
NHPI	<i>N</i> -hydroxyphthalimide
<i>n</i>	quantity
nm	nanometer
NMR	nuclear magnetic resonance
<i>o</i>	<i>ortho</i>
Oct	octyl
Ox	oxidation/oxidized
<i>p</i>	<i>para</i>
p	quintet
PEG	polyethylene glycol
Pent	pentyl

Ph	phenyl
Phth	phthaloyl
Piv	pivaloyl
ppm	parts per million
ppy	phenylpyridine
Pr	propyl
Py	pyridine
Pym	pyrimidine
PyO	pyridine- <i>N</i> -oxide
q	quartet
Q	quinoline
R	rest
Rac	racemic
Red	reduction/reduced
ref.	reference
rt	room temperature
RVC	reticulated vitreous carbon
s	singlet (spectral)
sat.	saturated
SCE	standard calomel
SET	single electron transfer
SPS	solvent purification system
Sub	substrate
<i>T</i>	temperature
<i>t</i>	<i>tert</i>
TAM	triazolyldimethylmethyl
TBAI	tetrabutylammonium iodide
<i>t</i> BuCN	pivalonitril
TEMPO	(2,2,6,6-tetramethylpiperidin-1-yl)oxyl
Tf	trifluoromethanesulfonyl
TFA	trifluoroacetic acid
TFE	2,2,2-trifluoroethanol
THF	tetrahydrofuran

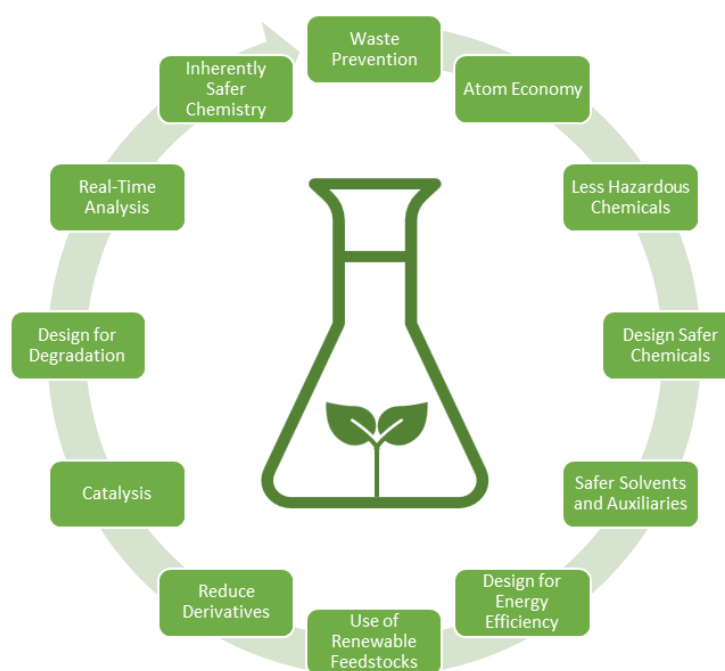
## LIST OF ABBREVIATIONS

---

TIPS	triisopropylsilyl
TLC	thin layer chromatography
TM	transition metal
TMEDA	<i>N, N, N', N'</i> -tetramethylethylenediamin
TOF	time-of-flight
TREAT HF	triethylamine trihydrofluoride
Ts	<i>p</i> -toluenesulfonyl
TS	transition state
V	volt
vs.	<i>versus</i>
W	watt
X	(pseudo)halide
XAT	halogen atom transfer

# 1 INTRODUCTION

Organic synthesis has advanced to a key technology in the fields of material sciences, crop-protection agents, and pharmaceutical industry, among others from the fundamental pioneering synthesis of urea by *Friedrich Wöhler* in 1828.<sup>[1]</sup> Since then, organic synthesis has been and continues to be of great importance to modern society, driving progress and modernization, which is also reflected by the recognition of numerous organic chemists with Nobel Prizes during the 20<sup>th</sup> and 21<sup>st</sup> century.<sup>[2]</sup> Despite the progress and significance, organic synthesis is a resource- and energy-consuming process, requiring vast amounts of solvents, stoichiometric additives, and reagents during often lengthy synthetic routes. During recent years, the awareness and knowledge of the increasing environmental impact of mankind demands for new innovations among various fields to develop overall more sustainable processes. As a consequence, numeric principles<sup>[3]</sup> and theoretical concepts<sup>[4]</sup> have evolved to guide profound developments and improvements within the field of organic synthesis. Major attention was attracted by the “12 Principles of Green Chemistry” established by *Anastas* and *Warner* (Scheme 1.1).<sup>[4e]</sup> Among those, catalysis is considered as a crucial tool to improve the step-, atom- and resource economy and minimize the environmental footprint overall.



**Scheme 1.1** The “12 Principles of Green Chemistry” according to *Anastas* and *Warner*.<sup>[4e]</sup>

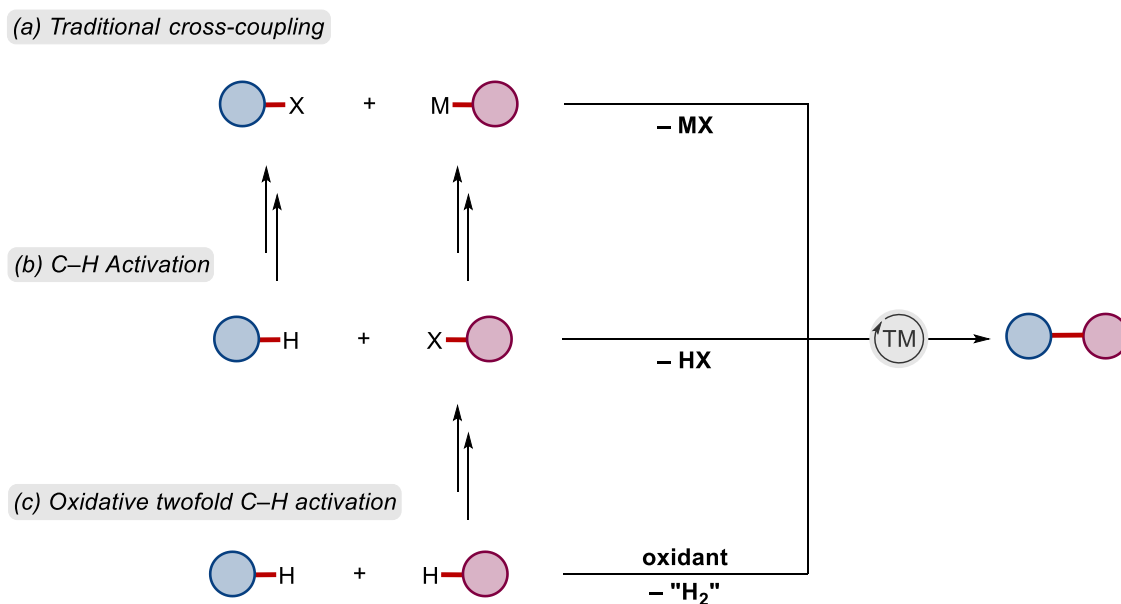
## 1.1 Transition Metal-Catalyzed C–H Activation

The selective and efficient formation of C–C and C–Het bonds is of key relevance to synthetic organic chemistry, as it provides access to the development of new scaffolds important to pharmaceutical-, crop- and materials industries. During the past decades, the discovery of transition metal-catalyzed reactions has revolutionized strategies in synthetic organic chemistry and established entirely new disconnections in comparison to “traditional” approaches.<sup>[5]</sup> Next to the early reports on the copper-catalyzed coupling of aryl halides by *Ullmann*<sup>[6]</sup> and *Goldberg*,<sup>[7]</sup> the functionalization of aryl halides or pseudohalides with organometallic nucleophiles,<sup>[8]</sup> most commonly employing a palladium catalyst, represent a landmark for organic synthesis, which has been recognized with the Nobel Prize to *Heck*, *Negishi*, and *Suzuki* in 2010.<sup>[9]</sup> Additional palladium-catalyzed couplings of (pseudo) aryl halides with terminal alkynes (*Sonogashira-Hagihara*)<sup>[10]</sup> or amines (*Buchwald-Hartwig*)<sup>[11]</sup> highlight the versatility of the concept and add to their translational nature.

Despite the major impetus of cross-coupling reactions on modern synthetic chemistry, lengthy pre-functionalization of the substrates limits the overall sustainability of the catalysis, as more (hazardous) reagents are required, and metal-halide waste is generated (Scheme 1.1.1a). In contrast, the direct, isohypsic functionalization of otherwise inert C–H bonds has emerged as a powerful tool overall, circumventing the installation of organometallic nucleophiles and therefore significantly increasing atom- and step economy (Scheme 1.1.1b).<sup>[12]</sup>

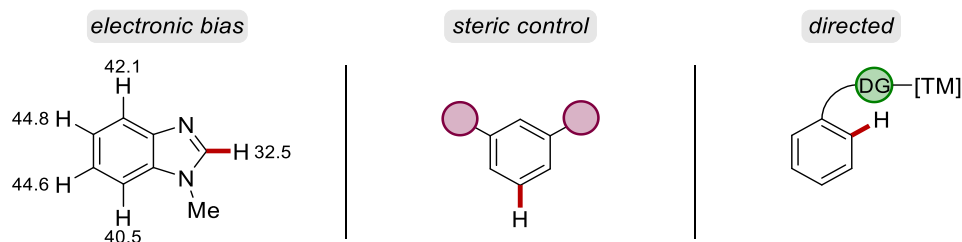
However, as one of the substrates obviates to be functionalized with a (pseudo)halide, the most desirable approach is the direct C–H/C–H functionalization of the reactants (Scheme 1.1.1c).<sup>[13]</sup> This oxidative, cross-dehydrogenative coupling resembles ideal atom-economy formally generating hydrogen as a by-product. In practice, since no oxidative addition of a substrate takes place, stoichiometric amounts of often toxic and expensive (metal)oxidants are required to turn-over the catalyst. Although, twofold C–H activations are characterized by major gains in efficiency in comparison to cross-coupling chemistry, they suffer from poor oxidant economy.<sup>[14]</sup>





**Scheme 1.1.1** Conceptual comparison of transition metal-catalyzed C-C bond formations.

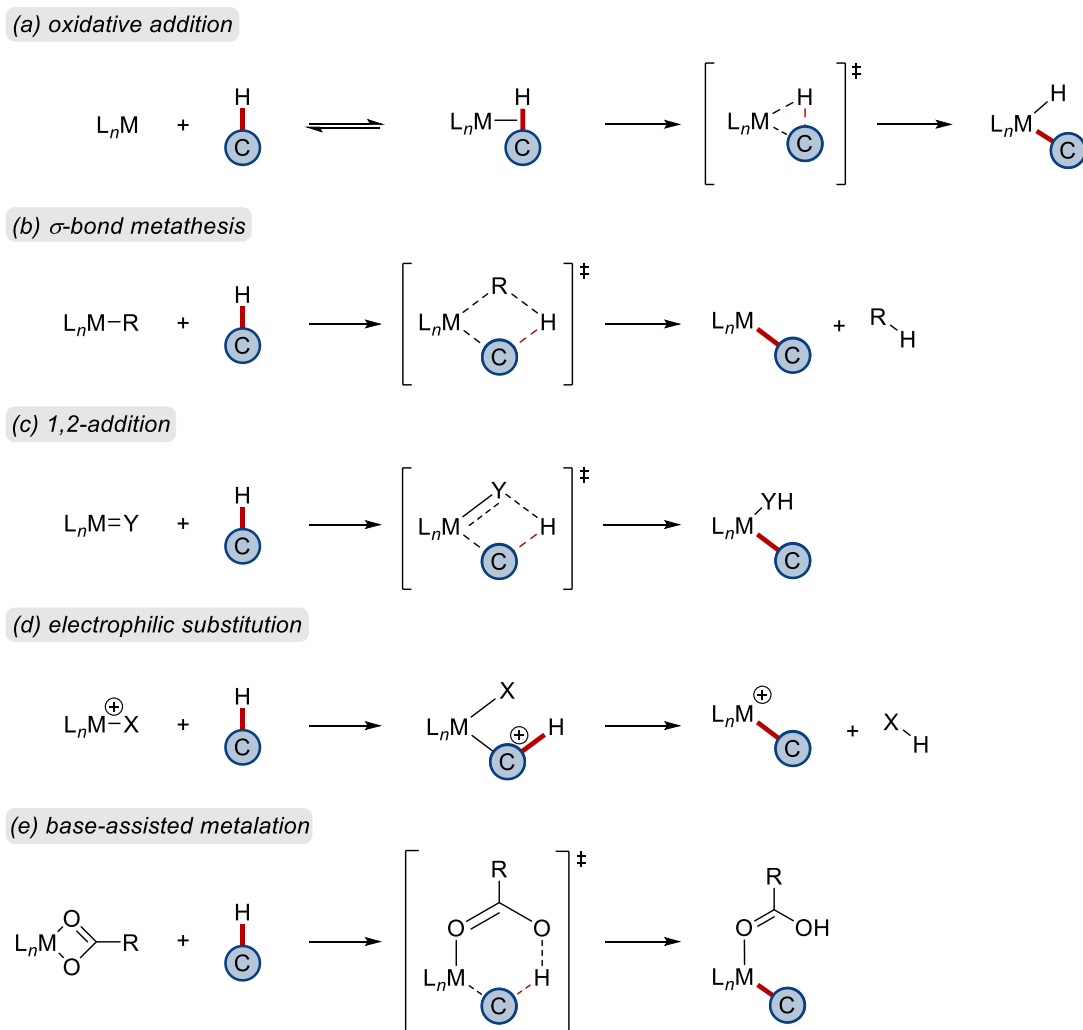
Whereas the regioselectivity is unambiguously determined by the position of the interconverted functional groups in cross-coupling reactions, in C-H activations multiple bonds could potentially be functionalized. To control the site-selectivity in C-H activations, mainly three different concepts have been developed.<sup>[15]</sup> On the one hand, metalation can selectively proceed at the weakest C-H bond, based on the electronic properties, reflected for example by the  $pK_a$ -values<sup>[16]</sup> in the corresponding substrate.<sup>[17]</sup> As such, often heterocyclic compounds exhibit reactivity at a specific position, such as *N*-methyl benzimidazole, which undergoes C-H cleavage at the kinetically most acidic 2-position (Scheme 1.1.2).<sup>[18]</sup> Likewise, steric properties can induce selective C-H cleavage at the most accessible position.<sup>[19]</sup> Since these approaches are largely depending on the inherent substrate features, their application and versatility is rather limited. The most common approach, however, relies on LEWIS-basic functional groups, capable of coordinating to transition metals.



**Scheme 1.1.2** Strategies for selectivity control in C-H activations. Theoretically predicted  $pK_a$ -values for *N*-methyl benzimidazole are given.

Through this coordination the catalyst is oriented in proximity to a specific C–H bond and enables the chelation-assisted C–H scission.<sup>[12e]</sup> In this regard, research during recent years specifically focused on the employment of weakly coordinating,<sup>[20]</sup> transient<sup>[21]</sup> or removeable directing groups.<sup>[22]</sup> Although the vast majority of reported directing groups guide to *ortho*-positions, the extension of the concept to *meta*- and *para*-selective C–H activation of arenes has also been reported.<sup>[23]</sup>

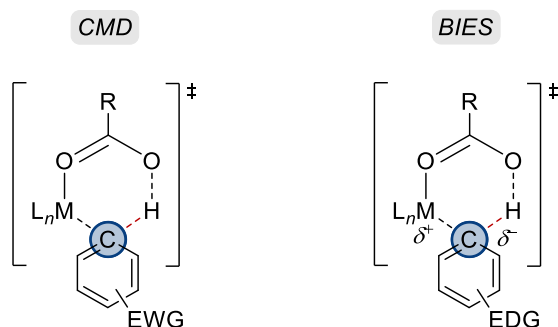
Due to the high interest in C–H functionalizations, the community has extensively studied the mechanism of the underlying C–H activation step. Despite radical-type outer-sphere radical mechanisms,<sup>[24]</sup> which are excluded from this consideration, generally five different modes of organometallic C–H bond cleavage have been proposed. Depending on the metal, its oxidation state, and potential ligands, C–H scission can either occur *via* oxidative addition,  $\sigma$ -bond metathesis, 1,2-addition, electrophilic substitution or base-assisted metalation (Scheme 1.1.3).<sup>[25]</sup> C–H activations proceeding through an oxidative addition pathway often feature electron-rich low valent complexes of late transition metals, e.g. iridium(I) in combination with electron donating ligands. Thereby, interaction of the  $\sigma^*$ -orbital induces a formal two-electron transfer from the metal to the ligand (Scheme 1.1.3a). In contrast, early electron-deficient transition metals, such as lanthanides and actinides with  $d^0$  electronic configuration, typically involve a  $\sigma$ -bond metathesis, which features the formation of a four-membered transition state from metal hydrides or metal alkyl complexes (Scheme 1.1.3b). Mechanistically related to the  $\sigma$ -bond metathesis, a 1,2-addition pathway deviates by a C–H bond addition to an unsaturated M=Y species (Scheme 1.1.3c). In this scenario Y represents a ligand with  $\pi$ -bonding capability, for example alkylidene- or imido complexes. Additionally, electron-poor late transition metals often showcase electrophilic bond activation, which is formally equivalent to the previously discussed  $\sigma$ -bond metathesis. Rarely, palladium(II) complexes exhibit reactivity with C<sub>aryl</sub>–H bonds comparable to classical electrophilic aromatic substitution, when electron-rich arenes were found to undergo accelerated C–H scission. In recent years, mechanistic studies provided support for a base-assisted C–H activation being commonly operative, specifically when bifunctional ligands, such as carboxylates, were employed in the catalysis (Scheme 1.1.3e). Already in 1979 *Sokolov* found evidences for the crucial role of a carboxylate ligand for C–H metalations,<sup>[26]</sup> which were later supported by calculations of *Sakaki*,<sup>[27]</sup> and further experimental results from *Fagnou*.<sup>[28]</sup>



**Scheme 1.1.3** Different mechanisms for organometallic C–H cleavage.

It was suggested that the carboxylate coordinated to the metal center and affected a concerted metalation-deprotonation (CMD, Scheme 1.1.4).<sup>[29]</sup> A similar mode of action has been independently coined by *Macgregor/Davies* observing additional agostic interactions in the 6-membered transition state, defining their results as ambiphilic metal ligand activation (AMLA).<sup>[30]</sup> In these scenarios, a kinetically controlled, preferential C–H cleavage of the more acidic hydrogens of electron-deficient, in competition to electron-rich arenes was observed.<sup>[31]</sup>

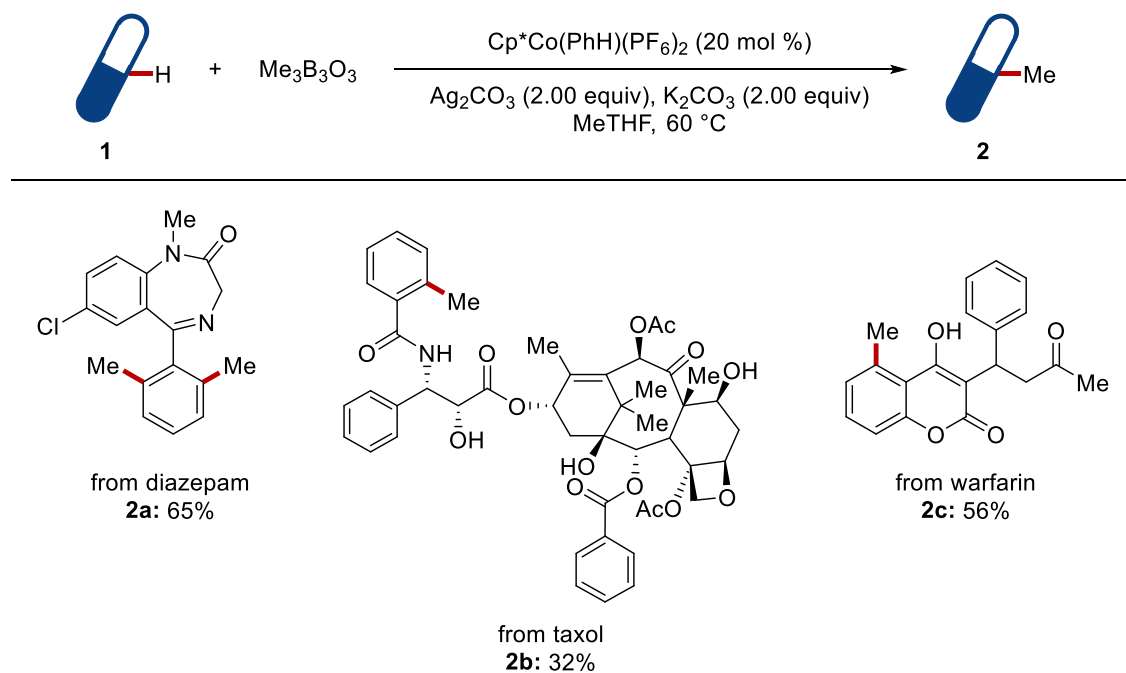
In contrast, *Ackermann* introduced the concept of base-assisted internal electrophilic substitution (BIES), for C–H functionalizations with inherent higher reactivity of arenes with electron-donating (EDG) over substrates with electron-withdrawing groups (EWG), as well as the key role of carboxylate ligands.<sup>[32]</sup>



**Scheme 1.1.4** Differences in transition state models for base-assisted metalation.

The unique transformative potential of modern C–H functionalization strategies is displayed in the application to complex natural product syntheses, as they provide substantially more step-economic access to the desired scaffolds.<sup>[33]</sup> Importantly, a variety of concepts have been established to functionalize C(sp)<sup>3</sup>–H bonds<sup>[34]</sup> and induce enantioselective transformations.<sup>[35]</sup> Recent developments also highlighted the synthetic utility for late-stage diversification (LSD) of natural products, such as carbohydrates<sup>[36]</sup> and peptides,<sup>[37]</sup> as well as active pharmaceutical ingredients (APIs).<sup>[38]</sup>

A fascinating recent example of late-stage methylation was published by *Ackermann* and *Johansson*.<sup>[39]</sup> Extensive investigations *via* high throughput experimentation (HTE) discovered the capability of a high-valent cationic cobalt(III) complex to functionalize aryls **1** bearing various directing groups, using silver carbonate as the stoichiometric oxidant. The approach could be utilized to install methyl-groups on complex APIs, such as taxol **1a**, diazepam **1b**, or warfarin **1c** (Scheme 1.1.5)

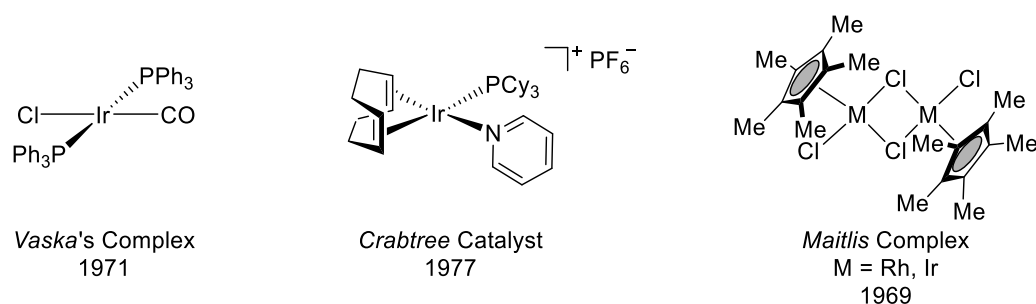


**Scheme 1.1.5** Examples of the late-stage functionalization of natural products and APIs.

Nevertheless, the drawback of stoichiometric amounts of oxidants, remained a key challenge to be addressed for efficient cross-dehydrogenative C–H activations with various transition metals and transformations (*vide infra*).

## 1.2 Iridium Complexes for C–H Activation

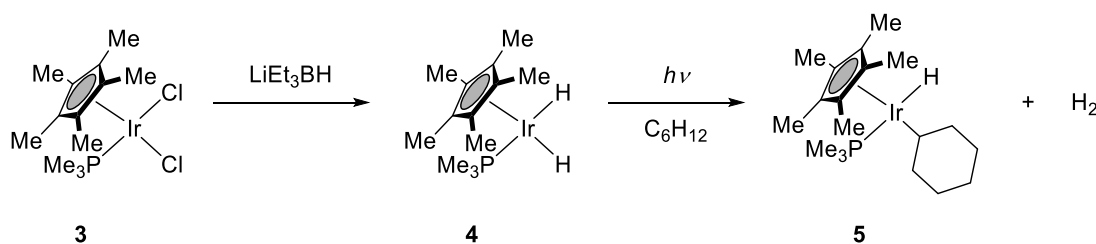
In the history of organometallic chemistry, iridium complexes have often served as model compounds for their more reactive rhodium analogues.<sup>[40]</sup> Specifically, the oxidative addition mechanism could be extensively studied, from the pioneering work of *Lauri Vaska* during the early 1960, when the synthesis and oxidative addition of hydrogen to  $\text{IrCl}(\text{CO})(\text{PPh}_3)_2$  was discovered (Figure 1.2.1).<sup>[41]</sup> However, catalytic performance e.g. for hydrogenation, was not found to be competitive to the rhodium analogs, such as the *Wilkinson* catalyst. This observation was rationalized with the unfavorable de-coordination of a phosphine ligand after oxidative addition, which could facilitate the coordination of a substrate.<sup>[42]</sup> As a result of its lower reactivity, important insights into the mechanism of related complexes could be obtained, as the isolation of stable iridium-intermediates could be achieved. The observed limited reactivity was overcome by the development of cationic catalysts with a reduced metal to phosphine ratio (1:2) by *Schrock*, since phosphine dissociation was not required anymore.<sup>[43]</sup> Subsequently, attempts by *Crabtree*, to further decrease the phosphine to metal ratio to 1:1 in order to synthesize more reactive complexes, led to the development of the *Crabtree* catalyst in 1977, which showed higher hydrogenation activities, especially for tri- and tetrasubstituted olefins, than the *Wilkinson* catalyst.<sup>[44]</sup> Although iridium complexes are generally less frequently used in hydrogenation reactions, in comparison to their rhodium analogues, the enantioselective hydrogenation of imines is superior with iridium and performed on industrial scale in the metolachlor process operated by SYNGENTA.<sup>[45]</sup>



**Figure 1.2.1** Structures of iridium complexes used in catalysis.

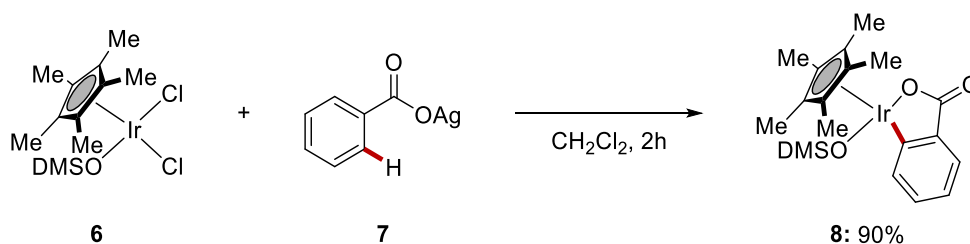
Through these results and the first reports on stable cyclopentadienyl rhodium and iridium complexes by *Maitlis* (Figure 1.2.1),<sup>[46]</sup> *Bergman* investigated the oxidative addition of alkanes to iridium catalysts, after early results from *Chatfield*<sup>[47]</sup> and *Shilov*<sup>[48]</sup> were already suggestive of organometallic C–H activations.<sup>[49]</sup> Indeed, direct formation of an iridium-

alkyl and iridium-aryl species was demonstrated, upon irradiation of an iridium dihydride complex in benzene or cyclohexane, respectively.<sup>[50]</sup> This event, together with related studies of *Graham*,<sup>[51]</sup> assigned a landmark for organometallic chemistry, as the successful isolation of complex **5** represented the first evidence for the feasible C–H activation by homogenous transition metal complexes (Scheme 1.2.1).



**Scheme 1.2.1** Pioneering proof of homogenous oxidative C–H addition to a transition metal by *Bergman* and *Graham* in 1982.

In due course several examples of stoichiometric chelation assisted C<sub>Aryl</sub>–H bond activations have been reported using iridium complexes.<sup>[25e, 52]</sup> Although, cyclometalation of weakly coordinating benzoate **7** was described in 1987 by *Maitlis* for the first time (Scheme 1.2.2), catalytic C–H activations remained scarce (*vide infra*).<sup>[53]</sup>

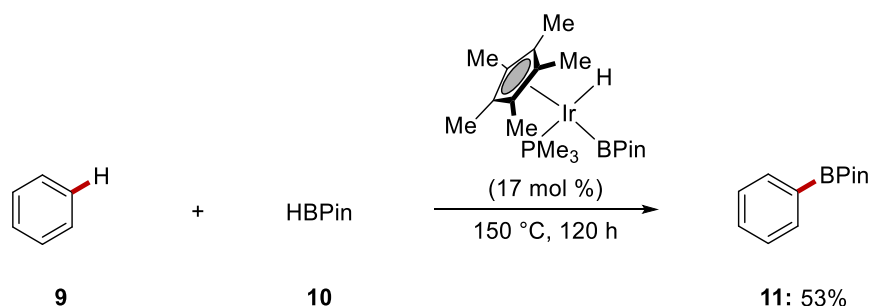


**Scheme 1.2.2** Synthesis of a cyclo-metalated iridium complex **8** upon reaction with weakly coordinating benzoate **7** by *Maitlis*.

### 1.2.1 Iridium-Catalyzed C–H Activation

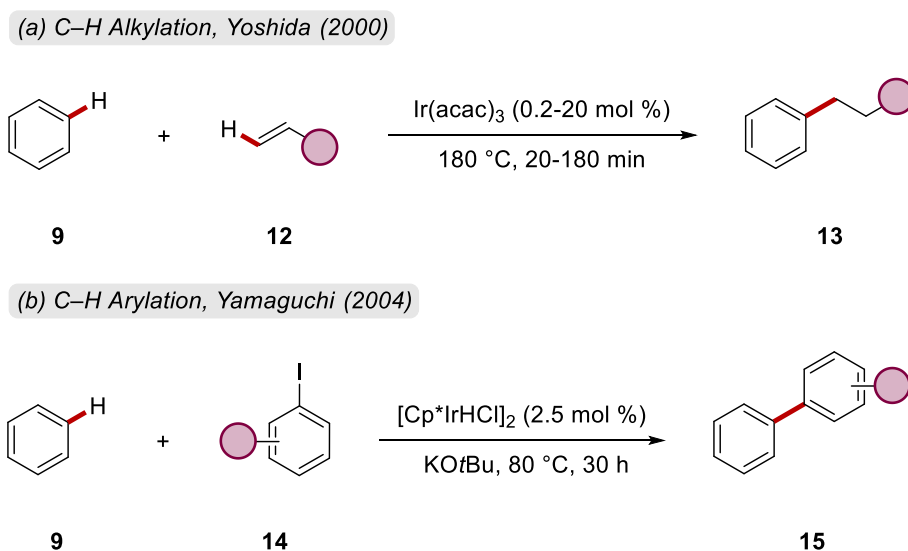
Despite the early progress of catalytic C–H activations with cobalt (1955),<sup>[54]</sup> palladium (1969),<sup>[55]</sup> ruthenium (1986),<sup>[56]</sup> platinum (1978)<sup>[48b]</sup> and rhodium complexes (1994)<sup>[57]</sup> among others<sup>[49]</sup> and the emergence of iridium catalysts for hydrogenation, dehydrogenation, hydroamination or allylic substitution,<sup>[40, 58]</sup> catalytic C–H activations catalyzed by iridium have not been reported until the late 1990's. During initial stoichiometric reactivity studies

of *Bergman*'s complex **4** for the borylation with HBPIn **10** in 1999, *Smith* found substantial formation of arylboron products from the catalytic reaction with the arene **9** solvent (Scheme 1.2.3).<sup>[59]</sup>



**Scheme 1.2.3** Iridium-catalyzed borylation of arenes reported by *Smith*.

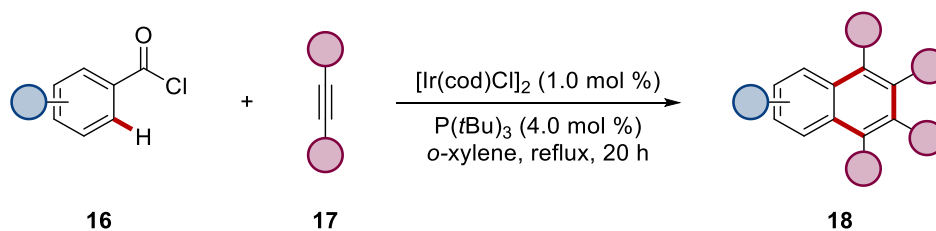
Later, several other reports followed on iridium-catalyzed borylation reactions.<sup>[19b, 60]</sup> Additionally, *Yoshida* reported on a C–H alkylation employing an iridium(III) catalyst and terminal alkenes **12** (Scheme 1.2.4a).<sup>[61]</sup> In contrast to conventional *Friedel-Crafts* alkylations, linear anti-*Markovnikov* products **13** were obtained. Another early example of catalytic iridium-catalyzed reactions, was accomplished by *Yamaguchi* in 2004, using aryl iodides **14** as coupling partners (Scheme 1.2.4b).<sup>[62]</sup>



**Scheme 1.2.4** Iridium-catalyzed C–H functionalizations of benzene.

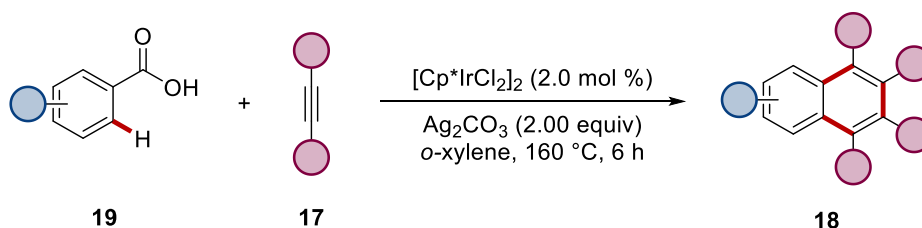
The redox-neutral assembly of naphthalenes **18** from benzoyl chlorides **16** and internal alkynes **17** was reported as early as 2002. Thereby, *Masakatsu* and co-workers employed an iridium(I) pre-catalyst with trialkylphosphine ligands (Scheme 1.2.5).<sup>[63]</sup>





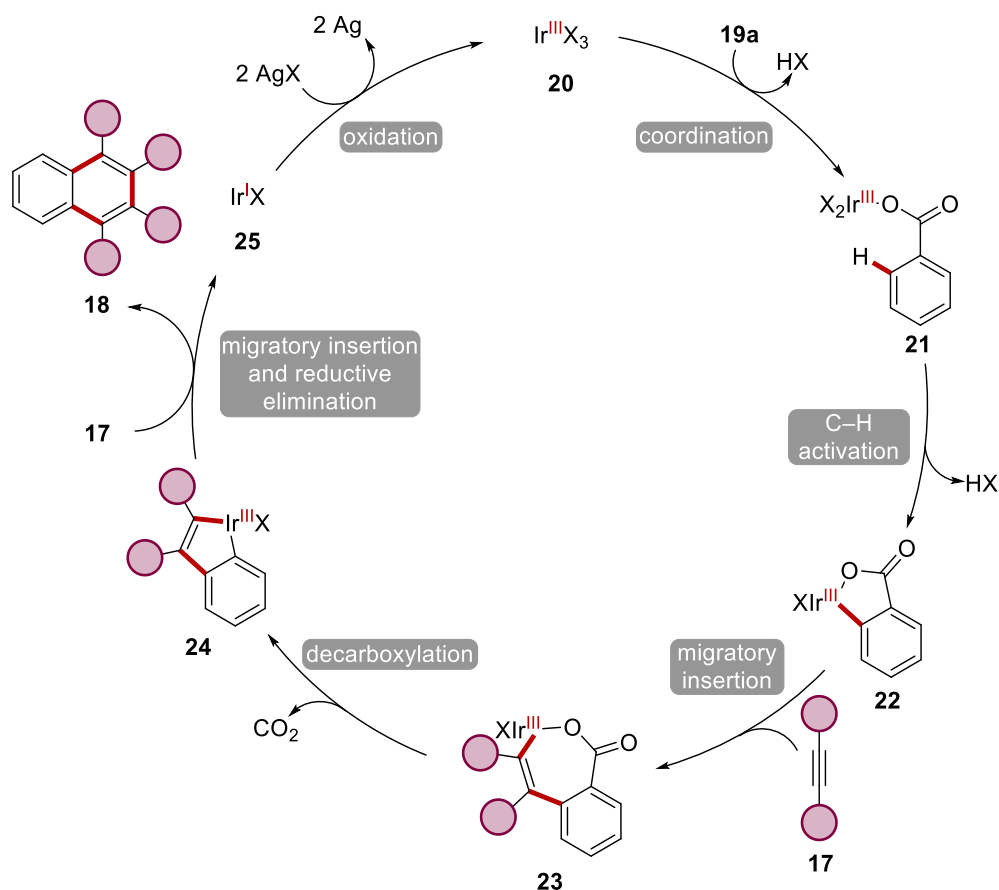
**Scheme 1.2.5** Iridium-catalyzed decarbonylative synthesis of naphthalenes from benzoyl chlorides.

Related to this work, *Miura* developed the first oxidative, iridium-catalyzed transformation in 2007.<sup>[64]</sup> In a decarboxylative fashion, benzoic acids **19** underwent the catalysis to furnish naphthalene derivatives **18**, using the *Maitlis* complex and silver acetate as a stoichiometric oxidant (Scheme 1.2.6). Interestingly, the authors found that the equivalent rhodium catalyst provided isocoumarins **40** in combination with copper acetate as an oxidant (*vide infra*).



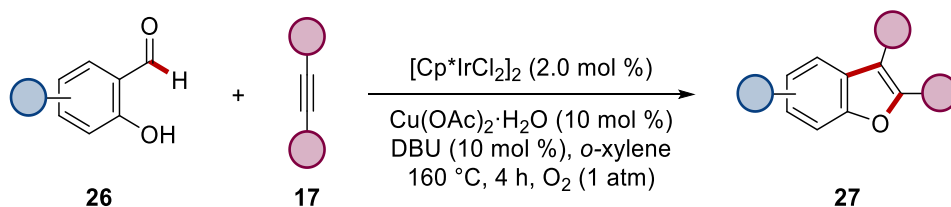
**Scheme 1.2.6** Iridium-catalyzed C–H alkyne annulation of benzoic acids **19**.

The authors proposed that upon coordination of the benzoate to the iridium catalyst, C–H cleavage furnishes a five-membered iridacycle **22** (Scheme 1.2.7). After coordination and subsequent insertion of alkyne **17**, the seven-membered intermediate **23** is generated, which undergoes decarboxylation towards species **24**. Finally, a second alkyne **17** inserts, and reductive elimination occurs to release naphthalene **18**. The catalyst is subsequently oxidized by the silver oxidant to regenerate the active species **20**.



**Scheme 1.2.7** Proposed catalytic cycle for the iridium-catalyzed functionalization of benzoic acid **19a**.

After this report, numerous methods have been developed utilizing the Cp\*Ir(III) catalyst, leveraging C–H arylations, alkylation, alkynylations, and aminations among others, highlighting the unique performance of iridium catalysis.<sup>[13e, 65]</sup> Not only the decarboxylative C–H activation, but interestingly also the decarbonylative annulation of salicylic aldehydes **26** has been disclosed by *Sato* in 2018 (Scheme 1.2.8).<sup>[66]</sup> The catalyst was regenerated by co-catalytic amounts of copper under an atmosphere of oxygen.

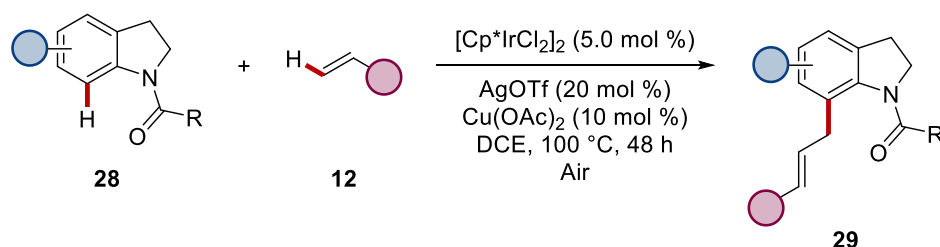


**Scheme 1.2.8** Decarbonylative synthesis of benzofuranes **27**.

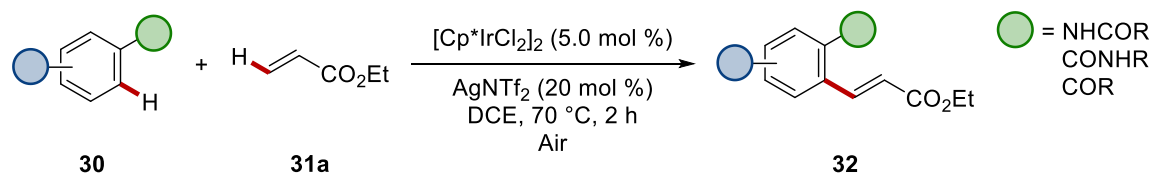
Next to powerful oxidative transformations, iridium catalysts have also emerged as a capable tool for asymmetric C–H functionalizations.<sup>[67]</sup> However, concerning cross-dehydrogenative iridium-catalyzed alkenylations, only few examples have been published in literature to

date.<sup>[22b, 68]</sup> First, *Shibata* reported on a C7-selective alkenylation of indolines **28** with widely available styrenes **12** in 2014 (Scheme 1.2.9a).<sup>[69]</sup> Importantly, the iridium catalyst was guided by the weakly coordinating amide directing group and the catalyst was regenerated with co-catalytic amounts of silver- and copper salts under air. Second, the group of *Sukbok Chang* developed iridium-catalyzed alkenylations of arenes **30** bearing various weakly O-coordinating directing groups, such as amides, anilides or ketones (Scheme 1.2.9b).<sup>[70]</sup> Further, progress has been made by *Ackermann* for the related alkenylation of benzamides and anilides in water using a cost efficient ruthenium catalyst.<sup>[71]</sup>

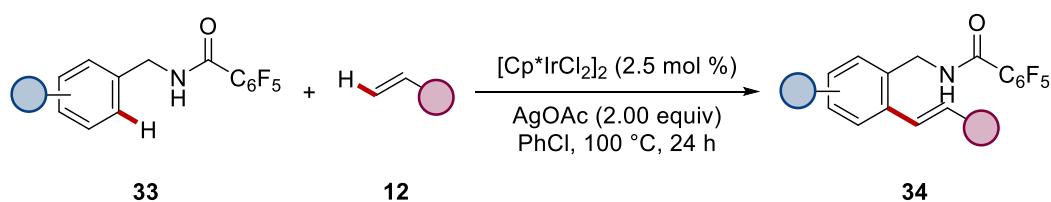
(a) C7-Alkenylation of indolines **28**, *Shibata* (2014)



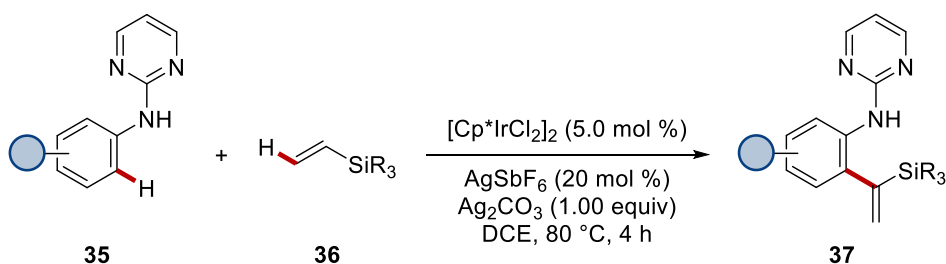
(b) Alkenylation with various DG's, *Chang* (2015)



(c) Alkenylation of benzylamines **33**, *Chen* (2019)



(d) Branch-selective alkenylation of anilines **35**, *Chatani* (2021)



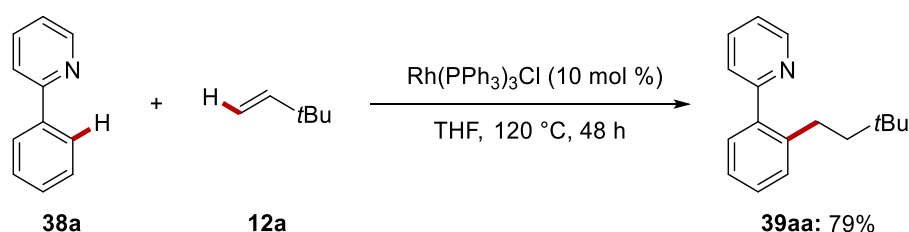
Scheme 1.2.9 Cp\*Ir(III)-catalyzed C–H alkenylations.

In contrast to the amide, ketone and anilide directed alkenylation reported by *Chang*, strongly coordinating phenyl pyridines led to hydroarylation products with acrylates. A similar alkenylation protocol of benzamides was also reported by *Leong*.<sup>[72]</sup> The latter of C<sub>aryl</sub>-H alkenylations could be expanded using benzylamides **33** as directing groups (Scheme 1.2.9c). After coupling the desired benzylamines with pentafluorobenzoic acid, effective iridium-catalyzed *ortho*-alkenylation was observed, using stoichiometric silver acetate as the terminal oxidant.<sup>[73]</sup> Finally, *Chatani* explored vinylsilanes **36** as coupling partners and observed the branch-selective formation of the corresponding products **37** (Scheme 1.2.9d).<sup>[74]</sup> The deviating selectivity was attributed to strain energy during the migratory insertion step, as suggested by DFT calculations.

Importantly, with respect to oxidant-economy, the presented transformations lack sustainability as over-stoichiometric amounts of metal oxidants are required, and the use of air often illustrates unfeasible and dangerous with flammable organic solvents, especially on larger scales.

### 1.3 Rhodium-Catalyzed C–H Activation

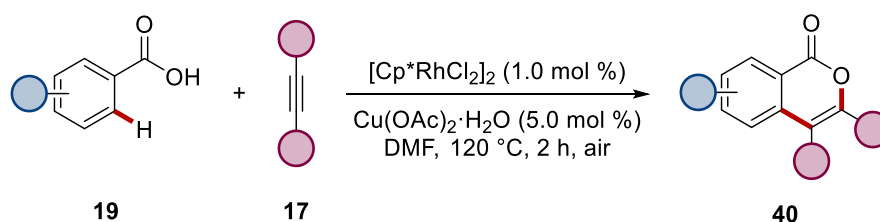
The broad implementation of rhodium catalysts in organic synthesis has emerged since the development of the *Wilkinson* catalyst for the hydrogenation of alkenes and alkynes in the 1960's.<sup>[75]</sup> Moreover, the unique features of homogenous rhodium catalysts gave rise to the synthesis of acetic acid, from methanol and carbon monoxide, also known as *Monsanto* process.<sup>[76]</sup> Although, the *Monsanto* reaction, which can be characterized as a rhodium analog to the palladium-catalyzed *Wacker* synthesis, has already been developed in the 1970's, rhodium-catalyzed C–H activation processes have remained relatively underexplored.<sup>[77]</sup> Pioneering work on directed rhodium-catalyzed C–H activation using 2-phenylpyridine **38a** was reported in 1994 by *Kang*.<sup>[57]</sup> It was found that the *Wilkinson* catalyst was able to efficiently alkylate the arene with neohexene **12a** under chelation-assistance (Scheme 1.3.1).



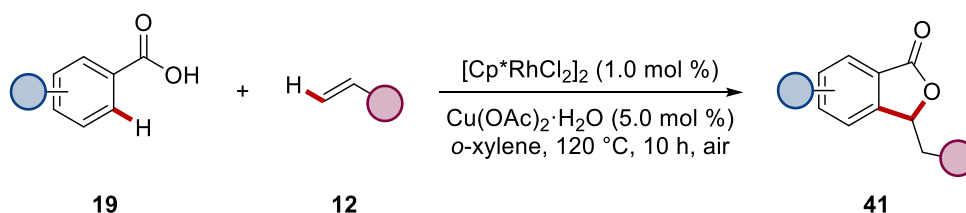
**Scheme 1.3.1** Chelation-assisted *ortho*-alkylation of phenylpyridine **38a** catalyzed by the *Wilkinson* complex.

On the basis of these findings, a variety of redox-neutral processes, such as arylations and alkenylations, featuring oxidative addition to a rhodium(I) catalyst have been developed. Importantly, by employing chiral phosphine ligands, also asymmetric versions have been described.<sup>[78]</sup> However, despite early studies on the oxidative olefination of arenes by *Matsumoto*,<sup>[79]</sup> further oxidative rhodium-catalyzed transformations have been barely developed until 2007. *Miura* disclosed the annulation of benzoic acids **19** with alkynes **17** and activated alkenes **12**, such as acrylates or acrylamides, using a rhodium(III) catalyst to assemble isocoumarins **40** and phthalides **41** respectively (Scheme 1.3.2).<sup>[64, 80]</sup> The initial publication used catalytic amounts of copper acetate under air to regenerate the active catalyst (Scheme 1.3.2c). In comparison to previous rhodium(I)-catalyzed reactions, the C–H activation was expected to occur *via* a redox-neutral electrophilic substitution manifold on a rhodium(III) species. Notably, these transformations have also been proven to be feasible utilizing using less expensive ruthenium catalysts.<sup>[81]</sup>

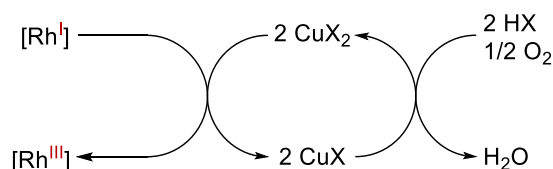
(a) Oxidative annulation of benzoic acids **19** with internal alkynes **17**, Miura (2007)



(b) Dehydrogenative construction of phthalides **41**, Miura (2007)

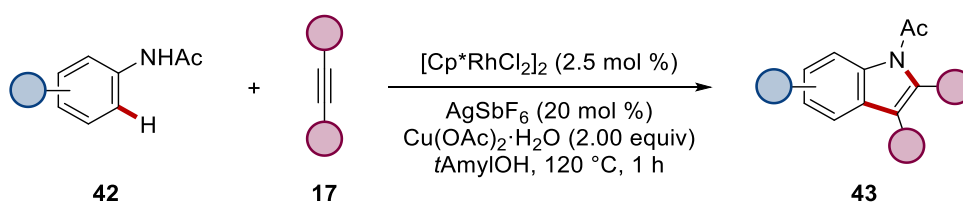
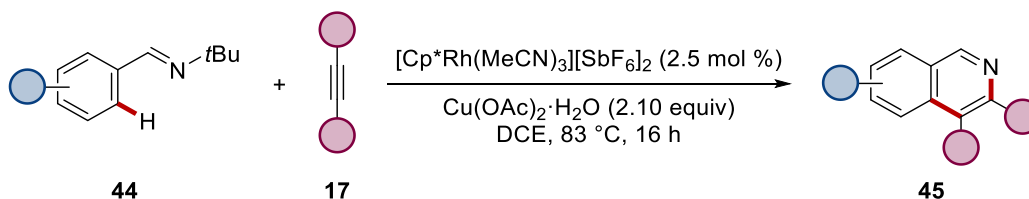


(c) Proposed regeneration of the catalyst



**Scheme 1.3.2** Pioneering oxidative rhodium(III)-catalyzed annulation of benzoic acids **19**.

From this early precedence, numerous oxidative rhodium(III)-catalyzed methods for the construction of various valuable (heterocyclic) scaffolds have been established. Not only due to the lower catalyst loadings, high efficiencies and selectivities, but also because of reaction pathways that are inaccessible with palladium catalysts, rhodium-catalyzed C–H functionalizations have witnessed drastic advances for C–C, C–O and C–N bond formations.<sup>[77]</sup> In terms of rhodium-catalyzed alkyne annulations, key contributions followed the pioneering work of *Miura*. Utilizing anilides **42**, *Fagnou* presented an elegant approach towards a one-step synthesis of indoles **43** (Scheme 1.3.3a).<sup>[82]</sup> Similarly, the same group could facilitate the formation of isoquinolines **45**, when a cationic rhodium(III) catalyst was employed (Scheme 1.3.3b).<sup>[83]</sup>

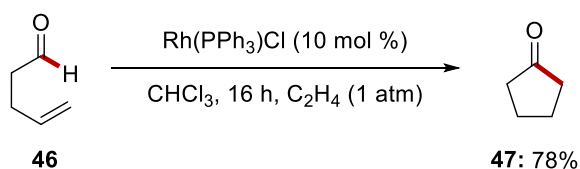
(a) Annulation of acetanilides **42**, Fagnou (2008)(b) Synthesis of isoquinolines **45**, Fagnou (2009)**Scheme 1.3.3** Examples of oxidative rhodium(III)-catalyzed alkyne annulations.

Remarkable endeavors in a related study towards the synthesis of isoquinolinium salts have been made to unravel the mechanism. Isolation of key intermediates has been achieved and exposed that the catalysis proceeds through a seven-membered rhodacycle.<sup>[84]</sup> The scope of directing groups which could assist the  $\text{C}_{\text{Aryl}}\text{-H}$  scission could be successfully extended to naphthols,<sup>[85]</sup> benzamides,<sup>[86]</sup> or phenylpyrazoles.<sup>[87]</sup> Further efforts have been made to extend chelation-assisted C–H activation strategies towards the functionalization of aldehydes.

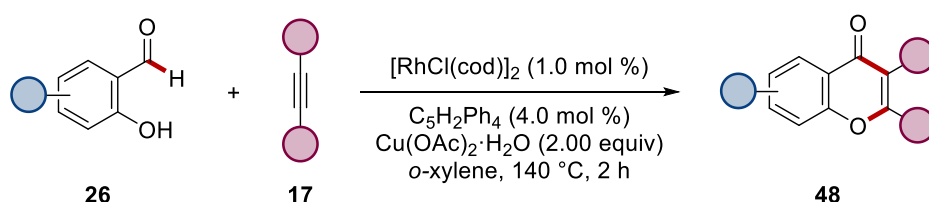
Although rhodium-catalyzed hydroacylations have been of long interest, they mostly relied on redox-neutral transformations, which were catalyzed by rhodium(I)-phosphine catalysts.<sup>[88]</sup> After a pioneering study on the formyl C–H activation of 4-pentenals using stoichiometric amounts of the *Wilkinson* complex by *Sakai* in 1972,<sup>[89]</sup> the first catalytic approach was developed by *Miller* four years later (Scheme 1.3.4a). In an undirected, intramolecular transformation it was found, that 4-pentenal **46** undergoes cyclisation to furnish the corresponding ketone **47**.<sup>[90]</sup> In contrast, *Miura* described that chromones **48** could be efficiently synthesized when a tetraphenyl cyclopentadienyl ligand was used within an oxidative regime (Scheme 1.3.4b).<sup>[91]</sup> The same ligand turned out to also have beneficial effects on the catalytic efficiency of the alkenylation of salicylic aldehydes **26**, as disclosed by *Glorius*.<sup>[92]</sup> When ethyl acrylate **31a** was employed as a reaction partner the corresponding aurones **49** were obtained in a cross-dehydrogenative fashion (Scheme 1.3.4c). A remarkable switch in chemoselectivity, in comparison to the work of *Miura*, was observed when the *Wilkinson* catalyst was employed together with a picoline *N*-oxide oxidant, delivering coumarins **51** after annulation with terminal alkynes **50** (Scheme

1.3.4d).<sup>[93]</sup> Its worth to mention that also allenes were viable coupling partners in rhodium-catalyzed annulation of 2-hydroxybenzaldehydes **26**.<sup>[94]</sup>

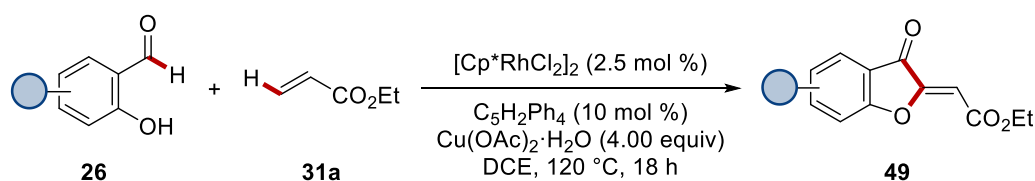
(a) Intramolecular hydroacylation, Miller (1976)



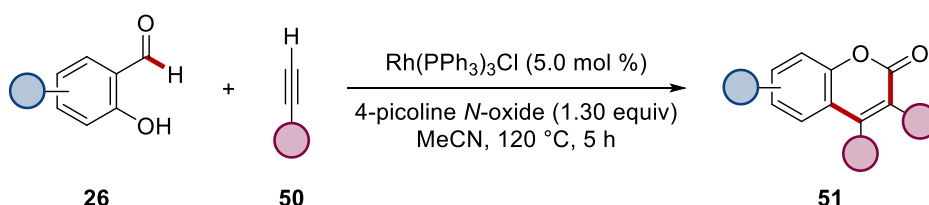
(b) Oxidative annulation of 2-hydroxybenzaldehydes **26**, Miura (2008)



(c) Rhodium-catalyzed assembly of aurones **49**, Glorius (2012)



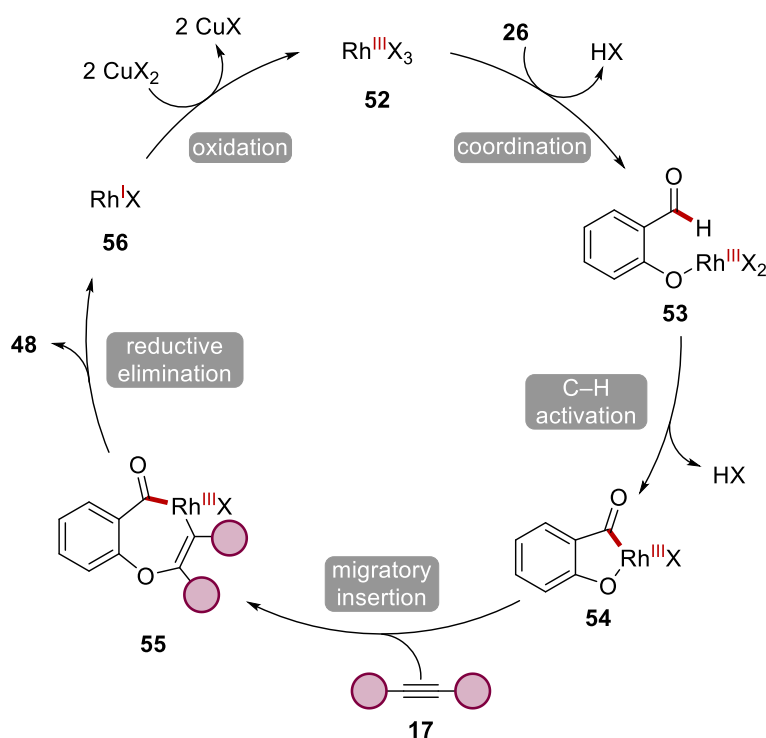
(d) Synthesis of coumarines **51** via formyl C–H activation, Li (2014)



**Scheme 1.3.4** Transition metal-catalyzed formyl C–H functionalizations.

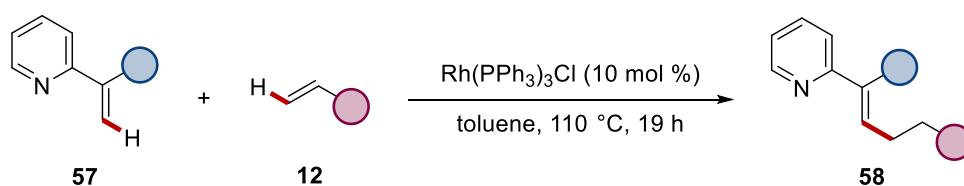
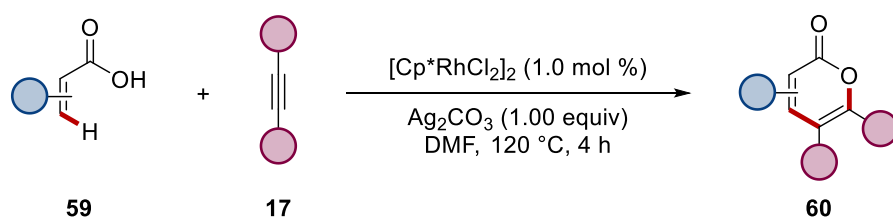
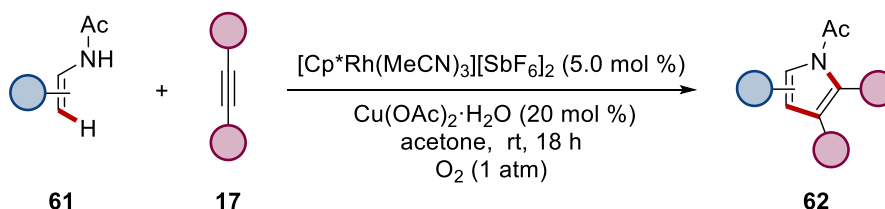
In terms of the catalytic scenario for the synthesis of chromones, *Miura* proposed that the rhodium(III) catalyst is initially coordinated by the phenolic oxygen atom (Scheme 1.3.5).<sup>[91]</sup> Afterwards, a five-membered rhodacycle **54** is generated and alkyne insertion delivers intermediate **55**. Subsequent reductive elimination releases the product **48** and the resulting rhodium(I) species **56** is oxidized by the copper(II) salt to regenerate the active catalyst **52**.





**Scheme 1.3.5** Plausible catalytic cycle for the rhodium-catalyzed annulation of 2-hydroxy benzaldehydes **26** developed by *Miura*.

Next to the activation of formyl C–H bonds, increased attention has been attracted by the C–H functionalization of alkenes. Owing to their higher  $\pi$ -bonding ability, which could inhibit C–H activation, and reactivity towards other reactions manifolds, such as conjugate addition or *Diels-Alder* reactions, functionalization of alkenes is considerably challenging.<sup>[95]</sup> Besides the progress of palladium-catalyzed reactions, rhodium complexes have been proven to be particularly effective catalysts for the insertion into olefinic C–H bonds. Besides the pioneering work on redox-neutral low-valent rhodium catalysis for chelation-assisted C–H activation of olefins starting during the 1990's,<sup>[96]</sup> the field gained new momentum with the discovery of oxidative rhodium(III) catalysis. Based on the initial report of the functionalization of vinyl pyridines **57** by *Kim* (Scheme 1.3.6a),<sup>[96e]</sup> *Miura* successfully utilized internal alkynes **17** to annulate acrylic acids **59** to form the corresponding lactones **60** (Scheme 1.3.6b).<sup>[97]</sup> This catalysis was efficiently accomplished by the use of a rhodium(III) complex and the silver carbonate additive to turn-over the catalyst.

(a) Alkylation of 2-vinylpyridines **57**, Kim (1996)(b) Oxidative functionalization of acrylic acids **59**, Miura (2009)(c) Synthesis of pyrroles **62**, Fagnou (2010)**Scheme 1.3.6** Rhodium-catalyzed C–H functionalization of olefins *via* chelation-assistance.

From this early introduction, many contributions in the field of (oxidative) rhodium(III)-catalyzed vinyl functionalization followed.<sup>[95a]</sup> As such, *Fagnou* was able to assemble the important motif of pyrroles **62** from readily available enamides **61** and internal alkynes **17** (Scheme 1.3.6c).<sup>[98]</sup> During further studies more abundant ruthenium-catalysts were found to be highly active catalysts for the analogous construction of pyrroles.<sup>[99]</sup> Although, these reports unambiguously represent advances with respect to step- and atom-economic aspects, the use of stoichiometric oxidants remains to jeopardize the overall sustainability of the processes.

## 1.4 Undirected C–H Functionalization

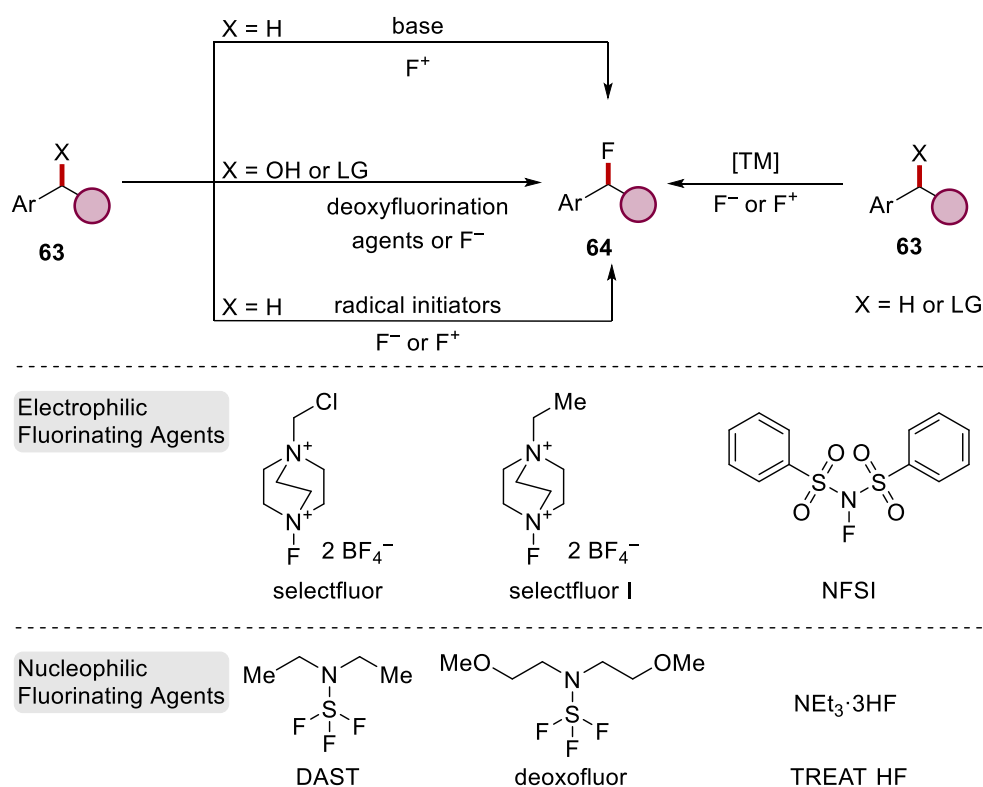
As discussed in the previous chapters, modern transition metal-catalyzed C–H functionalizations is a powerful strategy to chemoselectively construct molecular scaffolds and it is also applied to the late-stage derivatization of complex molecules. However, for the chemoselective C–H activation, the presence of LEWIS-basic groups to guide the catalyst are mostly indispensable (*vide supra*). Although, this strategy exhibits obvious benefits, the dependence on directing groups limits the application and requires their installation and removal. In contrast to the “guided” approach of C–H functionalization,<sup>[100]</sup> innovative concepts have been developed to selectively functionalize C–H bonds distant to LEWIS-basic groups, which are generally classified as remote or undirected C–H functionalizations. The selectivity is predominantly controlled by the inherent electronic or steric environment of the C–H bonds and therefore considered as “innate” reactivity.<sup>[38b, 100]</sup> Within this context, mainly metal-catalyzed carbene/nitrene-,<sup>[101]</sup> or hydrogen atoms transfer (HAT) reactions *via* homolytic bond cleavage have evolved to achieve the undirected C–H functionalization.<sup>[102]</sup> In particular, concepts based on HAT mechanisms, generally involve free radical, carbenoide or nitrenoide pathways and have proven to be a powerful tool to enable metal-free transformations.<sup>[103]</sup> For the generation of radicals, especially photo-,<sup>[68, 104]</sup> and electrochemical techniques<sup>[105]</sup> as well as the use of strongly oxidizing reagents have been employed, among others.<sup>[24, 106]</sup>

### 1.4.1 Benzylic C–H Fluorination

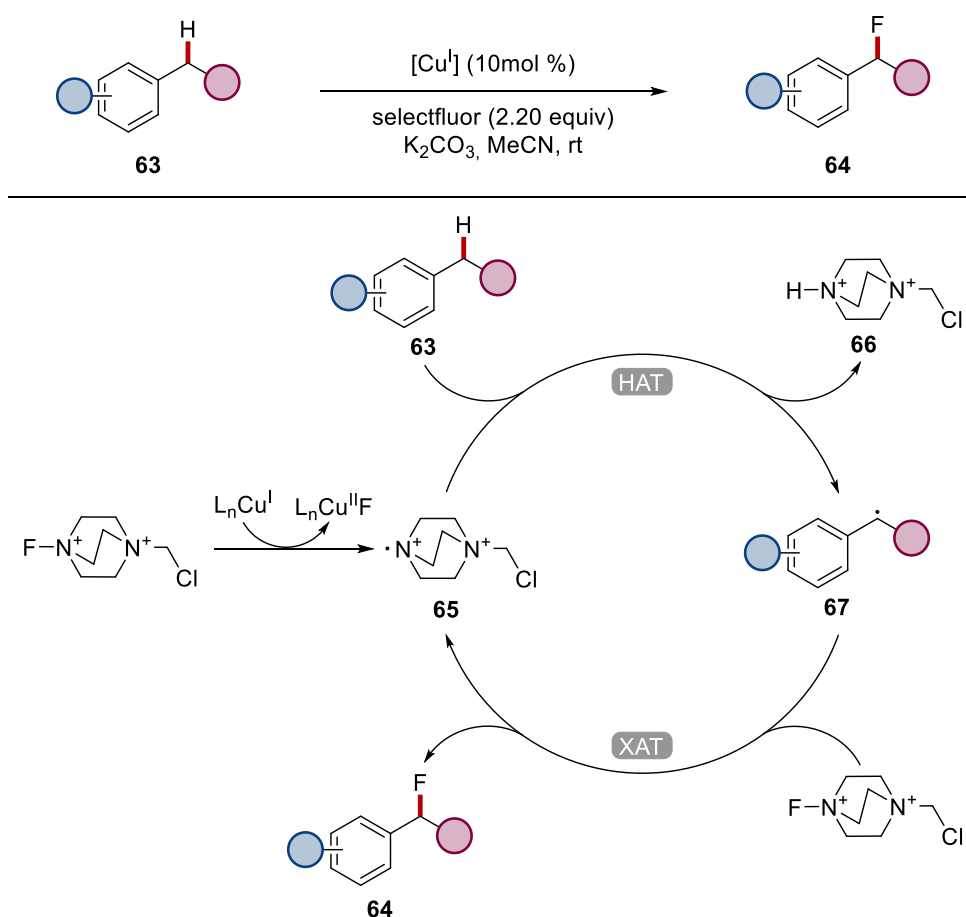
Benzylic C–H bonds represent the weakest C(sp<sup>3</sup>)–H bonds with dissociation energies (BDE) between 84–89 kcal/mol.<sup>[107]</sup> Due to their ubiquitous presence in feedstock and fine chemicals, methodologies for the direct benzylic C–H functionalization are specifically attractive.<sup>[108]</sup> At the same time, the unique properties of the fluorine atom<sup>[109]</sup> substantially impacts the development in medicinal,<sup>[110]</sup> agrochemical<sup>[111]</sup> and material sciences.<sup>[112]</sup> Classical constructions of C(sp<sup>3</sup>)–F bonds are mainly performed by either nucleophilic, electrophilic or radical fluorination (Scheme 1.4.1).<sup>[113]</sup> Thus, transition metals can be used to catalyze the fluorine incorporation either with nucleophilic or electrophilic fluorine sources.<sup>[113a]</sup> However, the introduction of fluorine atoms *via* nucleophilic substitution is generally challenging due to the low nucleophilicity of fluorine, competitive hydrogen bonding interactions and the low solubility of metal fluorides. To facilitate such transformations, leaving groups (LG) have to be installed or hydroxyl groups at benzylic

positions have to be *in-situ* activated for the substitution using specific deoxyfluorinating agents, for instance DAST.<sup>[114]</sup> In terms of price- and atom efficiency, the use of simple fluoride sources, such as metal fluorides or solubilized hydrogen fluoride, represent the most desirable, though.

Besides the nucleophilic fluorination, electrophilic fluorination is a sometimes-viable alternative. However, the direct deprotonation with strong bases, and the subsequent treatment with electrophilic fluorine sources, usually requires the presence of additional electron-withdrawing groups at the benzylic carbon and therefore limits the generality of the reaction. In contrast, the combination of radical initiators and electrophilic fluorinating reagents grants access to a broader scope of substrates and is typically considerably milder (Scheme 1.4.1).



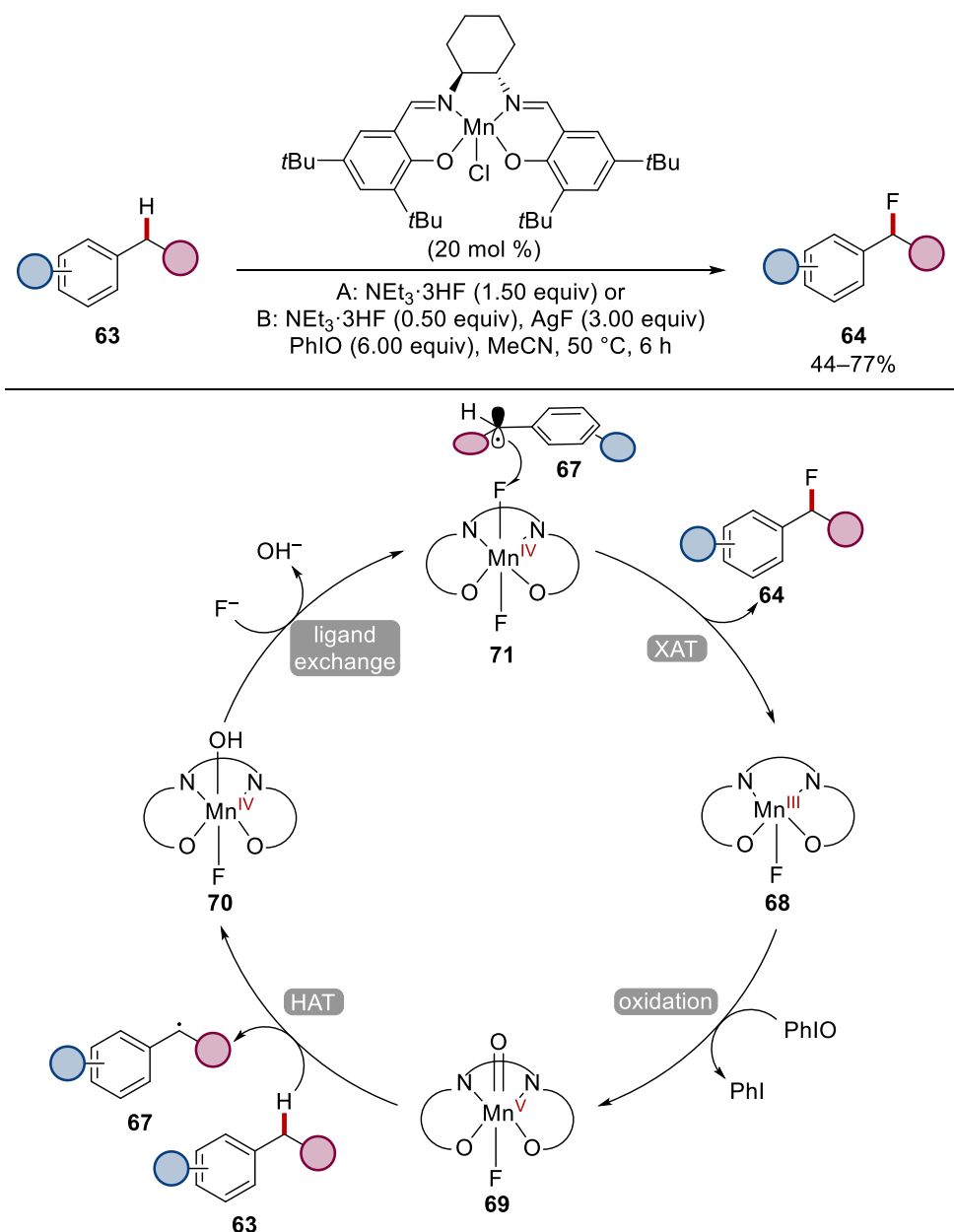
*N,N*-dihydroxypyromellitimide,<sup>[116]</sup> tetracyanobenzene<sup>[117]</sup> or fluorenone<sup>[118]</sup> among others,<sup>[119]</sup> have been described to facilitate fluorination. In terms of metal catalysts, copper,<sup>[120]</sup> iron<sup>[121]</sup> and decatungstate<sup>[119a]</sup> were reported to enable benzylic fluorinations with electrophilic fluorine reagents. Thus, *Lectka* employed copper(I) complexes and proposed a radical chain process with an inner-sphere single electron transfer from copper to a selectfluor molecule, generating a radical cation **65** (Scheme 1.4.2).<sup>[120b]</sup> This species, in turn, abstracts a proton from the benzylic substrate **63** to furnish the benzyl radical **67**. Finally, a fluorine atom is transferred from another selectfluor molecule to the benzylic radical **67** to furnish the product **64** and generate another radical cation **65**, which propagates the chain process.



**Scheme 1.4.2** Copper-initiated C–H fluorination and mechanistic proposal.

Similar mechanistic scenarios are proposed when photocatalysts are employed. However, the use of the electrophilic fluorine reagents, requires at least two equivalents, representing a dramatic disadvantage as to the low atom-economy and high costs of the reagents. In contrast the use of hydrogen fluoride sources, such as  $\text{NEt}_3 \cdot 3\text{HF}$  or metal fluorides, is

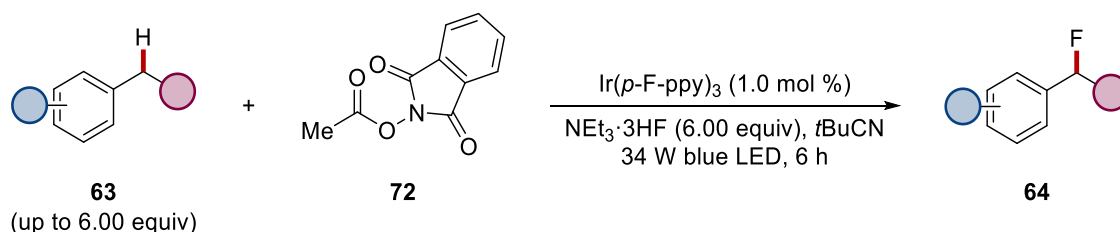
arguably more benign. In 2013, *Groves* reported an oxidative manganese-catalyzed benzylic fluorination using nucleophilic fluoride sources (Scheme 1.4.3).<sup>[122]</sup> When an excess amount of iodosobenzene was used as the terminal oxidant, corresponding fluorinated products **64** could be obtained in 44–70% yields. In a subsequent report the same group utilized the strategy for the late-stage <sup>18</sup>F-labeling of a variety of building blocks and bioactive compounds.<sup>[123]</sup> It was hypothesized that the manganese(III)-salen complex **68** undergoes oxidation towards an manganese(V)-oxo-species **69**, which can abstract a proton from the benzylic substrate **63** via HAT.<sup>[122, 124]</sup> Subsequent fluorine atom abstraction by the generated radical **67** from difluoro-manganese complex **71**, then furnishes the desired product **64**.



**Scheme 1.4.3** Proposed catalytic cycle of the manganese-catalyzed benzylic fluorination.

While this report attracted significant attention due to the absence of directing groups and the use of simple fluoride reagents, the relatively high catalyst loading, together with six equivalents of iodosobenzene, limits the overall sustainability of the approach.

Recently, the *Doyle* group developed a synthesis of benzyl fluorides **64** by abstracting benzylic protons with a photochemically generated methyl radical.<sup>[125]</sup> Subsequent oxidative radical-polar crossover would then furnish a benzyl cation, which was trapped with nucleophilic fluorides (Scheme 1.4.4). Albeit the significantly lower catalyst loading, as compared to the approach by *Groves*, the limiting reagent was the redox-active *N*-acyloxyphthalimide **72** and the benzylic substrates **63** were needed in excess of up to 6.00 equivalents.



**Scheme 1.4.4** Photoredox-catalyzed synthesis of benzyl fluorides.

## 1.4.2 Metal-Free Arylation of Benzylic Fluorides

In addition to the great interest in the synthesis of fluorinated compounds for their unique properties, C–F activation constitutes a valuable tool for the selective modification or coupling towards non-fluorinated compounds.<sup>[126]</sup> Although fluoride has a diminished leaving group ability in the series of bimolecular substitution reactions on alkyl halides, the activation of benzylic fluorides by hydrogen-bonding interactions has been developed as a fascinating strategy to install various nucleophiles, such as alcohols,<sup>[127]</sup> amines,<sup>[128]</sup> and importantly also electron-rich arenes, featuring *Friedel-Crafts*-type reactivity.<sup>[126c, 129]</sup>

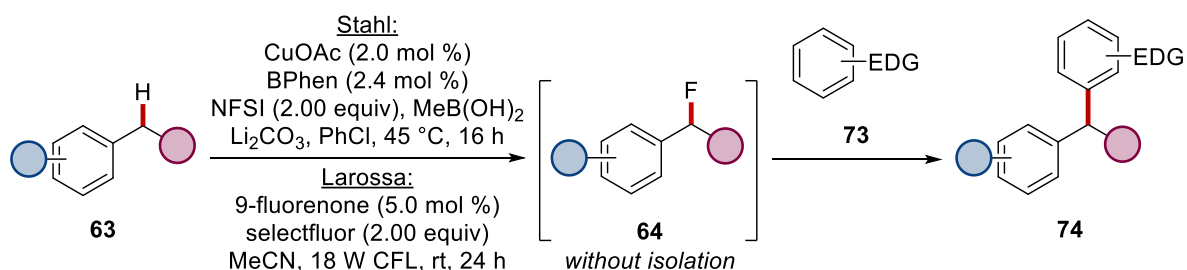
An important advancement for the synthetic utilization has been established by *Paquin* in 2014, when benzyl fluorides **64** were efficiently arylated using HFIP as a cosolvent with strong hydrogen bonding capabilities (Scheme 1.4.5a).<sup>[130]</sup> Notably, the disclosed reactivity could not be accomplished with other benzyl halides or leaving groups in benzylic positions.

Recently, Stahl reported on a copper-catalyzed C–H fluorination using NFSI as an oxidant, that was used to install various electron-rich arenes **73** after quenching and filtrating the fluorination reaction mixture (Scheme 1.4.5b).<sup>[120a]</sup> The authors could further highlight the strategic advantage of an initial fluorination step, by coupling benzyl fluorides **64** with other *O*- and *N*-nucleophiles, which are otherwise not accessible by a oxidative copper-catalyzed C–H functionalization. In the same year, Larossa and co-workers developed an elegant one-pot, two-steps approach towards the arylation of benzylic positions.<sup>[131]</sup> In a first step substrates **63** are fluorinated in a photo-catalyzed fashion, employing selectfluor as oxidant and fluoride source (Scheme 1.4.5b). Subsequently, the corresponding arene **73** is added and the mixture is heated to furnish the corresponding products **74**.

(a) Arylation of benzyl fluorides enabled by hydrogen bonding, Paquin (2014)



(b) Benzylic C–H fluorination/arylation cascade, Stahl/Larossa (2020)

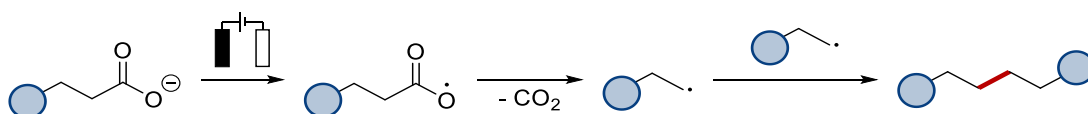


**Scheme 1.4.5** Benzyl fluorides **64** for subsequent arylations and C–H fluorination/arylation sequences.



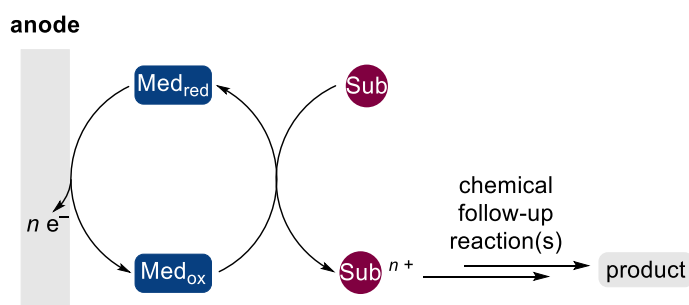
## 1.5 Electrochemical C–H Functionalizations

Electroorganic synthesis has emerged as a powerful and environmentally-benign tool for the oxidation and reduction of organic substrates. The first electrochemical electron-transfer reaction in the field of organic syntheses was conducted by *Faraday*<sup>[132]</sup> and in greater detail studied in 1848 by *Kolbe* (Scheme 1.5.1). Upon anodic oxidation of carboxylate-ions, carbon dioxide is eliminated to generate a carbon-centered radical that homocouples to form a new carbon–carbon bond.<sup>[133]</sup>



**Scheme 1.5.1** *Kolbe's* anodic dimerization of carboxylates.

Since this pioneering report, numerous electrochemical strategies have been developed for the generation of radical-cations, radical-anions, carbocations or carbanions to construct valuable scaffolds by C–C or C–Het bond formations in a sustainable manner.<sup>[105, 134]</sup> Importantly, the use of organic electrochemistry does not only reduce the environmental footprint of a given transformation, but can provide access to overall safer and milder processes.<sup>[135]</sup> With respect to chemoselectivity, the applied potential can be precisely controlled to prevent undesired side reactions. The potential of organic electrochemistry was showcased by the development of several industrial processes,<sup>[136]</sup> such as the reductive dimerization of acrylonitril by *Monsanto*,<sup>[137]</sup> and the *Simons* Fluorination,<sup>[138]</sup> as well as elegant applications to natural product syntheses.<sup>[139]</sup> Alternatively to direct electrolysis, oxidation of an organic substrates can also be facilitated by a homogeneous redox catalyst (indirect electrolysis, Scheme 1.5.2). This design can improve chemoselectivity, as it avoids over-oxidation of the substrates and enhances reaction efficiency due to reduced electrode-passivation. In some cases, a switch in selectivity can be achieved or the kinetic inhibition of the analogous heterogenous process can be successfully eliminated.<sup>[134b]</sup>

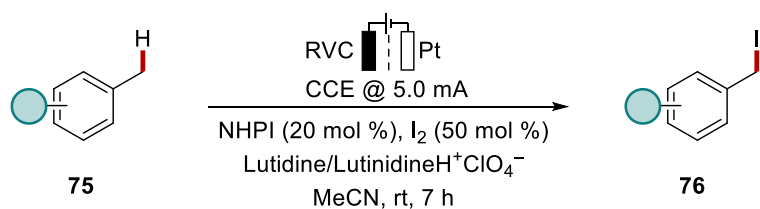


**Scheme 1.5.2** Indirect electrolysis.

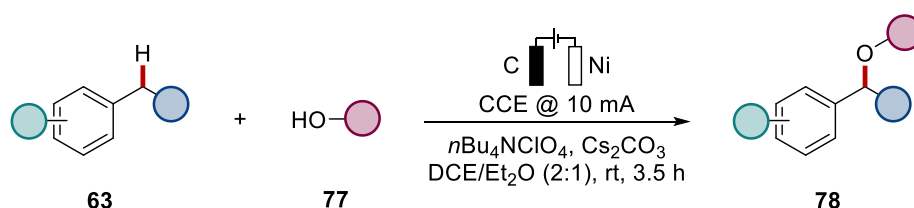
However, the reactivity and selectivity of electrooxidative processes in direct or indirect electrosyntheses is dictated by the HOMO levels, and therefore dependent on the innate properties of a given substrate.<sup>[134c]</sup>

Among undirected electrochemical C–H functionalizations, the coupling with nucleophilic reagents at benzylic positions represents an attractive approach, owing to their relatively low bond dissociation energy and the omnipresent existence in naturally occurring scaffolds, bioactive compounds, and commercial chemicals (*vide supra*).<sup>[108, 140]</sup> In 2018, *Stahl* reported on a mild iodination of toluenes **75**, using *N*-hydroxyphthalimide as a redox-mediator in a divided cell set-up (Scheme 1.5.3a).<sup>[141]</sup> In contrast, *Lei* and co-workers developed an electrochemical etherification, featuring a user-friendly undivided cell set-up to furnish oxygenated products **78** in good yields (Scheme 1.5.3b).<sup>[142]</sup> Based on pioneering studies by *Yoshida* with cationic auxiliaries for the amination,<sup>[143]</sup> *Xu* reported on the direct amination of secondary benzylic positions using electrochemically stable tosylamines **79** (Scheme 1.5.3c).<sup>[144]</sup> The reaction was proposed to be initiated by anodic oxidation of the arene, followed by subsequent deprotonation towards the benzylic radical **82**. Further oxidation and nucleophilic attack of the amine **79** to the generated carbocation **83** delivers the corresponding products **80**. Interestingly, the secondary positions were site-selectively functionalized over tertiary carbon atoms, which was attributed to stereoelectronic effects.

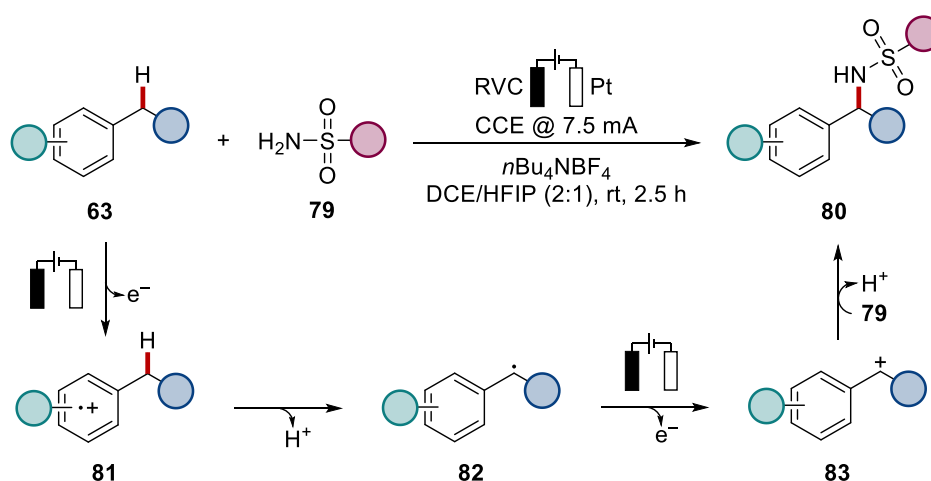
## (a) Mediated electrochemical iodination, Stahl (2018)



## (b) Electrochemical etherification, Lei (2020)



## (c) Electrochemical amination, Xu (2021)



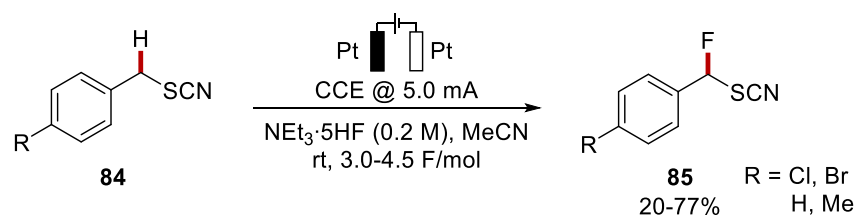
Scheme 1.5.3 Recent examples of electrochemical benzylic C–H functionalization.

## 1.5.1 Electrochemical C–H Fluorination

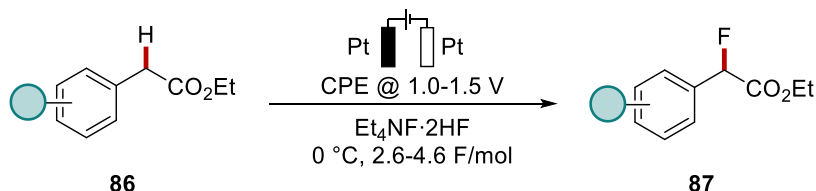
The introduction of fluorine atoms to anodically generated carbocations represents a highly desirable transformation, considering the importance of fluorinated scaffolds in various industries and the abundance of nucleophilic fluoride sources. However, electrode passivation along with reduced nucleophilicity, caused by the strong tendency for hydrogen-bonding interactions, render this approach specifically challenging. Furthermore, a vast majority of electrochemical fluorination reactions (ECF), install the fluorine in decarboxylative fashions,<sup>[145]</sup> add to double bonds of alkenes or use dithioacetals as auxiliaries.<sup>[146]</sup> As to the *Simons* process, the reaction is not connected to a specific transformation, but rather associated with the principal technique of electrochemical (per)fluorinations of various organic and inorganic substrates, such as carboxylic acids,

alcohols, ketones or amines, in anhydrous liquid hydrogen fluoride using nickel electrodes.<sup>[138, 147]</sup> Regarding the mechanism, it is believed that anodic currents generate highly oxidizing nickel fluorides, which subsequently react with the substrates. That not the organic substrates are electrochemically oxidized first was supported by *Sartori* and co-workers, who independently added the substrate after the electrolysis and observed product formation.<sup>[148]</sup> In contrast, research during the last decades used anodic currents to directly oxidize substrates to undergo chemical follow-up reactions. In this regard, the selective electrochemical C–H fluorination of benzylic positions is highly desirable with respect to atom and step economy, but commonly requires substrates bearing additional electron-withdrawing groups at the benzylic methylene group. As such, the ECF of thiocyanates **84** has been disclosed by *Fuchigami* using an undivided cell and triethylamine pentahydrofluoride (Scheme 1.5.4a).<sup>[149]</sup> In terms of the scope, the reaction was efficiently accomplished on *para*-chloro and bromo thiocyanate **84**, but was not indicated to be applicable for other substituents, than *para*-methyl and the unsubstituted arene. Apart from benzylic thiocyanates **84**, tetralone and phenylacetic acid esters **86** were also proven to be viable substrates for the fluorination under constant potential conditions.<sup>[150]</sup> The electrolysis was conducted in neat fluoride containing ionic liquid and methoxy-substituents on the arene were required for a sufficient reaction outcome (Scheme 1.5.4b).

(a) Anodic fluorination of benzyl thiocyanates **84**, *Fuchigami* (2000)



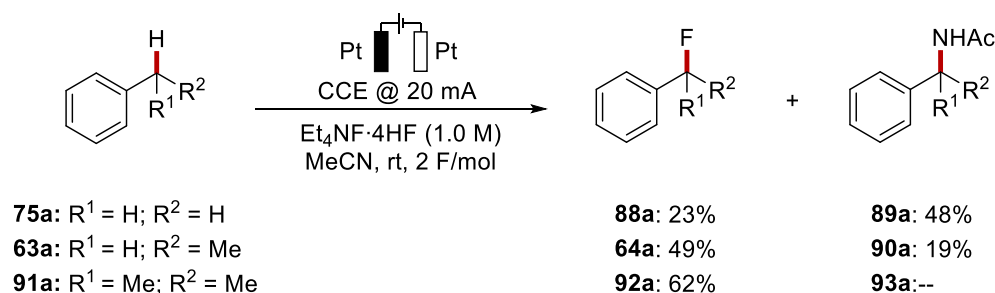
(b) Electrochemical fluorination of phenylacetic acid esters **86**, *Yoneda* (2003)



**Scheme 1.5.4** Representative examples of electrochemical fluorination of acidic benzylic methylene groups.

Apart from the electrochemical C–H fluorination of acidic benzylic substrates, the direct functionalization of otherwise non-activated benzylic positions remained challenging. After seminal reports,<sup>[151]</sup> *Fuchigami* discovered electrochemical C–H fluorinations without

additional electron withdrawing groups at the benzylic position in 2002.<sup>[152]</sup> Related to previous studies employing more activated substrates, a competitive acetamidation reaction, through the nucleophilic attack of acetonitrile, was observed (Scheme 1.5.5). While fluorination exclusively took place on cumene (**91a**), competitive C–H amidations occurred with less hindered benzylic substrates, such as ethylbenzene (**63a**) and toluene (**75a**).

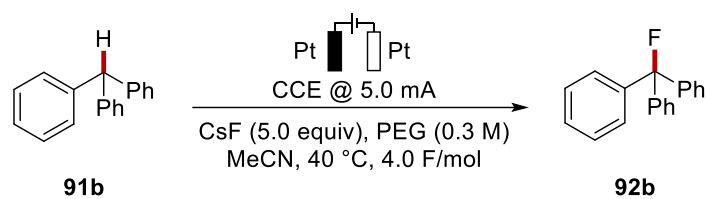


**Scheme 1.5.5** Benzylic fluorination of toluene (**75a**), ethylbenzene (**63a**), and cumene (**91a**) by *Fuchigami*.

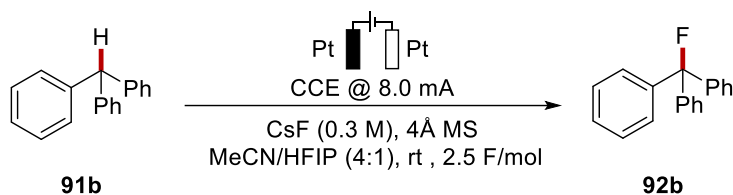
Progress in the following years has mainly focused on the use of more accessible fluoride sources, specifically alkali-metal fluorides. In 2012, *Fuchigami* achieved the fluorination of triphenylmethane **91b** using polyethylene glycol (PEG) as chelating additive to solubilize the potassium and cesium fluorides (Scheme 1.5.6a).<sup>[153]</sup> Recently, *Inagi* observed the beneficial effect of fluorinated alcohols in combination with cesium fluoride for the ECF in acetonitrile (Scheme 1.5.6b).<sup>[154]</sup> However, the scope of the ECF, besides triphenylmethane **91b**, was limited to diphenylmethane and *para*-methoxy phenyl acetic ester which were shown to undergo the transformation in moderate yield (56% and 38%). Other substrates, for instance activated thioethers or deoxybenzoines, were insufficiently fluorinated.

A related transformation was reported by *Lei* and co-workers who selectively cleaved the C–C bond of various phenyl cyclopropanes **93** under electrooxidative conditions to obtain 1,3-difluorinated products **94** (Scheme 1.5.6c).<sup>[155]</sup> In comparison to previous fluorination strategies, easily miscible and more cost-effective  $\text{NEt}_3 \cdot 3\text{HF}$  was used as the fluoride source.

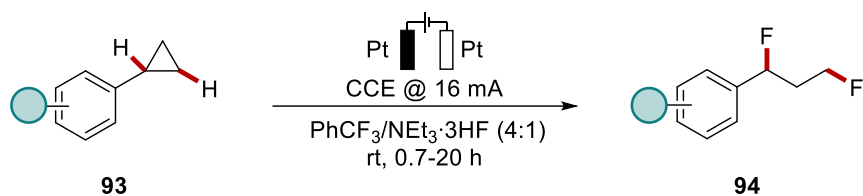
(a) *Electrochemical fluorination with alkali-metal fluorides, Fuchigami (2012)*



(b) *Electrochemical fluorination in fluorinated solvents, Inagi (2021)*



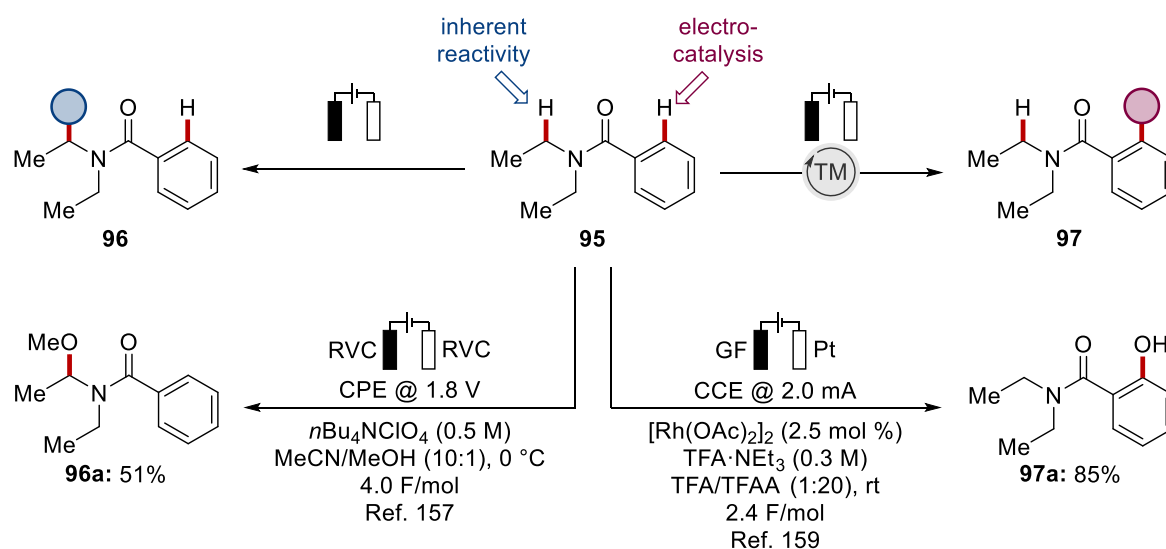
(c) *Electrochemical fluorination of cyclopropanes, Lei (2021)*



**Scheme 1.5.6** Electrochemical benzylic C–H fluorinations with nucleophilic fluorides.

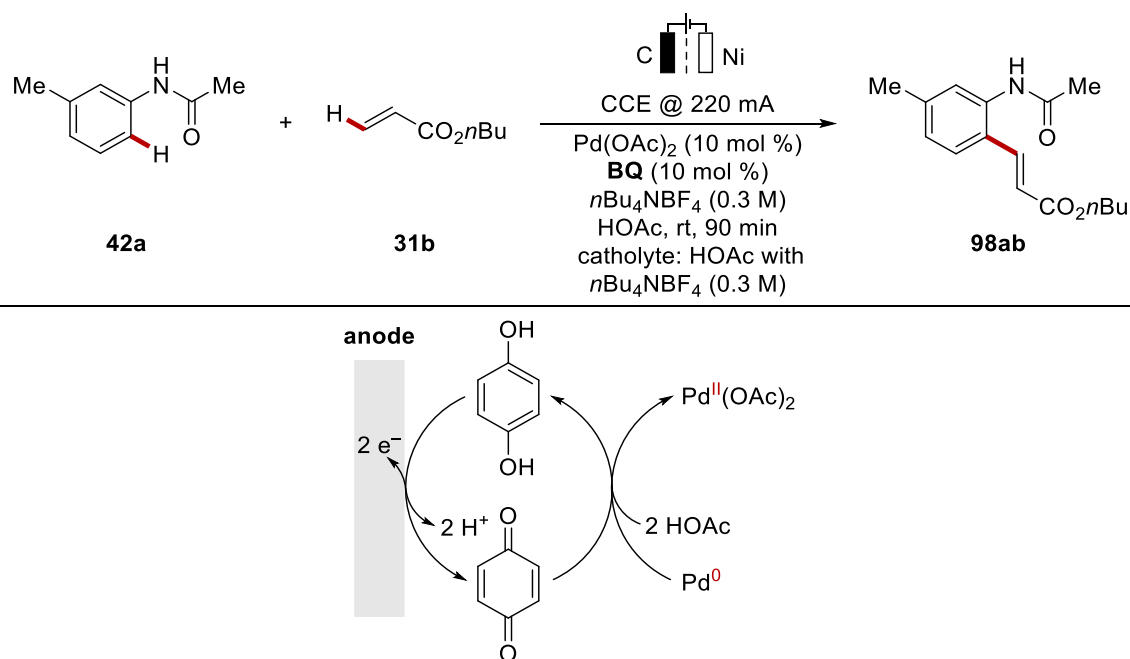
## 1.6 Electro-Catalyzed C–H Activation

Most substrates capable of undergoing electrochemical C–H functionalizations contain activated C–H bonds.<sup>[156]</sup> In this regard, the development of direct oxidative functionalizations of inert C–H bonds by transition-metal catalysis has emerged as a powerful toolbox for step- and atom-economic assembly of various scaffolds (*vide supra*). Since oxidative C–H activations mostly rely on stoichiometric amounts of toxic or expensive oxidants, the replacement of these by sustainable electricity, could increase the overall atom economy and allow the functionalization of C–H bonds, which are otherwise unreactive in traditional electrosynthetic transformations. The complementary chemoselectivity of electrocatalysis and electrosynthesis can be remarkably exemplified by the respective, reactive positions of tertiary benzamide **95** (Scheme 1.6.1): In classical *Shono*-type reactivity, acidic C–H bonds in the  $\alpha$ -position to the nitrogen would get functionalized with nucleophiles, such as methanol,<sup>[157]</sup> upon oxidation to an iminium ion intermediate.<sup>[158]</sup> However, when transition metals are employed under electrooxidative conditions, for instance a rhodium catalyst for the *ortho*-hydroxylation towards benzamide **97a**,<sup>[159]</sup> the selective functionalization of otherwise inert C–H bonds can be accomplished and has led to the great emergence of metallaelectrocatalysis.<sup>[14, 156, 160]</sup>



**Scheme 1.6.1** Reactivity comparison of classical organic electrosynthesis and transition metal electrocatalysis.

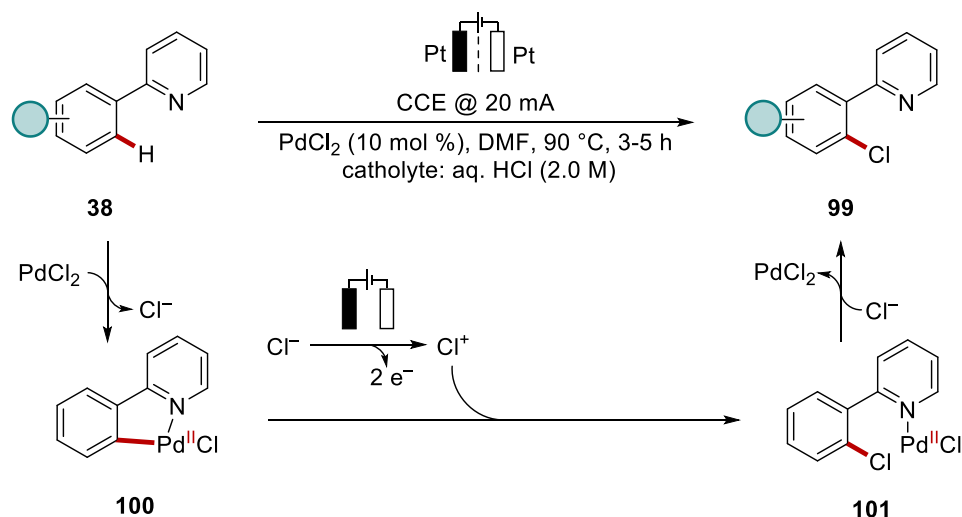
Early studies in the field of electrochemical transition metal-catalyzed C–H activation were reported by *Jutand* and *Amatore*.<sup>[161]</sup> In a *Fujiwara-Moritani*-type reaction, acetanilide **42a** was successfully alkenylated to furnish product **98ab**. The reaction was conducted in a divided cell set-up to avoid electrode deposition of the catalyst, under either constant current or constant potential electrolysis (CCE or CPE). Interestingly, a benzoquinone redox-mediator was required to homogenously recycle the palladium(II) catalyst after reductive elimination towards a palladium(0) species (Scheme 1.6.2).



**Scheme 1.6.2** Mediated palladaelectro-catalyzed alkenylation by *Amatore* and *Jutand* in a divided cell.

Next, *Kakiuchi* developed a palladium-catalyzed *ortho*-chlorination of phenylpyridines **38**, which again required a divided cell set-up.<sup>[162]</sup> Anodic oxidation was utilized to generate halonium ions from the corresponding anions, to furnish the chlorinated products **99** from the cyclometalated intermediate **100** (Scheme 1.6.3). Importantly, the oxidation state of the catalyst did not change during the process and relatively expensive electrophilic halogen sources were successfully replaced.

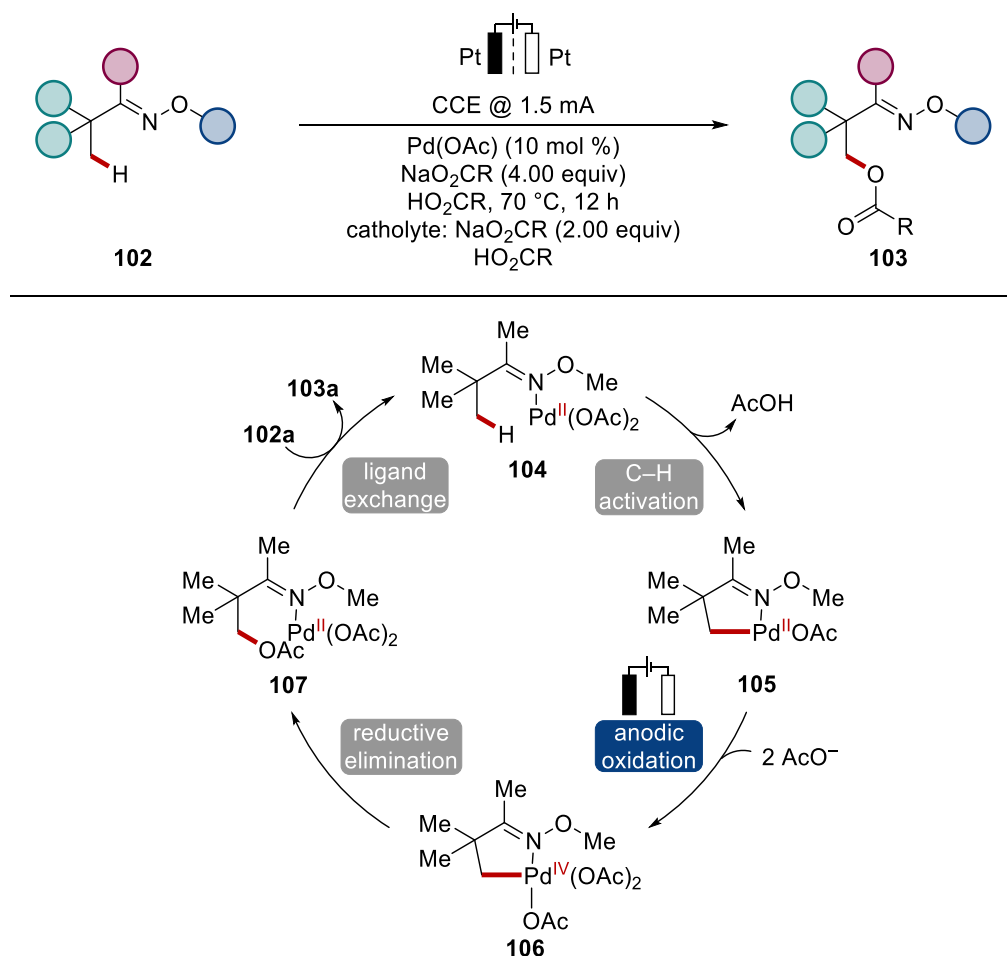




**Scheme 1.6.3** Palladium-catalyzed *ortho*-halogenation of 2-phenylpyridines.

The authors could further extend this approach towards brominations and iodinations, which were used for a domino-arylation approach.<sup>[163]</sup> So far, anodic oxidation for palladium electro-catalyzed reactions were solely used to oxidize mediators or the halide ions in divided cell set-ups.

In contrast, investigations by *Mei* revealed that the palladium catalyst can be directly oxidized at platinum anodes to carry out C(sp<sup>3</sup>)-H acetoxylation reactions of various oximes **102** with sodium carboxylates and the corresponding carboxylic acids (Scheme 1.6.4).<sup>[164]</sup> Despite the high functional group tolerance towards esters, nitriles and sulfonamides, the authors could further extend the strategy towards the C-O formation with alkoxides and tosylates. The reaction mechanism commences with a C-H cleavage to furnish a cyclometalated five-membered palladacycle **105** (Scheme 1.6.4). Isolation and characterization of a related cyclometalated species by means of cyclic voltammetry indicated two irreversible oxidation events, which were suggestive of an oxidation-induced reductive elimination. Therefore, the authors proposed that before the reductive elimination, complex **105** undergoes oxidation towards a palladium(III) or palladium(IV) species. After the reductive elimination, the product **103** decoordinates to close the catalytic cycle.



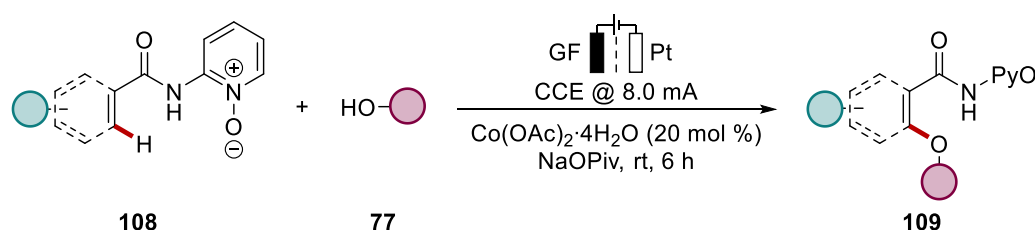
**Scheme 1.6.4** Palladaelectro-catalyzed C–H acetoxylation of oximes.

In subsequent studies the same group<sup>[165]</sup> and *Sanford*<sup>[166]</sup> demonstrated the functionalization of arene C(sp<sup>2</sup>)–H bonds under similar conditions. Following these early examples of palladaelectro-catalyzed transformations, the concept was further extended towards C–H alkylations<sup>[167]</sup> and benzoylations.<sup>[168]</sup> Additionally, first examples of asymmetric palladium-catalyzed using transient directing groups were reported by *Ackermann*.<sup>[169]</sup> A major challenge in palladaelectro-catalyzed reactions is the cathodic deposition of the metal catalysts, which is the reason for the common requirement for divided cell set-ups.

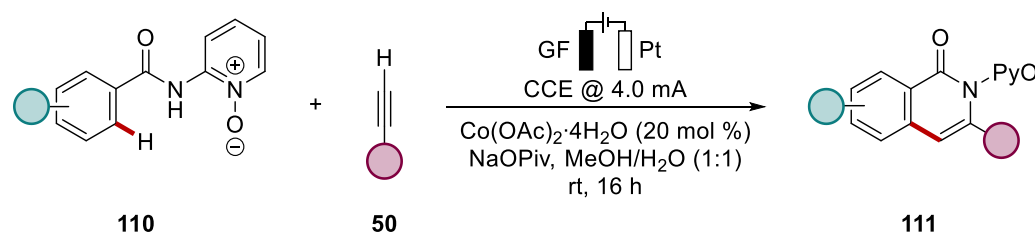
While palladium has been shown to undergo direct electrooxidation, tremendous efforts have been made to use more cost-efficient and environmentally benign transition metals in electro-catalyzed reactions. Cobalt catalysts have been extensively studied in the field of C–H activation.<sup>[35a, 170]</sup> However, cobalt electro-catalyzed C–H activation was firstly published by *Ackermann* in 2017, reporting on the oxygenation of benzamides **108** with various primary alcohols **77** under mild conditions (Scheme 1.6.5a).<sup>[171]</sup> The electrolysis was conducted at room temperature, mostly in a divided cell set-up, but in an undivided cell for a scale-up, employing abundant cobalt(II) acetate as the catalyst. Astonishingly, not only

arenes decorated with oxidation-sensitive substituents, such as thioethers or halides, were tolerated under the optimized conditions. Indeed, also alkenes **108** were unprecedentedly proven to be viable substrates for electrochemical C–H activations. Shortly after this report on the electrooxidative C–H oxygenation, *Ackermann*, and later *Lei* developed cobaltaelectro-catalyzed C–H/N–H annulations. Whereas *Ackermann* used terminal alkynes **50** (Scheme 1.6.5b),<sup>[172]</sup> *Lei* was able to use gaseous feedstocks **113** for the annulation reaction (Scheme 1.6.5c).<sup>[173]</sup>

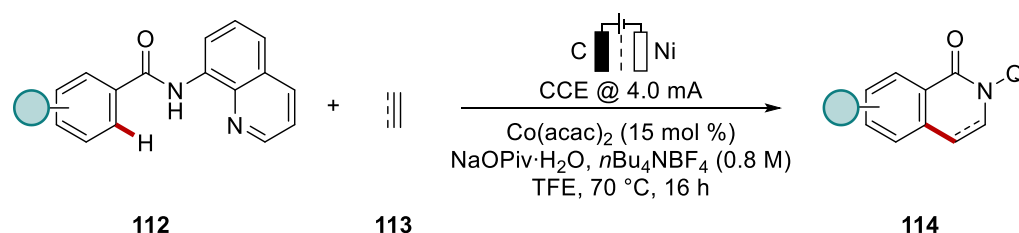
(a) Electrochemical cobalt-catalyzed oxygenation, *Ackermann* (2017)



(b) Cobaltaelectro-catalyzed alkyne annulation, *Ackermann* (2018)



(c) Cobalt-catalyzed electrooxidative annulation with ethylene or acetylene, *Lei* (2018)

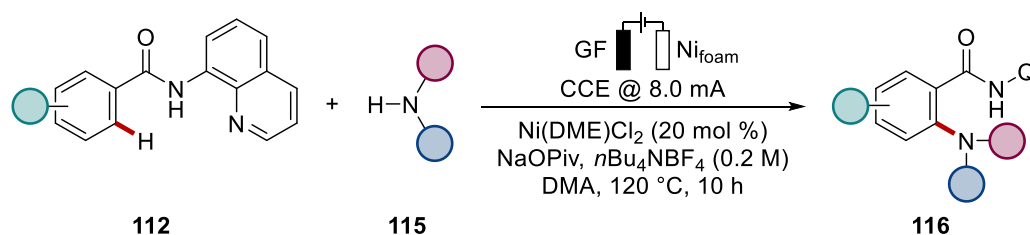
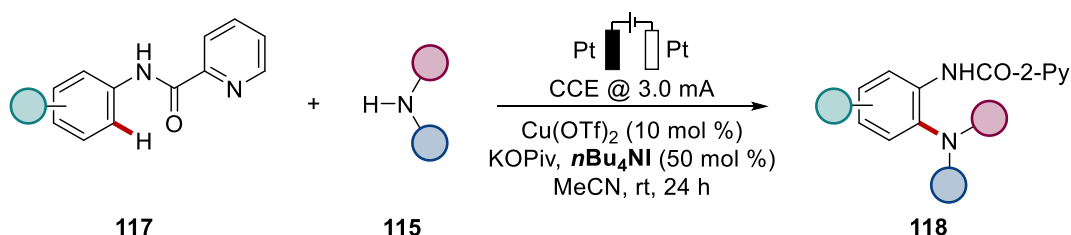
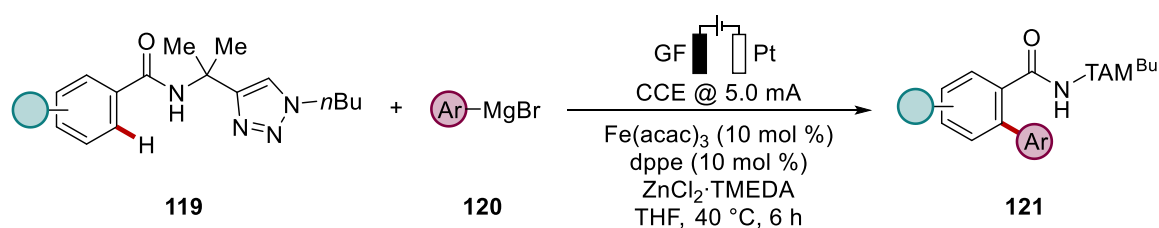
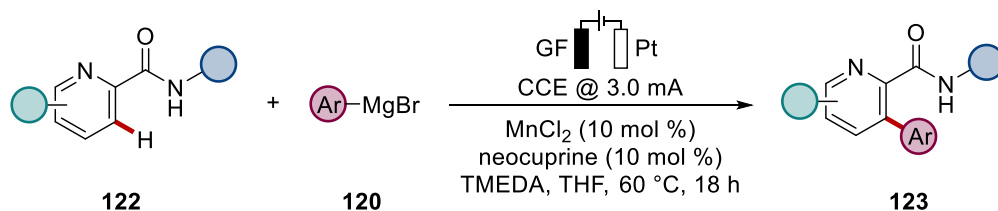


**Scheme 1.6.5** Pioneering studies on cobaltaelectro-catalyzed C–H activations.

In the course of these contributions, attractive carbonylations,<sup>[174]</sup> annulations using internal alkynes,<sup>[175]</sup> alkenes<sup>[176]</sup> and allenes,<sup>[177]</sup> among others,<sup>[160e, 160g, 178]</sup> were established. Anodic events were demonstrated to be crucial for the re-oxidation of the cobalt catalyst after reductive elimination or additionally being involved during an oxidation-induced reductive elimination manifold.<sup>[179]</sup>

Regarding other sustainable 3d transition metals for electrooxidative C–H activations, attractive concepts have been developed using nickel, copper, iron, and manganese catalysts (*vide infra*). The first nickel-catalyzed electrooxidative C–H activation, under the guidance of an 8-aminoquinoline directing group, was disclosed by *Ackermann*, reporting on the amination of benzamides **112** at elevated temperatures (Scheme 1.6.6a).<sup>[180]</sup> A further report on nickel electrocatalysis,<sup>[181]</sup> substantiated increased reactivity towards the oxygenation with secondary alcohols in comparison to the previously developed cobalteelectro-catalyzed C–O bond formation,<sup>[171]</sup> employing mostly primary alcohols. Aside from nickel, also copper catalysts have been validated by *Mei* and co-workers, to aminate anilides **117** under electrooxidative conditions (Scheme 1.6.6b). The corresponding products **118** could be obtained using a benign copper(II) catalyst which has been demonstrated to be indirectly re-oxidized by an iodide mediator.<sup>[182]</sup> In contrast, an cupraelectro-catalyzed annulation of benzamides **112** with terminal alkynes **50** was reported, without the requirement for a redox catalyst.<sup>[183]</sup> Regarding other environmental-friendly transition metals for metallaelectrocatalysis, *Ackermann* discovered the activity of an earth-abundant iron complex for the arylation of benzamides **119** under exceedingly mild conditions (Scheme 1.6.6c). Mechanistic insights supported by DFT, cyclovoltammetry and experiment were suggestive of an oxidation-induced reductive elimination.<sup>[184]</sup> Additionally, a pioneering manganaelectro-catalyzed C–H arylation of azines **122** has been developed by the same group, which did not rely on bidentate amide-directing groups (Scheme 1.6.6d).<sup>[184, 185]</sup>

## (a) Nickel-catalyzed electrooxidative C–H amination, Ackermann (2018)

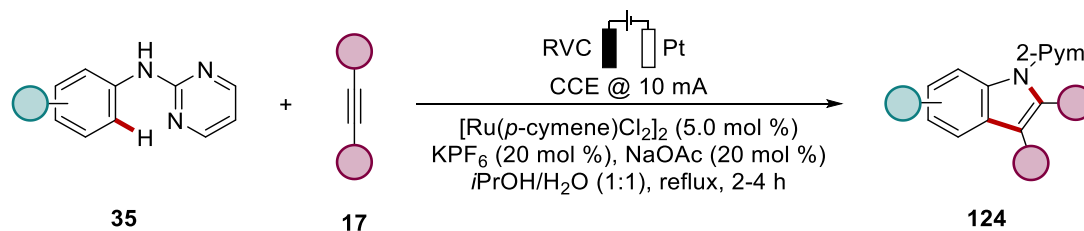
(b) Cupraelectro-catalyzed amination of anilides **117**, Mei (2018)(c) Ferraelectro-catalyzed arylation of benzamides **119**, Ackermann (2019)(d) Manganaelectro-catalyzed arylation of azines **122**, Ackermann (2019)**Scheme 1.6.6** Early examples of electrooxidative 3d transition metal-catalyzed C–H activations.

Although these reports represent unambiguous advances in the field of sustainable C–H activations using green electricity as the oxidant, the use of 3d metals usually require high catalyst loadings and strongly-coordinating bidentate directing groups, such as pyridineamides **117**, pyridine-*N*-oxide-amides **110** or quinolinylamides **112** or (*vide supra*). Although progress has been made in the traceless cleavage and recovery of the directing groups,<sup>[22b, 175, 186]</sup> the functionalization of monodentate or weakly *O*-coordinating directing-groups is arguably more atom- and step-economic. Next to key contributions of palladium electrocatalysis (*vide supra*), significant advances have been achieved utilizing ruthenium and rhodium catalysts for electro-catalyzed C–H activations (*vide infra*).

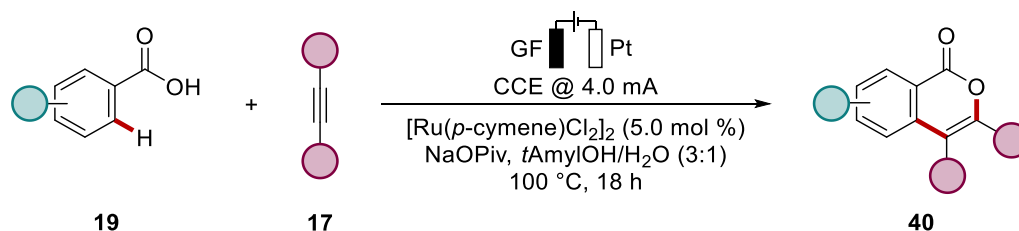
### 1.6.1 Ruthenium Electro-Catalyzed C–H Activation

From the first studies on oxidative ruthenium-catalyzed C–H activations of arenes reported by Milstein in 2001,<sup>[187]</sup> ruthenium catalysts have developed as a powerful and less expensive alternative to palladium and rhodium catalysts.<sup>[12h, 188a, 188b]</sup> Nevertheless, the use of stoichiometric oxidants in ruthenium-catalyzed C–H activations jeopardized the overall atom and cost economy, until *Xu* and *Ackermann* independently published pioneering electrooxidative ruthenium-catalyzed C–H annulations with internal alkynes **17** towards the formation of indoles **124** and isocoumarins **40**, respectively (Scheme 1.6.7).<sup>[189]</sup> Both reactions were performed in user-friendly undivided cells at constant currents. In the case of *Xu*'s work, the catalyst was guided by a pyrimidyl group, whereas isocoumarins **40** were formed upon weak coordination of benzoic acids **19**. Both concepts were characterized by high functional group tolerance towards nitrile- or bromoarenes, and excellent regioselectivity with unsymmetrical alkynes.

(a) Ruthenaelectro-catalyzed assembly of indoles **124**, *Xu* (2018)



(b) Electrooxidative ruthenium-catalyzed annulation of benzoic acids **19**, *Ackermann* (2018)

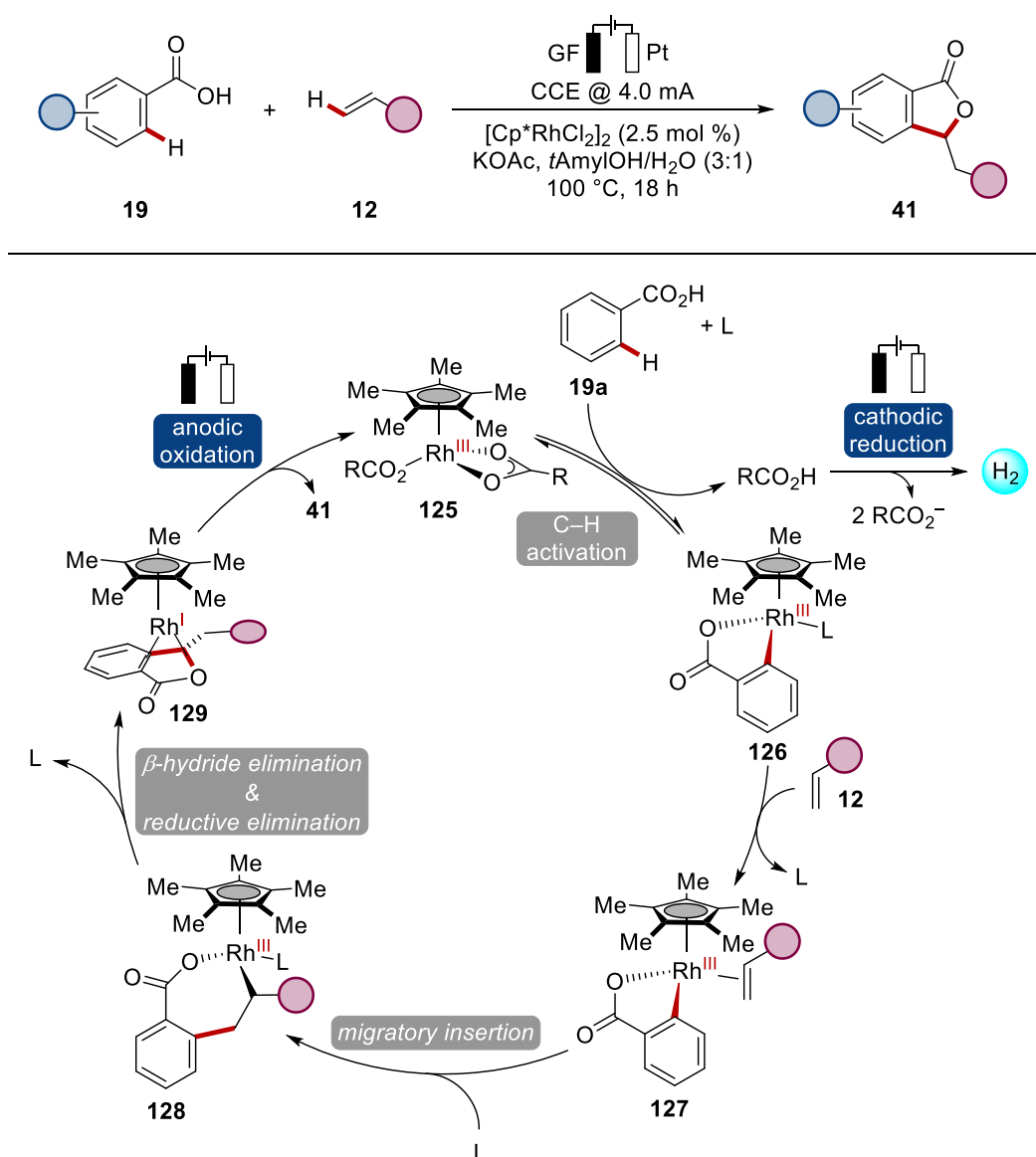


**Scheme 1.6.7** Pioneering studies on electrochemical ruthenium-catalyzed C–H activations.

Ruthenaelectro-catalyzed C–H activations of monodentate and weakly coordinating substrates have also been proven to be viable for the elegant construction of heterocycles,<sup>[190]</sup> pyridine-directed late-stage acetoxylation of phenols,<sup>[191]</sup> and *meta*-bromination of phenylpyridines.<sup>[192]</sup>

### 1.6.2 Rhodium Electro-Catalyzed C–H Activation

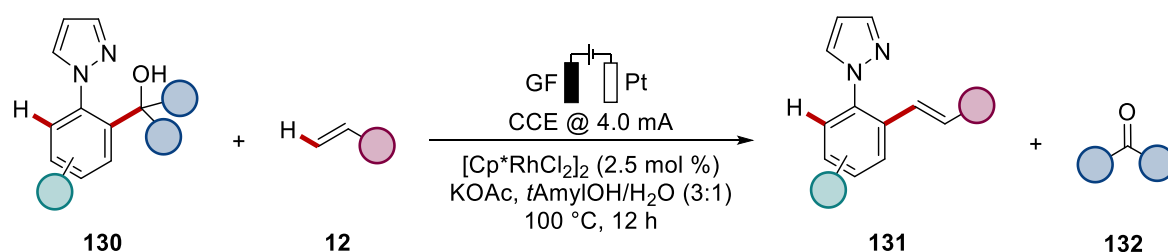
Over the past decades, rhodium catalysts have been extensively employed in C–H activation, setting the stage for a plethora of step-economic formations of C–C or C–Het bonds from weakly-coordinating substrates with low catalyst loadings (*vide supra*). Considering the unique efficiency of rhodium catalysis, the use of rhodium complexes for electrochemical C–H functionalizations, has been under-explored until a rhodaelectro-catalyzed alkenylation of benzoic acids **19** was discovered by *Ackermann* in 2018, highlighting the general feasibility of direct reoxidation of homogenous rhodium catalysts (Scheme 1.6.8).<sup>[193]</sup>



**Scheme 1.6.8** Proof of concept study on rhodaelectro-catalyzed C–H activation by *Ackermann* in 2018.

Under the optimized reactions conditions with KOAc as the base, a  $[\text{Cp}^*\text{RhCl}_2]_2$  catalyst in *tert*-amyl alcohol/water as a protic solvent mixture, the corresponding phthalides **41** could be efficiently obtained under constant current electrolysis. The reaction was proposed to be initiated by a carboxylate-assisted BIES-type<sup>[32]</sup> C–H activation towards the five-membered rhodacycle **126**. Thereafter, the migratory insertion of the alkene **12** delivers a seven-membered metallacycle **128**, which can undergo  $\beta$ -hydride- and reductive elimination. Upon anodic oxidation the corresponding product **41** is released, and the active catalyst **125** regenerated. Based on these findings, the extension of this concept to electrochemical dehydrogenative coupling towards the olefination of benzamides with styrenes was achieved by the same group.<sup>[194]</sup> Interestingly, the reaction outcome was highly dependent on the nature of the *N*-substituent on the amide, with longer alkyl or bulkier substituents exhibiting decreased reactivity as compared to the *N*-methyl benzamides. Related to the reports on the rhodaelectro-catalyzed alkenylation, *Ackermann* was able to demonstrate the unprecedented reactivity of a osmium-catalyst for the chemoselective assembly of phthalides **41** from benzoic acids **19** and acrylates **31** under electrooxidative conditions, in 2021.<sup>[195]</sup>

Rhodium electrocatalysis was impressively also extended towards C–C activations. In 2019, chemoselective C–C alkenylation of secondary and tertiary benzyl alcohols **130** was accomplished, disfavoring the competitive C–H functionalization and successfully replacing the frequently used metal oxidants (Scheme 1.6.9).<sup>[196]</sup> The catalyst was guided by a removable pyrazole directing group in *ortho*-position to efficiently couple the arenes with electron-rich and electron-deficient styrenes **12**.



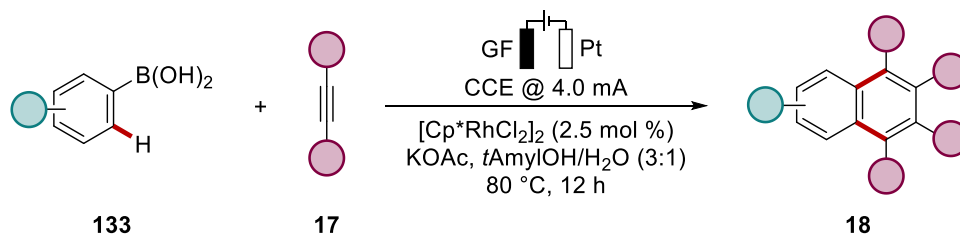
**Scheme 1.6.9** Position-selective rhodaelectro-catalyzed C–C alkenylation.

Next to alkenylations, several reports on electrochemical rhodium-catalyzed alkyne annulations have been disclosed.<sup>[193a]</sup> Among the first precedences, [2+2+2] cycloaddition of internal alkynes to boronic acids has been reported to furnish polycyclic scaffolds **18** (Scheme 1.6.10a).<sup>[197]</sup> In a comparison with chemical oxidants, the authors highlighted, that not only oxidant-economy was significantly improved, when electricity was used as the

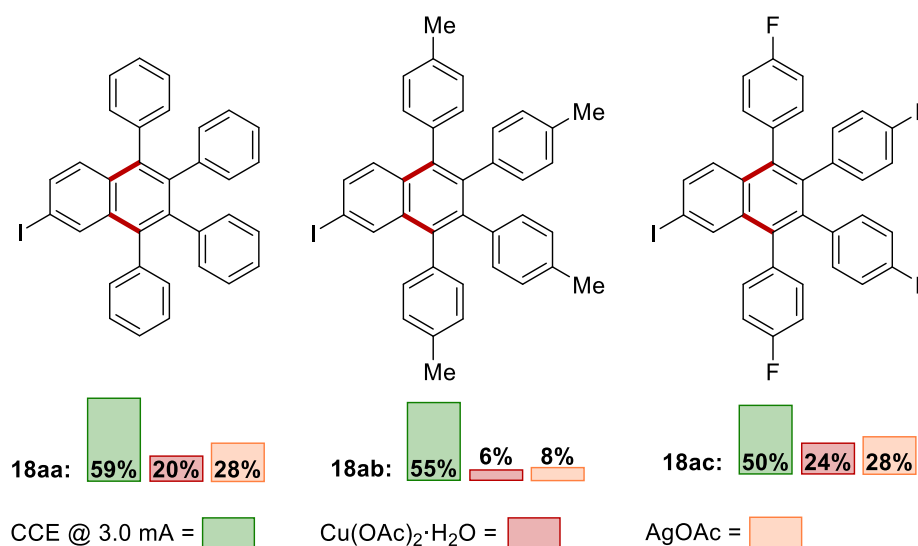


terminal oxidant. Indeed, chemical oxidants were outperformed, in terms of yield (Scheme 1.6.10b). Moreover, it was shown that a subsequent *Scholl* reaction could transform the obtained scaffolds into  $\pi$ -extended polyaromatic hydrocarbons **134** (Scheme 1.6.10c).

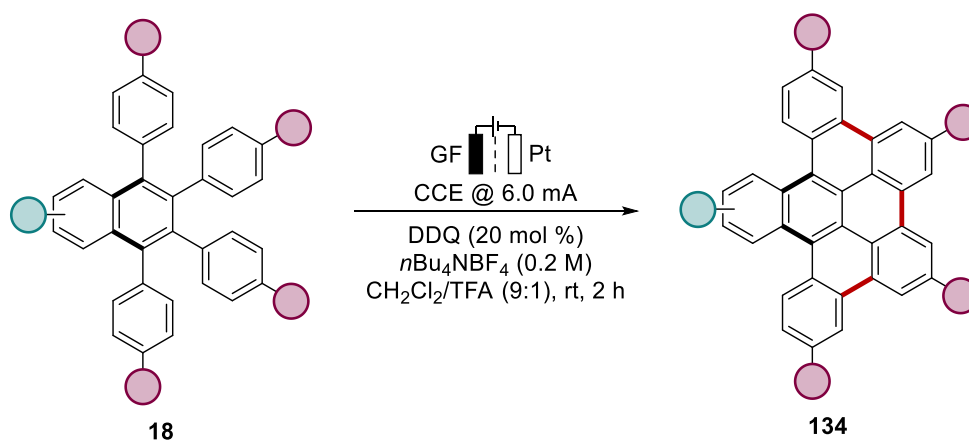
(a) Rhodaelectro-catalyzed annulation of boronic acids, Ackermann (2019)



(b) Efficiency comparison with chemical oxidants



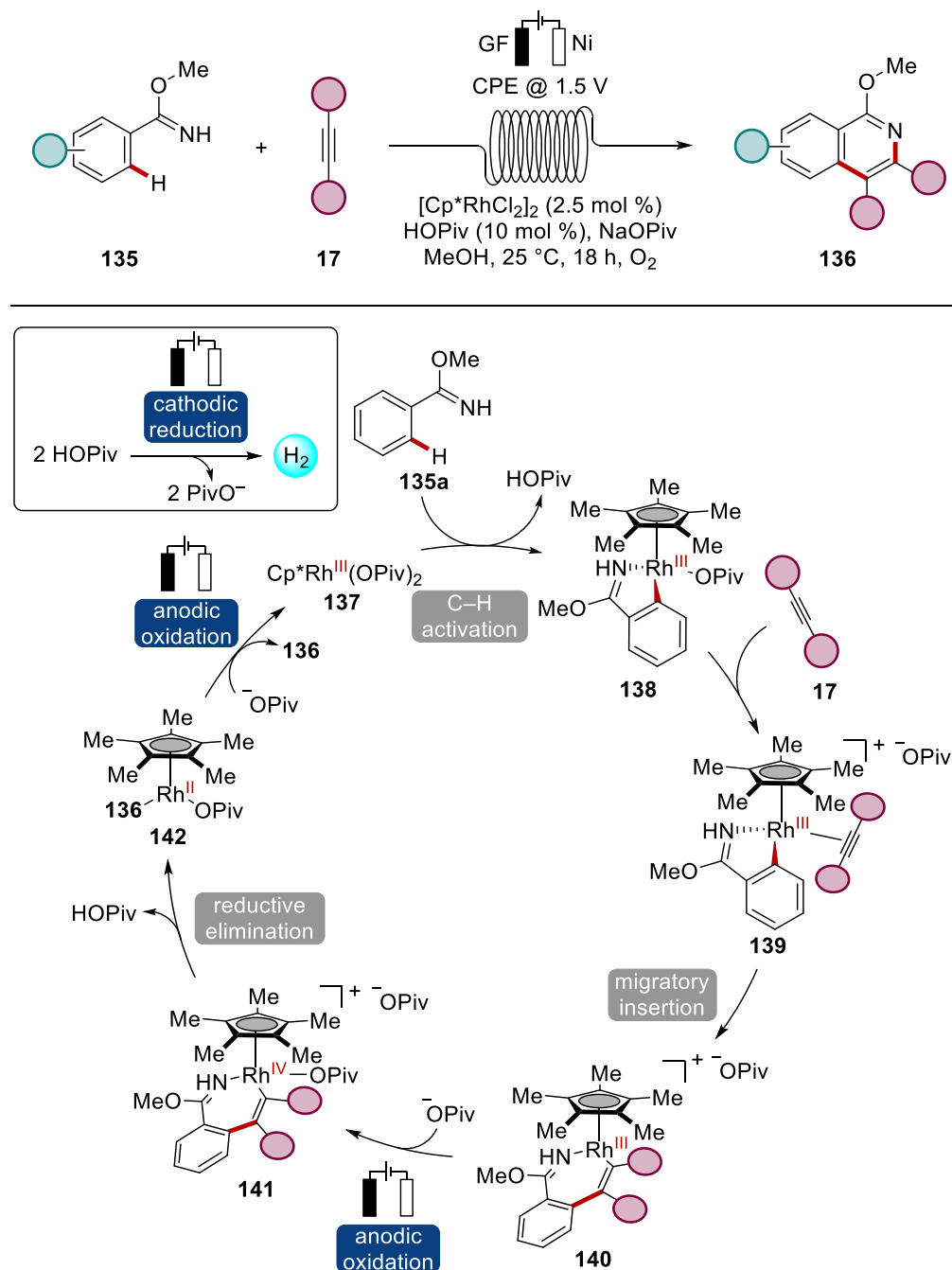
(c) DDQ-catalyzed electrochemical cyclodehydrogenation



**Scheme 1.6.10** Annulative C–H activation towards the assembly of polycyclic aromatic hydrocarbons **18** and **134**.

Based on this precedence, the same group also designed an electro-catalyzed domino-synthesis of aza-polycyclic motifs utilizing a rhodium catalyst.<sup>[198]</sup>

Substantial advances regarding the utilization of flow-chemistry for metallaelectro-catalyzed C–H activations, accompanied with detailed mechanistic insights, has been achieved in 2019. Thereby, weakly coordinating imidates **135** were inter- and intramolecularly annulated with internal alkynes **17** using a modular flow-cell to construct valuable isoquinolines **136** (Scheme 1.6.11). Through the successful isolation of key reaction intermediates, such as the C–H activated imidate **135a** and a seven-membered rhodacycle, the authors were able to perform mechanistic experiments and investigate the redox-behavior by cyclic voltammetry to propose an oxidatively-induced reductive elimination being operative, which was additionally supported by detailed DFT calculations. Independent studies conducted by *Xu*, likewise found support for this reaction pathway during an rhodaelectro-catalyzed C–H phosphorylation (*vide infra*).<sup>[199]</sup>

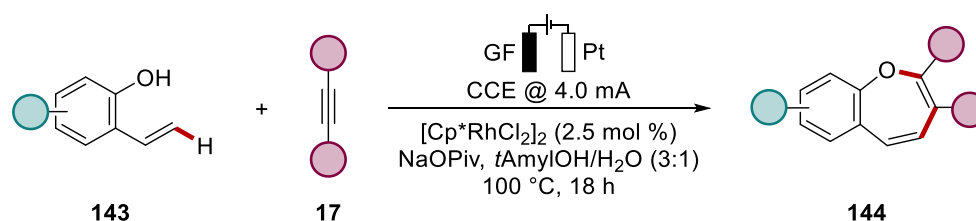


**Scheme 1.6.11** Rhodaelectro-catalyzed annulation of imidates **135** in flow featuring an oxidatively-induced reductive elimination.

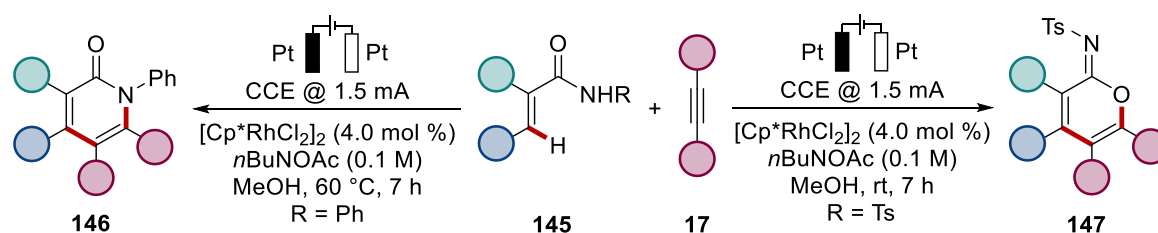
In the course of the presented work, further versatile annulative transformations have been developed promoting electrochemical oxidation of rhodium catalysts. As discovered by *Ackermann*, 2-vinylphenols **143** were viable substrates for the annulation towards valuable seven-membered heterocycles **144** (Scheme 1.6.12a).<sup>[200]</sup> The reaction was characterized by a robustness towards a plethora of functional groups attached to the phenol and the alkyne. Interestingly, also alkynes substituted with a BODIPY moiety could undergo this transformation towards highly fluorescent benzoxepines **144**. Finally, the scalability of the

strategy was validated in a gram-scale synthesis, which furnished the product with high efficiency. Shortly afterwards, *Mei* reported an elegant approach for the divergent annulation of acrylamides. Depending on the *N*-substituent either  $\alpha$ -pyridones **146** or cyclic imidates **147** were obtained under rhodaelectro-catalytic conditions in an undivided cell (Scheme 1.6.12b).<sup>[201]</sup> Terminal alkynes were also found suitable for the synthesis of imidates **147** at ambient temperature. Studies by means of DFT suggested that a stepwise-ionic reductive elimination for the tosylate substituted amides **145** is more favorable than the neutral concerted way, which is in line with the observed chemoselectivity.

(a) Electrochemical rhodium-catalyzed assembly of benzoxepines **144**, *Ackermann* (2021)



(b) Chemodivergent rhodaelectro-catalyzed annulation of acrylamides **145**, *Mei* (2021)

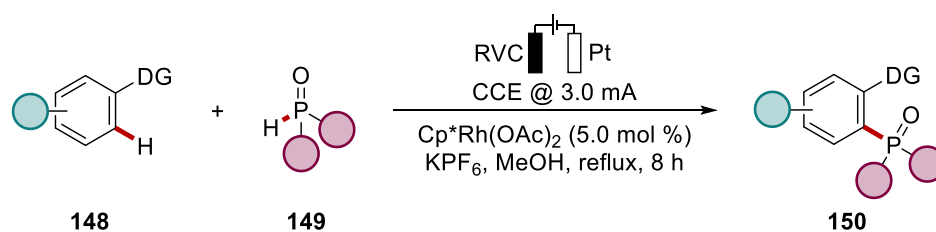


**Scheme 1.6.12** Electrochemical functionalization of alkenes *via* rhodium electrocatalysis.

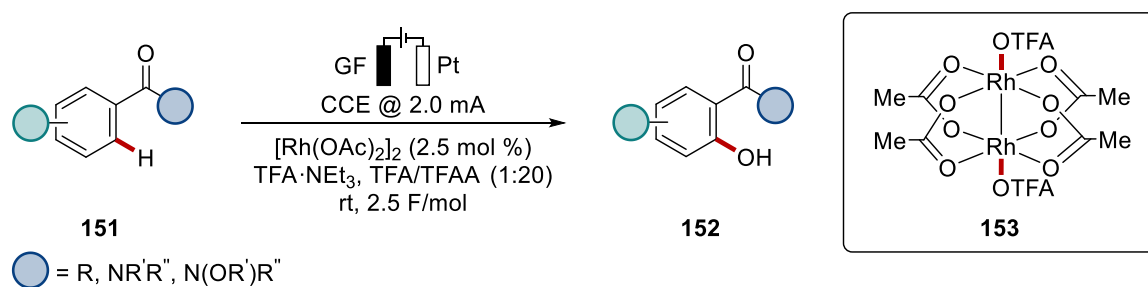
In addition to C–C bond formations, electrocatalysis using rhodium complexes has proven to be a highly efficient tool for the formation of C–Het bonds. The synthesis of triarylphosphine oxides **150** could be achieved from the corresponding diarylphosphine oxides **149** by the guidance of various *N*-directing groups, such as (amino) pyridines, pyrimidines, pyrazoles or purines (Scheme 1.6.13a).<sup>[199]</sup> Also benzodiazepine drugs were efficiently phosphorylated. The authors could successfully scale the synthesis to obtain more than 80 grams of the desired product and found evidence that the mechanism proceeds through an oxidatively-induced reductive elimination. Next to the C–P formation *Ackermann* and co-workers could oxygenate various arenes with weakly *O*-coordinating carbonyls, employing a bimetallic rhodium catalyst **153** without the cyclopentadienyl ligand (Scheme 1.6.13b).<sup>[159]</sup> Interestingly, when tertiary *N*-methyl benzamides were employed, a

subsequent intramolecular *Shono*-type reaction was facilitated by increasing the charge of the electrolysis. Mechanistic insights suggested an oxidation-induced C–H activation being operative for the developed C–H oxygenation.

(a) *Electrochemical rhodium-catalyzed phosphorylation, Xu (2019)*



(b) *Rhodaelectro-catalyzed bimetallic C–H oxygenation, Ackermann (2021)*

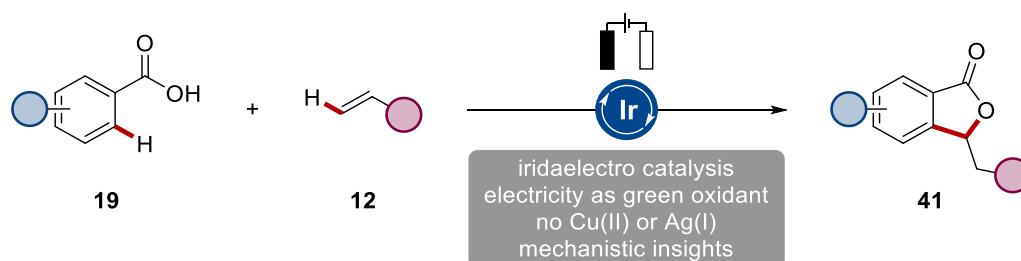


**Scheme 1.6.13** Electrochemical C–Het bond formation catalyzed by rhodium-complexes.

## 2 OBJECTIVES

The development of novel strategies for robust C–H functionalizations to access complex structures by efficient C–C and C–Het forming processes is of utmost interest for molecular sciences.<sup>[5]</sup> Although, traditional cross-couplings represent a capable tool to access also complex targets, the preinstallation of functional groups is step and atom intensive. In contrast, the development of direct, transition metal-catalyzed C–H activations has evolved as an increasingly powerful strategy to overcome these limitations.<sup>[12, 13d, 13e, 33a]</sup> Despite the remarkable advantages of C–H functionalizations over existing approaches, the use of often toxic and expensive oxidants contradicts the overall green nature and render applications on larger scale less attractive. Indeed, the merger of organic electrochemistry and transition metal catalysis has clearly addressed these key limitations and provided a powerful approach towards unique reaction manifolds.<sup>[14, 156]</sup> Thus, the aim of this thesis is the exploration and advancement of the field of electro-catalyzed C–H activations and the use of electricity to establish robust step-, atom- and oxidant-economic disconnections for organic synthesis.

Iridium catalysts played a key role in understanding and providing insights into C–H activation mechanisms. Concurrently, their use for the assembly of important heterocyclic scaffolds and important motifs has attracted major attention.<sup>[13e, 65]</sup> In the context of the importance of iridium catalysis for synthetic and metal organic chemistry, surprisingly iridium electrocatalysis, had thus far proven elusive. Within the doctoral studies, a key aspiration was the finding of viable reaction conditions to electrochemically recycle homogenous iridium catalysts. As iridium has been reported to be highly active towards the C–H activation of benzoic acids **19**, alkenylation with acrylates **12** was chosen as a model reaction (Scheme 2.1).

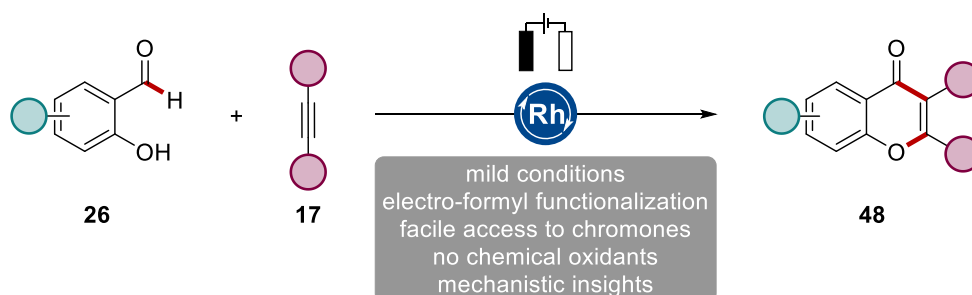


**Scheme 2.1** Iridium-catalyzed electrochemical C–H annulation of benzoic acids **19**.

In the course of the investigations, not only chemical oxidants should be replaced, but the mode of action and a comparison with previously reported electrocatalysts was anticipated

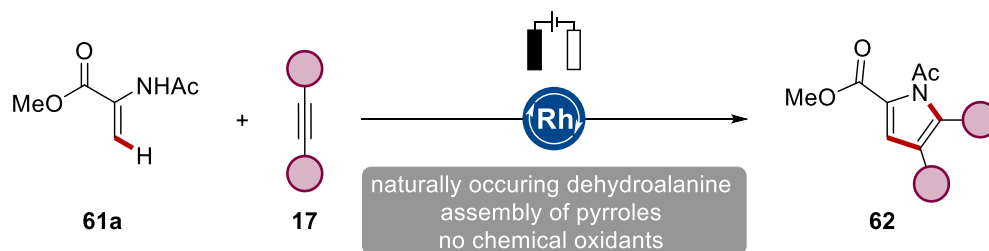
to provide meaningful mechanistic insights that could prove valuable for further developments of iridoelectro catalysis.

Metal-catalyzed hydroacylations represent a highly attractive approach towards the synthesis of substituted ketones.<sup>[88]</sup> Hence, functionalization of hydroxy benzaldehydes has demonstrated as particularly enabling for the assembly of various oxygen containing heterocycles.<sup>[91-94]</sup> Very recently, rhodium catalysts have emerged as highly efficient and selective catalysts for electrochemical transformations.<sup>[193a]</sup> However, as transition metal electrocatalysis has predominantly focused on the functionalization of arenes,<sup>[160e, 160f, 193a]</sup> the challenge raised, whether the concept could be exploited for electrochemical formyl C–H activation. Due to the sensitive nature of aldehydes towards oxidation, nucleophilic attack, or decarbonylation this approach was highly demanding. A reliable strategy would comprise relevant organometallic intermediates with lower oxidation-potentials than the corresponding aldehydes **26**, to avoid the overoxidation. Therefore, it was devised to initiate the studies with alkyne coupling partners **17** for the efficient construction of chromones **48** (Scheme 2.2).



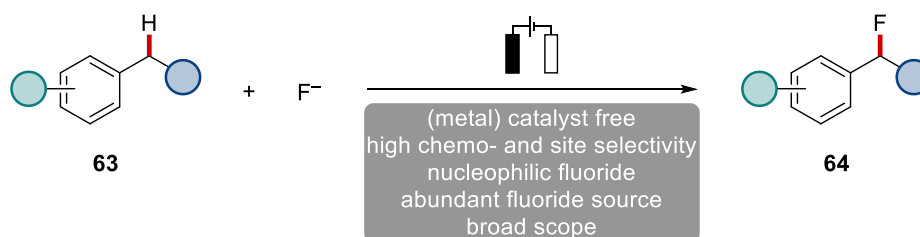
**Scheme 2.2** Electrochemical rhodium-catalyzed formyl C–H activation for the assembly of chromones.

Despite the C–H activation of arenes, the functionalization of alkenes represents a key technology within organic synthesis and a variety of C–H activations on alkenes had been established.<sup>[95a]</sup> In contrast, electrochemical versions of oxidative functionalizations, by means of organometallic C–H cleavage, are significantly scarce.<sup>[171, 201-202]</sup> From this starting point, a rhodoelectro-catalyzed functionalization of dehydroalanine **61a** was intended to provide a robust and modular avenue for the sustainable synthesis of pyrroles **62** (Scheme 2.3).



**Scheme 2.3** Rhodaelectro-catalyzed annulation of alkenes towards the synthesis of pyrroles.

The facile synthesis of fluorinated scaffolds is of paramount relevance to chemists in pharmaceutical,<sup>[110]</sup> crop protection,<sup>[111]</sup> as well as material industries.<sup>[112]</sup> Considering that aliphatic fluorides are primarily synthesized from the corresponding alcohols with cost- and atom-inefficient deoxyfluorinating agents,<sup>[114]</sup> the direct introduction of fluorine to omnipresent C–H bonds has experienced compelling attention.<sup>[113b, 113d]</sup> In this regard, the innate reactivity of substrates **63** bearing benzylic hydrogens, has been of major interest for direct fluorinations, most commonly using expensive electrophilic fluoride reagents.<sup>[113c, 113d]</sup> As opposed to rare reports utilizing chemical oxidants and desirable nucleophilic fluoride sources,<sup>[122, 123, 125]</sup> electrochemical fluorinations have so far not been able to provide synthetic utility due to major limitations regarding scope and/or chemoselectivity.<sup>[146]</sup> Herein, reaction conditions should be established to overcome previous disadvantages and set the stage for broadly applicable, metal-free electrochemical fluorinations using abundant and cost-effective fluoride sources (Scheme 2.4).



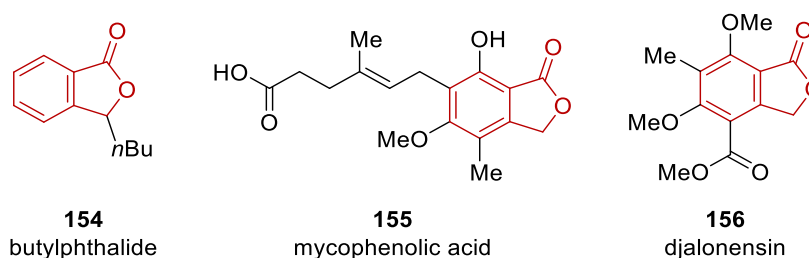
**Scheme 2.4** Metal-free electrochemical benzylic C–H fluorination.



### 3 RESULTS AND DISCUSSION

#### 3.1 Iridaelectro-Catalyzed C–H Alkenylation by Redox Catalyst Cooperation

Phthalides are commonly found in natural products exhibiting a variety of biological activities.<sup>[203]</sup> For instance simple butylphthalide **154** exhibits potency against ischemia (Figure 3.1.1).<sup>[203a]</sup> Another interesting representative scaffold is mycophenolic acid **155**, which is used as an immunosuppressant and revealed anti-cancer activity.<sup>[204]</sup>



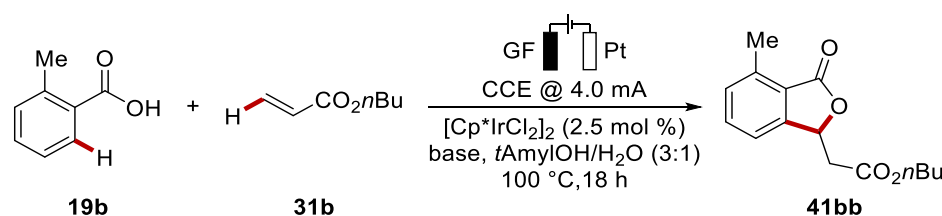
**Figure 3.1.1** Naturally occurring phthalides.

In order to access valuable building blocks and important motifs, such as phthalides, the direct cross-dehydrogenative reaction of alkenes with arenes has developed as an attractive tool for a step-economic syntheses, avoiding the pre-installation of halides on the arene.<sup>[205]</sup> However, most commonly stoichiometric oxidants, such as toxic and/or expensive metal salts, are typically required in order to regenerate the active transition metal catalysts.<sup>[12d, 13e, 38c, 206]</sup> To overcome the drawbacks of sacrificial oxidants, organic electrocatalysis has emerged as a powerful alternative for C–H activations.<sup>[14, 156]</sup> While electrooxidative transformations using palladium and cobalt catalysts have attracted major attention, these systems often require strongly coordinating directing groups.<sup>[160e, 160f]</sup> Although, iridium catalysis has emerged as particularly capable for C–H functionalizations, its use in electro-catalyzed C–H activations has not yet been realized. Therefore, the development of the first electrooxidative transformation using iridium catalysis was envisioned.

### 3.1.1 Optimization Studies for the Iridaelectro-Catalyzed C–H Alkenylation

Based on previous studies,<sup>[64, 80, 196]</sup> the initial reactivity of the electrochemical iridium-catalyzed alkenylation of weakly coordinating benzoic acids was firstly discovered by *Dr. Youai Qiu*, reacting *o*-toluic acid **19b**, to prevent double alkenylation, with butyl acrylate **31b** as the coupling partner. The protic solvent mixture of *t*-amyl alcohol and water with potassium acetate as the base provided sufficient conductivity to furnish the desired phthalide **41bb** in 47% yield under constant current conditions (Table 3.1.1, entry 1), using a graphite felt anode and platinum plate cathode.

**Table 3.1.1** Initial optimization studies for the iridaelectro-catalyzed C–H alkenylation.



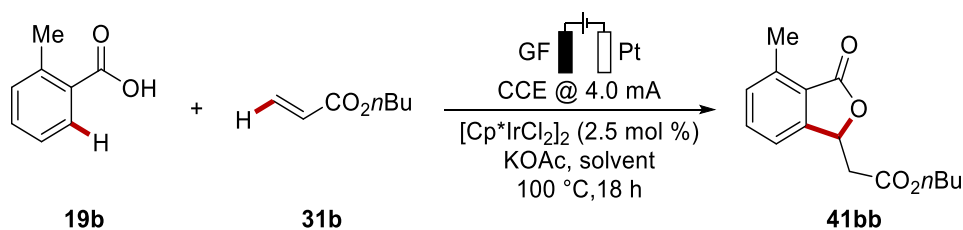
Entry	<i>T</i> [°C]	Base	Yield [%]
1	100	KOAc	47 <sup>[a]</sup>
2	100	KOAc	38 <sup>[b]</sup>
3	100	KOAc	36 <sup>[a,c]</sup>
4	100	KOAc	29 <sup>[d]</sup>
5	60	KOAc	--
6	100	NaOPiv	29
7	100	K <sub>2</sub> CO <sub>3</sub>	--

Undivided cell, GF anode (10 mm × 15 mm × 6.0 mm), Pt cathode (10 mm × 15 mm × 0.125 mm), constant current = 4.0 mA, **19b** (1.00 mmol), **31b** (0.50 mmol), catalyst (2.5 mol %), base (2.00 equiv), solvent (4.0 mL), 100 °C, under air, 18 h. Isolated yields are given. [a] <sup>1</sup>H-NMR yield with CH<sub>2</sub>Br<sub>2</sub> as internal standard. [b] **19b** (0.50 mmol), **31b** (1.00 mmol). [c] With KOAc (1.00 equiv). [d] With KPF<sub>6</sub> (20 mol %).

From this starting point, extensive optimization studies have been performed. At the outset, changing the ratio of the benzoic acid **19b** to acrylate **31b**, or reducing the amount of base, decreased the formed product yield (entry 2 and 3). Similar effects were observed, when the stoichiometry of the added base or the reaction temperature was lowered, resulting in a diminished activity (entry 4 and 5). Different bases, such as NaOPiv or K<sub>2</sub>CO<sub>3</sub>, were tested, but did not provide any beneficial reaction outcome. Subsequently, different solvent systems were investigated for the iridaelectrocatalysis (Table 3.1.2). As it turned out, neither the

change of the alcohol co-solvent to isopropanol, nor the variation of the *tert*-amyl alcohol/water ratio could increase product yield (entry 2 and 3). Using fluorinated alcohols as solvents, which have previously been shown benign for electrochemical transformations,<sup>[130d, 190a, 207]</sup> led to a further decrease of efficiency (entry 4 and 5).

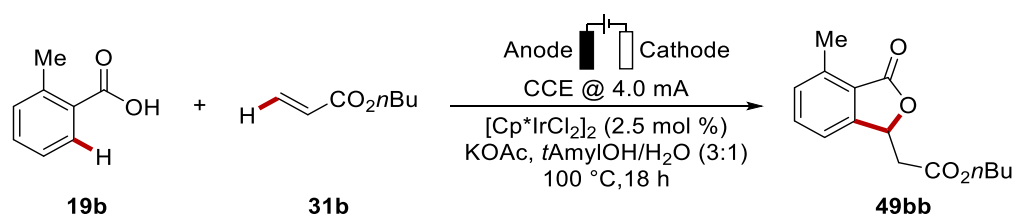
**Table 3.1.2** Variation of the solvent system for the iridaelectro-catalyzed C–H alkenylation.



Entry	Solvent	$T$ [°C]	Yield [%]
1	<i>t</i> AmylOH/H <sub>2</sub> O (3:1)	100	47 <sup>[a,b]</sup>
2	<i>i</i> PrOH/H <sub>2</sub> O (3:1)	100	28 <sup>[a,b]</sup>
3	<i>t</i> AmylOH/H <sub>2</sub> O (1:1)	100	37 <sup>[a,b]</sup>
4	TFE	70	18
5	HFIP	60	13

Undivided cell, GF anode (10 mm × 15 mm × 6.0 mm), Pt cathode (10 mm × 15 mm × 0.125 mm), constant current = 4.0 mA, **19b** (0.50 mmol), **31b** (0.25 mmol), catalyst (2.5 mol %), KOAc (2.00 equiv), solvent (4.0 mL), 100 °C, under air, 18 h. Isolated yields are given. [a] <sup>1</sup>H-NMR yield with CH<sub>2</sub>Br<sub>2</sub> as internal standard. [b] **19b** (1.00 mmol), **31b** (0.50 mmol).

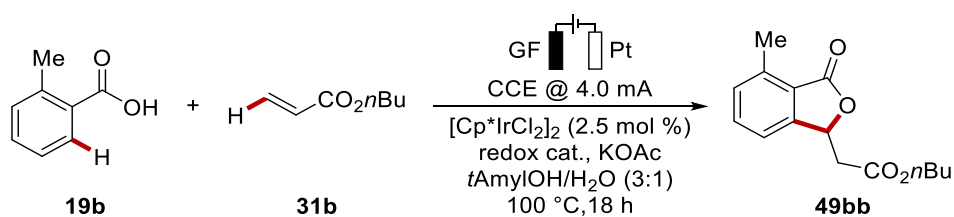
Next, the effect of the electrode materials on the reaction outcome was investigated (Table 3.1.3). Altering the electrode material to platinum as anode material and graphite felt as cathode led to a significant decrease in yield (entry 2). This observation can be rationalized by the proposed proton reduction half reaction in related studies,<sup>[183]</sup> which has the lowest overpotential on platinum.<sup>[208]</sup> However, using less expensive nickel foam as cathode, which exhibits a larger surface area, provided overall comparable efficiency in comparison to platinum plate (entry 3). When a nickel plate cathode, copper or stainless steel (entries 4–6) were employed, a slight to moderate decrease in product formation was observed. Variation of the anodic material to nickel foam or platinum plate (entry 8 and 9), turned out to be less effective, presumably due to different surface properties and significantly lower surface area in comparison to the one of graphite felt.

**Table 3.1.3** Variation of the electrode materials for the iridaelectro-catalyzed C–H alkenylation.

Entry	Anode	Cathode	Yield [%]
1	GF	Pt	47 <sup>[a,b]</sup>
2	Pt	GF	16 <sup>[a]</sup>
3	GF	Ni <sub>foam</sub>	49
4	GF	Ni	38
5	GF	Cu	46
6	GF	Fe	29
7	GF	GF	39
8	Pt	Pt	33
9	Ni <sub>foam</sub>	Ni <sub>foam</sub>	26

Undivided cell, GF anode (10 mm × 15 mm × 6.0 mm), Pt cathode (10 mm × 15 mm × 0.125 mm), constant current = 4.0 mA, **19b** (0.50 mmol), **31b** (0.25 mmol), catalyst (2.5 mol %), KOAc (2.00 equiv), solvent (4.0 mL), 100 °C, under air, 18 h. Isolated yields are given. [a] <sup>1</sup>H-NMR yield with CH<sub>2</sub>Br<sub>2</sub> as internal standard. [b] **19b** (0.50 mmol), **31b** (0.25 mmol).

Lowering the concentration and using an excess of the acrylate improved the yield to 57% in comparison to the reaction with an excess of benzoic acid or equimolar amounts of the reactants (Table 3.1.4, entry 1–3). The use of nickel foam as cathode was shown to be disadvantageous in comparison to platinum plate under the examined conditions (entry 4). Since *Jutand* and co-workers reported on the electrochemical benzoquinone (BQ) mediated palladium-catalyzed alkenylation,<sup>[161]</sup> the question arose whether a beneficial effect of a redox mediator could be observed in the iridaelectro-catalyzed C–H activation of benzoic acids. Delightfully, the yield increased dramatically to 87%, when catalytic amounts of BQ were employed (entry 4).

**Table 3.1.4** Further optimization studies regarding substrate ratio and redox mediator.

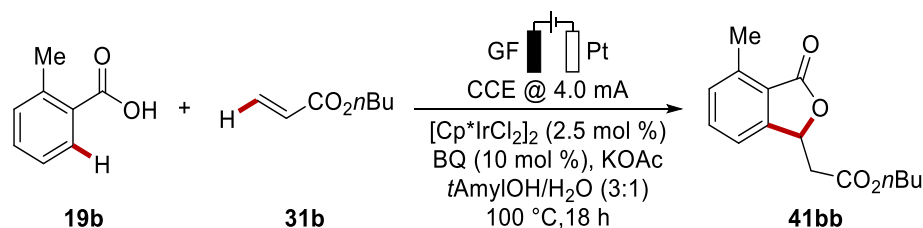
Entry	<b>19b/31b</b> [mmol]	Redox Cat.	Yield [%]
1	1.00/0.50	--	47 <sup>[a]</sup>
2	0.25/0.50	--	57
3	0.25/0.25	--	30
4	0.25/0.50	--	51 <sup>[b]</sup>
5	0.25/0.50	BQ	87

Undivided cell, GF anode (10 mm × 15 mm × 6.0 mm), Pt cathode (10 mm × 15 mm × 0.125 mm), constant current = 4.0 mA, catalyst (2.5 mol %), KOAc (2.00 equiv), redox catalyst (10 mol %), solvent (4.0 mL), 100 °C, under air, 18 h. Isolated yields are given. [a] <sup>1</sup>H-NMR yield with CH<sub>2</sub>Br<sub>2</sub> as internal standard. [b] Ni<sub>Foam</sub> as cathode.

To gain further insights, different reaction parameters were varied, and control experiments were conducted (Table 3.1.5). First, experiments conducted by *Dr. Youai Qiu* highlighted the crucial role of the catalyst and the base for the reaction outcome (entry 2 and 3). Second, the influence of electricity was examined by performing the reaction without applied current under the optimized conditions. Minor product formation of only 16% was observed (entry 4), which can be attributed to a single turn-over of the catalyst and promoted by catalytic amounts of BQ. A solvent ratio *tert*-AmylOH/H<sub>2</sub>O 3:1 was demonstrated to be most efficient in comparison to a higher (1:1, entry 5) or lower (7:1, entry 6) water content. A substantial decrease in yield was observed, when other alcohol/water mixtures were employed, such as *n*-butanol/water or glycerin/water. Likewise, the use of water, acetonitrile or methanol as solvents was proven to be less effective (entry 9–11). Regarding the nature and the amount of the catalyst, the reaction nicely tolerated a reduced catalyst loading of 1.0 mol % (entry 12). Simple iridium chloride was not able to catalyze the desired transformation, underlining the importance of the electron-rich pentamethylcyclopentadienyl ligand for the performance of the developed reaction (entry 13). Importantly, equimolar amounts of the reactants led only to a slight decrease in phthalide **41bb** generation (entry 15). An overall good yield of 72% was obtained, when platinum was substituted by nickel foam as the cathode material under the optimized reaction conditions. Using simple

stainless steel as the cathode or shorter reaction times, a significant loss of efficacy was observed (entry 17 and 18).

**Table 3.1.5** Variations of the standard conditions and control experiments for the iridaelectro-catalyzed C–H alkenylation.



Entry	Deviation from standard conditions	Yield [%]
1	none	87
2	no KOAc	_[a]
3	no catalyst	_[a]
4	no current	16
5	<i>t</i> AmylOH/H <sub>2</sub> O (1:1)	35
6	<i>t</i> AmylOH/H <sub>2</sub> O (7:1)	76
7	<i>n</i> BuOH instead of <i>t</i> AmylOH	22
8	Glycerine instead of <i>t</i> AmylOH	<5
9	H <sub>2</sub> O	29
10	MeCN	5 <sup>[b]</sup>
11	MeOH	33 <sup>[c]</sup>
12	1.0 mol % catalyst	66
13	IrCl <sub>3</sub> ·H <sub>2</sub> O (5.0 mol %)	-
14	NaOPiv instead of KOAc	72
15	1.0 equiv of acrylate	78
16	Ni <sub>foam</sub> cathode	72
17	Fe cathode	46
18	6 h	55

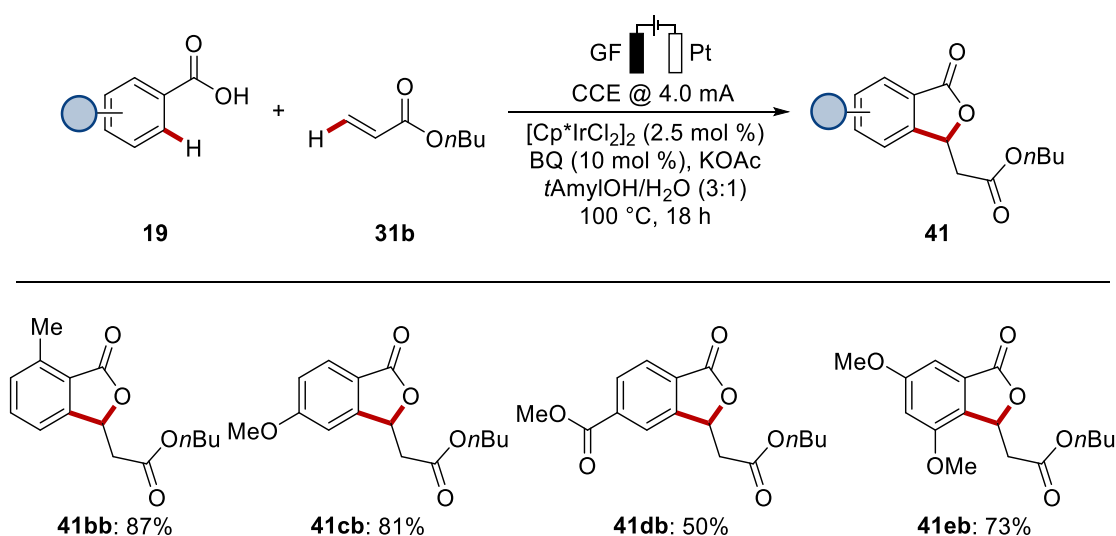
Undivided cell, GF anode (10 mm × 15 mm × 6.0 mm), Pt cathode (10 mm × 15 mm × 0.125 mm), constant current = 4.0 mA, **19b** (0.25 mmol), **31b** (0.50 mmol), catalyst (2.5 mol %), KOAc (2.00 equiv), BQ (10 mol %), solvent (4.0 mL), 100 °C, under air, 18 h. Isolated yields are given. [a] Performed by *Dr. Youai Qiu*. [b] At 70 °C. [c] At 60 °C.

Overall, the desired iridaelectrocatalysis could be accomplished with a slight excess of acrylate **31b** and KOAc in a *tert*-AmylOH/H<sub>2</sub>O (3:1), employing 10 mol % of benzoquinone as the redox mediator. Lowering the water content in the reaction medium or the catalyst

loading were tolerated and furnished the desired product in an overall good yield. Furthermore, the reaction was tolerant towards equimolar amounts of the reactants and nickel foam as cathode material.

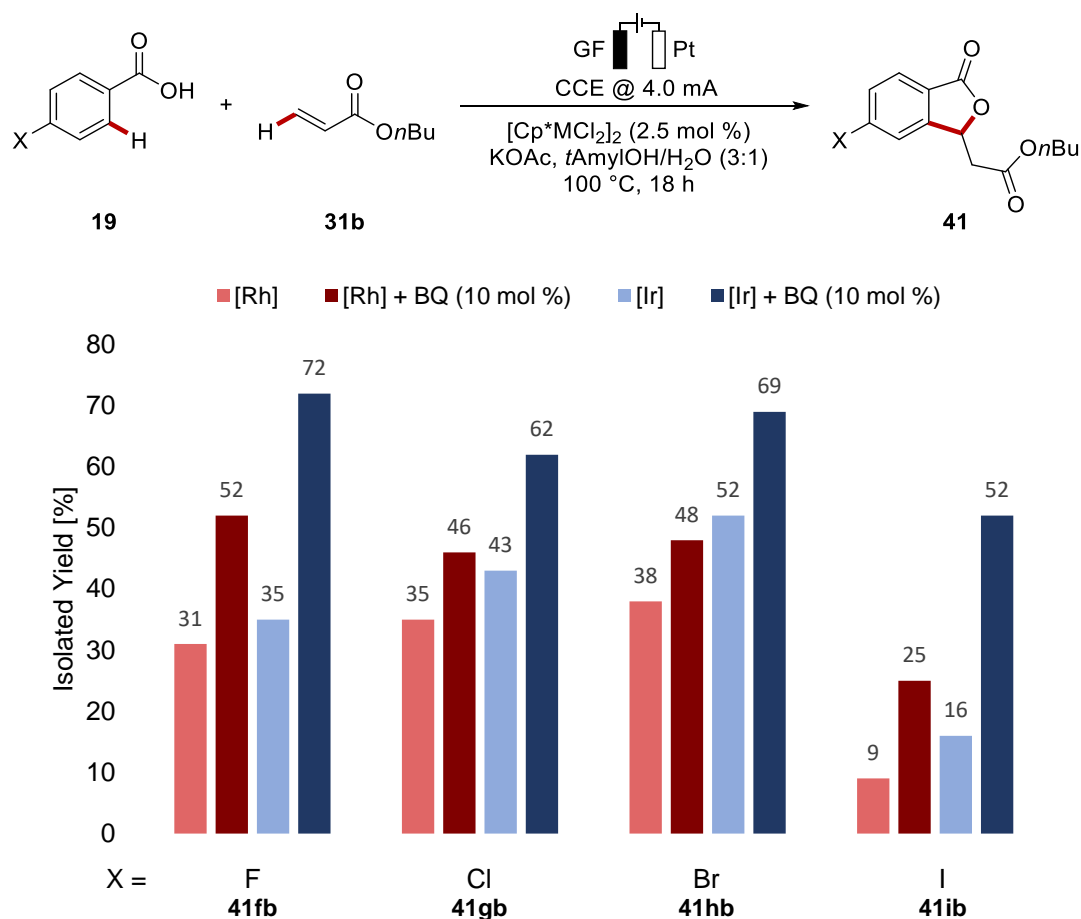
### 3.1.2 Substrate Scope for the Iridaelectro-Catalyzed C–H Alkenylation

With the optimized reactions conditions in hand, its versatility towards the viable benzoic acid component **19** was tested (Scheme 3.1.1). The reaction demonstrated to be very robust towards electron-rich and electron-deficient arenes **19b-19e**, featuring methoxy- or ester substituents, as highlighted by synthesis of the products **41bb-41eb**.



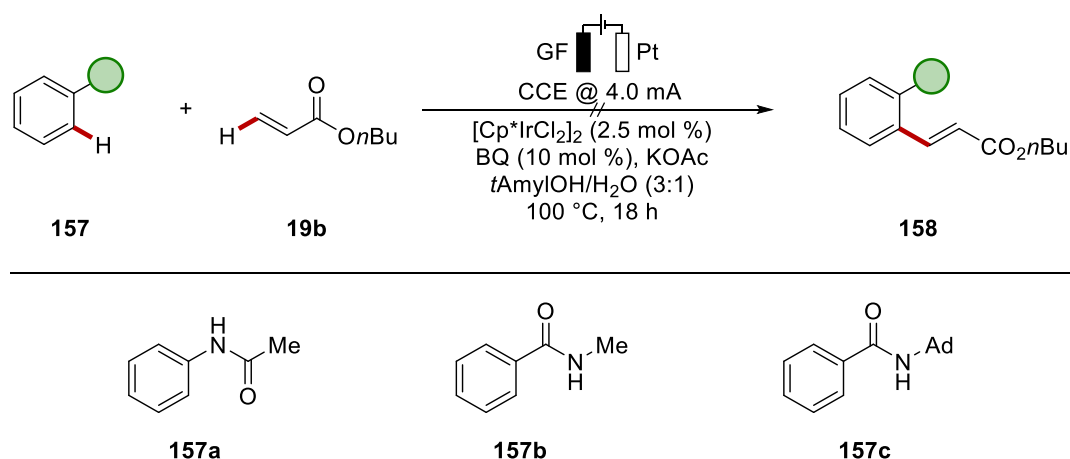
**Scheme 3.1.1** Iridium-catalyzed electrochemical alkenylation of benzoic acids **19**.

Several additional examples have been investigated by *Dr. Youai Qiu*, demonstrating high degrees of chemo and positional selectivity. Benzoic acids bearing sensitive electrophilic groups, such as cyano-, ester-, chloro- and synthetically useful bromo and iodo substituents, could be selectively converted.<sup>[209]</sup> The comparison between the previously reported rhodium electrocatalysis<sup>[193b]</sup> and the cooperative iridaelectro-catalyzed strategy was of particular interest. Experiments conducted by *Dr. Youai Qiu* highlighted the increased chemoselectivity of the synergistic catalysis for rhodium and iridium catalysts with various halogenated arenes (Scheme 3.1.2). However, the iridium catalysis was found to perform more efficiently with fluorine- or iodine-substituted arenes **19f-19i** as compared to the synergistic rhodium catalysis. Generally, the beneficial effect of the redox-mediator was less pronounced in the case of the rhodium-catalyzed alkenylation.



**Scheme 3.1.2** Influence of synergistic electrocatalysis with rhodium and iridium catalysts. Experiments performed by Dr. Youai Qiu.

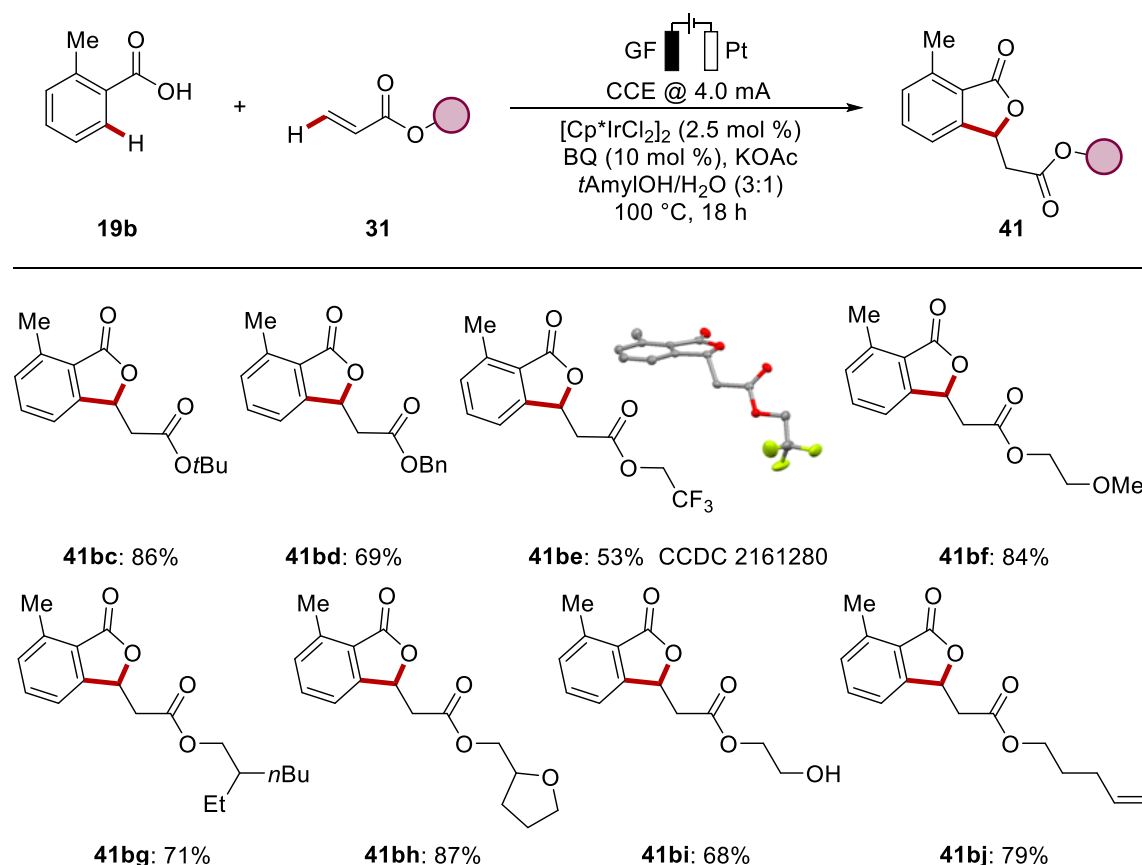
Alternative weakly coordinating directing groups such as benzamide **157b-157c** or acetanilide **157a**, were not able to undergo the iridaelectro-catalyzed C–H alkenylation under the optimized reaction conditions (Scheme 3.1.3), as the starting materials remained unreacted.



**Scheme 3.1.3** Limitations of the iridaelectro-catalyzed C–H alkenylation.



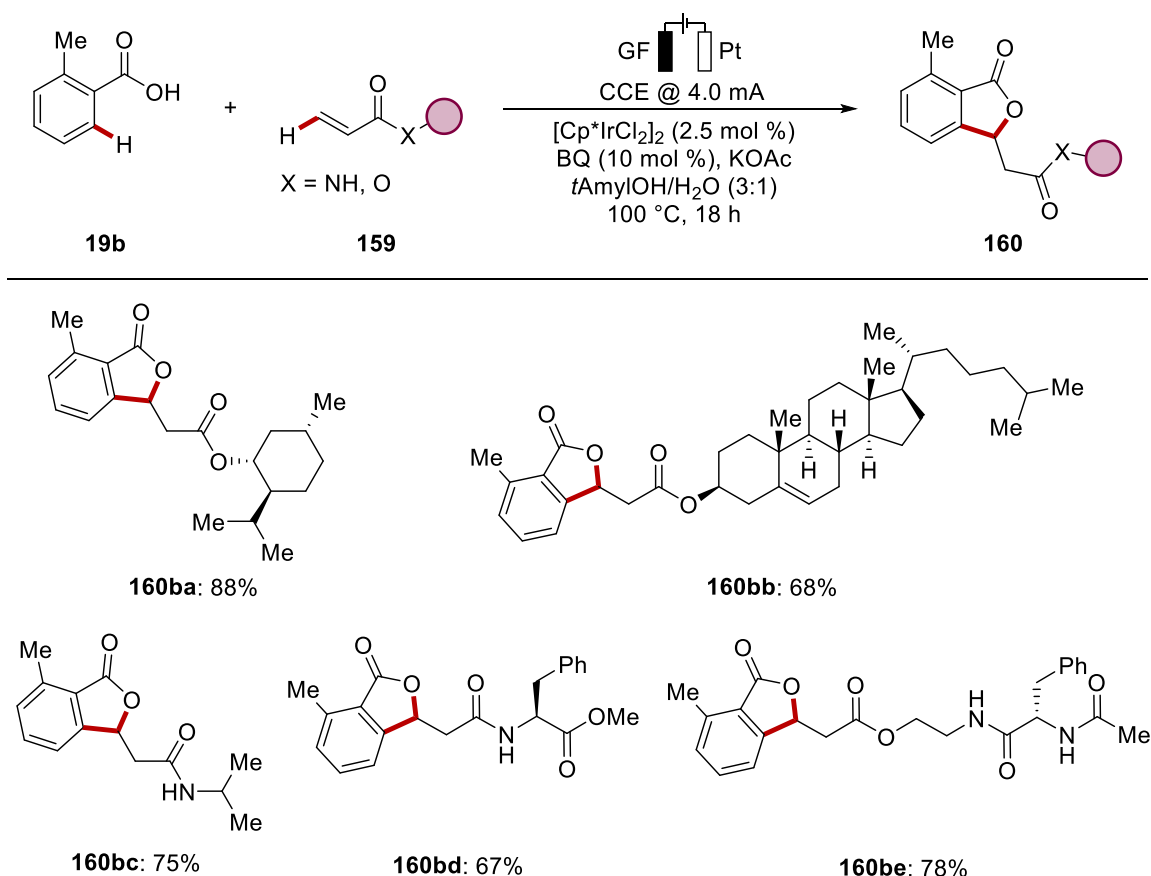
Next, the robustness of the developed strategy regarding the alkene component was explored (Scheme 3.1.4). Generally, a variety of acrylates **31** were converted to the desired products **41bc-41bj** in good to excellent yields. Thus, alkenes with a free hydroxyl group **31i** or a sensitive alkene **31j** furnished the corresponding phthalides **41bi** and **41bj** in 68% and 79% yield, respectively.



**Scheme 3.1.4** Scope of the iridacatalyzed C–H activation with acrylates **31**.

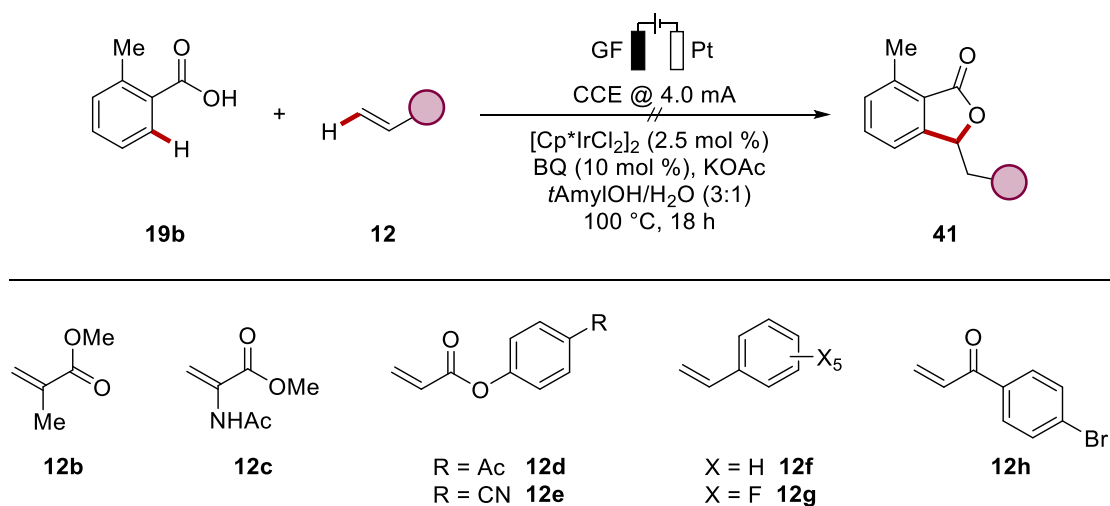
Additionally, acrylates **31g-31h** bearing different substitution patterns were fully tolerated as highlighted by the high efficiency regarding the formation of products **41bg** and **41bh**. Also, the acrylate **31e** derived from trifluoroethanol delivered product **41be** in moderate yield. With this remarkable performance in hand, more complex acrylates **159** were tested in the electrocatalysis (Scheme 3.1.5). Surprisingly, acrylates **159a-159b** derived from natural menthol and cholesterol, which carry sterically more demanding backbones, were converted to phthalides **160ba** and **160bb** in good to excellent yields. Even acrylamide **159c** was converted to the corresponding product **160bc** in 75% yield. Encouraged by these findings, amino acid derived alkenes were tested for the iridacatalyzed C–H alkenylation. Indeed, acrylates and acrylamides carrying phenylalanine in their backbone

furnished the products **160bd** and **160be** in 67% and 78% yields, respectively. To rule out a potential racemization of the amino acid, racemic acrylamide **159d** was prepared. Afterwards, the obtained products were analyzed by chiral high performance liquid chromatography (HPLC), to confirm that the stereoinformation of the phenylalanine remained intact during the catalysis.



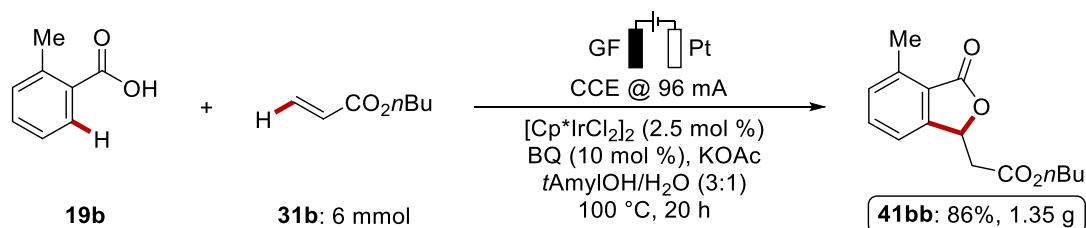
**Scheme 3.1.5** Electrochemical iridium-catalyzed C–H alkenylation with complex acrylates and acrylamides **159**.

Besides the broad substrate scope of the developed electrocatalytic C–H activation some limitations were also identified (Scheme 3.1.6). Most likely due to stereoelectronic reasons, additional substituents at the double bond were not tolerated (**12b** and **12c**). Furthermore, vinyl ketones **12d–12e** and (electron-deficient) remained unreacted in the iridium electrocatalysis (**12f–12g**).



**Scheme 3.1.6** Limitations for the alkenes **12** in the iridaelectro-catalyzed C–H activation.

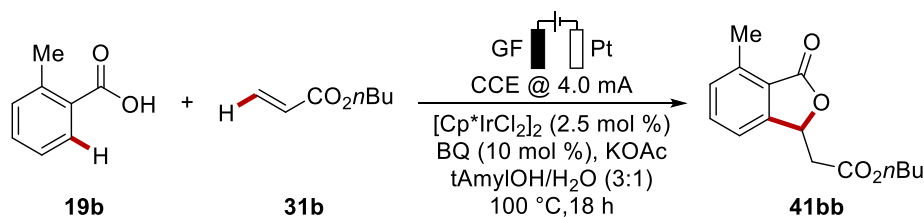
The synthetic utility of the developed strategy was illustrated by a gram-scale synthesis of phthalide **41bb** (Scheme 3.1.7). In a user-friendly undivided cell set-up, the corresponding product could be isolated after 20 h reaction time with excellent efficiency.



**Scheme 3.1.7** Gram-scale synthesis *via* iridaelectro-catalyzed C–H alkenylation.

### 3.1.3 Mechanistic Studies on the Iridaelectro-Catalyzed C–H Alkenylation

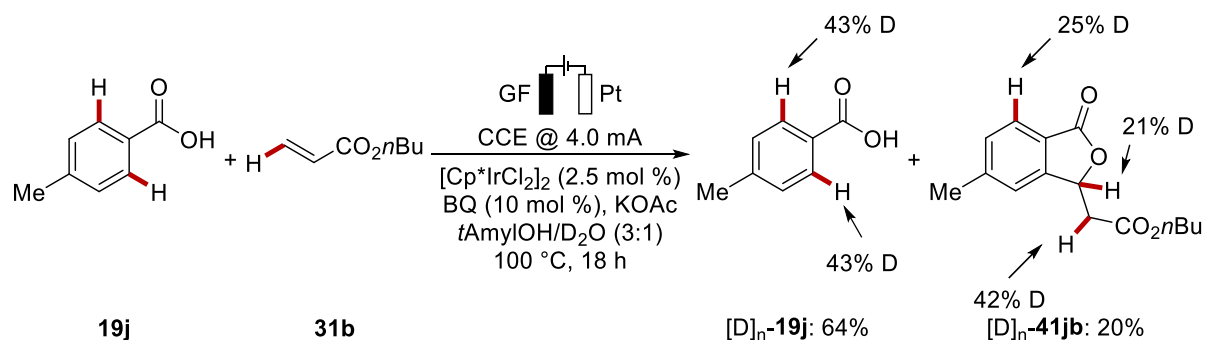
To gain a deeper understanding of the catalysts' mode of action, detailed mechanistic studies were performed. First, control experiments were conducted in order to prove the role of the redox mediator (Table 3.1.6). As such, the commonly employed electrocatalysts TEMPO and ferrocene were used instead of BQ (entry 3 and 4). Both mediators showed only a slight advantage over the conditions without benzoquinone (67%/68% vs. 57%), indicating benzoquinone to be a superior redox catalyst. Interestingly, the sterically demanding *tert*-butyl substituted benzoquinone exhibited lower activity, with substantially better performance than the electron-deficient tetrafluoro benzoquinone, which even showed to have a negative influence in comparison to the absence of the benzoquinone catalyst (entry 5 and 6). These results hint to a significant impact of the steric and electronic properties of the benzoquinone derivative on the electron transfer to the iridium catalyst. To exclude a simple ligand acceleration of benzoquinone, dibenzylideneacetone (DBA), as a prominent structurally related dienyl ligand, was used instead of the redox catalyst. The observed yield was comparable to the reaction outcome without the redox catalyst, rendering a simple ligand effect unlikely. Experiments with the reduced hydroquinone as a redox mediator further confirmed its role, as the desired product was formed in 79% yield (entry 7). At the same time, 1,2-dihydroxybenzene failed to improve the efficacy of the reaction, underlining the importance of the 1,4-substitution pattern for effective mediation (entry 9). Employing stoichiometric amounts of benzoquinone without applied current delivered 70% of the expected product **41bb**, which proves that benzoquinone can serve as a stoichiometric oxidant in this transformation (entry 11).

**Table 3.1.6** Control experiments for the role of the redox catalyst in the iridaelectro-catalyzed C–H alkenylation.

Entry	Deviation from standard conditions	Yield [%]
1	-	87
2	No BQ	57
3	TEMPO instead of BQ	68
4	Ferrocene instead of BQ	67 <sup>[a]</sup>
5	2,6-di- <i>t</i> Bu-BQ <b>161</b> instead of BQ	66 <sup>[a]</sup>
6	tetrafluoro-BQ <b>162</b> instead of BQ	26 <sup>[a]</sup>
7	DBA instead of BQ	62
8	Hydroquinone instead of BQ	79
9	1,2-Dihydroxybenzene instead of BQ	49
10	MeHQ instead of BQ	76
11	no current, BQ (200 mol %)	70

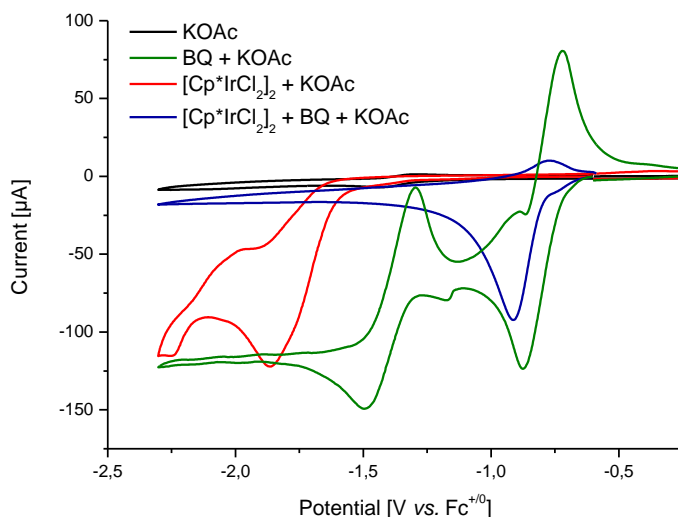
Undivided cell, GF anode (10 mm × 15 mm × 6.0 mm), Pt cathode (10 mm × 15 mm × 0.125 mm), constant current = 4.0 mA, **19b** (0.25 mmol), **31b** (0.50 mmol), catalyst (2.5 mol %), KOAc (2.00 equiv), BQ (10 mol %), solvent (4.0 mL), 100 °C, under air, 18 h. Isolated yields are given. [a] Performed by *Dr. Youai Qiu*.

The competition experiment between an electron-deficient and electron-rich benzoic acids performed by *Dr. Youai Qiu* revealed a preference of the *meta*-methyl substituted- over the *meta*-trifluoromethyl substituted benzoic acid. This observation can be rationalized in terms of a BIES manifold,<sup>[32]</sup> rather than a CMD mechanism.<sup>[210]</sup> A reaction in isotopically labeled cosolvent D<sub>2</sub>O disclosed 43% incorporation into the *ortho*-positions of the re-isolated *para*-toluic acid **19j** starting material (Scheme 3.1.8). This observation, together with KIE studies performed by *Dr. Youai Qiu* ( $k_{\text{H}}/k_{\text{D}} \approx 1.0$ ), is suggestive of a reversible C–H cleavage.



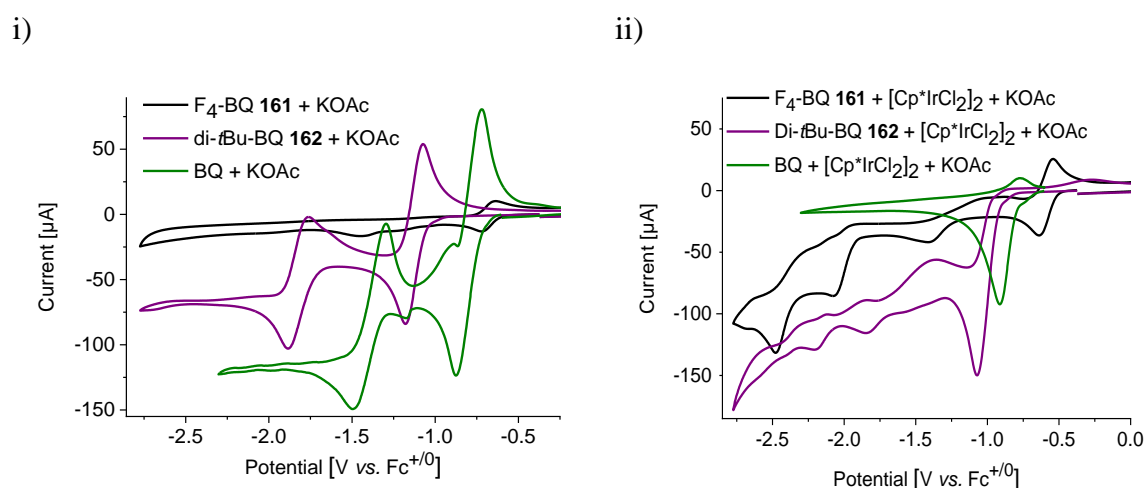
**Scheme 3.1.8** H/D exchange experiment for the electrochemical C–H/C–H alkenylation.

In collaboration with *Dr. Tjark H. Meyer*, cyclic voltammetry studies were performed to investigate whether an interaction of the redox mediator with the iridium catalyst occurs, which ultimately resulted in the observed high levels of chemoselectivity (*vide infra*). The results discussed herein have therefore been in parts discussed in the dissertation of *Dr. Tjark Meyer*.<sup>[211]</sup> When the cyclic voltammogram of benzoquinone was measured independently with potassium acetate, the two characteristic, reversible one-electron redox events at  $E_{1,1/2} = -1.39 \text{ V vs. Fc}^{+/0}$  and  $E_{2,1/2} = 0.79 \text{ V vs. Fc}^{+/0}$  were observed (Figure 3.1.2).<sup>[212]</sup> The iridium(III) reduction event at  $E_p = -1.86 \text{ V vs. Fc}^{+/0}$  was found to be much more negative and could be assigned to an iridium(III/II) reduction, with the help of DFT calculations by *Dr. João C. A. Oliveira*.<sup>[209]</sup>



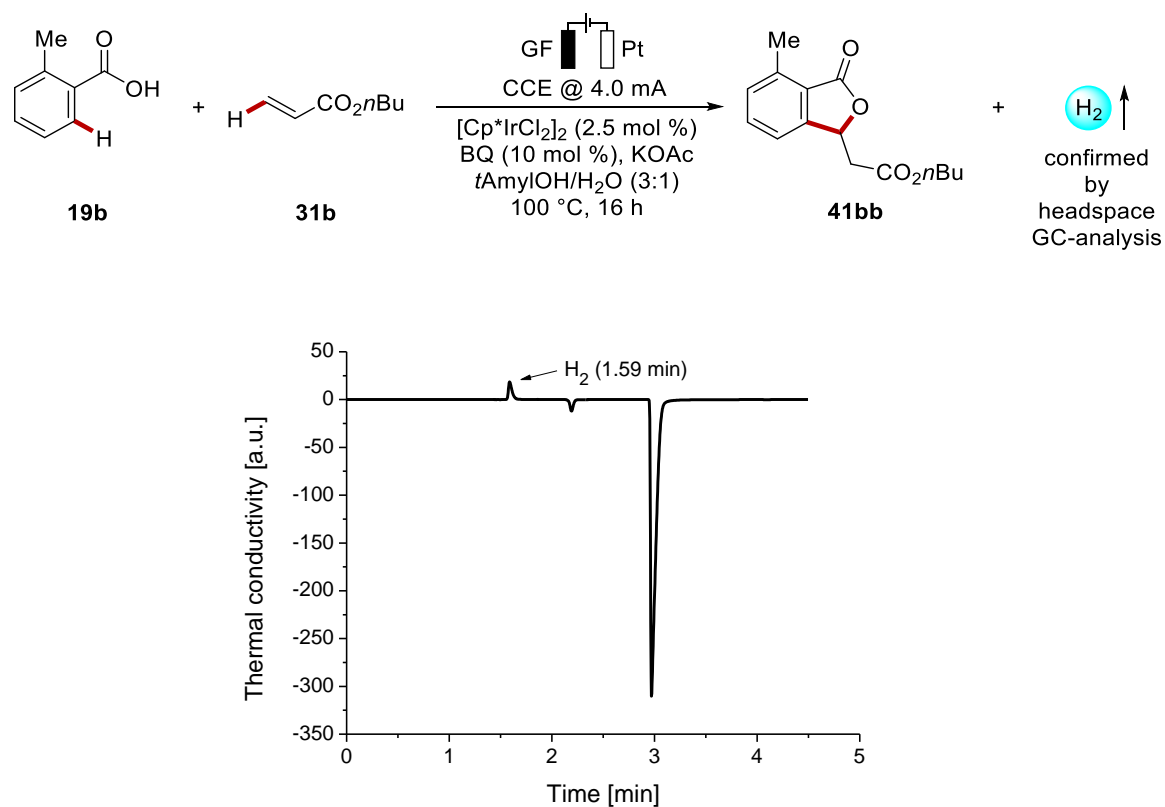
**Figure 3.1.2** Cyclic voltammetry in MeCN with  $n\text{Bu}_4\text{NPF}_6$  (0.1 M) at 100 mV/s and a GC working electrode. KOAc (black), benzoquinone and KOAc (green);  $[\text{Cp}^*\text{IrCl}_2]_2$  and KOAc (red);  $[\text{Cp}^*\text{IrCl}_2]_2$ , benzoquinone and KOAc (blue). Concentration of quinones (3.0 mM),  $[\text{Cp}^*\text{IrCl}_2]_2$  (1.5 mM) and KOAc (12 mM).

However, upon addition of benzoquinone to the iridium pre-catalyst, the disappearance of the benzoquinone back-scan peak and the iridium reduction was indicative of an efficient electron transfer from the mediator to the catalyst. The electron-transfer could potentially be facilitated by coordination of the benzoquinone to the catalyst as related studies by *Jutand*, *Rager* and *Amouri* have shown.<sup>[161]</sup> To further validate this hypothesis, the analogous experiments with previously examined redox catalysts tetrafluoro-1,4-benzoquinone and 2,6-di-*tert*-butyl benzoquinone were investigated (Table 3.1.6). In contrast to the unsubstituted- and the butyl-substituted derivative, tetrafluoro benzoquinone showed only one reversible redox-event at  $E_{1,1/2} = 0.67$  V vs.  $\text{Fc}^{+/0}$  with significantly lower currents (Figure 3.1.3i). The lower currents are also observed in literature reports,<sup>[213]</sup> and could be explained with weaker interactions of the naphthol groups on the electrode surface with the reduced tetrafluoro benzoquinone species.<sup>[214]</sup> Furthermore, the redox-potentials of the *tert*-butyl substituted benzoquinone are shifted by 470 mV towards negative potentials. In contrast to the disappearance of the iridium reduction response upon addition of benzoquinone, mixtures of the iridium pre-catalyst with the other derivatives still show current responses, presumably of iridium(III) species, at more negative potential than their own reduction events (Figure 3.1.3ii). These observations are in good agreement with the experimentally observed activities of the corresponding redox catalysts (Table 3.1.6).



**Figure 3.1.3** Cyclic voltammetry in MeCN with  $n\text{Bu}_4\text{NPF}_6$  (0.1 M) at 100 mV/s and a GC working electrode. i) tetrafluoro-1,4-benzoquinone (**161**) and KOAc (black); 2,6-di-*tert*-butyl-1,4-benzoquinone (**162**) and KOAc (purple); benzoquinone and KOAc (green). ii) [Cp\*IrCl<sub>2</sub>]<sub>2</sub>, tetrafluoro-1,4-benzoquinone (**161**) and KOAc (black); [Cp\*IrCl<sub>2</sub>]<sub>2</sub>, 2,6-di-*tert*-butyl benzoquinone (**162**) and KOAc (purple); [Cp\*IrCl<sub>2</sub>]<sub>2</sub>, 1,4-benzoquinone and KOAc (green). Concentration of quinones (3.0 mM), [Cp\*IrCl<sub>2</sub>]<sub>2</sub> (1.5 mM) and KOAc (12 mM).

After these insights regarding the anodic half reaction, the products of the cathodic process were envisioned to be characterized. As was hypothesized and indicated by the strong dependence on the platinum as the cathodic material (*vide infra*), proton reduction was supposed to be the major reaction occurring at the counter electrode. A headspace analysis of the gas atmosphere by gas chromatography after the reaction was finished, confirmed the generation of hydrogen during the iridium electrocatalysis (Figure 3.1.4).

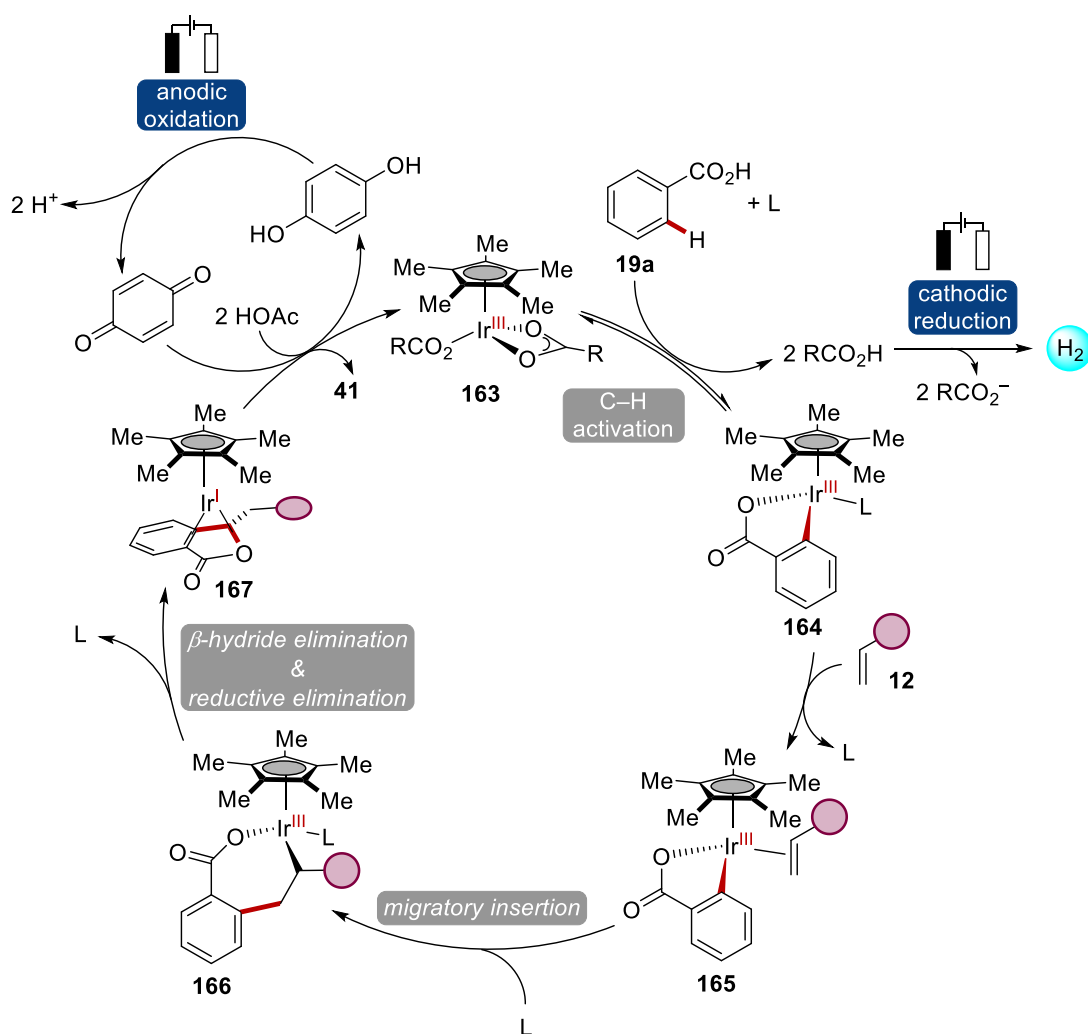


**Figure 3.1.4** Headspace gas chromatogram after the electrochemical iridium-catalyzed C–H alkenylation.



### 3.1.4 Proposed Catalytic Scenario for the Cooperative Iridaelectrocatalysis

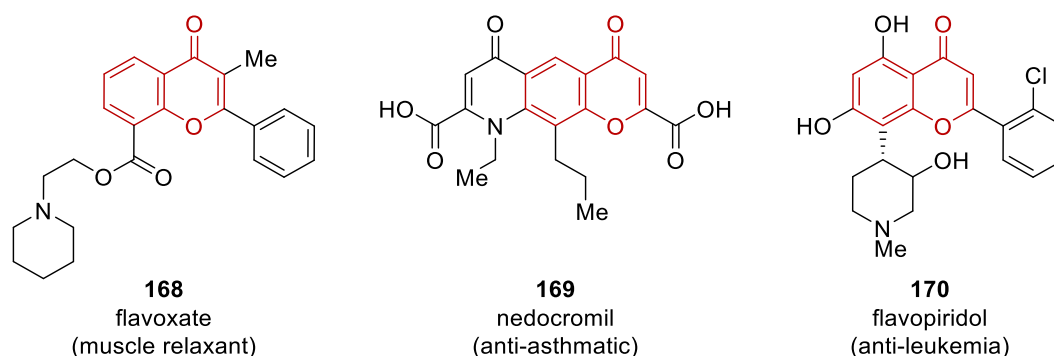
Based on the presented mechanistic findings, a plausible mechanistic scenario commenced by a reversible, organometallic C–H scission in a BIES-type fashion to furnish iridacycle **164** (Scheme 3.1.9). Subsequently, the alkene coordinates and undergoes migratory insertion to form the seven-membered metallacycle **166**.  $\beta$ -Hydride and reductive elimination afforded the iridium(I) sandwich complex **167**, which is re-oxidized by the aid of the benzoquinone redox catalyst, to regenerate the active iridium(III) species **163**. As the cathodic half reaction, the generated protons are reduced to form hydrogen.



**Scheme 3.1.9** Proposed catalytic cycle for the cooperative iridaelectro-catalyzed C–H alkenylation.

### 3.2 Rhodaelectro-Catalyzed Assembly of Chromones *via* formyl C–H Activation

C–H activation reactions have evolved as a transformative strategy for synthetic organic chemistry.<sup>[12, 13d, 35d, 215a, 215b]</sup> Within this context, metal-catalyzed hydroacylations have attracted major attention due to their high atom-economy and efficiency to access substituted ketones.<sup>[88b, 216]</sup> In recent years, functionalizations of 2-hydroxybenzaldehydes were identified as a particularly powerful tool for the construction of valuable oxygen-containing heterocycles, such as aurones,<sup>[92]</sup> coumarins,<sup>[93]</sup> and chromones.<sup>[91]</sup> Thus, the chromone scaffold is a common motif in commercialized drugs, such as flavoxate **168** or nedocromil **169**,<sup>[217]</sup> natural products and bioactive compounds, among others of relevance to acute myeloid leukemia (Figure 3.2.1).<sup>[218]</sup>

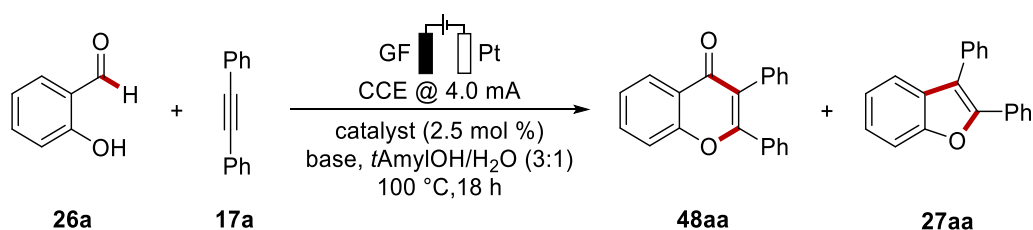


**Figure 3.2.1** Chromones as a privileged scaffold in pharmaceutical and bioactive compounds.

While electrocatalysis has provided a major impetus for resource-efficient C–H activations,<sup>[156, 160h, 202]</sup> the challenging electro-functionalization of redox-sensitive aldehydes continues to be scarce. Especially the lability of aldehydes towards decarbonylation, overoxidation, and nucleophilic attack, illustrate the functionalization under electrooxidative conditions particularly difficult.<sup>[88b, 216]</sup> Based on major advances regarding rhodaelectro-catalyzed C–H activations,<sup>[193a]</sup> a selective oxidative formation of chromones in a step and oxidant efficient fashion from readily available salicylic aldehydes was anticipated as highly desirable.

### 3.2.1 Optimization of the Electrochemical Rhodium-Catalyzed formyl C–H Activation of 2-Hydroxybenzaldehydes

At the outset, the reactivity of salicylic aldehyde (**26a**) with tolane (**17a**) was explored. The products were expected to be either, the chromone skeleton **48aa** or the decarbonylated benzofuran derivative **27aa**, as reported in literature.<sup>[66, 91, 219]</sup> As it turned out, an iridium catalyst furnished under constant potential conditions in an undivided cell set-up, using a *tert*-amyl alcohol/water mixture, the decarbonylated benzofurane **27aa** as the major product (Table 3.2.1, entry 1). The addition of benzoquinone or TEMPO as redox catalysts slightly improved the yield of the decarbonylation product (entry 2 and 3). Ultimately, also the use of Cs<sub>2</sub>CO<sub>3</sub> as base, did not increase the yield (entry 4). Afterwards, different catalysts were tested for the desired transformation. Although, ruthenium was reported to be capable of cleaving the formyl C–H bond under conventional conditions,<sup>[219]</sup> [Ru(*p*-cymene)Cl<sub>2</sub>]<sub>2</sub> did not exhibit reactivity within an electrooxidative regime (entry 5). Surprisingly, the utilization of a rhodium(III) complex furnished chromone **48aa** in excellent efficiency with KOAc as the base (entry 6). Encouraged by this finding, the use of NaOPiv further increased the isolated yield (entry 7). Notably, the reaction was completed already after 3.5 h, reassembling a metallaelectro-catalyzed transformation with very high faradaic efficiency (FE) of 87%.

**Table 3.2.1.** Initial optimization studies towards metallaelectro-catalyzed formyl C–H activation.


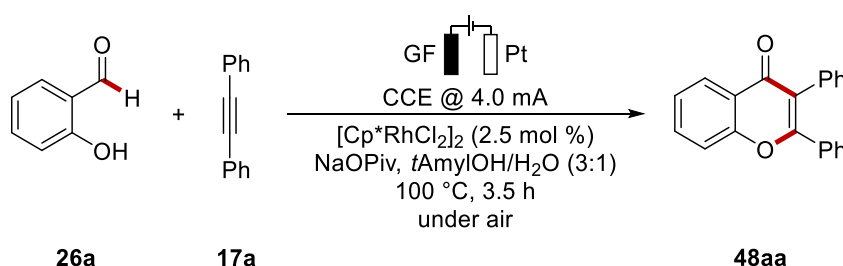
Entry	Catalyst	Base	Yield [%]	
			<b>48aa</b>	<b>27aa</b>
1	[Cp*IrCl <sub>2</sub> ] <sub>2</sub>	KOAc	<5	9
2	[Cp*IrCl <sub>2</sub> ] <sub>2</sub>	KOAc	<5	11 <sup>[a]</sup>
3	[Cp*IrCl <sub>2</sub> ] <sub>2</sub>	KOAc	<5	20 <sup>[b]</sup>
4	[Cp*IrCl <sub>2</sub> ] <sub>2</sub>	Cs <sub>2</sub> CO <sub>3</sub>	<5	14
5	[RuCl <sub>2</sub> ( <i>p</i> -cymene)] <sub>2</sub>	KOAc	--	-- <sup>[c]</sup>
6	[Cp*RhCl <sub>2</sub> ] <sub>2</sub>	KOAc	81	--
7	[Cp*RhCl <sub>2</sub> ] <sub>2</sub>	NaOPiv	89	--
8	[Cp*RhCl <sub>2</sub> ] <sub>2</sub>	NaOPiv	92 <sup>[d]</sup>	--

Undivided cell, GF anode (10 mm × 15 mm × 6.0 mm), Pt cathode (10 mm × 15 mm × 0.125 mm), constant current = 4.0 mA, **26a** (0.75 mmol), **17a** (0.25 mmol), catalyst (2.5 mol %), base (2.00 equiv), solvent (4.0 mL), 100 °C, under air, 18 h. Isolated yields are given. [a] with benzoquinone (10 mol %). [b] with TEMPO (10 mol %). [c] with catalyst (10 mol %). [d] reaction time 3.5 h.

With these results in hand, additional control experiments and variations of the reaction conditions were conducted to gain a better understanding of limitations and the role of specific parameters on the outcome of the developed transformation. The crucial role of electricity was demonstrated as the yield dramatically decreased, when the current was not applied (Table 3.2.2, entry 3). Although, a minor background reactivity was observed, when the reaction was performed under air and without current, a comparable yield was obtained under inert atmosphere, indicating that electricity serves as the terminal oxidant (entry 4). Regarding the variable temperature, a slight decrease to 80 °C still furnished the desired product **48aa** in excellent yields. However, conducting the reaction at only 40 °C substantially lowered the efficacy of the rhodoelectro-catalyzed annulation (entry 5 and 6). Importantly, the amount of catalyst could be successfully lowered, without observing major loss in efficiency (entry 7). Regarding the nature of the catalyst, the use of the *Wilkinson* catalyst or a combination of a rhodium (I) pre-catalyst with a tetraphenyl-substituted cyclopentadien ligand, as was used by *Miura*,<sup>[91]</sup> was likewise proven to show diminished

activity (entry 8 and 9). Concerning the stoichiometry of the reactants, reduced amounts of salicylic aldehyde (**26a**) did not result in significantly reduced product **48aa** formation (entry 10 and 11), whereas the reaction time of 3.5 h appeared to be crucial (entry 12 and 13). To underline the broad applicability of our strategy, the reaction was demonstrated to be efficiently viable in the commercially available IKA *Electrasyn*<sup>®</sup> set-up (entry 14).

**Table 3.2.2** Control experiments and variation of the standard conditions for the rhodaelectro-catalyzed formyl C–H activation.

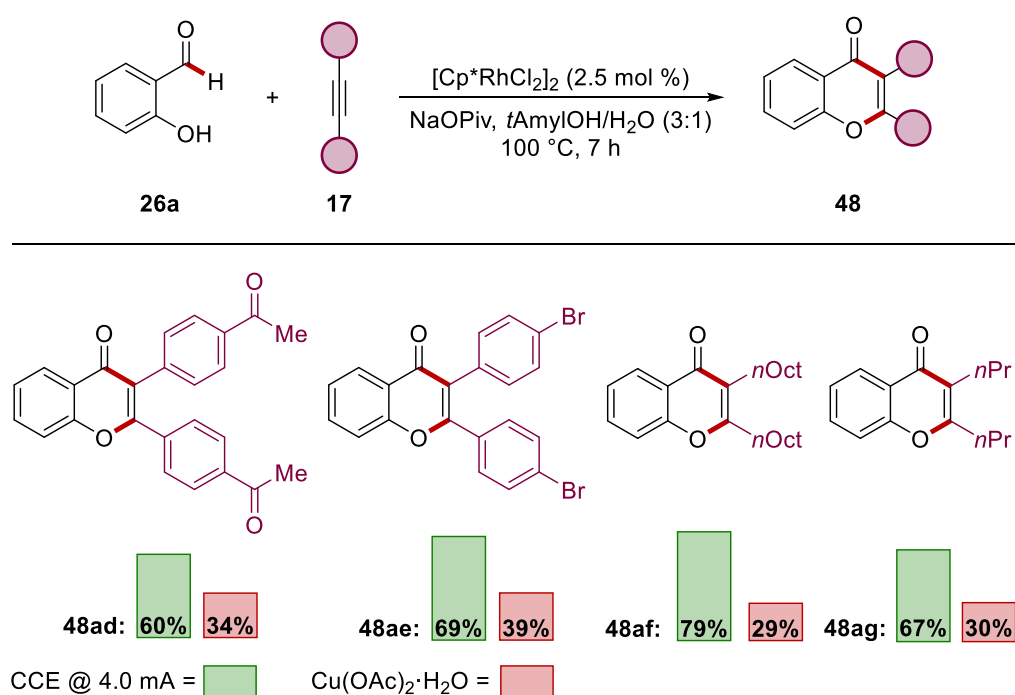


Entry	Deviation from standard conditions	Yield [%]
1	none	92
2	No catalyst	--
3	No current	22
4	Under N <sub>2</sub>	88
5	80 °C	86
6	40 °C	37
7	[Cp <sup>*</sup> RhCl <sub>2</sub> ] <sub>2</sub> (1.0 mol %)	85
8	[Rh(PPh <sub>3</sub> ) <sub>3</sub> Cl] (5.0 mol %)	--
9	[Rh(COD)Cl] <sub>2</sub> (2.5 mol %), C <sub>5</sub> H <sub>2</sub> Ph <sub>4</sub> (10 mol %)	6 <sup>[a]</sup>
10	1.5 equiv of <b>26a</b>	71
11	2.0 equiv of <b>26a</b>	86
12	1 h	37
13	2 h	68
14	Performed with IKA <i>Electrasyn</i> <sup>®</sup>	91 <sup>[b]</sup>

Undivided cell, GF anode (10 mm × 15 mm × 6.0 mm), Pt cathode (10 mm × 15 mm × 0.125 mm), constant current = 4.0 mA, **26a** (0.75 mmol), **17a** (0.25 mmol), catalyst (2.5 mol %), NaOPiv (2.00 equiv), solvent (4.0 mL), under air. Isolated yields are given. [a] Yield determined by <sup>1</sup>H-NMR spectroscopy with CH<sub>2</sub>Br<sub>2</sub> as an internal standard. [b] constant current = 8.0 mA, **26a** (1.50 mmol), **17a** (0.50 mmol), solvent (8.0 mL), with RVC instead of GF.

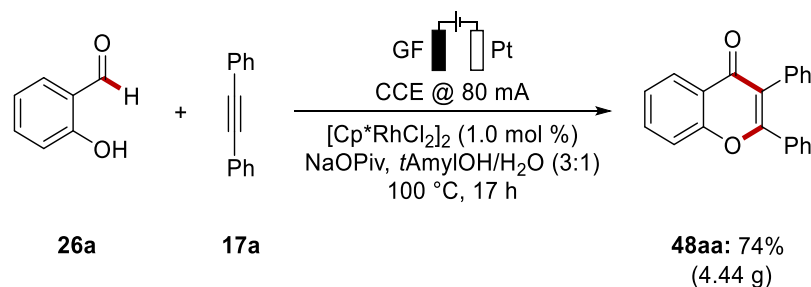
### 3.2.2 Electrosynthesis *versus* Chemical Oxidants for the Rhodium Catalysis

To assess the advantages of the developed rhodaelectro-catalytic strategy over the previously reported protocol,<sup>[91]</sup> the performance of the two approaches regarding challenging substrates was compared (Scheme 3.2.1). The presented strategy proved specifically superior, when electron-deficient diphenylacetylenes **17**, such as aryls decorated with acetyl (**17d**) or bromo substituents (**17e**), were tested in the rhodium catalysis. An even larger increase in efficacy was observed in comparison to the chemical oxidant, when alkynes **17f-17g** with aliphatic substituents were used in the catalysis.



**Scheme 3.2.1** Performance comparison between electricity and stoichiometric oxidant.

Likely, due to copper-catalyzed isomerization of the triple-bond, the desired products were obtained in significantly lower yields. Additionally, the synthetic utility and scalability of the approach could be demonstrated in a multi-gram scale synthesis in a user-friendly undivided cell (Scheme 3.2.2).

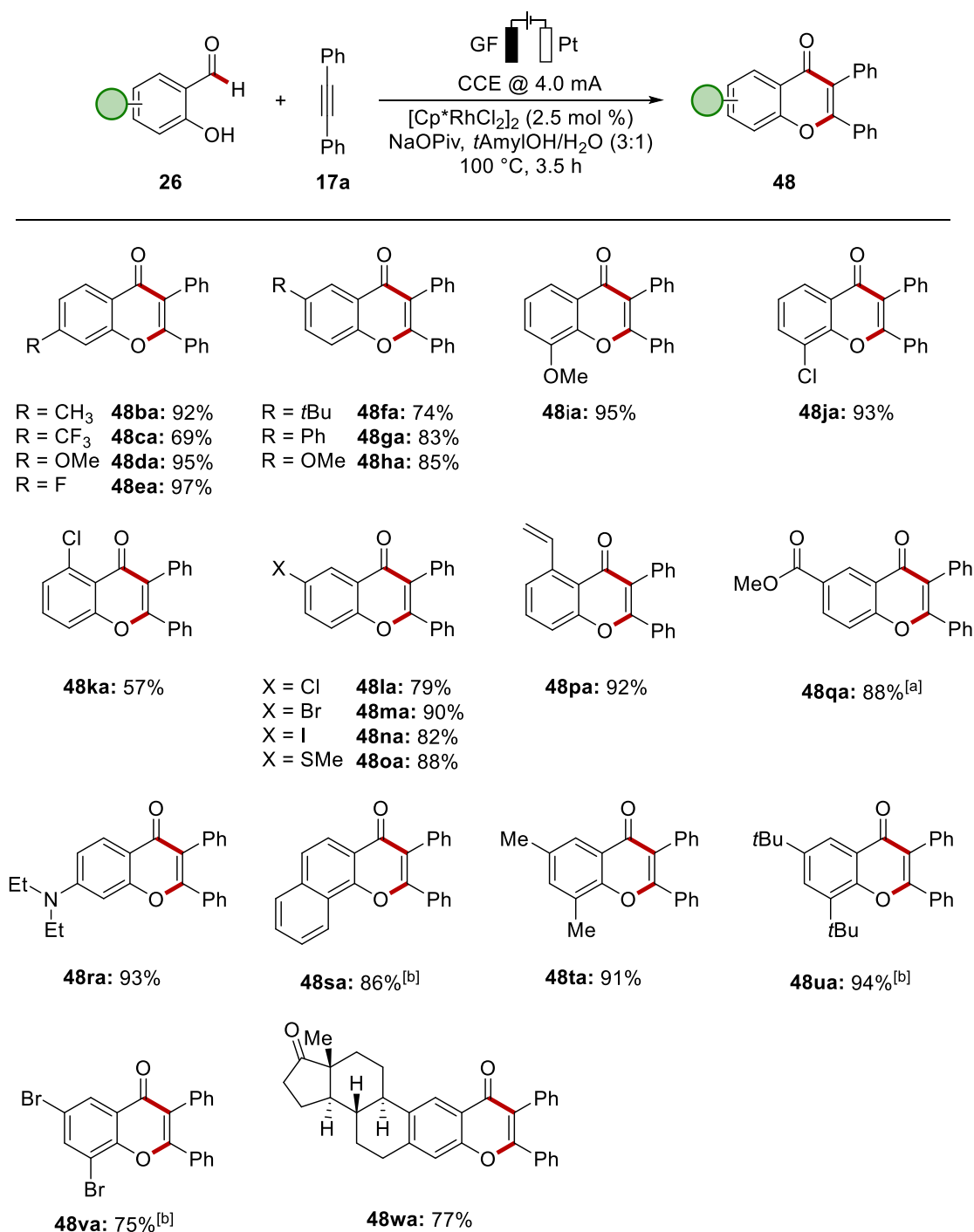


**Scheme 3.2.2** Rhodaelectro catalysis on multigram scale.

Product **48aa** was obtained in very good yield, employing a reduced catalyst loading and extended reaction time.

### 3.2.3 Scope of the Rhodaelectro-Catalyzed formyl C–H Annulation

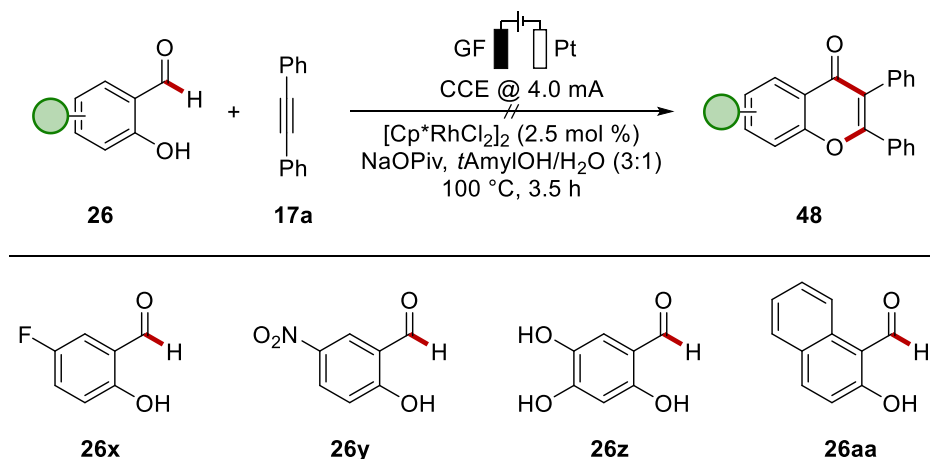
With the optimized conditions identified, scope of salicylic aldehydes **26** was investigated (Scheme 3.2.3). Thus, electron-deficient as well as electron-rich substituents, including fluoro-, trifluoromethyl- and methoxy groups, in the *para*-position to the aldehyde were converted to the desired products **48ba-48ea** in very good to excellent yields. Electron-neutral and electron-rich substituents in the 3- and 5-position effectively furnished chromones **48fa-48ja**. Notably, electrophilic halides, among them synthetically useful bromo- and iodo- substituted aldehydes, were fully tolerated in the rhodaelectro catalysis (**48ma-48na**). The robustness of the catalysis was further reflected by the formation of product **48pa** with outstanding efficiency. Under water-free conditions also the substrate with an ester substituent was smoothly be transformed to product **48qa**. Substrates bearing oxidation-sensitive thioether and amine were likewise converted to the desired products **48oa** and **48ra**, without loss of efficacy. Under slightly prolonged reaction times, also bulky disubstituted aldehydes delivered the products **48sa-48va** in very good yields. Finally, estrone derivative **26w** was successfully transformed to the desired product **48wa**, highlighting the excellent selectivity of the electrosynthesis in general.



**Scheme 3.2.3** Scope for salicylic aldehydes **26**. [a] *t*AmylOH with *n*Bu<sub>4</sub>NPF<sub>6</sub> (0.1 M). [b] 7 h.

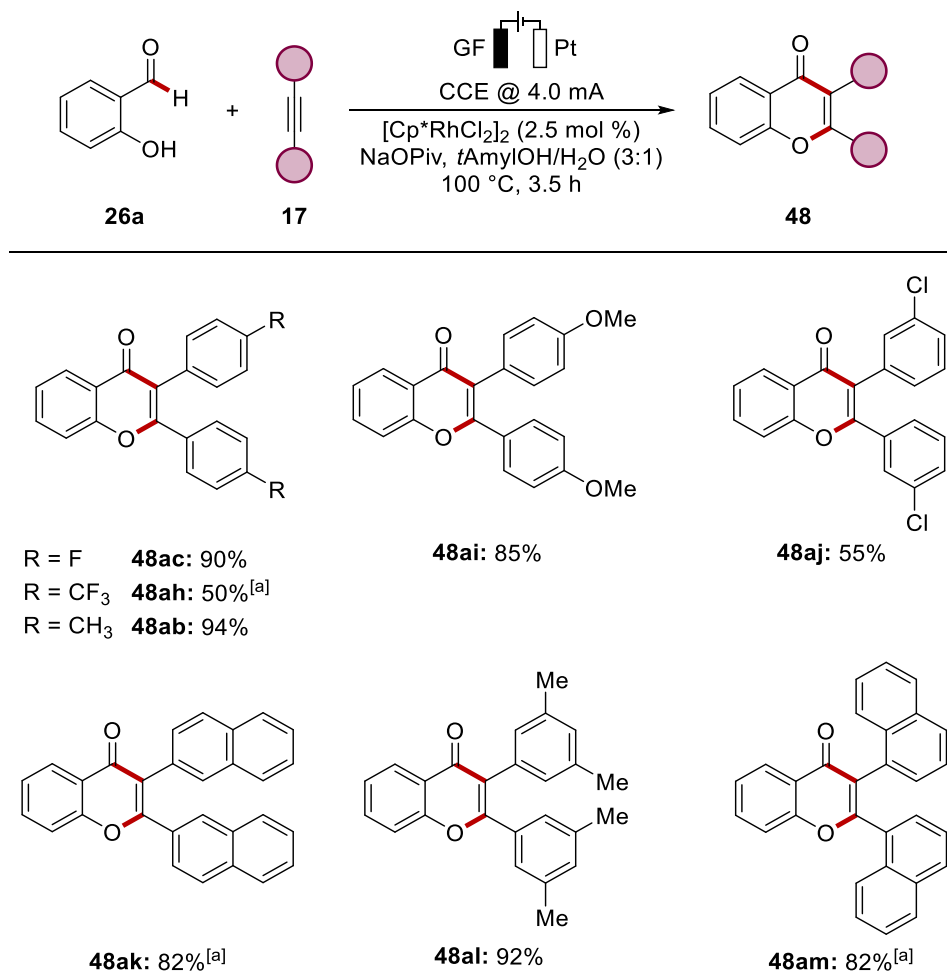
Under otherwise identical reaction conditions certain limitations were observed (Scheme 3.2.4). Thus, electron-deficient substituents at the 5-position were proven to ineffectively or not undergo the catalysis at all. Furthermore, free hydroxyl groups, likely due to competing coordination to the catalyst, or sterically demanding substituents in the *ortho*-position to the aldehyde were not tolerated under the optimized reaction conditions.





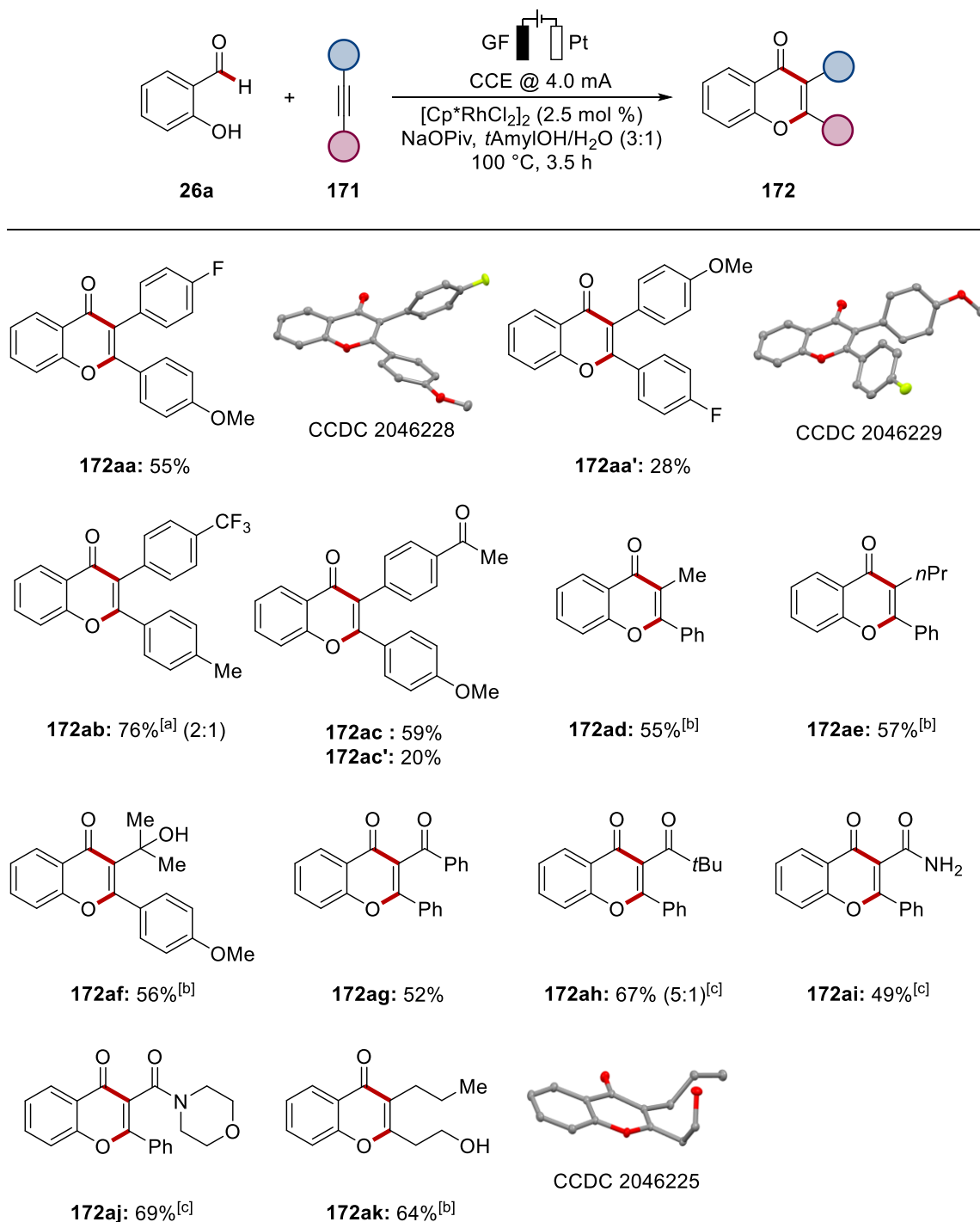
**Scheme 3.2.4** Unsuccessful examples for the rhodium-catalyzed annulation.

Next, the versatility of the presented strategy was further substantiated by various symmetrical alkynes **17** (Scheme 3.2.5). Hence, a variety of *para*-substituted diphenylacetylenes were tested. As it turned out, electron-rich and electron-deficient alkynes were efficiently converted into the desired products **48ac-48aj**. However, *p*-trifluoromethyl- and *m*-chloro derivatives **17h** and **17j**, exhibited slightly decreased reactivity. Remarkably, sterically encumbered naphthalene **17k** and **17m**, as well as and dimethylphenyl-derived substrates **17l** furnished the desired products in excellent yields (**48ak-48am**).



**Scheme 3.2.5** Scope for symmetrically substituted alkynes **17**. [a] 7 h.

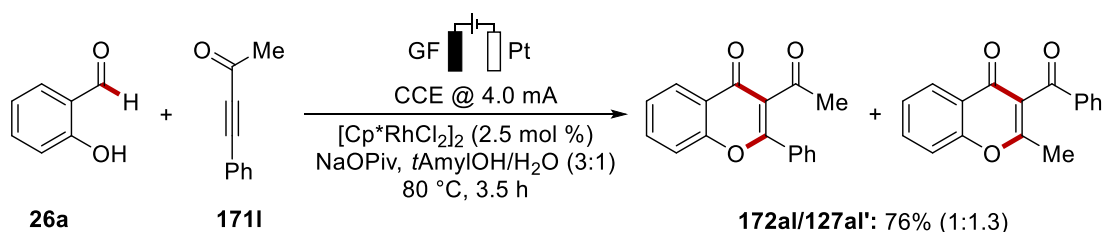
With these findings in hand, the regioselectivity of unsymmetrically decorated alkynes **171** was examined (Scheme 3.2.6). Alkynes bearing two differently substituted arenes, furnished the products **172aa-172ac** with the more electron-rich moiety in the 2-position of the chromone, as unambiguously proven by X-ray structures of products **172aa** and **172aa'**. Interestingly, the phenyl moieties are not in plane, but tilted due to steric repulsion. The ratio of the formed isomers was determined to be 2:1 for products **172ab** and 3:1 for the product derived from *p*-methoxy/*p*-acetyl diphenylacetylene **171c**. In the case of alkynes with an aromatic and an aliphatic residue, the phenyl group was generally located proximal to the oxygen-heteroatom of the resulting chromones **172ad-172ae**. For these substitution patterns the isolated isomers were formed exclusively in moderate to good yields (55-57%). Notably, unsymmetrical alkynes **171f-171j** featuring alcohol, ketone, or amide substituents underwent the catalysis with overall high efficiency and excellent regioselectivity. Surprisingly, the residues of hydroxyheptyne **171k** could be effectively differentiated by the rhodium catalyst, selectively furnishing **172ak**.



**Scheme 3.2.6** Scope for unsymmetrically substituted alkynes **171**. [a] Ratio determined by <sup>19</sup>F-NMR. [b] 7 h. [c] [Cp\*RhCl<sub>2</sub>]<sub>2</sub> (5.0 mol %).

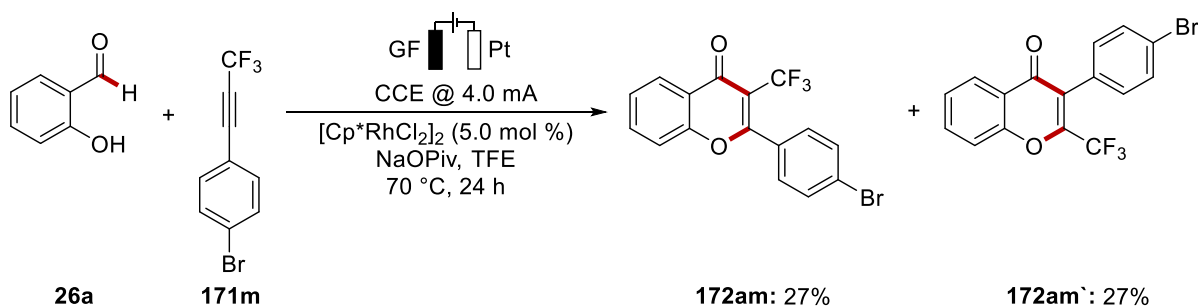
In order to gain insights into the high levels of regio-discrimination, DFT-calculations were carried out by *Dr. João C. A. Oliveira*. The calculated regioselectivity for the insertion-step of alkyne **171b** was in good agreement with the experimentally observed ratio of 2:1. NCI-plots indicated that non-covalent interactions were of minor relevance.<sup>[220]</sup> Additionally, the transition states for the migratory insertion of alkyne **171k** were calculated. Here, the regioisomer with the hydroxyl group distal to the carbonyl group was favored by

2.4 kcal mol<sup>-1</sup>, which can be attributed to hydrogen bonding interactions between the coordinating oxygen of the salicylic aldehyde with the hydroxyl group of the alkyne.<sup>[220]</sup> Interestingly, upon decreasing the reaction temperature with alkyne **171i**, a mixture of non-separable isomers was obtained (Scheme 3.2.7). Careful analyses by 2D-NMR spectroscopy were suggestive of structure **172al'** being the unexpected side product, specifically due to the correlation of the *ortho*-protons with the carbonyl of the phenylketone observed in the HMBC experiment.



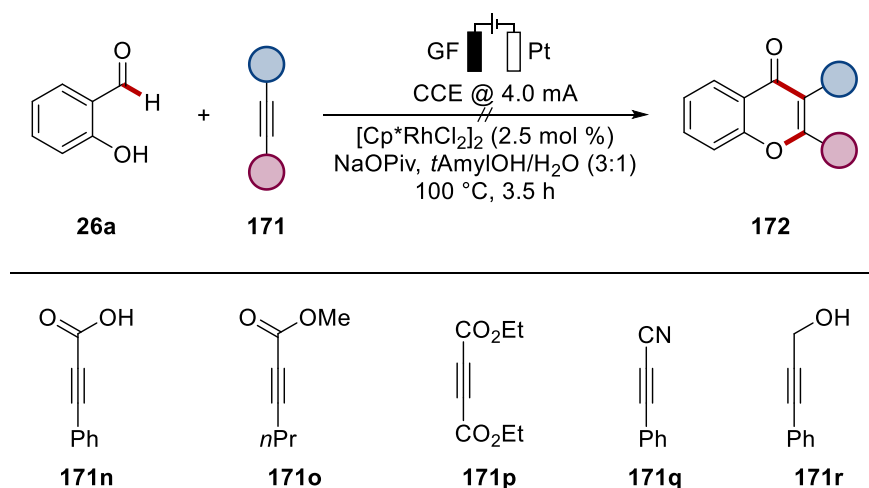
**Scheme 3.2.7** Unexpected side product formation at lower temperature under rhodoelectro-catalytic conditions.

Under the standard reaction conditions, trifluoromethylated alkyne **171m** could not be converted to the desired chromone scaffold. However, the combination of TFE as a solvent and a slightly increased amount of catalyst, furnished a 1:1 mixture of isomers in 54% yield (Scheme 3.2.8). It is noteworthy, that after the previously observed selectivity with unsymmetrical alkynes bearing electronically different substituents (*vide supra*), the ratio of the formed trifluoromethylated regioisomers was somewhat unexpected.



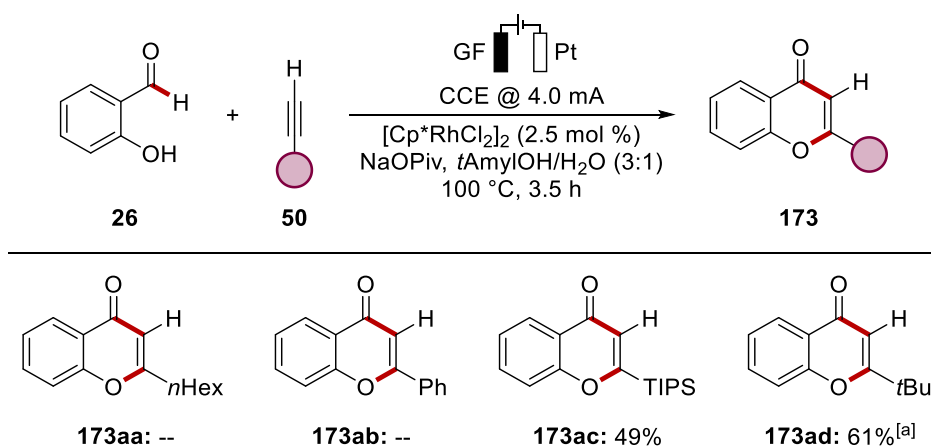
**Scheme 3.2.8** Reaction of trifluoromethylated alkyne **171m** in TFE as a solvent.

During the investigation of the scope of the alkyne component, minor limitations have been observed (Scheme 3.2.9). Especially, acid or ester substituted alkynes **171n-171p** were found to show no or diminished reactivity in the annulation of salicylic aldehyde **26a**. Furthermore, the electron-withdrawing nitrile or alcohol substituents underwent the catalysis ineffectively (**171q** and **171r**).



**Scheme 3.2.9** Limitations of the scope for the viable alkyne component.

Next, the performance of terminal alkynes in the catalysis was evaluated (Scheme 3.2.10). Interestingly, terminal alkynes **50** bearing aliphatic or aromatic groups did not furnish the desired products **173**. Analyses of the reaction mixtures by GC-MS indicated a [2+2+2] cycloaddition of the alkynes **50a** and **50b** as a competing side reaction. Choosing a bulkier substituent, like the (triisopropylsilyl)acetylene **50c** or *tert*-butyl acetylene **50d** delivered the corresponding products **173ac** and **173ad** in moderate to good yield.

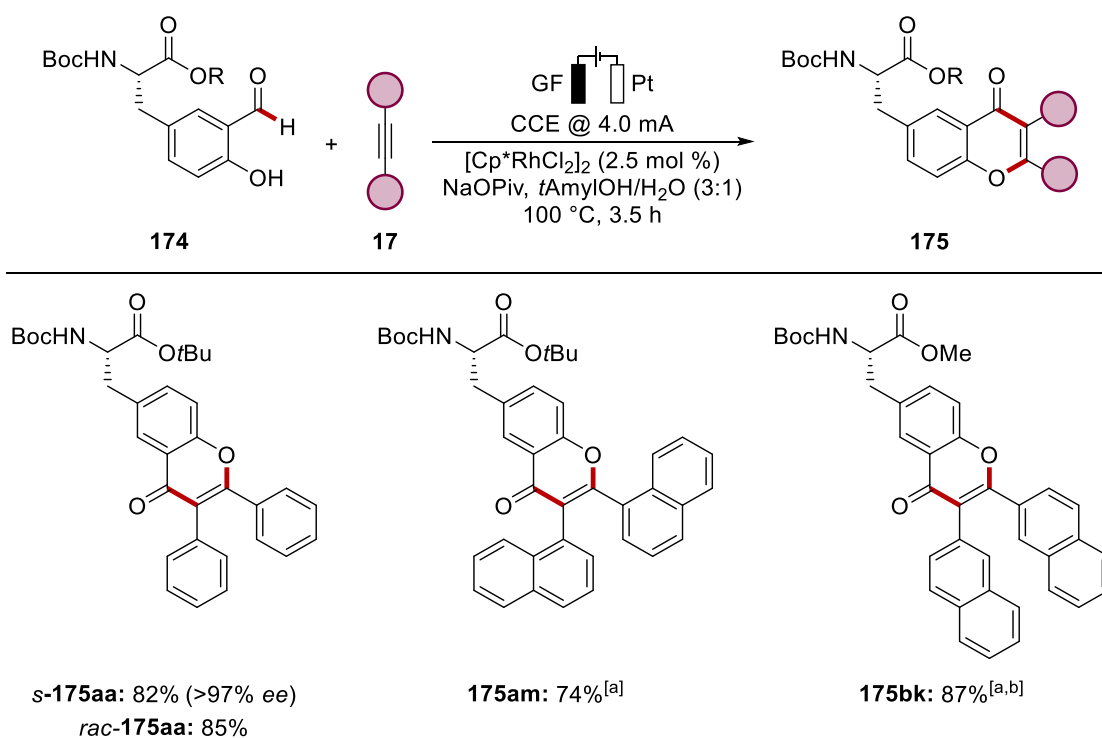


**Scheme 3.2.10** Terminal alkynes **50** in the rhodaelectro-catalyzed annulation. [a] **26a** (1.50 mmol), **50d** (0.50 mmol), rt, 7 h.

The key to success for the *tert*-butyl acetylene **50d** was to conduct the reaction at room temperature and at higher concentrations. Attempts to improve the yield of product **173ac** by increasing the catalyst loading, lowering the reaction temperature, or conducting the reaction in a divided cell set-up were not successful.

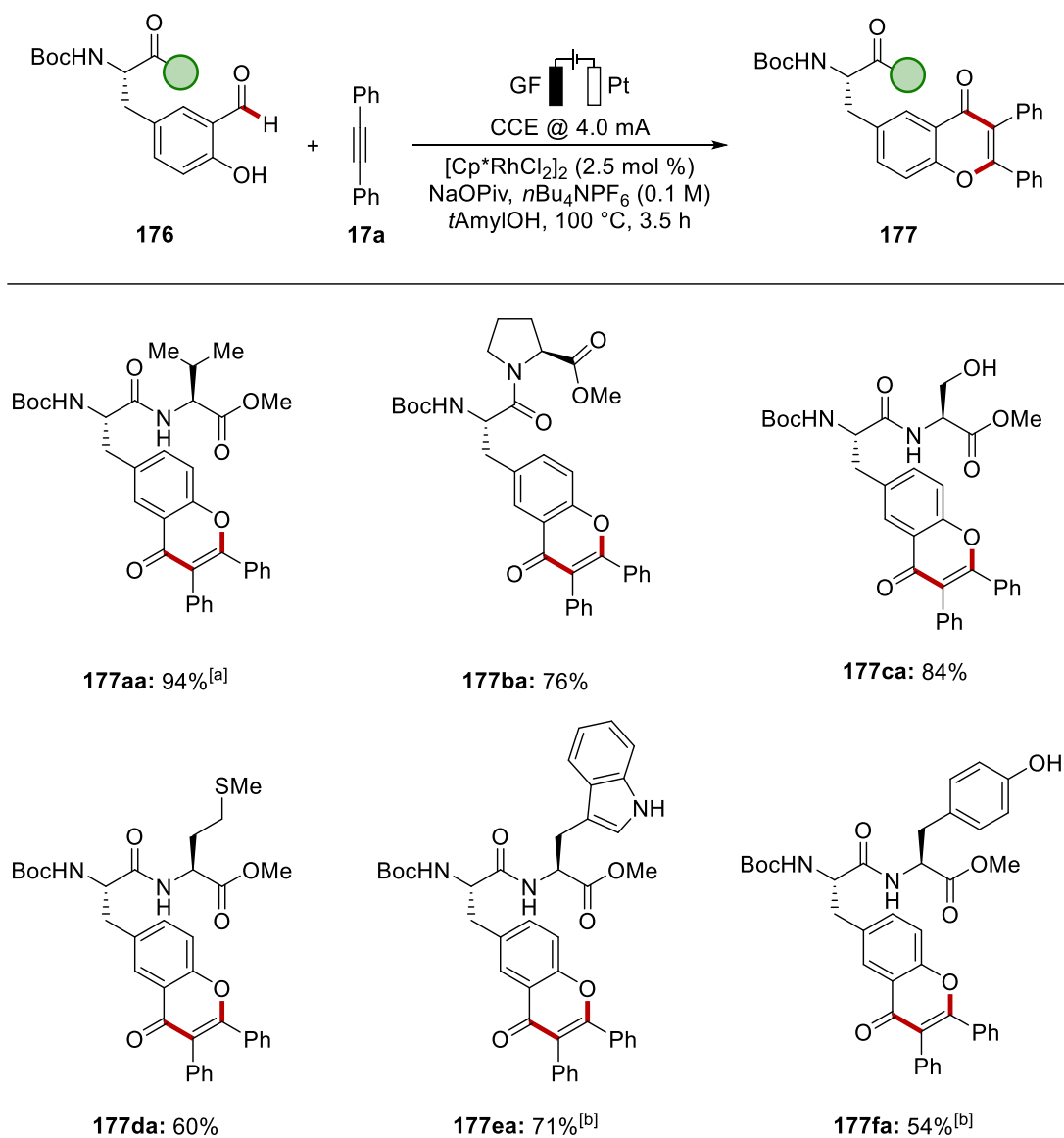
### 3.2.4 Application of Electrocatalytic formyl C–H Activation to the Functionalization of Peptides

Chemically modified peptidomimetics feature major advantages over their naturally occurring derivatives, such as reduced enzymatic degradation, feature superior binding affinities, cell permeability and pharmacokinetics.<sup>[221]</sup> Traditionally, the functionalization of structurally complex peptides heavily relied on derivatization of terminal amino acids, azide-based click chemistry or on the innate reactivity of cysteine.<sup>[37c, 37d, 222]</sup> Considering the practical relevance of late-stage peptide diversifications, and the remarkable efficiency and robustness of the examined strategy, it was explored, whether formylated tyrosines could be functionalized. To prevent hydrolysis under the aqueous conditions Boc/*tert*-butyl protected tyrosine was selected as the model substrate for the envisioned modification (Scheme 3.2.11). Indeed, the annulation of tyrosines **174** could be achieved in excellent yield. With regard to the suitability of the developed strategy for the labeling of peptides, it is crucial that the stereocenter remained intact during the catalysis. Therefore, the racemic tyrosine derivative was prepared, and the products subsequently analyzed by chiral HPLC. Remarkably, it was found that the product of the enantiopure tyrosine derivative **174a** did not racemize under the electrocatalytic conditions. With these high levels of robustness and chemoselectivity in hand, functionalization of tyrosine **174a-174b** with naphthalene derived alkynes **17m** and **17k** to enhance the optoelectronic properties of the resulting labels was investigated. The desired products **175bk** and **175am** could be obtained in very high yields. Importantly, also an ester moiety on the amino acid backbone was fully tolerated using an organic electrolyte instead of water, which is of great importance for a broader application to peptide chemistry.



**Scheme 3.2.11** Annulation of tyrosine derivatives **174** using rhodoelectro catalysis [a] 7 h. [b] *t*AmylOH with *n*Bu<sub>4</sub>NPF<sub>6</sub> (0.1 M).

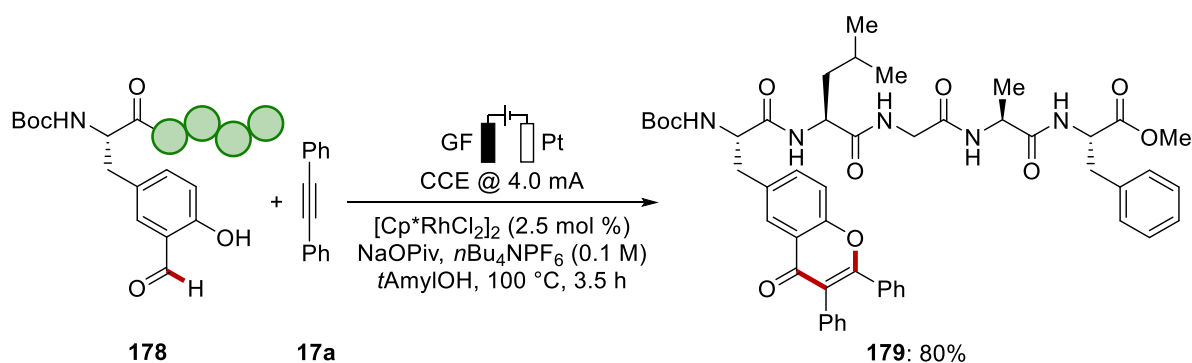
To further probe the applicability of the developed concept towards peptide labeling a variety of dipeptides **176** were tested (Scheme 3.2.12). Thus, substrates **176a-176f** were efficiently converted to the corresponding products, among them oxidation-sensitive serine (**177ca**) and methionine (**177da**) containing analogs. Furthermore, potentially coordinating *NH*-free tryptophane or tyrosine regioselectively furnished the products **177ea** and **177fa**, respectively, in moderate to high yields.



**Scheme 3.2.12** Electrolabeling of various dipeptides **176** via rhodium catalysis. [a] 7 h. [b]  $[\text{Cp}^*\text{RhCl}_2]_2$  (5.0 mol %).

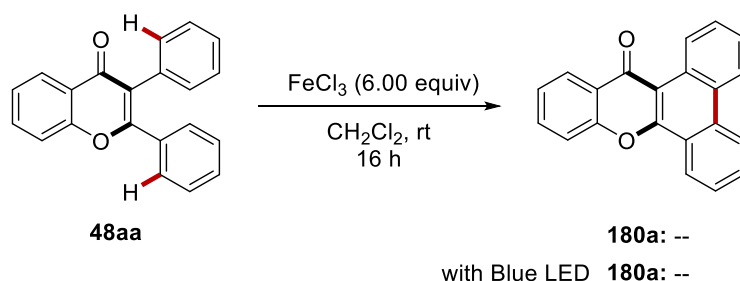
Finally, the concept was applied to the functionalization of oligopeptide **178** (Scheme 3.2.13). Indeed, the labeled derivative **179** was obtained in excellent efficiency, illustrating the unique power and selectivity of the rhodaelectrocatalysis for peptide labeling.





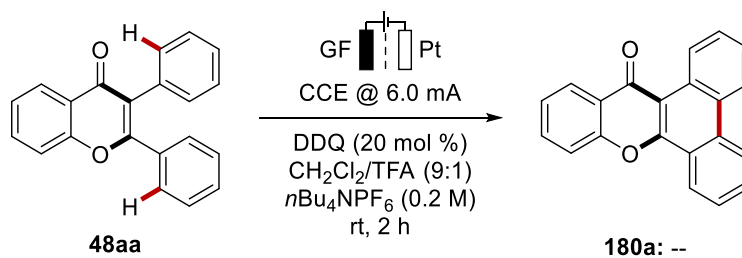
**Scheme 3.2.13** Electrolabeling of pentapeptide **178** via rhodium catalysis.

Since the attached aryl moieties on the resulting chromones seemed to be not in plane, as suggested by the X-ray structures (*vide supra*), the fluorescence of the resulting structures was not particularly high. To further tune the photoelectronic properties of the obtained compounds, a subsequent *Scholl*-type annulation reaction was anticipated, to convert the aryls of the former alkynes into  $\pi$ -extended labels. First attempts to achieve the desired transformation in a LEWIS-acid mediated fashion, using iron(III) chloride, failed to convert any chromone **48aa** to the anticipated product **180a** (Scheme 3.2.14). Likewise, under blue LED irradiation the starting material remained unreacted.



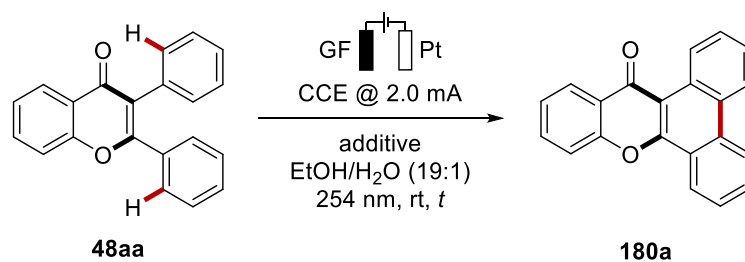
**Scheme 3.2.14** Initial attempts for LEWIS-acid mediated annulation of chromone **48aa**.

Next, electrochemical conditions reported by Ackermann,<sup>[197]</sup> using DDQ as a mediator in a divided cell set-up were investigated (Scheme 3.2.15). However, under the examined conditions the chromone **48aa** decomposed and no product was detected.



**Scheme 3.2.15** Attempted DDQ-mediated electrochemical annulation.

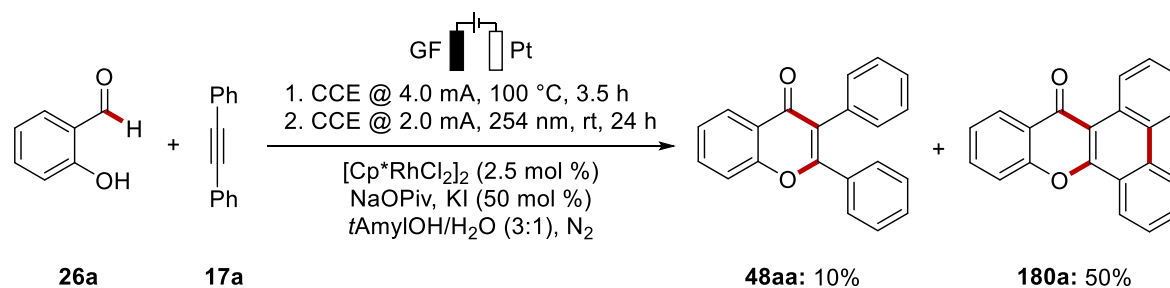
Instead, *Gordon et al.* and *Tojo* reported on photocyclization of stilbenes with iodine as the terminal oxidant.<sup>[223]</sup> Furthermore, the group of *Zhang* developed a photochemical approach without the need of an external oxidant under UV irradiation.<sup>[224]</sup> Hence, first attempts to reproduce the conditions of *Zhang* were carried out (Table 3.2.3, entry 1). Although, no comparable yields as reported in the literature were obtained (63%),<sup>[224]</sup> 32% of the product **180a** could be formed in a mixture of ethanol and water under UV-C irradiation in a LUZCHEM photoreactor. With this encouraging result in hand, the conditions were subsequently optimized. Indeed, extended reaction times did not lead to a major increase in yield (entry 2), and the use of toluene as a solvent was noticed to shut down the reactivity (entry 3). Pleasingly, it was found that iodine could serve as an effective oxidant for the annulation of the 2,3-substituted chromone **48aa** (entry 4). As the reduced loading of iodine led to a significant decrease in yield (entry 5), a photoelectrochemical approach was envisioned to reduce costs and safety hazards. Delightfully, with stoichiometric amounts of potassium iodide, as a non-toxic reagent, a similar yield could be obtained, when a constant current of 2.0 mA was applied (entry 6). It is noteworthy, that the efficacy of the strategy outperformed the literature report, which could only obtain 63% of the same product under the best conditions.<sup>[224]</sup> Additionally, a good yield of the desired products was obtained, when catalytic amounts of KI were used (entry 7). Finally, the essential role of electricity was proven, as the amount of synthesized product dramatically decreased without current (entry 8).

**Table 3.2.3** Development of a photoelectro-chemical annulation reaction of chromones.

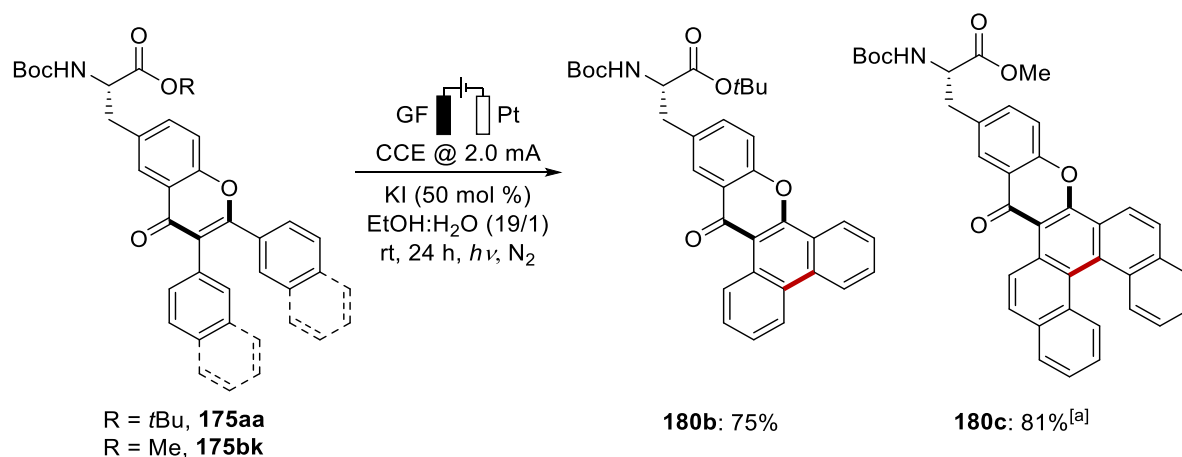
Entry	time	Additive	Variations	Yield [%]
1	3 h	-	No current	32
2	15 h	-	No current	37
3	15 h	-	No current in toluene	--
4	15 h	I <sub>2</sub> (110 mol %)	No current	88 <sup>[a]</sup>
5	22 h	I <sub>2</sub> (10 mol %)	No current	46 <sup>[b]</sup>
6	22 h	KI (110 mol %)	--	93
7	22 h	KI (25 mol %)	--	70 <sup>[a]</sup>
8	22 h	KI (25 mol %)	No current	35

Undivided quartz cell, GF anode (10 mm × 15 mm × 6.0 mm), Pt cathode (10 mm × 15 mm × 0.125 mm), constant current = 2.0 mA, **48aa** (0.10 mmol), solvent (4.0 mL), rt, under N<sub>2</sub>, 22 h. <sup>1</sup>H-NMR yields with CH<sub>2</sub>Br<sub>2</sub> as internal standard are given. [a] Isolated yield. [b] With **48aa** (0.20 mmol).

As a next step, the reaction was attempted to be conducted in a one-pot fashion, after the initial rhodium catalysis, without any work-up (Scheme 3.2.16). Surprisingly the desired chromone **180a** with  $\pi$ -extended peptide could be obtained in moderate yield, along with minor amounts of non-cyclized chromone **48aa**.

**Scheme 3.2.16** One-pot synthesis from chromone **180a** from **26a** and **17a**. Yields determined by NMR with CH<sub>2</sub>Br<sub>2</sub> as internal standard.

Using the optimized protocol, tyrosine derivatives with the corresponding  $\pi$ -extended aromatic system were successfully synthesized (Scheme 3.2.17). After cyclisation, products **180b** and **180c** were isolated in high yields.



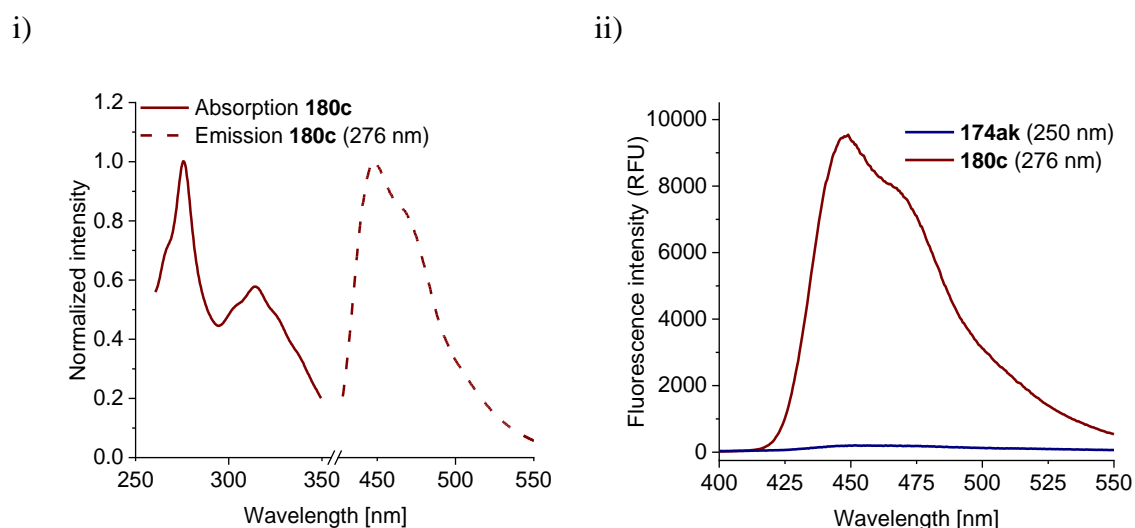
**Scheme 3.2.17** Synthesis of tyrosine derivatives with  $\pi$ -extended labels. [a] With MeOH instead of EtOH.

To investigate the effect of the cyclisation on the photoelectronic properties, analyses by means of UV/Vis were performed (Table 3.2.4 and Figure 3.2.2). The Stokes shift of the investigated compounds was found to be between 120-250 nm.

**Table 3.2.4** Absorption and emission properties of selected amino acids measured in  $\text{CHCl}_3$  at 10 mg/L. [a] Concentration 0.5 mg/L.

Amino acid	Absorption [nm]	Emission [nm]	Stokes shift [nm]
<b>175aa</b>	$\lambda = 250, 351$	$\lambda (250) = 373$	123
<b>175am</b>	$\lambda = 240, 294$	$\lambda (240) = 460$	220
<b>175bk</b>	$\lambda = 250, 318$	$\lambda (250) = 454$	204
<b>180b</b>	$\lambda = 270, 280$	$\lambda (280) = 396$	116
<b>180c</b> <sup>[a]</sup>	$\lambda = 276, 314$	$\lambda (276) = 448$	172

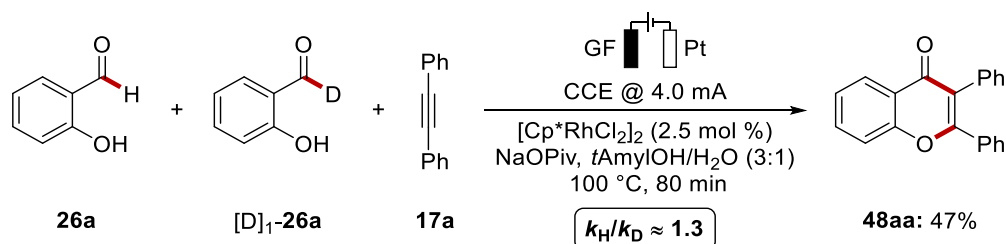
Interestingly, the absorption maxima upon subsequent cyclisation shifted by approximately 20 nm towards the visible region (**175aa** vs. **180b** and **175bk** vs. **180c**). Labels **180b** and **180c** showed improved fluorescence intensity in comparison to their non-cyclized precursors **175**. Especially tyrosine **180c** exhibited intense fluorescence, by multiple units stronger comparison to the precursor **175bk**, at 459 nm and therefore bears considerable potential as a fluorogenic probe (Figure 3.2.2ii).



**Figure 3.2.2** i) Absorption and emission spectra of tyrosine **180c**. ii) Comparison of the fluorescence intensity before and after the photoelectrochemical annulation.

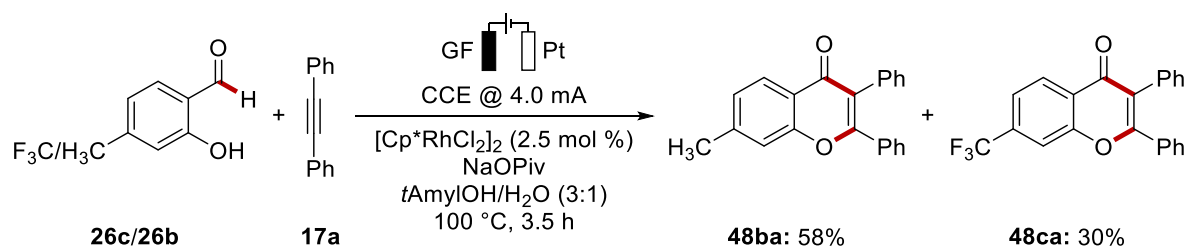
### 3.2.5 Mechanistic Insights for the Rhodaelectro-Catalyzed Alkyne Annulation of Salicylic Aldehydes

Inspired by the unique features of the catalysis, the catalysts' mode of action was intended to be unraveled. Thus, submitting deuterated and non-deuterated substrate **26a** to the reaction conditions revealed a minor kinetic isotope effect (Scheme 3.2.18). This result is indicative of a facile C–H cleavage.



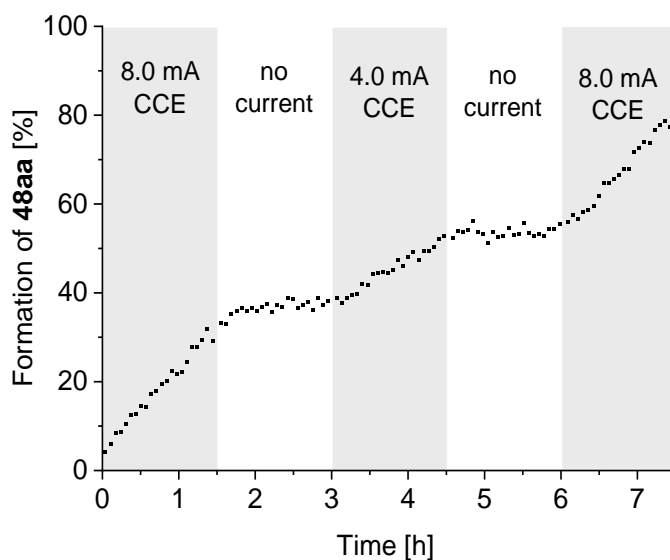
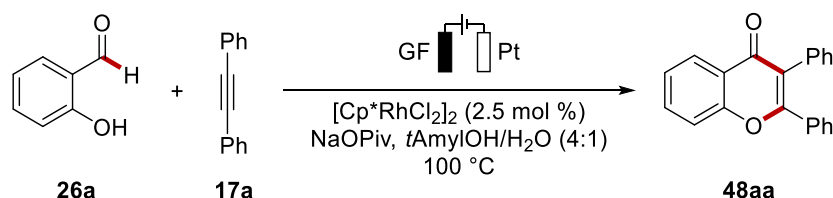
**Scheme 3.2.18** KIE studies for the rhodaelectro-catalyzed formyl C–H activation.

Furthermore, an intermolecular competition experiment between electronically complementary 2-hydroxybenzaldehydes **26b** and **26c** was performed (Scheme 3.2.19). The preferential functionalization of the electron-rich substrate **26b** is in-line with a BIES-type C–H rhodation.<sup>[32]</sup>



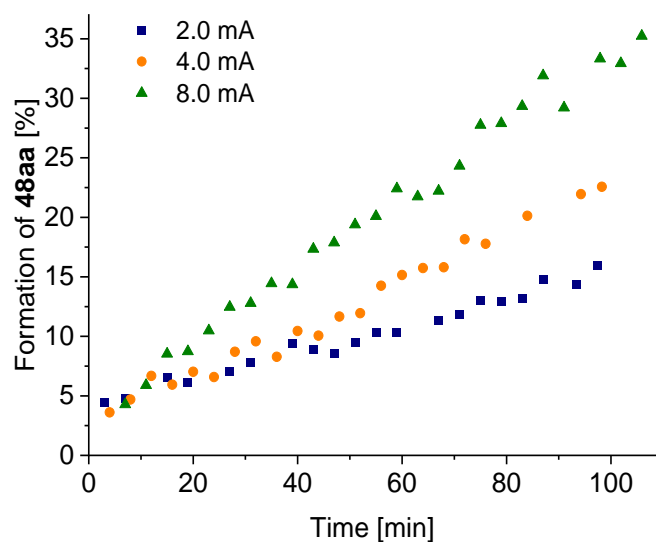
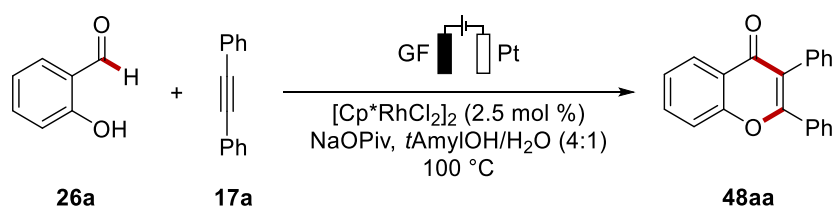
**Scheme 3.2.19** Competition experiment between differently substituted 2-hydroxybenzaldehydes **26**.

Afterwards, the role of electricity and the dependence on different currents was investigated. For this purpose, *in-operando* monitoring of the catalysis at different currents by *in-situ*  $^1\text{H-NMR}$  spectroscopy was used. Hence, an on/off experiment highlighted the key role of electricity for the efficient catalyst turnover (Figure 3.2.3).



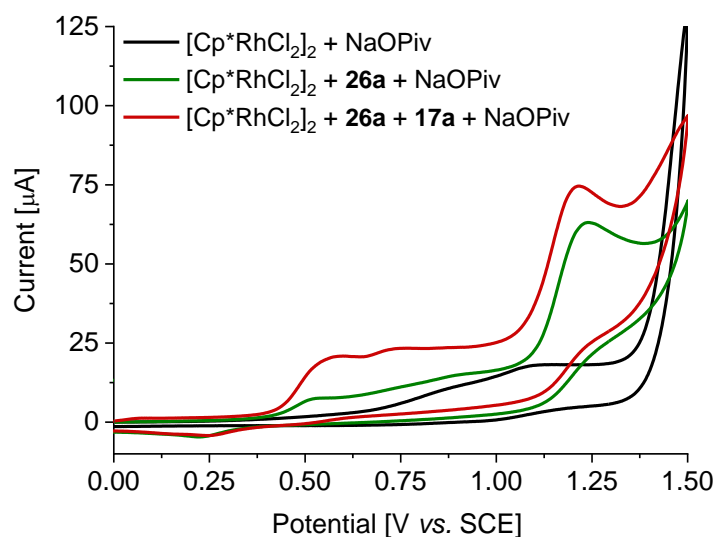
**Figure 3.2.3** Online reaction monitoring experiment for the rhodaelectro-catalyzed formyl C–H activation without and with applied currents.

Additionally, a dependence on the applied current could be observed. To investigate this further, the initial rates of the reaction progress with different currents were monitored (Figure 3.2.4). Indeed, the initial rates were highly dependent on the currents, illustrating turn-over limiting redox-events being effective.



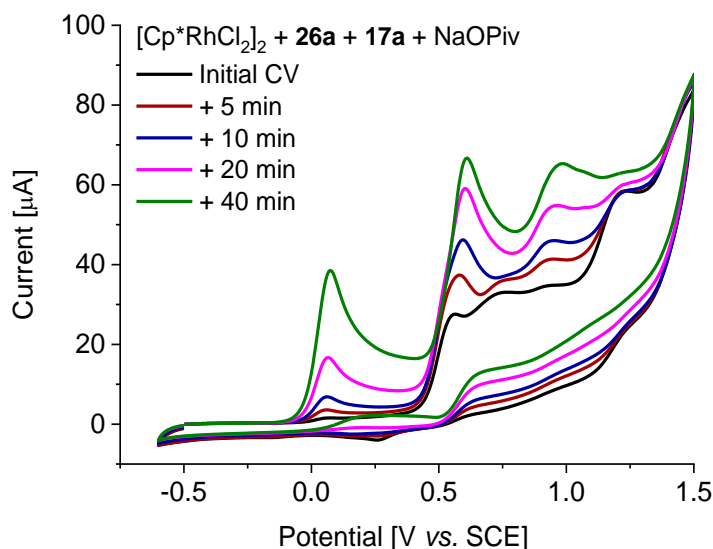
**Figure 3.2.4** Online reaction monitoring experiment for the rhodaelectro-catalyzed formyl C–H activation for the initial rates with different currents.

Significant insights into the catalytic active species were obtained by cyclic voltammetry studies utilizing a GC working electrode. Initially, the effect of the addition of the substrates **26a** and **17a** on the oxidation potential of the rhodium catalyst was investigated (Figure 3.2.5). Whereas the rhodium pre-catalyst did not show any significant oxidative response in the presence of the carboxylate base, after addition of the aldehyde a new irreversible oxidation event at  $E_p = 1.23$  V vs. SCE appeared. This observation could be attributed to a rhodium(III/IV) oxidation, as the 2-hydroxybenzaldehydes exhibited a significantly higher oxidation potential (Figure 3.2.5). When alkyne **17a** was added to the mixture, another redox event at  $E_p = 0.55$  V vs. SCE appeared, which is indicative of the formation of a new species.



**Figure 3.2.5** Cyclic voltammetry in MeCN with  $n\text{Bu}_4\text{NPF}_6$  (0.1 M) at 200 mV/s and a GC working electrode.  $[\text{Cp}^*\text{RhCl}_2]_2$  and NaOPiv (black);  $[\text{Cp}^*\text{RhCl}_2]_2$ , NaOPiv and salicylic aldehyde **26a** (green);  $[\text{Cp}^*\text{RhCl}_2]_2$ , NaOPiv, salicylic aldehyde **26a** and alkyne **17a** (blue). Concentration of  $[\text{Cp}^*\text{RhCl}_2]_2$  (2.5 mM), substrates (5.0 mM) and NaOPiv (15 mM).

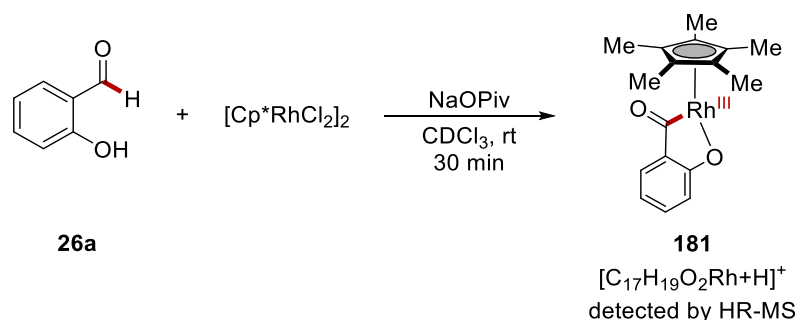
Interestingly, time-resolved measurements of the mixture showed that the anodic currents of the newly formed signals increase with the time and an additional irreversible response event at  $E_p = 0.08$  V vs. SCE occurred (Figure 3.2.6).



**Figure 3.2.6** Cyclic voltammetry of  $[\text{Cp}^*\text{RhCl}_2]_2$ , 2-hydroxybenzaldehyde **26a**, alkyne **17a** and NaOPiv in MeCN with  $n\text{Bu}_4\text{NPF}_6$  (0.1 M) at 200 mV/s and a GC working electrode. Initial cyclic voltammogram (black), cyclic voltammogram after 5 min (red); cyclic voltammogram after 10 min (blue); cyclic voltammogram after 20 min (pink); cyclic voltammogram after 40 min (green). Concentration of  $[\text{Cp}^*\text{RhCl}_2]_2$  (2.5 mM), substrates (5.0 mM) and NaOPiv (15 mM).

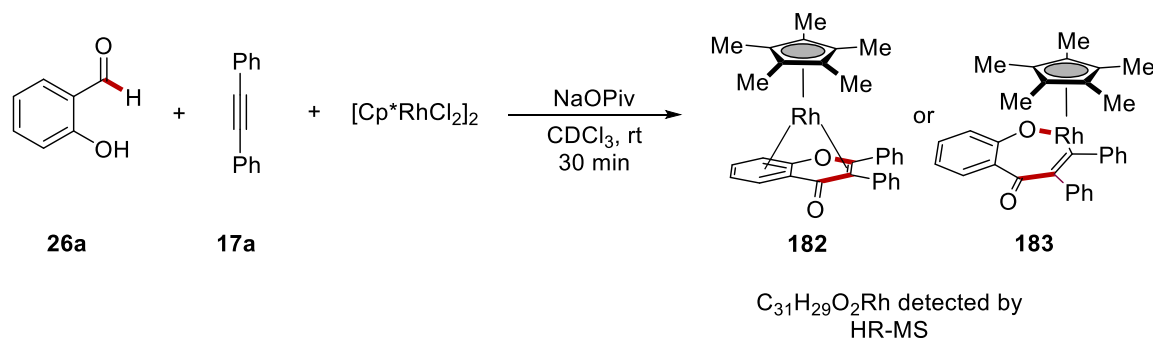


To further investigate whether the formation of a cyclometallated rhodium species with salicylic aldehyde **26a** at room temperature is feasible, as suggested by the cyclic voltammetric studies (Figure 3.2.5), high-resolution mass spectrometry was conducted (Scheme 3.2.20). Indeed, a peak in the mass spectrum was detected, which correlates to the proposed complex **181**.



**Scheme 3.2.20** Proposed structures after the HR-ESI-MS Experiment of salicylic aldehyde with the rhodium pre-catalyst.

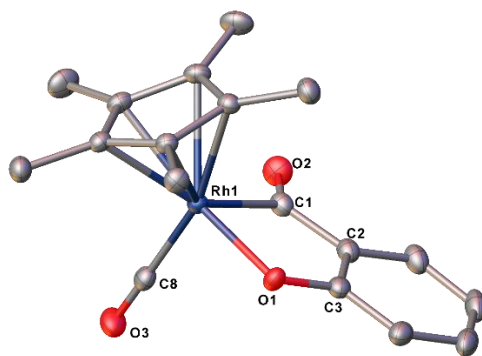
Subsequently, a corresponding experiment including the alkyne **17a**, was carried out, to confirm if insertion products could be observed (Scheme 3.2.21). As a result, a signal with a mass corresponding to the molecular formula of rhodium complexes **182** and **183** was assigned in the collected HR-MS spectra. Alternatively, the observed mass could also be attributed to a complex related to **181** with an additionally coordinated alkyne **17a**. However, this species is not expected to be detectable with the applied spectrometric method.



**Scheme 3.2.21** Proposed structures after the HR-EI-MS experiment of salicylic aldehyde **26a** with alkyne **17a** and the rhodium pre-catalyst.

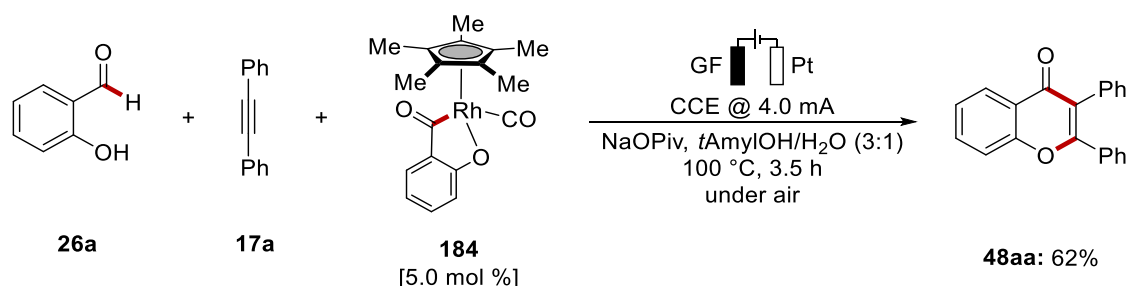
Albeit the presented mass spectrometric experiments provided first impressions on the involved intermediates, only the successful isolation and their subsequent electrochemical characterization could substantiate the structural properties and provide evidence for the

involved species. At this point, *Dr. Antonis Messinis* joined the project and focused on the isolation of reaction intermediates. Fortunately, a metalated salicylic aldehyde complex **184** was successfully synthesized and fully characterized (Figure 3.2.7).<sup>[220]</sup>



**Figure 3.2.7** Molecular structure of rhodium complex **184** (CCDC 2046502) isolated and crystallized by *Dr. Antonis Messinis* with hydrogen atoms omitted for clarity and thermal ellipsoids drawn at the 50% probability level.

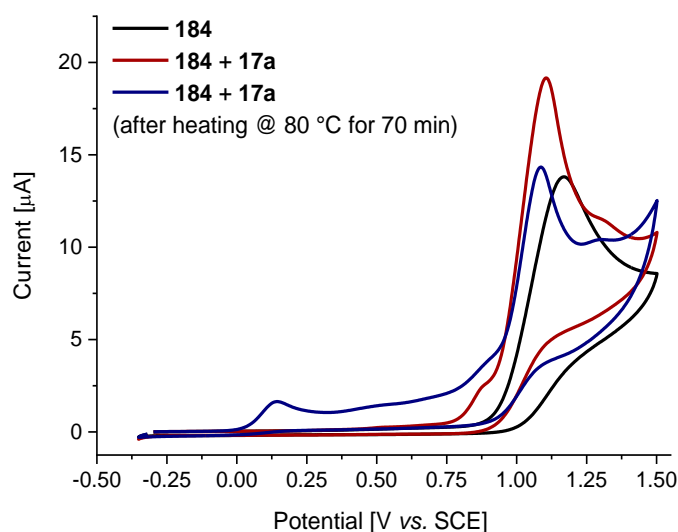
The isolated species was coordinated by a carbon monoxide ligand, presumably derived from the decarbonylation of a second aldehyde species. To test, if the observed species could be an on-cycle intermediate, its efficiency was tested for the rhodaelectrocatalysis. Since the species showed reduced activity in comparison to the pre-catalyst (62% vs. 92%, Scheme 3.2.22 and Table 3.2.2), it is concluded to be an off-cycle intermediate.



**Scheme 3.2.22** Investigation of the catalytic activity of **184**. Yield determined by NMR with  $\text{CH}_2\text{Br}_2$  as internal standard.

It is hypothesized that the carbonyl ligand strongly coordinates and prevents a facile insertion of the alkyne. Therefore, the related structure with a weaker coordinating ligand, is suggested to be a catalytically competent intermediate during the catalysis. Complex **184** was also studied by means of cyclic voltammetry (Figure 3.2.8). The measurements revealed a rhodium(III/IV) oxidation at  $E_p = 1.17$  V vs. SCE, which is in agreement to the proposed *in-*

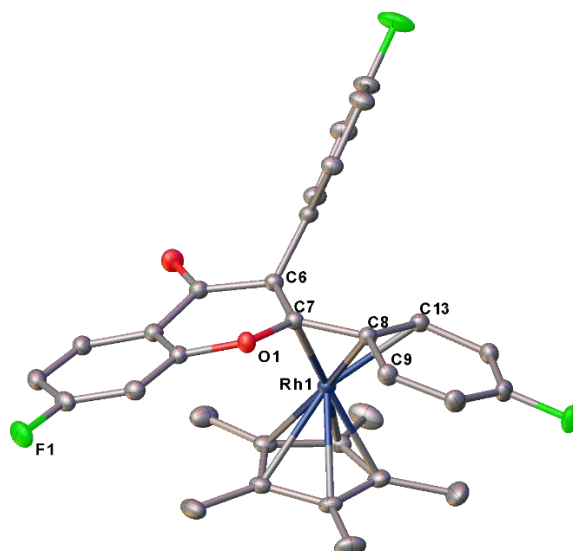
*situ* generation of the cyclometalated species, from the mixture of the pre-catalyst, base, and salicylic aldehyde (Figure 3.2.5).



**Figure 3.2.8** Cyclic voltammetry in MeCN with  $n\text{Bu}_4\text{NPF}_6$  (0.1 M) at 100 mV/s and a GC working electrode. **184** (black); **184** and **17a** (red); **184** and **17a** after heating at 80 °C for 70 min (blue). Concentration of substrates (2.5 mM).

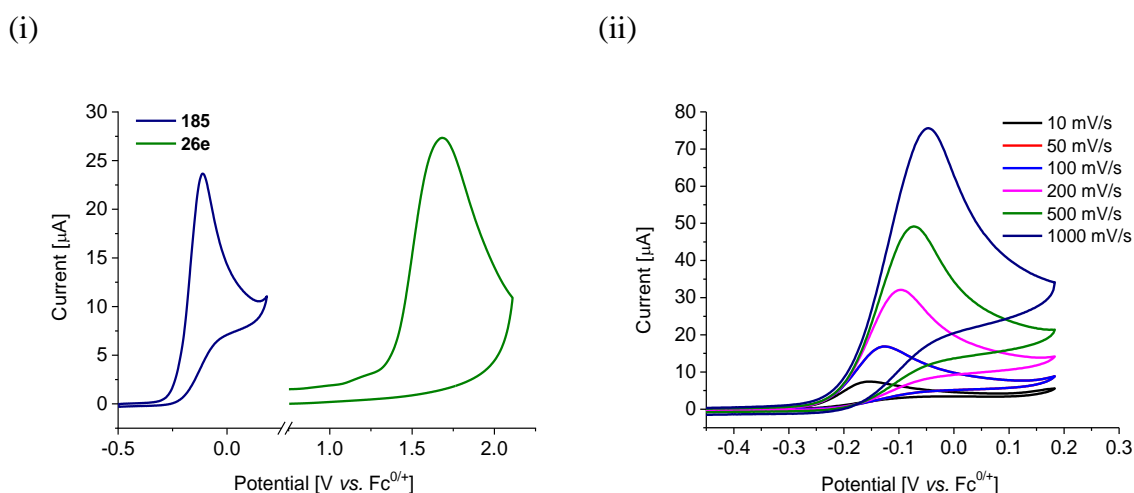
The oxidation potential slightly shifted to less positive potentials ( $E_p = 1.10$  V vs. SCE) when one equivalent of alkyne was added. However, the previously observed additional redox event, only appeared after heating of the reaction mixture for 70 minutes, which is consistent with the observed reduced catalytic efficacy (*vide supra*).

Delightfully, *Dr. Antonis Messinis* could additionally synthesize another species, which is hypothesized to be involved in the catalysis (Figure 3.2.9). From the reaction of the rhodium pre-catalyst with fluorinated aldehyde **26e** and alkyne **17c**, a rhodium (I) sandwich complex **185** was crystallized. The rhodium center is coordinated by the phenyl moiety in the 2-position and the C2/C3-double bond of the chromone. Subsequent characterization of the redox properties by cyclic voltammetry, demonstrated an oxidation of the rhodium complex at  $E_p = -0.11$  V vs.  $\text{Fc}^{0/+}$ , likely due to a two-electron transfer to generate a rhodium(III) species (Figure 3.2.10i).



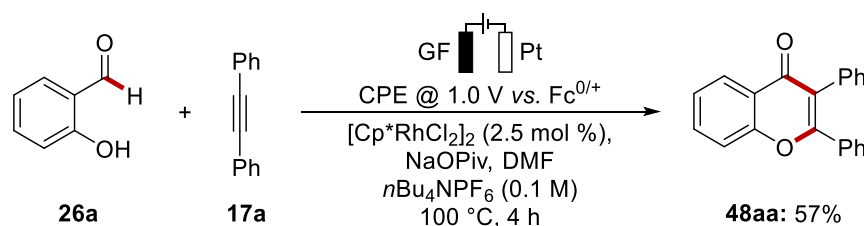
**Figure 3.2.9** Molecular structure of rhodium complex **185** (CCDC 2046507) isolated and crystallized by *Dr. Antonis Messinis* with hydrogen atoms omitted for clarity and thermal ellipsoids drawn at the 50% probability level.

Variation of the scan rates indicated an irreversible redox behavior even at high speeds (Figure 3.2.10ii), being supportive for a rapid product release. To investigate, whether the catalysis features an oxidatively-induced reductive elimination from a proposed seven-membered rhoda(III)-cycle, DFT calculations were executed by *Dr. João C. A. Oliveira* and revealed an oxidation potential of  $E_{1/2} = 0.48 \text{ V vs. Fc}^{0/+}$ .<sup>[220]</sup>



**Figure 3.2.10** Cyclic voltammetry in  $\text{CH}_2\text{Cl}_2$  with  $n\text{Bu}_4\text{NPF}_6$  (0.2 M) at a GC working electrode. Concentration of substrates (1.8 mM). i) **185** at 100 mV/s (blue) and 4-fluorosalicylaldehyd (**26e**) at 5 mV/s (green). ii) Rh-**185** at different scan rates. 10 mV/s (black); 50 mV/s (red); 100 mV/s (light blue); 200 mV/s (pink); 500 mV/s (green); 1000 mV/s (dark blue).

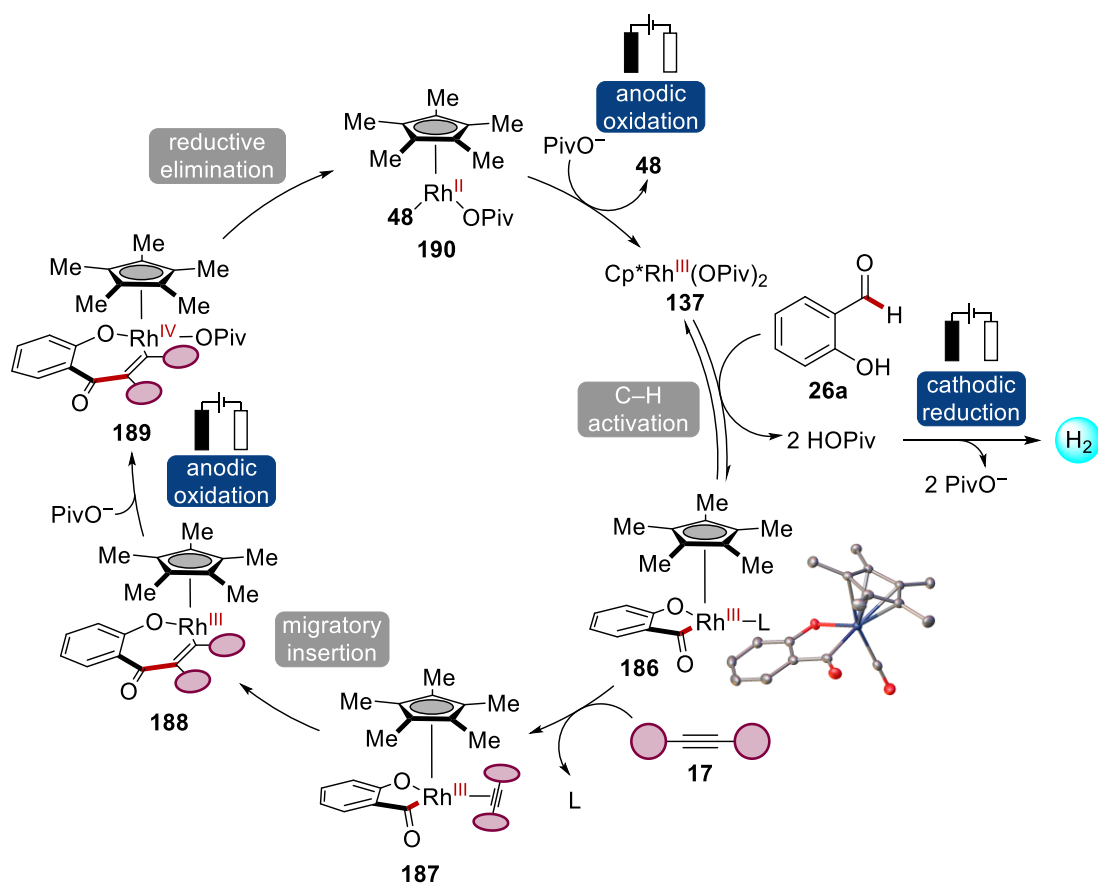
These results are fully in-line with experimentally observed values of a related species, which exhibited a redox event at  $E_{p/2} = 0.68$  V vs.  $\text{Fc}^{0/+}$ .<sup>[199, 225]</sup> Additional computational studies by *Dr. João C. A. Oliveira* with respect to the electro-formyl C–H activation supported a kinetically, favorable oxidatively-induced reductive elimination. The studies provide a clear explanation why the functionalization of oxidation-sensitive aldehydes can proceed, as the salicylic aldehyde **26e** displayed a reasonably lower oxidation potential in comparison to the isolated and computed intermediates ( $E_p = 1.68$  V vs.  $\text{Fc}^{0/+}$ , Figure 3.2.10i). To further substantiate this working hypothesis, rhodaelectrocatalysis was also performed at a constant potential of 1.0 V, which according to the data obtained from calculation and cyclic voltammetry, should be sufficient to facilitate an oxidation-induced reductive elimination as well as the re-oxidation of the catalyst, without over-oxidizing the corresponding aldehyde (Scheme 3.2.23). As the biphasic mixture of *t*AmylOH with  $\text{H}_2\text{O}$  was not suitable for this experiment, DMF was chosen as the solvent. The desired product could be obtained in 57% yield, supporting the hypothesis of an oxidatively-induced reductive elimination.



**Scheme 3.2.23** Assembly of chromone **48aa** under constant potential electrolysis in DMF.

### 3.2.6 Proposed Catalytic Cycle for the Rhodaelectro-Catalyzed Annulation of Salicylic Aldehydes

With the mechanistic insights obtained from experiment, cyclic voltammetry studies, DFT calculation and the X-ray structures, a plausible mechanistic scenario is proposed (Scheme 3.2.24). Thus, the catalysis is initiated by facile BIES-type C–H cleavage, as indicated by KIE and competition experiments, to furnish rhodacycle **186** according to a related crystal structure (**184**). Thereafter, coordination and migratory insertion furnish the 7-membered rhodacycle **188**. This species can then undergo oxidatively-induced reductive elimination to generate the sandwich-complex **190**. This species releases the desired chromone and regenerates the active rhodium(III) catalyst **137** upon anodic oxidation. At the same time, proton reduction is considered to take place at the platinum cathode.



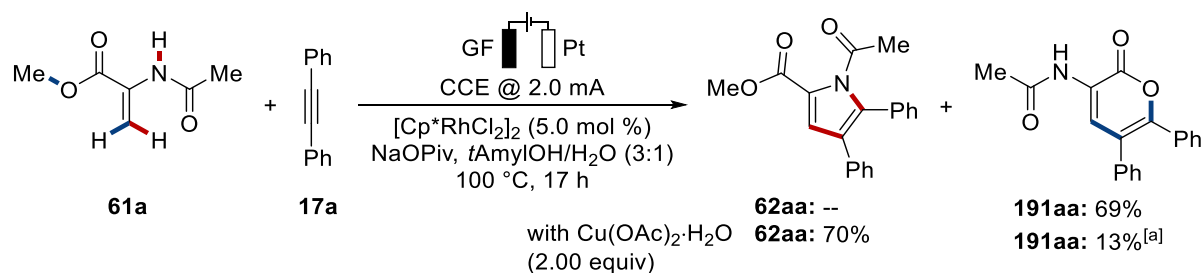
**Scheme 3.2.24** Proposed catalytic cycle for the rhodaelectro-catalyzed annulation of salicylic aldehydes.

### 3.3 Rhodaelectro-Catalyzed C–H Activation of Alkenes

The direct C–H/N–H annulation of alkynes represents a valuable tool for the rapid construction of heterocycles.<sup>[226]</sup> While several seminal contributions have been reported in the field of electro-catalyzed C–H activation, most approaches focused on the functionalization of arene C(sp<sup>2</sup>)–H bonds.<sup>[160e, 160f, 193a]</sup> In contrast, the assembly of useful motifs from simple alkenes is considerably more challenging due to the stronger  $\pi$ -bonding ability and reactivity towards conjugate additions or *Diels-Alder* reactions.<sup>[95]</sup> Regarding electrochemical reactions, which cathodically produce hydrogen, a competitive reduction of the alkenes represents an additional challenge to achieve efficient electro-catalyzed functionalizations. Starting from the pioneering work on cobaltaelectro-catalyzed oxygenation of alkenes,<sup>[171]</sup> *Mei* reported on the iridaelectro-catalyzed vinylic annulation towards lactones.<sup>[202]</sup> Subsequently, the same group developed a chemo-divergent functionalization of acrylamides employing electrooxidative rhodium catalysis.<sup>[201]</sup> With these rare literature precedences on electrocatalytic C–H activation of alkenes in mind, the strategy was conceived to be extended towards the synthesis of pyrroles from readily available dehydroalanines.

#### 3.3.1 Optimization Studies for the Rhodaelectro-Catalyzed Synthesis of Pyrroles

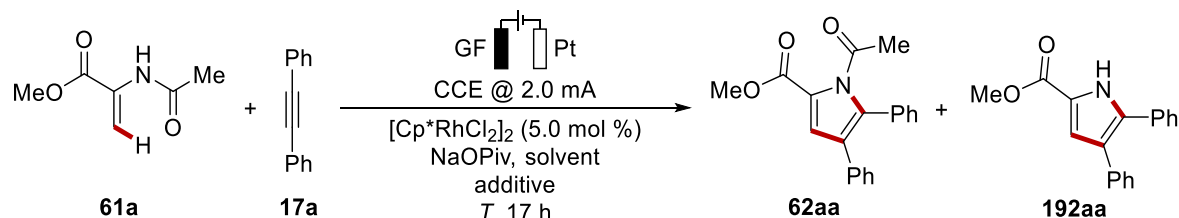
At the outset, the electrocatalysis of alkene **61a** was performed under constant current conditions in a *tert*-AmylOH/H<sub>2</sub>O mixture at 100 °C using a high valent rhodium(III) catalyst. Surprisingly, here the formation of lactone **191aa** was observed in high yield (Scheme 3.3.1). Interestingly, when copper acetate was employed as the terminal oxidant under the same conditions, pyrrole **62aa** was selectively formed. It is hypothesized that during the electrolysis the basicity increases due to proton reduction. This leads to a hydrolysis of the ester and lactonization of the stronger coordinating carboxylate delivers the observed lactone **191aa**. Although, this result is interesting, a related study has been published by *T.S. Mei* synthesizing  $\delta$ -lactones from the annulation of acrylic acids with alkynes in an iridaelectro-catalyzed fashion.<sup>[202]</sup>



**Scheme 3.3.1** Electrocatalysis of enamide **61a** with toluene (**17a**) furnished the unexpected lactone **191aa**. [a] <sup>1</sup>H-NMR yield with  $\text{CH}_2\text{Br}_2$  as internal standard.

Therefore, the reaction conditions were optimized towards chemoselective formation of the desired pyrrole **62aa**. Initial reactions were performed at lower reaction temperatures and anhydrous conditions, to prevent ester hydrolysis. However, using organic solvents such as acetone or *tert*-amyl alcohol in combination with supporting electrolyte did not furnish the desired products in significant amounts (Table 3.3.1, entry 1 and 2). Also, higher reaction temperatures and the employment of tetrabutylammonium acetate failed to increase product formation (entry 3 and 4).

**Table 3.3.1** Attempts for the rhodaelectro-catalyzed construction of pyrrole **62aa**.



Entry	Solvent	T [°C]	Additive	Yield [%]	
				<b>62aa</b>	<b>192aa</b>
1	<i>t</i> AmylOH	60	$\text{LiClO}_4$	<5	<5
2	Acetone	60	$\text{LiClO}_4$	--	--
3	<i>t</i> AmylOH	60	<i>n</i> Bu <sub>4</sub> NOAc	<5	trace
4	<i>t</i> AmylOH	120	<i>n</i> Bu <sub>4</sub> NOAc	<5	trace

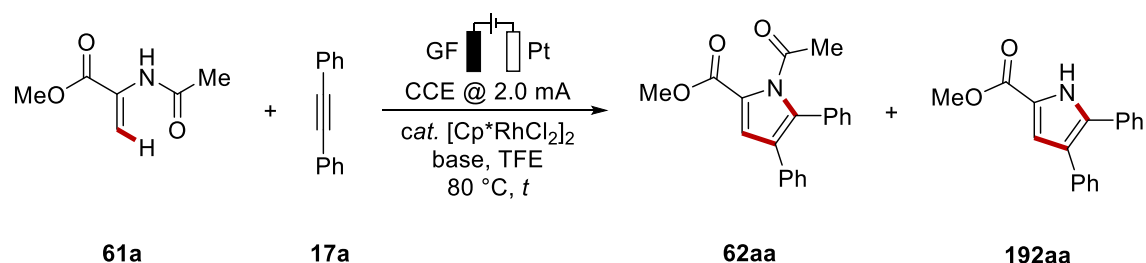
Undivided cell, GF anode (10 mm × 15 mm × 6.0 mm), Pt cathode (10 mm × 15 mm × 0.125 mm), constant current = 2.0 mA, **61a** (0.50 mmol), **17a** (0.25 mmol), catalyst (5.0 mol %), NaOPiv (2.00 equiv), additive (2.00 equiv), solvent (4.0 mL), under air, 17 h. <sup>1</sup>H-NMR yields with  $\text{CH}_2\text{Br}_2$  as internal standard are given.

When TFE was used as the solvent, pyrrole **62aa** was formed with the concomitant cleavage of the acetyl group (Table 3.3.2, entry 1). Encouraged by this finding, the use of sodium pivalate as a base and shortened reaction times, turned out to deliver the corresponding pyrrole **62aa** in slightly higher yield (entry 2). Remarkably, when nickel foam was used as



cathode material an overall increased conversion was observed, furnishing *N*-protected and deprotected pyrrole (entry 3 and 4). The chemoselectivity could be drastically improved, upon increasing the catalyst loading (entry 5). Then the effect of the reaction time was investigated. In fact, shorter reaction times further improved the formation of product **62aa** (entry 6). Pyrrole **62aa** was isolated in very good yield, when the cationic  $[\text{Cp}^*\text{Rh}(\text{MeCN})_3][\text{SbF}_6]_2$  was utilized in the catalysis, even at a reduced catalyst loading (entry 7). To prove that electricity serves as the relevant oxidant, the reaction was conducted under an atmosphere of nitrogen. Here, a small decrease in yield was observed (entry 8).

**Table 3.3.2** Optimization for the rhodaelectro-catalyzed assembly of pyrroles.

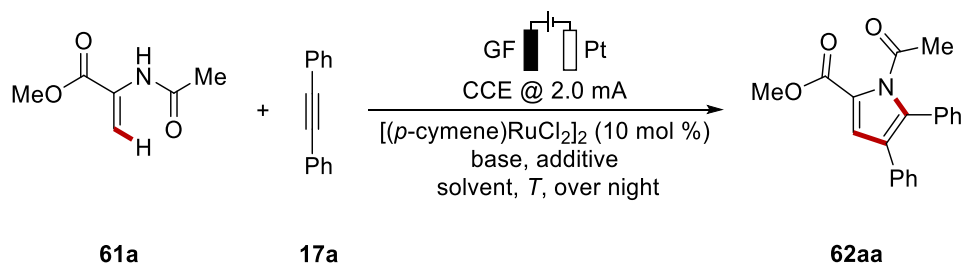


Entry	Catalyst Loading	<i>t</i> [h]	base	Yield [%]	
				<b>62aa</b>	<b>192aa</b>
1	5.0 mol %	23	NaOAc	--	7
2	2.5 mol %	16	NaOPiv	--	17
3	2.5 mol %	16	NaOAc	21 <sup>[a]</sup>	18 <sup>[a]</sup>
4	2.5 mol %	10	NaOAc	26 <sup>[a]</sup>	21 <sup>[a]</sup>
5	5.0 mol %	16	NaOAc	46	--
6	5.0 mol %	6	NaOAc	55	9
7	5.0 mol % <sup>[b]</sup>	6	NaOAc	70 (68)	<5
8	5.0 mol %	7.5	NaOAc	47 <sup>[c]</sup>	<5 <sup>[c]</sup>

Undivided cell, GF anode (10 mm × 15 mm × 6.0 mm), Pt cathode (10 mm × 15 mm × 0.125 mm), constant current = 2.0 mA, **61a** (0.50 mmol), **17a** (0.25 mmol), catalyst (5.0 mol %), NaOPiv (2.00 equiv), additive (2.00 equiv), solvent (4.0 mL), under air. <sup>1</sup>H-NMR yields with CH<sub>2</sub>Br<sub>2</sub> as internal standard are given. Isolated yields in parentheses. [a] With Ni<sub>foam</sub> cathode. [b] With  $[\text{Cp}^*\text{Rh}(\text{MeCN})_3][\text{SbF}_6]_2$  (5.0 mol %). [c] Under nitrogen atmosphere.

Since ruthenium has been known to be more cost-effective alternative in comparison to rhodium, the activity was studied towards the electro-catalyzed formation of pyrroles.<sup>[99]</sup> In the beginning TFE was evaluated as a solvent, which showed overall good activity in the rhodium-catalyzed transformation (*vide infra*). In the reaction using NaOAc as a base, in

combination with  $\text{KPF}_6$ , no pyrrole **62aa** formation was observed (Table 3.3.3, entry 1). Upon increasing the catalyst loading, 29% of the corresponding product **62aa** was formed (entry 2). In the course, also  $\text{RuCl}_3$  was tested towards its competence for the desired assembly. However, no significant activity was observed (entry 3 and 4). Since previous reports indicated dichloroethane (DCE) to be a suitable solvent for the ruthenium-catalyzed annulation,<sup>[99a]</sup> a mixture of TFE and DCE as the solvent system was used. Indeed, in combination with 1-AdCO<sub>2</sub>H, the yield of product **62aa** was successfully increased (entry 5). In contrast, the inverse solvent ratio was not proven to perform as efficiently (entry 6). Additionally, alternative hexafluorophosphate sources were not increasing the amount of product **62aa** (entry 7 and 8). Subsequently, the nature of the base was varied. However, the use of different counter-cations, as well as carbonate-based additives proved ineffective (entry 12–15). The use of nickel foam as cathodic material was found to slightly increase the efficacy (entry 16). Finally, it was found that additional 1-AdCO<sub>2</sub>H did not provide any significant benefit for the reaction outcome (entry 16 and 19).

**Table 3.3.3** Investigation on the performance of ruthenium in the electro-catalyzed construction of pyrrole **62aa**.

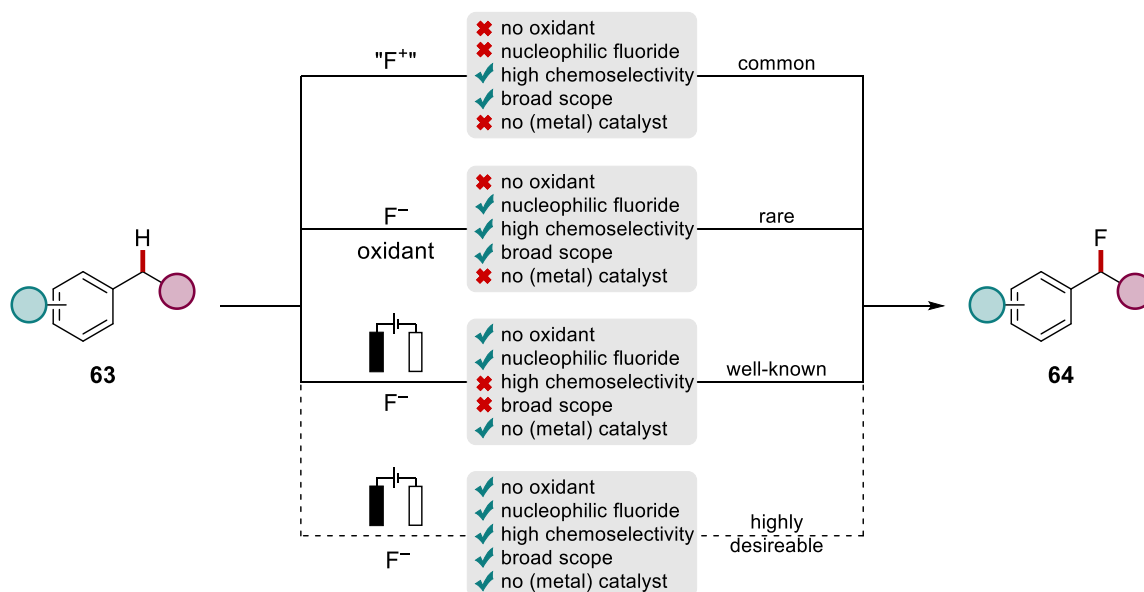
Entry	Solvent	$T$ [°C]	Base	Additive	Yield [%]
1	TFE	80	NaOAc	KPF <sub>6</sub> (20 mol %)	-- <sup>[a]</sup>
2	TFE	80	NaOAc	KPF <sub>6</sub> (30 mol %)	29
3	TFE	80	NaOAc	KPF <sub>6</sub> (30 mol %)	-- <sup>[b]</sup>
4	MeCN	80	NaOAc	KPF <sub>6</sub> (30 mol %)	-- <sup>[b]</sup>
5	TFE/DCE (3:1)	80	NaOAc	KPF <sub>6</sub> (40 mol %)	39
6	TFE/DCE (1:3)	80	NaOAc	KPF <sub>6</sub> (40 mol %) 1-AdCO <sub>2</sub> H (40 mol %)	28
7	TFE/DCE (3:1)	80	NaOAc	NaPF <sub>6</sub> (40 mol %) 1-AdCO <sub>2</sub> H (40 mol %)	29
8	TFE/DCE (3:1)	80	NaOAc	<i>n</i> Bu <sub>4</sub> NPF <sub>6</sub> (40 mol %) 1-AdCO <sub>2</sub> H (40 mol %)	32
9	TFE/DCE (3:1)	80	NaOAc	KPF <sub>6</sub> (40 mol %)	33
10	TFE/ <i>t</i> AmylOH (1:3)	80	NaOAc	KPF <sub>6</sub> (40 mol %)	<5
11	TFE/DCE (3:1)	80	NaOAc	KPF <sub>6</sub> (100 mol %)	29
12	TFE/DCE (3:1)	80	LiOAc	KPF <sub>6</sub> (100 mol %)	<5
13	TFE/DCE (3:1)	80	--	KPF <sub>6</sub> (40 mol %)	--
14	TFE/DCE (3:1)	80	NaHCO <sub>3</sub>	KPF <sub>6</sub> (40 mol %)	23
15	TFE/DCE (3:1)	80	Na <sub>2</sub> CO <sub>3</sub>	KPF <sub>6</sub> (40 mol %)	--
16	TFE/DCE (3:1)	80	NaOAc	KPF <sub>6</sub> (40 mol %)	38 <sup>[c]</sup>
17	TFE/DCE (3:1)	80	NaOAc	KPF <sub>6</sub> (40 mol %)	27 <sup>[c,d]</sup>
18	TFE/DCE (3:1)	80	NaOAc	KPF <sub>6</sub> (40 mol %) 1-AdCO <sub>2</sub> H (40 mol %)	39 <sup>[c]</sup>

Undivided cell, GF anode (10 mm × 15 mm × 6.0 mm), Pt cathode (10 mm × 15 mm × 0.125 mm), constant current = 2.0 mA, **61a** (0.375 mmol), **17a** (0.25 mmol), [Ru] (20 mol %), base (2.00 equiv), solvent (4.0 mL), under air, over night. <sup>1</sup>H-NMR yields with CH<sub>2</sub>Br<sub>2</sub> as internal standard are given. [a] With [(*p*-cymene)RuCl<sub>2</sub>]<sub>2</sub> (5.0 mol %). [b] With RuCl<sub>3</sub> (20 mol %). [c] With Ni<sub>foam</sub> cathode. [d] Enamide **61a** (0.25 mmol) and alkyne **17a** (0.50 mmol).

Overall, the envisioned electro-catalyzed construction of pyrroles was accomplished focusing on a rhodium catalyst. However, it is worth to mention, that the ruthenium catalyst showed higher chemoselectivity, as cleavage of the acetyl group was generally not observed. Furthermore, chemo-divergent activity was discovered, when a rhodium catalyst was employed in different solvents, furnishing either lactones **191aa** or pyrroles **62aa**. Regarding the electrochemical construction of lactones, the reactivity is complementary to the reported formation of pyrroles, when copper acetate was used as chemical oxidant.

### 3.4 Electrochemical C(sp<sup>3</sup>)-H Fluorination

As fluorine-containing compounds are of utmost interest to pharmaceutical<sup>[110]</sup> and agrochemical industries<sup>[111]</sup> as well as material sciences,<sup>[112]</sup> the efficient formation of C-F bonds is of major importance to the synthetic organic community.<sup>[113]</sup> Recent developments actively focused on approaches to functionalize benzylic C-H bonds due to their innate reactivity and abundance in commonly occurring compounds.<sup>[113c, 113d]</sup> In addition, benzyl fluorides are valuable strategic intermediates for the coupling with various nucleophiles.<sup>[120a, 126c, 126e, 131]</sup> However, typical approaches utilize stoichiometric amounts of electrophilic fluorine sources which decrease the overall cost and atom efficiency (Scheme 3.4.1).<sup>[113a, 113c]</sup> Efforts to employ nucleophilic metal or hydrogen fluorides, as cheap and abundant surrogates, are scarce and require stoichiometric oxidants.<sup>[122, 123, 125]</sup> These reports further suffer from the requirement of additional expensive (metal)catalysts and in parts use the substrates in over stoichiometric amounts (Scheme 3.4.1). Electrochemical protocols have evolved as interesting alternatives to replace chemical oxidants and employ readily available fluoride sources.<sup>[146]</sup> However, these approaches are heavily substrate-dependent and feature low levels of chemoselectivity, as undesired nitrogenation with the acetonitrile solvent is competitively observed. Therefore, it was envisaged to design an oxidant- and metal-free electrochemical fluorination manifold, which combines the high chemoselectivity, typically observed in fluorination reactions with electrophilic fluorine sources, with the sustainable nature of electrochemical fluorinations employing nucleophilic fluoride sources (Scheme 3.4.1).



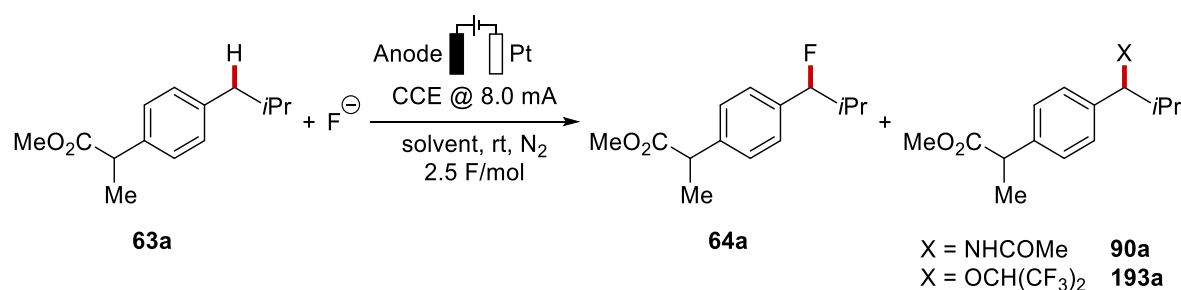
**Scheme 3.4.1** Motivation for the benzylic electrochemical C(sp<sup>3</sup>)-H fluorination.

### 3.4.1 Optimization for the Electrochemical Metal-free C(sp<sup>3</sup>)-H Fluorination

The potential of the electrochemical late-stage fluorination was firstly probed by reactivity studies towards the fluorination of ibuprofen methyl ester using readily available triethylamine trihydrofluoride as the source of nucleophilic fluoride in acetonitrile, with platinum electrodes (Table 3.1.1). The execution of the reaction under inert atmosphere prevented the formation of oxygenated side-products. Under these conditions, selective functionalization at the secondary methylene group took place. However, a competing acetamidation product **90a**, resulting from nucleophilic addition of acetonitrile, was observed in the same quantity as the desired fluorinated product (entry 1). This observation is in-line with reports in the literature, identifying this as a major competitive reaction, when acetonitrile is used as a solvent for benzylic fluorinations.<sup>[152, 227]</sup> To overcome this limitation, optimization studies with respect to the solvent system were performed next. Specifically, reaction conditions reported by *Inagi*,<sup>[154]</sup> using a mixture of acetonitrile and HFIP, with CsF, led to the study on the effect of fluorinated solvents for the desired transformation. However, under the conditions reported by *Inagi*, unfortunately only traces of the desired product **64a** could be obtained. In fact, oxygenation with HFIP towards **193a** was observed as the main competitive reaction, instead of acetamidation (entry 2). When the source of fluoride was changed to NEt<sub>3</sub>·3HF, mainly product **64a** was furnished, although in an unsatisfactory yield (entry 3). Interestingly, changing the anode material to RVC led to an overall decrease in conversion and selectivity (entry 4). Remarkably, the use of a

DCE/HFIP solvent mixture dramatically increased the yield of the desired product and suppressed the competitive oxygenation (entry 5). Notably, employing lower amounts of the fluoride source slightly decreased the yield (entry 6). Nevertheless, a further decrease to only 3.00 equivalents of  $\text{NEt}_3 \cdot 3\text{HF}$  could be compensated by the addition of an organic supporting electrolyte (entry 7). Next, the role of the anode material was examined. Albeit graphite felt proved superior, also platinum, glassy carbon (GC) and RVC enabled the transformation in very good efficiency (entry 8–10). Finally, alternative solvent mixtures were tested. As it turned out, DCE could be effectively substituted with  $\text{CH}_2\text{Cl}_2$  (entry 11).

**Table 3.4.1** Optimization for the electrochemical fluorination.



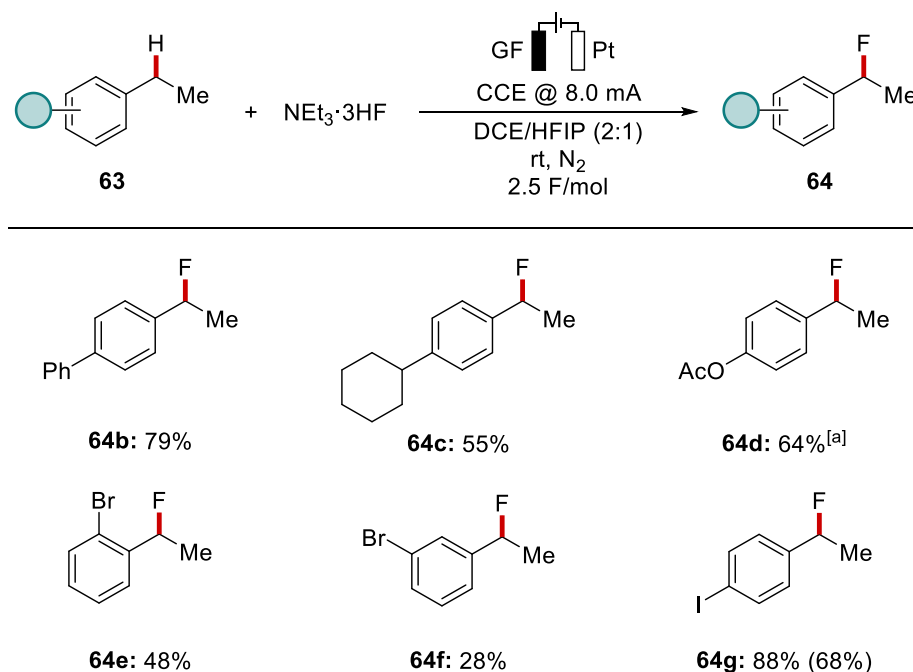
Entry	Fluoride Source	Anode material	Solvent	Yield [%]		
				<b>64a</b>	<b>90a</b>	<b>193a</b>
1	$\text{NEt}_3 \cdot 3\text{HF}$	Pt	MeCN	19	19	--
2	$\text{CsF}^{[a]}$	Pt	MeCN:HFIP (4:1)	<5	--	49
3	$\text{NEt}_3 \cdot 3\text{HF}$	Pt	MeCN:HFIP (4:1)	28	14	6
4	$\text{NEt}_3 \cdot 3\text{HF}$	RVC	MeCN:HFIP (4:1)	10	6	7
5	$\text{NEt}_3 \cdot 3\text{HF}$	RVC	DCE:HFIP (2:1)	82	--	--
6	$\text{NEt}_3 \cdot 3\text{HF}^{[b]}$	RVC	DCE:HFIP (2:1)	55	--	--
7	$\text{NEt}_3 \cdot 3\text{HF}^{[c]}$	RVC	DCE:HFIP (2:1)	66	--	--
8	$\text{NEt}_3 \cdot 3\text{HF}$	GC	DCE:HFIP (2:1)	72	--	--
9	$\text{NEt}_3 \cdot 3\text{HF}$	Pt	DCE:HFIP (2:1)	85	--	--
10	$\text{NEt}_3 \cdot 3\text{HF}$	GF	DCE:HFIP (2:1)	92	--	--
11	$\text{NEt}_3 \cdot 3\text{HF}$	GF	DCM:HFIP (2:1)	90	--	--
12	$\text{NEt}_3 \cdot 3\text{HF}$	GF	DCE:TFE (2:1)	37	--	-- <sup>[d]</sup>

Undivided cell, carbon-based anode, Pt cathode (10 mm × 15 mm × 0.125 mm), **63a** (0.50 mmol),  $\text{NEt}_3 \cdot 3\text{HF}$  (12.3 equiv), solvents (3.0 mL) under inert atmosphere. <sup>1</sup>H-NMR yields with  $\text{CH}_2\text{Br}_2$  as internal standard are given. [a] With  $\text{CsF}$  (0.3 M) and solvents (4.0 mL). [b] With  $\text{NEt}_3 \cdot 3\text{HF}$  (6.13 equiv). [c] With  $\text{NEt}_3 \cdot 3\text{HF}$  (3.07 equiv) and  $n\text{Bu}_4\text{NBF}_4$  (0.1 M). [d] Trifluoroethoxy-substituted side-product was formed in 23% yield.

In contrast the use of TFE, as an alternative fluorinated solvent, proved to furnish major amounts of oxygenated product, likely due to the increased nucleophilicity in comparison to HFIP (entry 12).<sup>[228]</sup>

### 3.4.2 Scope of the Undirected C(sp<sup>3</sup>)–H Fluorination

With the unique site-selectivity and efficiency of the fluorination of C(sp<sup>3</sup>)–H bonds in hand, the investigation of its scope was tested. First, various ethylbenzenes **63** were probed in the electrochemical reaction (Scheme 3.4.2). Substrates bearing electroneutral substituents, such as phenyl or cyclohexyl, were converted to the desired products **64b–64g** with high site-selectivity. Related to the observed selectivity regarding the ibuprofen derivative **63a**, **64c** featuring a tertiary and a secondary benzylic position was site-selectively functionalized at the secondary position. Furthermore, electrophilic bromo- and iodoarenes were well tolerated (**64e–64g**). While *meta*-bromo substituted derivative **63f** ineffectively underwent the transformation, synthetically useful *para*-iodo and *ortho*-bromo decorated ethylbenzenes were effectively converted to the products **64e** and **64g**.

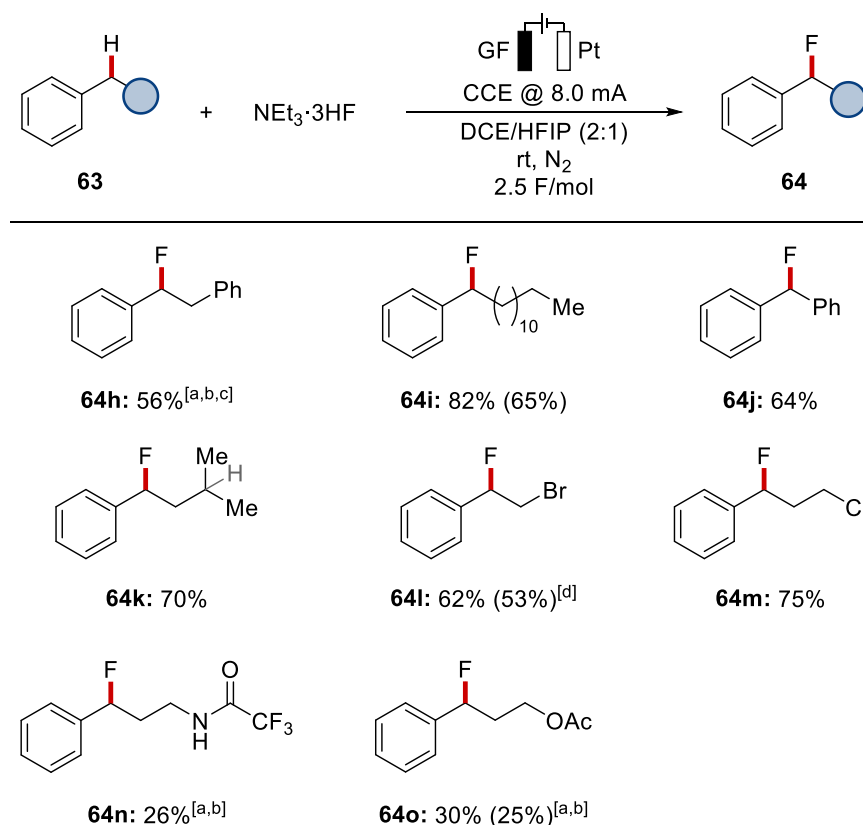


**Scheme 3.4.2** Scope for the electrochemical fluorination of various ethylbenzenes **64**. <sup>1</sup>H-NMR yields with CH<sub>2</sub>Br<sub>2</sub> as internal standard. Isolated yields in parentheses. [a] With 3.0 F/mol at –15 °C.

Next, different groups at the aliphatic sidechain were investigated towards their capability to undergo electrochemical fluorination (Scheme 3.4.3). Phenyl- or alkyl-substituted

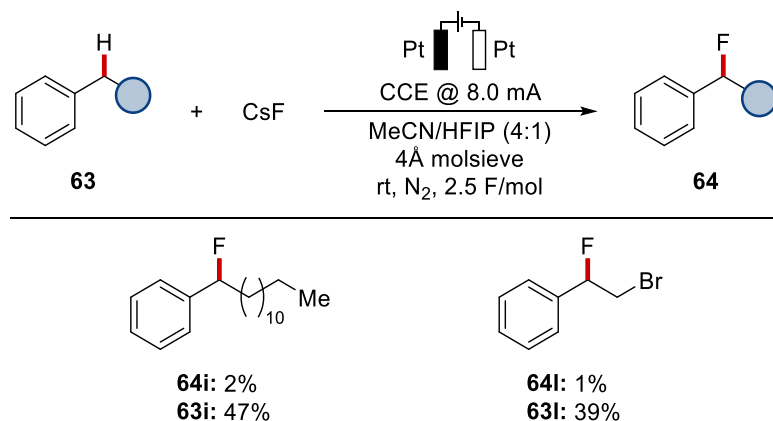


derivatives furnished the corresponding products **64h-64k** selectively. The outstanding site-selectivity was demonstrated as the tertiary carbon within the aliphatic residue of **63k** remained unfunctionalized. It is worth to mention that also aliphatic halides were fully compatible with the developed strategy (**64l-64m**). However, substituents at the sidechain, which can participate in hydrogen bonding interactions or could donate electron-density to a potential benzylic carbocation, caused a decreased reactivity, and the corresponding products **64n** and **64o** were obtained in reduced yields.



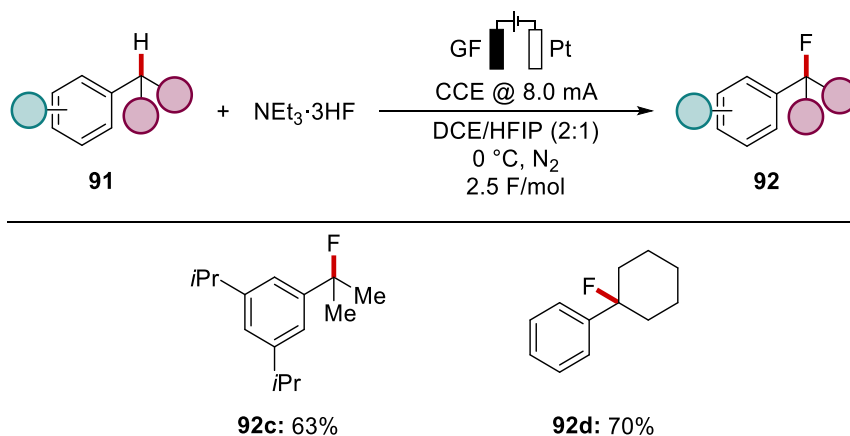
**Scheme 3.4.3** Electrochemical fluorination of differently substituted benzylic positions. <sup>1</sup>H-NMR yields with  $\text{CH}_2\text{Br}_2$  as internal standard. Isolated yields in parentheses. [a] CCE @ 16 mA. [b] At 0 °C. [c] 5.0 F/mol. [d] 3.0 F/mol.

We then compared the performance of the newly developed strategy with the recently reported conditions,<sup>[154]</sup> employing CsF in a MeCN/HFIP mixture on substrates **63i** and **63l**. Thus, the desired products were only formed in traces (Scheme 3.4.4). Interestingly, apart from unreacted starting material, mostly C–H oxygenated products, derived from the nucleophilic attack of HFIP, instead of nitrogenated product, were detected in GC-MS and NMR-analyses. These results highlight the crucial role of the developed solvents system in combination with an efficient fluoride source.



**Scheme 3.4.4** Electrochemical fluorination of secondary benzylic C–H bonds under the conditions reported by Inagi.<sup>[154]</sup> Unreacted alkylbenzene **63** determined by  $^1\text{H}$ -NMR spectroscopy. Yields of benzyl fluorides **64** determined by  $^{19}\text{F}$ -NMR spectroscopy with  $\text{PhCF}_3$  as internal standard.

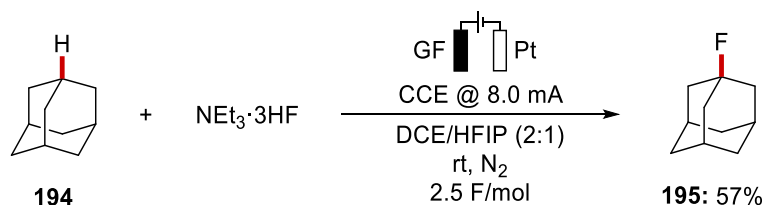
Subsequently, substrates bearing a tertiary benzylic carbon were tested for the newly developed fluorination reaction. At slightly lower reaction temperatures the benzylic isopropyl (**91c**) or cyclohexyl groups (**91d**) were fluorinated in good yields (Scheme 3.4.5). Experiments conducted by *Alexej Scheremetjew* demonstrated that also nitrile or acetyl substituted isopropyl benzenes furnished the corresponding products in moderate yields (42–46%).<sup>[229]</sup>



**Scheme 3.4.5** Electrochemical fluorination of tertiary benzylic C–H bonds.  $^{19}\text{F}$ -NMR yields with  $\text{PhCF}_3$  as internal standard.

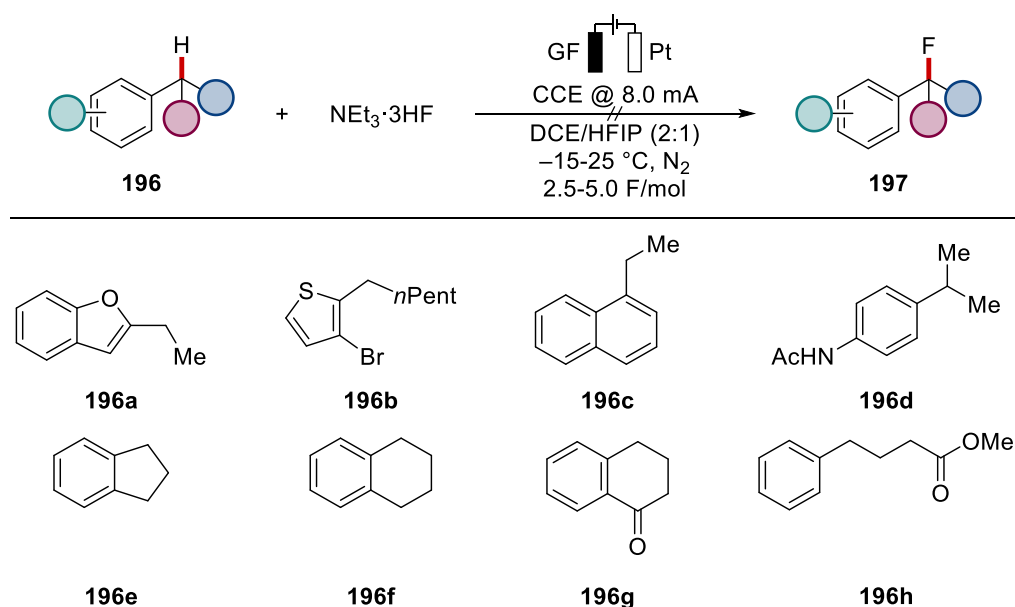
Adamantane **194** with stronger C–H bonds than the previously functionalized benzylic positions effectively underwent the ECF (Scheme 3.4.6). In the context of cost efficiency and safety of the fluorinating reagent, the developed method is considerably more attractive in comparison to a literature precedence,<sup>[230]</sup> which used more expensive and hazardous

NEt<sub>3</sub>·5HF. However, in the context of product yield the literature conditions are advantageous (74% vs. 56%).



**Scheme 3.4.6** Functionalization of unreactive C–H bonds of adamantane. <sup>19</sup>F-NMR yield with PhCF<sub>3</sub> as internal standard is provided.

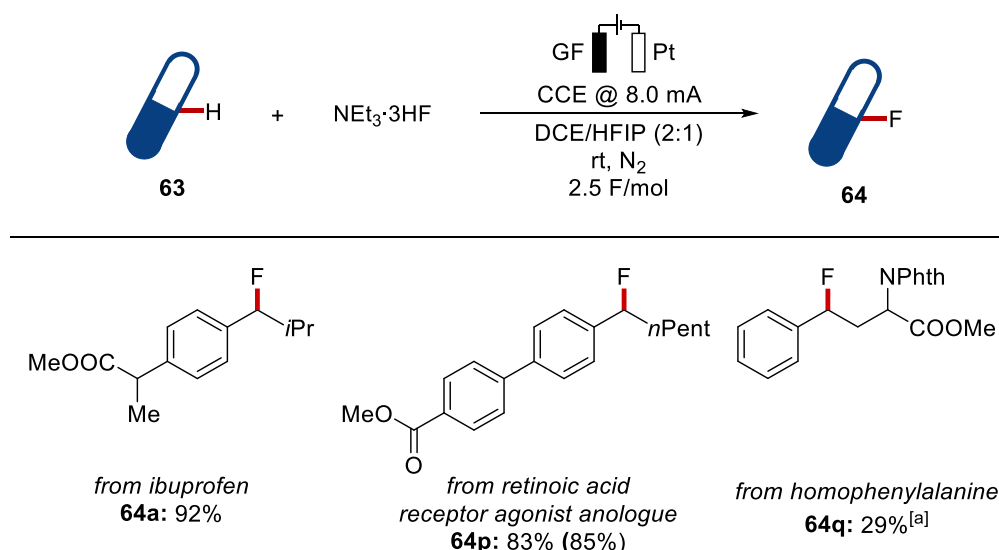
During the exploration of the substrate scope, several limitations of the reaction manifold were also found (Scheme 3.4.7). As such, electron-rich heterocycles, like benzofuran **196a** or thiophene **196b** remained mostly unreacted throughout the electrosynthesis. Scaffolds bearing substituents with positive mesomeric effects on the arene with tertiary benzylic positions were not converted to the desired products and decomposed during the reaction (**196d**). Additionally, cyclic structures as tetrahydronaphthalene **196f**, or tetralone **196g** were not tolerated under the optimized reaction conditions.



**Scheme 3.4.7** Limitations of the electrochemical C(sp<sup>3</sup>)-H fluorination.

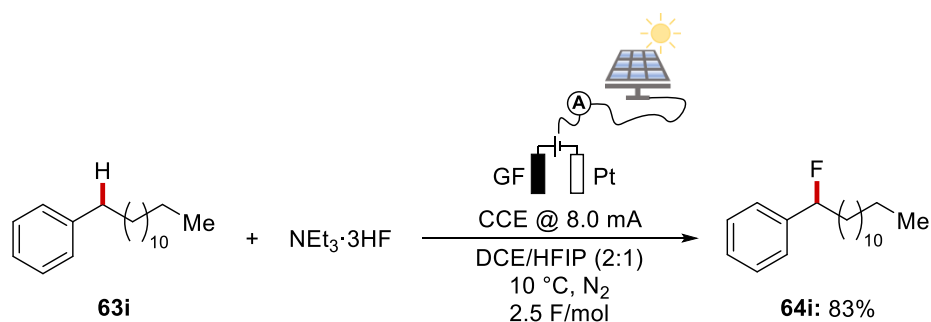
Surprisingly, ester **196h** was not fluorinated, but underwent nucleophilic collapse upon generation of the hypothesized benzylic cation to furnish a 5-membered lactone, which has been reported in the literature without fluorination agents.<sup>[231]</sup> Next, the synthetic utility was

explored towards the late-stage diversification of biologically active compounds (Scheme 3.4.8). Besides ibuprofen methyl ester **63a** as a drug analog, retinoic acid analogue receptor agonist **63p**,<sup>[232]</sup> was selectively converted to the desired product **64p**. Related to the observed decrease in reactivity, when polar groups are in proximity to the benzylic position, homophenylalanine derivative **63q** was functionalized in lower yields.



**Scheme 3.4.8** C-H fluorination of biologically active compounds.  $^1\text{H-NMR}$  yields with  $\text{CH}_2\text{Br}_2$  as internal standard. Isolated yields in parentheses. [a] At 0 °C.  $^{19}\text{F-NMR}$  yield with  $\text{PhCF}_3$  as internal standard is provided.

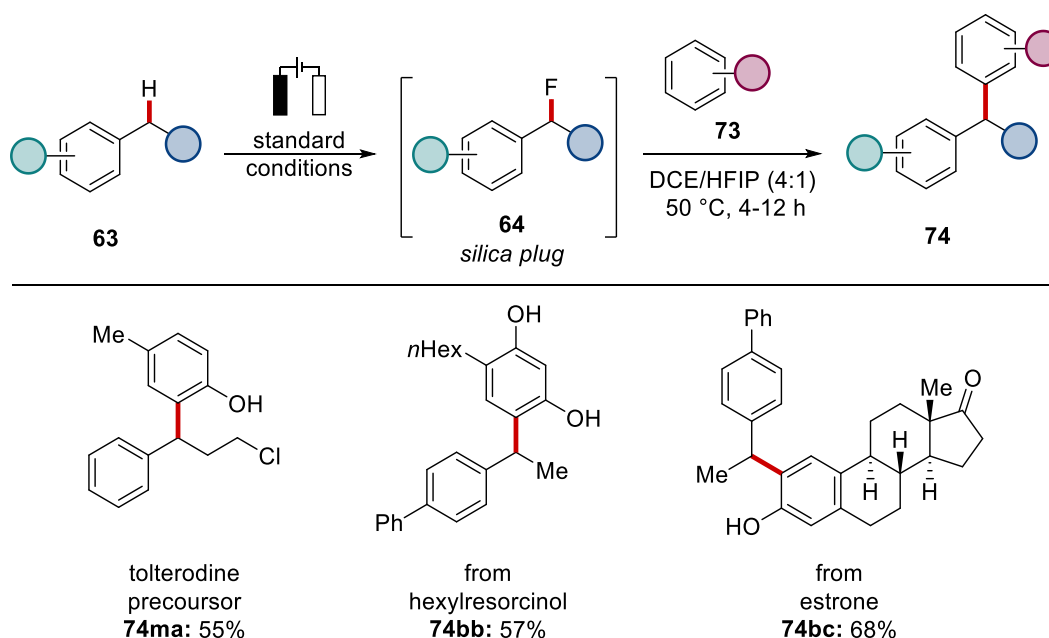
The synthetic utility of the concept could be impressively proved by *Alexej Scheremetjew* conducting a large-scale fluorination of ibuprofen methyl ester **63a** to obtain 2.46 g (86%) yield of the desired product **64a**.<sup>[229]</sup> Ultimately, high resource-economy could be demonstrated by using constant current solely derived from solar energy, on the 18<sup>th</sup> of March 2022 at the rooftop of the *Institute of Organic and Biomolecular Chemistry* in Göttingen, to furnish product **64i** in excellent yield (Scheme 3.4.9).



**Scheme 3.4.9** C-H fluorination facilitated by solar energy.  $^1\text{H-NMR}$  yield with  $\text{CH}_2\text{Br}_2$  as internal standard is provided.

### 3.4.3 Development of an Electrochemical C–H Fluorination/Arylation Sequence

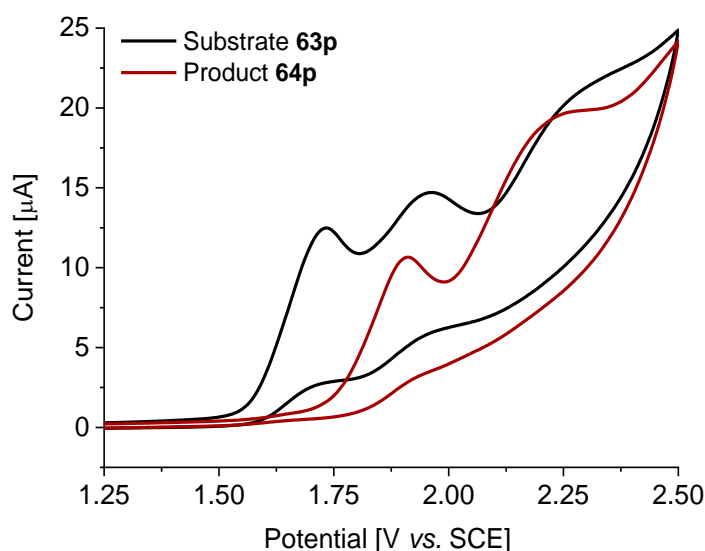
Due to the unique reactivity, benzyl fluorides are valuable strategic intermediates for subsequent coupling with multiple nucleophiles. The direct metal-free arylation of benzyl fluorides, facilitated by hydrogen bond donors, experienced significant recent attention. However, the reported strategies heavily relied on the installation of fluorides using cost- and atom inefficient electrophilic fluorine reagents. Therefore, the general applicability, of a subsequent arylation reaction, following the sustainable ECF without isolation of the intermediates was explored. As it turned out, a simple filtration of the crude reaction mixture over silica gel was sufficient to enable the fluoride displacement with electron-rich arenes in a mixture of DCE and HFIP (Scheme 3.4.10). In a first attempt, tolterodine precursor **74ma** was obtained in good yield after the C–H fluorination/arylation sequence from readily available 3-phenylpropyl chloride **63m**.<sup>[120a]</sup> Next, benzylic fluoride **64b** was envisioned to be coupled with electron-rich active pharmaceutical ingredients (APIs). Indeed, hexylresorcinol **73b**, an approved drug for the treatment of skin infections,<sup>[233]</sup> underwent the substitution, to furnish 57% of the desired product **74bb**.<sup>[131]</sup> Likewise, the steroidal sex hormone estrone **73c** could be chemoselectively benzylated with remarkable efficiency.



**Scheme 3.4.10** Utility of the benzyl fluorides towards the synthesis and functionalizations of bioactive molecules.

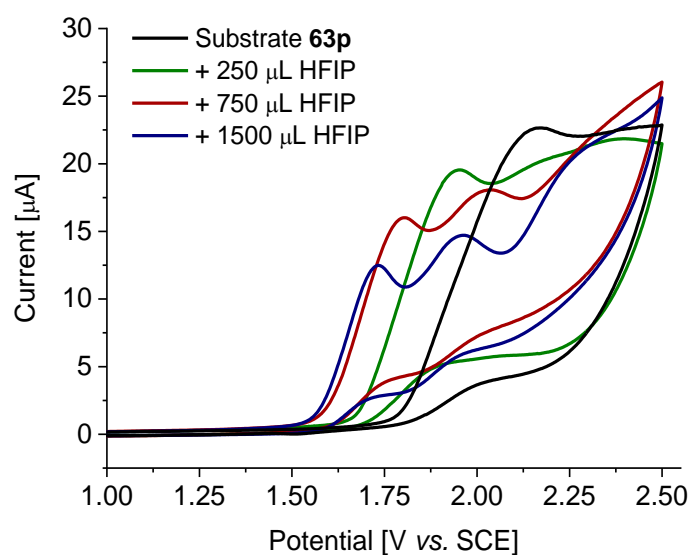
### 3.4.4 Mechanistic Insights by Cyclic Voltammetry

As was found by *Alexej Scheremetjew*, the benzylic fluorination displays a kinetic isotope effect of  $k_{\text{H}}/k_{\text{D}} \approx 3.1$ , which is indicative for a rate-limiting C–H cleavage.<sup>[229]</sup> In order to gain further insights into the unique efficacy, studies by means of cyclic voltammetry were conducted. First, the redox properties of the starting material **63p** and product **64p** were investigated (Figure 3.4.1). Indeed, the difference in oxidation potentials displayed to be  $\Delta E_{\text{p}} = 180$  mV, which is sufficient to prevent overoxidation of the product and enables the selective monofluorination.



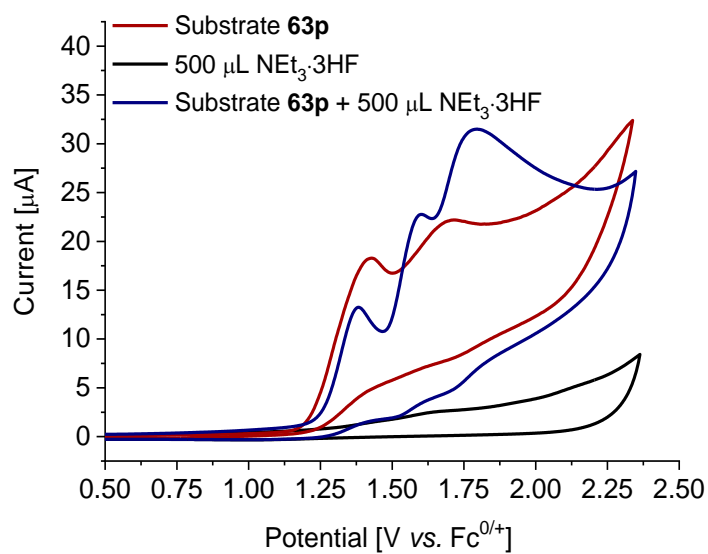
**Figure 3.4.1** Cyclic voltammetry in DCE:HFIP (2:1) with  $n\text{Bu}_4\text{NPF}_6$  (0.1 M) at 100 mV/s and a GC working electrode. Substrate **63p** (black); product **64p** (red).

Afterwards the crucial role of HFIP for the reaction was investigated (Figure 3.4.2). Substrate **63p** in DCE exhibited an irreversible response at  $E_{\text{p}} = 2.16$  V vs. SCE. Upon addition of small amounts of HFIP the oxidation event shifted slightly towards less positive potentials ( $E_{\text{p}} = 1.95$  V vs. SCE). This effect was boosted when a DCE/HFIP ratio of 4:1 was used (red,  $E_{1,\text{p}} = 1.80$  V vs. SCE). In addition to the further decrease in oxidation potential, a second oxidation event at  $E_{2,\text{p}} = 2.03$  V vs. SCE became apparent. This result suggests that HFIP enables the generation of a stable radical intermediate by a proton-coupled electron transfer,<sup>[234]</sup> which can undergo a second discrete oxidation.<sup>[207]</sup> When the optimized solvent ratio of DCE/HFIP = 2:1 was used, the oxidation potentials of **63p** were further lowered towards  $E_{1,\text{p}} = 1.73$  V vs. SCE and  $E_{2,\text{p}} = 1.96$  V vs. SCE, respectively.



**Figure 3.4.2** Cyclic voltammetry in DCE with  $n\text{Bu}_4\text{NPF}_6$  (0.1 M) at 100 mV/s and a GC working electrode. Substrate **63p** (black); substrate **63p** + 250  $\mu\text{L}$  HFIP (DCE/HFIP = 12:1, green); substrate **63p** + 750  $\mu\text{L}$  HFIP (DCE/HFIP = 4:1, red); substrate **63p** + 1500  $\mu\text{L}$  HFIP (DCE/HFIP = 2:1, blue).

Regarding the influence of the fluorine source, the initial redox response experienced only a relatively small shift towards more positive potentials ( $\Delta E_{1,p} = 40$  mV, Figure 3.4.3). In contrast, the effect on the second anodic event was demonstrated to be more pronounced ( $\Delta E_{2,p} = 100$  mV), indicating the stabilization of a generated benzyl cation by the fluoride source. Furthermore, the appearance of an additional anodic current was observed at  $E_{3,p} = 1.79$  V vs. Fc, which might be attributed to the formation of a generated product **64p** species (Figure 3.4.1).

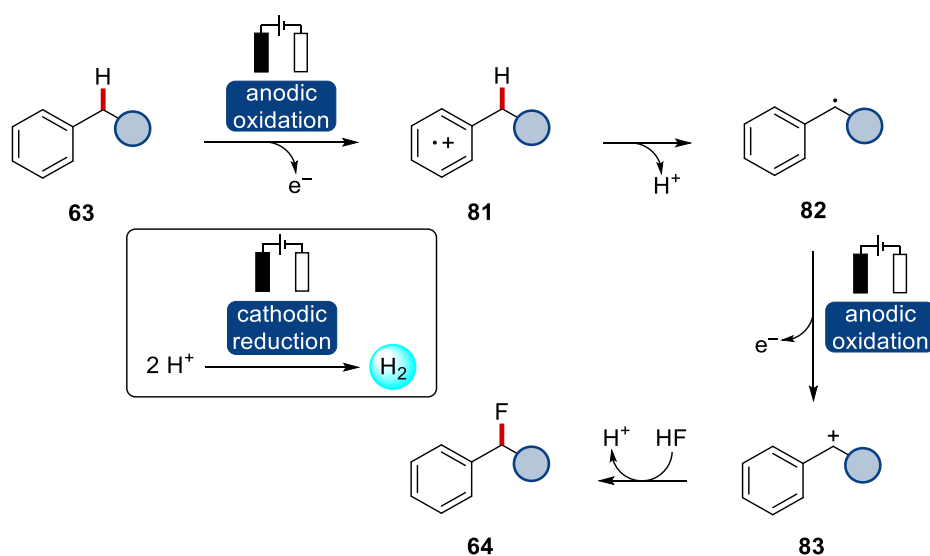


**Figure 3.4.3** Cyclic voltammetry in DCE/HFIP (2:1) with *n*Bu<sub>4</sub>NPF<sub>6</sub> (0.1 M) at 100 mV/s and a GC working electrode. With NEt<sub>3</sub>·3HF (black); substrate **63p** (red); substrate **63p** + 500 μL NEt<sub>3</sub>·3HF (blue).



### 3.4.5 Proposed Reaction Mechanism

Based on the cyclic voltammetry experiments and literature precedence, a mechanistic scenario of the electrooxidative C–H fluorination is proposed.<sup>[142, 144, 235a, 235b]</sup> Initially, the aromatic core is oxidized towards a radical cation **81**,<sup>[234]</sup> which is stabilized by the HFIP co-solvent (Scheme 3.4.11).<sup>[207]</sup> Thereafter, according to KIE studies, rate-limiting heterolytic C–H cleavage of the benzylic C–H bond furnishes radical **82**.<sup>[236]</sup> As protons and electrons travel to different distinct acceptors, this process can be classified as a multi-site proton-coupled electron transfer (MS-PCET).<sup>[237]</sup> In a second single electron oxidation, the corresponding benzyl cation **83** is formed, which interacts with hydrogen fluoride, to finally be trapped by a fluoride ion to deliver the desired product. At the platinum cathode, the hydrogen evolution reaction (HER) takes place by means of electrochemical proton reduction.

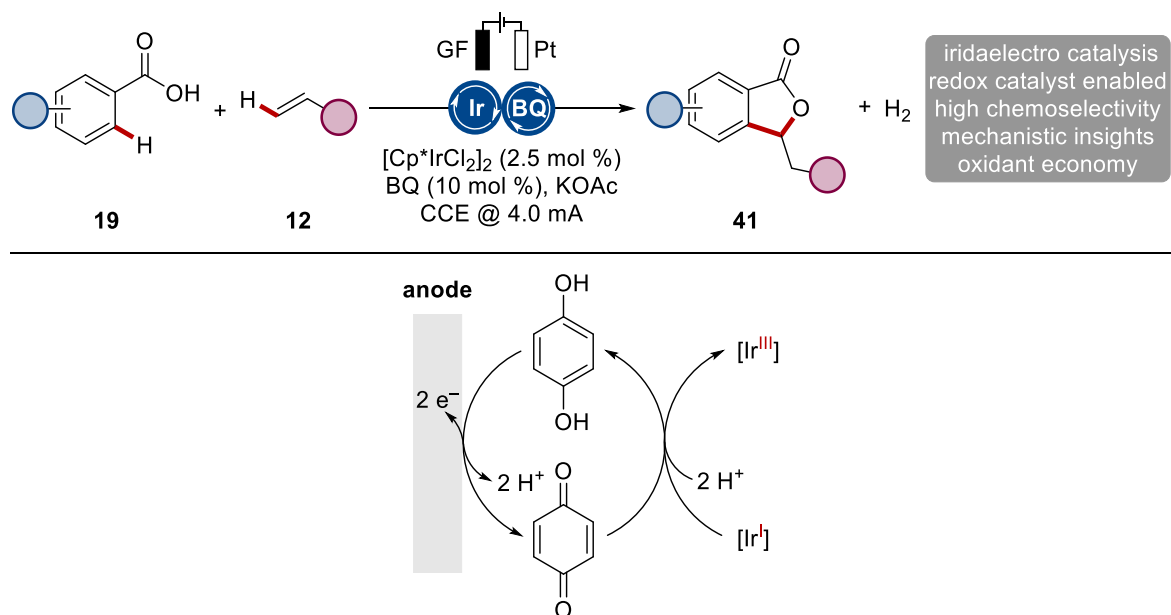


**Scheme 3.4.11** Proposed mechanistic scenario for the electrochemical benzylic C–H fluorination.

## 4 SUMMARY AND OUTLOOK

During the past decades, transition metal-catalyzed, oxidative functionalizations of inert and omnipresent C–H bonds for the construction of complex scaffolds have impressively emerged, providing a robust toolbox to organic chemists. However, the requirement for stoichiometric quantities of often toxic and expensive oxidants remains a major limitation in terms of sustainability. In contrast, the merger of electrocatalysis with organometallic C–H activations has evolved as a powerful strategy to overcome these persisting challenges. The use of electricity from renewable sources, the inherent safety and facile scalability provides unique possibilities for the environmentally benign formation of C–C and C–Het bonds, avoiding the generation of undesired side products and minimizing waste.

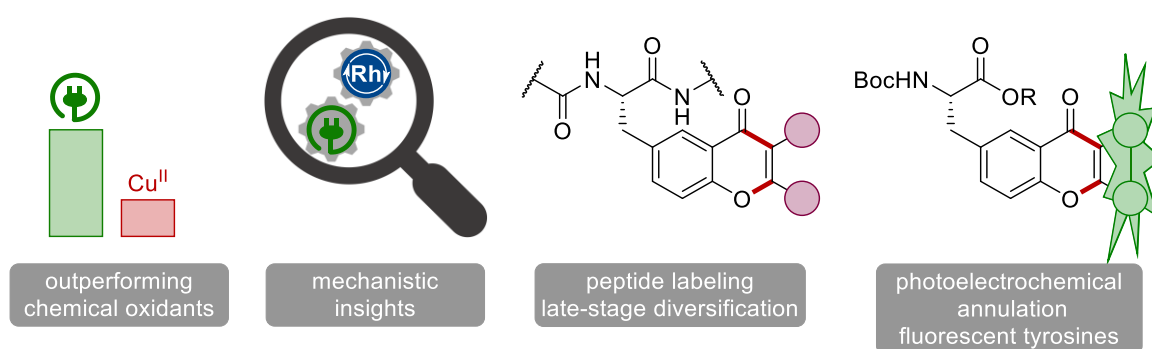
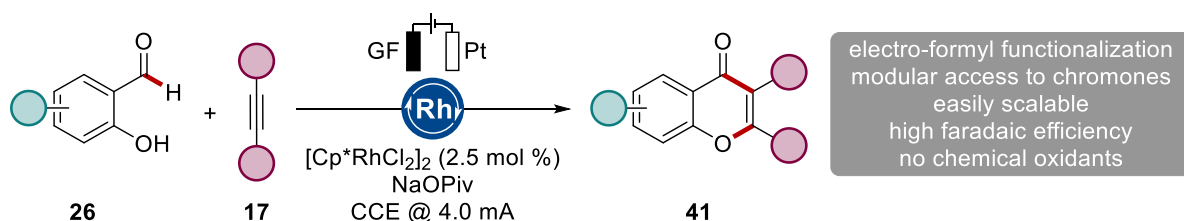
In the first project, the strategy of transition metal electrocatalysis was successfully applied towards an iridium-catalyzed annulation of alkenes **12** by weakly-coordinating benzoic acids **19** forming molecular hydrogen as the sole by-product (Scheme 4.1).<sup>[209]</sup> With a benzoquinone redox-mediator that homogeneously reoxidizes the catalyst, excellent chemoselectivity were obtained regarding halogenated arenes. The metallaelectrocatalysis was characterized by a simple undivided cell set-up, user-friendly constant current electrolysis, and KOAc as the only additive.



**Scheme 4.1** Iridaelectro-catalyzed C–H activation of benzoic acids by redox catalyst cooperation.

The catalytic system featured high functional group tolerance and mechanistic investigation by means of cyclic voltammetry shed light on the crucial role of the benzoquinone mediator within a iridium(III/I) reaction manifold.

With the recent progress in electrocatalytic arene functionalizations in mind, within the second project, the reactivity of transition metal catalysts for electrochemical formyl C–H cleavage was investigated. By sticking together readily available 2-hydroxy benzaldehydes **26** with alkynes **17**, chromones were constructed in a modular approach, catalyzed by a rhodium catalyst which is directly oxidized at the anode (Scheme 4.2).<sup>[238]</sup> The rhodaelectrocatalysis proved advantageous when challenging alkynes **17** were employed. Another key feature of the concept was the high regioselectivity regarding unsymmetrical alkynes. In the case of diarylalkynes, chromones were formed with the more electron-rich arene in the 2-position as the major isomer. The mild approach tolerated a plethora of functional groups, such as halogens, esters, or amines, which enabled effective alkyne annulations by tyrosine derivatives.

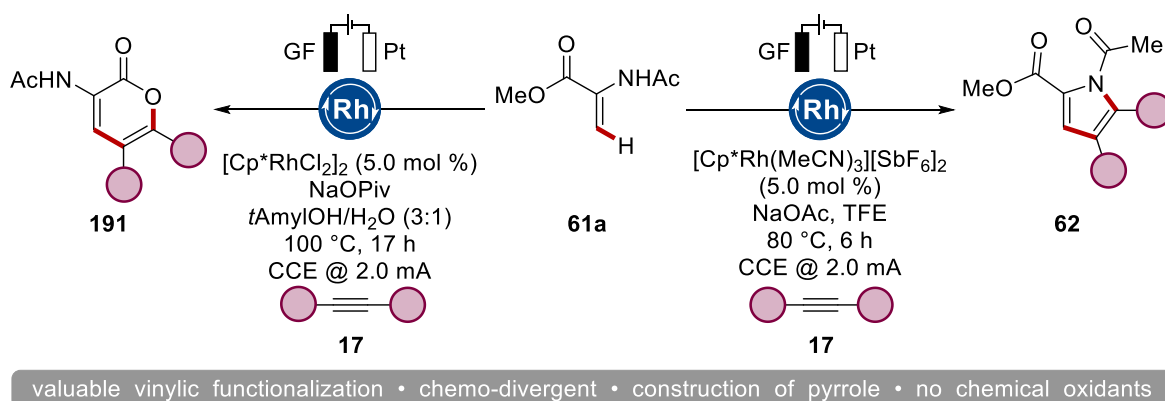


**Scheme 4.2** Electrochemical rhodium-catalyzed assembly of chromones and labeling of tyrosine-containing peptides.

It was shown that the developed strategy was tolerant towards several amino acid residues and complex peptides could be efficiently annulated in a late-stage fashion. A subsequent photoelectrochemical *Scholl*-type reaction, mediated by iodide, could transform the resulting tyrosine-based chromones into planar  $\pi$ -extended fluorescent probes with improved

photoelectronic properties. Finally, key reaction intermediates were obtained and their characterization *via* cyclic voltammetry provided unique insights into the catalysts' mode of action.

In a subsequent project, the functionalization of dehydroalanine **61a** was accomplished. Interestingly, in aqueous media lactone **191** was formed, providing an alternative route towards these scaffolds. The annulation of alkyne **17** is believed to be triggered by the ester hydrolysis with increasing basicity, as the electrolysis progresses and protons are reduced, to furnish the carboxylate. Nevertheless, careful optimization revealed that a cationic rhodium complex efficiently catalyzed the formation of the corresponding pyrrole **62**, when TFE was used as the solvent (Scheme 4.3).

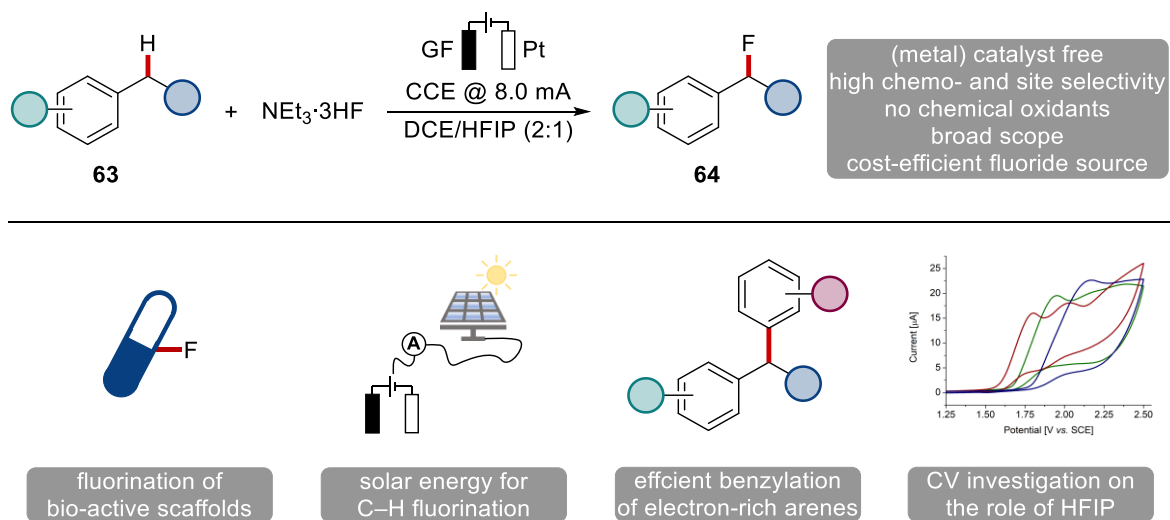


**Scheme 4.3** Chemo-divergent C–H functionalization of dehydroalanine **61a** towards pyrroles and lactones.

Further studies should focus on the exploration of the substrate scope, especially the annulation of dehydroalanine-containing peptides would be highly desirable.

In the final project, the challenge of chemoselective electrochemical fluorination of benzylic C–H bonds was addressed, reaching selectivities, which were thus far only achieved with electrophilic fluorinating reagents or by transition metal-catalyzed transformations using chemical oxidants. The key to success was the use of HFIP, to stabilize radical cations, in non-nucleophilic solvents to prevent side reactions, from the attack of a solvent molecule (Scheme 4.4). NEt<sub>3</sub>·3HF was used as an efficient, cost-effective, and abundant fluoride source, contemporarily avoiding additional organic electrolytes. The established strategy showed good functional group tolerance and excellent site-selectivity for secondary benzylic C–H bonds. Furthermore, adamantane was successfully functionalized at the methine position. The user-friendly nature of the developed ECF allowed for the benzylations of valuable bioactive compounds, after filtration of the reaction mixture over silica. The user-

friendly reaction set-up allowed the direct use of solar power to enable the benign fluorination, and insights by cyclic voltammetry demonstrated the crucial role of HFIP in stabilizing reaction intermediates.



**Scheme 4.4** Site- and chemoselective fluorination of  $\text{C}(\text{sp}^3)\text{-H}$  bonds.

## 5 EXPERIMENTAL PART

### 5.1 General Remarks

Reactions involving air- or moisture-sensitive compounds were conducted under an atmosphere of nitrogen using pre-dried glassware and standard *Schlenk* or glovebox techniques. Liquids and solutions were transferred *via* nitrogen-flushed syringes by BRAUN, with oven-dried stainless-steel cannulas (pre-dried at 140 °C). Solids were added under counter flow of nitrogen (standard *Schlenk* technique). Solutions were concentrated under reduced pressure by rotary evaporation at 40 °C. Non-volatile products were dried under high vacuum. Air and moisture sensitive substances were stored in a MBRAUN glovebox. If not noted otherwise, yields refer to isolated compounds, estimated to be >95% pure by GC and NMR.

*Caution:* Special safety considerations should be taken for experiments with fluoride reagents. They should be only handled by trained staff and under appropriate safety measurements (lab coat, gloves, and eye protection) inside a fume hood, as they are toxic reagents.

#### 5.1.1 Solvents and Reagents

##### Solvents

All solvents used for work-up and purification were distilled prior to use. Solvents used in reactions involving air- or moisture-sensitive compounds were dried and stored under an inert atmosphere of nitrogen or argon according to the following standard procedures: Solvents purified by solvent purification system (*SPS-800*) from MBRAUN: toluene, THF, diethyl ether, DCM, MeCN and DMF. Solvents dried and distilled over CaH<sub>2</sub>: DCE, DMA, and NMP. Solvents dried over 4Å molecular sieves and degassed using multiple cycles of freeze-pump-thaw: *t*AmOH, 1,4-dioxane, DME, acetone, methanol, ethanol, *i*PrOH, *n*BuOH, TFE and HFIP. Water was degassed before its use applying repeated freeze-pump-thaw cycles.

## Reagents

Chemicals obtained from commercial sources with a purity higher than 95% were used without further purification. The following compounds were known from the literature and synthesized according to previously reported procedures:

Alkynes **17b-m** and **171a-c**,<sup>[239]</sup> **171g-h**,<sup>[240]</sup> **171i**,<sup>[241]</sup> **171j**<sup>[242]</sup> and hydroxybenzaldehydes **[D]<sub>1</sub>-26a**,<sup>[219]</sup> **26c**,<sup>[243]</sup> **26g**,<sup>[244]</sup> **26n**,<sup>[245]</sup> **26o**,<sup>[246]</sup> **26p**<sup>[247]</sup> and tyrosine-derived hydroxybenzaldehyde **174a**<sup>[248]</sup> were synthesized according to previously described procedures. Peptides were synthesized under standard solution phase protocols (EDCI/HOBt). The following compounds were kindly synthesized and provided by the persons listed below:

*Karsten Rauch*: [Cp\*IrCl<sub>2</sub>]<sub>2</sub>, [Cp\*RhCl<sub>2</sub>]<sub>2</sub>, [RuCl<sub>2</sub>(*p*-cymene)]<sub>2</sub>, [Ru(OAc)<sub>2</sub>(*p*-cymene)], dry and/or degassed solvents.

*Dr. Alexander Bechthold*: **31e**, **31h**, **159a**, **159b**.

*Dr. Nikolaos Kaplaneris*: **159d**, **159e**.

*Dr. Cuiju Zhu*: **171f**.

*Ralf Steinbock*: **17e**, **17j**, **17m**.

*Jan Fleischer*: **17b**, **17i**, **17l**, **26t**, **171a**, **171c**.

*Linus Gross*: **61a**.

## 5.1.2 Analytical and Experimental Methods

### Column Chromatography

Analytical thin-layer chromatography (TLC) was used for reaction monitoring, analysis of column chromatography. TLC was performed on MERCK silica gel 60 coated aluminium sheets, with fluorescence indicator F-254. The plates were either visualized by UV light ( $\lambda = 254$  nm or 366 nm), if applicable, or by staining solution (KMnO<sub>4</sub> solution) followed by gentle heating with a heat gun.

Chromatographic purification of crude products was accomplished by flash column chromatography using silica gel from MERCK (*Geduran*<sup>®</sup> *Si 60*, 40–63  $\mu$ m) or MACHEREY-NAGEL (60 M, 40–63  $\mu$ m). The crude products were loaded with the respective eluent.

## Vacuum

The following average pressure was measured on the used rotary vane pump *RD4* from VACUUBRAND:  $0.8 \cdot 10^{-1}$  mbar (uncorrected value).

## Head Space Gas Chromatography

After a standard electrochemical reaction in a properly sealed electrolysis cell, a defined volume (1.0 mL) of the gaseous atmosphere were removed through a rubber septum using a HAMILTON *GASTIGHT* syringe. The gas analysis of the reaction mixture was performed on an AGILENT *7890B* GC System using a thermal conductivity detector and a 5 Å MS column.

## Melting Points

Melting points were measured on a *Stuart*<sup>®</sup> *SMP3* melting point apparatus from BARLOWORLD SCIENTIFIC. Values are uncorrected.

## Infrared Spectroscopy

Infrared (IR) spectra were recorded on a BRUKER *Alpha-P* FT-IR spectrometer with an ATR diamond probe for detection in the range of  $\tilde{\nu} = 4000\text{--}400$  cm<sup>-1</sup>. Analyses of the spectra were performed with the software *Opus 6.5* from BRUKER.

## Mass Spectrometry

High resolution (HR) electrospray ionization (ESI) mass spectra were recorded on a *micrOTOF* or a *maXis* from BRUKER DALTONICS or a *LTQ Orbitrap XL* from THERMO SCIENTIFIC. EI-MS spectra were recorded on a JEOL *AccuTOF* (EI) instrument. Ionization of the samples was achieved using electrospray ionization (ESI) or electron ionization (EI). The ratio of mass to charge ( $m/z$ ) is given, intensities  $I$  relative to the base signal ( $I = 100$ ) are written in parentheses.

## X-Ray Crystallographic Analyses

X-ray diffraction experiments for all compounds were carried out by *Dr. Christopher Golz* at 100(2) K on a BRUKER *D8 Venture* four-circle-diffractometer from BRUKER AXS



equipped with a Photon II detector purchased from BRUKER AXS and using microfocus I $\mu$ S Cu/Mo radiation from INCOATEC with HELIOS mirror optics and single-hole collimator from BRUKER AXS. Intensities were integrated<sup>[249]</sup> and absorption corrections based on equivalent reflections were applied using SADABS.<sup>[250]</sup> The structures were all solved using SHELXT<sup>[251]</sup> and refined against all F<sub>2</sub> in SHELXL<sup>[252]</sup> using Olex 2.<sup>[253]</sup> All of the non-hydrogen atoms were refined anisotropically while the carbon bond hydrogen atoms were located geometrically and refined using a riding model. Molecular structures are presented with hydrogen atoms omitted for clarity and thermal ellipsoids drawn at the 50% probability level.

### UV/Vis Spectroscopy

UV/Vis absorption data were recorded on a JASCO V-770 spectrophotometer. The scan speed was adjusted to 400 nm/min. Fluorescence excitation and emission data in solution were recorded on a JASCO FP-8500 spectrofluorometer. The scan speed was adjusted to 500 nm/min. The concentration in CHCl<sub>3</sub> is given for each sample and the excitation wavelengths were selected at the strongest signal.

### Nuclear Magnetic Resonance Spectroscopy

Nuclear magnetic resonance (NMR) spectra were recorded on BRUKER *Avance* 300, *Avance III HD 400*, *Avance Neo 400*, *Avance III HD 500* or *Avance Neo 600* spectrometer at 300 MHz, 400 MHz, 500 MHz, 600 MHz (<sup>1</sup>H-NMR), 75 MHz, 100 MHz, 125 MHz (<sup>13</sup>C-NMR) and 282 MHz, 377 MHz (<sup>19</sup>F-NMR), respectively. Chemical shifts are reported as  $\delta$ -values in parts per million (ppm) relative to SiMe<sub>4</sub> and are referenced to the residual proton peak or the carbon peak of the deuterated solvent:

**Table 5.1.1** Chemical Shifts of residual proton or carbon signals of deuterated solvents.

Solvent	$^1\text{H-NMR}$ [ppm]	$^{13}\text{C-NMR}$ [ppm]
$\text{CDCl}_3$	7.26	77.16
MeOD	3.31	49.00
$\text{CD}_2\text{Cl}_2$	5.32	54.00
$d_6$ -DMSO	2.50	39.51
$d_6$ -Acetone	2.05	206.26
$\text{C}_6\text{D}_6$	7.16	128.06

All measurements were performed at 298 K, unless stated otherwise. The measured resonance multiplicities were reported by the following abbreviations: s (singlet), d (doublet), t (triplet), q (quartet), quint (quintet), sext (sextet), sept (septet), dd (doublet of doublets), dt (doublet of triplets), ddd (doublet of doublets of doublets), td (triplet of doublets), dddd (doublet of doublets of doublets of doublets), m (multiplet) and br (broad singlet). The coupling constants  $J$  are reported in Hertz (Hz). Analysis of all spectra was performed with *MestReNova v14.2.0* from MESTRELAB RESEARCH.

### On-Line NMR Monitoring in Flow

The  $^1\text{H-NMR}$  spectroscopic experiments in flow were performed on a *Spinsolve 60ULTRA* from MAGRITEK. For pumping the solution to the spectrometer, an ISMATEC *REGLO Digital MS-2/12 (ISM 596)* peristaltic pump was employed. The flow rate was set to 0.4 mL/min. The spectra were batch-processed with the reaction monitoring wizard of the *MNova 12.0.3* (MESTRELAB RESEARCH) software. Arbitrary integral values were transformed to mmol and percentage values by referencing with 1,3,5-trimethoxybenzene as internal standard.

### Data Analysis

Data analysis and plotting were performed using MICROSOFT *Excel* or ORIGINLAB *OriginPro 8.5G* software.

## Chiral HPLC

HPLC chromatograms were recorded on an AGILENT *I290 Infinity* using *CHIRALPAK*<sup>®</sup> *IA-3*, *IB-3* and *ID-3* columns (3.0  $\mu\text{m}$  particle size;  $\text{\O}$ : 4.6 mm and 250 mm length).

### 5.1.3 Electrochemical Methods

#### Constant Current Electrolysis

Platinum electrodes (10 mm  $\times$  15 mm  $\times$  0.125 mm, 99.9%; CHEMPUR or ESG EDELMETALL-SERVICE), graphite felt electrodes (10 mm  $\times$  15 mm  $\times$  6.0 mm, *SIGRACELL*<sup>®</sup> *GFA 6 EA*, obtained from SGL CARBON), RVC electrodes (10 mm  $\times$  15 mm  $\times$  5.0 mm, ERG AEROSPACE CORPORATION, *Duocel*<sup>®</sup> *Reticulated Vitreous Carbon RVC100* (100 PPI)), nickel foam electrodes (10 mm  $\times$  15 mm  $\times$  1.0 mm, RECEMAT BV, *Ni5763*) were connected using stainless steel adapters, following the published protocol.<sup>[178]</sup> Electrocatalysis was conducted using an AXIOMET *AX-3003P* potentiostat or a METROHM *Multi Autolab/M204* using *Nova 2.1* software in constant current mode. For reactions performed with the standardized electrochemistry kit, *ElectraSyn 2.0*<sup>®</sup> from IKA, the commercialized electrodes, and 10 mL undivided cells were used. For heated reactions, the vial was connected *via* the IKA *ElectraSyn GOGO Module*<sup>®</sup> and mounted into a silicon oil bath.

Divided cells, separated by a P4 glass frit, were custom-made from the glass workshop of the *Georg-August-Universität Göttingen*.

For the electrocatalysis powered by sunlight, the commercially available amorphous silicon photovoltaic cell *TPS-103* from CONRAD ELECTRONIC (6 W, 17.5 V max. voltage, 428 mA max. current, 467 mm  $\times$  161 mm  $\times$  19 mm) was used. The output current was controlled with a customized and normalized constant current regulator and regularly double checked with an ammeter.

#### Constant Potential Electrolysis

Constant Potential electrolysis was conducted using a portable multi potentiostat METROHM *Dropsens  $\mu$ Stat 8000P* using *Dropview 8400* software or METROHM *Multi Autolab/M204* using *Nova 2.1* software. A silver-wire ( $d = 1.0$  mm, 99.9%, CHEMPUR) was used as the pseudo-reference electrode in close proximity to the working electrode. To ensure comparable constant potential conditions with the results gained by cyclic voltammetry,

calibration of the pseudo-reference electrode *versus* ferrocene was performed for each reaction system.

### **Cyclic Voltammetry**

The cyclic voltammetry measurements were carried out using a METROHM *Autolab PGSTAT204* workstation, and the following data analysis was performed with *Nova 2.1*. For the experiments, a glassy-carbon (GC) disc electrode ( $d = 3$  mm) or a platinum disc electrode ( $d = 3$  mm) was used as the working electrode (WE). Either a saturated calomel electrode (SCE) (Hg/Hg<sub>2</sub>Cl<sub>2</sub>, ceramic frit, OD = 6 mm); an aqueous Ag/AgCl (Ag/Ag<sup>+</sup>, aq. KCl (3 M), ceramic frit, OD = 6 mm) was used as the reference electrode (RE), if not stated otherwise. If a silver-wire ( $d = 1.0$  mm, 99.9%, CHEMPUR) was used as the pseudo-reference electrode, the voltammograms were referenced internally *versus* ferrocene. The counter electrode (CE) was a coiled platinum wire ( $d = 1.0$  mm, 99.9%, CHEMPUR). The electrodes were purchased from ALS JAPAN Co, Ltd. Measurements were recorded at a scan rate of 100 mV/s, if not indicated otherwise. The working temperature was 298 K, if not indicated otherwise. All solutions were degassed *via* freeze-pump-thaw method prior to use and nitrogen was bubbled through the solutions for at least 5 min before the experiment was performed. The voltametric studies were performed under a constant flow of dry nitrogen.

### **Photoelectrocatalysis**

Photoelectro-catalyzed annulations were performed under N<sub>2</sub> atmosphere in pre-dried quartz tubes using a LUZCHEM *LZC-ICH2* photoreactor with 254 nm irradiation with the electrolysis equipment mentioned above.

## 5.2 General Procedures

### 5.2.1 General Procedure A: Iridaelectro-Catalyzed C–H Alkenylation by Redox Catalyst Cooperation

The electrocatalysis was carried out in an undivided cell with a graphite felt anode (10 mm × 15 mm × 6.0 mm) and a Pt cathode (10 mm × 15 mm × 0.25 mm). Benzoic acid **19** (0.25 mmol, 1.00 equiv), alkene **12** (0.50 mmol, 2.00 equiv), KOAc (49.0 mg, 0.50 mmol, 2.00 equiv), BQ (2.7 mg, 10 mol %) and [Cp\*IrCl<sub>2</sub>]<sub>2</sub> (5.0 mg, 2.5 mol %) were dissolved in *t*AmOH/H<sub>2</sub>O (3:1, 4.0 mL). The electrocatalysis was performed at 100 °C with a constant current of 4.0 mA maintained for 18 h. Then, the DC-power supply was stopped, and the reaction mixture was diluted with EtOAc (2.0 mL). The platinum cathode and the graphite felt anode were washed with EtOAc (Pt: 1 × 5.0 mL; GF: 3 × 10 mL). The solvents were combined with the reaction mixture, silica gel was added, and the solvents were removed in vacuo. Subsequent column chromatography on silica gel afforded the corresponding products.

### 5.2.2 General Procedure B: Rhodaelectro-Catalyzed Assembly of Chromones *via* formyl C–H Activation

The electrocatalysis was carried out in an undivided cell, with a graphite felt (GF) anode (25 mm × 10 mm × 6.0 mm) and a platinum cathode (25 mm × 10 mm × 0.125 mm). 2-Hydroxybenzaldehyde **26** (0.75 mmol, 3.00 equiv), alkyne **17** (0.25 mmol, 1.00 equiv), NaOPiv (62.0 mg, 0.50 mmol, 2.00 equiv), [Cp\*RhCl<sub>2</sub>]<sub>2</sub> (3.9 mg, 2.5 mol %) and *t*AmylOH/H<sub>2</sub>O (3:1, 4.0 mL) were placed in a 10 mL cell. Electrocatalysis was performed at 100 °C with a constant current of 4.0 mA maintained for 3.5-7 h. Then, the DC-power supply was stopped, and the reaction mixture was diluted with EtOAc (2.0 mL). The platinum cathode and the graphite felt anode were washed with EtOAc (Pt: 1 × 5.0 mL; GF: 3 × 10 mL). The solvents were combined with the reaction mixture, silica gel was added, and the solvents were removed in vacuo. Subsequent column chromatography on silica gel afforded the corresponding products.

### 5.2.3 General Procedure C: Rhodaelectro-Catalyzed Assembly of Chromones via formyl C–H Activation under Water-free Conditions

The electrocatalysis was carried out in an undivided cell, with a graphite felt (GF) anode (25 mm × 10 mm × 6.0 mm) and a platinum cathode (25 mm × 10 mm × 0.125 mm). 2-Hydroxybenzaldehyde **26** (0.75 mmol, 3.00 equiv), alkyne **17** (0.25 mmol, 1.00 equiv), NaOPiv (62.0 mg, 0.50 mmol, 2.00 equiv), [Cp\*RhCl<sub>2</sub>]<sub>2</sub> (3.9 mg, 2.5 mol %), *n*Bu<sub>4</sub>NPF<sub>6</sub> (155 mg, 0.1 M) and *t*AmylOH (4.0 mL) were placed in a 10 mL cell. Electrocatalysis was performed at 100 °C with a constant current of 4.0 mA maintained for 3.5-7 h. Then, the DC-power supply was stopped, and the reaction mixture was diluted with EtOAc (2.0 mL). The platinum cathode and the graphite felt anode were washed with EtOAc (Pt: 1 × 5.0 mL; GF: 3 × 10 mL). The solvents were combined with the reaction mixture, silica gel was added, and the solvents were removed in vacuo. Subsequent column chromatography on silica gel afforded the corresponding products.

### 5.2.4 General Procedure D: Rhodium-Catalyzed Synthesis of Chromones using Cu(OAc)<sub>2</sub> as the Terminal Oxidant

2-Hydroxybenzaldehyde **26** (78 μL, 0.75 mmol, 3.00 equiv), alkyne **17** (0.25 mmol, 1.00 equiv), Cu(OAc)<sub>2</sub>·H<sub>2</sub>O (99.8 mg, 0.50 mmol, 2.00 equiv), NaOPiv (62.0 mg, 0.50 mmol, 2.00 equiv), [Cp\*RhCl<sub>2</sub>]<sub>2</sub> (3.9 mg, 2.5 mol %) and *t*AmylOH/H<sub>2</sub>O (3:1, 4.0 mL) were placed in a 10 mL schlenk tube under nitrogen atmosphere. The reaction was stirred at 100 °C for 7 h. Subsequently, the mixture was diluted with EtOAc (25 mL), and silica gel was added. The solvents were removed in vacuo and column chromatography on silica gel afforded the corresponding products.

### 5.2.5 General Procedure E: Photoelectrochemical Annulation of 2,3-Aryl-Substituted Chromones

The electrocatalysis was carried out in an undivided quartz-glas cell, with a graphite felt (GF) anode (25 mm × 10 mm × 6.0 mm) and a platinum cathode (25 mm × 10 mm × 0.125 mm). Chromone **48** (0.10 mmol, 1.00 equiv) and potassium iodide (4.2 mg, 25 mol %) were dissolved in EtOH/H<sub>2</sub>O (19:1, 4.0 mL). The mixture was degassed by purging nitrogen through the solution for 5 min. Electrocatalysis was performed in a ventilated UV-reactor with a constant current of 2.0 mA under irradiation of UV-C light (254 nm) for 22 h. Then,

irradiation and the DC-power supply were stopped, and the reaction mixture was diluted with EtOAc (2.0 mL). The platinum cathode and the graphite felt anode were washed with EtOAc (Pt:  $1 \times 5.0$  mL; GF:  $3 \times 10$  mL). The solvents were combined with the reaction mixture, silica gel was added, and the solvents were removed in vacuo. Subsequent column chromatography on silica gel afforded the corresponding products.

### 5.2.6 General Procedure F: Rhodaelectro-Catalyzed Annulation of Alkenes

The electrocatalysis was carried out in a 10 mL undivided cell, with a graphite felt (GF) anode (25 mm  $\times$  10 mm  $\times$  6.0 mm) and a platinum cathode (25 mm  $\times$  10 mm  $\times$  0.125 mm). Alkene **61** (0.50 mmol, 2.00 equiv), alkyne **17** (0.25 mmol, 1.00 equiv), NaOAc (41.0 mg, 0.50 mmol, 2.00 equiv) and a rhodium catalyst were dissolved in TFE (4.0 mL) or *t*AmylOH/H<sub>2</sub>O (3:1, 4.0 mL). Electrocatalysis was performed at 80-100 °C with a constant current of 2.0 mA maintained for 6 h. Then, the DC-power supply was stopped, and the reaction mixture was diluted with EtOAc (2.0 mL). The platinum cathode and the graphite felt anode were washed with EtOAc (Pt:  $1 \times 5.0$  mL; GF:  $3 \times 10$  mL). The solvents were combined with the reaction mixture, silica gel was added, and the solvents were removed in vacuo. Subsequent column chromatography on silica gel afforded the corresponding products.

### 5.2.7 General Procedure G: Electrochemical Fluorination of C(sp<sup>3</sup>)-H bonds

Benzylic substrate **63** (0.50 mmol, 1.00 equiv), DCE (2.0 mL), HFIP (1.0 mL), and NEt<sub>3</sub>·3HF (1.0 mL) were placed in a 10 mL undivided cell under inert atmosphere. A graphite felt (GF) anode (25 mm  $\times$  10 mm  $\times$  6.0 mm) and a platinum cathode (25 mm  $\times$  10 mm  $\times$  0.125 mm) were attached to an electrode holder which was assembled on the electrolysis cell. Electrosynthesis was performed, unless noted otherwise, at rt with a constant current of 8.0 mA until 2.5 F/mol were passed (4.2 h). After electrolysis, the reaction mixture was filtered over a plug of silica. The platinum cathode and the graphite felt anode were washed with EtOAc (Pt:  $1 \times 5.0$  mL; GF:  $3 \times 10$  mL) and the resulting fraction was filtered over the same silica plug. After rinsing the silica plug with an additional mixture of *n*hexane/ethylacetate (75 mL), the solvents were removed in vacuo. CH<sub>2</sub>Br<sub>2</sub> (36  $\mu$ L, 0.50 mmol) and PhCF<sub>3</sub> (62  $\mu$ L, 0.50 mmol) were added to the resulting residue and the mixture was submitted for NMR analyses.

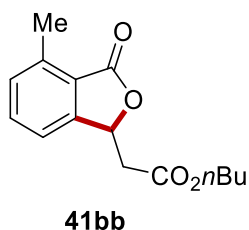
**5.2.8 General Procedure H: Benzylation of Electron-Rich Arenes**

Following general procedure G for the electrochemical fluorination, arene **73** (2.50 mmol, 5.00 equiv) was added to the filtrate of the silica plug (pentane/DCM = 9:1, 75 mL) and the solvents were removed in vacuo. Subsequently the residue was dissolved in DCE (2.0 mL) and stirred at room temperature. Then HFIP (0.5 mL) was added dropwise, and the reaction was heated to 50 °C. When the benzylic fluoride was consumed, as indicated by TLC or GC-MS, the reaction was stopped, the solvents removed, and the residue purified by column chromatography.



## 5.3 Iridaelectro-Catalyzed C–H Alkenylation by Redox Catalyst Cooperation

### 5.3.1 Characterization Data

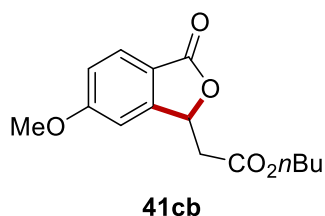


#### *n*-Butyl 2-(4-methyl-3-oxo-1,3-dihydroisobenzofuran-1-yl)acetate

The general procedure A was followed using **19b** (34.0 mg, 0.25 mmol) and **31b** (64.1 mg, 0.50 mmol) at 100 °C for 18 h. Purification by column chromatography on silica gel (*n*hexane/EtOAc = 5:1) yielded **41bb** (56.9 mg, 87%) as a colorless oil.

**<sup>1</sup>H-NMR** (300 MHz, CDCl<sub>3</sub>):  $\delta$  = 7.53 (dd,  $J$  = 7.6, 7.6 Hz, 1H), 7.33–7.23 (m, 2H), 5.81 (t,  $J$  = 6.5 Hz, 1H), 4.15 (t,  $J$  = 6.7 Hz, 2H), 2.87 (d,  $J$  = 6.5 Hz, 2H), 2.68 (s, 3H), 1.60–1.54 (m, 2H), 1.43–1.29 (m, 2H), 0.92 (t,  $J$  = 7.3 Hz, 3H). **<sup>13</sup>C-NMR** (75 MHz, CDCl<sub>3</sub>):  $\delta$  = 170.0 (C<sub>q</sub>), 169.4 (C<sub>q</sub>), 149.3 (C<sub>q</sub>), 139.9 (C<sub>q</sub>), 133.9 (CH), 131.1 (CH), 123.4 (C<sub>q</sub>), 119.3 (CH), 76.1 (CH), 65.1 (CH<sub>2</sub>), 39.7 (CH<sub>2</sub>), 30.5 (CH<sub>2</sub>), 19.0 (CH<sub>2</sub>), 17.3 (CH<sub>3</sub>), 13.7 (CH<sub>3</sub>). **IR** (ATR):  $\tilde{\nu}$  = 2962, 1756, 1733, 1568, 1260, 1202, 908 cm<sup>-1</sup>. **MS** (ESI)  $m/z$  (relative intensity): 285 (100) [M+Na]<sup>+</sup>, 263 (65) [M+H]<sup>+</sup>. **HR-MS** (ESI)  $m/z$  calc. for C<sub>15</sub>H<sub>19</sub>O<sub>4</sub> [M+H]<sup>+</sup>: 263.1278, found: 263.1280.

The spectral data are in accordance with those reported in the literature.<sup>[193b]</sup>

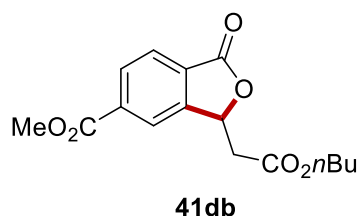


#### *n*-Butyl 2-(6-methoxy-3-oxo-1,3-dihydroisobenzofuran-1-yl)acetate

The general procedure A was followed using **19c** (76.1 mg, 0.50 mmol) and **31b** (32.0 mg, 0.25 mmol) at 100 °C for 18 h. Purification by column chromatography on silica gel (*n*hexane/EtOAc = 4:1 + 1% NEt<sub>3</sub>) yielded **41cb** (56.4 mg, 81%) as a colorless oil.

**<sup>1</sup>H-NMR** (400 MHz, CDCl<sub>3</sub>):  $\delta$  = 7.76 (d,  $J$  = 8.5 Hz, 1H), 7.01 (dd,  $J$  = 8.5, 2.2 Hz, 1H), 6.92–6.88 (m, 1H), 5.76 (t,  $J$  = 6.6 Hz, 1H), 4.13 (t,  $J$  = 6.7 Hz, 2H), 3.86 (s, 3H), 2.89 (dd,  $J$  = 16.5, 7.0 Hz, 1H), 2.81 (dd,  $J$  = 16.5, 6.3 Hz, 1H), 1.63–1.54 (m, 2H), 1.39–1.29 (m, 2H), 0.89 (t,  $J$  = 7.4 Hz, 3H). **<sup>13</sup>C-NMR** (100 MHz, CDCl<sub>3</sub>):  $\delta$  = 169.5 (C<sub>q</sub>), 169.4 (C<sub>q</sub>), 164.8 (C<sub>q</sub>), 151.6 (C<sub>q</sub>), 127.3 (CH), 118.1 (C<sub>q</sub>), 116.7 (CH), 106.2 (CH), 76.2 (CH), 65.1 (CH<sub>2</sub>), 55.8 (CH<sub>3</sub>), 39.6 (CH<sub>2</sub>), 30.5 (CH<sub>2</sub>), 19.0 (CH<sub>2</sub>), 13.6 (CH<sub>3</sub>). **IR** (ATR):  $\tilde{\nu}$  = 2958, 1758, 1728, 1607, 1257, 1012, 905 cm<sup>-1</sup>. **MS** (ESI)  $m/z$  (relative intensity): 301 (100) [M+Na]<sup>+</sup>, 279 (95) [M+H]<sup>+</sup>. **HR-MS** (ESI)  $m/z$  calc. for C<sub>15</sub>H<sub>19</sub>O<sub>5</sub> [M+H]<sup>+</sup>: 279.1227, found: 279.1215.

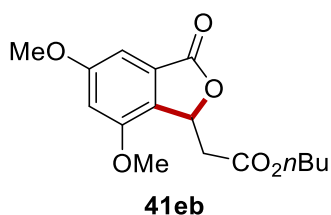
The spectral data are in accordance with those reported in the literature.<sup>[193b]</sup>



### Methyl 3-(2-butoxy-2-oxoethyl)-1-oxo-1,3-dihydroisobenzofuran-5-carboxylate

The general procedure A was followed using **19d** (90.1 mg, 0.50 mmol) and **31b** (32.0 mg, 0.25 mmol) at 100 °C for 18 h. Purification by column chromatography on silica gel (*n*hexane/EtOAc = 4:1 + 1% NEt<sub>3</sub>) yielded **41db** (38.3 mg, 50%) as a colorless oil.

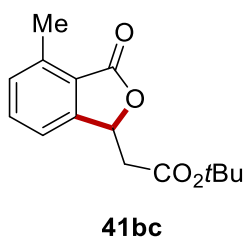
**<sup>1</sup>H-NMR** (400 MHz, CDCl<sub>3</sub>):  $\delta$  = 8.20 (dd,  $J$  = 7.9, 1.3 Hz, 1H), 8.16–8.13 (m, 1H), 7.96–7.92 (m, 1H), 5.93–5.87 (m, 1H), 4.14 (t,  $J$  = 7.4 Hz, 2H), 3.95 (s, 3H), 2.93 (d,  $J$  = 6.4 Hz, 2H), 1.63–1.55 (m, 2H), 1.39–1.28 (m, 2H), 0.90 (t,  $J$  = 7.4 Hz, 3H). **<sup>13</sup>C-NMR** (100 MHz, CDCl<sub>3</sub>):  $\delta$  = 168.9 (C<sub>q</sub>), 168.8 (C<sub>q</sub>), 165.6 (C<sub>q</sub>), 148.7 (C<sub>q</sub>), 135.5 (C<sub>q</sub>), 130.8 (CH), 129.7 (C<sub>q</sub>), 125.9 (CH), 123.4 (CH), 77.0 (CH), 65.3 (CH<sub>2</sub>), 52.8 (CH<sub>3</sub>), 39.2 (CH<sub>2</sub>), 30.5 (CH<sub>2</sub>), 19.0 (CH<sub>2</sub>), 13.6 (CH<sub>3</sub>). **IR** (ATR):  $\tilde{\nu}$  = 2959, 2935, 1770, 1725, 1439, 1285, 1059, 1010 cm<sup>-1</sup>. **MS** (ESI)  $m/z$  (relative intensity): 329 (100) [M+Na]<sup>+</sup>, 307 (45) [M+H]<sup>+</sup>. **HR-MS** (ESI)  $m/z$  calc. for C<sub>16</sub>H<sub>19</sub>O<sub>6</sub> [M+H]<sup>+</sup>: 307.1176, found: 307.1177.



***n*-Butyl 2-(5,7-dimethoxy-3-oxo-1,3-dihydroisobenzofuran-1-yl)acetate**

The general procedure A was followed using **19e** (91.1 mg, 0.50 mmol) and **31b** (32.0 mg, 0.25 mmol) at 100 °C for 18 h. Purification by column chromatography on silica gel (*n*hexane/EtOAc = 4:1) yielded **41eb** (56.3 mg, 73%) as a white solid.

**<sup>1</sup>H-NMR** (300 MHz, CDCl<sub>3</sub>):  $\delta$  = 6.93 (d,  $J$  = 1.9 Hz, 1H), 6.69 (d,  $J$  = 1.9 Hz, 1H), 5.83 (dd,  $J$  = 8.8, 3.2 Hz, 1H), 4.14 (t,  $J$  = 6.7 Hz, 2H), 3.88 (s, 3H), 3.87 (s, 3H), 3.27 (dd,  $J$  = 16.3, 3.2 Hz, 1H), 2.62 (dd,  $J$  = 16.3, 8.8 Hz, 1H), 1.70–1.55 (m, 2H), 1.45–1.31 (m, 2H), 0.94 (t,  $J$  = 7.3 Hz, 3H). **<sup>13</sup>C-NMR** (75 MHz, CDCl<sub>3</sub>):  $\delta$  = 170.1 (C<sub>q</sub>), 169.6 (C<sub>q</sub>), 162.8 (C<sub>q</sub>), 154.8 (C<sub>q</sub>), 129.5 (C<sub>q</sub>), 128.6 (C<sub>q</sub>), 104.9 (CH), 98.7 (CH), 76.2 (CH), 64.9 (CH<sub>2</sub>), 56.0 (CH<sub>3</sub>), 55.7 (CH<sub>3</sub>), 38.1 (CH<sub>2</sub>), 30.6 (CH<sub>2</sub>), 19.1 (CH<sub>2</sub>), 13.7 (CH<sub>3</sub>). **IR** (ATR):  $\tilde{\nu}$  = 2959, 2935, 1768, 1735, 1627, 1431, 1171, 1040 cm<sup>-1</sup>. **M.p.**: 87–89 °C. **MS** (ESI)  $m/z$  (relative intensity): 331 (100) [M+Na]<sup>+</sup>, 309 (75) [M+H]<sup>+</sup>. **HR-MS** (ESI)  $m/z$  calc. for C<sub>16</sub>H<sub>21</sub>O<sub>6</sub> [M+H]<sup>+</sup>: 309.1333, found: 309.1335.



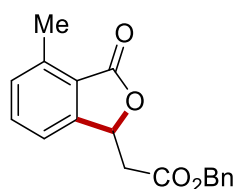
***tert*-Butyl 2-(4-methyl-3-oxo-1,3-dihydroisobenzofuran-1-yl)acetate**

The general procedure A was followed using **19b** (34.0 mg, 0.25 mmol) and **31c** (64.1 mg, 0.50 mmol) at 100 °C for 18 h. Purification by column chromatography on silica gel (*n*hexane/EtOAc = 10:1) yielded **41bc** (56.5 mg, 86%) as a colorless oil.

**<sup>1</sup>H-NMR** (300 MHz, CDCl<sub>3</sub>):  $\delta$  = 7.45 (dd,  $J$  = 7.6, 7.6 Hz, 1H), 7.21 (m, 2H), 5.69 (t,  $J$  = 6.4 Hz, 1H), 2.74 (d,  $J$  = 6.4 Hz, 2H), 2.61 (s, 3H), 1.37 (s, 9H). **<sup>13</sup>C-NMR** (75 MHz, CDCl<sub>3</sub>):  $\delta$  = 169.2 (C<sub>q</sub>), 167.5 (C<sub>q</sub>), 148.5 (C<sub>q</sub>), 138.8 (C<sub>q</sub>), 132.9 (CH), 130.0 (CH), 122.5 (C<sub>q</sub>), 118.3 (CH), 80.8 (C<sub>q</sub>), 75.3 (CH), 39.8 (CH<sub>2</sub>), 27.0 (CH<sub>3</sub>), 16.3 (CH<sub>3</sub>). **IR** (ATR):  $\tilde{\nu}$  = 2978, 2939, 1755, 1725, 1602, 1481, 1367, 1148, 1046, 1006 cm<sup>-1</sup>. **MS** (ESI)  $m/z$  (relative

intensity): 285 (70)  $[M+Na]^+$ , 280 (60)  $[M+NH_4]^+$ , 207 (100), 229 (25). **HR-MS** (ESI)  $m/z$  calc. for  $C_{15}H_{19}O_4$   $[M+H]^+$ : 263.1278, found: 263.1278.

The spectral data are in accordance with those reported in the literature.<sup>[193b]</sup>



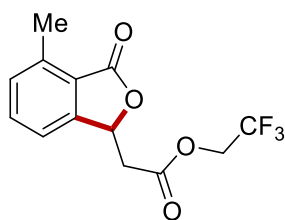
**41bd**

### **Benzyl 2-(4-methyl-3-oxo-1,3-dihydroisobenzofuran-1-yl)acetate**

The general procedure A was followed using **19b** (34.0 mg, 0.25 mmol) and **31d** (81.1 mg, 0.50 mmol) at 100 °C for 18 h. Purification by column chromatography on silica gel (*n*hexane/EtOAc = 9:1 to 6:1) yielded **41bd** (50.8 mg, 69%) as a white solid.

**<sup>1</sup>H-NMR** (300 MHz,  $CDCl_3$ ):  $\delta$  = 7.41 (dd,  $J$  = 7.6, 7.6 Hz, 1H), 7.30–7.24 (m, 5H), 7.21–7.10 (m, 2H), 5.74 (t,  $J$  = 6.5 Hz, 1H), 5.04–5.01 (m, 2H), 2.84 (dd,  $J$  = 6.6, 1.3 Hz, 2H), 2.59 (s, 3H). **<sup>13</sup>C-NMR** (75 MHz,  $CDCl_3$ ):  $\delta$  = 169.0 ( $C_q$ ), 168.2 ( $C_q$ ), 148.1 ( $C_q$ ), 138.9 ( $C_q$ ), 134.2 ( $C_q$ ), 132.9 (CH), 130.1 (CH), 127.6 (CH), 127.5 (CH), 127.4 (CH), 122.3 ( $C_q$ ), 118.2 (CH), 74.9 (CH), 66.0 ( $CH_2$ ), 38.7 ( $CH_2$ ), 16.3 ( $CH_3$ ). **IR** (ATR):  $\tilde{\nu}$  = 3033, 2943, 1753, 1735, 1601, 1163, 1008  $cm^{-1}$ . **M.p.**: 72–73 °C. **MS** (ESI)  $m/z$  (relative intensity): 335 (10), 319 (100)  $[M+Na]^+$ , 314 (50)  $[M+NH_4]^+$ , 297 (45)  $[M+H]^+$ . **HR-MS** (ESI)  $m/z$  calc. for  $C_{18}H_{17}O_4$   $[M+H]^+$ : 297.1121, found: 297.1121.

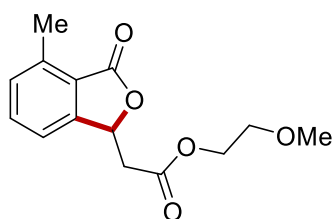
The spectral data are in accordance with those reported in the literature.<sup>[193b]</sup>

**41be**

### 2-Trifluoroethyl 2-(4-methyl-3-oxo-1,3-dihydroisobenzofuran-1-yl)acetate

The general procedure A was followed using **19b** (34.0 mg, 0.25 mmol) and **31e** (77.1 mg, 0.50 mmol) at 100 °C for 18 h. Purification by column chromatography on silica gel (*n*hexane/EtOAc = 10:1 to 6:1) yielded **41be** (38.2 mg, 53%) as a crystalline solid.

**<sup>1</sup>H-NMR** (400 MHz, CDCl<sub>3</sub>):  $\delta$  = 7.48 (dd,  $J$  = 7.6, 7.6 Hz, 1H), 7.26–7.17 (m, 2H), 5.78–5.70 (m, 1H), 4.57–4.35 (m, 2H), 2.97 (dd,  $J$  = 16.8, 5.4 Hz, 1H), 2.89 (dd,  $J$  = 16.8, 7.4 Hz, 1H), 2.62 (s, 3H). **<sup>13</sup>C-NMR** (100 MHz, CDCl<sub>3</sub>):  $\delta$  = 168.8 (C<sub>q</sub>), 166.8 (C<sub>q</sub>), 147.6 (C<sub>q</sub>), 139.2 (C<sub>q</sub>), 133.1 (CH), 130.4 (CH), 122.4 (C<sub>q</sub>), 121.7 (q,  $^1J_{C-F}$  = 277.2 Hz, C<sub>q</sub>), 118.1 (CH), 74.4 (CH), 59.7 (q,  $^2J_{C-F}$  = 36.9 Hz, CH<sub>2</sub>), 38.1 (CH<sub>2</sub>), 16.3 (CH<sub>3</sub>). **<sup>19</sup>F{<sup>1</sup>H}-NMR** (282 MHz, CDCl<sub>3</sub>):  $\delta$  = -73.7 (s). **IR** (ATR):  $\tilde{\nu}$  = 2963, 1765, 1746, 1416, 1269, 1167, 1002 cm<sup>-1</sup>. **M.p.**: 131–132 °C. **MS** (ESI)  $m/z$  (relative intensity): 312 (20), 311 (100) [M+Na]<sup>+</sup>, 306 (10) [M+NH<sub>4</sub>]<sup>+</sup>, 290 (10), 289 (30) [M+H]<sup>+</sup>. **HR-MS** (ESI)  $m/z$  calc. for C<sub>13</sub>H<sub>12</sub>F<sub>3</sub>O<sub>4</sub> [M+H]<sup>+</sup>: 289.0682, found: 289.0680.

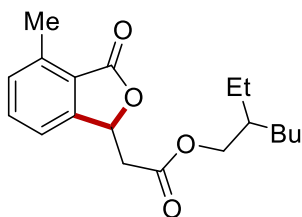
**41bf**

### 2-Methoxyethyl 2-(4-methyl-3-oxo-1,3-dihydroisobenzofuran-1-yl)acetate

The general procedure A was followed using **19b** (34.0 mg, 0.25 mmol) and **31f** (65.1 mg, 0.50 mmol) at 100 °C for 18 h. Purification by column chromatography on silica gel (*n*hexane/EtOAc = 4:1) yielded **41bf** (55.6 mg, 84%) as a colorless oil.

**<sup>1</sup>H-NMR** (400 MHz, CDCl<sub>3</sub>):  $\delta$  = 7.46 (dd,  $J$  = 7.6, 7.6 Hz, 1H), 7.24–7.20 (m, 2H), 5.75 (t,  $J$  = 6.6 Hz, 1H), 4.27–4.22 (m, 2H), 3.56–3.51 (m, 2H), 3.31 (s, 3H), 2.85 (d,  $J$  = 6.6 Hz, 2H), 2.61 (s, 3H). **<sup>13</sup>C-NMR** (100 MHz, CDCl<sub>3</sub>)  $\delta$  = 170.1 (C<sub>q</sub>), 169.5 (C<sub>q</sub>), 149.3 (C<sub>q</sub>), 140.0

(C<sub>q</sub>), 134.1 (CH), 131.3 (CH), 123.5 (C<sub>q</sub>), 119.4 (CH), 76.1 (CH), 70.3 (CH<sub>2</sub>), 64.2 (CH<sub>2</sub>), 59.1 (CH<sub>3</sub>), 39.8 (CH<sub>2</sub>), 17.4 (CH<sub>3</sub>). **IR** (ATR):  $\tilde{\nu}$  = 2926, 1755, 1736, 1601, 1201, 1172, 1007 cm<sup>-1</sup>. **MS** (ESI) *m/z* (relative intensity): 287 (100) [M+Na]<sup>+</sup>, 282 (30) [M+NH<sub>4</sub>]<sup>+</sup>, 265 (90) [M+H]<sup>+</sup>. **HR-MS** (ESI) *m/z* calc. for C<sub>14</sub>H<sub>17</sub>O<sub>5</sub> [M+H]<sup>+</sup>: 265.1071, found: 265.1071. The spectral data are in accordance with those reported in the literature.<sup>[81a]</sup>

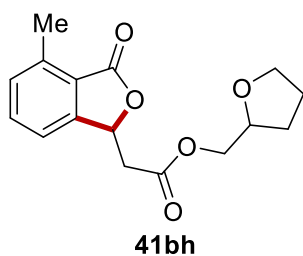
**41bg**

### 2-Ethylhexyl-2-(4-methyl-3-oxo-1,3-dihydroisobenzofuran-1-yl)acetate

The general procedure A was followed using **19b** (34.0 mg, 0.25 mmol) and **31g** (92.1 mg, 0.50 mmol) at 100 °C for 18 h. Purification by column chromatography on silica gel (*n*hexane/EtOAc = 9:1) yielded **41bg** (56.8 mg, 71%) as a colorless oil.

**<sup>1</sup>H-NMR** (400 MHz, CDCl<sub>3</sub>):  $\delta$  = 7.45 (dd, *J* = 7.6, 7.6 Hz, 1H), 7.24–7.17 (m, 2H), 5.74 (t, *J* = 6.6 Hz, 1H), 4.07–3.95 (m, 2H), 2.88–2.74 (m, 2H), 2.62 (s, 3H), 1.59–1.42 (m, 1H), 1.30–1.19 (m, 8H), 0.85–0.78 (m, 6H). **<sup>13</sup>C-NMR** (125 MHz, CDCl<sub>3</sub>):  $\delta$  = 170.0 (C<sub>q</sub>), 169.5 (C<sub>q</sub>), 149.3 (C<sub>q</sub>), 140.0 (C<sub>q</sub>), 134.0 (CH), 131.2 (CH), 123.5 (C<sub>q</sub>), 119.3 (CH), 76.2 (CH), 67.8 (CH<sub>2</sub>), 40.0 (CH<sub>2</sub>), 38.9 (CH), 30.5 (CH<sub>2</sub>), 29.1 (CH<sub>2</sub>), 23.9 (CH<sub>2</sub>), 23.1 (CH<sub>2</sub>), 17.5 (CH<sub>3</sub>), 14.2 (CH<sub>3</sub>), 11.2 (CH<sub>3</sub>). **IR** (ATR):  $\tilde{\nu}$  = 2958, 2929, 1760, 1735, 1201, 1170, 1008 cm<sup>-1</sup>. **MS** (ESI) *m/z* (relative intensity): 341 (100) [M+Na]<sup>+</sup>, 336 (25) [M+NH<sub>4</sub>]<sup>+</sup>, 319 (20) [M+H]<sup>+</sup>. **HR-MS** (ESI) *m/z* calc. for C<sub>19</sub>H<sub>27</sub>O<sub>4</sub> [M+H]<sup>+</sup>: 319.1904, found: 319.1903.

The spectral data are in accordance with those reported in the literature.<sup>[81a]</sup>

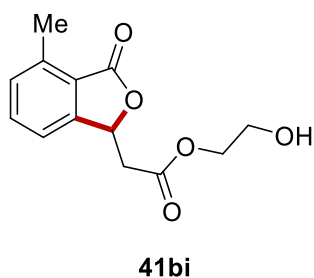


**(Tetrahydrofuran-2-yl)methyl-2-(4-methyl-3-oxo-1,3-dihydroisobenzofuran-1-yl)acetate**

The general procedure A was followed using **19b** (34.0 mg, 0.25 mmol) and **31h** (78.1 mg, 0.50 mmol) at 100 °C for 18 h. Purification by column chromatography on silica gel (*n*hexane/EtOAc = 4:1 to 2:1) yielded **41bh** (63.0 mg, 87%) as a colorless oil.

**<sup>1</sup>H-NMR** (400 MHz, CDCl<sub>3</sub>):  $\delta$  = 7.46 (dd,  $J$  = 7.6, 7.6 Hz, 1H), 7.24–7.19 (m, 2H), 5.75 (t,  $J$  = 6.6 Hz, 1H), 4.21–4.14 (m, 1H), 4.10–4.00 (m, 2H), 3.85–3.77 (m, 1H), 3.76–3.68 (m, 1H), 2.85 (dd,  $J$  = 6.6, 1.0 Hz, 2H), 2.61 (s, 3H), 2.00–1.89 (m, 1H), 1.89–1.78 (m, 2H), 1.60–1.49 (m, 1H). **<sup>13</sup>C-NMR** (100 MHz, CDCl<sub>3</sub>)  $\delta$  = 170.1 (C<sub>q</sub>), 169.4 (C<sub>q</sub>), 149.3 (C<sub>q</sub>), 140.0 (C<sub>q</sub>), 134.1 (CH), 131.2 (CH), 123.5 (C<sub>q</sub>), 119.4 (CH), 76.4 (CH), 76.1 (CH), 68.6 (CH<sub>2</sub>), 67.2 (CH<sub>2</sub>), 39.8 (CH<sub>2</sub>), 28.0 (CH<sub>2</sub>), 25.8 (CH<sub>2</sub>), 17.4 (CH<sub>3</sub>). **IR** (ATR):  $\tilde{\nu}$  = 2952, 1753, 1734, 1601, 1289, 1200, 1166, 1006 cm<sup>-1</sup>. **MS** (ESI)  $m/z$  (relative intensity): 313 (100) [M+Na]<sup>+</sup>, 308 (45) [M+NH<sub>4</sub>]<sup>+</sup>, 291 (90) [M+H]<sup>+</sup>. **HR-MS** (ESI)  $m/z$  calc. for C<sub>16</sub>H<sub>19</sub>O<sub>5</sub> [M+H]<sup>+</sup>: 291.1227, found: 291.1228.

The spectral data are in accordance with those reported in the literature.<sup>[81a]</sup>



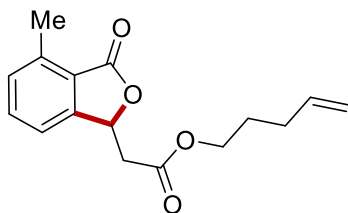
**2-Hydroxyethyl-2-(4-methyl-3-oxo-1,3-dihydroisobenzofuran-1-yl)acetate**

The general procedure A was followed using **19b** (34.0 mg, 0.25 mmol) and **31i** (58.1 mg, 0.50 mmol) at 100 °C for 18 h. Purification by column chromatography on silica gel (*n*hexane/EtOAc = 3:1 to 2:1) yielded **41bi** (42.6 mg, 68%) as a colorless oil.

**<sup>1</sup>H-NMR** (300 MHz, CDCl<sub>3</sub>):  $\delta$  = 7.47 (dd,  $J$  = 7.6, 7.6 Hz, 1H), 7.25–7.17 (m, 2H), 5.78–5.71 (m, 1H), 4.26–4.17 (m, 2H), 3.81–3.71 (m, 2H), 2.96–2.73 (m, 2H), 2.60 (s, 3H), 2.17

(bs, 1H). **<sup>13</sup>C-NMR** (75 MHz, CDCl<sub>3</sub>)  $\delta$  = 170.2 (C<sub>q</sub>), 169.6 (C<sub>q</sub>), 149.1 (C<sub>q</sub>), 140.0 (C<sub>q</sub>), 134.1 (CH), 131.2 (CH), 123.3 (C<sub>q</sub>), 119.3 (CH), 76.0 (CH), 66.7 (CH<sub>2</sub>), 60.8 (CH<sub>2</sub>), 39.7 (CH<sub>2</sub>), 17.3 (CH<sub>3</sub>). **IR** (ATR):  $\tilde{\nu}$  = 3467, 2955, 1732, 1601, 1201, 1172, 1006 cm<sup>-1</sup>. **MS** (ESI)  $m/z$  (relative intensity): 273 (100) [M+Na]<sup>+</sup>, 268 (10) [M+NH<sub>4</sub>]<sup>+</sup>, 251 (30) [M+H]<sup>+</sup>. **HR-MS** (ESI)  $m/z$  calc. for C<sub>13</sub>H<sub>15</sub>O<sub>5</sub> [M+H]<sup>+</sup>: 251.0914, found: 251.0914.

The spectral data are in accordance with those reported in the literature.<sup>[193b]</sup>



**41bj**

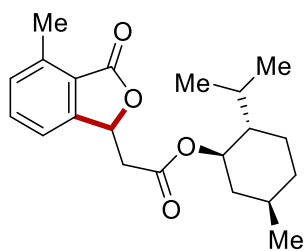
#### **Pent-4-en-1-yl-2-(4-methyl-3-oxo-1,3-dihydroisobenzofuran-1-yl)acetate**

The general procedure A was followed using **19b** (34.0 mg, 0.25 mmol) and **31j** (70.1 mg, 0.50 mmol) at 100 °C for 18 h. Purification by column chromatography on silica gel (*n*hexane/EtOAc = 9:1) yielded **41bj** (54.2 mg, 79%) as a colorless oil.

**<sup>1</sup>H-NMR** (300 MHz, CDCl<sub>3</sub>):  $\delta$  = 7.46 (dd,  $J$  = 7.6, 7.6 Hz, 1H), 7.24–7.18 (m, 2H), 5.80–5.64 (m, 2H), 5.01–4.87 (m, 2H), 4.09 (t,  $J$  = 6.7 Hz, 2H), 2.80 (d,  $J$  = 6.5 Hz, 2H), 2.61 (s, 3H), 2.10–1.96 (m, 2H), 1.74–1.59 (m, 2H). **<sup>13</sup>C-NMR** (125 MHz, CDCl<sub>3</sub>)  $\delta$  = 170.0 (C<sub>q</sub>), 169.3 (C<sub>q</sub>), 149.3 (C<sub>q</sub>), 140.0 (C<sub>q</sub>), 137.2 (CH), 134.0 (CH), 131.2 (CH), 123.5 (C<sub>q</sub>), 119.3 (CH), 115.5 (CH<sub>2</sub>), 76.1 (CH), 64.8 (CH<sub>2</sub>), 39.9 (CH<sub>2</sub>), 30.1 (CH<sub>2</sub>), 27.8 (CH<sub>2</sub>), 17.5 (CH<sub>3</sub>). **IR** (ATR):  $\tilde{\nu}$  = 2925, 1755, 1732, 1201, 1168, 1007 cm<sup>-1</sup>. **MS** (ESI)  $m/z$  (relative intensity): 297 (100) [M+Na]<sup>+</sup>, 292 (20) [M+NH<sub>4</sub>]<sup>+</sup>, 275 (20) [M+H]<sup>+</sup>. **HR-MS** (ESI)  $m/z$  calc. for C<sub>16</sub>H<sub>19</sub>O<sub>4</sub> [M+H]<sup>+</sup>: 275.1278, found: 275.1275.

The spectral data are in accordance with those reported in the literature.<sup>[81a]</sup>



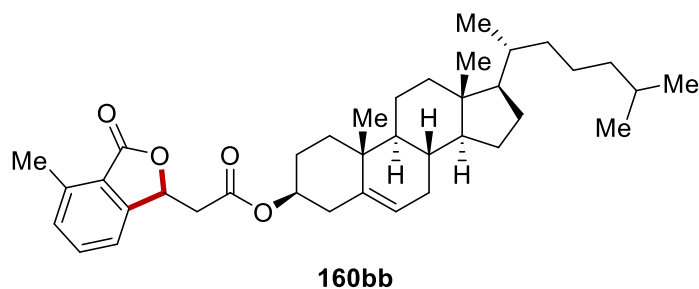
**160ba**

**(1*R*,2*S*,5*R*)-2-Isopropyl-5-methylcyclohexyl-2-(4-methyl-3-oxo-1,3-dihydroisobenzofuran-1-yl)acetate**

The general procedure A was followed using **19b** (34.1 mg, 0.25 mmol) and **159a** (105 mg, 0.50 mmol) at 100 °C for 18 h. Purification by column chromatography on silica gel (*n*hexane/EtOAc = 9:1) yielded **160ba** (75.9 mg, 88%) as a white solid.

**<sup>1</sup>H-NMR** (300 MHz, CDCl<sub>3</sub>):  $\delta$  = 7.51–7.39 (m, 1H), 7.24–7.17 (m, 2H), 5.72 (q, *J* = 6.2 Hz, 1H), 4.75–4.60 (m, 1H), 2.90–2.71 (m, 2H), 2.61 (s, 3H), 1.99–1.53 (m, 4H), 1.49–1.16 (m, 2H), 1.05–0.73 (m, 9H), 0.72–0.65 (m, 3H). **<sup>13</sup>C-NMR** (75 MHz, CDCl<sub>3</sub>)  $\delta$  = 170.2 (C<sub>q</sub>), 169.0 (C<sub>q</sub>), 149.4 (C<sub>q</sub>), 139.9 (C<sub>q</sub>), 134.0 (CH), 131.2 (CH), 123.6 (C<sub>q</sub>), 119.4 (CH), 76.2 (CH), 75.3 (CH), 47.0 (CH), 40.8 (CH<sub>2</sub>), 39.9 (CH<sub>2</sub>), 34.2 (CH<sub>2</sub>), 31.5 (CH), 26.3 (CH), 23.3 (CH<sub>2</sub>), 22.1 (CH<sub>3</sub>), 20.8 (CH<sub>3</sub>), 17.4 (CH<sub>3</sub>), 16.3 (CH<sub>3</sub>). **IR** (ATR):  $\tilde{\nu}$  = 2953, 2926, 1758, 1727, 1601, 1370, 1200, 1151, 1007 cm<sup>-1</sup>. **M.p.**: 84–86 °C. **MS** (ESI) *m/z* (relative intensity): 367 (100) [M+Na]<sup>+</sup>, 362 (25) [M+NH<sub>4</sub>]<sup>+</sup>. **HR-MS** (ESI) *m/z* calc. for C<sub>21</sub>H<sub>29</sub>O<sub>4</sub> [M+H]<sup>+</sup>: 345.2060, found: 345.2056.

The spectral data are in accordance with those reported in the literature.<sup>[81a]</sup>

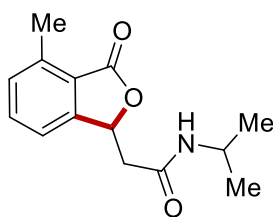


**(3*S*,8*S*,9*S*,10*R*,13*R*,14*S*,17*R*)-10,13-Dimethyl-17-((*R*)-6-methylheptan-2-yl)-  
2,3,4,7,8,9,10,11,12,13,14,15,16,17-tetradecahydro-1*H*-cyclopenta[*a*]phenanthren-3-yl  
2-((*S*)-4-methyl-3-oxo-1,3-dihydroisobenzofuran-1-yl)acetate**

The general procedure A was followed using **19b** (34.0 mg, 0.25 mmol) and **159b** (220 mg, 0.50 mmol) at 100 °C for 18 h. Purification by column chromatography on silica gel (*n*hexane/EtOAc = 9:1) yielded **160bb** (97.7 mg, 68%) as a white solid.

**<sup>1</sup>H-NMR** (600 MHz, CDCl<sub>3</sub>): δ = 7.48–7.30 (m, 1H), 7.23–7.19 (m, 2H), 5.75–5.70 (m, 1H), 5.33–5.28 (m, 1H), 4.64–4.56 (m, 1H), 2.83–2.75 (m, 2H), 2.62 (s, 3H), 2.30–2.14 (m, 2H), 1.97–1.86 (m, 2H), 1.84–1.72 (m, 3H), 1.55–1.34 (m, 7H), 1.32–1.23 (m, 3H), 1.22–1.15 (m, 1H), 1.14–0.96 (m, 7H), 0.95–0.86 (m, 6H), 0.84 (d, *J* = 6.5 Hz, 3H), 0.79 (dd, *J* = 6.6, 2.7 Hz, 6H), 0.60 (s, 3H). **<sup>13</sup>C-NMR** (125 MHz, CDCl<sub>3</sub>) δ = 170.1 (C<sub>q</sub>), 168.7 (C<sub>q</sub>), 149.4 (C<sub>q</sub>), 139.9 (C<sub>q</sub>), 139.4 (C<sub>q</sub>), 133.9 (CH), 131.1 (CH), 123.6 (C<sub>q</sub>), 123.0 (CH), 122.9 (CH), 119.3 (CH), 76.2 (CH), 75.1 (CH), 56.8 (CH), 56.3 (CH), 50.2 (CH), 42.5 (C<sub>q</sub>), 40.2 (CH<sub>2</sub>), 39.9 (CH<sub>2</sub>), 39.7 (CH<sub>2</sub>), 38.2 (CH<sub>2</sub>), 38.1 (CH<sub>2</sub>), 37.1 (CH<sub>2</sub>), 36.8 (C<sub>q</sub>), 36.4 (CH<sub>2</sub>), 36.0 (CH), 32.1 (CH<sub>2</sub>), 32.0 (CH), 28.4 (CH<sub>2</sub>), 28.2 (CH), 27.9 (CH<sub>2</sub>), 27.8 (CH<sub>2</sub>), 24.5 (CH<sub>2</sub>), 24.0 (CH<sub>2</sub>), 23.0 (CH<sub>3</sub>), 22.8 (CH<sub>3</sub>), 21.2 (CH<sub>2</sub>), 19.5 (CH<sub>3</sub>), 18.9 (CH<sub>3</sub>), 17.5 (CH<sub>3</sub>), 12.1 (CH<sub>3</sub>). **IR** (ATR):  $\tilde{\nu}$  = 2935, 1758, 1731, 1200, 1171, 1047 cm<sup>-1</sup>. **M.p.**: 134–135 °C. **MS** (ESI) *m/z* (relative intensity): 597 (100) [M+Na]<sup>+</sup>. **HR-MS** (ESI) *m/z* calc. for C<sub>38</sub>H<sub>54</sub>O<sub>4</sub> [M+Na]<sup>+</sup>: 597.3914, found: 597.3907.

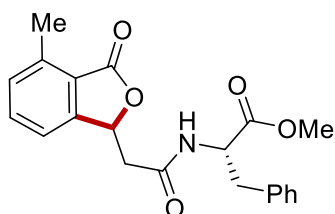
The spectral data are in accordance with those reported in the literature.<sup>[193b]</sup>

**160bc**

### ***N*-Isopropyl-2-(4-methyl-3-oxo-1,3-dihydroisobenzofuran-1-yl)acetamide**

The general procedure A was followed using **19b** (68.1 mg, 0.50 mmol) and **159c** (28.3 mg, 0.25 mmol) at 100 °C for 18 h. Purification by column chromatography on silica gel (*n*hexane/EtOAc = 3:1 to 2:1) yielded **160bc** (46.3 mg, 75%) as a white solid.

**<sup>1</sup>H-NMR** (300 MHz, CDCl<sub>3</sub>):  $\delta$  = 7.45 (dd, *J* = 7.6, 7.6 Hz, 1H), 7.26–7.17 (m, 2H), 5.81–5.70 (m, 1H), 4.12–3.92 (m, 1H), 2.63–2.59 (m, 2H), 2.57 (s, 3H), 1.12 (d, *J* = 6.6 Hz, 3H), 1.07 (d, *J* = 6.6 Hz, 3H). **<sup>13</sup>C-NMR** (125 MHz, CDCl<sub>3</sub>)  $\delta$  = 170.2 (C<sub>q</sub>), 167.4 (C<sub>q</sub>), 149.6 (C<sub>q</sub>), 139.8 (C<sub>q</sub>), 134.1 (CH), 131.1 (CH), 123.2 (C<sub>q</sub>), 119.7 (CH), 77.2 (CH), 42.5 (CH<sub>2</sub>), 41.9 (CH), 22.8 (CH<sub>3</sub>), 17.5 (CH<sub>3</sub>). **IR** (ATR):  $\tilde{\nu}$  = 3274, 2968, 2925, 1741, 1649, 1551, 1395, 1215, 1088, 998 cm<sup>-1</sup>. **M.p.**: 156–158 °C. **MS** (ESI) *m/z* (relative intensity): 270 (100) [M+Na]<sup>+</sup>, 265 (15) [M+NH<sub>4</sub>]<sup>+</sup>, 248 (80) [M+H]<sup>+</sup>. **HR-MS** (ESI) *m/z* calc. for C<sub>14</sub>H<sub>18</sub>NO<sub>3</sub> [M+H]<sup>+</sup>: 248.1281, found: 248.1281.

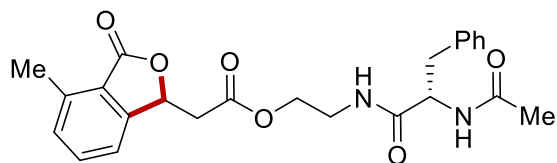
**160bd**

### **Methyl (2-((-4-methyl-3-oxo-1,3-dihydroisobenzofuran-1-yl)acetyl)-*L*-phenylalaninate**

The general procedure A was followed using **19b** (68.1 mg, 0.50 mmol) and **159d** (58.4 mg, 0.25 mmol) at 100 °C for 18 h. After the compound was purified by column chromatography on silica gel (CH<sub>2</sub>Cl<sub>2</sub>/MeOH = 99:1 to 98:2), remaining starting material was removed by extraction from sat. NaHCO<sub>3</sub> with CH<sub>2</sub>Cl<sub>2</sub> to obtain the desired product **160bd** (61.2 mg, 67%) as a brownish solid.

**<sup>1</sup>H-NMR** (600 MHz, CDCl<sub>3</sub>):  $\delta$  = 7.49–7.43 (m, 1H), 7.30–7.26 (m, 1H), 7.26–7.07 (m, 6H), 6.44–6.32 (m, 1H), 5.79–5.72 (m, 1H), 4.93–4.85 (m, 1H), 3.70–3.69 (m, 3H), 3.19–3.12 (m, 1H), 3.11–3.01 (m, 1H), 2.76–2.68 (m, 1H), 2.68–2.58 (m, 4H). **<sup>13</sup>C-NMR** (125 MHz,

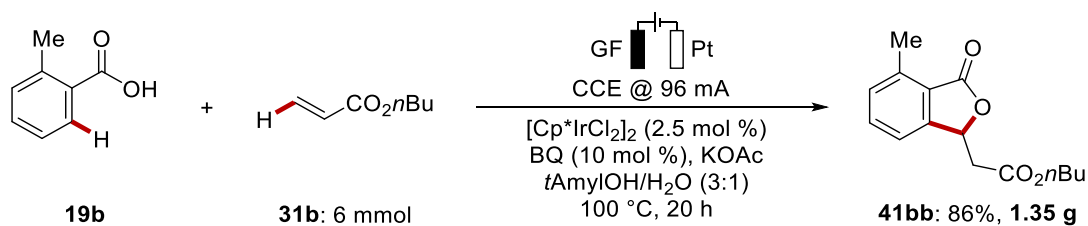
$\text{CDCl}_3$ )  $\delta$  = 171.6 ( $\text{C}_q$ ), 169.9 ( $\text{C}_q$ ), 168.0 ( $\text{C}_q$ ), 149.5 ( $\text{C}_q$ ), 139.8 ( $\text{C}_q$ ), 135.5 ( $\text{C}_q$ ), 134.0 ( $\text{CH}$ ), 131.0 ( $\text{CH}$ ), 129.4 ( $\text{CH}$ ), 128.7 ( $\text{CH}$ ), 127.1 ( $\text{CH}$ ), 123.2 ( $\text{C}_q$ ), 119.6 ( $\text{CH}$ ), 76.6 ( $\text{CH}$ ), 53.5 ( $\text{CH}$ ), 52.5 ( $\text{CH}_3$ ), 41.7 ( $\text{CH}_2$ ), 37.9 ( $\text{CH}_2$ ), 17.5 ( $\text{CH}_3$ ). **IR** (ATR):  $\tilde{\nu}$  = 3314, 3062, 2952, 1743, 1652, 1534, 1203, 1048, 1005  $\text{cm}^{-1}$ . **M.p.**: 136–138 °C. **MS** (ESI)  $m/z$  (relative intensity): 417 (25), 389 (20), 366 (100)  $[\text{M}-\text{H}]^-$ , 283 (40). **HR-MS** (ESI)  $m/z$  calc. for  $\text{C}_{21}\text{H}_{20}\text{NO}_5$   $[\text{M}-\text{H}]^-$ : 366.1347, found: 366.1344.

**160be**

### 2-((*S*)-2-Acetamido-3-phenylpropanamido)ethyl-2-(4-methyl-3-oxo-1,3-dihydroisobenzofuran-1-yl)acetate

The general procedure A was followed using **19b** (68.1 mg, 0.50 mmol) and **159e** (76.1 mg, 0.25 mmol) at 100 °C for 18 h. After the compound was purified by column chromatography on silica gel ( $\text{CH}_2\text{Cl}_2/\text{MeOH}$  = 98:2 to 96:4), remaining starting material was removed by extraction from sat.  $\text{NaHCO}_3$  with  $\text{CH}_2\text{Cl}_2$  to obtain the desired product **160be** (85.5 mg, 78%) as a brownish solid.

**$^1\text{H-NMR}$**  (600 MHz,  $\text{CDCl}_3$ ):  $\delta$  = 7.50–7.45 (m, 1H), 7.23 (m, 1H), 7.21–7.05 (m, 6H), 6.74–6.69 (m, 1H), 6.62–6.57 (m, 1H), 5.71–5.65 (m, 1H), 4.65–4.54 (m, 1H), 4.15–4.00 (m, 2H), 3.48–3.28 (m, 2H), 3.07–3.00 (m, 1H), 2.98–2.92 (m, 1H), 2.90–2.83 (m, 1H), 2.67–2.59 (m, 4H), 1.88 (d,  $J$  = 4.2 Hz, 3H).  **$^{13}\text{C-NMR}$**  (125 MHz,  $\text{CDCl}_3$ )  $\delta$  = 171.5 ( $\text{C}_q$ ), 170.5 ( $\text{C}_q$ ), 170.2 ( $\text{C}_q$ ), 169.0 ( $\text{C}_q$ ), 149.0 ( $\text{C}_q$ ), 140.0 ( $\text{C}_q$ ), 136.9 ( $\text{C}_q$ ), 134.2 ( $\text{CH}$ ), 131.3 ( $\text{CH}$ ), 129.3 ( $\text{CH}$ ), 128.5 ( $\text{CH}$ ), 126.8 ( $\text{CH}$ ), 123.2 ( $\text{C}_q$ ), 119.2 ( $\text{CH}$ ), 76.3 ( $\text{CH}$ ), 63.6 ( $\text{CH}_2$ ), 54.8 ( $\text{CH}$ ), 39.8 ( $\text{CH}_2$ ), 38.4 ( $\text{CH}_2$ ), 38.1 ( $\text{CH}_2$ ), 23.2 ( $\text{CH}_3$ ), 17.5 ( $\text{CH}_3$ ). **IR** (ATR):  $\tilde{\nu}$  = 3297, 3074, 2930, 1753, 1648, 1541, 1171, 1048, 1009  $\text{cm}^{-1}$ . **M.p.**: 172–173 °C. **MS** (ESI)  $m/z$  (relative intensity): 461 (100)  $[\text{M}+\text{Na}]^+$ , 439 (25)  $[\text{M}+\text{H}]^+$ . **HR-MS** (ESI)  $m/z$  calc. for  $\text{C}_{24}\text{H}_{27}\text{N}_2\text{O}_4$   $[\text{M}+\text{H}]^+$ : 439.1864, found: 439.1859.

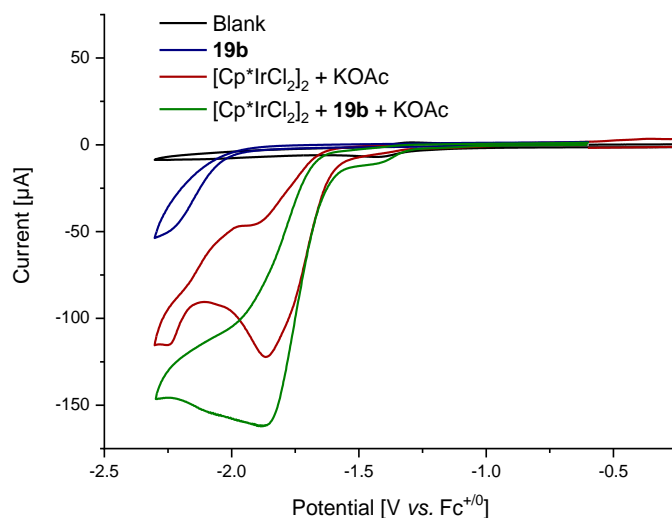
5.3.2 Gram Scale Synthesis of **41bb**

In an undivided cell with a GF anode (25 mm  $\times$  50 mm  $\times$  6.0 mm) and a platinum cathode (25 mm  $\times$  50 mm  $\times$  0.25 mm), **19b** (1.02 g, 7.50 mmol), **31b** (768 mg, 6.00 mmol), KOAc (1.18 g, 12.0 mmol), BQ (65 mg, 0.60 mmol) and [Cp\*IrCl<sub>2</sub>]<sub>2</sub> (119 mg, 0.15 mmol) were dissolved in *t*AmylOH/H<sub>2</sub>O (3:1, 50 mL). Electrocatalysis was performed at 100 °C with a constant current of 96 mA maintained for 20 h. The RVC anode was washed with EtOAc (3  $\times$  30 mL) in an ultrasonic bath. Evaporation of the solvent and subsequent column chromatography on silica gel (*n*hexane/EtOAc = 10:1) yielded **41bb** (1.35 g, 86%) as a colorless oil.

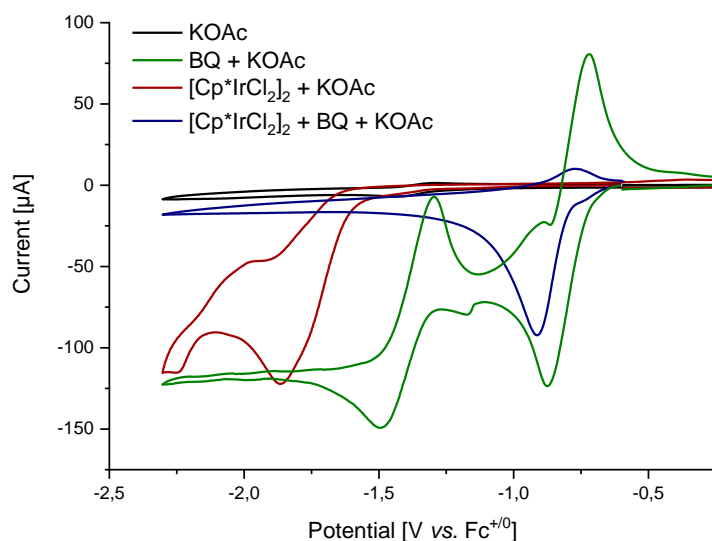


**Figure 5.3.1** Set-up for the multi-gram scale reaction of **41bb**.

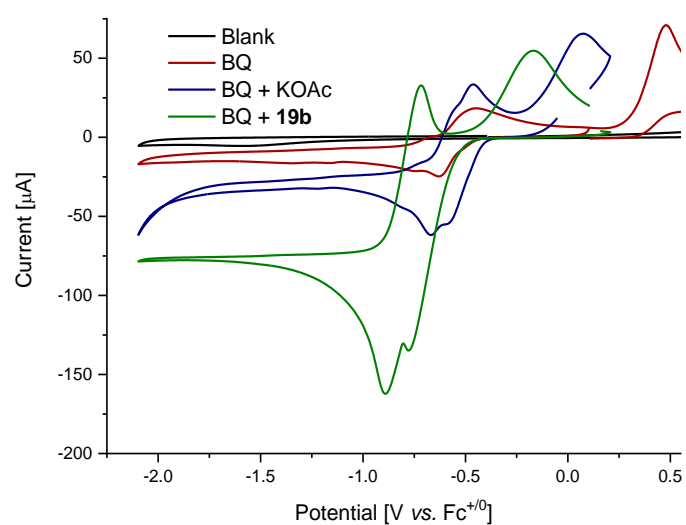
### 5.3.3 Cyclic Voltammetry



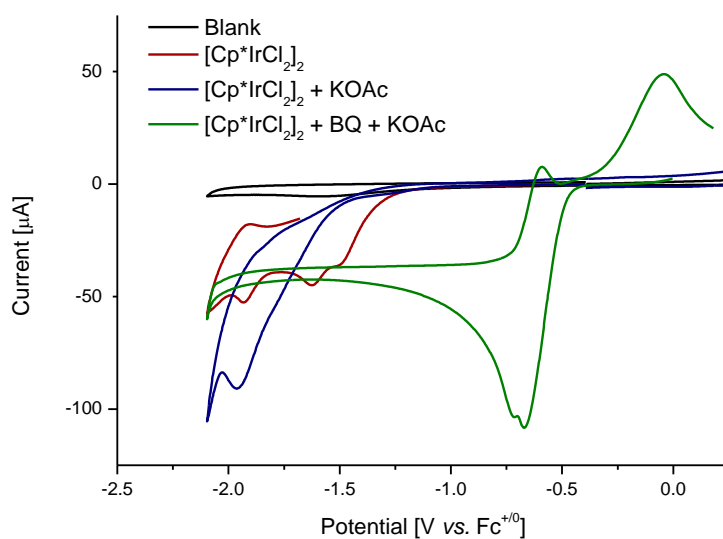
**Figure 5.3.2** Cyclic voltammograms in MeCN with *n*Bu<sub>4</sub>NPF<sub>6</sub> (0.1 M) at 100 mV/s with a GC working electrode. blank (black), **19b** (blue), [Cp\*IrCl<sub>2</sub>]<sub>2</sub> + KOAc (red), [Cp\*IrCl<sub>2</sub>]<sub>2</sub> + **19b** + KOAc (green). Concentrations of substrates 3.0 mM, [Cp\*IrCl<sub>2</sub>]<sub>2</sub> (1.5 mM), KOAc (12 mM).



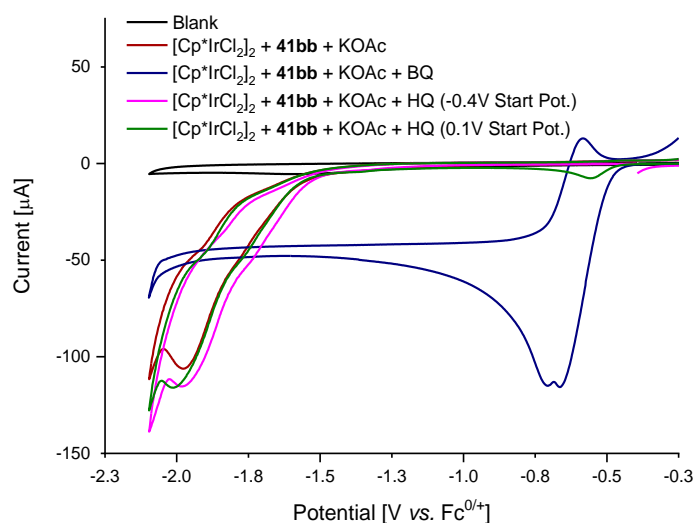
**Figure 5.3.3** Cyclic voltammetry in MeCN with *n*Bu<sub>4</sub>NPF<sub>6</sub> (0.1 M) at 100 mV/s and a GC working electrode. KOAc (black), benzoquinone and KOAc (green); [Cp\*IrCl<sub>2</sub>]<sub>2</sub> and KOAc (red); [Cp\*IrCl<sub>2</sub>]<sub>2</sub> and KOAc (red); [Cp\*IrCl<sub>2</sub>]<sub>2</sub>; benzoquinone and KOAc (blue). Concentration of quinones (3.0 mM), [Cp\*IrCl<sub>2</sub>]<sub>2</sub> (1.5 mM) and KOAc (12 mM).



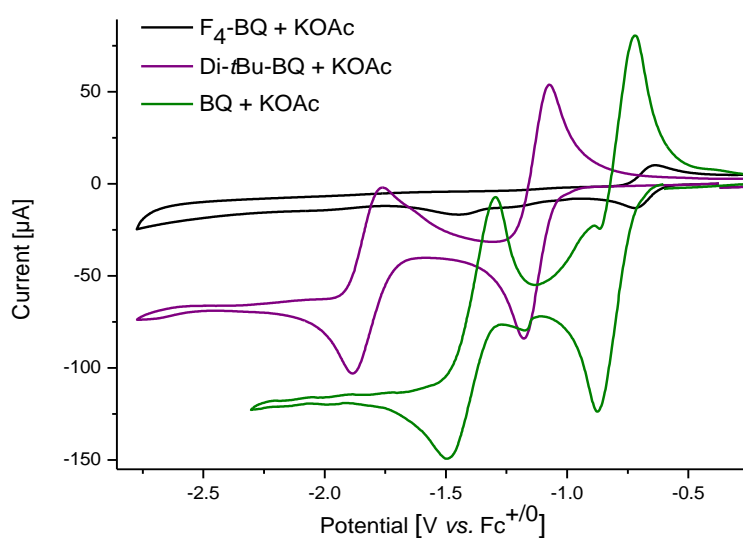
**Figure 5.3.4** Cyclic voltammograms in MeOH with  $n\text{Bu}_4\text{NPF}_6$  (0.1) at 100 mV/s with GC working electrode. Blank (black); BQ (red); BQ + KOAc (blue); BQ + **1a** (green). Concentrations of substrates (3.0 mM)  $[\text{Cp}^*\text{IrCl}_2]_2$  (1.5 mM), KOAc 12 mM).



**Figure 5.3.5** Cyclic voltammograms in MeOH with  $n\text{Bu}_4\text{NPF}_6$  (0.1 M) at 100 mV/s and with GC working electrode. Blank (black);  $[\text{Cp}^*\text{IrCl}_2]_2$  (red);  $[\text{Cp}^*\text{IrCl}_2]_2$  + KOAc (blue);  $[\text{Cp}^*\text{IrCl}_2]_2$  + BQ + KOAc (green). Concentrations of substrates (3.0 mM),  $[\text{Cp}^*\text{IrCl}_2]_2$  (1.5 mM), KOAc (12 mM).

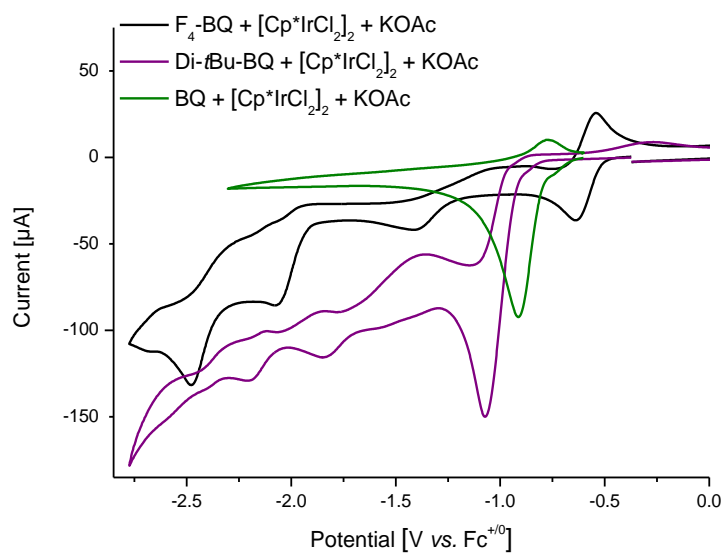


**Figure 5.3.6** Cyclic voltammograms in MeOH with  $n\text{Bu}_4\text{NPF}_6$  (0.1 M) at 100 mV/s with GC working electrode. Blank (black);  $[\text{Cp}^*\text{IrCl}_2]_2 + \mathbf{41bb} + \text{KOAc}$  (red);  $[\text{Cp}^*\text{IrCl}_2]_2 + \mathbf{41bb} + \text{KOAc} + \text{BQ}$  (blue);  $[\text{Cp}^*\text{IrCl}_2]_2 + \mathbf{41bb} + \text{KOAc} + \text{HQ}$  (-0.4 V Start Potential) (pink);  $[\text{Cp}^*\text{IrCl}_2]_2 + \mathbf{41bb} + \text{KOAc} + \text{HQ}$  (0.1 V Start Potential) (green). Concentrations of substrates (3 mM),  $[\text{Cp}^*\text{IrCl}_2]_2$  (1.5 mM). KOAc (12 mM).



**Figure 5.3.7** Cyclic voltammetry in MeCN with  $n\text{Bu}_4\text{NPF}_6$  (0.1 M) at 100 mV/s and a GC working electrode. tetrafluoro benzoquinone and KOAc (black); 2,6-di-*tert*-butyl benzoquinone and KOAc (purple); benzoquinone and KOAc (green). Concentrations of quinones (3 mM) and KOAc (12 mM).

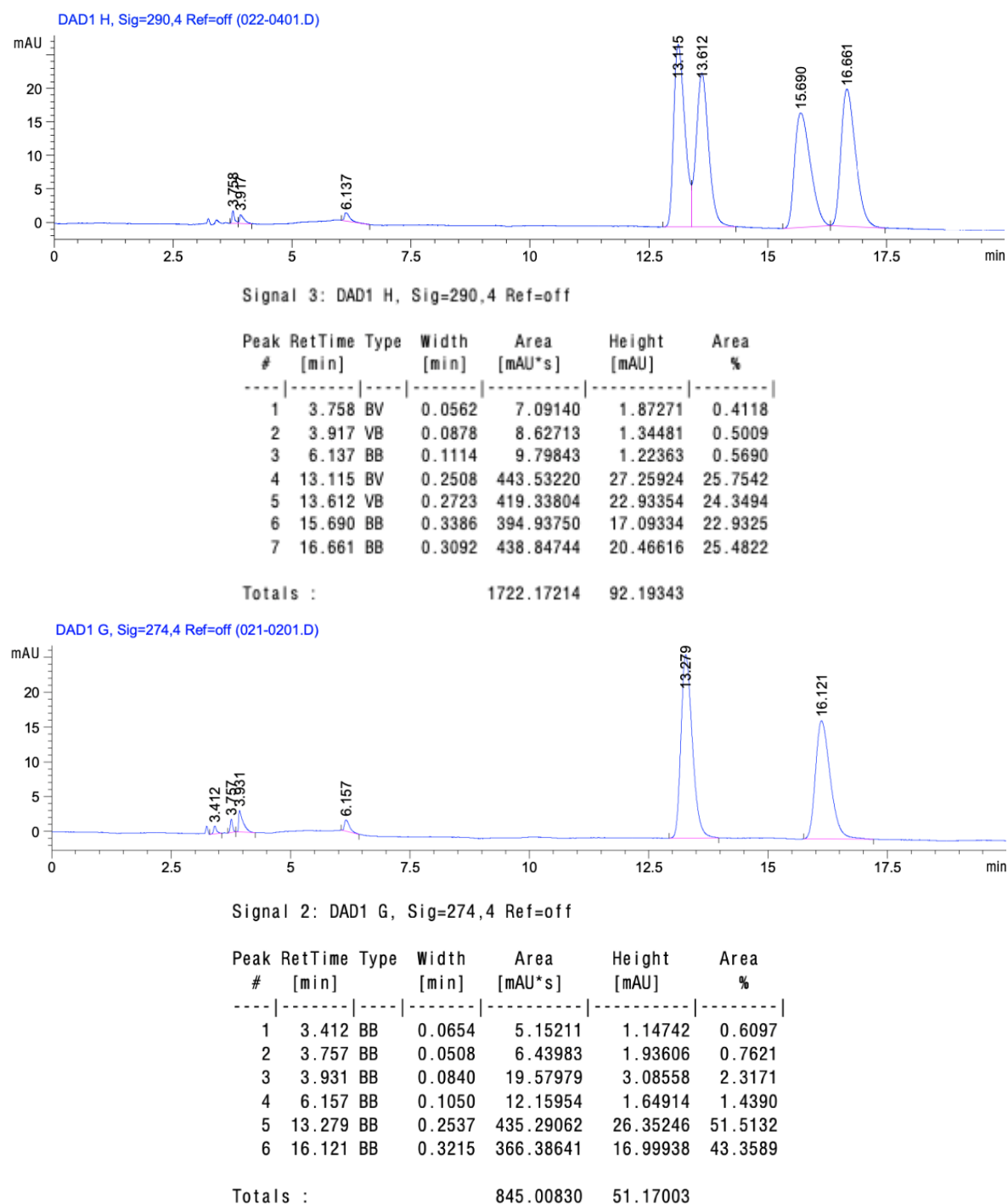




**Figure 5.3.8** Cyclic voltammetry in MeCN with  $n\text{Bu}_4\text{NPF}_6$  (0.1 M) at 100 mV/s and a GC working electrode.  $[\text{Cp}^*\text{IrCl}_2]_2$ , tetrafluoro benzoquinone and KOAc (black);  $[\text{Cp}^*\text{IrCl}_2]_2$ , 2,6-di-*tert*-butyl benzoquinone and KOAc (purple);  $[\text{Cp}^*\text{IrCl}_2]_2$ , benzoquinone and KOAc (green). Concentration of quinones (3.0 mM),  $[\text{Cp}^*\text{IrCl}_2]_2$  (1.5 mM) and KOAc (12 mM).

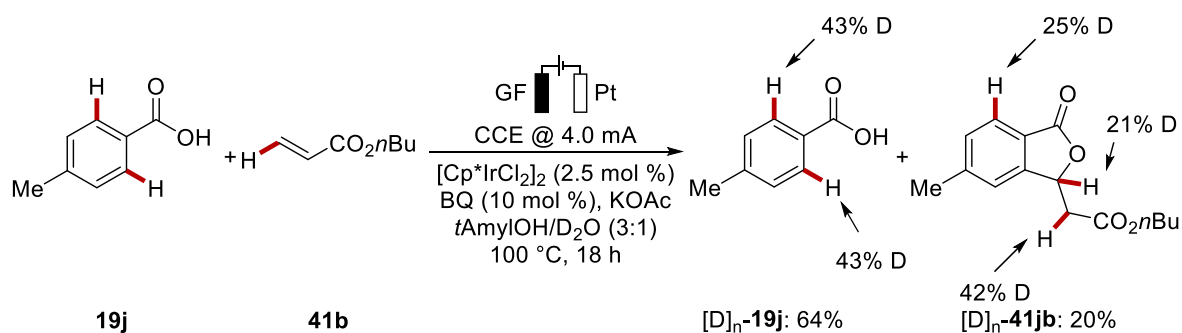
### 5.3.4 Racemization Studies for Phthalide 160bd

A racemic alkene *rac*-**160bd** was employed in the iridoelectro-catalyzed C–H activation and the products were analyzed by HPLC, showing that no racemization of the amino acid backbone occurs.



**Figure 5.3.9** HPLC chromatograms of *rac*-**160bd** and **160bd**. A *CHIRALPAK*<sup>®</sup> *ID* column and *n*hexane/ethyl acetate (60:40, 1.0 mL/min, detection at 250 nm) were used for separation.

## 5.3.5 H/D Exchange Experiment



In an undivided cell with GF anode (10 mm × 15 mm × 6 mm) and a platinum cathode (10 mm × 15 mm × 0.25 mm), **19j** (68 mg, 0.50 mmol), **31b** (32 mg, 0.25 mmol), KOAc (49 mg, 0.50 mmol), BQ (2.7 mg, 10 mol %) and [Cp\*IrCl<sub>2</sub>]<sub>2</sub> (5.0 mg, 2.5 mol %) were dissolved in *t*AmOH/D<sub>2</sub>O (3:1, 4.0 mL). Electrocatalysis was performed at 100 °C with a constant current of 4.0 mA maintained for 18 h. The RVC anode was washed with EtOAc (3 × 10 mL) in an ultrasonic bath. Column chromatography (*n*hexane/EtOAc = 9:1 to 4:1 + 0.25% AcOH) yielded **[D]<sub>n</sub>-19j** (43.7 mg, 64%) as a white solid and **[D]<sub>n</sub>-41jb** (26.3 mg, 20%) as a colorless oil. The D-incorporating was estimated by <sup>1</sup>H-NMR spectroscopy and confirmed by mass spectrometry.

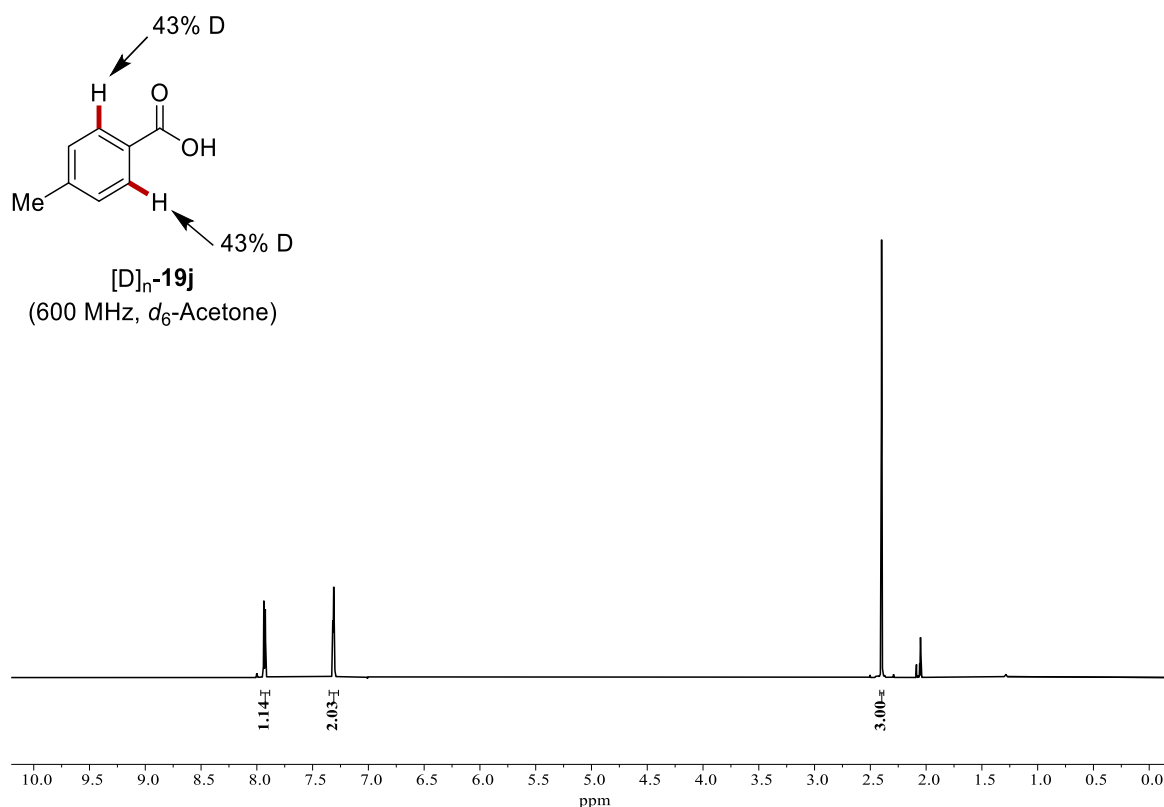
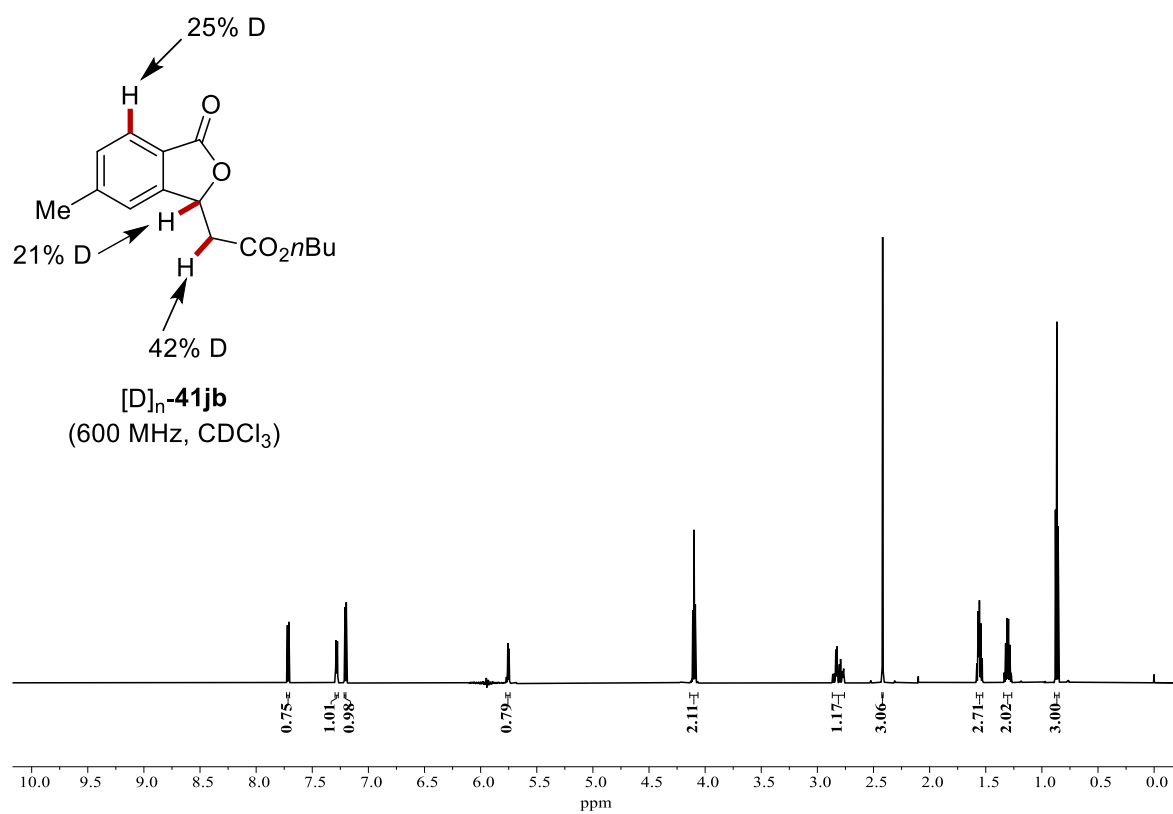
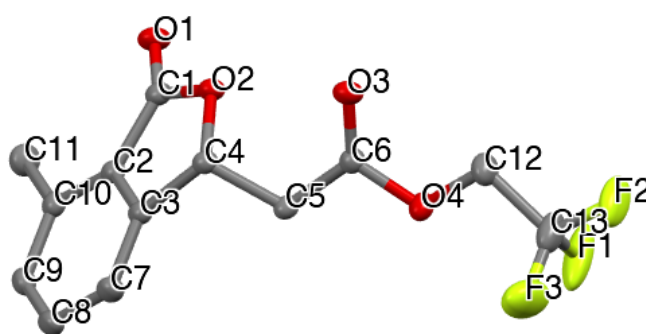


Figure 5.3.10 <sup>1</sup>H-NMR of isolated **[D]<sub>n</sub>-19j** from the H/D experiment.



**Figure 5.3.11** <sup>1</sup>H-NMR of isolated [D]<sub>n</sub>-41**jb** from the H/D experiment.

## 5.3.6 Crystallographic Data of Phthalide 41be

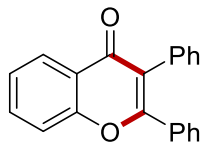


41be

Identification code	CCDC 2161280
Empirical formula	C <sub>13</sub> H <sub>11</sub> F <sub>3</sub> O <sub>4</sub>
Formula weight	288.22
Temperature/K	100.03
Crystal system	triclinic
Space group	P-1
a/Å	9.5412(15)
b/Å	10.7708(13)
c/Å	12.8438(19)
α/°	86.373(4)
β/°	82.056(4)
γ/°	88.893(4)
Volume/Å <sup>3</sup>	1304.6(3)
Z	4
ρ <sub>calc</sub> /cm <sup>3</sup>	1.467
μ/mm <sup>-1</sup>	0.135
F(000)	592.0
Crystal size/mm <sup>3</sup>	0.322 × 0.31 × 0.15
Radiation	MoKα (λ = 0.71073)
2θ range for data collection/°	4.31 to 62.996
Index ranges	-13 ≤ h ≤ 14, -15 ≤ k ≤ 15, 0 ≤ l ≤ 18
Reflections collected	8585
Independent reflections	8585 [R <sub>int</sub> = ?, R <sub>sigma</sub> = 0.0216]
Data/restraints/parameters	8585/72/404
Goodness-of-fit on F <sup>2</sup>	1.046
Final R indexes [I >= 2σ (I)]	R <sub>1</sub> = 0.0376, wR <sub>2</sub> = 0.1022
Final R indexes [all data]	R <sub>1</sub> = 0.0424, wR <sub>2</sub> = 0.1060
Largest diff. peak/hole / e Å <sup>-3</sup>	0.44/-0.24

## 5.4 Rhodaelectro-Catalyzed Assembly of Chromones *via* formyl C–H Activation

### 5.4.1 Characterization Data



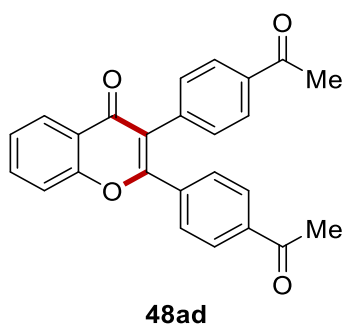
**48aa**

#### 2,3-Diphenyl-4*H*-chromen-4-one

The general procedure B was followed using **26a** (78  $\mu$ L, 0.75 mmol) and **17a** (44.5 mg, 0.25 mmol) at 100  $^{\circ}$ C for 3.5 h. Purification by column chromatography on silica gel (*n*hexane/EtOAc = 12:1 to 10:1) yielded **48aa** (68.2 mg, 92%) as a white solid.

**$^1$ H-NMR** (400 MHz,  $\text{CDCl}_3$ ):  $\delta$  = 8.33 (d,  $J$  = 8.8 Hz, 1H), 7.73 (dd,  $J$  = 7.5 Hz, 7.5 Hz, 1H), 7.57 (d,  $J$  = 8.4 Hz, 1H), 7.49–7.41 (m, 3H), 7.39–7.23 (m, 8H).  **$^{13}$ C-NMR** (101 MHz,  $\text{CDCl}_3$ ):  $\delta$  = 177.4 ( $\text{C}_q$ ), 161.6 ( $\text{C}_q$ ), 156.2 ( $\text{C}_q$ ), 133.8 (CH), 133.4 ( $\text{C}_q$ ), 133.0 ( $\text{C}_q$ ), 131.3 (CH), 130.2 (CH), 129.7 (CH), 128.3 (CH), 128.2 (CH), 127.7 (CH), 126.5 (CH), 125.2 (CH), 123.6 ( $\text{C}_q$ ), 123.0 ( $\text{C}_q$ ), 118.1 (CH). **IR** (ATR):  $\tilde{\nu}$  = 1633, 1607, 1559, 1373, 1294, 1222, 915, 756, 695  $\text{cm}^{-1}$ . **M.p.**: 143–144  $^{\circ}$ C. **MS** (ESI)  $m/z$  (relative intensity): 299 (100)  $[\text{M}+\text{H}]^+$ , 321 (40)  $[\text{M}+\text{Na}]^+$ , 619 (30)  $[2\text{M}+\text{Na}]^+$ . **HR-MS** (ESI)  $m/z$  calcd for  $\text{C}_{21}\text{H}_{15}\text{O}_2$   $[\text{M}+\text{H}]^+$ : 299.1067, found: 299.1054.

The spectral data are in accordance with those reported in the literature.<sup>[254]</sup>

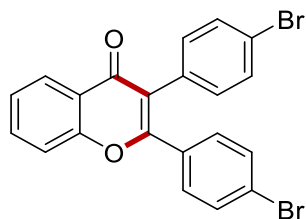


### 2,3-Bis(4-acetophenon)-4*H*-chromen-4-one

The general procedure B was followed using **26a** (78  $\mu$ L, 0.75 mmol) and **17d** (65.5 mg, 0.25 mmol) at 100  $^{\circ}$ C for 7 h. Purification by column chromatography on silica gel (*n*hexane/EtOAc = 2:1) yielded **48ad** (57.0 mg, 60%) as a brown solid.

The general procedure D was followed using **26a** (78  $\mu$ L, 0.75 mmol) and **17d** (65.5 mg, 0.25 mmol) at 100  $^{\circ}$ C for 7 h. Purification by column chromatography on silica gel (*n*hexane/EtOAc = 4:1 to 3:2) yielded **48ad** (32.6 mg, 34%) as a brown solid among other side products.

**$^1$ H-NMR** (300 MHz,  $\text{CDCl}_3$ ):  $\delta$  = 8.28 (d,  $J$  = 7.8 Hz, 1H), 7.89 (d,  $J$  = 8.3 Hz, 2H), 7.85 (d,  $J$  = 8.4 Hz, 2H), 7.74 (dd,  $J$  = 7.8 Hz, 7.8 Hz, 1H), 7.55 (d,  $J$  = 8.4 Hz, 1H), 7.51–7.45 (m, 3H), 7.32 (d,  $J$  = 8.2 Hz, 2H), 2.58 (s, 3H), 2.57 (s, 3H).  **$^{13}$ C-NMR** (75 MHz,  $\text{CDCl}_3$ ):  $\delta$  = 197.9 ( $\text{C}_q$ ), 197.2 ( $\text{C}_q$ ), 176.8 ( $\text{C}_q$ ), 160.6 ( $\text{C}_q$ ), 156.1 ( $\text{C}_q$ ), 138.1 ( $\text{C}_q$ ), 137.8 ( $\text{C}_q$ ), 137.2 ( $\text{C}_q$ ), 136.4 ( $\text{C}_q$ ), 134.3 (CH), 131.6 (CH), 129.9 (CH), 128.4 (CH), 128.2 (CH), 126.5 (CH), 125.7 (CH), 123.4 ( $\text{C}_q$ ), 122.9 ( $\text{C}_q$ ), 118.2 (CH), 26.8 ( $\text{CH}_3$ ), 26.7 ( $\text{CH}_3$ ). **IR** (ATR):  $\tilde{\nu}$  = 2923, 2853, 1680, 1633, 1598, 1463, 1375, 1259, 1146, 956  $\text{cm}^{-1}$ . **M.p.**: 165–166  $^{\circ}$ C. **MS** (ESI)  $m/z$  (relative intensity): 383 (100)  $[\text{M}+\text{H}]^+$ , 787 (50)  $[2\text{M}+\text{Na}]^+$ . **HR-MS** (ESI)  $m/z$  calcd for  $\text{C}_{25}\text{H}_{19}\text{O}_4$   $[\text{M}+\text{H}]^+$ : 383.1283, found: 383.1278.

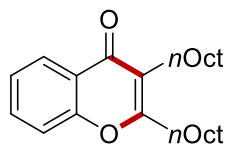
**48ae**

### 2,3-Bis(4-bromophenyl)-4H-chromen-4-one

The general procedure B was followed using **26a** (78  $\mu$ L, 0.75 mmol) and **17e** (84.0 mg, 0.25 mmol) at 100 °C for 7 h. Purification by column chromatography on silica gel (*n*hexane/EtOAc = 8:1) yielded **48ae** (79.6 mg, 69%) as a white solid.

The general procedure D was followed using **26a** (78  $\mu$ L, 0.75 mmol) and **17e** (84.0 mg, 0.25 mmol) at 100 °C for 7 h. Purification by column chromatography on silica gel (*n*hexane/EtOAc = 8:1) yielded **48ae** (44.5 mg, 39%).

**<sup>1</sup>H-NMR** (400 MHz, CDCl<sub>3</sub>):  $\delta$  = 8.19 (dd,  $J$  = 8.0, 1.7 Hz, 1H), 7.64 (ddd,  $J$  = 8.7, 7.1, 1.7 Hz, 1H), 7.44 (dd,  $J$  = 8.5, 1.0 Hz, 1H), 7.40–7.34 (m, 5H), 7.18 (m,  $J$  = 8.5 Hz, 2H), 7.01–7.18 (m,  $J$  = 8.5 Hz, 2H). **<sup>13</sup>C-NMR** (101 MHz, CDCl<sub>3</sub>):  $\delta$  = 176.9 (C<sub>q</sub>), 160.5 (C<sub>q</sub>), 156.0 (C<sub>q</sub>), 134.1 (CH), 132.9 (CH), 131.9 (C<sub>q</sub>), 131.8 (CH), 131.7 (CH), 131.6 (C<sub>q</sub>), 131.2 (CH), 126.5 (CH), 125.5 (CH), 125.1 (C<sub>q</sub>), 123.4 (C<sub>q</sub>), 122.3 (C<sub>q</sub>), 122.1 (C<sub>q</sub>), 118.1 (CH). **IR** (ATR):  $\tilde{\nu}$  = 1637, 1608, 1459, 1368, 1216, 1061, 1005, 814, 753, 495 cm<sup>-1</sup>. **M.p.**: 184–186 °C. **MS** (ESI)  $m/z$  (relative intensity): 456 (100) [M+H]<sup>+</sup> (<sup>79</sup>Br<sup>81</sup>Br), 478 (40) [M+Na]<sup>+</sup> (<sup>79</sup>Br<sup>81</sup>Br), 934 (60) [2M+Na]<sup>+</sup> (<sup>79</sup>Br<sup>81</sup>Br). **HR-MS** (ESI)  $m/z$  calcd for C<sub>21</sub>H<sub>13</sub><sup>79</sup>Br<sup>81</sup>BrO<sub>2</sub> [M+H]<sup>+</sup>: 456.9258, found: 456.9252.

**48af**

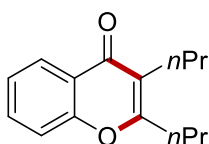
### 2,3-Dioctyl-4H-chromen-4-one

The general procedure B was followed using **26a** (78  $\mu$ L, 0.75 mmol) and **17f** (62.6 mg, 0.25 mmol) at 100 °C for 3.5 h. Purification by column chromatography on silica gel (*n*hexane/EtOAc = 40:1 to 20:1) yielded **48af** (72.9 mg, 79%) as a colorless oil.



The general procedure D was followed using **26a** (78  $\mu\text{L}$ , 0.75 mmol) and **17f** (62.6 mg, 0.25 mmol) at 100  $^{\circ}\text{C}$  for 7 h. Purification by column chromatography on silica gel (*n*hexane/EtOAc = 40:1 to 20:1) yielded **48af** (26.8 mg, 29%).

**$^1\text{H-NMR}$**  (400 MHz,  $\text{CDCl}_3$ ):  $\delta$  = 8.18 (dd,  $J$  = 8.0, 1.7 Hz, 1H), 7.59 (ddd,  $J$  = 8.6, 7.0, 1.7 Hz, 1H), 7.39–7.29 (m, 2H), 2.73–2.64 (m, 2H), 2.57–2.47 (m, 2H), 1.74 (m, 2H), 1.53–1.45 (m, 2H), 1.42–1.20 (m, 20H), 0.87 (m, 6H).  **$^{13}\text{C-NMR}$**  (101 MHz,  $\text{CDCl}_3$ ):  $\delta$  = 178.0 ( $\text{C}_q$ ), 165.7 ( $\text{C}_q$ ), 156.0 ( $\text{C}_q$ ), 132.9 (CH), 126.0 (CH), 124.4 (CH), 123.1 ( $\text{C}_q$ ), 121.5 ( $\text{C}_q$ ), 117.7 (CH), 32.0 ( $\text{CH}_2$ ), 32.0 ( $\text{CH}_2$ ), 32.0 ( $\text{CH}_2$ ), 30.0 ( $\text{CH}_2$ ), 29.6 ( $\text{CH}_2$ ), 29.5 ( $\text{CH}_2$ ), 29.5 ( $\text{CH}_2$ ), 29.5 ( $\text{CH}_2$ ), 29.4 ( $\text{CH}_2$ ), 29.3 ( $\text{CH}_2$ ), 27.7 ( $\text{CH}_2$ ), 24.9 ( $\text{CH}_2$ ), 22.8 ( $\text{CH}_2$ ), 22.8 ( $\text{CH}_2$ ), 14.2 ( $\text{CH}_3$ ), 14.2 ( $\text{CH}_3$ ). **IR** (ATR):  $\tilde{\nu}$  = 2922, 2854, 1637, 1573, 1463, 1387, 1227, 1151, 759, 718  $\text{cm}^{-1}$ . **MS** (ESI)  $m/z$  (relative intensity): 371 (100)  $[\text{M}+\text{H}]^+$ , 393 (20)  $[\text{M}+\text{Na}]^+$ , 741 (40)  $[2\text{M}+\text{H}]^+$ . **HR-MS** (ESI)  $m/z$  calcd for  $\text{C}_{25}\text{H}_{39}\text{O}_2$   $[\text{M}+\text{H}]^+$ : 371.2945, found: 371.2947.



**48ag**

### 2,3-Dipropyl-4H-chromen-4-one

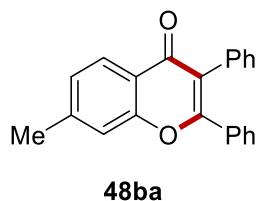
The general procedure B was followed using **26a** (78  $\mu\text{L}$ , 0.75 mmol) and **17g** (27.5 mg, 0.25 mmol) at 100  $^{\circ}\text{C}$  for 7 h. Purification by column chromatography on silica gel (*n*hexane/EtOAc = 25:1 to 15:1) yielded **48ag** (39.0 mg, 68%) as a colorless oil.

The general procedure D was followed using **26a** (78  $\mu\text{L}$ , 0.75 mmol) and **17g** (27.5 mg, 0.25 mmol) at 100  $^{\circ}\text{C}$  for 7 h. Purification by column chromatography on silica gel (*n*hexane/EtOAc = 25:1 to 15:1) yielded **48ag** (17.3 mg, 30%) as a colorless oil among other side products.

**$^1\text{H-NMR}$**  (400 MHz,  $\text{CDCl}_3$ ):  $\delta$  = 8.18 (dd,  $J$  = 7.9, 1.7 Hz, 1H), 7.59 (ddd,  $J$  = 8.7, 7.0, 1.7 Hz, 1H), 7.37 (dd,  $J$  = 8.7, 1.1 Hz, 1H), 7.33 (ddd,  $J$  = 8.1, 7.0, 1.1 Hz, 1H), 2.72–2.64 (m, 2H), 2.57–2.47 (m, 2H), 1.85–1.74 (m, 2H), 1.60–1.47 (m, 2H), 1.04 (t,  $J$  = 7.4 Hz, 3H), 0.98 (t,  $J$  = 7.4 Hz, 3H).  **$^{13}\text{C-NMR}$**  (101 MHz,  $\text{CDCl}_3$ ):  $\delta$  = 178.0 ( $\text{C}_q$ ), 165.5 ( $\text{C}_q$ ), 156.1 ( $\text{C}_q$ ), 133.0 (CH), 126.0 (CH), 124.5 (CH), 123.1 ( $\text{C}_q$ ), 121.4 ( $\text{C}_q$ ), 117.7 (CH), 33.8 ( $\text{CH}_2$ ), 26.8 ( $\text{CH}_2$ ), 22.7 ( $\text{CH}_2$ ), 21.1 ( $\text{CH}_2$ ), 14.3 ( $\text{CH}_3$ ), 14.0 ( $\text{CH}_3$ ). **IR** (ATR):  $\tilde{\nu}$  = 2961, 2930, 1632, 1573, 1462, 1385, 1338, 1229, 1160, 760  $\text{cm}^{-1}$ . **MS** (ESI)  $m/z$  (relative intensity): 231

(100)  $[M+H]^+$ , 253 (40)  $[M+Na]^+$ , 483 (60)  $[2M+Na]^+$ . **HR-MS** (ESI)  $m/z$  calcd for  $C_{15}H_{19}O_2$   $[M+H]^+$ : 231.1380, found: 231.1380.

The spectral data are in accordance with those reported in the literature.<sup>[254]</sup>

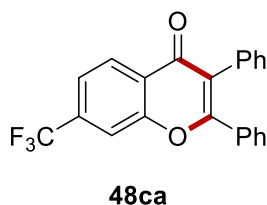


### 7-Methyl-2,3-diphenyl-4H-chromen-4-one

The general procedure B was followed using **26b** (102 mg, 0.75 mmol) and **17a** (44.5 mg, 0.25 mmol) at 100 °C for 3.5 h. Purification by column chromatography on silica gel (*n*hexane/EtOAc = 10:1) yielded **48ba** (72.1 mg, 92%) as a white solid.

**<sup>1</sup>H-NMR** (400 MHz,  $CDCl_3$ ):  $\delta$  = 8.08 (d,  $J$  = 8.1 Hz, 1H), 7.31–7.27 (m, 2H), 7.25–7.19 (m, 3H), 7.19–7.11 (m, 7H), 2.41 (s, 3H). **<sup>13</sup>C-NMR** (101 MHz,  $CDCl_3$ ):  $\delta$  = 177.3 ( $C_q$ ), 161.2 ( $C_q$ ), 156.3 ( $C_q$ ), 145.0 ( $C_q$ ), 133.5 ( $C_q$ ), 133.1 ( $C_q$ ), 131.3 (CH), 130.0 (CH), 129.6 (CH), 128.3 (CH), 128.1 (CH), 127.6 (CH), 126.7 (CH), 126.2 (CH), 122.9 ( $C_q$ ), 121.4 ( $C_q$ ), 117.8 (CH), 22.0 ( $CH_3$ ). **IR** (ATR):  $\tilde{\nu}$  = 1625, 1555, 1420, 1368, 1222, 1167, 776, 745, 694, 618  $cm^{-1}$ . **M.p.**: 175–176 °C. **MS** (ESI)  $m/z$  (relative intensity): 313 (30)  $[M+H]^+$ , 335 (100)  $[M+Na]^+$ , 647 (60)  $[2M+Na]^+$ . **HR-MS** (ESI)  $m/z$  calcd for  $C_{22}H_{17}O_2$   $[M+H]^+$ : 313.1223, found: 313.1226.

The spectral data are in accordance with those reported in the literature.<sup>[255]</sup>

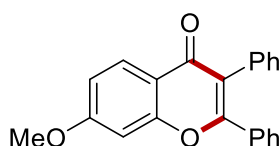


### 2,3-Diphenyl-7-(trifluoromethyl)-4H-chromen-4-one

The general procedure B was followed using **26c** (143 mg, 0.75 mmol) and **17a** (44.5 mg, 0.25 mmol) at 100 °C for 3.5 h. Purification by column chromatography on silica gel (*n*hexane/EtOAc = 15:1) yielded **48ca** (63.5 mg, 69%) as a white solid.

**<sup>1</sup>H-NMR** (400 MHz, CDCl<sub>3</sub>):  $\delta$  = 8.33 (d,  $J$  = 8.3 Hz, 1H), 7.77 (d,  $J$  = 1.5 Hz, 1H), 7.58 (dd,  $J$  = 8.3, 1.5 Hz, 1H), 7.35–7.30 (m, 2H), 7.29–7.17 (m, 6H), 7.16–7.12 (m, 2H). **<sup>13</sup>C-NMR** (101 MHz, CDCl<sub>3</sub>):  $\delta$  = 176.6 (C<sub>q</sub>), 162.3 (C<sub>q</sub>), 155.6 (C<sub>q</sub>), 135.4 (q,  $^2J_{C-F}$  = 33.3 Hz, C<sub>q</sub>), 132.8 (C<sub>q</sub>), 132.3 (C<sub>q</sub>), 131.2 (CH), 130.6 (CH), 129.7 (CH), 128.5 (CH), 128.3 (CH), 128.1 (CH), 127.9 (CH), 125.8 (C<sub>q</sub>), 123.7 (C<sub>q</sub>), 123.3 (q,  $^1J_{C-F}$  = 273.1 Hz, C<sub>q</sub>), 121.5 (q,  $^3J_{C-F}$  = 3.4 Hz, CH), 116.1 (q,  $^3J_{C-F}$  = 4.1 Hz, CH). **<sup>19</sup>F{<sup>1</sup>H}-NMR**  $\delta$  = (377 MHz, CDCl<sub>3</sub>) – 63.02. **IR** (ATR):  $\tilde{\nu}$  = 1633, 1550, 1434, 1349, 1312, 1114, 1039, 915, 748, 691 cm<sup>-1</sup>. **M.p.**: 137–139 °C. **MS** (ESI)  $m/z$  (relative intensity): 367 (40) [M+H]<sup>+</sup>, 389 (100) [M+Na]<sup>+</sup>, 405 (20) [M+K]<sup>+</sup>. **HR-MS** (ESI)  $m/z$  calcd for C<sub>22</sub>H<sub>14</sub>F<sub>3</sub>O<sub>2</sub> [M+H]<sup>+</sup>: 367.0940, found: 367.0943.

The spectral data are in accordance with those reported in the literature.<sup>[255]</sup>



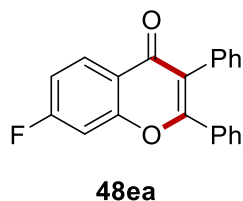
**48da**

### 7-Methoxy-2,3-diphenyl-4H-chromen-4-one

The general procedure B was followed using **26d** (114 mg, 0.75 mmol) and **17a** (44.5 mg, 0.25 mmol) at 100 °C for 3.5 h. Purification by column chromatography on silica gel (*n*hexane/EtOAc = 8:1 to 5:1) yielded **48da** (74.8 mg, 91%) as a yellowish solid.

**<sup>1</sup>H-NMR** (400 MHz, CDCl<sub>3</sub>):  $\delta$  = 8.09 (d,  $J$  = 8.9 Hz, 1H), 7.31–7.26 (m, 2H), 7.25–7.10 (m, 8H), 6.89 (dd,  $J$  = 8.9, 2.4 Hz, 1H), 6.82 (d,  $J$  = 2.4 Hz, 1H), 3.81 (s, 3H). **<sup>13</sup>C-NMR** (101 MHz, CDCl<sub>3</sub>):  $\delta$  = 176.8 (C<sub>q</sub>), 164.2 (C<sub>q</sub>), 161.1 (C<sub>q</sub>), 157.8 (C<sub>q</sub>), 133.4 (C<sub>q</sub>), 133.0 (C<sub>q</sub>), 131.3 (CH), 130.0 (CH), 129.6 (CH), 128.3 (CH), 128.1 (CH), 127.8 (CH), 127.6 (CH), 122.8 (C<sub>q</sub>), 117.5 (C<sub>q</sub>), 114.6 (CH), 100.1 (CH), 55.9 (CH<sub>3</sub>). **IR** (ATR):  $\tilde{\nu}$  = 1621, 1439, 1379, 1250, 1193, 1016, 829, 746, 690, 629 cm<sup>-1</sup>. **M.p.**: 216–218 °C. **MS** (ESI)  $m/z$  (relative intensity): 329 (100) [M+H]<sup>+</sup>, 351 (20) [M+Na]<sup>+</sup>, 679 (50) [2M+Na]<sup>+</sup>. **HR-MS** (ESI)  $m/z$  calcd for C<sub>22</sub>H<sub>17</sub>O<sub>3</sub> [M+H]<sup>+</sup>: 329.1172, found: 329.1176.

The spectral data are in accordance with those reported in the literature.<sup>[255]</sup>

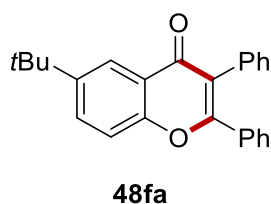


### 7-Fluoro-2,3-diphenyl-4H-chromen-4-one

The general procedure B was followed using **26e** (105 mg, 0.75 mmol) and **17a** (44.5 mg, 0.25 mmol) at 100 °C for 3.5 h. Purification by column chromatography on silica gel (*n*hexane/EtOAc = 15:1) yielded **48ea** (76.7 mg, 97%) as a white solid.

**<sup>1</sup>H-NMR** (400 MHz, CDCl<sub>3</sub>):  $\delta$  = 8.21 (dd,  $J$  = 8.9, 6.3 Hz, 1H), 7.31–7.26 (m, 2H), 7.26–7.15 (m, 6H), 7.14–7.10 (m, 3H), 7.05 (ddd,  $J$  = 8.9, 8.2, 2.4 Hz, 1H). **<sup>13</sup>C-NMR** (101 MHz, CDCl<sub>3</sub>):  $\delta$  = 176.5 (C<sub>q</sub>), 165.8 (d,  $^1J_{C-F}$  = 254.8 Hz, C<sub>q</sub>), 161.8 (C<sub>q</sub>), 157.1 (d,  $^3J_{C-F}$  = 13.4 Hz, C<sub>q</sub>), 133.0 (C<sub>q</sub>), 132.6 (C<sub>q</sub>), 131.2 (CH), 130.3 (CH), 129.6 (CH), 129.0 (d,  $J$  = 10.7 Hz, CH), 128.4 (CH), 128.2 (CH), 127.8 (CH), 123.1 (C<sub>q</sub>), 120.5 (d,  $^4J_{C-F}$  = 2.3 Hz, C<sub>q</sub>), 114.0 (d,  $^2J_{C-F}$  = 22.8 Hz, CH), 104.6 (d,  $^2J_{C-F}$  = 25.1 Hz, CH). **<sup>19</sup>F{<sup>1</sup>H}-NMR** (282 MHz, CDCl<sub>3</sub>):  $\delta$  = –103.1. **IR** (ATR):  $\tilde{\nu}$  = 1640, 1611, 1437, 1373, 1242, 1157, 853, 746, 690, 618 cm<sup>-1</sup>. **M.p.**: 169–170 °C. **MS** (ESI)  $m/z$  (relative intensity): 317 (30) [M+H]<sup>+</sup>, 339 (100) [M+Na]<sup>+</sup>, 655 (40) [2M+Na]<sup>+</sup>. **HR-MS** (ESI)  $m/z$  calcd for C<sub>21</sub>H<sub>14</sub>FO<sub>2</sub> [M+H]<sup>+</sup>: 317.0972, found: 317.0975.

The spectral data are in accordance with those reported in the literature.<sup>[254]</sup>



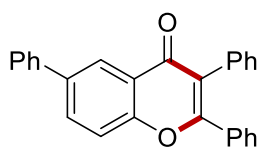
### 6-(*tert*-Butyl)-2,3-diphenyl-4H-chromen-4-one

The general procedure B was followed using **26f** (134 mg, 0.75 mmol) and **17a** (44.5 mg, 0.25 mmol) at 100 °C for 3.5 h. Purification by column chromatography on silica gel (*n*hexane/EtOAc = 20:1) yielded **48fa** (65.2 mg, 74%) as a white solid.

**<sup>1</sup>H-NMR** (400 MHz, CDCl<sub>3</sub>):  $\delta$  = 8.20 (dd,  $J$  = 2.5, 0.5 Hz, 1H), 7.67 (dd,  $J$  = 8.9, 2.5 Hz, 1H), 7.39 (dd,  $J$  = 8.9, 0.5 Hz, 1H), 7.32–7.28 (m, 2H), 7.26–7.11 (m, 8H), 1.31 (s, 9H). **<sup>13</sup>C-NMR** (101 MHz, CDCl<sub>3</sub>):  $\delta$  = 177.7 (C<sub>q</sub>), 161.4 (C<sub>q</sub>), 154.4 (C<sub>q</sub>), 148.5 (C<sub>q</sub>), 133.5 (C<sub>q</sub>),

133.2 (C<sub>q</sub>), 131.7 (CH), 131.4 (CH), 130.1 (CH), 129.6 (CH), 128.3 (CH), 128.1 (CH), 127.6 (CH), 122.9 (C<sub>q</sub>), 122.9 (C<sub>q</sub>), 122.1 (CH), 117.7 (CH), 35.0 (C<sub>q</sub>), 31.5 (CH<sub>3</sub>). **IR** (ATR):  $\tilde{\nu}$  = 1636, 1608, 1486, 1362, 1260, 1219, 924, 828, 765, 697, 516 cm<sup>-1</sup>. **M.p.**: 152–154 °C. **MS** (ESI) *m/z* (relative intensity): 355 (50) [M+H]<sup>+</sup>, 377 (100) [M+Na]<sup>+</sup>, 731 (80) [2M+Na]<sup>+</sup>. **HR-MS** (ESI) *m/z* calcd for C<sub>25</sub>H<sub>23</sub>O<sub>2</sub> [M+H]<sup>+</sup>: 355.1693, found: 355.1694.

The spectral data are in accordance with those reported in the literature.<sup>[254]</sup>

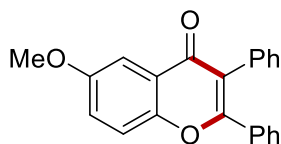


**48ga**

### 2,3,6-Triphenyl-4H-chromen-4-one

The general procedure B was followed using **26g** (149 mg, 0.75 mmol) and **17a** (44.5 mg, 0.25 mmol) at 100 °C for 3.5 h. Purification by column chromatography on silica gel (*n*hexane/EtOAc = 13:1) yielded **48ga** (77.6 mg, 83%) as a white solid. **<sup>1</sup>H-NMR** (500 MHz, CDCl<sub>3</sub>):  $\delta$  = 8.41 (d, *J* = 2.3 Hz, 1H), 7.84 (dd, *J* = 8.7, 2.3 Hz, 1H), 7.61–7.57 (m, 2H), 7.51 (d, *J* = 8.7 Hz, 1H), 7.38 (dd, *J* = 7.7 Hz, 7.7 Hz, 2H), 7.34–7.26 (m, 3H), 7.26–7.14 (m, 8H). **<sup>13</sup>C-NMR** (126 MHz, CDCl<sub>3</sub>):  $\delta$  = 177.4 (C<sub>q</sub>), 161.6 (C<sub>q</sub>), 155.6 (C<sub>q</sub>), 139.6 (C<sub>q</sub>), 138.3 (C<sub>q</sub>), 133.4 (C<sub>q</sub>), 133.0 (C<sub>q</sub>), 132.7 (CH), 131.3 (CH), 130.2 (CH), 129.7 (CH), 129.1 (CH), 128.4 (CH), 128.2 (CH), 127.9 (CH), 127.7 (CH), 127.3 (CH), 124.2 (CH), 123.7 (C<sub>q</sub>), 123.0 (C<sub>q</sub>), 118.6 (CH). **IR** (ATR):  $\tilde{\nu}$  = 1642, 1608, 1476, 1361, 1226, 925, 764, 693, 640, 492 cm<sup>-1</sup>. **M.p.**: 178–180 °C. **MS** (ESI) *m/z* (relative intensity): 375 (100) [M+H]<sup>+</sup>, 397 (10) [M+Na]<sup>+</sup>, 771 (20) [2M+Na]<sup>+</sup>. **HR-MS** (ESI) *m/z* calcd for C<sub>27</sub>H<sub>19</sub>O<sub>2</sub> [M+H]<sup>+</sup>: 375.1380, found: 375.1381.

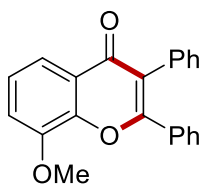
The spectral data are in accordance with those reported in the literature.<sup>[254]</sup>

**48ha****6-Methoxy-2,3-diphenyl-4H-chromen-4-one**

The general procedure B was followed using **26h** (114 mg, 0.75 mmol) and **17a** (44.5 mg, 0.25 mmol) at 100 °C for 3.5 h. Purification by column chromatography on silica gel (*n*hexane/EtOAc = 10:1 to 6:1) yielded **48ha** (69.6 mg, 85%) as a pale-yellow solid.

**<sup>1</sup>H-NMR** (400 MHz, CDCl<sub>3</sub>):  $\delta$  = 7.56 (d, *J* = 3.1 Hz, 1H), 7.37 (d, *J* = 9.1 Hz, 1H), 7.32–7.27 (m, 2H), 7.24–7.12 (m, 9H), 3.93 (s, 3H). **<sup>13</sup>C-NMR** (101 MHz, CDCl<sub>3</sub>):  $\delta$  = 177.1 (C<sub>q</sub>), 161.3 (C<sub>q</sub>), 157.0 (C<sub>q</sub>), 151.0 (C<sub>q</sub>), 133.4 (C<sub>q</sub>), 133.1 (C<sub>q</sub>), 131.3 (CH), 130.0 (CH), 129.6 (CH), 128.3 (CH), 128.1 (CH), 127.6 (CH), 124.1 (C<sub>q</sub>), 123.8 (CH), 122.2 (C<sub>q</sub>), 119.5 (CH), 105.4 (CH), 56.0 (CH<sub>3</sub>). **IR** (ATR):  $\tilde{\nu}$  = 1626, 1481, 1435, 1361, 1275, 1022, 830, 783, 743, 570 cm<sup>-1</sup>. **M.p.**: 179°–181 °C. **MS** (ESI) *m/z* (relative intensity): 329 (100) [M+H]<sup>+</sup>, 351 (20) [M+Na]<sup>+</sup>, 679 (40) [2M+Na]<sup>+</sup>. **HR-MS** (ESI) *m/z* calcd for C<sub>22</sub>H<sub>17</sub>O<sub>3</sub> [M+H]<sup>+</sup>: 329.1172, found: 329.1174.

The spectral data are in accordance with those reported in the literature.<sup>[254]</sup>

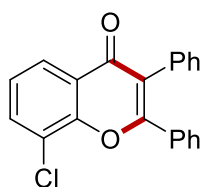
**48ia****8-Methoxy-2,3-diphenyl-4H-chromen-4-one**

The general procedure B was followed using **26i** (114 mg, 0.75 mmol) and **17a** (44.5 mg, 0.25 mmol) at 100 °C for 3.5 h. Purification by column chromatography on silica gel (*n*hexane/EtOAc = 8:1) yielded **48ia** (78.3 mg, 95%) as a white solid.

**<sup>1</sup>H-NMR** (400 MHz, CDCl<sub>3</sub>):  $\delta$  = 7.75 (dd, *J* = 8.1, 1.4 Hz, 1H), 7.37–7.32 (m, 2H), 7.25–7.13 (m, 9H), 7.09 (dd, *J* = 8.1, 1.4 Hz, 1H), 3.90 (s, 3H). **<sup>13</sup>C-NMR** (101 MHz, CDCl<sub>3</sub>):  $\delta$  = 177.4 (C<sub>q</sub>), 161.2 (C<sub>q</sub>), 149.0 (C<sub>q</sub>), 146.6 (C<sub>q</sub>), 133.3 (C<sub>q</sub>), 133.0 (C<sub>q</sub>), 131.3 (CH), 130.1 (CH), 129.8 (CH), 128.3 (CH), 128.2 (CH), 127.7 (CH), 124.8 (CH), 124.6 (C<sub>q</sub>), 122.9 (C<sub>q</sub>), 117.1 (CH), 114.3 (CH), 56.4 (CH<sub>3</sub>). **IR** (ATR):  $\tilde{\nu}$  = 1626, 1558, 1489, 1376, 1266, 1227,

1091, 1069, 757, 695  $\text{cm}^{-1}$ . **M.p.:** 187–189 °C. **MS** (ESI)  $m/z$  (relative intensity): 329 (40)  $[\text{M}+\text{H}]^+$ , 451 (100)  $[\text{M}+\text{Na}]^+$ , 679 (80)  $[\text{2M}+\text{Na}]^+$ . **HR-MS** (ESI)  $m/z$  calcd for  $\text{C}_{22}\text{H}_{17}\text{O}_3$   $[\text{M}+\text{H}]^+$ : 329.1172, found: 329.1173.

The spectral data are in accordance with those reported in the literature.<sup>[91]</sup>

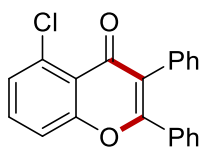


**48ja**

### 8-Chloro-2,3-diphenyl-4H-chromen-4-one

The general procedure B was followed using **26j** (118 mg, 0.75 mmol) and **17a** (44.5 mg, 0.25 mmol) at 100 °C for 3.5 h. Purification by column chromatography on silica gel (*n*hexane/EtOAc = 12:1 to 7:1) yielded **48ja** (77.4 mg, 93%) as a white solid.

**<sup>1</sup>H-NMR** (400 MHz,  $\text{CDCl}_3$ ):  $\delta$  = 8.11 (dd,  $J$  = 8.0, 1.5 Hz, 1H), 7.68 (dd,  $J$  = 7.7, 1.5 Hz, 1H), 7.43–7.36 (m, 2H), 7.30–7.14 (m, 9H). **<sup>13</sup>C-NMR** (101 MHz,  $\text{CDCl}_3$ ):  $\delta$  = 177.0 ( $\text{C}_q$ ), 161.3 ( $\text{C}_q$ ), 151.8 ( $\text{C}_q$ ), 133.9 (CH), 132.8 ( $\text{C}_q$ ), 132.6 ( $\text{C}_q$ ), 131.2 (CH), 130.5 (CH), 129.9 (CH), 128.6 (CH), 128.3 (CH), 128.0 (CH), 125.2 (CH), 125.1 (CH), 125.0 ( $\text{C}_q$ ), 123.2 ( $\text{C}_q$ ), 123.0 ( $\text{C}_q$ ). **IR** (ATR):  $\tilde{\nu}$  = 1642, 1560, 1471, 1440, 1370, 1041, 1024, 758, 689, 652  $\text{cm}^{-1}$ . **M.p.:** 154–155 °C. **MS** (ESI)  $m/z$  (relative intensity): 333 (70)  $[\text{M}+\text{H}]^+$  ( $^{35}\text{Cl}$ ), 355 (100)  $[\text{M}+\text{Na}]^+$  ( $^{35}\text{Cl}$ ), 371 (20)  $[\text{M}+\text{K}]^+$  ( $^{35}\text{Cl}$ ). **HR-MS** (ESI)  $m/z$  calcd for  $\text{C}_{21}\text{H}_{14}^{35}\text{ClO}_2$   $[\text{M}+\text{H}]^+$ : 333.0677, found: 333.0681.

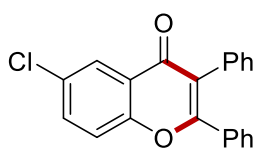


**48ka**

### 5-Chloro-2,3-diphenyl-4H-chromen-4-one

The general procedure B was followed using **26k** (118 mg, 0.75 mmol) and **17a** (44.5 mg, 0.25 mmol) at 100 °C for 3.5 h. Purification by column chromatography on silica gel (*n*hexane/EtOAc = 15:1) yielded **48ka** (47.6 mg, 57%) as a white solid.

**<sup>1</sup>H-NMR** (500 MHz, CDCl<sub>3</sub>):  $\delta$  = 7.45 (dd,  $J$  = 8.5, 7.7 Hz, 1H), 7.36 (dd,  $J$  = 8.5, 1.2 Hz, 1H), 7.31 (ddd,  $J$  = 8.5, 6.8, 1.2 Hz, 3H), 7.27–7.23 (m, 1H), 7.22–7.16 (m, 5H), 7.15–7.13 (m, 2H). **<sup>13</sup>C-NMR** (126 MHz, CDCl<sub>3</sub>):  $\delta$  = 176.4 (C<sub>q</sub>), 160.0 (C<sub>q</sub>), 157.7 (C<sub>q</sub>), 134.1 (C<sub>q</sub>), 132.9 (CH), 132.7 (C<sub>q</sub>), 132.5 (C<sub>q</sub>), 131.3 (CH), 130.3 (CH), 129.6 (CH), 128.3 (CH), 128.2 (CH), 128.1 (CH), 127.8 (CH), 123.9 (C<sub>q</sub>), 120.6 (C<sub>q</sub>), 117.3 (CH). **IR** (ATR):  $\tilde{\nu}$  = 1653, 1618, 1595, 1453, 1373, 949, 785, 752, 699, 648 cm<sup>-1</sup>. **M.p.**: 165–166 °C. **MS** (ESI)  $m/z$  (relative intensity): 333 (100) [M+H]<sup>+</sup> (<sup>35</sup>Cl), 355 (10) [M+Na]<sup>+</sup> (<sup>35</sup>Cl), 687 (100) [2M+Na]<sup>+</sup> (<sup>35</sup>Cl). **HR-MS** (ESI)  $m/z$  calcd for C<sub>21</sub>H<sub>14</sub><sup>35</sup>ClO<sub>2</sub> [M+H]<sup>+</sup>: 333.0677, found: 333.0680.

**481a**

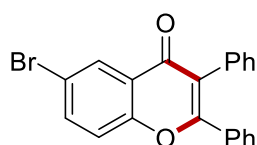
### 6-Chloro-2,3-diphenyl-4H-chromen-4-one

The general procedure B was followed using **261** (117 mg, 0.75 mmol) and **17a** (44.5 mg, 0.25 mmol) at 100 °C for 3.5 h. Purification by column chromatography on silica gel (*n*hexane/EtOAc = 12:1) yielded **481a** (65.6 mg, 79%) as a white solid.

**<sup>1</sup>H-NMR** (400 MHz, CDCl<sub>3</sub>):  $\delta$  = 8.15 (d,  $J$  = 2.5 Hz, 1H), 7.53 (dd,  $J$  = 8.9, 2.5 Hz, 1H), 7.39 (d,  $J$  = 8.9 Hz, 1H), 7.31–7.27 (m, 2H), 7.26–7.23 (m, 1H), 7.22–7.19 (m, 3H), 7.19–7.15 (m, 2H), 7.14–7.10 (m, 2H). **<sup>13</sup>C-NMR** (101 MHz, CDCl<sub>3</sub>):  $\delta$  = 176.3 (C<sub>q</sub>), 161.8 (C<sub>q</sub>), 154.5 (C<sub>q</sub>), 134.0 (CH), 133.0 (C<sub>q</sub>), 132.5 (C<sub>q</sub>), 131.2 (CH), 131.1 (C<sub>q</sub>), 130.4 (CH), 129.6 (CH), 128.4 (CH), 128.2 (CH), 127.9 (CH), 125.8 (CH), 124.6 (C<sub>q</sub>), 123.0 (C<sub>q</sub>), 119.9 (CH). **IR** (ATR):  $\tilde{\nu}$  = 1643, 1561, 1432, 1361, 1272, 1221, 1050, 926, 818, 699 cm<sup>-1</sup>. **M.p.**: 181–182 °C. **MS** (ESI)  $m/z$  (relative intensity): 333 (100) [M+H]<sup>+</sup> (<sup>35</sup>Cl), 355 (70) [M+Na]<sup>+</sup> (<sup>35</sup>Cl), 687 (90) [2M+Na]<sup>+</sup> (<sup>35</sup>Cl). **HR-MS** (ESI)  $m/z$  calcd for C<sub>21</sub>H<sub>14</sub><sup>35</sup>ClO<sub>2</sub> [M+H]<sup>+</sup>: 333.0677, found: 333.0679.

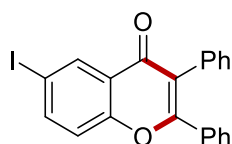
The spectral data are in accordance with those reported in the literature.<sup>[91]</sup>



**48ma****6-Bromo-2,3-diphenyl-4H-chromen-4-one**

The general procedure B was followed using **26m** (168 mg, 0.75 mmol) and **17a** (44.5 mg, 0.25 mmol) at 100 °C for 3.5 h. Purification by column chromatography on silica gel (*n*hexane/EtOAc = 15:1) yielded **48ma** (85.0 mg, 90%) as a white solid.

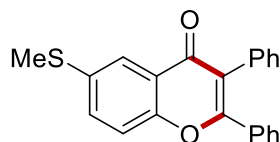
**<sup>1</sup>H-NMR** (400 MHz, CDCl<sub>3</sub>):  $\delta$  = 8.31 (d,  $J$  = 2.5 Hz, 1H), 7.68 (dd,  $J$  = 8.8, 2.5 Hz, 1H), 7.34 (d,  $J$  = 8.8 Hz, 1H), 7.29 (m, 2H), 7.27–7.23 (m, 1H), 7.22–7.16 (m, 5H), 7.14–7.10 (m, 2H). **<sup>13</sup>C-NMR** (101 MHz, CDCl<sub>3</sub>):  $\delta$  = 176.1 (C<sub>q</sub>), 161.8 (C<sub>q</sub>), 154.9 (C<sub>q</sub>), 136.7 (CH), 133.0 (C<sub>q</sub>), 132.5 (C<sub>q</sub>), 131.2 (CH), 130.4 (CH), 129.6 (CH), 129.0 (CH), 128.4 (CH), 128.2 (CH), 127.9 (CH), 124.9 (C<sub>q</sub>), 123.1 (C<sub>q</sub>), 120.1 (CH), 118.5 (C<sub>q</sub>). **IR** (ATR):  $\tilde{\nu}$  = 1637, 1603, 1466, 1424, 1356, 1270, 1220, 756, 698, 652 cm<sup>-1</sup>. **M.p.**: 190–191 °C. **MS** (ESI)  $m/z$  (relative intensity): 377 (100) [M+H]<sup>+</sup> (<sup>79</sup>Br), 399 (90) [M+Na]<sup>+</sup> (<sup>79</sup>Br), 777 (100) [2M+Na]<sup>+</sup> (<sup>79</sup>Br). **HR-MS** (ESI)  $m/z$  calcd for C<sub>21</sub>H<sub>14</sub><sup>79</sup>BrO<sub>2</sub> [M+H]<sup>+</sup>: 377.0172, found: 377.0174.

**48na****6-Iodo-2,3-diphenyl-4H-chromen-4-one**

The general procedure B was followed using **26n** (186 mg, 0.75 mmol) and **17a** (44.5 mg, 0.25 mmol) at 100 °C for 3.5 h. Purification by column chromatography on silica gel (*n*hexane/EtOAc = 20:1) yielded **48na** (85.0 mg, 82%) as a white solid.

**<sup>1</sup>H-NMR** (300 MHz, CDCl<sub>3</sub>):  $\delta$  = 8.50 (d,  $J$  = 2.2 Hz, 1H), 7.85 (dd,  $J$  = 8.8, 2.2 Hz, 1H), 7.31–7.14 (m, 9H), 7.16–7.06 (m, 2H). **<sup>13</sup>C-NMR** (101 MHz, CDCl<sub>3</sub>):  $\delta$  = 175.9 (C<sub>q</sub>), 161.8 (C<sub>q</sub>), 155.6 (C<sub>q</sub>), 142.3 (CH), 135.3 (CH), 133.0 (C<sub>q</sub>), 132.6 (C<sub>q</sub>), 131.2 (CH), 130.4 (CH), 129.7 (CH), 128.5 (CH), 128.2 (CH), 127.9 (CH), 125.3 (C<sub>q</sub>), 123.3 (C<sub>q</sub>), 120.2 (CH), 89.0 (C<sub>q</sub>). **IR** (ATR):  $\tilde{\nu}$  = 1632, 1597, 1550, 1415, 1359, 1269, 1224, 764, 695, 648 cm<sup>-1</sup>. **M.p.**:

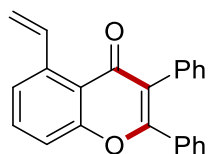
178–180 °C. **MS** (ESI)  $m/z$  (relative intensity): 425 (100)  $[M+H]^+$ , 447 (70)  $[M+Na]^+$ , 871 (70)  $[2M+Na]^+$ . **HR-MS** (ESI)  $m/z$  calcd for  $C_{21}H_{14}IO_2$   $[M+H]^+$ : 425.0033, found: 425.0037.

**48oa**

### 6-(Methylthio)-2,3-diphenyl-4H-chromen-4-one

The general procedure B was followed using **26o** (168 mg, 0.75 mmol) and **17a** (44.5 mg, 0.25 mmol) at 100 °C for 3.5 h. Purification by column chromatography on silica gel (*n*hexane/EtOAc = 15:1) yielded **48oa** (75.9 mg, 88%) as a yellow solid.

**<sup>1</sup>H-NMR** (400 MHz,  $CDCl_3$ ):  $\delta$  = 7.98 (d,  $J$  = 2.4 Hz, 1H), 7.49 (dd,  $J$  = 8.8, 2.4 Hz, 1H), 7.36 (d,  $J$  = 8.8 Hz, 1H), 7.32–7.28 (m, 2H), 7.27–7.11 (m, 8H), 2.48 (s, 3H). **<sup>13</sup>C-NMR** (101 MHz,  $CDCl_3$ ):  $\delta$  = 176.7 ( $C_q$ ), 161.5 ( $C_q$ ), 154.1 ( $C_q$ ), 136.2 ( $C_q$ ), 133.3 ( $C_q$ ), 132.9 ( $C_q$ ), 132.7 (CH), 131.3 (CH), 130.2 (CH), 129.6 (CH), 128.3 (CH), 128.2 (CH), 127.7 (CH), 123.9 ( $C_q$ ), 123.1 ( $C_q$ ), 122.1 (CH), 118.6 (CH), 16.2 ( $CH_3$ ). **IR** (ATR):  $\tilde{\nu}$  = 1633, 1599, 1457, 1420, 1357, 1272, 1223, 768, 696  $cm^{-1}$ . **M.p.**: 130–132 °C. **MS** (ESI)  $m/z$  (relative intensity): 345 (60)  $[M+H]^+$ , 367 (70)  $[M+Na]^+$ , 711 (100)  $[2M+Na]^+$ . **HR-MS** (ESI)  $m/z$  calcd for  $C_{22}H_{17}SO_2$   $[M+H]^+$ : 345.0944, found: 345.0947.

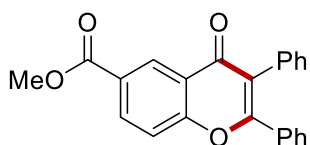
**48pa**

### 2,3-Diphenyl-5-vinyl-4H-chromen-4-one

The general procedure B was followed using **26p** (111 mg, 0.75 mmol) and **17a** (44.5 mg, 0.25 mmol) at 100 °C for 3.5 h. Purification by column chromatography on silica gel (*n*hexane/EtOAc = 10:1) yielded **48pa** (72.5 mg, 92%) as a brown solid.

**<sup>1</sup>H-NMR** (400 MHz,  $CDCl_3$ ):  $\delta$  = 8.12 (dd,  $J$  = 17.3, 10.9 Hz, 1H), 7.65 (dd,  $J$  = 8.7, 7.2 Hz, 1H), 7.52–7.40 (m, 4H), 7.39–7.21 (m, 8H), 5.64 (dd,  $J$  = 17.3, 1.6 Hz, 1H), 5.40 (dd,  $J$  =

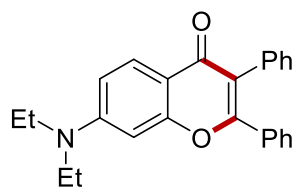
10.9, 1.6 Hz, 1H).  $^{13}\text{C-NMR}$  (101 MHz,  $\text{CDCl}_3$ ):  $\delta$  = 179.1 ( $\text{C}_q$ ), 160.0 ( $\text{C}_q$ ), 157.1 ( $\text{C}_q$ ), 141.1 ( $\text{C}_q$ ), 137.4 (CH), 133.1 (CH), 133.0 ( $\text{C}_q$ ), 133.0 ( $\text{C}_q$ ), 132.9 (CH), 131.3 (CH), 130.1 (CH), 129.5 (CH), 128.3 (CH), 128.1 (CH), 127.6 (CH), 124.1 (CH), 123.7 ( $\text{C}_q$ ), 120.4 ( $\text{C}_q$ ), 117.6 (CH), 116.6 ( $\text{CH}_2$ ). **IR** (ATR):  $\tilde{\nu}$  = 3055, 2926, 1626, 1564, 1470, 1369, 1228, 1058, 976, 819  $\text{cm}^{-1}$ . **M.p.**: 154–155. **MS** (ESI)  $m/z$  (relative intensity): 325 (100)  $[\text{M}+\text{H}]^+$ , 671 (70)  $[\text{2M}+\text{Na}]^+$ . **HR-MS** (ESI)  $m/z$  calcd for  $\text{C}_{23}\text{H}_{17}\text{O}_2$   $[\text{M}+\text{H}]^+$ : 325.1229, found: 325.1223.

**48qa**

#### Methyl 4-oxo-2,3-diphenyl-4H-chromene-6-carboxylate

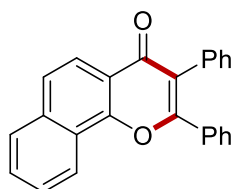
The general procedure C was followed using **26q** (135 mg, 0.75 mmol) and **17a** (44.5 mg, 0.25 mmol) at 100 °C for 3.5 h. Purification by column chromatography on silica gel (*n*hexane/EtOAc = 8:1 to 6:1) yielded **48qa** (78.2 mg, 88%) as a white solid.

$^1\text{H-NMR}$  (400 MHz,  $\text{CDCl}_3$ ):  $\delta$  = 8.88 (d,  $J$  = 2.1 Hz, 1H), 8.27 (dd,  $J$  = 8.8, 2.1 Hz, 1H), 7.50 (d,  $J$  = 8.8 Hz, 1H), 7.33–7.29 (m, 2H), 7.29–7.24 (m, 1H), 7.24–7.16 (m, 5H), 7.16–7.12 (m, 2H), 3.88 (s, 3H).  $^{13}\text{C-NMR}$  (101 MHz,  $\text{CDCl}_3$ ):  $\delta$  = 176.8 ( $\text{C}_q$ ), 166.0 ( $\text{C}_q$ ), 161.7 ( $\text{C}_q$ ), 158.6 ( $\text{C}_q$ ), 134.4 (CH), 132.9 ( $\text{C}_q$ ), 132.4 ( $\text{C}_q$ ), 131.2 (CH), 130.4 (CH), 129.7 (CH), 129.0 (CH), 128.4 (CH), 128.2 (CH), 127.9 (CH), 127.2 ( $\text{C}_q$ ), 123.4 ( $\text{C}_q$ ), 123.3 ( $\text{C}_q$ ), 118.6 (CH), 52.5 ( $\text{CH}_3$ ). **IR** (ATR):  $\tilde{\nu}$  = 1716, 1642, 1606, 1430, 1291, 1256, 1212, 762, 695, 653  $\text{cm}^{-1}$ . **M.p.**: 200–201 °C. **MS** (ESI)  $m/z$  (relative intensity): 357 (100)  $[\text{M}+\text{H}]^+$ , 379 (20)  $[\text{M}+\text{Na}]^+$ , 735 (30)  $[\text{2M}+\text{Na}]^+$ . **HR-MS** (ESI)  $m/z$  calcd for  $\text{C}_{23}\text{H}_{17}\text{O}_4$   $[\text{M}+\text{H}]^+$ : 357.1121, found: 357.1124.

**48ra****7-(Diethylamino)-2,3-diphenyl-4H-chromen-4-one**

The general procedure B was followed using **26r** (145 mg, 0.75 mmol) and **17a** (44.5 mg, 0.25 mmol) at 100 °C for 3.5 h. Purification by column chromatography on silica gel (*n*hexane/EtOAc = 5:1 to 2:1) yielded **48ra** (86.1 mg, 93%) as a yellow solid.

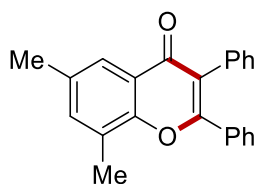
**<sup>1</sup>H-NMR** (400 MHz, CDCl<sub>3</sub>):  $\delta$  = 8.01 (d,  $J$  = 9.1 Hz, 1H), 7.33–7.29 (m, 2H), 7.26–7.10 (m, 8H), 6.69 (dd,  $J$  = 9.1, 2.5 Hz, 1H), 6.46 (d,  $J$  = 2.5 Hz, 1H), 3.39 (q,  $J$  = 7.1 Hz, 4H), 1.17 (t,  $J$  = 7.0 Hz, 6H). **<sup>13</sup>C-NMR** (101 MHz, CDCl<sub>3</sub>):  $\delta$  = 176.5 (C<sub>q</sub>), 160.2 (C<sub>q</sub>), 158.6 (C<sub>q</sub>), 152.0 (C<sub>q</sub>), 134.1 (C<sub>q</sub>), 133.6 (C<sub>q</sub>), 131.5 (CH), 129.7 (CH), 129.6 (CH), 128.2 (CH), 128.1 (CH), 127.7 (CH), 127.3 (CH), 122.5 (C<sub>q</sub>), 112.9 (C<sub>q</sub>), 110.7 (CH), 96.3 (CH), 44.9 (CH<sub>2</sub>), 12.7 (CH<sub>3</sub>). **IR** (ATR):  $\tilde{\nu}$  = 1618, 1596, 1442, 1377, 1352, 1267, 1155, 818, 771, 696 cm<sup>-1</sup>. **M.p.**: 164–165 °C. **MS** (ESI)  $m/z$  (relative intensity): 370 (100) [M+H]<sup>+</sup>, 392 (30) [M+Na]<sup>+</sup>. **HR-MS** (ESI)  $m/z$  calcd for C<sub>25</sub>H<sub>24</sub>NO<sub>2</sub> [M+H]<sup>+</sup>: 370.1802, found: 370.1806.

**48sa****2,3-Diphenyl-4H-benzo[h]chromen-4-one**

The general procedure B was followed using **26s** (129 mg, 0.75 mmol) and **17a** (44.5 mg, 0.25 mmol) at 100 °C for 7 h. Purification by column chromatography on silica gel (*n*hexane/EtOAc = 12:1) yielded **48sa** (75.3 mg, 86%) as a light brown solid.

**<sup>1</sup>H-NMR** (400 MHz, CDCl<sub>3</sub>):  $\delta$  = 8.53 (dd,  $J$  = 7.7, 1.6 Hz, 1H), 8.24 (d,  $J$  = 8.7 Hz, 1H), 7.94 (dd,  $J$  = 7.7, 1.6 Hz, 1H), 7.78 (d,  $J$  = 8.7 Hz, 1H), 7.73–7.65 (m, 2H), 7.54–7.49 (m, 2H), 7.42–7.28 (m, 8H). **<sup>13</sup>C-NMR** (101 MHz, CDCl<sub>3</sub>):  $\delta$  = 177.2 (C<sub>q</sub>), 160.7 (C<sub>q</sub>), 153.4 (C<sub>q</sub>), 136.0 (C<sub>q</sub>), 133.4 (C<sub>q</sub>), 132.9 (C<sub>q</sub>), 131.3 (CH), 130.2 (CH), 129.7 (CH), 129.3 (CH), 128.4 (CH), 128.3 (CH), 128.3 (CH), 127.8 (CH), 127.2 (CH), 125.3 (CH), 124.1 (C<sub>q</sub>), 124.1

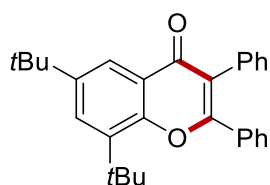
(C<sub>q</sub>), 122.5 (CH), 121.5 (CH), 119.9 (C<sub>q</sub>). **IR** (ATR):  $\tilde{\nu}$  = 1627, 1441, 1384, 1239, 1150, 1064, 757, 692, 638, 524 cm<sup>-1</sup>. **M.p.**: 206–208. **MS** (ESI)  $m/z$  (relative intensity): 349 (90) [M+H]<sup>+</sup>, 471 (90) [M+Na]<sup>+</sup>, 719 (100) [2M+Na]<sup>+</sup>. **HR-MS** (ESI)  $m/z$  calcd for C<sub>25</sub>H<sub>17</sub>O<sub>2</sub> [M+H]<sup>+</sup>: 349.1223, found: 349.1222.

**48ta**

### 6,8-Dimethyl-2,3-diphenyl-4*H*-chromen-4-one

The general procedure B was followed using **26t** (113 mg, 0.75 mmol) and **17a** (44.5 mg, 0.25 mmol) at 100 °C for 3.5 h. Purification by column chromatography on silica gel (*n*hexane/EtOAc = 15:1) yielded **48ta** (72.7 mg, 91%) as a white solid.

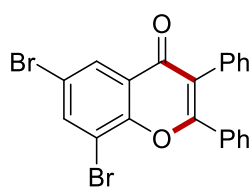
**<sup>1</sup>H-NMR** (400 MHz, CDCl<sub>3</sub>):  $\delta$  = 7.82 (dd,  $J$  = 1.5, 1.5 Hz, 1H), 7.34–7.30 (m, 2H), 7.28–7.26 (m, 1H), 7.25–7.21 (m, 2H), 7.21–7.13 (m, 6H), 2.43 (s, 3H), 2.35 (s, 3H). **<sup>13</sup>C-NMR** (101 MHz, CDCl<sub>3</sub>):  $\delta$  = 177.8 (C<sub>q</sub>), 160.9 (C<sub>q</sub>), 152.9 (C<sub>q</sub>), 136.0 (CH), 134.5 (C<sub>q</sub>), 133.7 (C<sub>q</sub>), 133.3 (C<sub>q</sub>), 131.4 (CH), 130.0 (CH), 129.7 (CH), 128.3 (CH), 128.2 (CH), 127.6 (CH), 127.1 (C<sub>q</sub>), 123.3 (CH), 123.2 (C<sub>q</sub>), 122.6 (C<sub>q</sub>), 21.1 (CH<sub>3</sub>), 15.7 (CH<sub>3</sub>). **IR** (ATR):  $\tilde{\nu}$  = 1631, 1603, 1472, 1371, 1267, 918, 802, 728, 696, 570 cm<sup>-1</sup>. **M.p.**: 198–199 °C. **MS** (ESI)  $m/z$  (relative intensity): 327 (100) [M+H]<sup>+</sup>, 349 (30) [M+Na]<sup>+</sup>, 675 (20) [2M+Na]<sup>+</sup>. **HR-MS** (ESI)  $m/z$  calcd for C<sub>23</sub>H<sub>19</sub>O<sub>2</sub> [M+H]<sup>+</sup>: 327.1380, found: 327.1382.

**48ua**

### 6,8-Di-*tert*-butyl-2,3-diphenyl-4*H*-chromen-4-one

The general procedure B was followed using **26u** (176 mg, 0.75 mmol) and **17a** (44.5 mg, 0.25 mmol) at 100 °C for 7 h. Purification by column chromatography on silica gel (*n*hexane/EtOAc = 30:1 to 20:1) yielded **48ua** (96.1 mg, 94%) as a light brown solid.

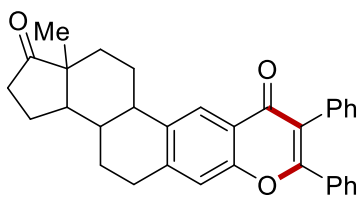
**<sup>1</sup>H-NMR** (400 MHz, CDCl<sub>3</sub>):  $\delta$  = 8.12 (d,  $J$  = 2.5 Hz, 1H), 7.66 (d,  $J$  = 2.5 Hz, 1H), 7.33 (dd,  $J$  = 2.5, 2.5 Hz, 2H), 7.27–7.10 (m, 8H), 1.46 (s, 9H), 1.31 (s, 9H). **<sup>13</sup>C-NMR** (101 MHz, CDCl<sub>3</sub>):  $\delta$  = 178.0 (C<sub>q</sub>), 161.3 (C<sub>q</sub>), 153.2 (C<sub>q</sub>), 147.6 (C<sub>q</sub>), 138.5 (C<sub>q</sub>), 133.7 (C<sub>q</sub>), 133.2 (C<sub>q</sub>), 131.4 (CH), 129.9 (CH), 129.7 (CH), 128.8 (CH), 128.2 (CH), 128.2 (CH), 127.5 (CH), 123.8 (C<sub>q</sub>), 122.6 (C<sub>q</sub>), 120.4 (CH), 35.2 (C<sub>q</sub>), 35.1 (C<sub>q</sub>), 31.5 (CH<sub>3</sub>), 30.4 (CH<sub>3</sub>). **IR** (ATR):  $\tilde{\nu}$  = 1631, 1593, 1467, 1444, 1364, 1234, 1062, 774, 691, 650 cm<sup>-1</sup>. **M.p.**: 178–181 °C. **MS** (ESI)  $m/z$  (relative intensity): 411 (100) [M+H]<sup>+</sup>, 433 (10) [M+Na]<sup>+</sup>, 821 (10) [2M+H]<sup>+</sup>. **HR-MS** (ESI)  $m/z$  calcd for C<sub>29</sub>H<sub>31</sub>O<sub>2</sub> [M+H]<sup>+</sup>: 411.2319, found: 411.2321.

**48va**

#### 6,8-Dibromo-2,3-diphenyl-4H-chromen-4-one

The general procedure B was followed using **26v** (223 mg, 0.75 mmol) and **17a** (44.5 mg, 0.25 mmol) at 100 °C for 7 h. Purification by column chromatography on silica gel (*n*hexane/EtOAc = 10:1) yielded **48va** (85.3 mg, 75%) as a white solid.

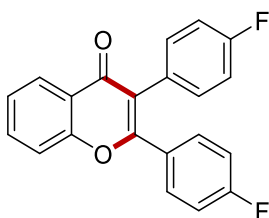
**<sup>1</sup>H-NMR** (400 MHz, CDCl<sub>3</sub>):  $\delta$  = 8.27 (d,  $J$  = 2.3 Hz, 1H), 7.97 (d,  $J$  = 2.3 Hz, 1H), 7.41–7.36 (m, 2H), 7.31–7.17 (m, 6H), 7.16–7.11 (m, 2H). **<sup>13</sup>C-NMR** (101 MHz, CDCl<sub>3</sub>):  $\delta$  = 175.8 (C<sub>q</sub>), 161.6 (C<sub>q</sub>), 151.8 (C<sub>q</sub>), 139.3 (CH), 132.5 (C<sub>q</sub>), 132.2 (C<sub>q</sub>), 131.1 (CH), 130.8 (CH), 129.9 (CH), 128.7 (CH), 128.4 (CH), 128.4 (CH), 128.2 (CH), 125.6 (C<sub>q</sub>), 123.0 (C<sub>q</sub>), 118.4 (C<sub>q</sub>), 113.0 (C<sub>q</sub>). **IR** (ATR):  $\tilde{\nu}$  = 1637, 1550, 1467, 1351, 1258, 1217, 1049, 924, 769, 697 cm<sup>-1</sup>. **M.p.**: 219–220 °C. **MS** (ESI)  $m/z$  (relative intensity): 456 (100) [M+H]<sup>+</sup> (<sup>79</sup>Br<sup>81</sup>Br), 478 (10) [M+Na]<sup>+</sup> (<sup>79</sup>Br<sup>81</sup>Br), 934 (20) [2M+Na]<sup>+</sup> (<sup>79</sup>Br<sup>81</sup>Br). **HR-MS** (ESI)  $m/z$  calcd for C<sub>21</sub>H<sub>13</sub><sup>79</sup>Br<sup>81</sup>BrO<sub>2</sub> [M+H]<sup>+</sup>: 456.9258, found: 456.9254.

**48wa**

**13a-Methyl-8,9-diphenyl-2,3,3a,3b,4,5,11b,12,13,13a-decahydrocyclopenta[5,6]naphtho-[1,2-g]chromene-1,10-dione**

The general procedure B was followed using **26w** (112 mg, 0.375 mmol) and **17a** (44.5 mg, 0.25 mmol) at 100 °C for 3.5 h. Purification by column chromatography on silica gel (*n*hexane/EtOAc = 4:1 to 2:1) yielded **48wa** (91.8 mg, 77%) as a white solid.

**<sup>1</sup>H-NMR** (500 MHz, CDCl<sub>3</sub>): δ = 8.09 (d, *J* = 1.3 Hz, 1H), 7.31–7.28 (m, 2H), 7.27–7.21 (m, 2H), 7.21–7.16 (m, 5H), 7.15–7.11 (m, 2H), 3.05–2.93 (m, 2H), 2.55–2.48 (m, 1H), 2.48–2.41 (m, 1H), 2.30 (td, *J* = 11.0, 4.3 Hz, 1H), 2.09 (dt, *J* = 18.8, 8.8 Hz, 1H), 2.01 (ddq, *J* = 12.1, 5.7, 3.5, 2.9 Hz, 2H), 1.94 (dt, *J* = 13.0, 3.5 Hz, 1H), 1.62–1.52 (m, 3H), 1.51–1.41 (m, 3H), 0.85 (s, 3H). **<sup>13</sup>C-NMR** (126 MHz, CDCl<sub>3</sub>): δ = 220.6 (C<sub>q</sub>), 177.3 (C<sub>q</sub>), 161.2 (C<sub>q</sub>), 154.4 (C<sub>q</sub>), 144.2 (C<sub>q</sub>), 137.9 (C<sub>q</sub>), 133.6 (C<sub>q</sub>), 133.2 (C<sub>q</sub>), 131.4 (CH), 130.0 (CH), 129.6 (CH), 128.3 (CH), 128.1 (CH), 127.6 (CH), 122.7 (C<sub>q</sub>), 122.6 (CH), 121.4 (C<sub>q</sub>), 117.3 (CH), 50.7 (CH), 48.0 (C<sub>q</sub>), 44.2 (CH), 38.0 (CH), 35.9 (CH<sub>2</sub>), 31.5 (CH<sub>2</sub>), 29.8 (CH<sub>2</sub>), 26.2 (CH<sub>2</sub>), 25.9 (CH<sub>2</sub>), 21.7 (CH<sub>2</sub>), 13.9 (CH<sub>3</sub>). **IR** (ATR):  $\tilde{\nu}$  = 1730, 1641, 1616, 1439, 1368, 1242, 1218, 767, 737, 694 cm<sup>-1</sup>. **M.p.**: 284–286 °C. **MS** (ESI) *m/z* (relative intensity): 475 (100) [M+H]<sup>+</sup>, 492 (20) [M+Na]<sup>+</sup>, 971 (10) [2M+Na]<sup>+</sup>. **HR-MS** (ESI) *m/z* calcd for C<sub>33</sub>H<sub>31</sub>O<sub>3</sub> [M+H]<sup>+</sup>: 475.2268, found: 475.2270.

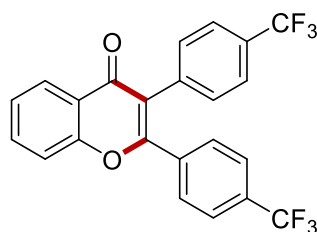
**48ac**

**2,3-Bis(4-fluorophenyl)-4*H*-chromen-4-one**

The general procedure B was followed using **26a** (78 μL, 0.75 mmol) and **17c** (53.6 mg, 0.25 mmol) at 100 °C for 3.5 h. Purification by column chromatography on silica gel (*n*hexane/EtOAc = 10:1) yielded **48ac** (75.6 mg, 90%) as a white solid.

**<sup>1</sup>H-NMR** (400 MHz, CDCl<sub>3</sub>):  $\delta$  = 8.28 (ddd,  $J$  = 7.9, 1.7, 0.5 Hz, 1H), 7.71 (ddd,  $J$  = 8.5, 7.1, 1.7 Hz, 1H), 7.53 (ddd,  $J$  = 8.5, 1.1, 0.5 Hz, 1H), 7.46–7.43 (m, 3H), 7.22–7.16 (m, 2H), 7.05–6.96 (m, 4H). **<sup>13</sup>C-NMR** (101 MHz, CDCl<sub>3</sub>):  $\delta$  = 177.3 (C<sub>q</sub>), 163.6 (d,  $J$  = 252.4 Hz, C<sub>q</sub>), 162.4 (d,  $J$  = 247.4 Hz, C<sub>q</sub>), 160.7 (C<sub>q</sub>), 156.0 (C<sub>q</sub>), 134.0 (CH), 133.0 (d,  $J$  = 8.1 Hz, CH), 131.8 (d,  $J$  = 8.7 Hz, CH), 129.3 (d,  $J$  = 3.4 Hz, C<sub>q</sub>), 128.7 (d,  $J$  = 3.5 Hz, C<sub>q</sub>), 126.5 (CH), 125.4 (CH), 123.4 (C<sub>q</sub>), 122.0 (C<sub>q</sub>), 118.0 (CH), 115.6 (d,  $J$  = 21.5 Hz, CH), 115.6 (d,  $J$  = 21.9 Hz, CH). **<sup>19</sup>F{<sup>1</sup>H}-NMR** (376 MHz, CDCl<sub>3</sub>):  $\delta$  = -108.8, -113.9. **IR** (ATR):  $\tilde{\nu}$  = 1626, 1605, 1503, 1462, 1375, 1225, 1154, 825, 759, 518 cm<sup>-1</sup>. **M.p.**: 158–159 °C. **MS** (ESI)  $m/z$  (relative intensity): 335 (100) [M+H]<sup>+</sup>, 357 (50) [M+Na]<sup>+</sup>, 691 (70) [2M+Na]<sup>+</sup>. **HR-MS** (ESI)  $m/z$  calcd for C<sub>21</sub>H<sub>13</sub>O<sub>2</sub>F<sub>2</sub> [M+H]<sup>+</sup>: 335.0878, found: 335.0878.

The spectral data are in accordance with those reported in the literature.<sup>[254]</sup>



**48ah**

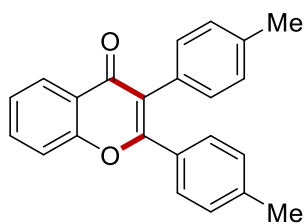
### 2,3-Bis[4-(trifluoromethyl)phenyl]-4H-chromen-4-one

The general procedure B was followed using **26a** (78  $\mu$ L, 0.75 mmol) and **17h** (75.5 mg, 0.24 mmol) at 100 °C for 7 h. Purification by column chromatography on silica gel (*n*hexane/EtOAc = 8:1) yielded **48ah** (52.4 mg, 50%) as a white solid.

**<sup>1</sup>H-NMR** (400 MHz, CDCl<sub>3</sub>):  $\delta$  = 8.30 (dd,  $J$  = 8.0, 1.7 Hz, 1H), 7.76 (ddd,  $J$  = 8.7, 7.2, 1.7 Hz, 1H), 7.61–7.51 (m, 7H), 7.53–7.44 (m, 1H), 7.35 (dt,  $J$  = 7.8, 0.9 Hz, 2H). **<sup>13</sup>C-NMR** (101 MHz, CDCl<sub>3</sub>):  $\delta$  = 176.8 (C<sub>q</sub>), 160.3 (C<sub>q</sub>), 156.1 (C<sub>q</sub>), 136.4–136.3 (m, C<sub>q</sub>), 136.3–136.2 (m, C<sub>q</sub>), 134.4 (CH), 132.4 (q, <sup>2</sup> $J_{C-F}$  = 32.9 Hz, C<sub>q</sub>), 131.7 (CH), 130.2 (q, <sup>2</sup> $J_{C-F}$  = 32.6 Hz, C<sub>q</sub>), 130.1 (CH), 126.6 (CH), 125.8 (CH), 125.5 (q, <sup>3</sup> $J_{C-F}$  = 3.8 Hz, CH), 125.5 (q, <sup>3</sup> $J_{C-F}$  = 3.8 Hz, CH), 124.2 (q, <sup>1</sup> $J_{C-F}$  = 271.8 Hz, C<sub>q</sub>), 123.6 (q, <sup>1</sup> $J_{C-F}$  = 272.6 Hz, C<sub>q</sub>), 123.4 (C<sub>q</sub>), 122.7 (C<sub>q</sub>), 118.2 (CH). **<sup>19</sup>F{<sup>1</sup>H}-NMR** (376 MHz, CDCl<sub>3</sub>):  $\delta$  = -62.7, -63.1. **IR** (ATR):  $\tilde{\nu}$  = 1638, 1613, 1463, 1321, 1160, 1104, 1065, 1012, 840, 770 cm<sup>-1</sup>. **M.p.**: 170–172 °C. **MS** (ESI)  $m/z$  (relative intensity): 435 (50) [M+H]<sup>+</sup>, 457 (50) [M+Na]<sup>+</sup>, 891 (100) [2M+Na]<sup>+</sup>. **HR-MS** (ESI)  $m/z$  calcd for C<sub>23</sub>H<sub>13</sub>O<sub>2</sub>F<sub>6</sub> [M+H]<sup>+</sup>: 435.0814, found: 435.0816.

The spectral data are in accordance with those reported in the literature.<sup>[254]</sup>

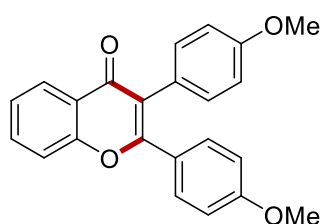


**48ab****2,3-Di-*p*-tolyl-4*H*-chromen-4-one**

The general procedure B was followed using **26a** (78  $\mu$ L, 0.75 mmol) and **17b** (51.6 mg, 0.25 mmol) at 100 °C for 3.5 h. Purification by column chromatography on silica gel (*n*hexane/EtOAc = 12:1) yielded **48ab** (76.9 mg, 94%) as a white solid.

**<sup>1</sup>H-NMR** (400 MHz, CDCl<sub>3</sub>):  $\delta$  = 8.30 (dd,  $J$  = 8.1, 1.7 Hz, 1H), 7.68 (ddd,  $J$  = 8.6, 7.1, 1.7 Hz, 1H), 7.52 (dd,  $J$  = 8.6, 1.1 Hz, 1H), 7.41 (ddd,  $J$  = 8.1, 7.1, 1.1 Hz, 1H), 7.35–7.30 (m, 2H), 7.16–7.12 (m, 4H), 7.09 (d,  $J$  = 8.1 Hz, 2H), 2.36 (s, 3H), 2.34 (s, 3H). **<sup>13</sup>C-NMR** (101 MHz, CDCl<sub>3</sub>):  $\delta$  = 177.6 (C<sub>q</sub>), 161.5 (C<sub>q</sub>), 156.1 (C<sub>q</sub>), 140.4 (C<sub>q</sub>), 137.2 (C<sub>q</sub>), 133.6 (CH), 131.1 (CH), 130.6 (C<sub>q</sub>), 130.1 (C<sub>q</sub>), 129.6 (CH), 129.1 (CH), 128.9 (CH), 126.4 (CH), 125.0 (CH), 123.6 (C<sub>q</sub>), 122.6 (C<sub>q</sub>), 118.0 (CH), 21.5 (CH<sub>3</sub>), 21.4 (CH<sub>3</sub>). **IR** (ATR):  $\tilde{\nu}$  = 1637, 1604, 1459, 1371, 1225, 1042, 1013, 814, 751, 500 cm<sup>-1</sup>. **M.p.**: 139–140 °C. **MS** (ESI)  $m/z$  (relative intensity): 327 (100) [M+H]<sup>+</sup>, 349 (20) [M+Na]<sup>+</sup>, 675 (50) [2M+Na]<sup>+</sup>. **HR-MS** (ESI)  $m/z$  calcd for C<sub>23</sub>H<sub>19</sub>O<sub>2</sub> [M+H]<sup>+</sup>: 327.1380, found: 327.1381.

The spectral data are in accordance with those reported in the literature.<sup>[255]</sup>

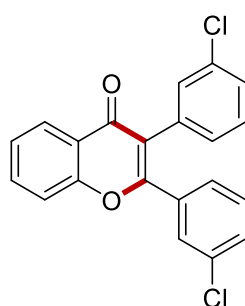
**48ai****2,3-Bis(4-methoxyphenyl)-4*H*-chromen-4-one**

The general procedure B was followed using **26a** (78  $\mu$ L, 0.75 mmol) and **17i** (59.6 mg, 0.25 mmol) at 100 °C for 3.5 h. Purification by column chromatography on silica gel (*n*hexane/EtOAc = 5:1 to 3:1) yielded **48ai** (74.8 mg, 74%) as a white solid.

**<sup>1</sup>H-NMR** (400 MHz, CDCl<sub>3</sub>):  $\delta$  = 8.27 (dd,  $J$  = 7.9, 1.6 Hz, 1H), 7.67 (ddd,  $J$  = 8.7, 7.1, 1.7 Hz, 1H), 7.51 (d,  $J$  = 8.4 Hz, 1H), 7.42–7.34 (m, 3H), 7.17 (d,  $J$  = 8.7 Hz, 2H), 6.87 (d,

$J = 8.7$  Hz, 2H), 6.79 (d,  $J = 8.9$  Hz, 2H), 3.81 (s, 3H), 3.79 (s, 3H).  $^{13}\text{C-NMR}$  (101 MHz,  $\text{CDCl}_3$ ):  $\delta = 177.6$  ( $\text{C}_q$ ), 161.2 ( $\text{C}_q$ ), 160.9 ( $\text{C}_q$ ), 159.0 ( $\text{C}_q$ ), 156.0 ( $\text{C}_q$ ), 133.5 (CH), 132.4 (CH), 131.3 (CH), 126.4 (CH), 125.7 ( $\text{C}_q$ ), 125.5 ( $\text{C}_q$ ), 124.9 (CH), 123.5 ( $\text{C}_q$ ), 121.6 ( $\text{C}_q$ ), 117.9 (CH), 114.0 (CH), 113.6 (CH), 55.4 ( $\text{CH}_3$ ), 55.3 ( $\text{CH}_3$ ). **IR** (ATR):  $\tilde{\nu} = 1600, 1504, 1462, 1381, 1239, 1171, 1024, 826, 759, 522$   $\text{cm}^{-1}$ . **M.p.**: 151–153 °C. **MS** (ESI)  $m/z$  (relative intensity): 359 (90)  $[\text{M}+\text{H}]^+$ , 381 (40)  $[\text{M}+\text{Na}]^+$ , 739 (100)  $[2\text{M}+\text{Na}]^+$ . **HR-MS** (ESI)  $m/z$  calcd for  $\text{C}_{23}\text{H}_{19}\text{O}_4$   $[\text{M}+\text{H}]^+$ : 359.1278, found: 359.1279.

The spectral data are in accordance with those reported in the literature.<sup>[91]</sup>

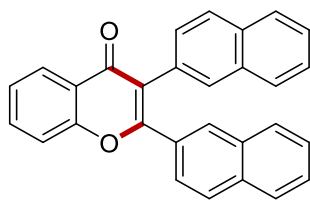


**48aj**

### 2,3-Bis(3-chlorophenyl)-4H-chromen-4-one

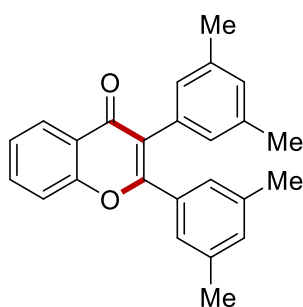
The general procedure B was followed using **26a** (78  $\mu\text{L}$ , 0.75 mmol) and **17j** (61.8 mg, 0.25 mmol) at 100 °C for 3.5 h. Purification by column chromatography on silica gel (*n*hexane/EtOAc = 8:1) yielded **48aj** (52.0 mg, 55%) as a white solid.

$^1\text{H-NMR}$  (400 MHz,  $\text{CDCl}_3$ ):  $\delta = 8.20$  (dd,  $J = 8.2, 1.7$  Hz, 1H), 7.69–7.63 (m, 1H), 7.48 (d,  $J = 8.6$ , 1H), 7.46–7.41 (m, 1H), 7.41–7.35 (m, 1H), 7.30–7.25 (m, 1H), 7.24–7.16 (m, 3H), 7.16–7.06 (m, 2H), 7.01–6.97 (m, 1H).  $^{13}\text{C-NMR}$  (101 MHz,  $\text{CDCl}_3$ ):  $\delta = 176.9$  ( $\text{C}_q$ ), 160.2 ( $\text{C}_q$ ), 156.1 ( $\text{C}_q$ ), 134.6 ( $\text{C}_q$ ), 134.5 ( $\text{C}_q$ ), 134.4 ( $\text{C}_q$ ), 134.2 (CH), 131.3 (CH), 130.6 (CH), 129.8 (CH), 129.6 (CH), 129.5 (CH), 129.4 (CH), 128.3 (CH), 128.1 (CH), 126.5 (CH), 125.6 (CH), 123.4 ( $\text{C}_q$ ), 122.3 ( $\text{C}_q$ ), 118.1 (CH). **IR** (ATR):  $\tilde{\nu} = 1640, 1564, 1466, 1372, 1225, 1085, 1052, 787, 755, 697$   $\text{cm}^{-1}$ . **M.p.**: 148–150 °C. **MS** (ESI)  $m/z$  (relative intensity): 367.0 (100)  $[\text{M}+\text{H}]^+$  ( $^{35}\text{Cl}$ ), 389.0 (30)  $[\text{M}+\text{Na}]^+$  ( $^{35}\text{Cl}$ ), 757 (80)  $[2\text{M}+\text{Na}]^+$  ( $^{35}\text{Cl}$ ). **HR-MS** (ESI)  $m/z$  calcd for  $\text{C}_{21}\text{H}_{13}\text{O}_2^{35}\text{Cl}_2$   $[\text{M}+\text{H}]^+$ : 367.0287, found: 367.0289.

**48ak****2,3-Di(naphthalen-2-yl)-4H-chromen-4-one**

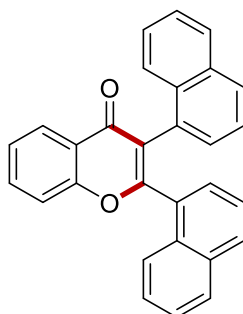
The general procedure B was followed using **26a** (78  $\mu$ L, 0.75 mmol) and **17k** (69.6 mg, 0.25 mmol) at 100 °C for 7 h. Purification by column chromatography on silica gel (nhexane/EtOAc = 10:1 to 5:1) yielded **48ak** (81.5 mg, 82%) as a brown solid.

**<sup>1</sup>H-NMR** (400 MHz, CDCl<sub>3</sub>):  $\delta$  = 8.37 (dd,  $J$  = 8.0, 1.6 Hz, 1H), 8.14 (s, 1H), 7.86 (s, 1H), 7.80 (d,  $J$  = 8.0 Hz, 1H), 7.78–7.70 (m, 5H), 7.63 (d,  $J$  = 8.5 Hz, 1H), 7.57 (d,  $J$  = 8.5 Hz, 1H), 7.52–7.40 (m, 5H), 7.37–7.30 (m, 2H). **<sup>13</sup>C-NMR** (101 MHz, CDCl<sub>3</sub>):  $\delta$  = 177.6 (C<sub>q</sub>), 161.7 (C<sub>q</sub>), 156.3 (C<sub>q</sub>), 133.9 (CH), 133.8 (C<sub>q</sub>), 133.5 (C<sub>q</sub>), 132.9 (C<sub>q</sub>), 132.7 (C<sub>q</sub>), 130.9 (CH), 130.8 (C<sub>q</sub>), 130.4 (C<sub>q</sub>), 130.1 (CH), 129.1 (CH), 128.9 (CH), 128.3 (CH), 128.0 (CH), 127.7 (CH), 126.7 (CH), 126.5 (CH), 126.3 (CH), 126.2 (CH), 125.9 (CH), 125.3 (CH), 123.7 (C<sub>q</sub>), 123.1 (C<sub>q</sub>), 118.1 (CH). **IR** (ATR):  $\tilde{\nu}$  = 1622, 1464, 1383, 1342, 1218, 904, 858, 741, 660, 473 cm<sup>-1</sup>. **M.p.**: 110–111 °C. **MS** (ESI)  $m/z$  (relative intensity): 399 (100) [M+H]<sup>+</sup>, 421 (10) [M+Na]<sup>+</sup>, 819 (20) [2M+Na]<sup>+</sup>. **HR-MS** (ESI)  $m/z$  calcd for C<sub>29</sub>H<sub>19</sub>O<sub>2</sub> [M+H]<sup>+</sup>: 399.1380, found: 399.1381.

**48al****2,3-Bis(3,5-dimethylphenyl)-4H-chromen-4-one**

The general procedure B was followed using **26a** (78  $\mu$ L, 0.75 mmol) and **17l** (58.5 mg, 0.25 mmol) at 100 °C for 3.5 h. Purification by column chromatography on silica gel (nhexane/EtOAc = 20:1) yielded **48al** (81.3 mg, 92%) as a brown solid.

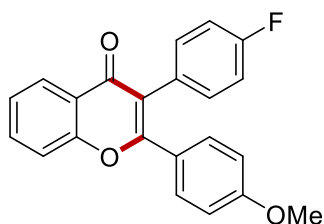
**<sup>1</sup>H-NMR** (400 MHz, CDCl<sub>3</sub>):  $\delta$  = 8.32 (dd,  $J$  = 8.1, 1.7 Hz, 1H), 7.71 (ddd,  $J$  = 8.6, 7.1, 1.7 Hz, 1H), 7.57 (dd,  $J$  = 8.6, 1.1 Hz, 1H), 7.43 (ddd,  $J$  = 8.1, 7.1, 1.1 Hz, 1H), 7.04 (s, 2H), 6.97 (s, 1H), 6.93 (s, 1H), 6.85 (s, 2H), 2.26 (s, 6H), 2.22 (s, 6H). **<sup>13</sup>C-NMR** (101 MHz, CDCl<sub>3</sub>):  $\delta$  = 177.7 (C<sub>q</sub>), 161.6 (C<sub>q</sub>), 156.1 (C<sub>q</sub>), 137.6 (C<sub>q</sub>), 137.5 (C<sub>q</sub>), 133.6 (CH), 133.2 (C<sub>q</sub>), 132.9 (C<sub>q</sub>), 131.7 (CH), 129.3 (CH), 128.8 (CH), 127.4 (CH), 126.4 (CH), 125.0 (CH), 123.6 (C<sub>q</sub>), 123.2 (C<sub>q</sub>), 118.0 (CH), 21.4 (CH<sub>3</sub>), 21.3 (CH<sub>3</sub>). **IR** (ATR):  $\tilde{\nu}$  = 2914, 1633, 1605, 1463, 1369, 1223, 1181, 1084, 847, 766 cm<sup>-1</sup>. **M.p.**: 153–155 °C. **MS** (ESI)  $m/z$  (relative intensity): 355 (100) [M+H]<sup>+</sup>, 731 (60) [2M+Na]<sup>+</sup>. **HR-MS** (ESI)  $m/z$  calcd for C<sub>25</sub>H<sub>23</sub>O<sub>2</sub> [M+H]<sup>+</sup>: 355.1698, found: 355.1694.

**48am**

### 2,3-Di(naphthalen-1-yl)-4H-chromen-4-one

The general procedure B was followed using **26a** (78  $\mu$ L, 0.75 mmol) and **17m** (69.6 mg, 0.25 mmol) at 100 °C for 7 h. Purification by column chromatography on silica gel (*n*hexane/EtOAc = 12:1 to 8:1) yielded **48am** (83.7 mg, 82%) as a yellow solid.

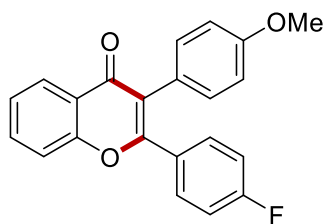
**<sup>1</sup>H-NMR** (400 MHz, CDCl<sub>3</sub>):  $\delta$  = 8.44 (dd,  $J$  = 8.0, 1.6 Hz, 1H), 8.02 (d,  $J$  = 7.3 Hz, 1H), 7.93–7.88 (m, 1H), 7.80 (dd,  $J$  = 7.3, 2.0 Hz, 1H), 7.79–7.74 (m, 2H), 7.72 (d,  $J$  = 8.2 Hz, 1H), 7.67–7.63 (m, 1H), 7.57–7.48 (m, 4H), 7.47–7.41 (m, 2H), 7.22 (d,  $J$  = 7.1 Hz, 1H), 7.15–7.11 (m, 2H), 7.08 (t,  $J$  = 7.7 Hz, 1H). **<sup>13</sup>C-NMR** (101 MHz, CDCl<sub>3</sub>):  $\delta$  = 177.4 (C<sub>q</sub>), 163.8 (C<sub>q</sub>), 156.6 (C<sub>q</sub>), 134.0 (CH), 133.5 (C<sub>q</sub>), 133.3 (C<sub>q</sub>), 132.6 (C<sub>q</sub>), 131.0 (C<sub>q</sub>), 131.0 (C<sub>q</sub>), 130.7 (C<sub>q</sub>), 130.4 (CH), 128.6 (CH), 128.5 (CH), 128.5 (CH), 128.3 (CH), 127.7 (CH), 127.1 (CH), 126.7 (CH), 126.3 (CH), 126.3 (CH), 125.7 (CH), 125.7 (CH), 125.5 (CH), 125.3 (CH), 125.2 (CH), 124.9 (C<sub>q</sub>), 124.7 (CH), 123.8 (C<sub>q</sub>), 118.3 (CH). **IR** (ATR):  $\tilde{\nu}$  = 1642, 1616, 1566, 1461, 1363, 1212, 1112, 891, 762, 674 cm<sup>-1</sup>. **M.p.**: 224–226 °C. **MS** (ESI)  $m/z$  (relative intensity): 399 (100) [M+H]<sup>+</sup>, 421 (30) [M+Na]<sup>+</sup>, 819 (50) [2M+Na]<sup>+</sup>. **HR-MS** (ESI)  $m/z$  calcd for C<sub>29</sub>H<sub>19</sub>O<sub>2</sub> [M+H]<sup>+</sup>: 399.1380, found: 399.1382.

**172aa****3-(4-Fluorophenyl)-2-(4-methoxyphenyl)-4H-chromen-4-one**

The general procedure B was followed using **26a** (78  $\mu$ L, 0.75 mmol) and **171a** (56.6 mg, 0.25 mmol) at 100 °C for 3.5 h. Purification by column chromatography on silica gel (*n*hexane/EtOAc = 8:1 to 5:1) yielded **172aa** (47.2 mg, 55%) as a white solid and **172aa'** (24.3 mg, 28%) as white solid.

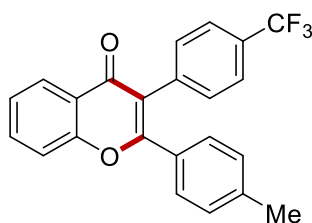
**<sup>1</sup>H-NMR** (400 MHz, CDCl<sub>3</sub>):  $\delta$  = 8.27 (dd,  $J$  = 8.1, 1.7 Hz, 1H), 7.69 (ddd,  $J$  = 8.6, 7.2, 1.7 Hz, 1H), 7.53 (dd,  $J$  = 8.6, 1.1 Hz, 1H), 7.42 (ddd,  $J$  = 8.1, 7.2, 1.1 Hz, 1H), 7.37–7.32 (m, 2H), 7.25–7.19 (m, 2H), 7.06–6.99 (m, 2H), 6.83–6.78 (m, 2H), 3.80 (s, 3H). **<sup>13</sup>C-NMR** (101 MHz, CDCl<sub>3</sub>):  $\delta$  = 177.4 (C<sub>q</sub>), 162.3 (d,  $^1J_{C-F}$  = 246.8 Hz, C<sub>q</sub>), 161.6 (C<sub>q</sub>), 161.1 (C<sub>q</sub>), 156.1 (C<sub>q</sub>), 133.7 (CH), 133.0 (d,  $^3J_{C-F}$  = 8.2 Hz, CH), 131.3 (CH), 129.3 (d,  $^4J_{C-F}$  = 3.6 Hz, C<sub>q</sub>), 126.4 (CH), 125.3 (C<sub>q</sub>), 125.2 (CH), 123.5 (C<sub>q</sub>), 121.1 (C<sub>q</sub>), 118.0 (CH), 115.5 (d,  $^2J_{C-F}$  = 21.5 Hz, CH), 113.7 (CH), 55.4 (CH<sub>3</sub>). **<sup>19</sup>F{<sup>1</sup>H}-NMR** (377 MHz, CDCl<sub>3</sub>):  $\delta$  = –114.5 (m, 1F). **M.p.**: 201–202 °C. **IR** (ATR):  $\tilde{\nu}$  = 1598, 1561, 1462, 1375, 1251, 1226, 1021, 829, 763, 518 cm<sup>-1</sup>. **MS** (ESI)  $m/z$  (relative intensity): 347 (100) [M+H]<sup>+</sup>, 369 (20) [M+Na]<sup>+</sup>, 715 (60) [2M+Na]<sup>+</sup>. **HR-MS** (ESI)  $m/z$  calcd for C<sub>22</sub>H<sub>16</sub>FO<sub>3</sub> [M+H]<sup>+</sup>: 347.1078, found: 347.1079.

The spectral data are in accordance with those reported in the literature.<sup>[219]</sup>

**172aa'****2-(4-Fluorophenyl)-3-(4-methoxyphenyl)-4*H*-chromen-4-one**

**<sup>1</sup>H-NMR** (400 MHz, CDCl<sub>3</sub>):  $\delta$  = 8.29 (ddd,  $J$  = 7.9, 1.8, 0.5 Hz, 1H), 7.70 (ddd,  $J$  = 8.7, 7.1, 1.7 Hz, 1H), 7.52 (ddd,  $J$  = 8.5, 1.1, 0.5 Hz, 1H), 7.47–7.37 (m, 3H), 7.18–7.09 (m, 2H), 7.05–6.93 (m, 2H), 6.90–6.82 (m, 2H), 3.81 (s, 3H). **<sup>13</sup>C-NMR** (101 MHz, CDCl<sub>3</sub>):  $\delta$  = 177.6 (C<sub>q</sub>), 163.5 (d,  $^1J_{C-F}$  = 251.8 Hz, C<sub>q</sub>), 160.3 (C<sub>q</sub>), 159.3 (C<sub>q</sub>), 156.1 (C<sub>q</sub>), 133.8 (CH), 132.4 (CH), 131.8 (d,  $^3J_{C-F}$  = 8.6 Hz, CH), 129.7 (d,  $^4J_{C-F}$  = 3.3 Hz, C<sub>q</sub>), 126.6 (CH), 125.2 (CH), 124.9 (C<sub>q</sub>), 123.6 (C<sub>q</sub>), 122.6 (C<sub>q</sub>), 118.0 (CH), 115.5 (d,  $^2J_{C-F}$  = 21.8 Hz, CH), 114.1 (CH), 55.4 (CH<sub>3</sub>). **<sup>19</sup>F{<sup>1</sup>H}-NMR** (377 MHz, CDCl<sub>3</sub>):  $\delta$  = -109.4 (m, 1F). **IR** (ATR):  $\tilde{\nu}$  = 1633, 1603, 1505, 1462, 1376, 1227, 1020, 825, 763, 515 cm<sup>-1</sup>. **M.p.**: 145–146 °C. **MS** (ESI)  $m/z$  (relative intensity): 347 (100) [M+H]<sup>+</sup>, 369 (50) [M+Na]<sup>+</sup>, 715 (60) [2M+Na]<sup>+</sup>. **HR-MS** (ESI)  $m/z$  calcd for C<sub>22</sub>H<sub>16</sub>FO<sub>3</sub> [M+H]<sup>+</sup>: 347.1078, found: 347.1077.

The spectral data are in accordance with those reported in the literature.<sup>[219]</sup>

**172ab (2:1)****2-(*p*-Tolyl)-3-[4-(trifluoromethyl)phenyl]-4*H*-chromen-4-one (mixture of isomers)**

The general procedure B was followed using **26a** (78  $\mu$ L, 0.75 mmol) and **171b** (65.1 mg, 0.25 mmol) at 100 °C for 3.5 h. Purification by column chromatography on silica gel (*n*hexane/EtOAc = 10:1) yielded **172ab** as a 2:1 mixture of isomers (72.7 mg, 76%) appearing as a white solid.

**<sup>1</sup>H-NMR** (300 MHz, CDCl<sub>3</sub>):  $\delta$  = 8.25–8.16 (m, 1H), 7.63–7.59 (m, 1H), 7.50–7.42 (m, 4H), 7.38–7.32 (m, 1H), 7.28 (d,  $J$  = 8.2 Hz, 1H), 7.18 (d,  $J$  = 8.2 Hz, 1H), 7.07–6.98 (m, 3H), 2.29–2.23 (m, 3H). **<sup>19</sup>F{<sup>1</sup>H}-NMR** (282 MHz, CDCl<sub>3</sub>):  $\delta$  = -62.5, -62.9. **IR** (ATR):  $\tilde{\nu}$  =

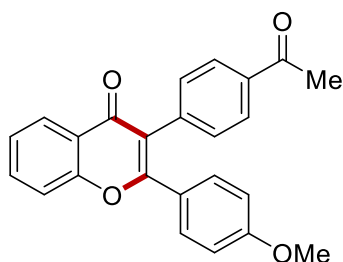
1641, 1614, 1465, 1377, 1322, 1165, 1119, 1068, 760  $\text{cm}^{-1}$ . **M.p.:** 143–144 °C. **MS** (ESI)  $m/z$  (relative intensity): 381 (100)  $[\text{M}+\text{H}]^+$ , 403 (40)  $[\text{M}+\text{Na}]^+$ , 783 (60)  $[2\text{M}+\text{Na}]^+$ . **HR-MS** (ESI)  $m/z$  calcd for  $\text{C}_{23}\text{H}_{16}\text{F}_3\text{O}_2$   $[\text{M}+\text{H}]^+$ : 381.1097, found: 381.1098.

Major isomer:

$^{13}\text{C}\{^1\text{H},^{19}\text{F}\}$ -NMR (151 MHz,  $\text{CDCl}_3$ ):  $\delta$  = 177.0 ( $\text{C}_q$ ), 162.4 ( $\text{C}_q$ ), 156.1 ( $\text{C}_q$ ), 141.1 ( $\text{C}_q$ ), 137.2 ( $\text{C}_q$ ), 134.0 (CH), 131.8 (CH), 129.9 ( $\text{C}_q$ ), 129.6 ( $\text{C}_q$ ), 129.6 (CH), 129.2 (CH), 126.4 (CH), 125.4 (CH), 125.3 (CH), 124.3 ( $\text{C}_q$ ), 123.5 ( $\text{C}_q$ ), 121.5 ( $\text{C}_q$ ), 118.1 (CH), 21.6 ( $\text{CH}_3$ ).

Minor isomer:

$^{13}\text{C}\{^1\text{H},^{19}\text{F}\}$ -NMR (151 MHz,  $\text{CDCl}_3$ ):  $\delta$  = 177.5 ( $\text{C}_q$ ), 159.5 ( $\text{C}_q$ ), 156.1 ( $\text{C}_q$ ), 138.0 ( $\text{C}_q$ ), 137.0 ( $\text{C}_q$ ), 134.0 (CH), 131.7 ( $\text{C}_q$ ), 131.0 (CH), 130.1 (CH), 129.4 (CH), 129.2 ( $\text{C}_q$ ), 126.6 (CH), 125.4 (CH), 125.2 (CH), 123.8 ( $\text{C}_q$ ), 123.8 ( $\text{C}_q$ ), 123.6 ( $\text{C}_q$ ), 118.1 (CH), 21.4 ( $\text{CH}_3$ ).



**172ac**

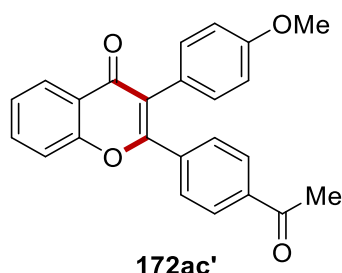
### 3-(4-Acetylphenyl)-2-(4-methoxyphenyl)-4H-chromen-4-one

The general procedure B was followed using **26a** (78  $\mu\text{L}$ , 0.75 mmol) and **171c** (62.5 mg, 0.25 mmol) at 100 °C for 3.5 h. Purification by column chromatography on silica gel (*n*hexane/EtOAc = 6:1 to 4:1) yielded **172ac** (54.2 mg, 59%) as a white solid and isomer **172ac'** (18.1 mg, 20%) as a white solid.

$^1\text{H}$ -NMR (400 MHz,  $\text{CDCl}_3$ ):  $\delta$  = 8.26 (dd,  $J$  = 8.0, 1.7 Hz, 1H), 7.92–7.89 (m, 2H), 7.70 (ddd,  $J$  = 8.6, 7.1, 1.7 Hz, 1H), 7.53 (dd,  $J$  = 8.6, 1.1 Hz, 1H), 7.42 (ddd,  $J$  = 8.0, 7.1, 1.1 Hz, 1H), 7.37–7.34 (m, 2H), 7.34–7.31 (m, 2H), 6.79–6.76 (m, 2H), 3.78 (s, 3H), 2.59 (s, 3H).

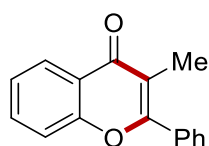
$^{13}\text{C}$ -NMR (101 MHz,  $\text{CDCl}_3$ ):  $\delta$  = 198.1 ( $\text{C}_q$ ), 176.9 ( $\text{C}_q$ ), 161.9 ( $\text{C}_q$ ), 161.3 ( $\text{C}_q$ ), 156.0 ( $\text{C}_q$ ), 138.9 ( $\text{C}_q$ ), 136.0 ( $\text{C}_q$ ), 133.9 (CH, C), 131.7 (CH), 131.4 (CH), 128.4 (CH), 126.4 (CH), 125.3 (CH), 125.0 ( $\text{C}_q$ ), 123.4 ( $\text{C}_q$ ), 121.1 ( $\text{C}_q$ ), 118.0 (CH), 113.8 (CH), 55.4 ( $\text{CH}_3$ ), 26.8 ( $\text{CH}_3$ ). **IR** (ATR):  $\tilde{\nu}$  = 1679, 1629, 1576, 1501, 1467, 1379, 1297, 1261, 1181, 1105  $\text{cm}^{-1}$ .

**M.p.:** 198–200 °C. **MS** (ESI)  $m/z$  (relative intensity): 371 (100)  $[M+H]^+$ , 763 (15)  $[2M+Na]^+$ . **HR-MS** (ESI)  $m/z$  calcd for  $C_{24}H_{19}O_4$   $[M+H]^+$ : 371.1283, found: 371.1278.



### 2-(4-Acetylphenyl)-3-(4-methoxyphenyl)-4H-chromen-4-one

**$^1H$ -NMR** (400 MHz,  $CDCl_3$ ):  $\delta$  = 8.29 (dd,  $J$  = 8.1, 1.7 Hz, 1H), 7.88–7.85 (m, 2H), 7.72 (ddd,  $J$  = 8.6, 7.1, 1.7 Hz, 1H), 7.54 (d,  $J$  = 8.6 Hz, 1H), 7.53–7.51 (m, 2H), 7.44 (ddd,  $J$  = 8.1, 7.1, 1.1 Hz, 1H), 7.14–7.11 (m, 2H), 6.87–6.83 (m, 2H), 3.81 (s, 3H), 2.59 (s, 3H).  **$^{13}C$ -NMR** (101 MHz,  $CDCl_3$ ):  $\delta$  = 197.5 ( $C_q$ ), 177.6 ( $C_q$ ), 159.9 ( $C_q$ ), 159.4 ( $C_q$ ), 156.1 ( $C_q$ ), 138.0 ( $C_q$ ), 137.7 ( $C_q$ ), 134.0 (CH), 132.4 (CH), 130.0 (CH), 128.1 (CH), 126.6 (CH), 125.4 (CH), 124.5 ( $C_q$ ), 123.6 ( $C_q$ ), 123.4 ( $C_q$ ), 118.1 (CH), 114.1 (CH), 55.4 ( $CH_3$ ), 26.8 ( $CH_3$ ). **IR** (ATR):  $\tilde{\nu}$  = 1683, 1637, 1572, 1512, 1463, 1377, 1295, 1264, 1175, 1105  $cm^{-1}$ . **M.p.:** 196–198 °C. **MS** (ESI)  $m/z$  (relative intensity): 371 (100)  $[M+H]^+$ , 763 (15)  $[2M+Na]^+$ . **HR-MS** (ESI)  $m/z$  calcd for  $C_{24}H_{19}O_4$   $[M+H]^+$ : 371.1283, found: 371.1279.



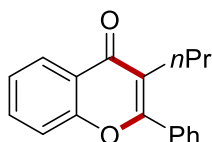
### 3-Methyl-2-phenyl-4H-chromen-4-one

The general procedure B was followed using **26a** (78  $\mu$ L, 0.75 mmol) and **171d** (29.1 mg, 0.25 mmol) at 100 °C for 7 h. Purification by column chromatography on silica gel (*n*hexane/EtOAc = 15:1) yielded **172ad** (32.8 mg, 55%) as a colorless oil.  **$^1H$ -NMR** (300 MHz,  $CDCl_3$ ):  $\delta$  = 8.26 (dd,  $J$  = 8.0, 1.7 Hz, 1H), 7.68–7.61 (m, 3H), 7.55–7.49 (m, 3H), 7.45 (dd,  $J$  = 8.5, 1.1 Hz, 1H), 7.39 (ddd,  $J$  = 8.0, 7.1, 1.1 Hz, 1H), 2.17 (s, 3H).  **$^{13}C$ -NMR** (101 MHz,  $CDCl_3$ ):  $\delta$  = 179.0 ( $C_q$ ), 161.1 ( $C_q$ ), 156.3 ( $C_q$ ), 133.6 ( $C_q$ ), 133.5 (CH), 130.3 (CH), 129.1 (CH), 128.6 (CH), 126.0 (CH), 124.8 (CH), 122.6 ( $C_q$ ), 118.0 (CH), 117.7



(C<sub>q</sub>), 11.9 (CH<sub>3</sub>). **IR** (ATR):  $\tilde{\nu}$  = 1631, 1571, 1467, 1380, 1230, 1131, 1015, 761, 697 cm<sup>-1</sup>. **MS** (ESI)  $m/z$  (relative intensity): 237 (100) [M+H]<sup>+</sup>, 259 (20) [M+Na]<sup>+</sup>, 495 (40) [2M+Na]<sup>+</sup>. **HR-MS** (ESI)  $m/z$  calcd for C<sub>16</sub>H<sub>13</sub>O<sub>2</sub> [M+H]<sup>+</sup>: 237.0910, found: 237.0914.

The spectral data are in accordance with those reported in the literature.<sup>[219]</sup>

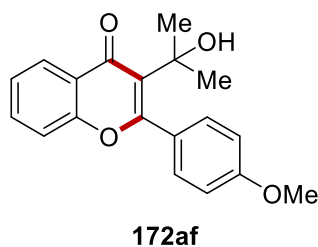


**172ae**

### 3-Propyl-2-phenyl-4H-chromen-4-one

The general procedure B was followed using **26a** (78  $\mu$ L, 0.75 mmol) and **171e** (36.1 mg, 0.25 mmol) at 100 °C for 3.5 h. Purification by column chromatography on silica gel (nhexane/EtOAc = 35:1 to 25:1) yielded **172ae** (37.4 mg, 57%) as a colorless oil.

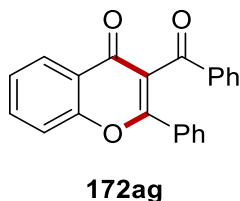
**<sup>1</sup>H-NMR** (400 MHz, CDCl<sub>3</sub>):  $\delta$  = 8.25 (ddd,  $J$  = 8.0, 1.7, 0.5 Hz, 1H), 7.64 (ddd,  $J$  = 8.7, 7.1, 1.7 Hz, 1H), 7.61–7.58 (m, 2H), 7.54–7.50 (m, 3H), 7.44–7.41 (m, 1H), 7.39 (ddd,  $J$  = 8.1, 7.1, 1.1 Hz, 1H), 2.56–2.50 (m, 2H), 1.65–1.53 (m, 2H), 0.90 (t,  $J$  = 7.4 Hz, 3H). **<sup>13</sup>C-NMR** (101 MHz, CDCl<sub>3</sub>):  $\delta$  = 178.6 (C<sub>q</sub>), 161.9 (C<sub>q</sub>), 156.3 (C<sub>q</sub>), 133.8 (C<sub>q</sub>), 133.4 (CH), 130.2 (CH), 128.7 (CH), 128.6 (CH), 126.0 (CH), 124.8 (CH), 123.1 (C<sub>q</sub>), 122.3 (C<sub>q</sub>), 118.0 (CH), 27.9 (CH<sub>2</sub>), 22.6 (CH<sub>2</sub>), 14.3 (CH<sub>3</sub>). **IR** (ATR):  $\tilde{\nu}$  = 2960, 1629, 1569, 1464, 1379, 1224, 1129, 1111, 760, 698 cm<sup>-1</sup>. **MS** (ESI)  $m/z$  (relative intensity): 265 (100) [M+H]<sup>+</sup>, 287 (30) [M+Na]<sup>+</sup>, 551 (70) [2M+Na]<sup>+</sup>. **HR-MS** (ESI)  $m/z$  calcd for C<sub>18</sub>H<sub>17</sub>O<sub>2</sub> [M+H]<sup>+</sup>: 265.1223, found: 265.1223.



### 3-(2-Hydroxypropan-2-yl)-2-(4-methoxyphenyl)-4H-chromen-4-one

The general procedure B was followed using **26a** (78  $\mu$ L, 0.75 mmol) and **171f** (47.5 mg, 0.25 mmol) at 100  $^{\circ}$ C for 7 h. Purification by column chromatography on silica gel (*n*hexane/EtOAc = 6:1 to 5:1) yielded **172af** (43.4 mg, 56%) as a yellow solid.

**$^1$ H-NMR** (400 MHz,  $\text{CDCl}_3$ ):  $\delta$  = 8.24 (dd,  $J$  = 7.9, 1.7 Hz, 1H), 7.67 (ddd,  $J$  = 8.7, 7.1, 1.8 Hz, 1H), 7.43–7.40 (m, 1H), 7.39–7.36 (m, 3H), 7.04–6.97 (m, 2H), 6.44 (s, 1H), 3.88 (s, 3H), 1.32 (s, 6H).  **$^{13}$ C-NMR** (101 MHz,  $\text{CDCl}_3$ ):  $\delta$  = 181.3 ( $\text{C}_q$ ), 162.4 ( $\text{C}_q$ ), 161.1 ( $\text{C}_q$ ), 155.5 ( $\text{C}_q$ ), 134.2 (CH), 130.2 (CH), 127.8 ( $\text{C}_q$ ), 127.5 ( $\text{C}_q$ ), 126.1 (CH), 125.2 (CH), 123.1 ( $\text{C}_q$ ), 117.8 (CH), 113.9 (CH), 72.6 ( $\text{C}_q$ ), 55.5 ( $\text{CH}_3$ ), 31.1 ( $\text{CH}_3$ ). **IR** (ATR):  $\tilde{\nu}$  = 1612, 1582, 1461, 1364, 1248, 1172, 1064, 1025, 763, 620  $\text{cm}^{-1}$ . **M.p.**: 147–149  $^{\circ}$ C. **MS** (ESI)  $m/z$  (relative intensity): 311 (10)  $[\text{M}+\text{H}]^+$ , 333 (90)  $[\text{M}+\text{Na}]^+$ , 643 (100)  $[2\text{M}+\text{Na}]^+$ . **HR-MS** (ESI)  $m/z$  calcd for  $\text{C}_{19}\text{H}_{19}\text{O}_4$   $[\text{M}+\text{H}]^+$ : 311.1278, found: 311.1274.



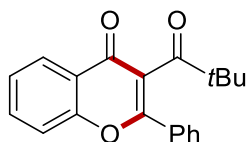
### 3-Acetyl-2-phenyl-4H-chromen-4-one

The general procedure B was followed using **26a** (78  $\mu$ L, 0.75 mmol) and **171g** (51.6 mg, 0.25 mmol) at 100  $^{\circ}$ C for 3.5 h. Purification by column chromatography on silica gel (*n*hexane/EtOAc = 8:1 to 4:1) yielded **172ag** as (42.7 mg, 52%) as a yellowish oil.

**$^1$ H-NMR** (400 MHz,  $\text{CDCl}_3$ ):  $\delta$  = 8.24 (dd,  $J$  = 8.0, 1.7 Hz, 1H), 7.92 (d,  $J$  = 7.9 Hz, 2H), 7.75 (dd,  $J$  = 6.9, 1.7 Hz, 1H), 7.66 (d,  $J$  = 7.2 Hz, 2H), 7.59 (d,  $J$  = 8.4 Hz, 1H), 7.52 (dd,  $J$  = 7.4, 7.4 Hz, 1H), 7.46 (dd,  $J$  = 7.7, 7.7 Hz, 1H), 7.44–7.32 (m, 5H).  **$^{13}$ C-NMR** (101 MHz,  $\text{CDCl}_3$ ):  $\delta$  = 193.6 ( $\text{C}_q$ ), 176.6 ( $\text{C}_q$ ), 162.6 ( $\text{C}_q$ ), 156.2 ( $\text{C}_q$ ), 137.1 ( $\text{C}_q$ ), 134.5 (CH), 133.9 (CH), 131.9 ( $\text{C}_q$ ), 131.6 (CH), 129.5 (CH), 128.9 (CH), 128.8 (CH), 128.6 (CH), 126.2 (CH), 125.8 (CH), 123.4 ( $\text{C}_q$ ), 122.7 ( $\text{C}_q$ ), 118.3 (CH). **IR** (ATR):  $\tilde{\nu}$  = 1674, 1632, 1564, 1464,

1375, 1225, 1117, 859, 762, 694  $\text{cm}^{-1}$ . **MS** (ESI)  $m/z$  (relative intensity): 327 (100)  $[\text{M}+\text{H}]^+$ , 349 (10)  $[\text{M}+\text{Na}]^+$ , 670 (30)  $[2\text{M}+\text{NH}_4]^+$ . **HR-MS** (ESI)  $m/z$  calcd for  $\text{C}_{22}\text{H}_{14}\text{O}_3$   $[\text{M}+\text{H}]^+$ : 327.1016, found: 327.1016.

The spectral data are in accordance with those reported in the literature.<sup>[256]</sup>



**172ah**

### 2-Phenyl-3-pivaloyl-4H-chromen-4-one

The general procedure B was followed using **26a** (78  $\mu\text{L}$ , 0.75 mmol), **171h** (46.6 mg, 0.25 mmol) and  $[\text{Cp}^*\text{RhCl}_2]_2$  (7.7 mg, 5.0 mol %) at 80  $^\circ\text{C}$  for 3.5 h. Purification by column chromatography on silica gel (*n*hexane/EtOAc = 15:1 to 10:1) yielded **172ah** as a 5:1 mixture of isomers (51.0 mg, 67%) appearing as a brownish oil.

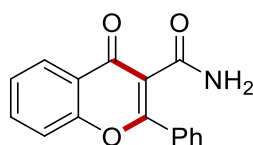
**$^1\text{H-NMR}$**  (300 MHz,  $\text{CDCl}_3$ ):  $\delta$  = 8.27 (dd,  $J$  = 7.9, 1.7 Hz, 0.16H), 8.21 (dd,  $J$  = 8.0, 1.7 Hz, 0.84H), 7.74–7.65 (m, 3H), 7.56–7.42 (m, 4H), 7.41–7.29 (m, 1H), 1.07 (s, 1.42H), 0.96 (s, 7.59H). **IR** (ATR):  $\tilde{\nu}$  = 1698, 1636, 1566, 1466, 1370, 1224, 914, 875, 761, 699  $\text{cm}^{-1}$ . **MS** (ESI)  $m/z$  (relative intensity): 307 (100)  $[\text{M}+\text{H}]^+$ , 329 (10)  $[\text{M}+\text{Na}]^+$ , 630 (25)  $[2\text{M}+\text{NH}_4]^+$ . **HR-MS** (ESI)  $m/z$  calcd for  $\text{C}_{20}\text{H}_{18}\text{O}_3$   $[\text{M}+\text{H}]^+$ : 307.1329, found: 307.1330.

Major isomer:

**$^{13}\text{C-NMR}$**  (126 MHz,  $\text{CDCl}_3$ ):  $\delta$  = 210.5 ( $\text{C}_q$ ), 176.6 ( $\text{C}_q$ ), 159.8 ( $\text{C}_q$ ), 156.2 ( $\text{C}_q$ ), 134.3 (CH), 132.9 ( $\text{C}_q$ ), 131.5 (CH), 129.2 (CH), 128.9 (CH), 126.0 (CH), 125.5 (CH), 124.7 ( $\text{C}_q$ ), 123.1 ( $\text{C}_q$ ), 118.2 (CH), 46.0 ( $\text{C}_q$ ), 27.0 ( $\text{CH}_3$ ).

Minor isomer:

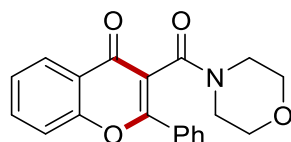
**$^{13}\text{C-NMR}$**  (126 MHz,  $\text{CDCl}_3$ ):  $\delta$  = 204.3 ( $\text{C}_q$ ), 176.6 ( $\text{C}_q$ ), 158.6 ( $\text{C}_q$ ), 155.4 ( $\text{C}_q$ ), 134.3 (CH), 131.0 (CH), 130.3 ( $\text{C}_q$ ), 128.6 (CH), 128.4 (CH), 126.5 (CH), 125.8 (CH), 124.0 ( $\text{C}_q$ ), 121.9 ( $\text{C}_q$ ), 118.1 (CH), 44.4 ( $\text{C}_q$ ), 26.6 ( $\text{CH}_3$ ).

**172ai**

#### 4-Oxo-2-phenyl-4H-chromene-3-carboxamide

The general procedure B was followed using **26a** (78  $\mu$ L, 0.75 mmol), **171i** (36.3 mg, 0.25 mmol) and [Cp\* $\text{RhCl}_2$ ]<sub>2</sub> (7.7 mg, 5.0 mol %) at 100 °C for 3.5 h. Purification by column chromatography on silica gel (*n*hexane/EtOAc = 1:1 to 1:3) yielded **172ai** (32.8 mg, 49%) as a white solid.

**<sup>1</sup>H-NMR** (400 MHz, CDCl<sub>3</sub>):  $\delta$  = 8.26 (d,  $J$  = 7.9 Hz, 1H), 8.03 (brs, 1H), 7.77–7.70 (m, 3H), 7.59–7.43 (m, 5H), 5.84 (brs, 1H). **<sup>13</sup>C-NMR** (101 MHz, CDCl<sub>3</sub>):  $\delta$  = 177.2 (C<sub>q</sub>), 169.2 (C<sub>q</sub>), 165.7 (C<sub>q</sub>), 155.6 (C<sub>q</sub>), 134.7 (CH), 133.4 (C<sub>q</sub>), 131.4 (CH), 128.8 (CH), 128.5 (CH), 126.3 (CH), 126.1 (CH), 123.4 (C<sub>q</sub>), 118.2 (CH), 116.2 (C<sub>q</sub>). **IR** (ATR):  $\tilde{\nu}$  = 3321, 1671, 1624, 1564, 1466, 1394, 1224, 1103, 760, 697 cm<sup>-1</sup>. **M.p.**: 220–222 °C. **MS** (ESI)  $m/z$  (relative intensity): 266 (100) [M+H]<sup>+</sup>, 288 (30) [M+Na]<sup>+</sup>, 553 (30) [2M+Na]<sup>+</sup>. **HR-MS** (ESI)  $m/z$  calcd for C<sub>16</sub>H<sub>11</sub>NO<sub>3</sub> [M+H]<sup>+</sup>: 266.0812, found: 266.0815.

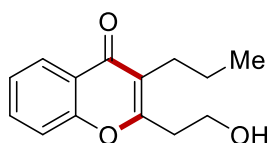
**172aj**

#### 3-(Morpholine-4-carbonyl)-2-phenyl-4H-chromen-4-one

The general procedure B was followed using **26a** (78  $\mu$ L, 0.75 mmol), **171j** (53.8 mg, 0.25 mmol) and [Cp\* $\text{RhCl}_2$ ]<sub>2</sub> (7.7 mg, 5.0 mol %) at 80 °C for 3.5 h. Purification by column chromatography on silica gel (*n*hexane/EtOAc = 1:1 to 1:3) yielded **172aj** (57.8 mg, 69%) as a brownish solid.

**<sup>1</sup>H-NMR** (400 MHz, CDCl<sub>3</sub>):  $\delta$  = 8.21 (d,  $J$  = 7.9 Hz, 1H), 7.83 (d,  $J$  = 7.5 Hz, 2H), 7.71 (dd,  $J$  = 7.8 Hz, 7.8 Hz, 1H), 7.55–7.47 (m, 4H), 7.42 (dd,  $J$  = 7.6 Hz, 7.6 Hz, 1H), 3.79–3.66 (m, 3H), 3.54 (ddd,  $J$  = 11.2, 6.3, 3.0 Hz, 1H), 3.51–3.44 (m, 1H), 3.33 (ddd,  $J$  = 13.4, 6.9, 3.0 Hz, 1H), 3.13 (ddd,  $J$  = 13.4, 6.3, 3.1 Hz, 1H), 2.99 (ddd,  $J$  = 10.5, 6.9, 3.0 Hz, 1H).

**<sup>13</sup>C-NMR** (101 MHz, CDCl<sub>3</sub>):  $\delta$  = 175.4 (C<sub>q</sub>), 163.9 (C<sub>q</sub>), 161.0 (C<sub>q</sub>), 156.1 (C<sub>q</sub>), 134.4 (CH), 131.8 (CH), 131.8 (C<sub>q</sub>), 129.0 (CH), 128.2 (CH), 126.1 (CH), 125.7 (CH), 123.1 (C<sub>q</sub>), 118.8 (C<sub>q</sub>), 118.1 (CH), 66.5 (CH<sub>2</sub>), 66.4 (CH<sub>2</sub>), 47.1 (CH<sub>2</sub>), 42.1 (CH<sub>2</sub>). **IR** (ATR):  $\tilde{\nu}$  = 1629, 1617, 1565, 1462, 1436, 1375, 1111, 1018, 758, 696 cm<sup>-1</sup>. **M.p.**: 178–180 °C. **MS** (ESI)  $m/z$  (relative intensity): 336 (100) [M+H]<sup>+</sup>, 358 (5) [M+Na]<sup>+</sup>. **HR-MS** (ESI)  $m/z$  calcd for C<sub>20</sub>H<sub>17</sub>NO<sub>4</sub> [M+H]<sup>+</sup>: 336.1230, found: 336.1233.

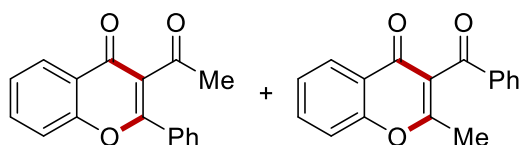
**172ak**

### 2-(2-Hydroxyethyl)-3-propyl-4H-chromen-4-one

The general procedure B was followed using **26a** (78  $\mu$ L, 0.75 mmol) and **171k** (30.6 mg, 0.25 mmol) at 100 °C for 7 h. Purification by column chromatography on silica gel (*n*hexane/EtOAc = 6:1) yielded **172ak** (37.4 mg, 64%) as a white solid.

**<sup>1</sup>H-NMR** (400 MHz, CDCl<sub>3</sub>):  $\delta$  = 8.10 (dd,  $J$  = 8.1, 1.7, 1H), 7.56 (ddd,  $J$  = 8.6, 7.1, 1.7 Hz, 1H), 7.33 (ddd,  $J$  = 8.6, 1.1, 0.5 Hz, 1H), 7.29 (ddd,  $J$  = 8.1, 7.1, 1.1 Hz, 1H), 4.06 (t,  $J$  = 6.5 Hz, 2H), 2.99 (t,  $J$  = 6.4 Hz, 2H), 2.55–2.48 (m, 2H), 1.57–1.44 (m, 2H), 0.96 (t,  $J$  = 7.3 Hz, 3H). **<sup>13</sup>C-NMR** (101 MHz, CDCl<sub>3</sub>):  $\delta$  = 178.0 (C<sub>q</sub>), 162.7 (C<sub>q</sub>), 156.0 (C<sub>q</sub>), 133.2 (CH), 126.0 (CH), 124.7 (CH), 122.9 (C<sub>q</sub>), 122.8 (C<sub>q</sub>), 117.7 (CH), 60.2 (CH<sub>2</sub>), 35.4 (CH<sub>2</sub>), 26.7 (CH<sub>2</sub>), 22.6 (CH<sub>2</sub>), 14.3 (CH<sub>3</sub>). **IR** (ATR):  $\tilde{\nu}$  = 3370, 2918, 1611, 1564, 1464, 1394, 1159, 1059, 757, 656 cm<sup>-1</sup>. **M.p.**: 104–105 °C. **MS** (ESI)  $m/z$  (relative intensity): 233 (80) [M+H]<sup>+</sup>, 255 (50) [M+Na]<sup>+</sup>, 487 (100) [2M+Na]<sup>+</sup>. **HR-MS** (ESI)  $m/z$  calcd for C<sub>14</sub>H<sub>17</sub>O<sub>3</sub> [M+H]<sup>+</sup>: 233.1172, found: 233.1174.

The spectral data are in accordance with those reported in the literature.<sup>[219]</sup>

**172al/172al'****3-Acetyl-2-phenyl-4H-chromen-4-one** (mixture of isomers)

The general procedure B was followed using **26a** (78  $\mu$ L, 0.75 mmol) and **171l** (36.1 mg, 0.25 mmol) at 100  $^{\circ}$ C for 7 h. Purification by column chromatography on silica gel (*n*hexane/EtOAc = 10:1 to 4:1) yielded a 1:1.26 mixture of **172al** and **172al'** (50.4 mg, 71%) as a yellow oil.

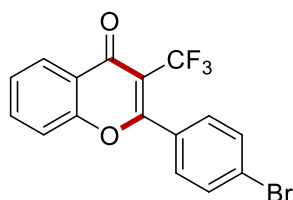
**$^1$ H-NMR** (400 MHz,  $\text{CDCl}_3$ ):  $\delta$  8.26–8.16 (m, 1H), 7.91–7.89 (m, 1H), 7.75–7.63 (m, 2H), 7.61–7.39 (m, 5H), 2.48–2.36 (m, 3H). **IR** (ATR):  $\tilde{\nu}$  = 1632, 1615, 1462, 1395, 1363, 1221, 1072, 925, 758, 709, 695  $\text{cm}^{-1}$ . **MS** (ESI)  $m/z$  (relative intensity): 265 (100)  $[\text{M}+\text{H}]^+$ , 287 (20)  $[\text{M}+\text{Na}]^+$ , 551 (20)  $[\text{2M}+\text{Na}]^+$ . **HR-MS** (ESI)  $m/z$  calcd for  $\text{C}_{17}\text{H}_{12}\text{O}_3$   $[\text{M}+\text{H}]^+$ : 265.0859, found: 265.0858.

Major isomer:

**$^{13}\text{C}$ -NMR** (101 MHz,  $\text{CDCl}_3$ ):  $\delta$  = 194.0 ( $\text{C}_q$ ), 176.0 ( $\text{C}_q$ ), 165.5 ( $\text{C}_q$ ), 156.1 ( $\text{C}_q$ ), 137.1 ( $\text{C}_q$ ), 134.2 (CH), 133.9 (CH), 129.5 (CH), 128.9 (CH), 126.1 (CH), 125.6 (CH), 123.6 ( $\text{C}_q$ ), 123.2 ( $\text{C}_q$ ), 118.0 (CH), 19.2 ( $\text{CH}_3$ ).

Minor isomer:

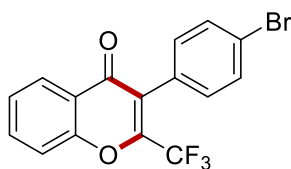
**$^{13}\text{C}$ -NMR** (101 MHz,  $\text{CDCl}_3$ ):  $\delta$  = 200.6 ( $\text{C}_q$ ), 176.0 ( $\text{C}_q$ ), 162.6 ( $\text{C}_q$ ), 156.0 ( $\text{C}_q$ ), 134.5 (CH), 132.0 (CH), 131.7 ( $\text{C}_q$ ), 129.0 (CH), 128.7 (CH), 126.1 (CH), 125.8 (CH), 125.0 ( $\text{C}_q$ ), 118.2 (CH), 32.4 ( $\text{CH}_3$ ).

**172am****2-(4-Bromophenyl)-3-(trifluoromethyl)-4H-chromen-4-one**

The general procedure B was followed using **26a** (78  $\mu$ L, 0.75 mmol) and **171m** (65.4 mg, 0.25 mmol) in TFE at 70  $^{\circ}$ C for 24 h. Purification by column chromatography on silica gel

(*n*hexane/EtOAc = 10:1) furnished **172am** (25.2 mg, 27%) and **172am'** (24.6 mg, 27%) as white solids.

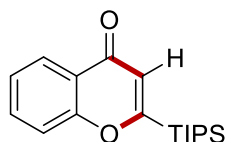
**<sup>1</sup>H-NMR** (400 MHz, CDCl<sub>3</sub>):  $\delta$  = 8.27 (dd,  $J$  = 8.0, 1.7 Hz, 1H), 7.75 (ddd,  $J$  = 8.3, 7.1, 1.2 Hz, 1H), 7.68 (d,  $J$  = 8.5 Hz, 2H), 7.52–7.45 (m, 4H). **<sup>13</sup>C-NMR** (101 MHz, CDCl<sub>3</sub>):  $\delta$  = 174.3 (C<sub>q</sub>), 166.0 (q,  $^3J_{C-F}$  = 2.5 Hz, C<sub>q</sub>), 155.6 (C<sub>q</sub>), 135.0 (CH), 131.4 (C<sub>q</sub>), 130.3 (q,  $^5J_{C-F}$  = 1.8 Hz, CH), 126.5 (CH), 126.4 (C<sub>q</sub>), 126.3 (CH), 123.4 (q,  $^4J_{C-F}$  = 1.0 Hz, C<sub>q</sub>), 122.5 (q,  $^1J_{C-F}$  = 273.9 Hz, C<sub>q</sub>), 118.1 (CH), 113.5 (q,  $^2J_{C-F}$  = 29.5 Hz, C<sub>q</sub>). **IR** (ATR):  $\tilde{\nu}$  = 1662, 1615, 1463, 1379, 1124, 1107, 1063, 1010, 825, 762 cm<sup>-1</sup>. **<sup>19</sup>F{<sup>1</sup>H}-NMR** (377 MHz, CDCl<sub>3</sub>)  $\delta$  = -56.2. **M.p.**: 90–92 °C. **MS** (ESI)  $m/z$  (relative intensity): 369 (20) [M+H]<sup>+</sup>, 391 (100) [M+Na]<sup>+</sup>, 761 (20) [2M+Na]<sup>+</sup>. **HR-MS** (ESI)  $m/z$  calcd for C<sub>16</sub>H<sub>8</sub><sup>79</sup>BrF<sub>3</sub>O<sub>2</sub> [M+H]<sup>+</sup>: 368.9733, found: 368.9733.



**172am'**

### 3-(4-Bromophenyl)-2-(trifluoromethyl)-4H-chromen-4-one

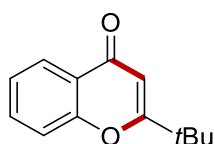
**<sup>1</sup>H-NMR** (400 MHz, CDCl<sub>3</sub>):  $\delta$  = 8.23 (dd,  $J$  = 8.1, 1.3 Hz, 1H), 7.80 (ddd,  $J$  = 8.5, 7.1, 1.4 Hz, 1H), 7.59 (d,  $J$  = 8.2 Hz, 3H), 7.50 (dd,  $J$  = 7.6, 7.6 Hz, 1H), 7.15 (d,  $J$  = 8.1 Hz, 2H). **<sup>13</sup>C-NMR** (101 MHz, CDCl<sub>3</sub>):  $\delta$  = 176.8 (C<sub>q</sub>), 155.2 (C<sub>q</sub>), 148.6 (q,  $^2J_{C-F}$  = 36.1 Hz, C<sub>q</sub>), 135.2 (CH), 131.7 (CH), 131.6 (CH), 131.6 (CH), 128.1 (C<sub>q</sub>), 126.6 (CH), 126.5 (CH), 124.6 (q,  $^3J_{C-F}$  = 1.5 Hz, C<sub>q</sub>), 123.5 (C<sub>q</sub>), 123.3 (C<sub>q</sub>), 119.40 (q,  $^1J_{C-F}$  = 276.7 Hz, C<sub>q</sub>), 118.5 (CH). **<sup>19</sup>F{<sup>1</sup>H}-NMR** (377 MHz, CDCl<sub>3</sub>)  $\delta$  = -63.5. **IR** (ATR):  $\tilde{\nu}$  = 1653, 1466, 1299, 1225, 1197, 1151, 1105, 1071, 937, 764 cm<sup>-1</sup>. **M.p.**: 125–127 °C. **MS** (ESI)  $m/z$  (relative intensity): 369 (30) [M+H]<sup>+</sup>, 391 (100) [M+Na]<sup>+</sup>, 761 (10) [2M+Na]<sup>+</sup>. C<sub>16</sub>H<sub>8</sub><sup>79</sup>BrF<sub>3</sub>O<sub>2</sub> [M+H]<sup>+</sup>: 368.9733, found: 368.9734.

**173ac****2-(Triisopropylsilyl)-4H-chromen-4-one**

The general procedure B was followed using **26a** (78  $\mu$ L, 0.75 mmol) and **50c** (45.6 mg, 0.25 mmol) in at rt. Purification by column chromatography on silica gel (*n*hexane/EtOAc = 15:1 to 10:1) furnished and **173ac** (37.3 mg, 49%) as an orange oil.

**<sup>1</sup>H-NMR** (400 MHz, CDCl<sub>3</sub>):  $\delta$  = 8.20 (dd,  $J$  = 8.1, 1.7 Hz, 1H), 7.63 (ddd,  $J$  = 8.6, 7.1, 1.7 Hz, 1H), 7.43 (dd,  $J$  = 8.6, 1.1 Hz, 1H), 7.36 (ddd,  $J$  = 8.1, 7.1, 1.1 Hz, 1H), 6.55 (s, 1H), 1.40 (hept,  $J$  = 7.4 Hz, 2H), 1.15 (d,  $J$  = 7.4 Hz, 18H). **<sup>13</sup>C-NMR** (101 MHz, CDCl<sub>3</sub>):  $\delta$  = 176.5 (C<sub>q</sub>), 175.4 (C<sub>q</sub>), 158.3 (C<sub>q</sub>), 133.5 (CH), 125.8 (CH), 124.9 (CH), 124.8 (C<sub>q</sub>), 122.4 (CH), 118.3 (CH), 18.5 (CH<sub>3</sub>), 10.7 (CH). **IR** (ATR):  $\tilde{\nu}$  = 1648, 1613, 1461, 1345, 800, 758, 678, 654, 610, 561 cm<sup>-1</sup>. **MS** (ESI)  $m/z$  (relative intensity): 303 (10) [M+H]<sup>+</sup>, 325 (50) [M+Na]<sup>+</sup>, 627 (100) [2M+Na]<sup>+</sup>, 929 (90) [3M+Na]<sup>+</sup>. **HR-MS** (ESI)  $m/z$  calcd for C<sub>18</sub>H<sub>26</sub>O<sub>2</sub>Si [M+Na]<sup>+</sup>: 325.1594, found: 325.1597.

The spectral data are in accordance with those reported in the literature.<sup>[257]</sup>

**173ad****2-(tert-Butyl)-4H-chromen-4-one**

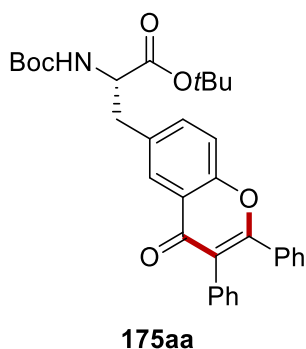
The general procedure B was followed using **26a** (156  $\mu$ L, 1.50 mmol), **50d** (41.1 mg, 0.50 mmol), [Cp\* $\text{RhCl}_2$ ]<sub>2</sub> (7.7 mg, 2.5 mol %) and NaOPiv (124 mg, 1.00 mmol) at rt for 7 h. Purification by column chromatography on silica gel (*n*hexane/EtOAc = 10:1 to 4:1) yielded **173ad** (61.5 mg, 61%) as a brown oil.

**<sup>1</sup>H-NMR** (400 MHz, CDCl<sub>3</sub>):  $\delta$  = 8.15 (dd,  $J$  = 8.0, 1.8 Hz, 1H), 7.66–7.57 (m, 1H), 7.42 (d,  $J$  = 8.4 Hz, 1H), 7.34 (dd,  $J$  = 7.5 Hz, 1H), 6.26 (s, 1H), 1.33 (s, 9H). **<sup>13</sup>C-NMR** (101 MHz, CDCl<sub>3</sub>):  $\delta$  = 179.0 (C<sub>q</sub>), 176.2 (C<sub>q</sub>), 156.5 (C<sub>q</sub>), 133.6 (CH), 125.6 (CH), 124.9 (CH), 123.5 (C<sub>q</sub>), 117.9 (CH), 106.7 (CH), 36.6 (C<sub>q</sub>), 27.9 (CH<sub>3</sub>). **IR** (ATR):  $\tilde{\nu}$  = 1647, 1462,



1355, 1229, 1133, 1077, 937, 852, 779, 757  $\text{cm}^{-1}$ . **MS** (ESI)  $m/z$  (relative intensity): 203 (100)  $[\text{M}+\text{H}]^+$ , 225 (15)  $[\text{M}+\text{Na}]^+$ , 427 (20)  $[2\text{M}+\text{Na}]^+$ . **HR-MS** (ESI)  $m/z$  calcd for  $\text{C}_{13}\text{H}_{14}\text{O}_2$   $[\text{M}+\text{H}]^+$ : 203.1067, found: 203.1056.

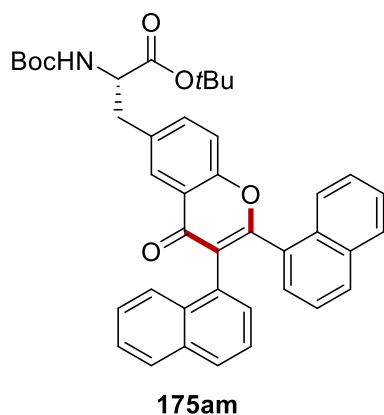
The spectral data are in accordance with those reported in the literature.<sup>[258]</sup>



**tert-Butyl (S)-2-[(tert-butoxycarbonyl)amino]-3-(4-oxo-2,3-diphenyl-4H-chromen-6-yl)propanoate**

The general procedure B was followed using **174a** (183 mg, 0.50 mmol) and **17a** (44.5 mg, 0.25 mmol) at 100 °C for 3.5 h. Purification by column chromatography on silica gel (*n*hexane/EtOAc = 6:1 to 4:1) yielded **175aa** (112 mg, 82%) as a white solid.

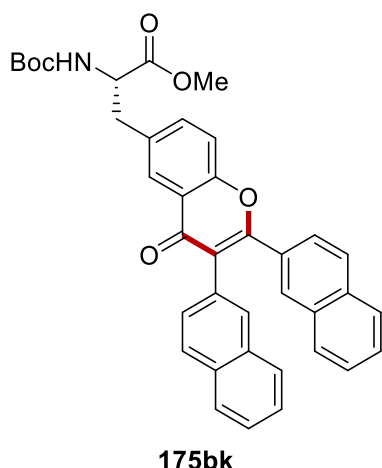
**<sup>1</sup>H-NMR** (600 MHz,  $\text{CDCl}_3$ ):  $\delta$  = 7.98 (d,  $J$  = 2.2 Hz, 1H), 7.49–7.45 (m, 1H), 7.39 (d,  $J$  = 8.5 Hz, 1H), 7.31–7.27 (m, 2H), 7.26–7.21 (m, 2H), 7.20–7.16 (m, 4H), 7.13–7.11 (m, 2H), 5.03 (d,  $J$  = 7.8 Hz, 1H), 4.41 (ddd,  $J$  = 7.8, 5.8, 5.7 Hz, 1H), 3.18 (dd,  $J$  = 13.9, 5.7 Hz, 1H), 3.08 (dd,  $J$  = 13.9, 5.8 Hz, 1H), 1.38 (s, 9H), 1.35 (s, 9H). **<sup>13</sup>C-NMR** (151 MHz,  $\text{CDCl}_3$ ):  $\delta$  = 177.1 ( $\text{C}_q$ ), 170.6 ( $\text{C}_q$ ), 161.5 ( $\text{C}_q$ ), 155.2 ( $\text{C}_q$ ), 155.2 ( $\text{C}_q$ ), 135.2 (CH), 133.8 ( $\text{C}_q$ ), 133.4 ( $\text{C}_q$ ), 133.0 ( $\text{C}_q$ ), 131.3 (CH), 130.1 (CH), 129.6 (CH), 128.3 (CH), 128.1 (CH), 127.7 (CH), 126.8 (CH), 123.3 ( $\text{C}_q$ ), 123.0 ( $\text{C}_q$ ), 118.1 (CH), 82.7 ( $\text{C}_q$ ), 79.9 ( $\text{C}_q$ ), 54.9 (CH), 38.0 ( $\text{CH}_2$ ), 28.4 ( $\text{CH}_3$ ), 28.1 ( $\text{CH}_3$ ). **IR** (ATR):  $\tilde{\nu}$  = 1689, 1636, 1614, 1444, 1364, 1239, 1152, 1052, 698  $\text{cm}^{-1}$ . **M.p.**: 145–147 °C. **MS** (ESI)  $m/z$  (relative intensity): 542 (70)  $[\text{M}+\text{H}]^+$ , 564 (100)  $[\text{M}+\text{Na}]^+$ , 1105 (80)  $[2\text{M}+\text{Na}]^+$ . **HR-MS** (ESI)  $m/z$  calcd for  $\text{C}_{33}\text{H}_{36}\text{NO}_6$   $[\text{M}+\text{H}]^+$ : 542.2537, found: 542.2521.



**tert-Butyl (S)-2-[(tert-butoxycarbonyl)amino]-3-(2,3-di(naphthalen-1-yl)-4-oxo-4H-chrom-en-6-yl)propanoate**

The general procedure B was followed using **174a** (183 mg, 0.50 mmol) and **17m** (69.6 mg, 0.25 mmol) at 100 °C for 7 h. Purification by column chromatography on silica gel (CH<sub>2</sub>Cl<sub>2</sub>/EtOAc = 50:1 to 20:1) yielded **175am** (119 mg, 74%) as a white solid.

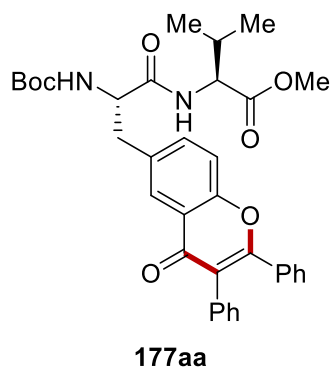
**<sup>1</sup>H-NMR** (400 MHz, CDCl<sub>3</sub>):  $\delta$  = 8.08 (dd,  $J$  = 4.2, 2.2 Hz, 1H), 7.88 (dd,  $J$  = 8.4, 4.2, 1H), 7.77–7.70 (m, 1H), 7.68–7.61 (m, 2H), 7.57 (d,  $J$  = 8.0, 1H), 7.53–7.46 (m, 2H), 7.44–7.33 (m, 3H), 7.30 (dd,  $J$  = 6.8, 3.4 Hz, 2H), 7.05 (dd,  $J$  = 6.1, 6.1 Hz, 2H), 7.02–6.91 (m, 3H), 5.06 (d,  $J$  = 5.7 Hz, 1H), 4.45 (ddd,  $J$  = 6.4, 5.7 Hz), 3.28–3.17 (m, 1H), 3.16–3.06 (m, 1H), 1.40 (s, 9H), 1.36 (m, 9H). **<sup>13</sup>C-NMR** (101 MHz, CDCl<sub>3</sub>):  $\delta$  = 177.1 (C<sub>q</sub>), 170.6 (C<sub>q</sub>), 163.6 (C<sub>q</sub>), 155.6 (C<sub>q</sub>), 155.2 (C<sub>q</sub>), 135.5 (CH), 134.1 (C<sub>q</sub>), 133.5 (C<sub>q</sub>), 133.3 (C<sub>q</sub>), 132.6 (C<sub>q</sub>), 131.0 (C<sub>q</sub>), 130.9 (C<sub>q</sub>), 130.7 (C<sub>q</sub>), 130.3 (CH), 128.5 (CH), 128.5 (CH), 128.4 (CH), 128.2 (CH), 127.6 (CH), 127.1 (CH), 127.0 (CH), 126.3 (CH), 126.1 (CH), 125.7 (CH), 125.6 (CH), 125.2 (CH), 125.1 (CH), 124.8 (C<sub>q</sub>), 124.6 (CH), 123.4 (C<sub>q</sub>), 118.3 (CH), 82.8 (C<sub>q</sub>), 79.9 (C<sub>q</sub>), 55.0 (CH), 38.1 (CH<sub>2</sub>), 28.4 (CH<sub>3</sub>), 28.2 (CH<sub>3</sub>). **IR** (ATR):  $\tilde{\nu}$  = 1708, 1643, 1616, 1485, 1360, 1231, 1148, 800, 772, 750 cm<sup>-1</sup>. **M.p.**: 122–124 °C. **MS** (ESI)  $m/z$  (relative intensity): 642 (20) [M+H]<sup>+</sup>, 664 (100) [M+Na]<sup>+</sup>, 1305 (70) [2M+Na]<sup>+</sup>. **HR-MS** (ESI)  $m/z$  calcd for C<sub>41</sub>H<sub>40</sub>NO<sub>6</sub> [M+H]<sup>+</sup>: 642.2850, found: 642.2879.



**Methyl (S)-2-[(*tert*-butoxycarbonyl)amino]-3-(2,3-di(naphthalen-2-yl)-4-oxo-4H-chromen-6-yl)propanoate**

The general procedure C was followed using **174b** (169 mg, 0.50 mmol) and **17k** (72.4 mg, 0.25 mmol) at 100 °C for 3.5 h. Purification by column chromatography on silica gel (*n*hexane/EtOAc = 4:1 to 2:1) yielded **175bk** (135 mg, 87%) as a white solid.

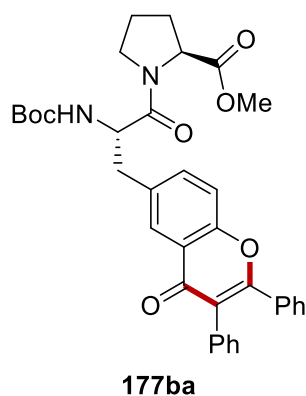
**<sup>1</sup>H-NMR** (400 MHz, CDCl<sub>3</sub>):  $\delta$  = 8.00–7.95 (m, 1H), 7.72–7.68 (m, 1H), 7.66 (d, *J* = 7.9 Hz, 1H), 7.62 (d, *J* = 8.5 Hz, 1H), 7.60–7.55 (m, 3H), 7.44–7.39 (m, 3H), 7.37–7.25 (m, 4H), 7.20 (dd, *J* = 8.5, 1.8 Hz, 1H), 7.16 (dd, *J* = 8.7, 1.8 Hz, 1H), 5.08 (d, *J* = 8.0 Hz, 1H), 4.55 (ddd, *J* = 8.0, 6.3, 5.3 Hz, 1H), 3.65 (s, 3H), 3.19 (dd, *J* = 13.9, 5.3 Hz, 1H), 3.08 (dd, *J* = 13.9, 6.3 Hz, 1H), 1.33 (s, 9H). **<sup>13</sup>C-NMR** (101 MHz, CDCl<sub>3</sub>):  $\delta$  = 177.3 (C<sub>q</sub>), 172.0 (C<sub>q</sub>), 161.6 (C<sub>q</sub>), 155.3 (C<sub>q</sub>), 155.2 (C<sub>q</sub>), 135.0 (CH), 133.6 (C<sub>q</sub>), 133.6 (C<sub>q</sub>), 133.4 (C<sub>q</sub>), 132.8 (C<sub>q</sub>), 132.5 (C<sub>q</sub>), 130.7 (CH), 130.6 (C<sub>q</sub>), 130.3 (C<sub>q</sub>), 130.0 (CH), 129.0 (CH), 128.8 (CH), 128.2 (CH), 127.9 (CH), 127.7 (CH). (One aromatic CH is missing due to overlap, the overlap was verified by HSQC, showing the peak at 127.7 corresponds to two carbons). 127.7 (CH). (One aromatic CH is missing due to overlap, the overlap was verified by HSQC, showing the peak at 127.7 corresponds to two carbons). 126.6 (CH), 126.6 (CH), 126.2 (CH), 126.1 (CH), 125.9 (CH), 123.4 (C<sub>q</sub>), 123.0 (C<sub>q</sub>), 118.4 (CH), 80.1 (C<sub>q</sub>), 54.6 (CH), 52.5 (CH<sub>3</sub>), 37.9 (CH<sub>2</sub>), 28.3 (CH<sub>3</sub>). **IR** (ATR):  $\tilde{\nu}$  = 1706, 1617, 1487, 1442, 1364, 1214, 1162, 821, 746, 474 cm<sup>-1</sup>. **M.p.**: 137–139 °C. **MS** (ESI) *m/z* (relative intensity): 600 (40) [M+H]<sup>+</sup>, 622 (40) [M+Na]<sup>+</sup>, 1221 (100) [2M+Na]<sup>+</sup>. **HR-MS** (ESI) *m/z* calcd for C<sub>38</sub>H<sub>33</sub>NO<sub>6</sub>Na [M+Na]<sup>+</sup>: 622.2206, found: 622.2172.



**Methyl (S)-2-[(*tert*-butoxycarbonyl)amino]-3-(4-oxo-2,3-diphenyl-4*H*-chromen-6-yl)propanoyl]-*L*-valinate**

The general procedure C was followed using **176a** (211 mg, 0.50 mmol) and **17a** (44.5 mg, 0.25 mmol) at 100 °C for 7 h. Purification by column chromatography on silica gel (*n*hexane/EtOAc = 4:1 to 1:1) yielded **177aa** (141 mg, 94%) as a white solid.

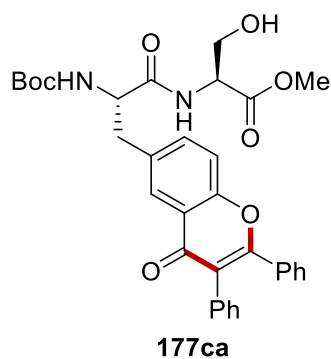
**<sup>1</sup>H-NMR** (400 MHz, CDCl<sub>3</sub>):  $\delta$  = 8.00 (d,  $J$  = 2.3 Hz, 1H), 7.50 (d,  $J$  = 2.3 Hz, 1H), 7.37 (dd,  $J$  = 8.5, 2.3 Hz, 1H), 7.30–7.26 (m, 2H), 7.25–7.15 (m, 6H), 7.14–7.10 (m, 2H), 6.66 (d,  $J$  = 8.5 Hz, 1H), 5.23 (d,  $J$  = 8.0 Hz, 1H), 4.44 (ddd,  $J$  = 8.6, 5.1 Hz, 1H), 4.39–4.31 (ddd,  $J$  = 8.0, 7.8, 5.9 Hz, 1H), 3.62 (s, 3H), 3.20 (dd,  $J$  = 14.0, 5.9 Hz, 1H), 3.04 (dd,  $J$  = 14.0, 7.8 Hz, 1H), 2.14–1.99 (m, 1H), 1.32 (s, 9H), 0.83 (d,  $J$  = 6.8 Hz, 2H), 0.80 (d,  $J$  = 7.7 Hz, 3H). **<sup>13</sup>C-NMR** (101 MHz, CDCl<sub>3</sub>):  $\delta$  = 177.2 (C<sub>q</sub>), 172.0 (C<sub>q</sub>), 171.1 (C<sub>q</sub>), 161.5 (C<sub>q</sub>), 155.6 (C<sub>q</sub>), 155.2 (C<sub>q</sub>), 135.0 (CH), 134.2 (C<sub>q</sub>), 133.3 (C<sub>q</sub>), 133.0 (C<sub>q</sub>), 131.3 (CH), 130.1 (CH), 129.6 (CH), 128.3 (CH), 128.1 (CH), 127.7 (CH), 126.7 (CH), 123.4 (C<sub>q</sub>), 123.0 (C<sub>q</sub>), 118.4 (CH), 77.4 (C<sub>q</sub>), 57.3 (CH), 55.8 (CH), 52.2 (CH<sub>3</sub>), 37.5 (CH<sub>2</sub>), 31.3 (CH), 28.3 (CH<sub>3</sub>), 19.0 (CH<sub>3</sub>), 17.9 (CH<sub>3</sub>). **IR** (ATR):  $\tilde{\nu}$  = 3307, 1646, 1617, 1520, 1487, 1443, 1368, 1228, 1163, 694 cm<sup>-1</sup>. **M.p.**: 110–111 °C. **MS** (ESI)  $m/z$  (relative intensity): 599 (50) [M+H]<sup>+</sup>, 621 (100) [M+Na]<sup>+</sup>, 1219 (40) [2M+Na]<sup>+</sup>. **HR-MS** (ESI)  $m/z$  calcd for C<sub>35</sub>H<sub>39</sub>N<sub>2</sub>O<sub>7</sub> [M+H]<sup>+</sup>: 599.2752, found: 599.2745.



**Methyl**    **{(S)-2-[(*tert*-butoxycarbonyl)amino]-3-(4-oxo-2,3-diphenyl-4*H*-chromen-6-yl)propanoyl}-L-prolinate**

The general procedure C was followed using **176b** (168 mg, 0.40 mmol) and **17a** (35.6 mg, 0.20 mmol) at 100 °C for 3.5 h. Purification by column chromatography on silica gel (CH<sub>2</sub>Cl<sub>2</sub>/MeOH = 98:2) yielded **177ba** (92.5 mg, 76%) as a white solid.

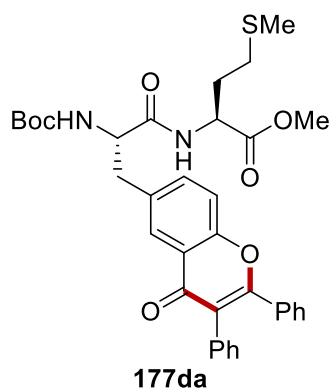
**<sup>1</sup>H-NMR** (400 MHz, CDCl<sub>3</sub>):  $\delta$  = 8.05 (d,  $J$  = 2.3 Hz, 1H), 7.57 (dd,  $J$  = 8.5, 2.2 Hz, 1H), 7.40 (d,  $J$  = 8.7 Hz, 1H), 7.32–7.28 (m, 2H), 7.26–7.22 (m, 2H), 7.20–7.16 (m, 4H), 7.15–7.11 (m, 2H), 5.24 (d,  $J$  = 8.8 Hz, 1H), 4.64 (ddd,  $J$  = 8.8, 7.1, 5.5 Hz, 1H), 4.60–4.53 (m, 1H), 3.68 (s, 3H), 3.51–3.42 (m, 1H), 3.27 (dd,  $J$  = 13.9, 5.5 Hz, 1H), 3.02 (dd,  $J$  = 13.9, 7.1 Hz, 1H), 2.27–2.17 (m, 1H), 2.10–1.97 (m, 2H), 1.92–1.80 (m, 1H), 1.29 (s, 9H). **<sup>13</sup>C-NMR** (101 MHz, CDCl<sub>3</sub>):  $\delta$  = 177.2 (C<sub>q</sub>), 172.5 (C<sub>q</sub>), 170.4 (C<sub>q</sub>), 161.4 (C<sub>q</sub>), 155.3 (C<sub>q</sub>), 155.2 (C<sub>q</sub>), 135.6 (CH), 133.8 (C<sub>q</sub>), 133.4 (C<sub>q</sub>), 133.0 (C<sub>q</sub>), 131.3 (CH), 130.1 (CH), 129.6 (CH), 128.3 (CH), 128.1 (CH), 127.6 (CH), 126.9 (CH), 123.3 (C<sub>q</sub>), 123.0 (C<sub>q</sub>), 118.1 (CH), 79.9 (C<sub>q</sub>), 59.0 (CH<sub>3</sub>), 53.1 (CH), 52.4 (CH), 47.1 (CH<sub>2</sub>), 38.3 (CH<sub>2</sub>), 29.1 (CH<sub>2</sub>), 28.3 (CH<sub>3</sub>), 25.0 (CH<sub>2</sub>). **IR** (ATR):  $\tilde{\nu}$  = 1705, 1641, 1488, 1439, 1368, 1228, 1167, 753, 697 cm<sup>-1</sup>. **M.p.**: 109–111 °C. **MS** (ESI)  $m/z$  (relative intensity): 597 (30) [M+H]<sup>+</sup>, 619 (100) [M+Na]<sup>+</sup>, 1215 (50) [2M+Na]<sup>+</sup>. **HR-MS** (ESI)  $m/z$  calcd for C<sub>35</sub>H<sub>37</sub>N<sub>2</sub>O<sub>7</sub> [M+H]<sup>+</sup>: 597.2595, found: 597.2692.



**Methyl**    {(S)-2-[(*tert*-butoxycarbonyl)amino]-3-(4-oxo-2,3-diphenyl-4*H*-chromen-6-yl)propanoyl}-*L*-serinate

The general procedure C was followed using **176c** (80.0 mg, 0.20 mmol) and **17a** (17.5 mg, 0.10 mmol) at 100 °C for 3.5 h. Purification by column chromatography on silica gel (CH<sub>2</sub>Cl<sub>2</sub>/MeOH = 98:2 to 95:5) yielded **177ca** (48.4 mg, 84%) as a white solid.

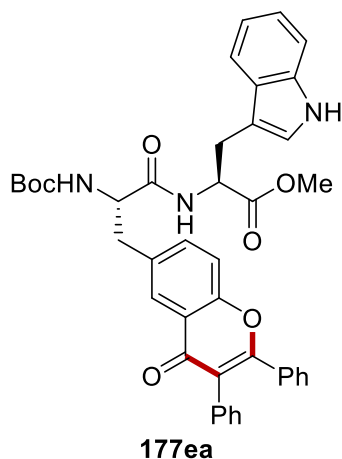
**<sup>1</sup>H-NMR** (600 MHz, CDCl<sub>3</sub>):  $\delta$  = 8.00 (d, *J* = 2.3 Hz, 1H), 7.51 (dd, *J* = 8.6, 2.3 Hz, 1H), 7.40 (d, *J* = 8.6 Hz, 1H), 7.32 (d, *J* = 7.4 Hz, 1H), 7.28–7.26 (m, 2H), 7.26–7.23 (m, 1H), 7.23–7.19 (m, 3H), 7.18–7.15 (m, 2H), 7.11–7.09 (m, 2H), 5.30 (d, *J* = 7.9 Hz, 1H), 4.56 (ddd, *J* = 7.4, 7.2, 7.2 Hz, 1H), 4.46 (ddd, *J* = 7.9, 6.4, 6.4 Hz, 1H), 3.93–3.84 (m, 2H), 3.84–3.79 (m, 1H), 3.67 (s, 3H), 3.18 (d, *J* = 6.4 Hz, 2H), 1.30 (s, 9H). **<sup>13</sup>C-NMR** (151 MHz, CDCl<sub>3</sub>):  $\delta$  = 177.8 (C<sub>q</sub>), 171.5 (C<sub>q</sub>), 170.9 (C<sub>q</sub>), 161.9 (C<sub>q</sub>), 155.6 (C<sub>q</sub>), 155.3 (C<sub>q</sub>), 135.6 (CH), 134.1 (C<sub>q</sub>), 133.2 (C<sub>q</sub>), 132.8 (C<sub>q</sub>), 131.3 (CH), 130.2 (CH), 129.6 (CH), 128.4 (CH), 128.2 (CH), 127.8 (CH), 126.4 (CH), 123.3 (C<sub>q</sub>), 123.0 (C<sub>q</sub>), 118.5 (CH), 80.5 (C<sub>q</sub>), 62.5 (CH<sub>2</sub>), 55.6 (CH<sub>3</sub>), 55.1 (CH), 52.8 (CH), 37.7 (CH<sub>2</sub>), 28.3 (CH<sub>3</sub>). **IR** (ATR):  $\tilde{\nu}$  = 3305, 1642, 1619, 1488, 1444, 1370, 1223, 1165, 750, 695 cm<sup>-1</sup>. **M.p.**: 120–122 °C. **MS** (ESI) *m/z* (relative intensity): 587 (50) [M+H]<sup>+</sup>, 609 (100) [M+Na]<sup>+</sup>, 1195 (60) [2M+Na]<sup>+</sup>. **HR-MS** (ESI) *m/z* calcd for C<sub>33</sub>H<sub>35</sub>N<sub>2</sub>O<sub>8</sub> [M+H]<sup>+</sup>: 587.2388; found: 587.2586.



**Methyl (S)-2-[(tert-butoxycarbonyl)amino]-3-(4-oxo-2,3-diphenyl-4H-chromen-6-yl)propanoyl-L-methioninate**

The general procedure C was followed using **176d** (112 mg, 0.25 mmol) and **17a** (22.6 mg, 0.13 mmol) at 100 °C for 3.5 h. Purification by column chromatography on silica gel (n-hexane/EtOAc = 2:1 to 4:3) yielded **177da** (48.8 mg, 60%) as a white solid.

**<sup>1</sup>H-NMR** (400 MHz, CDCl<sub>3</sub>):  $\delta$  = 8.01 (d,  $J$  = 2.2 Hz, 1H), 7.51 (dd,  $J$  = 8.6, 2.2 Hz, 1H), 7.39 (d,  $J$  = 8.6 Hz, 1H), 7.31–7.26 (m, 2H), 7.26–7.15 (m, 6H), 7.14–7.10 (m, 2H), 6.85 (d,  $J$  = 7.8 Hz, 1H), 5.21 (d,  $J$  = 8.1 Hz, 1H), 4.60 (td,  $J$  = 7.8, 5.0, 5.0 Hz, 1H), 4.38 (ddd,  $J$  = 8.1, 7.5, 6.0 Hz, 1H), 3.65 (s, 3H), 3.19 (dd,  $J$  = 14.0, 6.0 Hz, 1H), 3.06 (dd,  $J$  = 14.0, 7.5 Hz, 1H), 2.37 (dd,  $J$  = 7.5, 7.5 Hz, 2H), 2.10–2.00 (m, 1H), 1.97 (s, 3H), 1.92–1.80 (m, 1H), 1.33 (s, 9H). **<sup>13</sup>C-NMR** (101 MHz, CDCl<sub>3</sub>):  $\delta$  = 177.2 (C<sub>q</sub>), 172.0 (C<sub>q</sub>), 171.1 (C<sub>q</sub>), 161.6 (C<sub>q</sub>), 155.5 (C<sub>q</sub>), 155.2 (C<sub>q</sub>), 135.1 (CH), 134.1 (C<sub>q</sub>), 133.3 (C<sub>q</sub>), 133.0 (C<sub>q</sub>), 131.3 (CH), 130.2 (CH), 129.6 (CH), 128.4 (CH), 128.2 (CH), 127.7 (CH), 126.7 (CH), 123.3 (C<sub>q</sub>), 123.0 (C<sub>q</sub>), 118.4 (CH), 80.5 (C<sub>q</sub>), 55.7 (CH), 52.7 (CH<sub>3</sub>), 51.7 (CH), 37.7 (CH<sub>2</sub>), 31.6 (CH<sub>2</sub>), 29.9 (CH<sub>2</sub>), 28.3 (CH<sub>3</sub>), 15.5 (CH<sub>3</sub>). **IR** (ATR):  $\tilde{\nu}$  = 3307, 1646, 1618, 1488, 1442, 1369, 1225, 1164, 751, 696 cm<sup>-1</sup>. **M.p.**: 89–91 °C. **MS** (ESI)  $m/z$  (relative intensity): 631 (80) [M+H]<sup>+</sup>, 653 (90) [M+Na]<sup>+</sup>, 1283 (100) [2M+Na]<sup>+</sup>. **HR-MS** (ESI)  $m/z$  calcd for C<sub>35</sub>H<sub>39</sub>N<sub>2</sub>O<sub>7</sub>S [M+H]<sup>+</sup>: 631.2472, found: 631.2451.

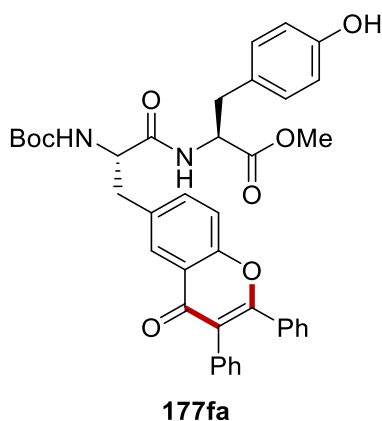


**Methyl (S)-2-[(tert-butoxycarbonyl)amino]-3-(4-oxo-2,3-diphenyl-4H-chromen-6-yl)propanoyl-L-tryptophanate**

The general procedure C was followed using **176e** (90.2 mg, 0.18 mmol), **17a** (15.7 mg, 90  $\mu$ mol) and [Cp\*RhCl<sub>2</sub>]<sub>2</sub> (2.8 mg, 5.0 mol %) at 100 °C for 3.5 h. Purification by column chromatography on silica gel (*n*hexane/EtOAc = 2:1 to 1:1) yielded **177ea** (58.1 mg, 71%) as a white solid.

**<sup>1</sup>H-NMR** (400 MHz, CDCl<sub>3</sub>):  $\delta$  = 8.65–8.34 (m, 1H), 7.99–7.84 (m, 1H), 7.48–7.39 (m, 1H), 7.36–7.31 (m, 1H), 7.30–7.15 (m, 10H), 7.15–7.03 (m, 3H), 6.99 (ddd,  $J$  = 7.2, 6.7, 6.7 Hz, 1H), 6.92–6.85 (m, 1H), 6.70 (d,  $J$  = 7.8 Hz, 1H), 5.14 (dd,  $J$  = 16.0, 8.0 Hz, 1H), 4.81 (ddd,  $J$  = 8.0, 5.5, 5.5 Hz, 1H), 4.46–4.29 (m, 1H), 3.53 (s, 3H), 3.23–3.14 (m, 2H), 3.14–3.02 (m, 1H), 2.95–2.75 (m, 1H), 1.26 (s, 9H). **<sup>13</sup>C-NMR** (101 MHz, CDCl<sub>3</sub>):  $\delta$  = 177.4 (C<sub>q</sub>), 172.2 (C<sub>q</sub>), 170.9 (C<sub>q</sub>), 161.7 (C<sub>q</sub>), 155.5 (C<sub>q</sub>), 155.2 (C<sub>q</sub>), 136.2 (C<sub>q</sub>), 135.2 (CH), 134.3 (C<sub>q</sub>), 133.3 (C<sub>q</sub>), 133.0 (C<sub>q</sub>), 131.3 (CH), 130.2 (CH), 129.7 (CH), 128.4 (CH), 128.2 (CH), 127.8 (CH), 127.6 (C<sub>q</sub>), 126.7 (CH), 123.4 (CH), 123.3 (C<sub>q</sub>), 123.0 (C<sub>q</sub>), 122.2 (CH), 119.6 (CH), 118.4 (CH), 111.6 (CH), 109.5 (C<sub>q</sub>), 80.3 (C<sub>q</sub>), 55.7 (CH), 53.0 (CH<sub>3</sub>), 52.5 (CH), 38.1 (CH<sub>2</sub>), 28.3 (CH<sub>3</sub>), 27.7 (CH<sub>2</sub>). **IR** (ATR):  $\tilde{\nu}$  = 3316, 1664, 1618, 1489, 1444, 1370, 1226, 1166, 747, 696 cm<sup>-1</sup>. **M.p.**: 147–149 °C. **MS** (ESI)  $m/z$  (relative intensity): 686 (100) [M+H]<sup>+</sup>, 708 (100) [M+Na]<sup>+</sup>, 1388 (30) [2M+Na]<sup>+</sup>. **HR-MS** (ESI)  $m/z$  calcd for C<sub>41</sub>H<sub>40</sub>N<sub>3</sub>O<sub>7</sub> [M+H]<sup>+</sup>: 686.2861, found: 686.2867.

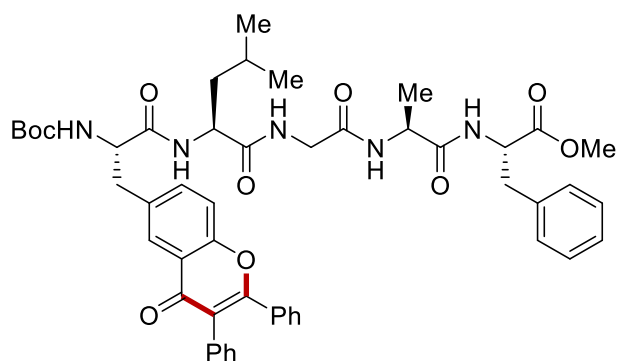




**Methyl (S)-2-[(*tert*-butoxycarbonyl)amino]-3-(4-oxo-2,3-diphenyl-4*H*-chromen-6-yl)propanoyl-L-tyrosinate**

The general procedure C was followed using **176f** (60.4 mg, 0.12 mmol), **17a** (11.0 mg, 60  $\mu$ mol) and [Cp\**Rh*Cl<sub>2</sub>]<sub>2</sub> (1.9 mg, 5.0 mol %) at 100 °C for 3.5 h. Purification by column chromatography on silica gel (*n*hexane/EtOAc = 3:2 to 1:1) yielded **177fa** (21.5 mg, 54%) as a white solid.

**<sup>1</sup>H-NMR** (400 MHz, CDCl<sub>3</sub>):  $\delta$  = 7.96 (s, 1H), 7.49 (d, *J* = 8.6 Hz, 1H), 7.38 (d, *J* = 8.6 Hz, 1H), 7.31–7.28 (m, 2H), 7.27–7.16 (m, 7H), 7.15–7.12 (m, 2H), 6.86 (d, *J* = 8.0 Hz, 1H), 6.79 (d, *J* = 8.5 Hz, 2H), 6.61 (d, *J* = 8.5 Hz, 1H), 5.26 (d, *J* = 5.4 Hz, 1H), 4.72 (ddd, *J* = 7.9, 6.5, 5.4 Hz, 1H), 4.43–4.33 (m, 1H), 3.58 (s, 3H), 3.13 (dd, *J* = 14.0, 5.6 Hz, 1H), 3.00 (dd, *J* = 14.0, 5.3 Hz, 1H), 2.87 (d, *J* = 6.5 Hz, 1H), 2.83 (d, *J* = 6.5 Hz, 1H), 1.25 (s, 9H). **<sup>13</sup>C-NMR** (101 MHz, CDCl<sub>3</sub>):  $\delta$  = 177.8 (C<sub>q</sub>), 172.0 (C<sub>q</sub>), 171.2 (C<sub>q</sub>), 162.0 (C<sub>q</sub>), 155.7 (C<sub>q</sub>), 155.3 (C<sub>q</sub>), 135.0 (CH), 134.4 (C<sub>q</sub>), 133.2 (C<sub>q</sub>), 133.0 (C<sub>q</sub>), 131.3 (CH), 130.5 (CH), 130.3 (CH), 129.7 (CH), 128.5 (CH), 128.2 (CH), 127.9 (CH), 127.0 (C<sub>q</sub>), 126.9 (CH), 123.2 (C<sub>q</sub>), 123.1 (C<sub>q</sub>), 118.5 (CH), 115.8 (CH), 80.4 (C<sub>q</sub>), 55.8 (CH), 53.6 (CH), 52.6 (CH<sub>3</sub>), 38.1 (CH<sub>2</sub>), 37.1 (CH<sub>2</sub>), 28.3 (CH<sub>3</sub>). **IR** (ATR):  $\tilde{\nu}$  = 3312, 2925, 1654, 1616, 1512, 1445, 1371, 1225, 1167, 755 cm<sup>-1</sup>. **M.p.**: 141–143 °C. **MS** (ESI) *m/z* (relative intensity): 663 (100) [M+H]<sup>+</sup>, 685 (80) [M+Na]<sup>+</sup>, 1347 (30) [2M+Na]<sup>+</sup>. **HR-MS** (ESI) *m/z* calcd for C<sub>39</sub>H<sub>39</sub>N<sub>2</sub>O<sub>8</sub> [M+H]<sup>+</sup>: 663.2701, found: 663.2708.

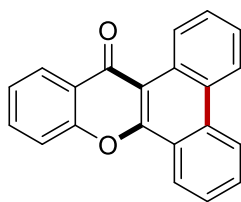


179

**Methyl (S)-2-[(*tert*-butoxycarbonyl)amino]-3-(4-oxo-2,3-diphenyl-4*H*-chromen-6-yl)propanoyl}-L-leucylglycyl-L-alanyl-L-phenylalaninate**

The general procedure C was followed using **178** (192 mg, 0.27 mmol) and **17a** (23.1 mg, 0.13 mmol) at 100 °C for 3.5 h. Purification by column chromatography on silica gel (CH<sub>2</sub>Cl<sub>2</sub>/MeOH = 95:5) yielded **179** (92.3 mg, 80%) as a white solid.

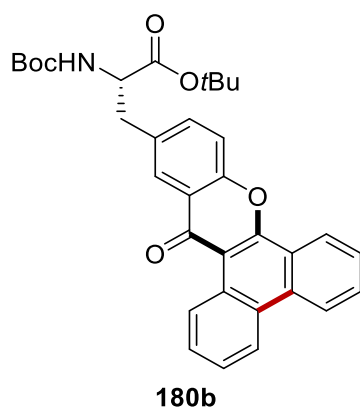
**<sup>1</sup>H-NMR** (400 MHz, *d*<sub>6</sub>-DMSO):  $\delta$  = 8.32 (d, *J* = 7.6 Hz, 1H), 8.20–8.12 (m, 2H), 8.08 (d, *J* = 2.1 Hz, 1H), 7.89 (d, *J* = 7.6 Hz, 1H), 7.84–7.74 (m, 1H), 7.63 (d, *J* = 8.5 Hz, 1H), 7.40–7.35 (m, 3H), 7.34–7.26 (m, 5H), 7.24 (d, *J* = 6.8 Hz, 2H), 7.21–7.19 (m, 2H), 7.19–7.17 (m, 1H), 7.15 (dd, *J* = 7.6, 1.9 Hz, 2H), 7.06 (d, *J* = 8.5 Hz, 1H), 4.49–4.39 (m, 1H), 4.38–4.29 (m, 2H), 4.29–4.21 (m, 1H), 3.70 (d, *J* = 5.9 Hz, 1H), 3.56 (s, 3H), 3.15 (dd, *J* = 13.7, 3.7 Hz, 1H), 3.01 (dd, *J* = 13.8, 5.9 Hz, 1H), 2.93 (dd, *J* = 12.1, 6.9 Hz, 1H), 2.88 (dd, *J* = 12.1, 9.0 Hz, 1H), 1.73–1.59 (m, 1H), 1.57–1.45 (m, 2H), 1.28 (s, 9H), 1.17 (d, *J* = 7.1 Hz, 3H), 0.89 (d, *J* = 6.4 Hz, 3H), 0.84 (d, *J* = 6.4 Hz, 3H). **<sup>13</sup>C-NMR** (101 MHz, *d*<sub>6</sub>-DMSO):  $\delta$  = 176.3 (C<sub>q</sub>), 172.4 (C<sub>q</sub>), 172.3 (C<sub>q</sub>), 171.8 (C<sub>q</sub>), 171.6 (C<sub>q</sub>), 168.2 (C<sub>q</sub>), 161.2 (C<sub>q</sub>), 155.4 (C<sub>q</sub>), 154.5 (C<sub>q</sub>), 137.1 (C<sub>q</sub>), 136.0 (C<sub>q</sub>), 135.8 (CH), 133.2 (C<sub>q</sub>), 133.0 (C<sub>q</sub>), 131.2 (CH), 130.2 (CH), 129.4 (CH), 129.1 (CH), 128.3 (CH), 128.2 (CH), 128.1 (CH), 127.5 (CH), 126.6 (CH), 125.7 (CH), 122.5 (C<sub>q</sub>), 122.4 (C<sub>q</sub>), 118.0 (CH), 78.2 (C<sub>q</sub>), 56.0 (CH), 53.7 (CH), 51.9 (CH<sub>3</sub>), 51.3 (CH), 47.8 (CH), 42.0 (CH<sub>2</sub>), 41.0 (CH<sub>2</sub>), 36.7 (CH<sub>2</sub>), 36.6 (CH<sub>2</sub>), 28.1 (CH<sub>3</sub>), 24.1 (CH), 23.1 (CH<sub>3</sub>), 21.6 (CH<sub>3</sub>), 18.3 (CH<sub>3</sub>). **IR** (ATR):  $\tilde{\nu}$  = 3291, 1642, 1521, 1370, 1221, 1167, 1050, 1026, 747, 697 cm<sup>-1</sup>. **M.p.**: 66–68 °C. **MS** (ESI) *m/z* (relative intensity): 888 (100) [M+H]<sup>+</sup>, 910 (70) [M+Na]<sup>+</sup>. **HR-MS** (ESI) *m/z* calcd for C<sub>50</sub>H<sub>58</sub>N<sub>5</sub>O<sub>10</sub> [M+H]<sup>+</sup>: 888.4178, found: 888.4165.

**180a****14H-Dibenzo[a,c]xanthen-14-one**

The general procedure E was followed using **48aa** (29.8 mg, 0.10 mmol). Purification by column chromatography on silica gel (*n*hexane/EtOAc = 10:1) yielded **180a** as a white solid (20.8 mg, 70%) as a white solid.

**<sup>1</sup>H-NMR** (400 MHz, CDCl<sub>3</sub>):  $\delta$  = 10.11 (dd,  $J$  = 8.3, 1.4 Hz, 1H), 8.60 (dd,  $J$  = 8.3, 1.4 Hz, 1H), 8.55 (dd,  $J$  = 8.3, 1.9 Hz, 2H), 8.40 (dd,  $J$  = 8.0, 1.7 Hz, 1H), 7.77–7.68 (m, 3H), 7.66–7.57 (m, 3H), 7.44 (ddd,  $J$  = 8.0, 6.9, 1.1 Hz, 1H). **<sup>13</sup>C-NMR** (101 MHz, CDCl<sub>3</sub>):  $\delta$  = 178.3 (C<sub>q</sub>), 155.1 (C<sub>q</sub>), 154.4 (C<sub>q</sub>), 133.9 (C<sub>q</sub>), 133.8 (CH), 130.6 (CH), 129.0 (C<sub>q</sub>), 128.6 (CH), 127.8 (CH), 127.5 (C<sub>q</sub>), 127.3 (CH), 126.7 (CH), 126.7 (CH), 124.7 (CH), 124.1 (CH), 124.0 (C<sub>q</sub>), 123.9 (C<sub>q</sub>), 122.8 (CH), 122.3 (CH), 117.5 (CH), 112.6 (C<sub>q</sub>). **IR** (ATR):  $\tilde{\nu}$  = 1641, 1609, 1574, 1462, 1405, 1294, 1233, 872, 760, 722 cm<sup>-1</sup>. **MS** (ESI)  $m/z$  (relative intensity): 297 (70) [M+H]<sup>+</sup>, 319 (40) [M+Na]<sup>+</sup>, 593 (60) [2M+H]<sup>+</sup>, 615 (100) [2M+Na]<sup>+</sup>. **HR-MS** (ESI)  $m/z$  calcd for C<sub>13</sub>H<sub>14</sub>O<sub>2</sub> [M+H]<sup>+</sup>: 297.0910, found: 297.0916.

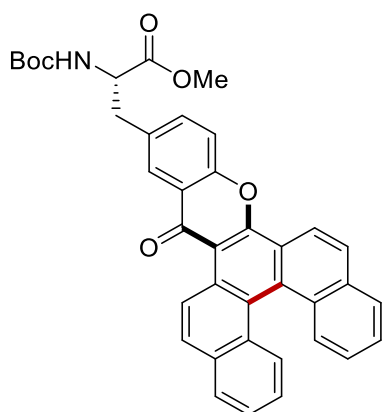
The spectral data are in accordance with those reported in the literature.<sup>[224]</sup>



***tert*-Butyl (S)-2-[(*tert*-butoxycarbonyl)amino]-3-(14-oxo-14*H*-dibenzo[*a,c*]xanthen-12-yl)propanoate**

General Procedure E was followed using amino acid **175aa** (65.8 mg, 0.12 mmol) and KI (10.1 mg, 60  $\mu$ mol) for 24 h. Purification by column chromatography on silica gel (*n*hexane/EtOAc = 6:1 to 4:1) furnished **180b** (48.3 mg, 75%) as a white solid.

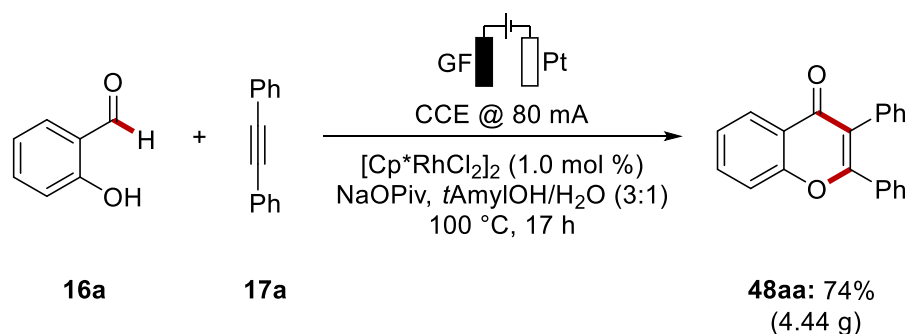
**<sup>1</sup>H-NMR** (400 MHz, CDCl<sub>3</sub>):  $\delta$  = 10.09 (dd,  $J$  = 8.4, 1.4 Hz, 1H), 8.59 (d,  $J$  = 8.4 Hz, 1H), 8.56 (d,  $J$  = 8.4 Hz, 2H), 8.21–8.15 (m, 1H), 7.78–7.68 (m, 2H), 7.67–7.60 (m, 2H), 7.59–7.51 (m, 2H), 5.15 (d,  $J$  = 7.9 Hz, 1H), 4.53 (ddd,  $J$  = 7.9, 6.1, 5.8 Hz, 1H), 3.27 (dd,  $J$  = 14.0, 5.8 Hz, 1H), 3.17 (dd,  $J$  = 14.0, 6.1 Hz, 1H), 1.47 (s, 9H), 1.44 (s, 9H). **<sup>13</sup>C-NMR** (101 MHz, CDCl<sub>3</sub>):  $\delta$  = 178.0 (C<sub>q</sub>), 170.8 (C<sub>q</sub>), 155.3 (C<sub>q</sub>), 155.0 (C<sub>q</sub>), 153.0 (C<sub>q</sub>), 135.2 (CH), 133.8 (C<sub>q</sub>), 133.4 (C<sub>q</sub>), 130.6 (CH), 129.0 (C<sub>q</sub>), 128.6 (CH), 127.8 (CH), 127.5 (C<sub>q</sub>), 127.3 (CH), 127.2 (CH), 126.7 (CH), 124.0 (CH), 123.9 (C<sub>q</sub>), 123.7 (C<sub>q</sub>), 122.8 (CH), 122.3 (CH), 117.6 (CH), 112.6 (C<sub>q</sub>), 82.7 (C<sub>q</sub>), 80.0 (C<sub>q</sub>), 55.1 (CH), 39.6 (CH<sub>2</sub>), 28.5 (CH<sub>3</sub>), 28.2 (CH<sub>3</sub>). **IR** (ATR):  $\tilde{\nu}$  = 1706, 1641, 1488, 1446, 1364, 1244, 1151, 755, 728 cm<sup>-1</sup>. **M.p.**: 197–199 °C. **MS** (ESI)  $m/z$  (relative intensity): 540 (60) [M+H]<sup>+</sup>, 562 (70) [M+Na]<sup>+</sup>, 1101 (100) [2M+Na]<sup>+</sup>. **HR-MS** (ESI)  $m/z$  calcd for C<sub>33</sub>H<sub>34</sub>NO<sub>6</sub> [M+H]<sup>+</sup>: 540.2381, found: 540.2380.

**180c**

**Methyl (S)-2-[(*tert*-butoxycarbonyl)amino]-3-(16-oxo-16*H*-dinaphtho[2,1-*a*:1',2'-*c*]xanthen-14-yl)propanoate**

General Procedure E was followed using amino acid **175bk** (49.5 mg, 0.08 mmol) and KI (6.9 mg, 40  $\mu$ mol) in MeOH/H<sub>2</sub>O (19:1, 4.0 mL) for 24 h. Purification by column chromatography on silica gel (*n*hexane/EtOAc = 5:1 to 3:1) furnished **180c** (39.9 mg, 81%) as a yellow solid.

**<sup>1</sup>H-NMR** (400 MHz, CDCl<sub>3</sub>, mixture of diastereomers):  $\delta$  = 10.16–10.07 (m, 1H), 8.61–8.56 (m, 1H), 8.27–8.22 (m, 1H), 8.21–8.18 (m, 1H), 8.15 (d,  $J$  = 9.3 Hz, 1H), 8.13–8.09 (m, 1H), 8.02–7.93 (m, 3H), 7.63–7.55 (m, 3H), 7.52 (t,  $J$  = 7.4 Hz, 1H), 7.31–7.26 (m, 1H), 7.25–7.21 (m, 1H), 5.18 (d,  $J$  = 8.2 Hz, 1H), 4.71 (d,  $J$  = 7.2 Hz, 1H), 3.82 (s, 3H), 3.38–3.17 (m, 2H), 1.45 (s, 9H). **<sup>13</sup>C-NMR** (101 MHz, CDCl<sub>3</sub>):  $\delta$  = 178.2 (C<sub>q</sub>), 172.2 (C<sub>q</sub>), 155.3 (C<sub>q</sub>), 154.5 (C<sub>q</sub>), 153.7 (C<sub>q</sub>), 135.1 (CH), 133.9 (C<sub>q</sub>), 133.0 (C<sub>q</sub>), 132.0 (C<sub>q</sub>), 131.6 (C<sub>q</sub>), 130.3 (C<sub>q</sub>), 130.3 (C<sub>q</sub>), 130.0 (CH), 129.4 (C<sub>q</sub>), 129.3 (CH), 129.3 (CH), 128.4 (CH), 128.0 (CH), 127.9 (CH), 127.6 (CH), 127.1 (CH), 126.3 (CH), 125.3 (CH), 124.6 (CH), 123.8 (C<sub>q</sub>), 123.7 (CH), 123.6 (C<sub>q</sub>), 123.1 (C<sub>q</sub>), 119.3 (CH), 117.9 (CH), 113.3 (C<sub>q</sub>), 80.3 (C<sub>q</sub>), 54.7 (CH), 52.6 (CH<sub>3</sub>), 38.2 (CH<sub>2</sub>), 28.4 (CH<sub>3</sub>). **IR** (ATR):  $\tilde{\nu}$  = 2925, 1743, 1709, 1641, 1485, 1441, 1247, 1165, 823, 753 cm<sup>-1</sup>. **M.p.**: 142–144 °C. **MS** (ESI)  $m/z$  (relative intensity): 598 (80) [M+H]<sup>+</sup>, 620 (100) [M+Na]<sup>+</sup>, 1217 (90) [2M+Na]<sup>+</sup>. **HR-MS** (ESI)  $m/z$  calcd for C<sub>38</sub>H<sub>32</sub>NO<sub>6</sub> [M+H]<sup>+</sup>: 598.2224, found: 598.2228.

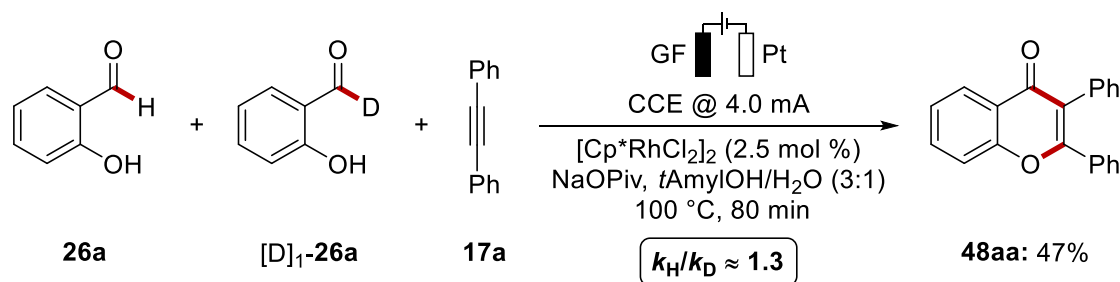
5.4.2 Multi-gram Scale Synthesis of **48aa**

In an undivided cell with a graphite felt anode (25 mm × 50 mm × 6.0 mm) and a platinum cathode (25 mm × 50 mm × 0.25 mm), aldehyde **26a** (4.88 g, 40.0 mmol), alkyne **17a** (3.44 g, 20.0 mmol), NaOPiv (4.96 g, 40.0 mmol), and  $[\text{Cp}^*\text{RhCl}_2]_2$  (124 mg, 0.20 mmol) were dissolved in *t*AmylOH/ $\text{H}_2\text{O}$  (60 mL, 3:1). Electrocatalysis was performed at 100 °C with a constant current of 80 mA maintained for 17 h. The graphite felt anode was washed with EtOAc (3 × 30 mL) in an ultrasonic bath. Evaporation of the solvent and subsequent column chromatography (*n*hexane/EtOAc = 10:1) yielded **48aa** (4.44 g, 74%) as a white solid.

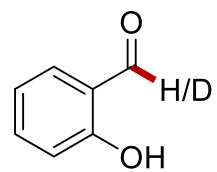


**Figure 5.4.1** Set-up for the multi-gram scale reaction of **48aa**.

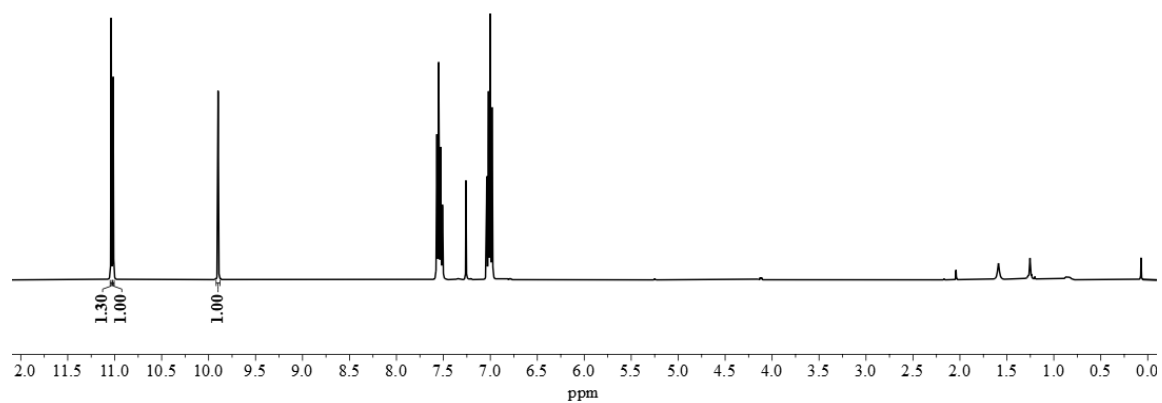
## 5.4.3 KIE Studies



The electrocatalysis was carried out in an undivided cell, with a graphite felt (GF) anode (25 mm × 10 mm × 6.0 mm) and a platinum cathode (25 mm × 10 mm × 0.125 mm). 2-Hydroxybenzaldehyde **26a** (45.8 mg, 0.375 mmol) and  $[\text{D}]_1\text{-26a}$  (46.1 mg, 0.375 mmol), alkyne **17a** (44.5 mg, 0.25 mmol), NaOPiv (62.0 mg, 0.50 mmol),  $[\text{Cp}^*\text{RhCl}_2]_2$  (3.9 mg, 2.5 mol %) and *t*AmylOH/H<sub>2</sub>O (4.0 mL, 3:1) were placed in a 10 mL cell. Electrocatalysis was performed at 100 °C with a constant current of 4.0 mA maintained for 80 min. Then, the DC-power supply was stopped, and the reaction mixture was diluted with EtOAc (2.0 mL). The platinum cathode and the graphite felt anode were washed with EtOAc (Pt: 1 × 5.0 mL; GF: 3 × 10 mL). The solvents were combined with the reaction mixture, silica gel was added, and the solvents were removed in vacuo. Subsequent column chromatography on silica gel (*n*hexane/EtOAc = 25:1 to 10:1) afforded a mixture of the recovered starting materials **26a** and  $[\text{D}]_1\text{-26a}$  (34.9 mg) as well as product **48aa** (34.9 mg, 47%). A KIE value of  $k_{\text{H}}/k_{\text{D}} \approx 1.3$  was determined by <sup>1</sup>H-NMR spectroscopic analysis of the mixture of **26a** and  $[\text{D}]_1\text{-26a}$ .



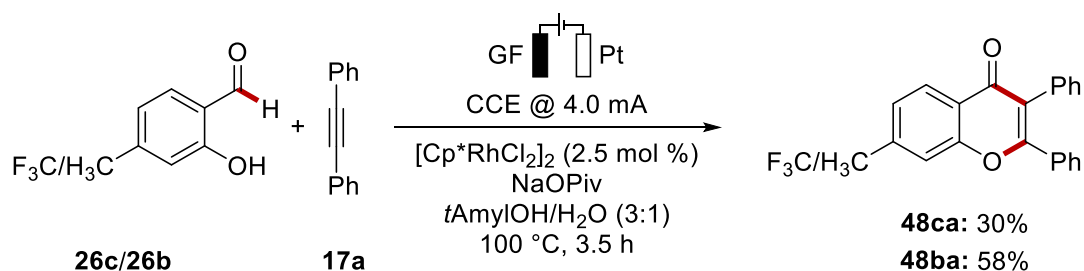
**26a/[D]<sub>1</sub>-26a**  
(CDCl<sub>3</sub>, 400 MHz)



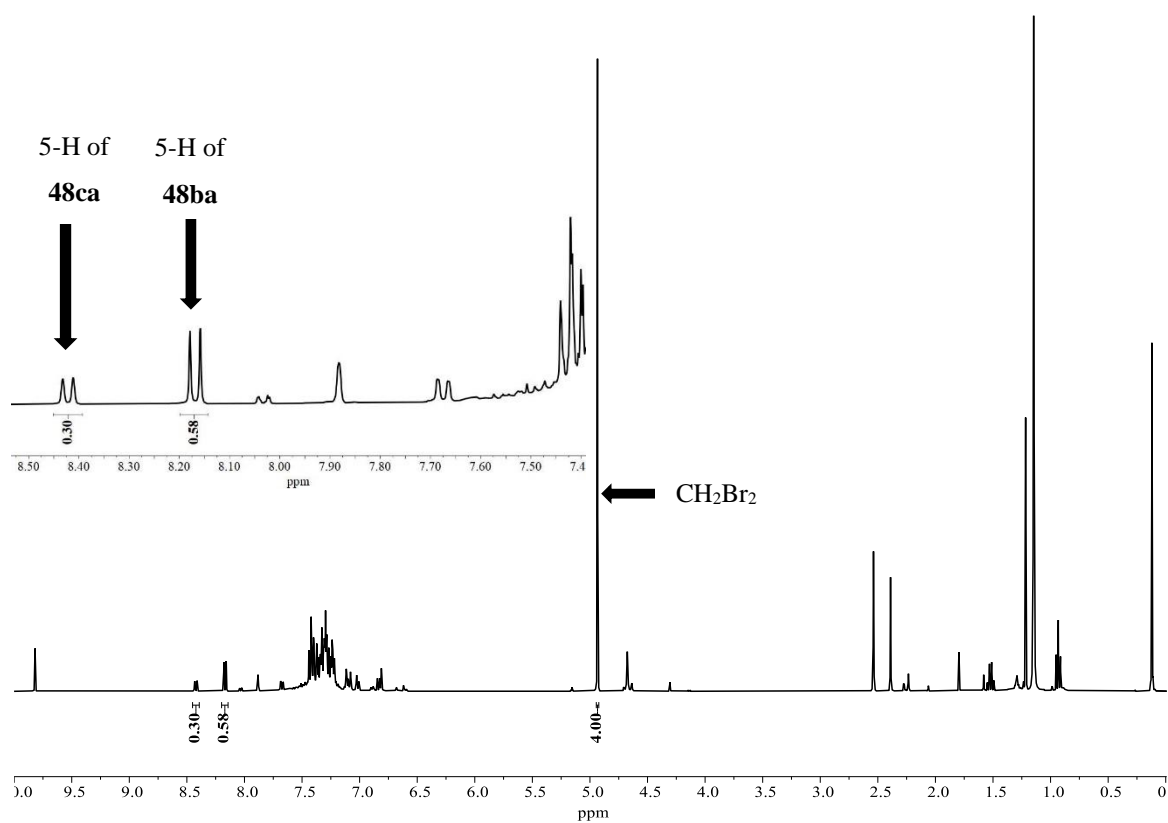
**Figure 5.4.2** <sup>1</sup>H-NMR spectrum of the of the isolated starting materials **26a/[D]<sub>1</sub>-26a** after the reaction.



## 5.4.4 Competition Experiment

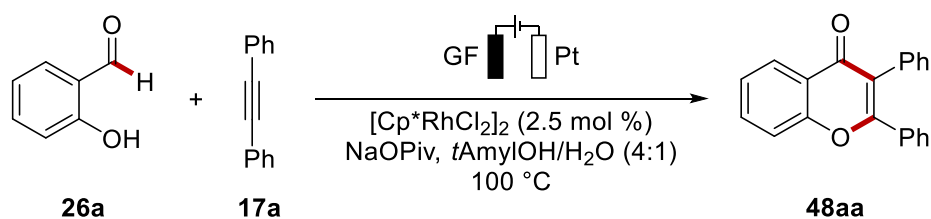


The electrocatalysis was carried out in an undivided cell, with a graphite felt (GF) anode (25 mm × 10 mm × 6.0 mm) and a platinum cathode (25 mm × 10 mm × 0.125 mm). 2-Hydroxybenzaldehydes **26c** (71.3 mg, 0.375 mmol) and **26b** (51.1 mg, 0.375 mmol), alkyne **17a** (44.5 mg, 0.25 mmol), NaOPiv (62 mg, 0.50 mmol), [Cp\**RhCl*<sub>2</sub>]<sub>2</sub> (3.9 mg, 2.5 mol %) and *t*AmylOH/H<sub>2</sub>O (4.0 mL, 3:1) were placed in a 10 mL cell. Electrocatalysis was performed at 100 °C with a constant current of 4.0 mA maintained for 3.5 h. Then, the DC-power supply was stopped, and the reaction mixture was diluted with EtOAc (2.0 mL). The platinum cathode and the graphite felt anode were washed with EtOAc (Pt: 1 × 5.0 mL; GF: 3 × 10 mL). The solvents were combined with the reaction mixture, and the solvents were removed in vacuo. CDCl<sub>3</sub> (1.2 mL) and internal standard CH<sub>2</sub>Br<sub>2</sub> (36 μL, 0.50 mmol) were added and the mixture was filtered through a cotton plug and analyzed by <sup>1</sup>H-NMR spectroscopy (CDCl<sub>3</sub>, 400 MHz).

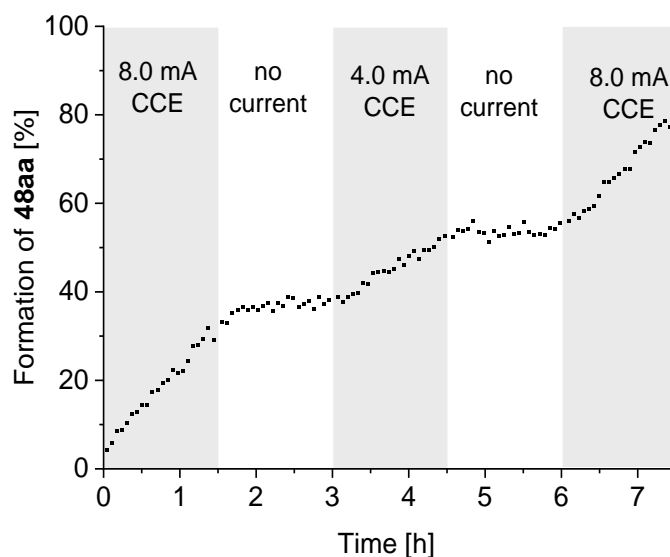


**Figure 5.4.3**  $^1\text{H-NMR}$  spectrum of the of crude mixture after the competition experiment between starting materials **26b** and **26c**.

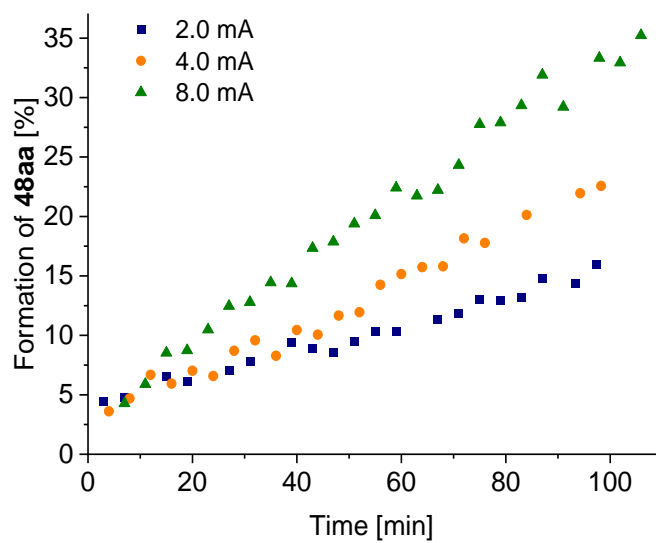
## 5.4.5 On-line NMR Monitoring in Flow



A 10 mL Schlenk tube was charged with aldehyde **26a** (183 mg, 1.50 mmol), alkyne **17a** (134 mg, 0.75 mmol), NaOPiv (186 mg, 1.50 mmol),  $[\text{Cp}^*\text{RhCl}_2]_2$  (11.6 mg, 2.5 mol %), 1,3,5-trimethoxybenzene (42.0 mg, 0.25 mmol) and *t*AmylOH/H<sub>2</sub>O (8.0 mL, 6.5:1.5). The electrocatalyses were performed with various constant currents. The yields were determined against the aromatic protons of the internal standard 1,3,5-trimethoxybenzene.

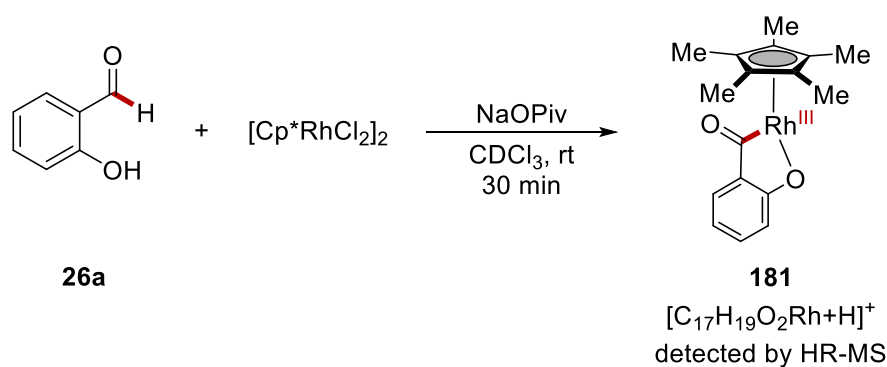


**Figure 5.4.4** On-line reaction monitoring experiment for the rhodaelectro-catalyzed formyl C–H activation without and with applied currents.

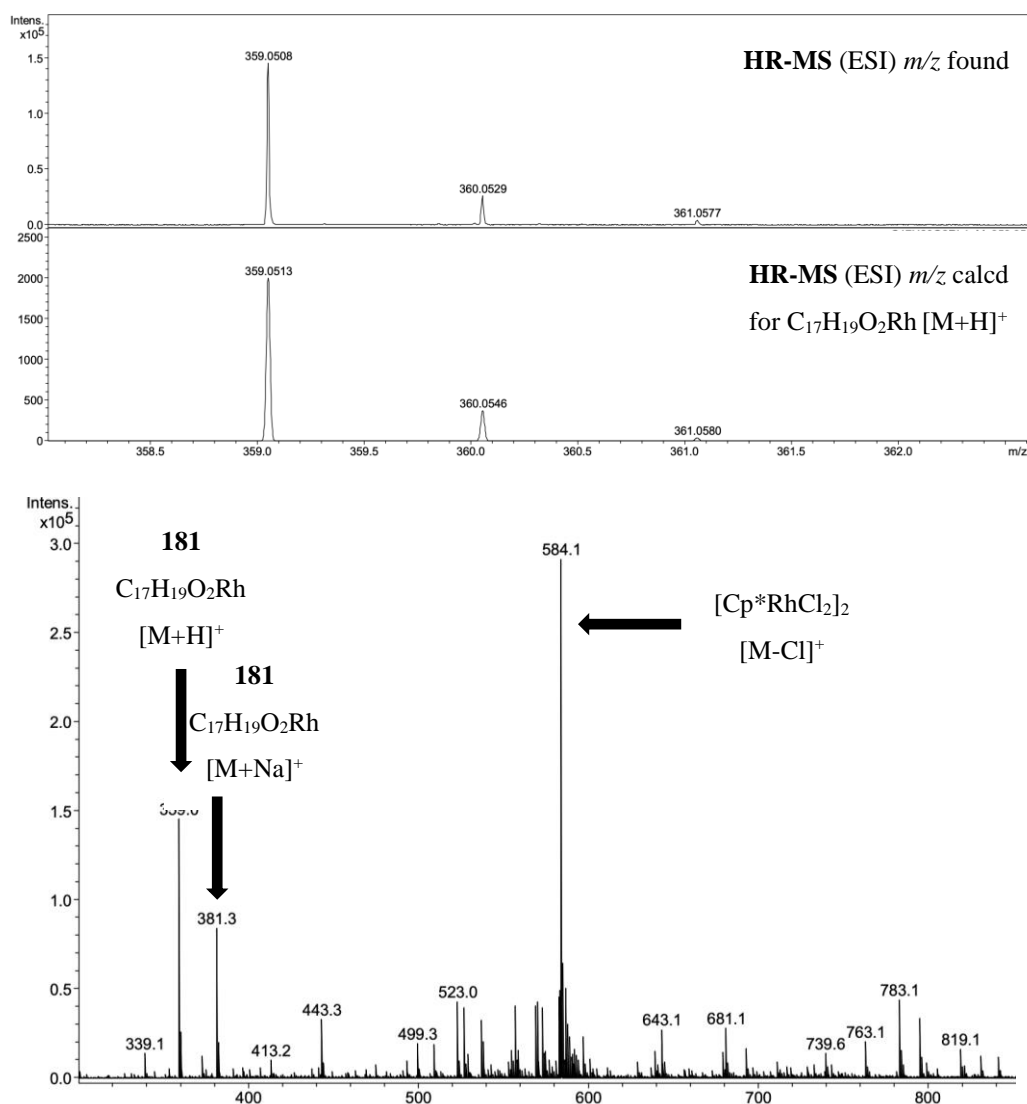


**Figure 5.4.5** Online reaction monitoring experiment for the rhodaelectro-catalyzed formyl C–H activation for the initial rates with different currents.

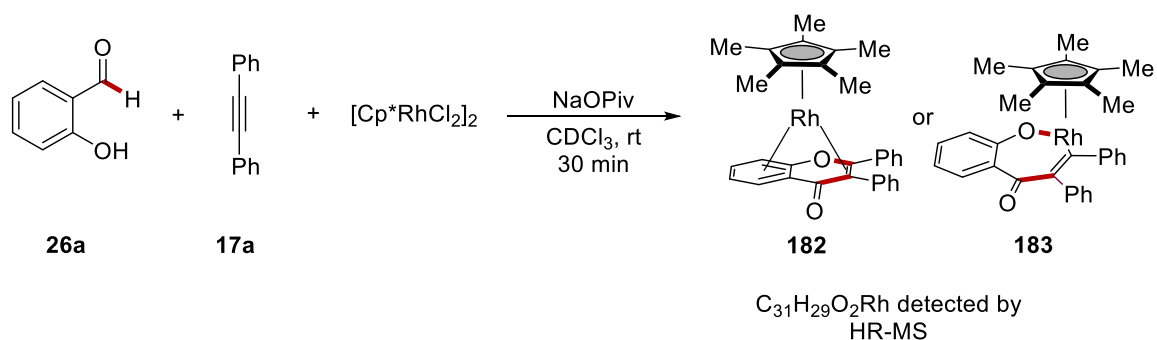
## 5.4.6 Detection of Intermediates by HR-MS



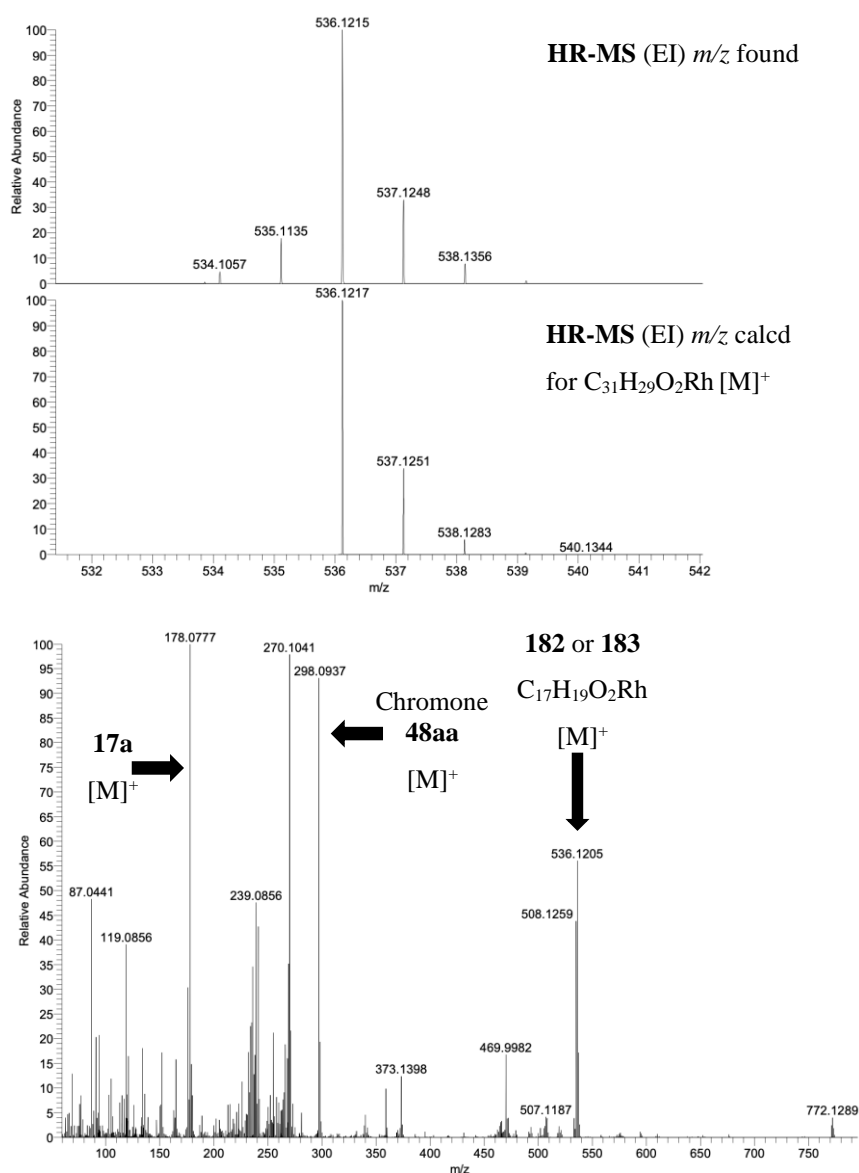
Salicylic aldehyde **26a** (2.4 mg, 0.02 mmol),  $[\text{Cp}^*\text{RhCl}_2]_2$  (6.2 mg, 0.01 mmol) and sodium pivalate (5.0 mg, 0.04 mmol) were added to a reaction vial and dissolved in  $\text{CDCl}_3$  (0.75 mL). The mixture was stirred for 30 min at rt and an aliquot was submitted for HR-MS analysis.



**Figure 5.4.6** ESI-MS (positive ionization-mode) of proposed cyclometalated rhodium-species **183**.

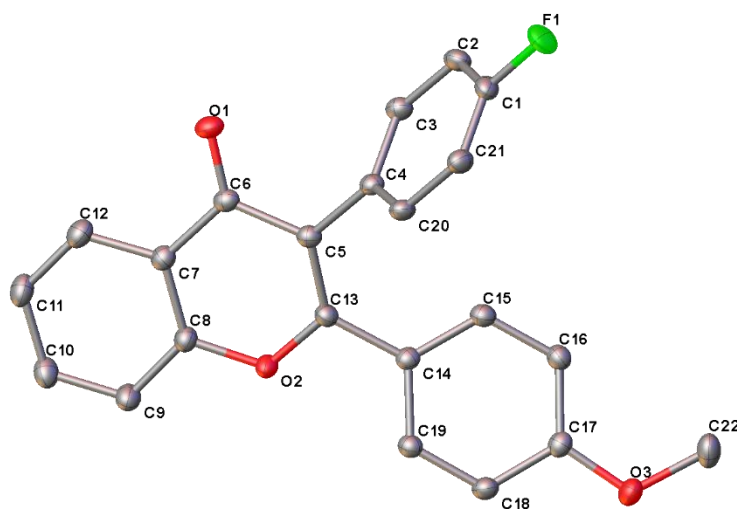


Salicylic aldehyde **26a** (2.4 mg, 0.02 mmol),  $[Cp^*RhCl_2]_2$  (6.2 mg, 0.01 mmol), alkyne **17a** (3.6 mg, 0.02 mmol), and sodium pivalate (5.0 mg, 0.04 mmol) were added to a reaction vial and dissolved in  $CDCl_3$  (0.75 mL). The mixture was stirred for 30 min at rt and an aliquot was submitted for HR-MS analysis.



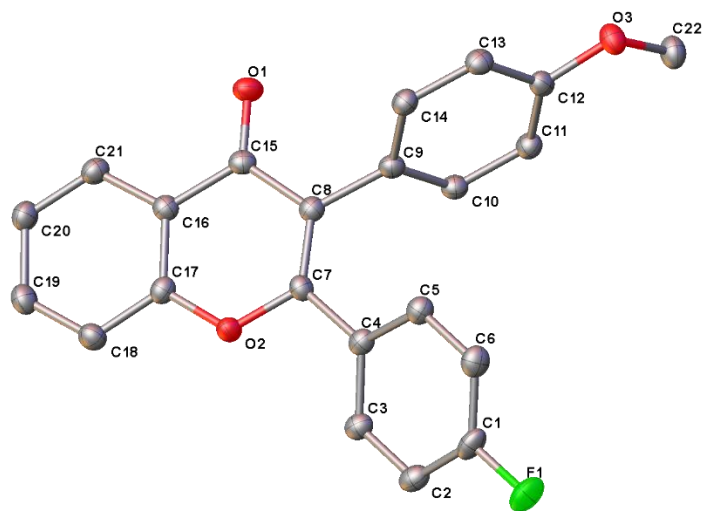
**Figure 5.4.7** EI-MS (positive ionization-mode) of a proposed rhodium-species **182** or **183**.

## 5.4.7 Crystallographic Data of Chromones



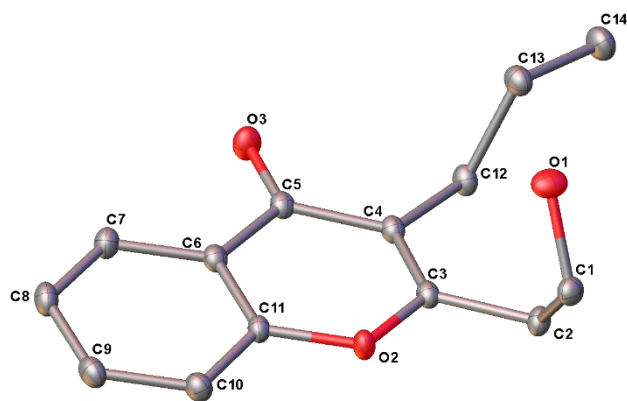
172aa

Identification code	CCDC 2046228
Empirical formula	C <sub>22</sub> H <sub>15</sub> FO <sub>3</sub>
Formula weight	346.34
Temperature/K	100.0
Crystal system	monoclinic
Space group	P2 <sub>1</sub> /c
a/Å	5.7254(5)
b/Å	15.2781(13)
c/Å	19.087(2)
α/°	90
β/°	98.301(3)
γ/°	90
Volume/Å <sup>3</sup>	1652.1(3)
Z	4
ρ <sub>calc</sub> /cm <sup>3</sup>	1.392
μ/mm <sup>-1</sup>	0.100
F(000)	720.0
Crystal size/mm <sup>3</sup>	0.202 × 0.179 × 0.116
Radiation	MoKα (λ = 0.71073)
2θ range for data collection/°	5.332 to 59.182
Index ranges	-7 ≤ h ≤ 7, -21 ≤ k ≤ 21, -25 ≤ l ≤ 26
Reflections collected	48386
Independent reflections	4561 [R <sub>int</sub> = 0.0308, R <sub>sigma</sub> = 0.0168]
Data/restraints/parameters	4561/0/236
Goodness-of-fit on F <sup>2</sup>	1.068
Final R indexes [I ≥ 2σ (I)]	R <sub>1</sub> = 0.0395, wR <sub>2</sub> = 0.0942
Final R indexes [all data]	R <sub>1</sub> = 0.0467, wR <sub>2</sub> = 0.1007
Largest diff. peak/hole / e Å <sup>-3</sup>	0.36/-0.22

**172aa'**

Identification code	CCDC 2046229
Empirical formula	C <sub>22</sub> H <sub>15</sub> FO <sub>3</sub>
Formula weight	346.34
Temperature/K	100.0
Crystal system	monoclinic
Space group	P2 <sub>1</sub> /c
a/Å	5.5391(2)
b/Å	13.8898(6)
c/Å	21.8396(9)
α/°	90
β/°	93.3070(10)
γ/°	90
Volume/Å <sup>3</sup>	1677.48(12)
Z	4
ρ <sub>calc</sub> /cm <sup>3</sup>	1.371
μ/mm <sup>-1</sup>	0.098
F(000)	720.0
Crystal size/mm <sup>3</sup>	0.3 × 0.085 × 0.054
Radiation	MoKα (λ = 0.71073)
2θ range for data collection/°	4.75 to 57.408
Index ranges	-7 ≤ h ≤ 7, -18 ≤ k ≤ 18, -28 ≤ l ≤ 29
Reflections collected	34891
Independent reflections	4333 [R <sub>int</sub> = 0.0474, R <sub>sigma</sub> = 0.0293]
Data/restraints/parameters	4333/0/237
Goodness-of-fit on F <sup>2</sup>	1.138
Final R indexes [I ≥ 2σ (I)]	R <sub>1</sub> = 0.0547, wR <sub>2</sub> = 0.1114
Final R indexes [all data]	R <sub>1</sub> = 0.0711, wR <sub>2</sub> = 0.1196
Largest diff. peak/hole / e Å <sup>-3</sup>	0.26/-0.26



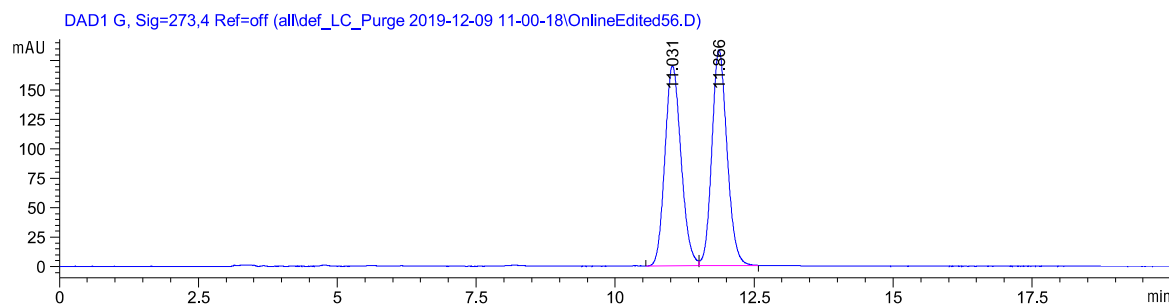
**172ak**

Identification code	CCDC 2046225
Empirical formula	$C_{14}H_{16}O_3$
Formula weight	232.27
Temperature/K	100.0
Crystal system	monoclinic
Space group	$P2_1/c$
$a/\text{\AA}$	4.8492(3)
$b/\text{\AA}$	15.5183(12)
$c/\text{\AA}$	15.0910(11)
$\alpha/^\circ$	90
$\beta/^\circ$	93.172(3)
$\gamma/^\circ$	90
Volume/ $\text{\AA}^3$	1133.88(14)
Z	4
$\rho_{\text{calc}}/\text{g/cm}^3$	1.361
$\mu/\text{mm}^{-1}$	0.095
F(000)	496.0
Crystal size/ $\text{mm}^3$	$0.474 \times 0.185 \times 0.165$
Radiation	MoK $\alpha$ ( $\lambda = 0.71073$ )
$2\Theta$ range for data collection/ $^\circ$	5.25 to 59.17
Index ranges	$-6 \leq h \leq 6, -21 \leq k \leq 21, -20 \leq l \leq 20$
Reflections collected	35861
Independent reflections	3134 [ $R_{\text{int}} = 0.0299, R_{\text{sigma}} = 0.0158$ ]
Data/restraints/parameters	3134/0/156
Goodness-of-fit on $F^2$	1.070
Final R indexes [ $I \geq 2\sigma(I)$ ]	$R_1 = 0.0391, wR_2 = 0.1001$
Final R indexes [all data]	$R_1 = 0.0414, wR_2 = 0.1019$
Largest diff. peak/hole / $e \text{\AA}^{-3}$	0.43/-0.23

### 5.4.8 Studies on Potential Racemization

A racemic tyrosine derivative *rac*-**174a** was employed in the rhodaelectro-catalyzed C–H activation and analyzed by HPLC, showing that no racemization occurs during the catalysis.

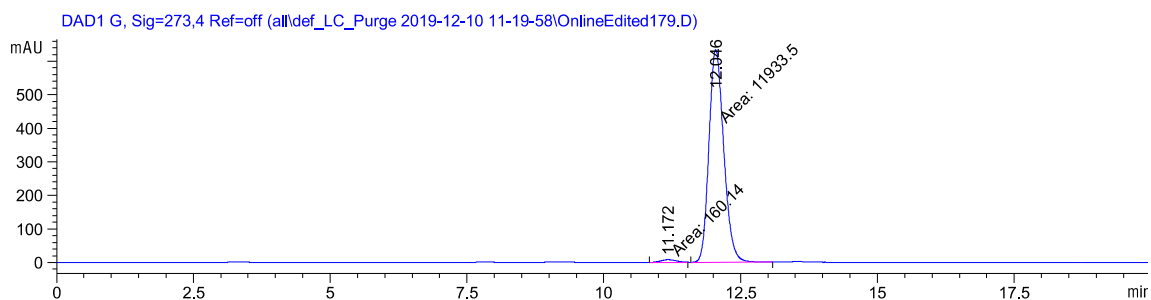
The *ee* % of **175aa** was determined >97%.



Signal 2: DAD1 G, Sig=273,4 Ref=off

Peak #	RetTime [min]	Type	Width [min]	Area [mAU*s]	Height [mAU]	Area %
1	11.031	VV R	0.3046	3434.80225	170.10265	49.6033
2	11.866	VB	0.2919	3489.74536	183.43951	50.3967

Totals : 6924.54761 353.54216



Signal 2: DAD1 G, Sig=273,4 Ref=off

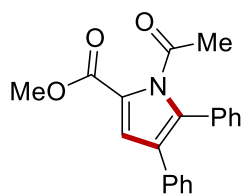
Peak #	RetTime [min]	Type	Width [min]	Area [mAU*s]	Height [mAU]	Area %
1	11.172	MM	0.3282	160.13980	8.13293	1.3242
2	12.046	MM	0.3138	1.19335e4	633.90845	98.6758

Totals : 1.20937e4 642.04137

**Figure 5.4.8** HPLC chromatograms of *rac*-**175aa** and **175aa**. A *CHIRALPAK*<sup>®</sup> IA column and *n*hexane/*i*PrOH (70:30, 1.0 mL/min, detection at 250 nm) were used for separation.

## 5.5 Rhodium-Catalyzed Electrochemical C–H Activation of Alkenes

### 5.5.1 Characterization Data



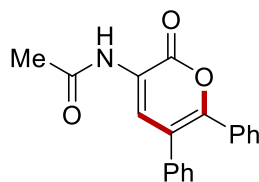
**62aa**

The general procedure F was followed using alkene **61a** (71.5 mg, 0.50 mmol), **17a** (44.5 mg, 0.25 mmol) and  $[\text{Cp}^*\text{Rh}(\text{MeCN})_3][\text{SbF}_6]_2$  (10.4 mg, 5.0 mol %) in TFE at 80 °C for 6 h. Purification by column chromatography on silica gel (*n*hexane/EtOAc = 12:1) yielded **62aa** (54.1 mg, 68%) as colorless oil.

Alkene **61a** (71.5 mg, 0.50 mmol), **17a** (44.5 mg, 0.25 mmol),  $\text{Cu}(\text{OAc})_2 \cdot \text{H}_2\text{O}$  (100 mg, 0.50 mmol) and  $[\text{Cp}^*\text{RhCl}_2]_2$  (7.7 mg, 5.0 mol %) were dissolved in *t*AmylOH/ $\text{H}_2\text{O}$  (4.0 mL, 3:1) under inert atmosphere and heated at 100 °C for 17 h. Afterwards the mixture was diluted with EtOAc (25 mL) and silica gel was added. The solvents were removed in vacuo and purification of the residue by column chromatography on silica gel (*n*hexane/EtOAc = 12:1) yielded **62aa** (56.1 mg, 70%) as colorless oil.

**$^1\text{H-NMR}$**  (400 MHz,  $\text{CDCl}_3$ ):  $\delta$  = 7.42–7.34 (m, 3H), 7.33–7.29 (m, 2H), 7.23–7.12 (m, 6H), 3.89 (s, 3H), 2.32 (s, 3H).  **$^{13}\text{C-NMR}$**  (101 MHz,  $\text{CDCl}_3$ ):  $\delta$  = 174.0 ( $\text{C}_q$ ), 161.2 ( $\text{C}_q$ ), 134.7 ( $\text{C}_q$ ), 134.1 ( $\text{C}_q$ ), 130.8 ( $\text{C}_q$ ), 129.0 (CH), 128.7 (CH), 128.4 (CH), 128.2 (CH), 126.6 (CH), 125.0 ( $\text{C}_q$ ), 123.1 ( $\text{C}_q$ ), 118.5 (CH), 52.0 ( $\text{CH}_3$ ), 29.0 ( $\text{CH}_3$ ). **IR** (ATR):  $\tilde{\nu}$  = 1759, 1702, 1440, 1375, 1252, 1201, 1131, 1056, 758, 696  $\text{cm}^{-1}$ . **MS** (ESI)  $m/z$  (relative intensity): 320 (50)  $[\text{M}+\text{H}]^+$ , 342 (100)  $[\text{M}+\text{Na}]^+$ , 661 (80)  $[2\text{M}+\text{Na}]^+$ . **HR-MS** (ESI)  $m/z$  calcd for  $\text{C}_{20}\text{H}_{17}\text{NO}_3$   $[\text{M}+\text{H}]^+$ : 320.1281, found: 320.1280.

The spectral data are in accordance with those reported in the literature.<sup>[99a, 98b]</sup>

**191aa*****N*-(2-oxo-5,6-diphenyl-2*H*-pyran-3-yl)acetamide**

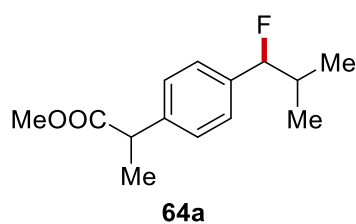
The general procedure F was followed using alkene **61a** (71.5 mg, 0.50 mmol), **17a** (44.5 mg, 0.25 mmol) and [Cp\**Rh*Cl<sub>2</sub>]<sub>2</sub> (7.7 mg, 5.0 mol %) in *t*AmylOH/H<sub>2</sub>O (4.0 mL, 3:1) at 100 °C for 17 h. Purification by column chromatography on silica gel (*n*hexane/EtOAc = 5:1 to 4:1) yielded **191aa** (52.3 mg, 69%) as a yellow solid.

**<sup>1</sup>H-NMR** (400 MHz, CDCl<sub>3</sub>):  $\delta$  = 8.44 (s, 1H), 8.07 (s, 1H), 7.33–7.29 (m, 5H), 7.29–7.26 (m, 1H), 7.24–7.20 (m, 4H), 2.23 (s, 3H). **<sup>13</sup>C-NMR** (101 MHz, CDCl<sub>3</sub>):  $\delta$  = 169.4 (C<sub>q</sub>), 159.5 (C<sub>q</sub>), 150.8 (C<sub>q</sub>), 136.5 (C<sub>q</sub>), 132.0 (C<sub>q</sub>), 129.6 (CH), 129.5 (CH), 129.1 (CH), 129.0 (CH), 128.3 (CH), 128.1 (CH), 123.7 (C<sub>q</sub>), 119.1 (C<sub>q</sub>), 24.8 (CH<sub>3</sub>). **IR** (ATR):  $\tilde{\nu}$  = 1704, 1666, 1521, 1482, 1373, 1240, 765, 729, 691, 654 cm<sup>-1</sup>. **M.p.**: 180–182 °C. **MS** (ESI) *m/z* (relative intensity): 306 (30) [M+H]<sup>+</sup>, 328 (100) [M+Na]<sup>+</sup>, 633 (50) [2M+Na]<sup>+</sup>. **HR-MS** (ESI) *m/z* calcd for C<sub>19</sub>H<sub>15</sub>NO<sub>3</sub> [M+H]<sup>+</sup>: 306.1125, found: 306.1122.

## 5.6 Electrochemical C(sp<sup>3</sup>)-H Fluorination

### 5.6.1 Quantitative <sup>1</sup>H and <sup>19</sup>F{H}-NMR Analyses for Benzyl Fluorides

Prior to quantification the automatic baseline correction and phase correction was performed using MNOVA 14.2.0 from MESTRELABS. Relevant integrals of nuclei from products and the standard are shown in the spectra. For further details see the captions and information given in the spectra.

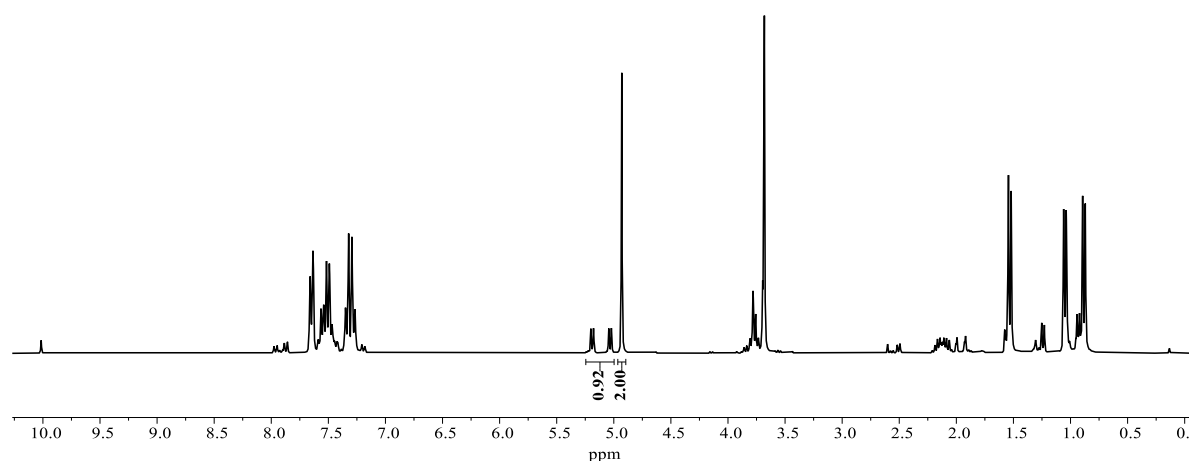


### Methyl 2-(4-(1-fluoro-2-methylpropyl)phenyl)propanoate

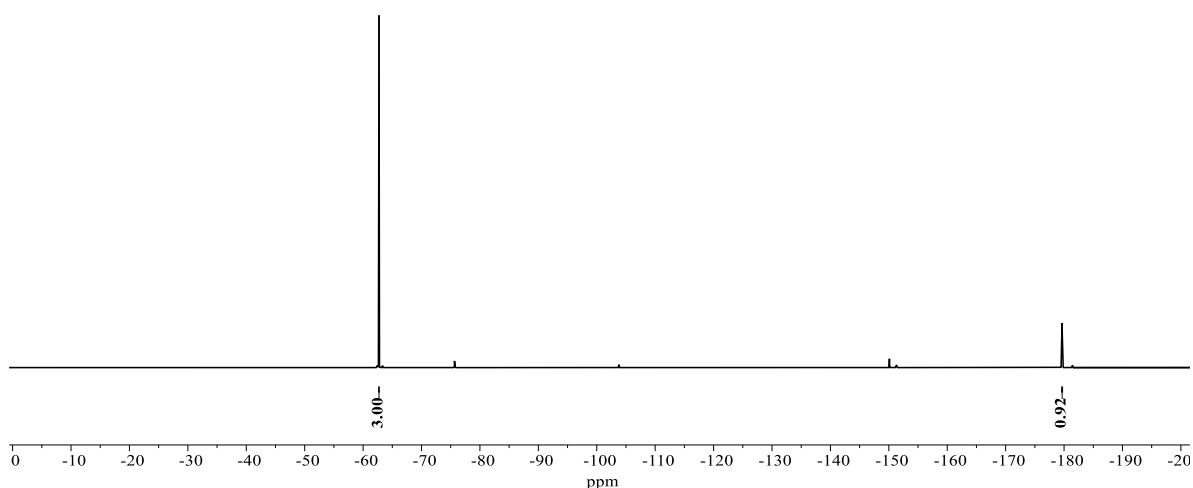
The general procedure G was followed using methyl 2-(4-(2-methylpropyl)phenyl)propanoate **63a** (110 mg, 0.50 mmol).

**Benzylic Fluoride C–H Shift:**  $^1\text{H-NMR}$  (300 MHz,  $\text{CDCl}_3$ )  $\delta = 5.11$  (dd,  $J = 47.0, 6.8$  Hz). Calibrated  $^1\text{H-NMR}$  yield from benzylic proton: 92%. **Benzylic Fluoride Shift:**  $^{19}\text{F}\{^1\text{H}\}$ -NMR (282 MHz,  $\text{CDCl}_3$ , mixture of diastereomers)  $\delta = -179.6, -179.7$ . Calibrated  $^{19}\text{F}\{^1\text{H}\}$ -NMR yield from benzylic fluoride: 92%. **HR-MS** (EI)  $m/z$  calcd for  $\text{C}_{14}\text{H}_{19}\text{FO}_2$   $[\text{M}]^+$ : 238.1364, found: 238.1362.

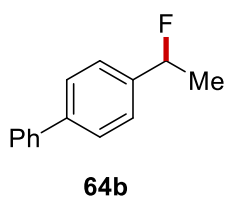
The spectral data are in accordance with those reported in literature.<sup>[122]</sup>



**Figure 5.6.1** Crude  $^1\text{H-NMR}$  Spectrum ( $\text{CDCl}_3$ , 300 MHz) of the reaction mixture with  $\text{CH}_2\text{Br}_2$  (36  $\mu\text{L}$ , 0.50 mmol) as internal standard (4.93 ppm). The signals of the resolved product and internal standard are integrated.



**Figure 5.6.2** Crude  $^{19}\text{F}\{^1\text{H}\}$ -NMR Spectrum ( $\text{CDCl}_3$ , 300 MHz) of the reaction mixture with  $\text{PhCF}_3$  (62  $\mu\text{L}$ , 0.50 mmol) as internal standard ( $-62.7$  ppm). The signals of the resolved product and internal standard are integrated.

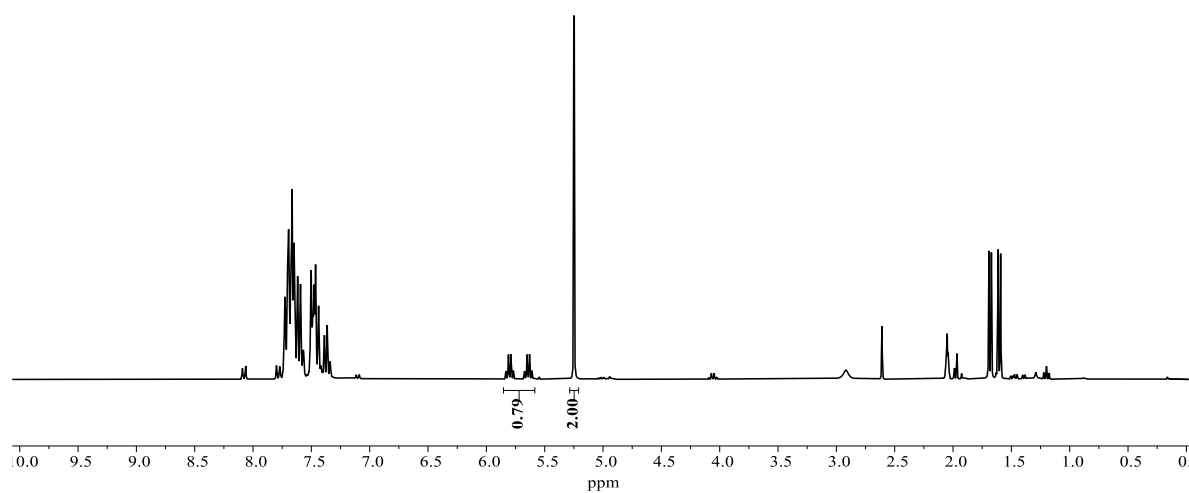


#### 4-(1-fluoroethyl)-1,1'-biphenyl

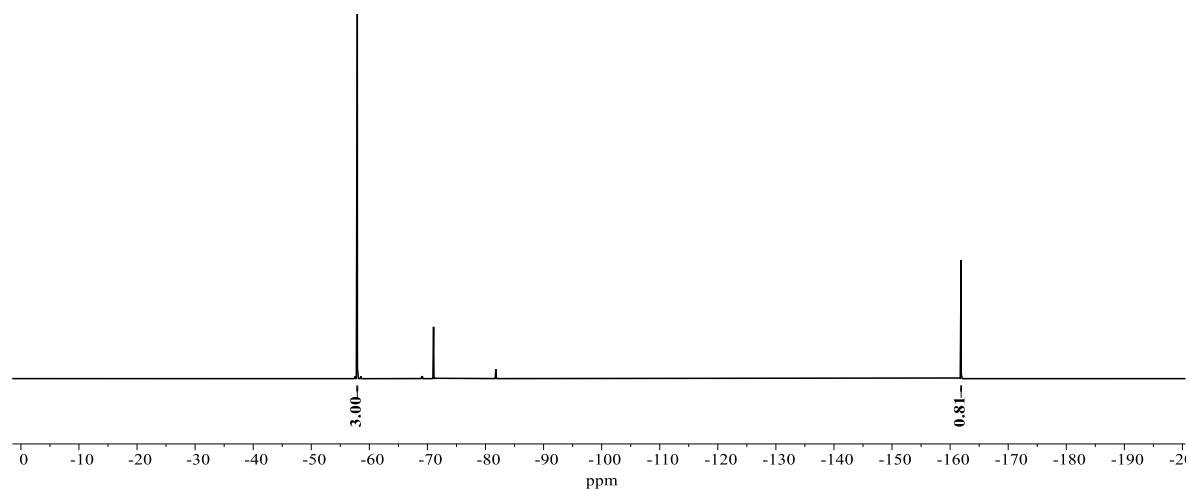
The general procedure G was followed using 4-ethyl-1,1'-biphenyl **63b** (91.2 mg, 0.50 mmol).

**Benzyl Fluoride C–H Shift:**  $^1\text{H}$ -NMR (300 MHz,  $d_6$ -Acetone)  $\delta = 5.72$  (dq,  $J = 48.2$ , 6.4 Hz). Calibrated  $^1\text{H}$ -NMR yield from the benzylic proton: 79%. **Benzylic Fluoride Shift:**  $^{19}\text{F}\{^1\text{H}\}$ -NMR (282 MHz,  $d_6$ -Acetone)  $\delta = -161.9$ . Calibrated  $^{19}\text{F}\{^1\text{H}\}$ -NMR yield from benzylic fluoride: 81%. **HR-MS** (EI)  $m/z$  calcd for  $\text{C}_{14}\text{H}_{13}\text{F}[\text{M}]^+$ : 200.0996, found: 200.0996.

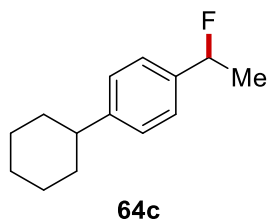
The spectral data are in accordance with those reported in literature.<sup>[118]</sup>



**Figure 5.6.3** Crude  $^1\text{H}$ -NMR Spectrum (300 MHz,  $d_6$ -Acetone) of the reaction mixture with  $\text{CH}_2\text{Br}_2$  (36  $\mu\text{L}$ , 0.50 mmol) as internal standard (5.25 ppm). The signals of the benzylic proton and internal standard are integrated.



**Figure 5.6.4** Crude  $^{19}\text{F}$ -NMR Spectrum (282 MHz,  $d_6$ -Acetone) of the reaction mixture with  $\text{PhCF}_3$  (62  $\mu\text{L}$ , 0.50 mmol) as internal standard (-57.9 ppm). The signals of the benzylic fluoride and internal standard are integrated.

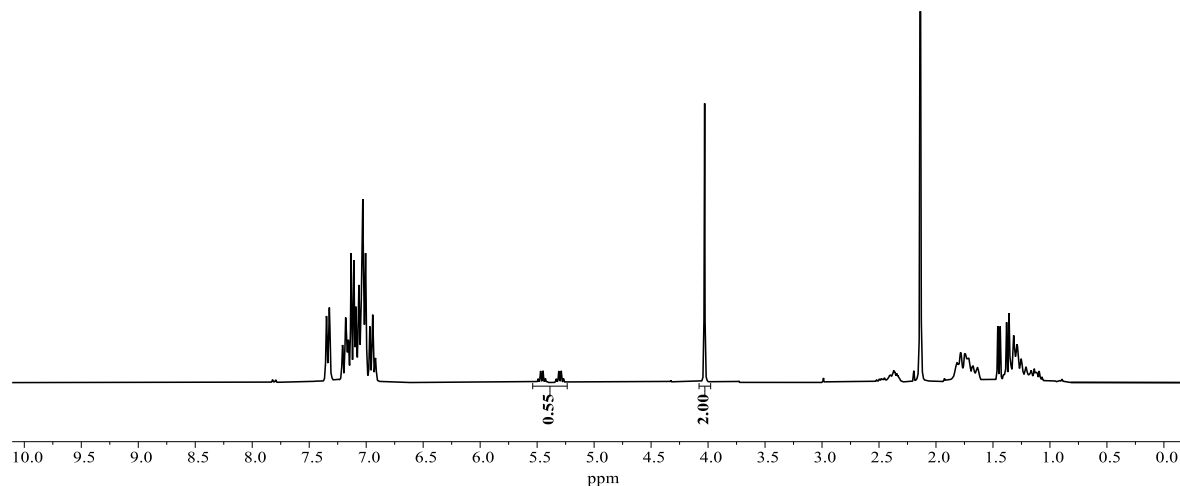


### 1-Cyclohexyl-4-(1-fluoroethyl)benzene

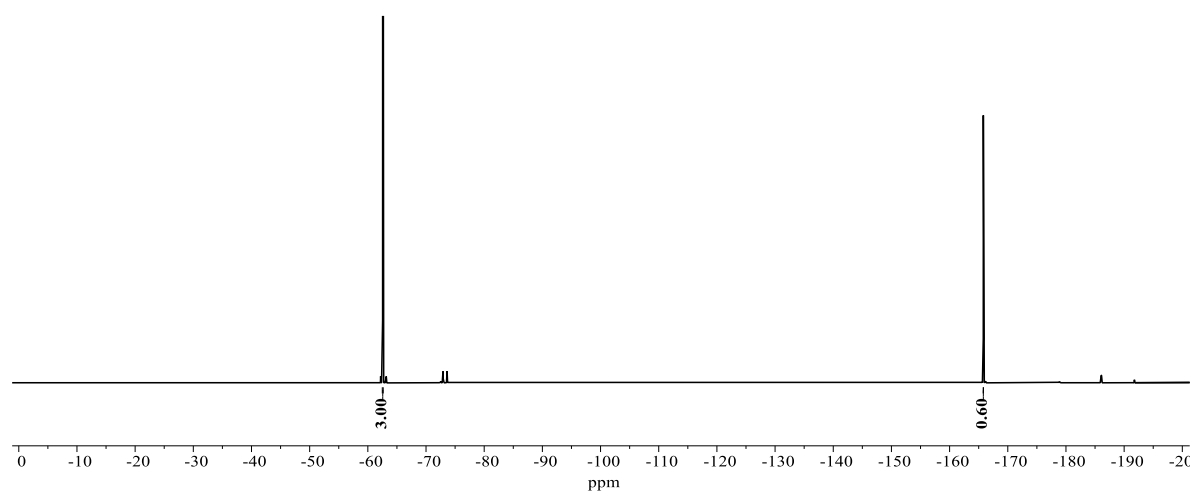
The general procedure G was followed using 1-cyclohexyl-4-ethylbenzene **63c** (94.3 mg, 0.50 mmol).



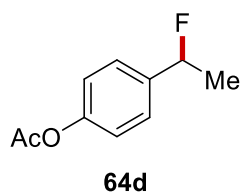
**Benzyl Fluoride C–H Shift:**  $^1\text{H-NMR}$  (300 MHz,  $\text{C}_6\text{D}_6$ )  $\delta = 5.35$  (dq,  $J = 47.8, 6.4$  Hz). Calibrated  $^1\text{H-NMR}$  yield from benzylic proton: 55%. **Benzylic Fluoride Shift:**  $^{19}\text{F}\{^1\text{H}\}$ -NMR (282 MHz,  $\text{CDCl}_3$ )  $\delta = -165.8$ . Calibrated  $^{19}\text{F}\{^1\text{H}\}$ -NMR yield from benzylic fluoride: 60%. **HR-MS** (EI)  $m/z$  calcd for  $\text{C}_{14}\text{H}_{19}\text{F} [\text{M}]^+$ : 206.1465, found: 206.1465.



**Figure 5.6.5** Crude  $^1\text{H-NMR}$  Spectrum (300 MHz,  $\text{C}_6\text{D}_6$ ) of the reaction mixture with  $\text{CH}_2\text{Br}_2$  (36  $\mu\text{L}$ , 0.50 mmol) as internal standard (4.03 ppm). The signals of the benzylic proton and internal standard are integrated.



**Figure 5.6.6** Crude  $^{19}\text{F-NMR}$  Spectrum (282 MHz,  $\text{C}_6\text{D}_6$ ) of the reaction mixture with  $\text{PhCF}_3$  (62  $\mu\text{L}$ , 0.50 mmol) as internal standard ( $-62.5$  ppm). The signals of the benzylic fluoride and internal standard are integrated.

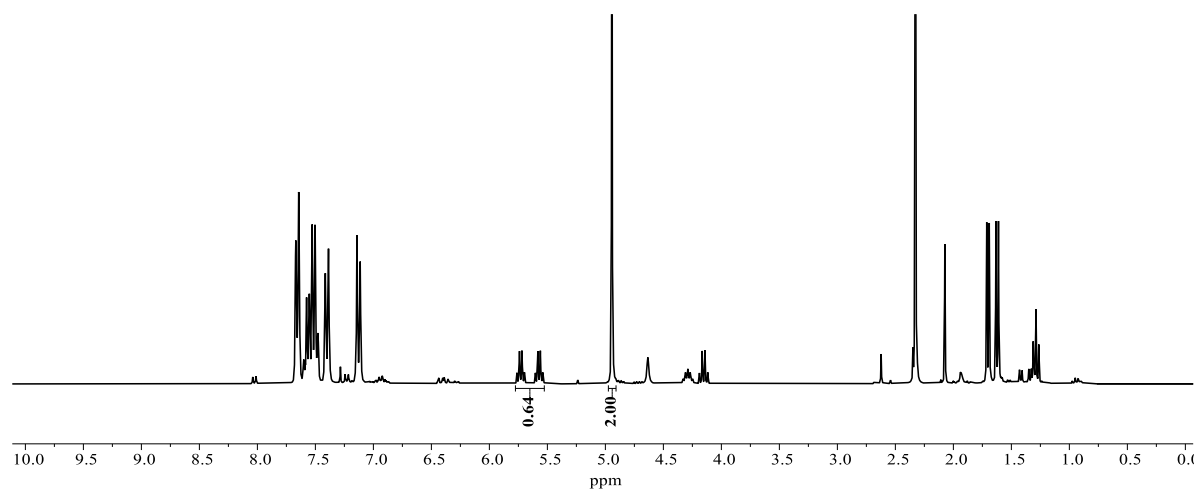


#### 4-(1-Fluoroethyl)phenyl acetate

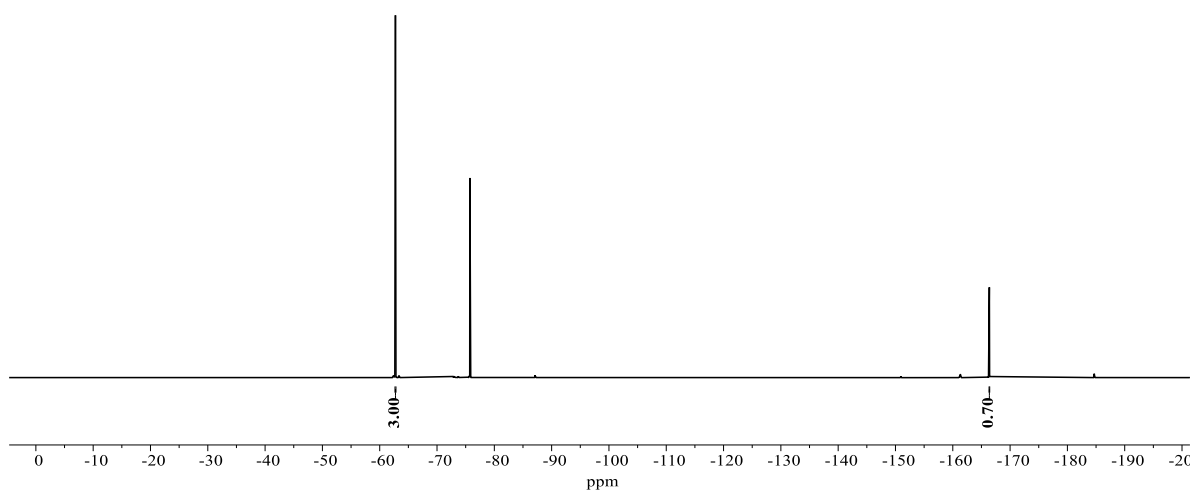
The general procedure G was followed using 4-ethylphenyl acetate **63d** (82.1 mg, 0.50 mmol) with 3.0 F/mol total charge at  $-15\text{ }^{\circ}\text{C}$ .

**Benzyl Fluoride C–H Shift:**  $^1\text{H-NMR}$  (300 MHz,  $\text{CDCl}_3$ ):  $\delta = 5.64$  (dq,  $J = 47.8, 6.4$  Hz). Calibrated  $^1\text{H-NMR}$  yield from benzylic proton: 64%. **Benzylic Fluoride Shift:**  $^{19}\text{F}\{^1\text{H}\}$ -NMR (282 MHz,  $\text{CDCl}_3$ ):  $\delta = -166.4$ . Calibrated  $^{19}\text{F}\{^1\text{H}\}$ -NMR yield from benzylic fluoride: 70%. **HR-MS** (EI)  $m/z$  calcd for  $\text{C}_{10}\text{H}_{11}\text{FO}_2$   $[\text{M}]^+$ : 182.0738, found: 182.0739.

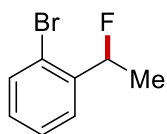
The spectral data are in accordance with those reported in literature.<sup>[119a]</sup>



**Figure 5.6.7** Crude  $^1\text{H-NMR}$  Spectrum (300 MHz,  $\text{CDCl}_3$ ) of the reaction mixture with  $\text{CH}_2\text{Br}_2$  (36  $\mu\text{L}$ , 0.50 mmol) as internal standard (4.93 ppm). The signals of the benzylic proton and internal standard are integrated.



**Figure 5.6.8**  $^{19}\text{F}$ -NMR Spectrum (282 MHz,  $\text{CDCl}_3$ ) of the reaction mixture with  $\text{PhCF}_3$  (62  $\mu\text{L}$ , 0.50 mmol) as internal standard ( $-62.7$  ppm). The signals of the benzylic fluoride and internal standard are integrated.



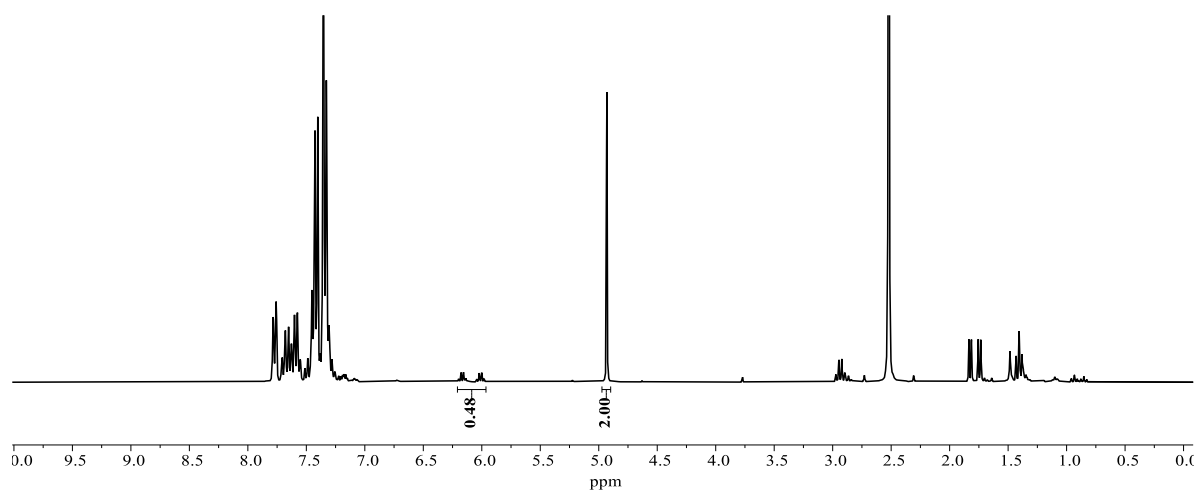
**64e**

### 1-Bromo-2-(1-fluoroethyl)benzene

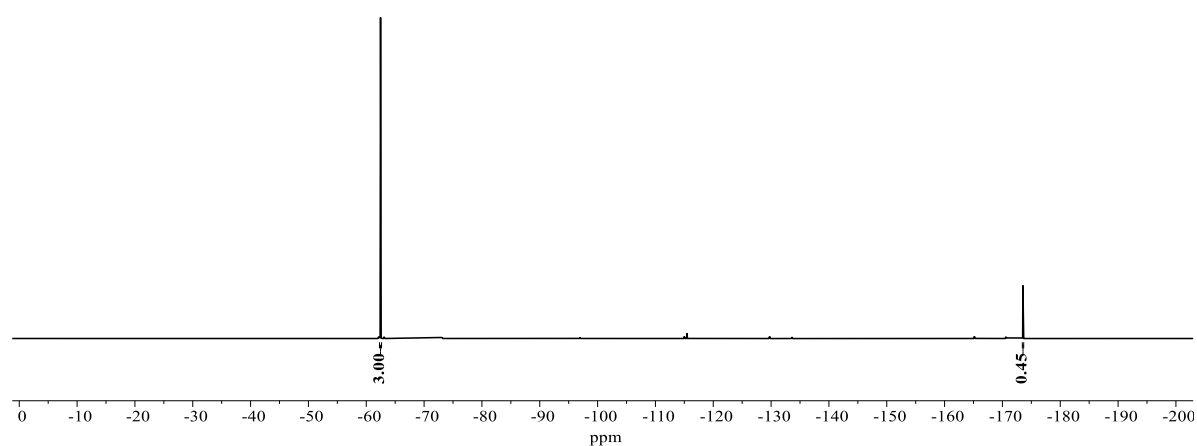
The general procedure G was followed using 1-bromo-2-ethylbenzene **63e** (92.5 mg, 0.50 mmol). The silica plug was flushed with EtOAc/*n*hexane/toluene (75 mL, 5:60:10).

**Benzylic Fluoride C–H Shift:**  $^1\text{H}$ -NMR (300 MHz,  $\text{CDCl}_3$ ):  $\delta = 6.08$  (dq,  $J = 46.4, 6.4$  Hz). Calibrated  $^1\text{H}$ -NMR yield from benzylic proton: 48%. **Benzylic Fluoride Shift:**  $^{19}\text{F}\{^1\text{H}\}$ -NMR (282 MHz,  $\text{CDCl}_3$ ):  $\delta = -173.5$ . Calibrated  $^{19}\text{F}\{^1\text{H}\}$ -NMR yield from benzylic fluoride: 45%. **HR-MS** (EI)  $m/z$  calcd for  $\text{C}_8\text{H}_8\text{F}^{79}\text{Br}$   $[\text{M}]^+$ : 201.9788, found: 201.9787.

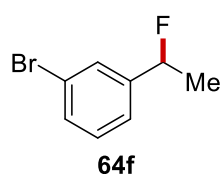
The spectral data are in accordance with those reported in literature.<sup>[120a]</sup>



**Figure 5.6.9** Crude <sup>1</sup>H-NMR Spectrum (300 MHz, CDCl<sub>3</sub>) of the reaction mixture with CH<sub>2</sub>Br<sub>2</sub> (36 μL, 0.50 mmol) as internal standard (4.93 ppm). The signals of the benzylic proton and internal standard are integrated.



**Figure 5.6.10** <sup>19</sup>F-NMR Spectrum (282 MHz, CDCl<sub>3</sub>) of the reaction mixture with PhCF<sub>3</sub> (62 μL, 0.50 mmol) as internal standard (-62.5 ppm). The signals of the benzylic fluoride and internal standard are integrated.



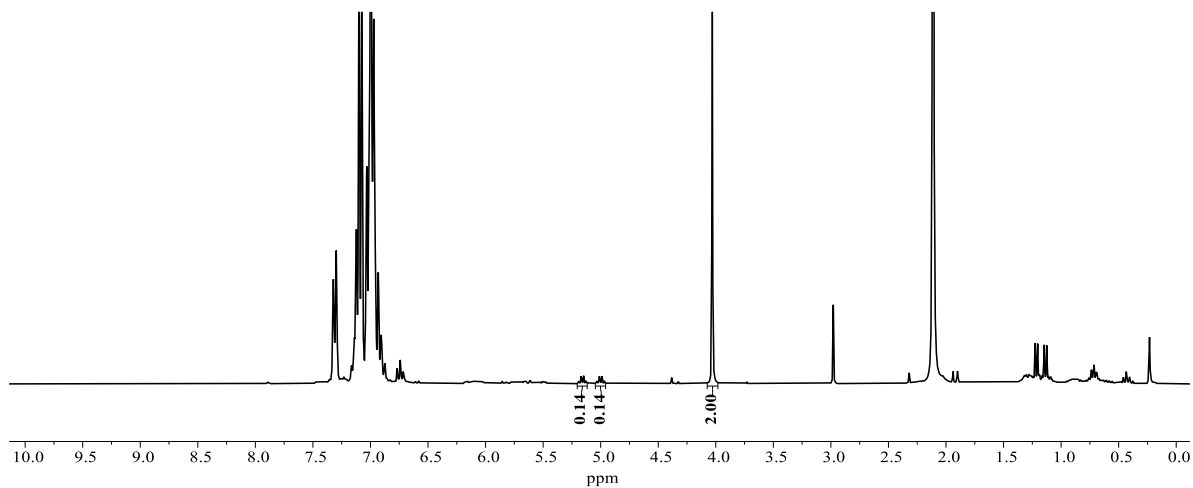
### 2-Bromo-2-(1-fluoroethyl)benzene

The general procedure G was followed using 2-bromo-2-ethylbenzene **63f** (92.5 mg, 0.50 mmol). The silica plug was flushed with EtOAc/*n*hexane/toluene (75 mL, 5:60:10).

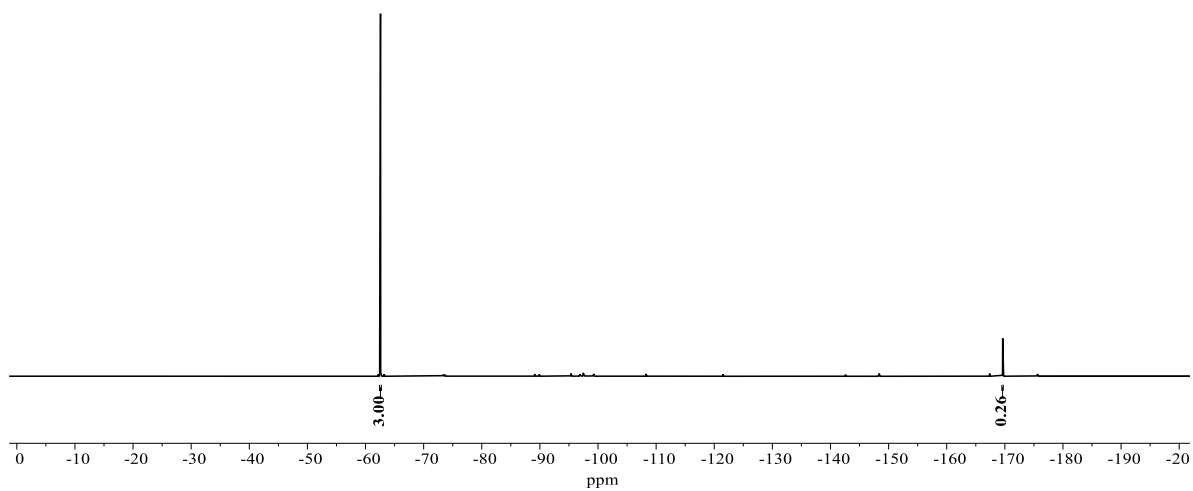
**Benzyl Fluoride C–H Shift:** <sup>1</sup>H-NMR (300 MHz, C<sub>6</sub>D<sub>6</sub>): δ = 5.09 (dq, *J* = 47.5, 6.6 Hz).  
**Calibrated <sup>1</sup>H-NMR yield from benzylic proton: 28%. Benzylic Fluoride Shift:** <sup>19</sup>F{<sup>1</sup>H}-

NMR (282 MHz,  $C_6D_6$ ):  $\delta = -169.6$ . Calibrated  $^{19}F\{^1H\}$ -NMR yield from benzylic fluoride: 26%. **HR-MS** (EI)  $m/z$  calcd for  $C_8H_8F^{79}Br [M]^+$ : 201.9788, found: 201.9786.

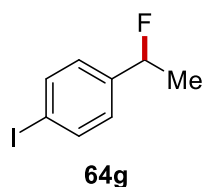
The spectral data are in accordance with those reported in literature.<sup>[118]</sup>



**Figure 5.6.11** Crude  $^1H$ -NMR Spectrum (300 MHz,  $C_6D_6$ ) of the reaction mixture with  $CH_2Br_2$  (36  $\mu L$ , 0.50 mmol) as internal standard (4.03 ppm). The signals of the benzylic proton and internal standard are integrated.



**Figure 5.6.12**  $^{19}F$ -NMR Spectrum (282 MHz,  $C_6D_6$ ) of the reaction mixture with  $PhCF_3$  (62  $\mu L$ , 0.50 mmol) as internal standard (-62.6 ppm). The signals of the benzylic fluoride and internal standard are integrated.

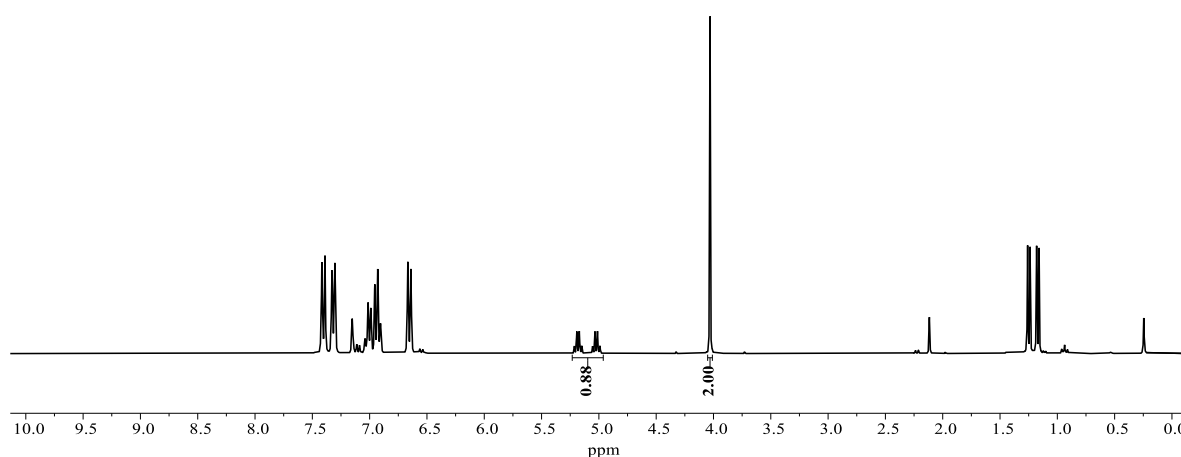


### 1-(1-Fluoroethyl)-4-iodobenzene

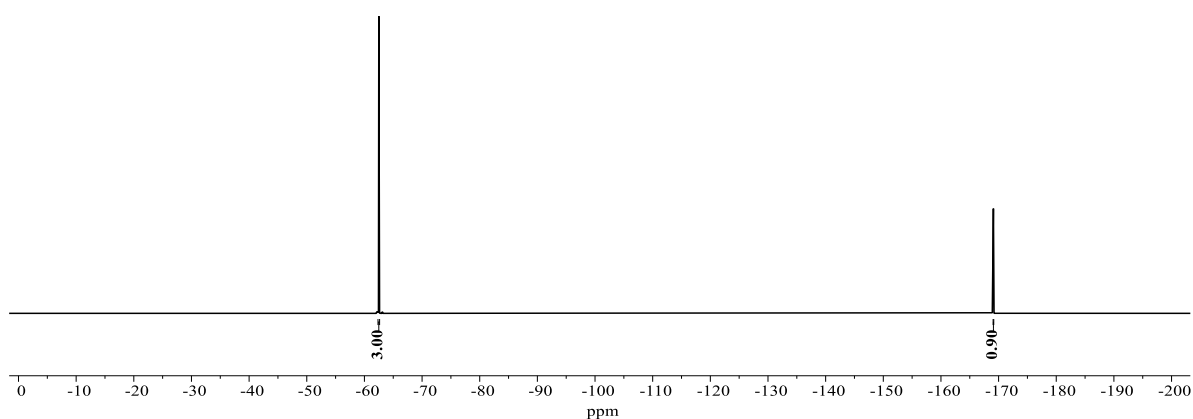
The general procedure G was followed using 1-ethyl-4-iodobenzene **63g** (116 mg, 0.50 mmol). After conducting the NMR analysis, the solvents were removed in vacuo, and the residue was purified by column chromatography (*n*hexane) to obtain **64g** (85.6 mg, 68%) as a colorless oil.

**<sup>1</sup>H-NMR** (400 MHz, C<sub>6</sub>D<sub>6</sub>):  $\delta$  = 7.44–7.37 (m, 2H), 6.66–6.60 (m, 2H), 5.08 (dq,  $J$  = 47.8, 6.5 Hz, 1H), 1.19 (dd,  $J$  = 23.4, 6.6 Hz, 3H). Calibrated <sup>1</sup>H-NMR yield from benzylic proton: 88%. **<sup>19</sup>F{<sup>1</sup>H}-NMR** (282 MHz, C<sub>6</sub>D<sub>6</sub>):  $\delta$  = -169.1. Calibrated <sup>19</sup>F{<sup>1</sup>H}-NMR yield from benzylic fluoride: 90%. **<sup>13</sup>C-NMR** (101 MHz, C<sub>6</sub>D<sub>6</sub>):  $\delta$  = 141.6 (d, <sup>2</sup> $J_{C-F}$  = 20.0 Hz, C<sub>q</sub>), 137.8 (CH), 127.2 (d, <sup>3</sup> $J_{C-F}$  = 6.9 Hz, CH), 93.9 (d, <sup>5</sup> $J_{C-F}$  = 2.5 Hz, C<sub>q</sub>), 90.1 (d, <sup>1</sup> $J_{C-F}$  = 169.7 Hz, CH), 22.8 (d, <sup>2</sup> $J_{C-F}$  = 25.1 Hz, CH<sub>3</sub>). **IR** (ATR):  $\tilde{\nu}$  = 1591, 1484, 1400, 1335, 1064, 1003, 879, 818, 768, 529. **HR-MS** (EI)  $m/z$  calcd for C<sub>8</sub>H<sub>8</sub>FI [M]<sup>+</sup>: 249.9649, found: 249.9651.

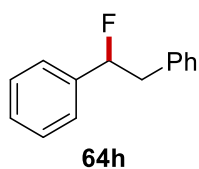
The spectral data are in accordance with those reported in literature.<sup>[122]</sup>



**Figure 5.6.13** Crude <sup>1</sup>H-NMR Spectrum (300 MHz, C<sub>6</sub>D<sub>6</sub>) of the reaction mixture with CH<sub>2</sub>Br<sub>2</sub> (36  $\mu$ L, 0.50 mmol) as internal standard (4.03 ppm). The signals of the benzylic proton and internal standard are integrated.



**Figure 5.6.14** Crude  $^{19}\text{F}$ -NMR Spectrum (282 MHz,  $\text{C}_6\text{D}_6$ ) of the reaction mixture with  $\text{PhCF}_3$  (62  $\mu\text{L}$ , 0.50 mmol) as internal standard ( $-62.5$  ppm). The signals of the benzylic fluoride and internal standard are integrated.

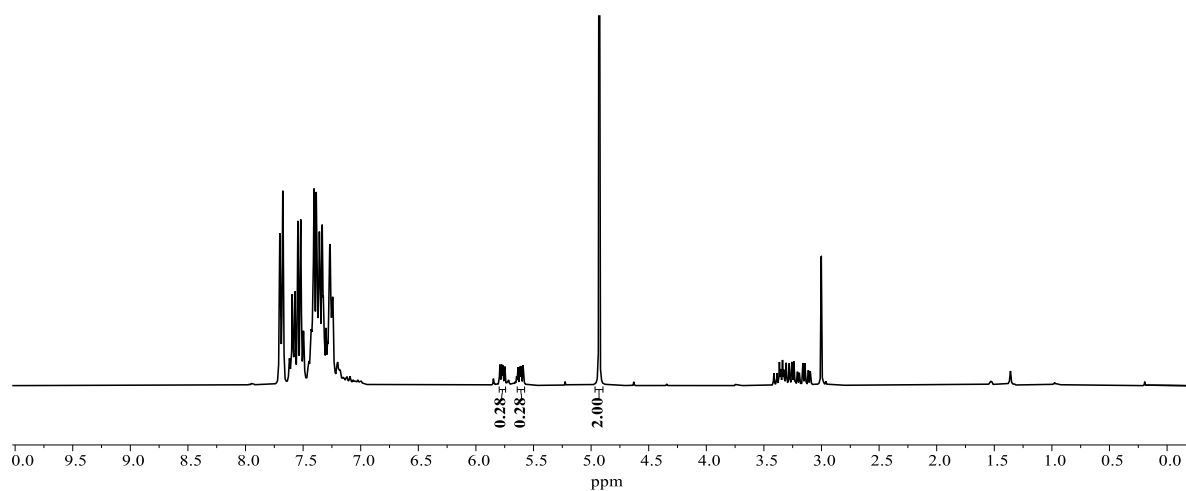


### (1-Fluoroethane-1,2-diyl)dibenzene

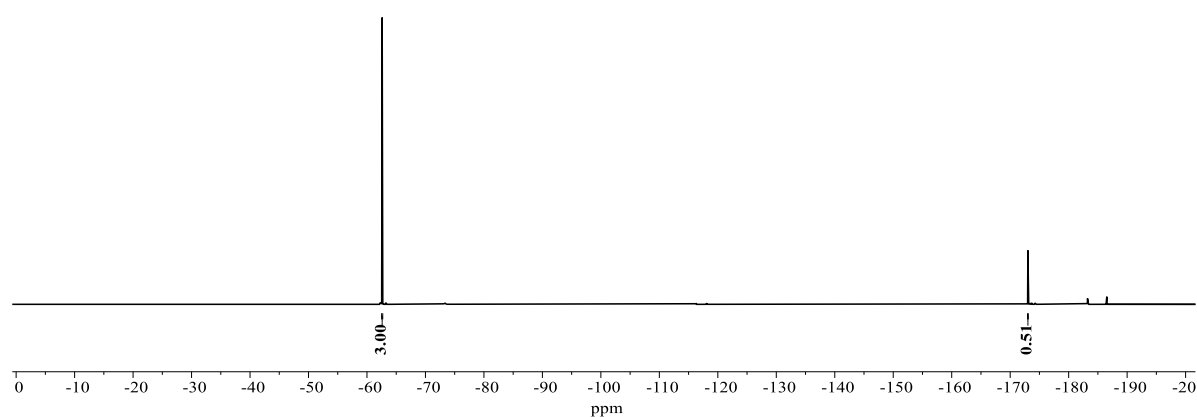
The general procedure G was followed using bibenzyl **63h** (91.1 mg, 0.50 mmol) with a total charge of 5.0 F/mol using constant current electrolysis at 16 mA at 0 °C.

**Benzylic Fluoride C–H Shift:**  $^1\text{H}$ -NMR (300 MHz,  $\text{CDCl}_3$ )  $\delta = 5.69$  (ddd,  $J = 47.4, 4.7, 4.7$  Hz). Calibrated  $^1\text{H}$ -NMR yield from benzylic proton: 56%. **Benzylic Fluoride Shift:**  $^{19}\text{F}\{^1\text{H}\}$ -NMR (282 MHz,  $\text{CDCl}_3$ )  $\delta = -173.0$ . Calibrated  $^{19}\text{F}\{^1\text{H}\}$ -NMR yield from benzylic fluoride: 51%. **HR-MS** (EI)  $m/z$  calcd for  $\text{C}_{14}\text{H}_{13}\text{F} [\text{M}]^+$ : 200.0996, found: 200.0995.

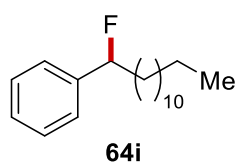
The spectral data are in accordance with those reported in literature.<sup>[259]</sup>



**Figure 5.6.15** Crude  $^1\text{H-NMR}$  Spectrum (300 MHz,  $\text{CDCl}_3$ ) of the reaction mixture with  $\text{CH}_2\text{Br}_2$  (36  $\mu\text{L}$ , 0.50 mmol) as internal standard (4.93 ppm). The signals of the benzylic proton and internal standard are integrated.



**Figure 5.6.16**  $^{19}\text{F-NMR}$  Spectrum (282 MHz,  $\text{CDCl}_3$ ) of the reaction mixture with  $\text{PhCF}_3$  (62  $\mu\text{L}$ , 0.50 mmol) as internal standard (-62.6 ppm). The signals of the benzylic fluoride and internal standard are integrated.



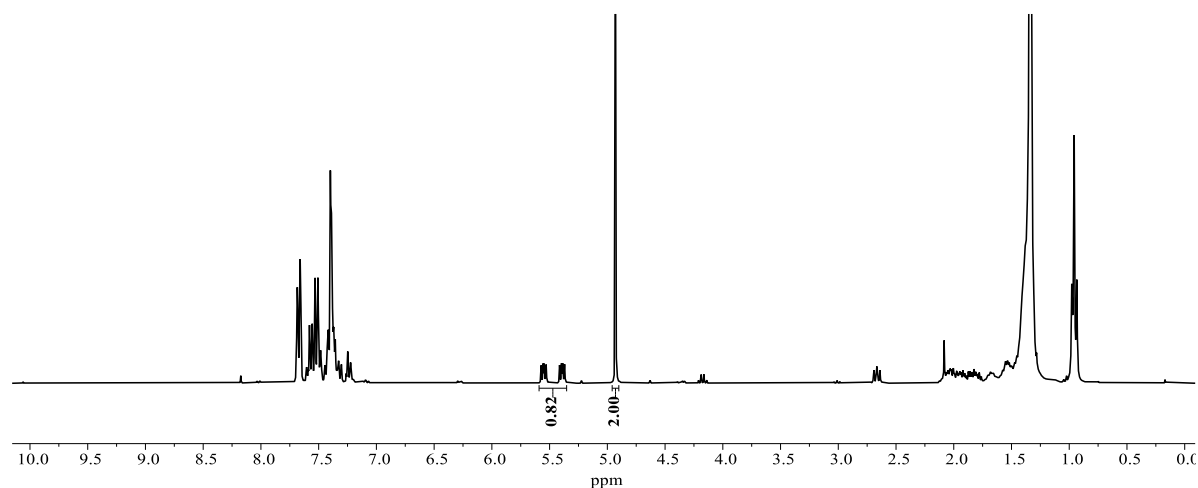
### 1-Fluorotridecylbenzene

The general procedure G was followed using tridecylbenzene **63i** (131 mg, 0.50 mmol). After conducting the NMR analysis, the solvents were removed in vacuo, and the residue was purified by column chromatography (*n*hexane) to obtain **64i** (90.4 mg, 65%) as a colorless oil.

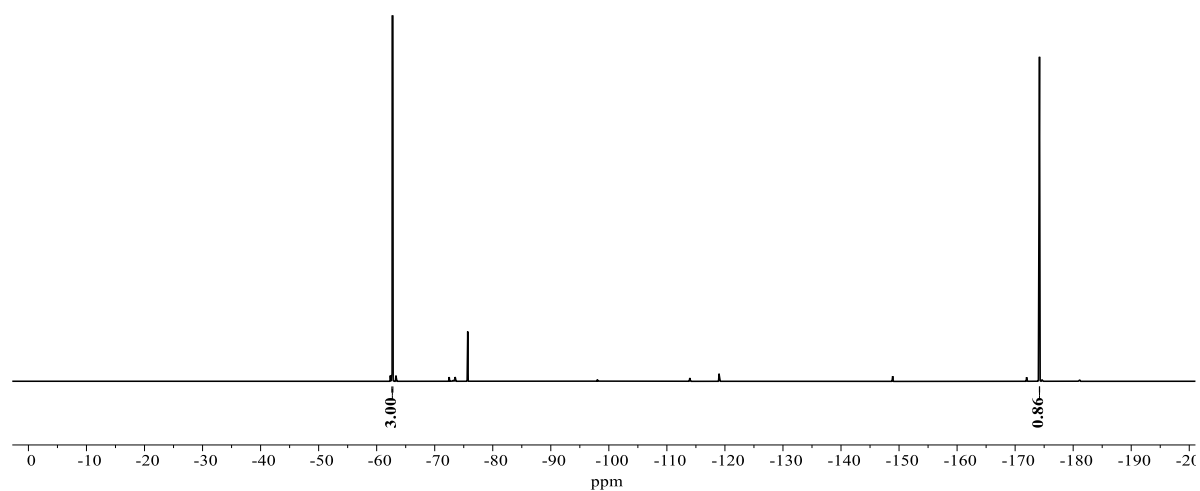


**$^1\text{H-NMR}$**  (400 MHz,  $\text{CDCl}_3$ ):  $\delta = 7.42\text{--}7.31$  (m, 5H), 5.47 (ddd,  $J = 48.1, 5.1, 4.9$  Hz, 1H), 1.99 (m, 1H), 1.91–1.74 (m, 1H), 1.55–1.41 (m, 2H), 1.29 (m, 18H), 0.91 (t,  $J = 6.7$  Hz, 3H). Calibrated  $^1\text{H-NMR}$  yield from benzylic proton: 82%.  **$^{13}\text{C-NMR}$**  (101 MHz,  $\text{CDCl}_3$ ):  $\delta = 140.8$  (d,  $^2J_{\text{C-F}} = 19.8$  Hz,  $\text{C}_q$ ), 128.5 (CH), 128.3 (d,  $^4J_{\text{C-F}} = 1.9$  Hz, CH), 125.7 (d,  $^3J_{\text{C-F}} = 6.8$  Hz, CH), 94.8 (d,  $^1J_{\text{C-F}} = 170.1$  Hz, CH), 37.4 (d,  $^2J_{\text{C-F}} = 23.5$  Hz,  $\text{CH}_2$ ), 32.1 ( $\text{CH}_2$ ), 29.8 ( $\text{CH}_2$ ), 29.8 ( $\text{CH}_2$ ), 29.7 ( $\text{CH}_2$ ), 29.6 ( $\text{CH}_2$ ), 29.5 ( $\text{CH}_2$ ), 29.5 ( $\text{CH}_2$ ), 25.3 (d,  $^3J_{\text{C-F}} = 4.3$  Hz,  $\text{CH}_2$ ), 22.8 ( $\text{CH}_2$ ), 14.3 ( $\text{CH}_3$ ).  **$^{19}\text{F}\{^1\text{H}\}\text{-NMR}$**  (282 MHz,  $\text{CDCl}_3$ ):  $\delta = -174.2$ . Calibrated  $^{19}\text{F}\{^1\text{H}\}\text{-NMR}$  yield from benzylic fluoride: 86%. **IR** (ATR):  $\tilde{\nu} = 2922, 2853, 1458, 1372, 1026, 975, 913, 753, 697, 551$ . **HR-MS** (EI)  $m/z$  calcd for  $\text{C}_{19}\text{H}_{31}\text{F} [\text{M}]^+$ : 278.2404, found: 278.2404.

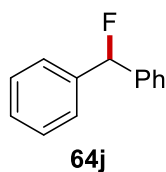
The spectral data are in accordance with those reported in literature.<sup>[260]</sup>



**Figure 5.6.17** Crude  $^1\text{H-NMR}$  Spectrum (300 MHz,  $\text{CDCl}_3$ ) of the reaction mixture with  $\text{CH}_2\text{Br}_2$  (36  $\mu\text{L}$ , 0.50 mmol) as internal standard (4.93 ppm). The signals of the benzylic proton and internal standard are integrated.



**Figure 5.6.18**  $^{19}\text{F}$ -NMR Spectrum (282 MHz,  $\text{CDCl}_3$ ) of the reaction mixture with  $\text{PhCF}_3$  (62  $\mu\text{L}$ , 0.50 mmol) as internal standard (-62.7 ppm). The signals of the benzylic fluoride and internal standard are integrated.



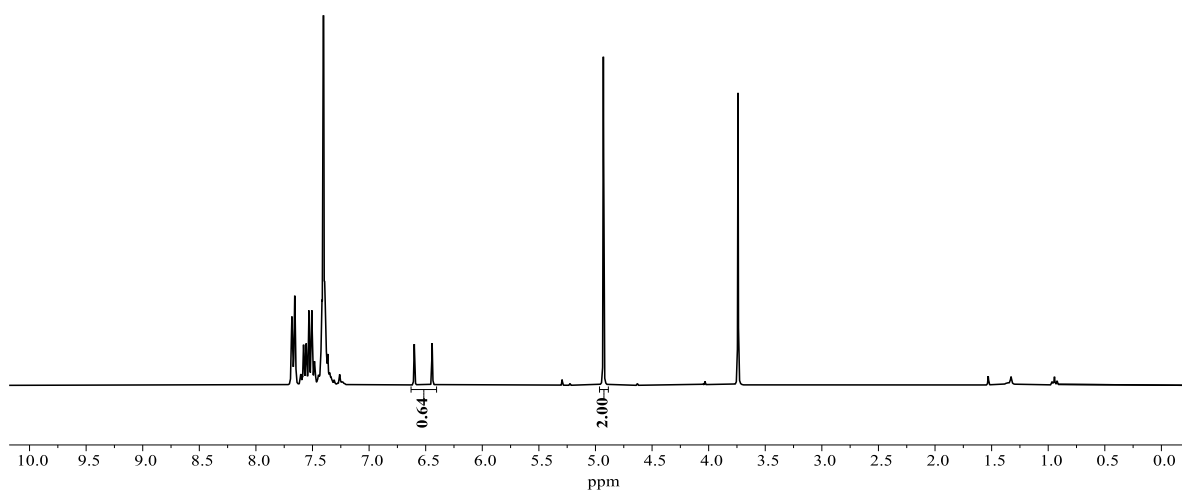
### (Fluoromethylene)dibenzene

The general procedure G was followed using diphenylmethane **63j** (84.1 mg, 0.50 mmol).

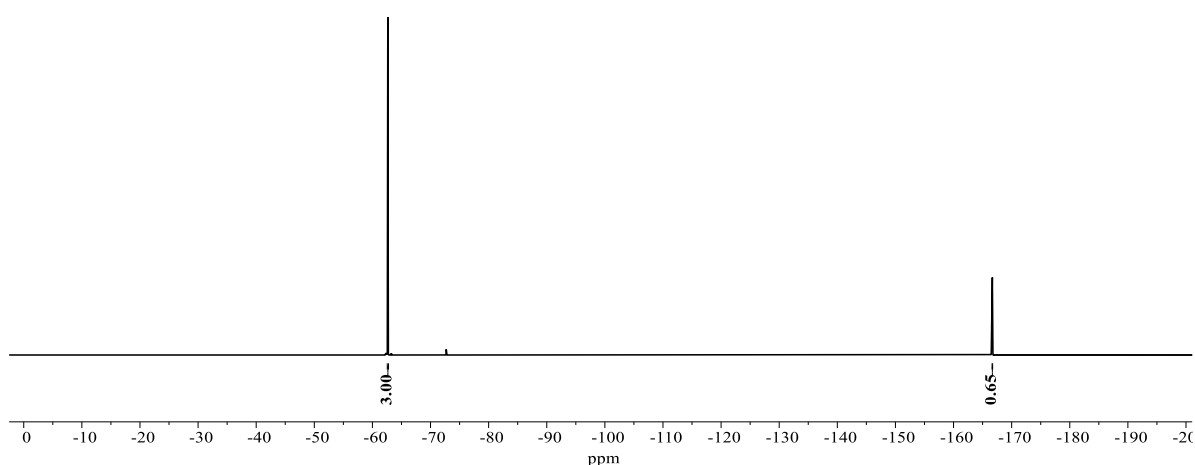
**Benzyl Fluoride C–H Shift:**  $^1\text{H}$ -NMR (300 MHz,  $\text{CDCl}_3$ ):  $\delta = 6.52$  (d,  $J = 47.7$  Hz).

Calibrated  $^1\text{H}$ -NMR yield from benzylic proton: 64%. **Benzylic Fluoride Shift:**  $^{19}\text{F}\{^1\text{H}\}$ -NMR (282 MHz,  $\text{CDCl}_3$ ):  $\delta = -166.7$ . Calibrated  $^{19}\text{F}\{^1\text{H}\}$ -NMR yield from benzylic fluoride: 65%. **HR-MS** (EI)  $m/z$  calcd for  $\text{C}_{13}\text{H}_{11}\text{F} [\text{M}]^+$ : 186.0839, found: 186.0840.

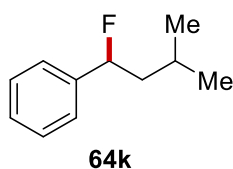
The spectral data are in accordance with those reported in literature.<sup>[125]</sup>



**Figure 5.6.19** Crude  $^1\text{H-NMR}$  Spectrum (300 MHz,  $\text{CDCl}_3$ ) of the reaction mixture with  $\text{CH}_2\text{Br}_2$  (36  $\mu\text{L}$ , 0.50 mmol) as internal standard (4.93 ppm). The signals of the benzylic proton and internal standard are integrated.



**Figure 5.6.20**  $^{19}\text{F-NMR}$  Spectrum (282 MHz,  $\text{CDCl}_3$ ) of the reaction mixture with  $\text{PhCF}_3$  (62  $\mu\text{L}$ , 0.50 mmol) as internal standard (-62.6 ppm). The signals of the benzylic fluoride and internal standard are integrated.



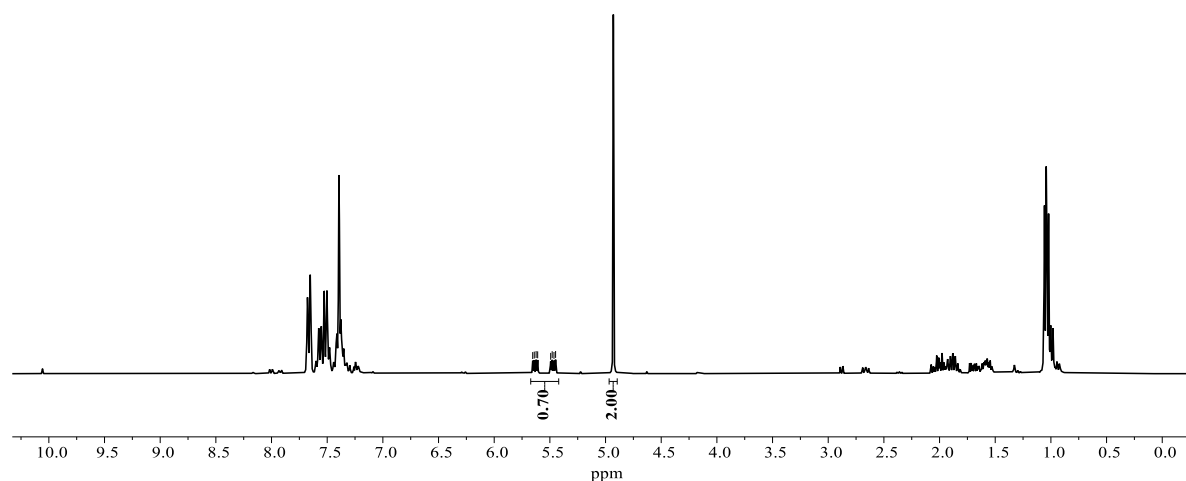
### (1-Fluoro-3-methylbutyl)benzene

The general procedure G was followed using isopentylbenzene **63k** (74.1 mg, 0.50 mmol).

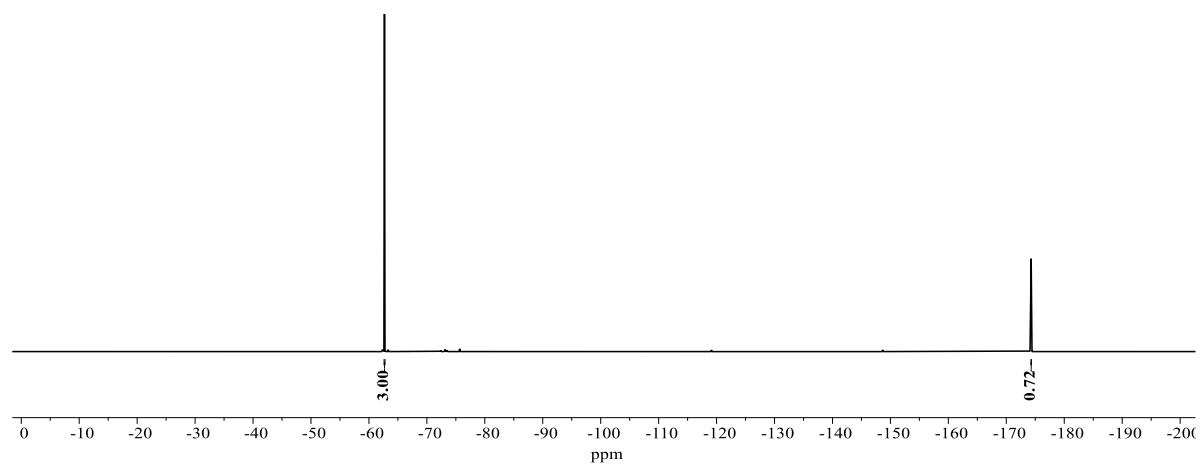
**Benzylic Fluoride C–H Shift:**  $^1\text{H-NMR}$  (300 MHz,  $\text{CDCl}_3$ )  $\delta = 5.55$  (ddd,  $J = 48.6, 4.3, 4.2$  Hz). Calibrated  $^1\text{H-NMR}$  yield from benzylic proton: 70%. **Benzylic Fluoride Shift:**

$^{19}\text{F}\{^1\text{H}\}$ -NMR (282 MHz,  $\text{CDCl}_3$ )  $\delta = -174.3$ . Calibrated  $^{19}\text{F}\{^1\text{H}\}$ -NMR yield from benzylic fluoride: 72%. **HR-MS** (EI)  $m/z$  calcd for  $\text{C}_{11}\text{H}_{15}\text{F}[\text{M}]^+$ : 166.1152, found: 166.1152.

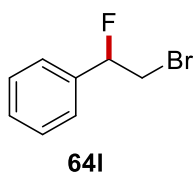
The spectral data are in accordance with those reported in literature.<sup>[120a]</sup>



**Figure 5.6.21** Crude  $^1\text{H}$ -NMR Spectrum (300 MHz,  $\text{CDCl}_3$ ) of the reaction mixture with  $\text{CH}_2\text{Br}_2$  (36  $\mu\text{L}$ , 0.50 mmol) as internal standard (4.93 ppm). The signals of the benzylic proton and internal standard are integrated.



**Figure 5.6.22**  $^{19}\text{F}$ -NMR Spectrum (282 MHz,  $\text{CDCl}_3$ ) of the reaction mixture with  $\text{PhCF}_3$  (62  $\mu\text{L}$ , 0.50 mmol) as internal standard (-62.7 ppm). The signals of the benzylic fluoride and internal standard are integrated.

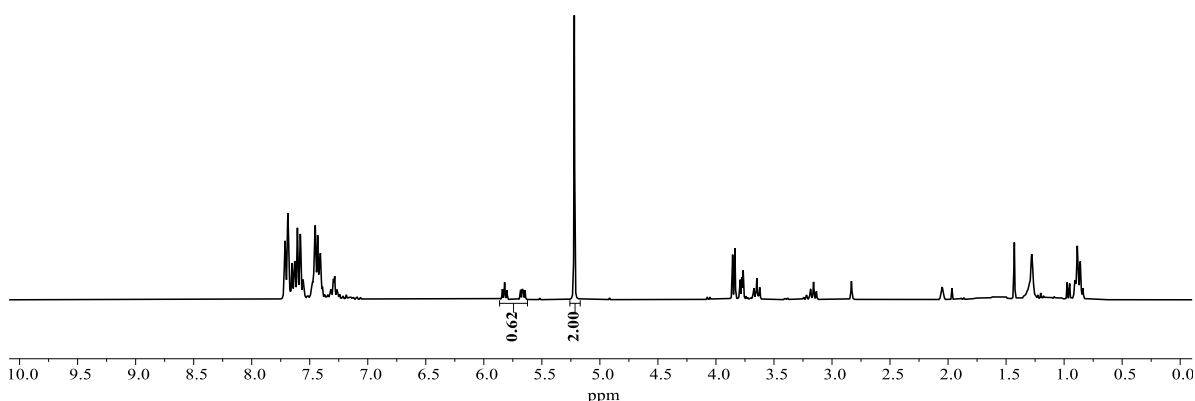


### (2-Bromo-1-fluoroethyl)benzene

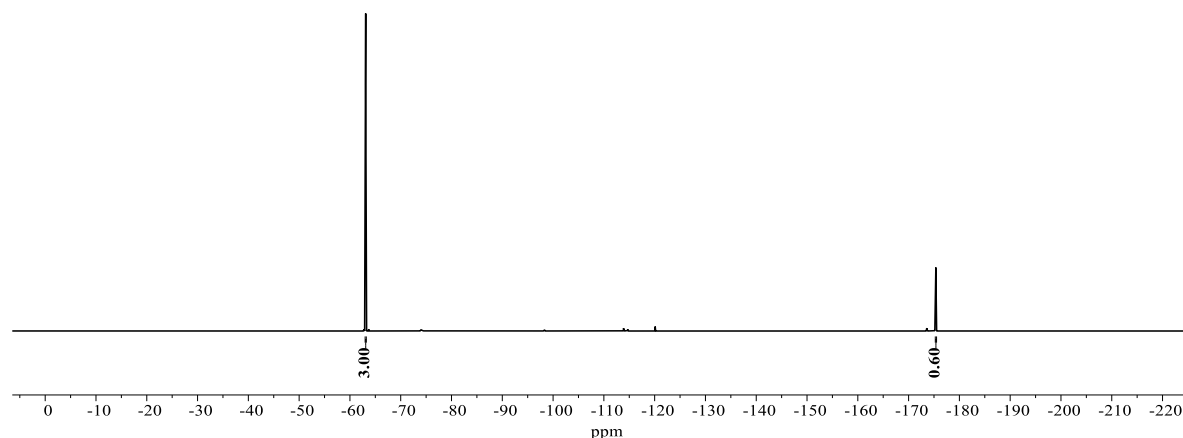
The general procedure G was followed using (2-bromoethyl)benzene **63I** (92.5 mg, 0.50 mmol) with 3.0 F/mol total charge and a RVC anode. After conducting the NMR analysis, the solvents were removed in vacuo, and the residue was purified by column chromatography (pentane to pentane/Et<sub>2</sub>O = 9:1) to obtain **64I** (53.4 mg, 53%) as a colorless oil.

**<sup>1</sup>H-NMR** (400 MHz, CDCl<sub>3</sub>):  $\delta$  = 7.46–7.31 (m, 5H), 5.63 (ddd,  $J$  = 47.0, 4.4, 4.1 Hz, 1H), 3.73–3.56 (m, 2H). Calibrated **<sup>1</sup>H-NMR** (300 MHz, *d*<sub>6</sub>-Acetone) yield from benzylic proton: 62%. **<sup>13</sup>C-NMR** (101 MHz, CDCl<sub>3</sub>):  $\delta$  = 137.3 (d,  $^2J_{C-F}$  = 20.3 Hz, C<sub>q</sub>), 129.4 (d,  $^4J_{C-F}$  = 1.7 Hz, CH), 128.9 (CH), 125.9 (d,  $^3J_{C-F}$  = 6.8 Hz, CH), 92.9 (d,  $^1J_{C-F}$  = 178.0 Hz, CH), 34.4 (d,  $^2J_{C-F}$  = 28.4 Hz, CH<sub>2</sub>). **<sup>19</sup>F{<sup>1</sup>H}-NMR** (282 MHz, CDCl<sub>3</sub>):  $\delta$  = -174.0. Calibrated **<sup>19</sup>F{<sup>1</sup>H}-NMR** (282 MHz, *d*<sub>6</sub>-Acetone) yield from benzylic fluoride: 60%. **IR** (ATR):  $\tilde{\nu}$  = 1502, 1453, 1419, 1214, 1059, 986, 758, 698, 594, 508. **HR-MS** (EI)  $m/z$  calcd for C<sub>8</sub>H<sub>8</sub><sup>79</sup>BrF [M]<sup>+</sup>: 201.9788, found: 201.9786.

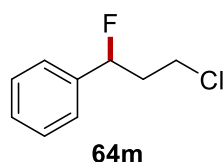
The spectral data are in accordance with those reported in literature.<sup>[261]</sup>



**Figure 5.6.23** Crude <sup>1</sup>H-NMR Spectrum (300 MHz, *d*<sub>6</sub>-Acetone) of the reaction mixture with CH<sub>2</sub>Br<sub>2</sub> (36  $\mu$ L, 0.50 mmol) as internal standard (5.25 ppm). The signals of the benzylic proton and internal standard are integrated.



**Figure 5.6.24** Crude  $^{19}\text{F}$ -NMR Spectrum (282 MHz,  $d_6$ -Acetone) of the reaction mixture with  $\text{PhCF}_3$  (62  $\mu\text{L}$ , 0.50 mmol) as internal standard ( $-63.1$  ppm). The signals of the benzylic fluoride and internal standard are integrated.

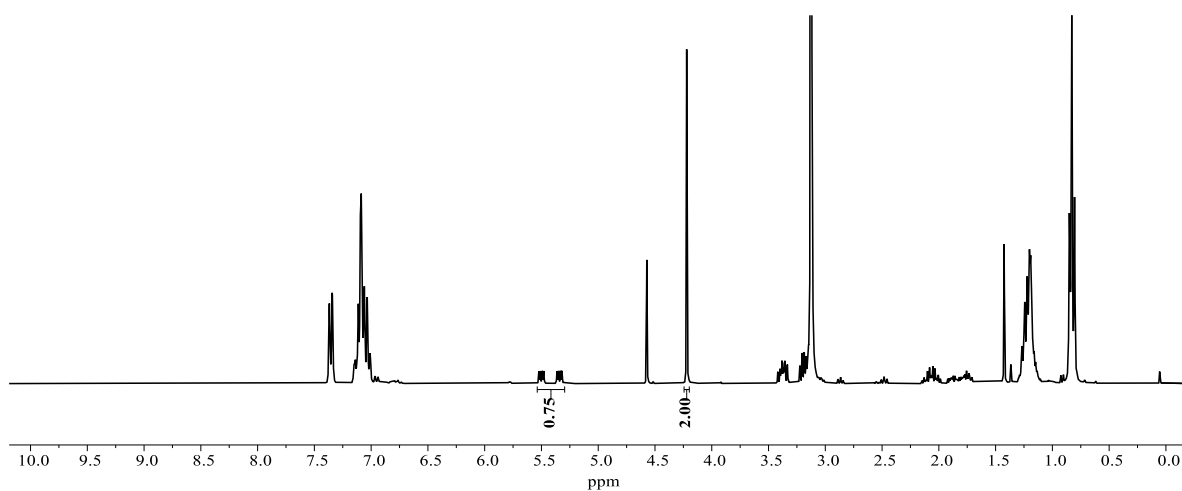


### (3-Chloro-1-fluoropropyl)benzene

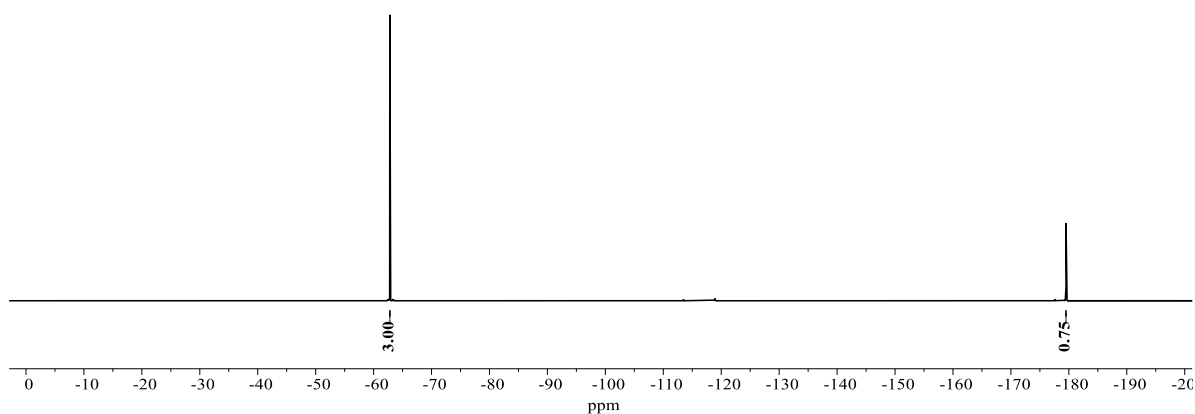
The general procedure G was followed using (3-chloro-1-propyl)benzene **63m** (77.3 mg, 0.50 mmol) with 3.0 F/mol total charge.

**Benzylic Fluoride C–H Shift:**  $^1\text{H}$ -NMR (300 MHz,  $\text{C}_6\text{D}_6$ )  $\delta = 5.42$  (ddd,  $J = 48.3, 9.1, 4.0$  Hz, 1H). Calibrated  $^1\text{H}$ -NMR yield from benzylic proton: 75%. **Benzylic Fluoride Shift:**  $^{19}\text{F}\{^1\text{H}\}$ -NMR (282 MHz,  $\text{C}_6\text{D}_6$ )  $\delta = -179.5$ . Calibrated  $^{19}\text{F}\{^1\text{H}\}$ -NMR yield from benzylic fluoride: 75%. **HR-MS** (EI)  $m/z$  calcd for  $\text{C}_9\text{H}_{10}\text{ClF} [\text{M}]^+$ : 172.0450, found: 172.0448.

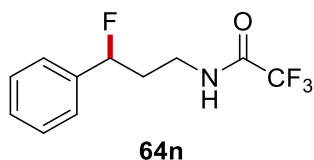
The spectral data are in accordance with those reported in literature.<sup>[119b]</sup>



**Figure 5.6.25** Crude  $^1\text{H}$ -NMR Spectrum (300 MHz,  $\text{C}_6\text{D}_6$ ) of the reaction mixture with  $\text{CH}_2\text{Br}_2$  (36  $\mu\text{L}$ , 0.50 mmol) as internal standard (4.22 ppm). The signals of the benzylic proton and internal standard are integrated.



**Figure 5.6.26**  $^{19}\text{F}$ -NMR Spectrum (282 MHz,  $\text{CDCl}_3$ ) of the reaction mixture with  $\text{PhCF}_3$  (62  $\mu\text{L}$ , 0.50 mmol) as internal standard (-62.8 ppm). The signals of the benzylic fluoride and internal standard are integrated.

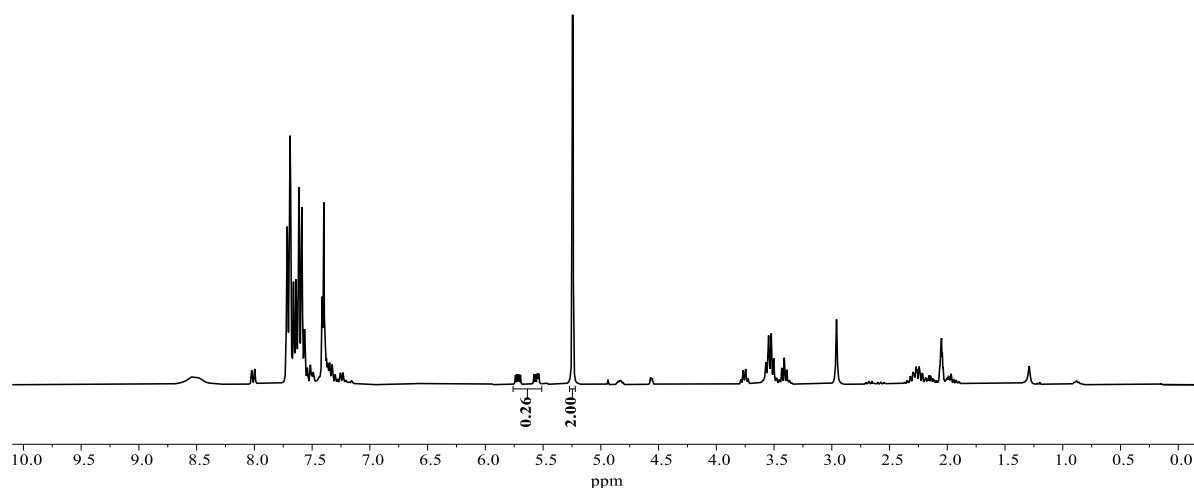


### 2,2,2-Trifluoro-N-(3-fluoro-3-phenylpropyl)acetamide

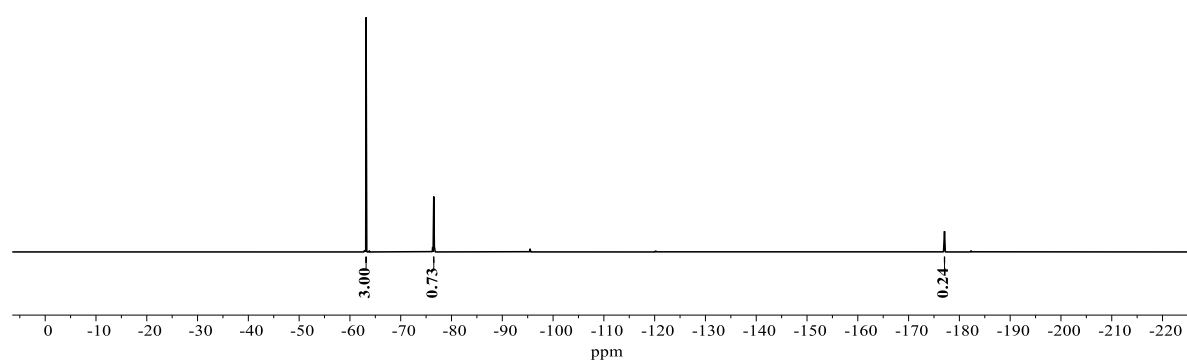
The general procedure G was followed using 2,2,2-trifluoro-N-(3-phenylpropyl)acetamide **63n** (116 mg, 0.50 mmol) with a total charge of 3.0 F/mol at  $-15\text{ }^\circ\text{C}$ .

**Benzyl Fluoride C–H Shift:**  $^1\text{H-NMR}$  (300 MHz,  $d_6$ -Acetone)  $\delta = 5.64$  (ddd,  $J = 47.9, 4.5, 4.5$  Hz). Calibrated  $^1\text{H-NMR}$  yield from benzylic proton: 26%. **Benzylic Fluoride Shift:**  $^{19}\text{F}\{^1\text{H}\}$ -NMR (282 MHz,  $d_6$ -Acetone)  $\delta = -177.1$ . Calibrated  $^{19}\text{F}\{^1\text{H}\}$ -NMR yield from benzylic fluoride: 24%. **HR-MS** (EI)  $m/z$  calcd for  $\text{C}_{11}\text{H}_{11}\text{F}_4\text{NO}$   $[\text{M}]^+$ : 249.0771, found: 249.0771.

The spectral data are in accordance with those reported in literature.<sup>[120a]</sup>

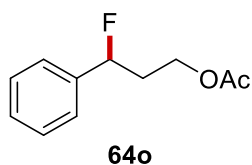


**Figure 5.6.27** Crude  $^1\text{H-NMR}$  Spectrum (300 MHz,  $d_6$ -Acetone) of the reaction mixture with  $\text{CH}_2\text{Br}_2$  (36  $\mu\text{L}$ , 0.50 mmol) as internal standard (5.25 ppm). The signals of the benzylic proton and internal standard are integrated.



**Figure 5.6.28**  $^{19}\text{F-NMR}$  Spectrum (282 MHz,  $d_6$ -Acetone) of the reaction mixture with  $\text{PhCF}_3$  (62  $\mu\text{L}$ , 0.50 mmol) as internal standard ( $-63.2$  ppm). The signals of the benzylic fluoride and internal standard are integrated.



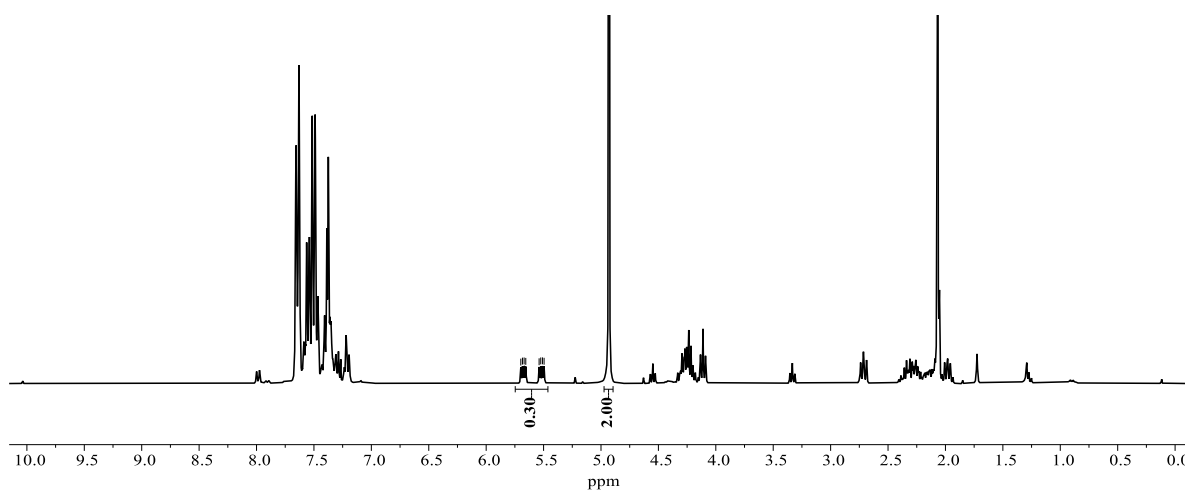


### 3-Fluoro-3-phenylpropyl acetate

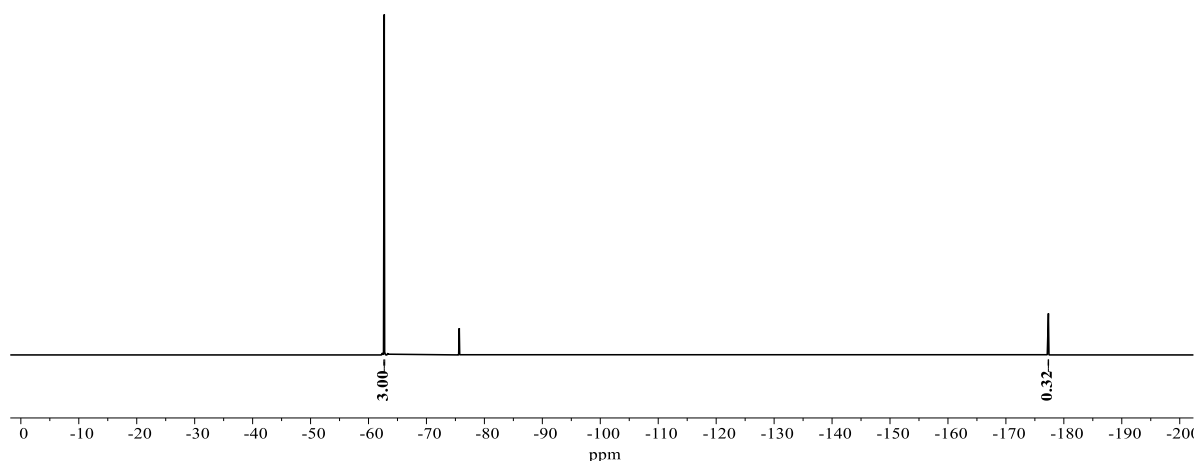
The general procedure G was followed using 3-phenylpropyl acetate **63o** (89.1 mg, 0.50 mmol) with a total charge of 3.0 F/mol using constant current electrolysis at 16 mA at  $-15\text{ }^{\circ}\text{C}$ . After conducting the NMR analysis, the solvents were removed in vacuo, and the residue was purified by column chromatography (*n*hexane/EtOAc = 9:1) to obtain the product **64o** as a colorless oil (24.3 mg, 25%).

**$^1\text{H-NMR}$**  (400 MHz,  $\text{CDCl}_3$ ):  $\delta = 7.42\text{--}7.32$  (m, 5H), 5.66–5.49 (ddd,  $J = 47.8, 4.3, 4.3$  Hz, 1H), 4.30–4.17 (m, 2H), 2.37–2.25 (m, 1H), 2.24–2.08 (m, 1H), 2.05 (s, 3H). Calibrated  $^1\text{H-NMR}$  yield from benzylic proton: 30%.  **$^{13}\text{C-NMR}$**  (101 MHz,  $\text{CDCl}_3$ )  $\delta = 171.0$  ( $\text{C}_q$ ), 139.6 (d,  $^2J_{\text{C-F}} = 19.6$  Hz,  $\text{C}_q$ ), 128.7 (CH), 128.7 (d,  $^4J_{\text{C-F}} = 2.0$  Hz, CH), 125.6 (d,  $^3J_{\text{C-F}} = 6.8$  Hz, CH), 91.5 (d,  $^1J_{\text{C-F}} = 171.0$  Hz, CH), 60.6 (d,  $^3J_{\text{C-F}} = 4.9$  Hz,  $\text{CH}_2$ ), 36.3 (d,  $^2J_{\text{C-F}} = 24.1$  Hz,  $\text{CH}_2$ ), 21.0 ( $\text{CH}_3$ ).  **$^{19}\text{F}\{^1\text{H}\}\text{-NMR}$**  (282 MHz,  $\text{CDCl}_3$ )  $\delta = -177.4$ . Calibrated  $^{19}\text{F}\{^1\text{H}\}\text{-NMR}$  yield from benzylic fluoride: 32%. **IR** (ATR):  $\tilde{\nu} = 1737, 1454, 1368, 1231, 1042, 966, 915, 758, 699, 607$ . **HR-MS** (ESI)  $m/z$  calcd for  $\text{C}_{11}\text{H}_{13}\text{FO}_2$  [ $\text{M}+\text{Na}$ ] $^+$ : 219.0792, found: 219.0788.

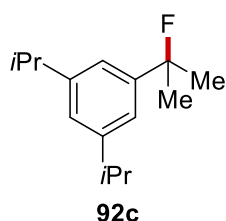
The spectral data are in accordance with those reported in literature.<sup>[120a]</sup>



**Figure 5.6.29** Crude  $^1\text{H-NMR}$  Spectrum (300 MHz,  $\text{CDCl}_3$ ) of the reaction mixture with  $\text{CH}_2\text{Br}_2$  (36  $\mu\text{L}$ , 0.50 mmol) as internal standard (4.93 ppm). The signals of the benzylic proton and internal standard are integrated.



**Figure 5.6.30**  $^{19}\text{F}$ -NMR Spectrum (282 MHz,  $\text{CDCl}_3$ ) of the reaction mixture with  $\text{PhCF}_3$  (62  $\mu\text{L}$ , 0.50 mmol) as internal standard ( $-62.7$  ppm). The signals of the benzylic fluoride and internal standard are integrated.

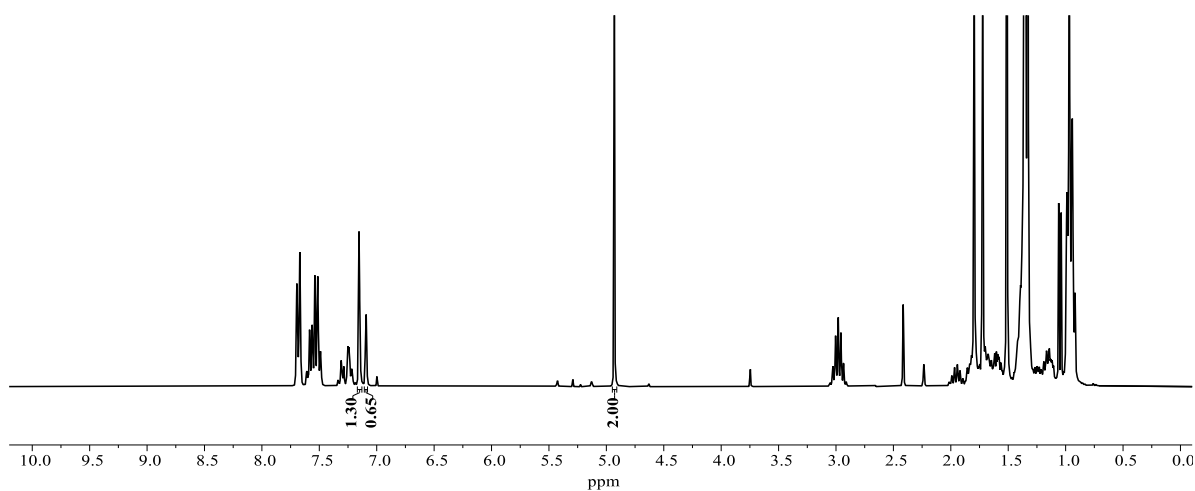


### 1-(2-fluoropropan-2-yl)-3,5-diisopropylbenzene

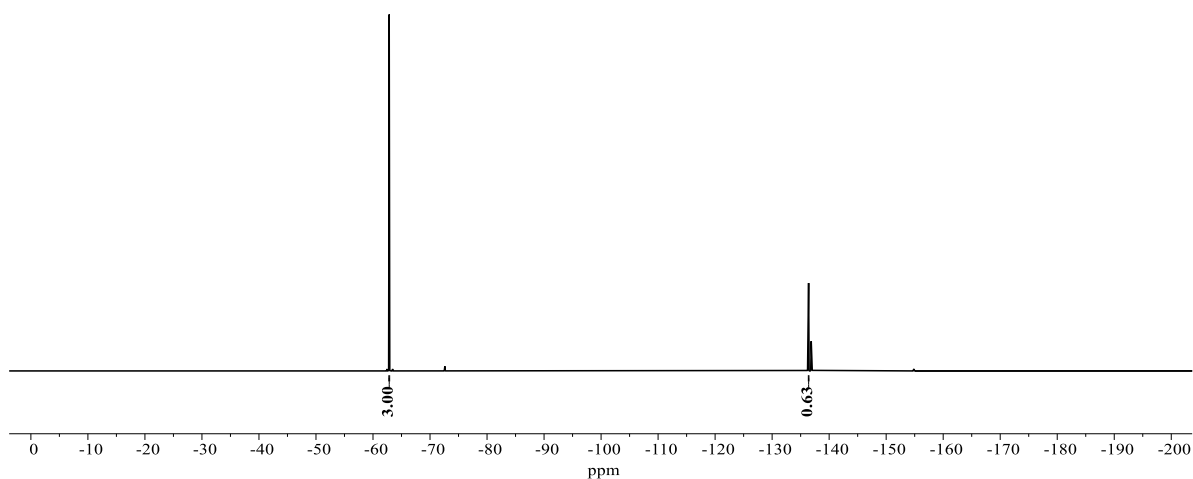
The general procedure G was followed using 1,3,5-triisopropylbenzene **91c** (102 mg, 0.50 mmol) at  $0^\circ\text{C}$ . After filtration over a silica plug (*n*hexane/DCM = 95:5), the organic layer was washed with water ( $3 \times 50$  mL) and dried over  $\text{Na}_2\text{SO}_4$ . The solvents were removed in vacuo and the resulting residue was analyzed by NMR.

**Aromatic C–H Shift:**  $^1\text{H}$ -NMR (300 MHz,  $\text{CDCl}_3$ ):  $\delta = 7.11\text{--}7.07$  (m). Calibrated  $^1\text{H}$ -NMR yield from aromatic proton: 65%. **Benzylic Fluoride Shift:**  $^{19}\text{F}\{^1\text{H}\}$ -NMR (282 MHz,  $\text{CDCl}_3$ )  $\delta = -136.4$ . Calibrated  $^{19}\text{F}\{^1\text{H}\}$ -NMR yield from benzylic fluoride: 63%. **HR-MS** (EI)  $m/z$  calcd for  $\text{C}_{15}\text{H}_{23}\text{F} [\text{M}]^+$ : 222.1778, found: 222.1775.

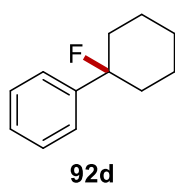
The spectral data are in accordance with those reported in literature.<sup>[125]</sup>



**Figure 5.6.31** Crude  $^1\text{H}$ -NMR Spectrum (300 MHz,  $\text{CDCl}_3$ ) of the reaction mixture with  $\text{CH}_2\text{Br}_2$  (36  $\mu\text{L}$ , 0.50 mmol) as internal standard (4.94 ppm). The signals of the aromatic protons and internal standard are integrated.



**Figure 5.6.32**  $^{19}\text{F}$ -NMR Spectrum (282 MHz,  $\text{CDCl}_3$ ) of the reaction mixture with  $\text{PhCF}_3$  (62  $\mu\text{L}$ , 0.50 mmol) as internal standard (-62.7 ppm). The signals of the benzylic fluoride and internal standard are integrated.

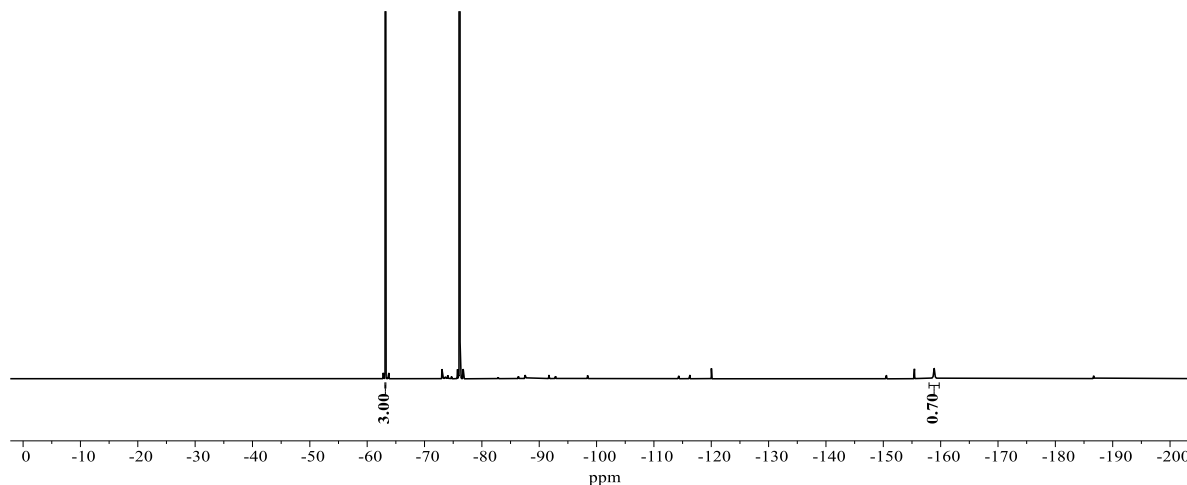


### (1-Fluorocyclohexyl)benzene

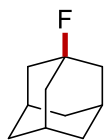
The general procedure G was followed using cyclohexylbenzene **91d** (80.1 mg, 0.50 mmol) at 0  $^\circ\text{C}$ .

**Benzylic Fluoride Shift:**  $^{19}\text{F}\{^1\text{H}\}$ -NMR (282 MHz,  $\text{CDCl}_3$ )  $\delta = -158.9$  (broad). Calibrated  $^{19}\text{F}\{^1\text{H}\}$ -NMR yield from benzylic fluoride: 70%. **HR-MS** (EI)  $m/z$  calcd for  $\text{C}_{12}\text{H}_{15}\text{F} [\text{M}]^+$ : 178.1152, found: 178.1153.

The spectral data are in accordance with a derivative reported in literature.<sup>[125]</sup>



**Figure 5.6.33**  $^{19}\text{F}$ -NMR Spectrum (282 MHz,  $\text{CDCl}_3$ ) of the reaction mixture with  $\text{PhCF}_3$  (62  $\mu\text{L}$ , 0.50 mmol) as internal standard (-63.2 ppm). The signals of the benzylic fluoride and internal standard are integrated.



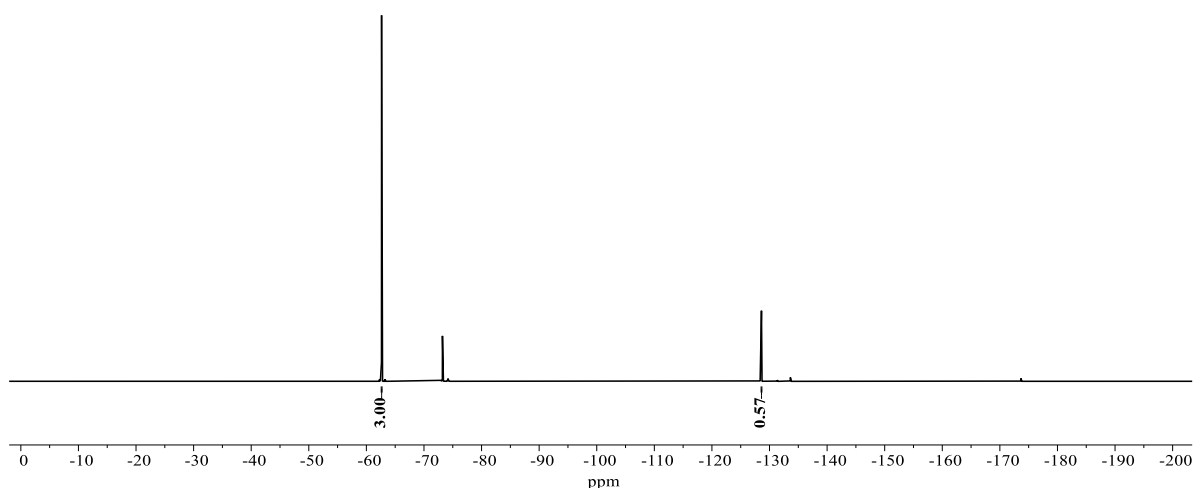
**195**

### 1-Fluoroadamantane

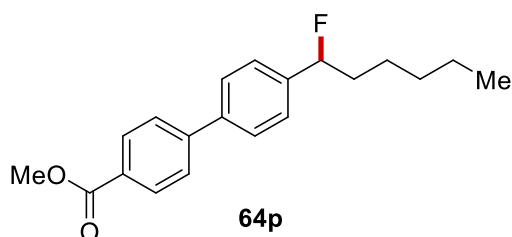
The general procedure G was followed using adamantane **194** (68.1 mg, 0.50 mmol) at 0 °C.

**Aliphatic Fluoride Shift:**  $^{19}\text{F}\{^1\text{H}\}$ -NMR (282 MHz,  $\text{C}_6\text{D}_6$ )  $\delta = -128.6$ . Calibrated  $^{19}\text{F}\{^1\text{H}\}$ -NMR yield from benzylic fluoride: 57%. **HR-MS** (EI)  $m/z$  calcd for  $\text{C}_{10}\text{H}_{15}\text{F} [\text{M}]^+$ : 154.1152, found: 154.1152.

The spectral data are in accordance with those reported in literature.<sup>[262]</sup>



**Figure 5.6.34**  $^{19}\text{F}$ -NMR Spectrum (282 MHz,  $\text{C}_6\text{D}_6$ ) of the reaction mixture with  $\text{PhCF}_3$  (62  $\mu\text{L}$ , 0.50 mmol) as internal standard (-62.6 ppm). The signals of the benzylic fluoride and internal standard are integrated.

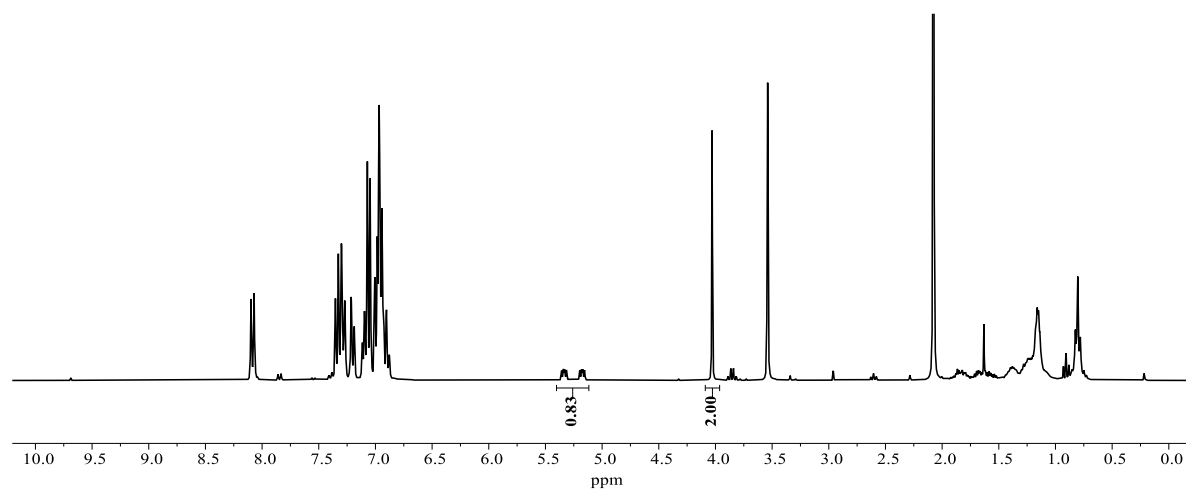


### Methyl-4'-(1-fluorohexyl)-[1,1'-biphenyl]-4-carboxylate

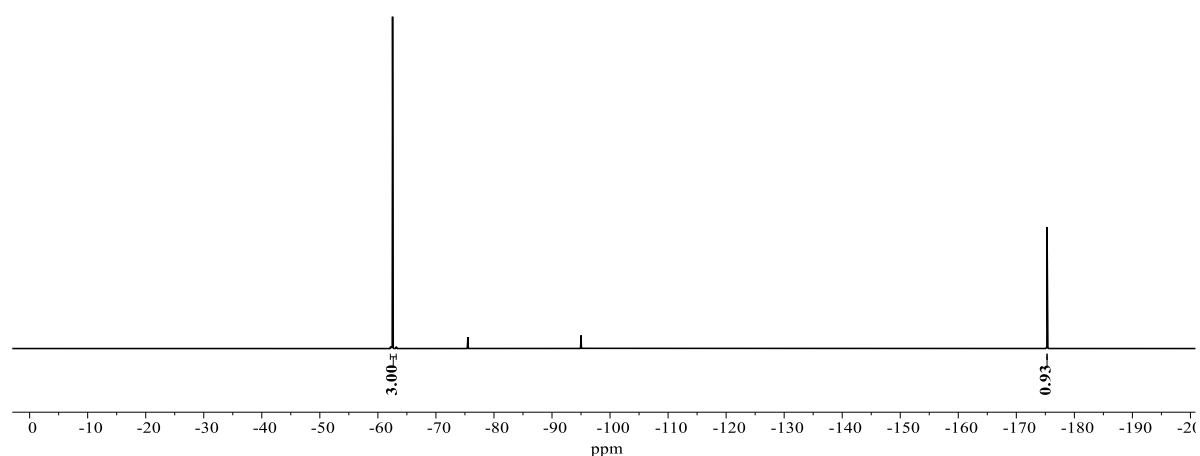
The general procedure G was followed using methyl-4'-hexyl-[1,1'-biphenyl]-4-carboxylate **63p** (148 mg, 0.50 mmol). The spectral data are in accordance with those reported in literature. After conducting the NMR analysis, the solvents were removed in vacuo, and the residue was purified by column chromatography (*n*hexane/EtOAc = 25:1) to obtain the product **64p** as a white solid (134 mg, 85%).

**$^1\text{H}$ -NMR** (400 MHz,  $\text{C}_6\text{D}_6$ ):  $\delta$  = 8.19–8.15 (m, 2H), 7.44–7.33 (m, 4H), 7.25 (d,  $J$  = 8.0 Hz, 2H), 5.31 (ddd,  $J$  = 48.0, 5.0, 4.7 Hz, 1H), 3.57 (s, 3H), 1.96–1.81 (m, 1H), 1.75–1.58 (m, 1H), 1.49–1.25 (m, 2H), 1.19 (m, 4H), 0.85 (t,  $J$  = 6.8 Hz, 3H). Calibrated  $^1\text{H}$ -NMR yield from benzylic proton: 83%.  **$^{13}\text{C}$ -NMR** (101 MHz,  $\text{C}_6\text{D}_6$ ):  $\delta$  = 166.6 ( $\text{C}_q$ ), 145.2 ( $\text{C}_q$ ), 141.2 (d,  $^2J_{\text{C-F}}$  = 20.0 Hz,  $\text{C}_q$ ), 140.0 (d,  $^5J_{\text{C-F}}$  = 1.9 Hz,  $\text{C}_q$ ), 130.5 (CH), 129.8 ( $\text{C}_q$ ), 127.6 (CH), 127.3 (CH), 126.4 (d,  $^3J_{\text{C-F}}$  = 6.9 Hz, CH), 94.3 (d,  $^1J_{\text{C-F}}$  = 171.7 Hz, CH), 51.7 ( $\text{CH}_3$ ), 37.7 (d,  $^2J_{\text{C-F}}$  = 23.5 Hz,  $\text{CH}_2$ ), 31.9 ( $\text{CH}_2$ ), 25.2 (d,  $^3J_{\text{C-F}}$  = 4.1 Hz,  $\text{CH}_2$ ), 22.9 ( $\text{CH}_2$ ), 14.2 ( $\text{CH}_3$ ).  **$^{19}\text{F}\{^1\text{H}\}$ -NMR** (282 MHz,  $\text{CDCl}_3$ ):  $\delta$  = -175.3. Calibrated  $^{19}\text{F}\{^1\text{H}\}$ -NMR yield from benzylic fluoride: 93%. **IR** (ATR):  $\tilde{\nu}$  = 2956, 2923, 1719, 1432, 1282, 1222, 1187, 1109,

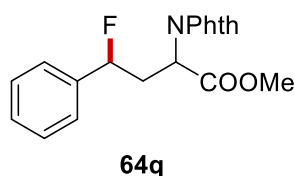
824, 767. **M.p.:** 89–91 °C. **HR-MS** (ESI)  $m/z$  calcd for  $C_{20}H_{23}FO_2$   $[M+Na]^+$ : 314.1677, found: 314.1677.



**Figure 5.6.35** Crude  $^1H$ -NMR Spectrum (300 MHz,  $C_6D_6$ ) of the reaction mixture with  $CH_2Br_2$  (36  $\mu$ L, 0.50 mmol) as internal standard (4.03 ppm). The signals of the benzylic proton and internal standard are integrated.



**Figure 5.6.36**  $^{19}F$ -NMR Spectrum (282 MHz,  $C_6D_6$ ) of the reaction mixture with  $PhCF_3$  (62  $\mu$ L, 0.50 mmol) as internal standard (-62.5 ppm). The signals of the benzylic fluoride and internal standard are integrated.

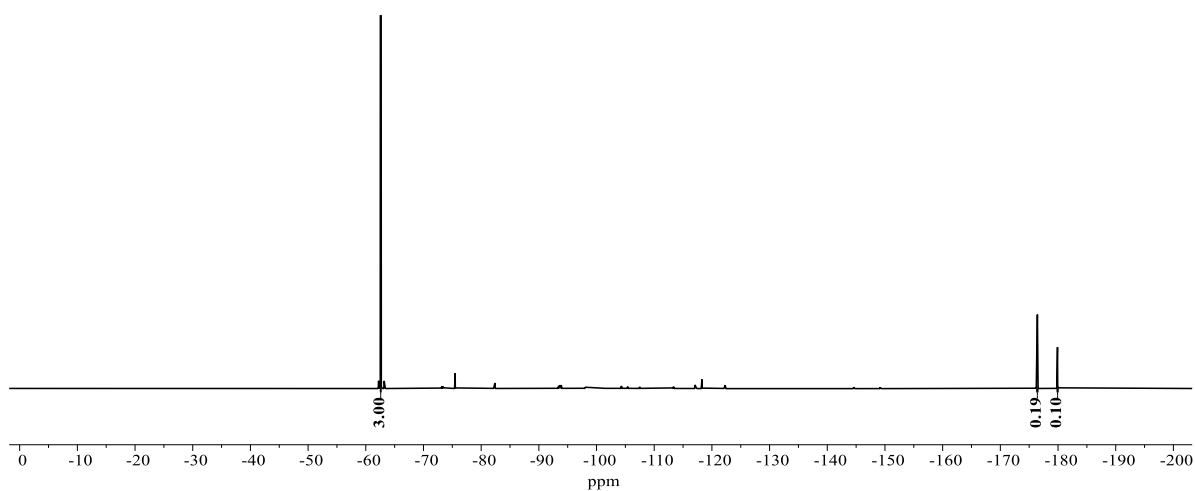


### Methyl 2-(1,3-dioxoisindolin-2-yl)-4-fluoro-4-phenylbutanoate

The general procedure G was followed using methyl 2-(1,3-dioxoisindolin-2-yl)-4-phenylbutanoate **63q** (162 mg, 0.50 mmol) at 0 °C.

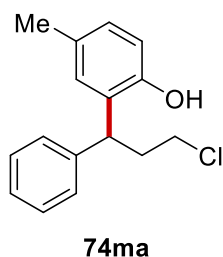
Due to a complex  $^1\text{H}$ -NMR spectrum, exhibiting overlapping signals with the internal standard, the yield was determined by  $^{19}\text{F}$ -NMR. The product was formed as a 2:1 mixture of diastereomers, according to  $^{19}\text{F}$ -NMR analysis. **Benzylic Fluoride Shift:**  $^{19}\text{F}\{^1\text{H}\}$ -NMR (282 MHz,  $\text{CDCl}_3$ )  $\delta = -176.4$  (major),  $-179.9$  (minor). Calibrated  $^{19}\text{F}\{^1\text{H}\}$ -NMR yield from benzylic fluoride: 29%. **HR-MS** (ESI)  $m/z$  calcd for  $\text{C}_{19}\text{H}_{16}\text{FNO}_4$   $[\text{M}+\text{Na}]^+$ : 364.0956, found: 364.0958.

The spectral data are in accordance with those reported in literature.<sup>[122]</sup>



**Figure 5.6.37**  $^{19}\text{F}$ -NMR Spectrum (282 MHz,  $\text{CDCl}_3$ ) of the reaction mixture with  $\text{PhCF}_3$  (62  $\mu\text{L}$ , 0.50 mmol) as internal standard (-62.7 ppm). The signals of the benzylic fluoride and internal standard are integrated.

## 5.6.2 Fluoride Displacement for the Benzylation of Electron-rich Arenes



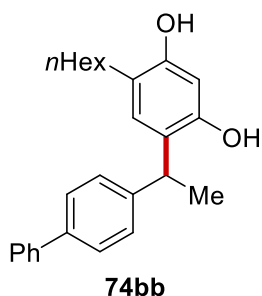
### (2-(3-Chloro-1-phenylpropyl)-4-methylphenol

The general procedure H was followed using (3-chloro-1-propyl)benzene **63m** (77.3 mg, 0.50 mmol) with 3.0 F/mol total charge and 4-methylphenol **73a** (270 mg, 2.50 mmol). After the mixture was stirred overnight another portion of HFIP (0.5 mL) was added, and the reaction was stirred for another 6 h at 50 °C. After the reaction was finished, the solvents were removed in vacuo and the residue was purified by column chromatography on silica gel (EtOAc/nhexane = 2:98) to furnish **74ma** (72.3 mg, 55%) as a colorless oil.

**<sup>1</sup>H-NMR** (400 MHz, CDCl<sub>3</sub>):  $\delta$  = 7.40–7.33 (m, 4H), 7.30–7.25 (m, 1H), 7.09 (d,  $J$  = 2.1 Hz, 1H), 6.97 (dd,  $J$  = 8.0, 2.1 Hz, 1H), 6.69 (d,  $J$  = 8.0 Hz, 1H), 4.68 (brs, 1H), 4.53 (t,  $J$  = 7.8 Hz, 1H), 3.56 (m, 2H), 2.66–2.50 (m, 2H), 2.35 (s, 3H). **<sup>13</sup>C-NMR** (101 MHz, CDCl<sub>3</sub>):  $\delta$  = 151.2 (C<sub>q</sub>), 143.0 (C<sub>q</sub>), 130.3 (C<sub>q</sub>), 129.5 (C<sub>q</sub>), 128.8 (CH), 128.7 (CH), 128.3 (CH), 128.1 (CH), 126.8 (CH), 116.2 (CH), 43.4 (CH<sub>2</sub>), 41.5 (CH), 37.3 (CH<sub>2</sub>), 20.9 (CH<sub>3</sub>). **IR** (ATR):  $\tilde{\nu}$  = 1500, 1447, 1256, 1184, 1103, 811, 763, 734, 701, 518. **MS** (ESI)  $m/z$  (relative intensity): 225 (100) [M-Cl]<sup>+</sup>, 283 (90) [M+Na]<sup>+</sup>. **HR-MS** (ESI)  $m/z$  calcd for C<sub>16</sub>H<sub>17</sub>O<sup>35</sup>Cl [M+Na]<sup>+</sup>: 283.0860, found: 283.0846.

The spectral data are in accordance with those reported in literature.<sup>[120a]</sup>



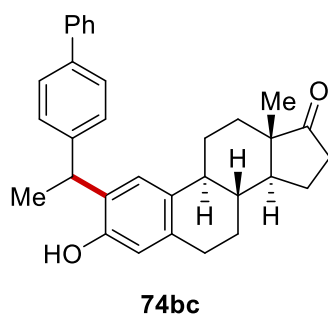


#### 4-(1-([1,1'-Biphenyl]-4-yl)ethyl)-6-hexylbenzene-1,3-diol

The general procedure H was followed using 4-ethyl-1,1'-biphenyl **63b** (91.2 mg, 0.50 mmol) and 4-hexylbenzene-1,3-diol **73b** (485 mg, 2.50 mmol). After the reaction was finished, the solvents were removed in vacuo and the residue was purified by column chromatography on silica gel (EtOAc/nhexane = 1:8 to 1:2) to furnish **74bb** (106 mg, 57%) as a colorless oil.

**<sup>1</sup>H-NMR** (400 MHz, CDCl<sub>3</sub>):  $\delta$  = 7.63–7.59 (m, 2H), 7.58–7.54 (m, 2H), 7.48–7.43 (m, 2H), 7.39–7.33 (m, 3H), 7.04 (s, 1H), 6.26 (s, 1H), 4.97 (s, 1H), 4.85 (s, 1H), 4.35 (q,  $J$  = 7.2 Hz, 1H), 2.63–2.56 (m, 2H), 1.68 (d,  $J$  = 7.2 Hz, 3H), 1.66–1.59 (m, 1H), 1.43–1.33 (m, 6H), 0.98–0.91 (m, 3H). **<sup>13</sup>C-NMR** (101 MHz, CDCl<sub>3</sub>):  $\delta$  = 152.5 (C<sub>q</sub>), 152.0 (C<sub>q</sub>), 145.1 (C<sub>q</sub>), 141.0 (C<sub>q</sub>), 139.3 (C<sub>q</sub>), 129.3 (CH), 128.8 (CH), 127.9 (CH), 127.5 (CH), 127.2 (CH), 127.1 (CH), 124.2 (C<sub>q</sub>), 121.0 (C<sub>q</sub>), 103.8 (CH), 38.0 (CH), 31.9 (CH<sub>2</sub>), 30.2 (CH<sub>2</sub>), 29.6 (CH<sub>2</sub>), 29.3 (CH<sub>2</sub>), 22.8 (CH<sub>2</sub>), 21.4 (CH<sub>3</sub>), 14.2 (CH<sub>3</sub>). **IR** (ATR):  $\tilde{\nu}$  = 2956, 2925, 1510, 1492, 1429, 1196, 1155, 1100, 839, 697. **M.p.**: 198–199 °C. **MS** (ESI)  $m/z$  (relative intensity): 397 (80) [M+Na]<sup>+</sup>, 771 (100) [2M+Na]<sup>+</sup>. **HR-MS** (ESI)  $m/z$  calcd for C<sub>26</sub>H<sub>30</sub>O<sub>2</sub> [M+Na]<sup>+</sup>: 397.2138, found: 397.2136.

The spectral data are in accordance with those reported in literature.<sup>[131]</sup>



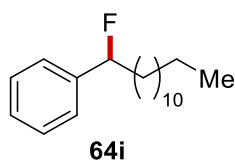
**(8R,9S,13S,14S)-2-(1-([1,1'-Biphenyl]-4-yl)ethyl)-3-hydroxy-13-methyl-6,7,8,9,11,12,13,14,15,16-decahydro-17H-cyclopenta[a]phenanthren-17-one**

The general procedure H was followed using 4-ethyl-1,1'-biphenyl **63b** (91.2 mg, 0.50 mmol), estrone **73c** (540 mg, 2.00 mmol) and DCE/HFIP (3.5 mL, 6:1) for the benzylation reaction. After the reaction was finished, the solvents were removed in vacuo and the residue was purified by column chromatography on silica gel (EtOAc/nhexane = 1:6 to 1:3) to furnish **74bc** (153 mg, 68%) as a white solid.

**<sup>1</sup>H-NMR** (600 MHz, CDCl<sub>3</sub>):  $\delta$  = 7.59–7.56 (m, 2H), 7.55–7.52 (m, 2H), 7.44–7.40 (m, 2H), 7.38–7.35 (m, 2H), 7.34–7.31 (m, 1H), 7.24 (s, 1H), 7.20 (d,  $J$  = 7.1 Hz, 1H), 6.54 (d,  $J$  = 6.3 Hz, 1H), 5.26–5.19 (m, 1H), 4.45 (dq,  $J$  = 12.0, 7.2 Hz, 1H), 2.91–2.78 (m, 2H), 2.55–2.48 (m, 1H), 2.44–2.39 (m, 1H), 2.28 (qd,  $J$  = 11.1, 4.4 Hz, 1H), 2.20–2.12 (m, 1H), 2.08–2.02 (m, 1H), 2.01–1.96 (m, 2H), 1.68 (dd,  $J$  = 7.3, 3.3 Hz, 3H), 1.65–1.57 (m, 2H), 1.57–1.51 (m, 2H), 1.46–1.39 (m, 1H), 0.93 (d,  $J$  = 5.7 Hz, 3H). **<sup>13</sup>C-NMR** (151 MHz, CDCl<sub>3</sub>, mixture of diastereomers):  $\delta$  = 221.9 (C<sub>q</sub>), 151.4 (C<sub>q</sub>), 145.0 (C<sub>q</sub>), 144.9 (C<sub>q</sub>), 141.0 (C<sub>q</sub>), 141.0 (C<sub>q</sub>), 139.1 (C<sub>q</sub>), 139.1 (C<sub>q</sub>), 135.7 (C<sub>q</sub>), 135.7 (C<sub>q</sub>), 131.9 (C<sub>q</sub>), 131.8 (C<sub>q</sub>), 129.6 (C<sub>q</sub>), 129.6 (C<sub>q</sub>), 128.8 (CH), 128.0 (CH), 128.0 (CH), 127.3 (CH), 127.3 (CH), 127.2 (CH), 127.1 (CH), 125.0 (CH), 124.9 (CH), 116.0 (CH), 116.0 (CH), 50.5 (CH), 48.2 (CH<sub>2</sub>), 48.2 (CH<sub>2</sub>), 44.3 (CH), 44.2 (CH), 38.5 (CH), 38.5 (CH), 38.4 (CH), 38.2 (CH<sub>2</sub>), 36.0 (CH<sub>2</sub>), 31.7 (CH<sub>2</sub>), 29.2 (CH<sub>2</sub>), 29.1 (CH<sub>2</sub>), 26.6 (CH<sub>2</sub>), 26.6 (CH<sub>2</sub>), 26.1 (CH<sub>2</sub>), 26.1 (CH<sub>2</sub>), 21.7 (CH<sub>2</sub>), 21.7 (CH<sub>2</sub>), 21.2 (CH<sub>3</sub>), 21.1 (CH<sub>3</sub>), 14.0 (CH<sub>3</sub>), 14.0 (CH<sub>3</sub>). **IR** (ATR):  $\tilde{\nu}$  = 2928, 1724, 1508, 1488, 1420, 1254, 1216, 838, 755, 698. **MS** (ESI)  $m/z$  (relative intensity): 473 (100) [M+Na]<sup>+</sup>, 923 (60) [2M+Na]<sup>+</sup>, 1378 [3M+Na]<sup>+</sup>. **HR-MS** (ESI)  $m/z$  calcd for C<sub>32</sub>H<sub>34</sub>O<sub>2</sub> [M+Na]<sup>+</sup>: 473.2451, found: 473.2441.

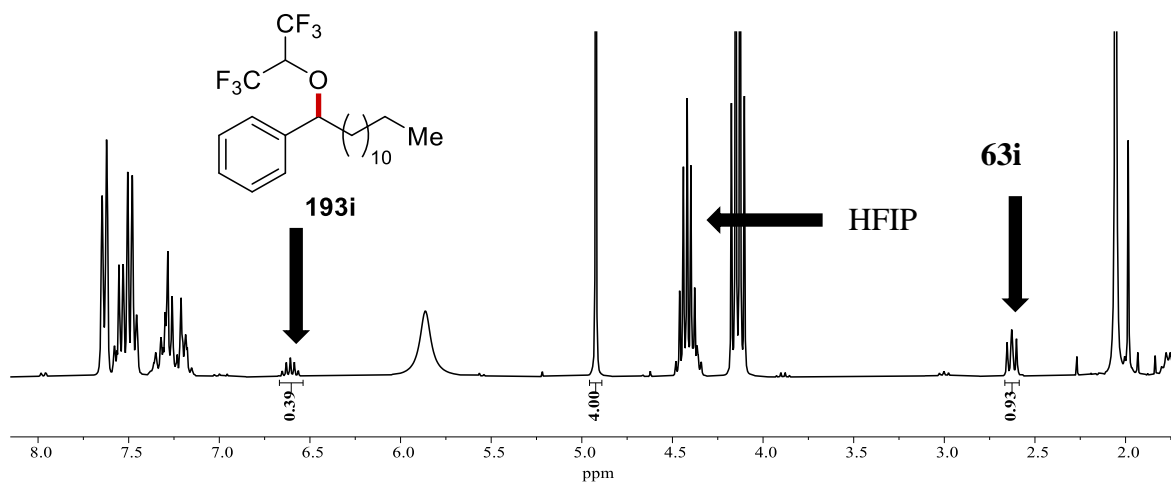
### 5.6.3 Comparison with Previously Reported Conditions

To investigate the advantages of the developed strategy, substrates **63i** and **63l** were tested under the previously described reaction conditions.<sup>[154]</sup> According to the reported protocol, benzylic substrate **63** (0.25 mmol, 1.00 equiv), grinded and oven-dried molecular sieves (20.0 mg), CsF (223 mg, 0.3M), and MeCN/HFIP (4:1, 5.0 mL) were placed in a 10 mL undivided cell under inert atmosphere. Platinum electrodes (25 mm × 10 mm × 0.125 mm) were attached to the electrode holder which was assembled on the electrolysis cell. Electrosynthesis was performed at rt with a constant current of 8.0 mA until 2.5 F/mol were passed (2.1 h). After electrolysis, the reaction mixture was filtered over a plug of silica. The platinum electrodes were washed with EtOAc (5.0 mL) and the resulting fraction was filtered over the same silica plug. After rinsing the silica plug with an additional mixture of *n*hexane/ethylacetate (75 mL), the solvents were removed in vacuo. CH<sub>2</sub>Br<sub>2</sub> (36 μL, 0.50 mmol) and PhCF<sub>3</sub> (62 μL, 0.50 mmol) were added to the resulting residue and the mixture was submitted for NMR analyses.

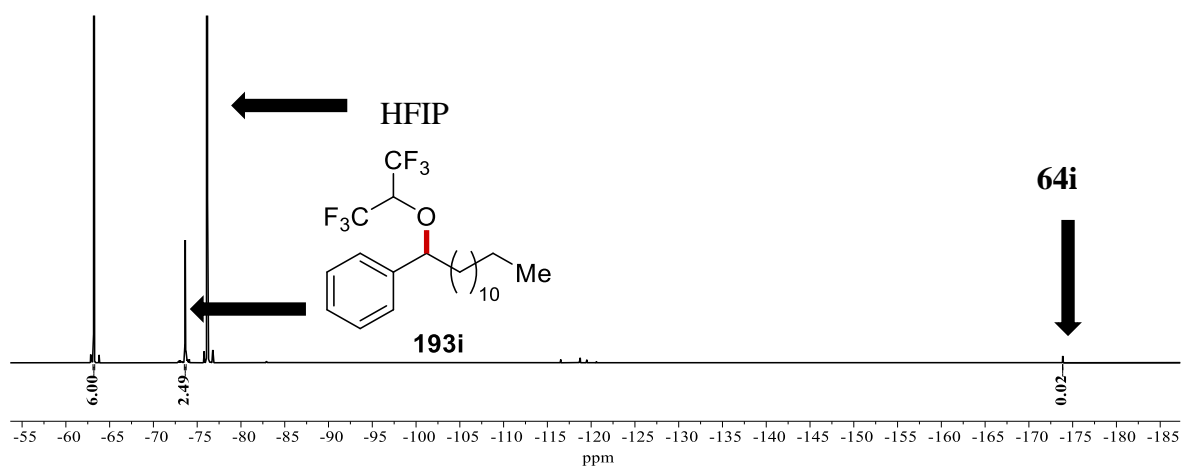


The general procedure was followed using tridecylbenzene **63i** (65.1 mg, 0.25 mmol). Analysis of the NMR data indicated only trace formation of **64i**, next to hypothesized oxygenated side product **193i** (39%) and remaining starting material **63i** (47%).

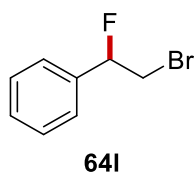
**Benzylic Fluoride Shift:** Calibrated  $^{19}\text{F}\{^1\text{H}\}$ -NMR yield from benzylic fluoride: 2%.



**Figure 5.6.38** Crude  $^1\text{H}$ -NMR Spectrum (300 MHz,  $\text{CDCl}_3$ ) of the reaction mixture with  $\text{CH}_2\text{Br}_2$  (36  $\mu\text{L}$ , 0.50 mmol) as internal standard (4.93 ppm).



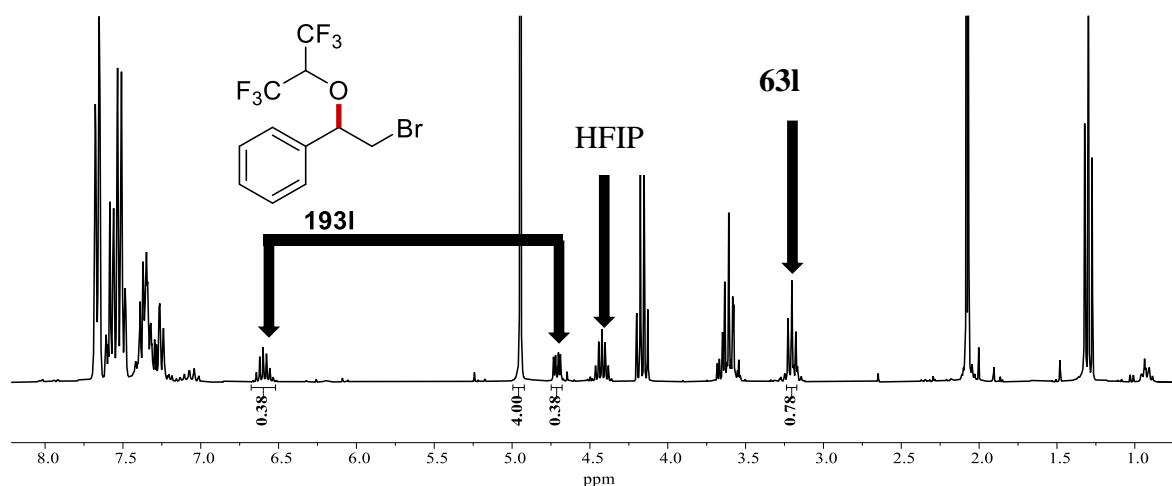
**Figure 5.6.39** Crude  $^{19}\text{F}\{^1\text{H}\}$ -NMR Spectrum ( $\text{CDCl}_3$ , 300 MHz) of the reaction mixture with  $\text{PhCF}_3$  (62  $\mu\text{L}$ , 0.50 mmol) as internal standard ( $-62.7$  ppm). The signals of the resolved (side) product(s) and internal standard are integrated.



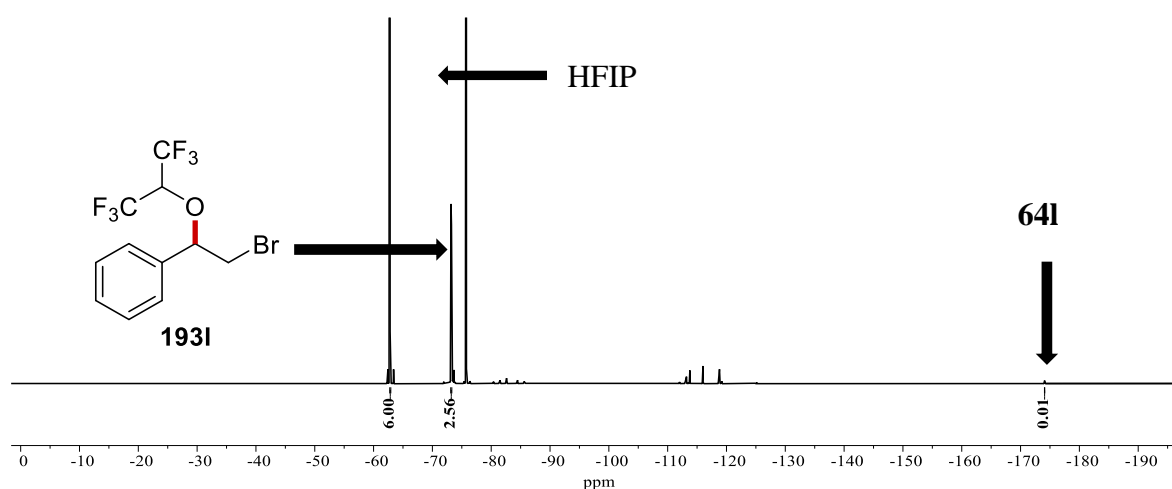
The general procedure was followed using methyl (2-bromoethyl)benzene **63I** (46.3 mg, 0.25 mmol).

Analysis of the NMR data indicated only trace formation of **64I**, next to hypothesized oxygenated side product **193I** (38%) and remaining starting material **63I** (39%).

**Benzylic Fluoride Shift:** Calibrated  $^{19}\text{F}\{^1\text{H}\}$ -NMR yield from benzylic fluoride: 1%.

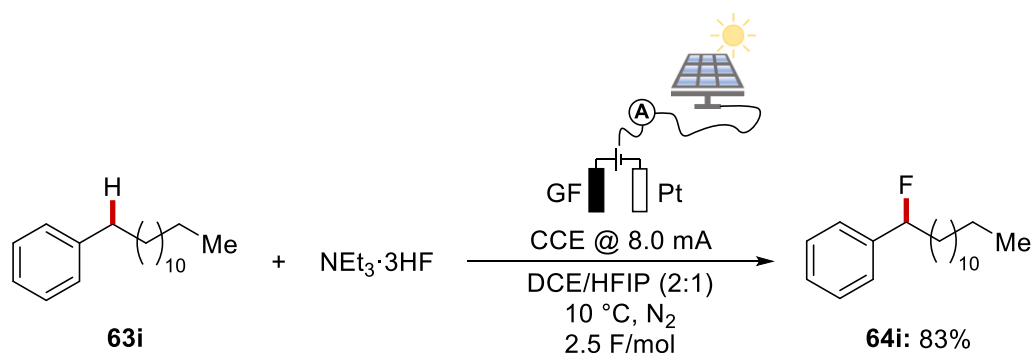


**Figure 5.6.40** Crude  $^1\text{H}$ -NMR Spectrum (300 MHz,  $\text{CDCl}_3$ ) of the reaction mixture with  $\text{CH}_2\text{Br}_2$  (36  $\mu\text{L}$ , 0.50 mmol) as internal standard (4.93 ppm).



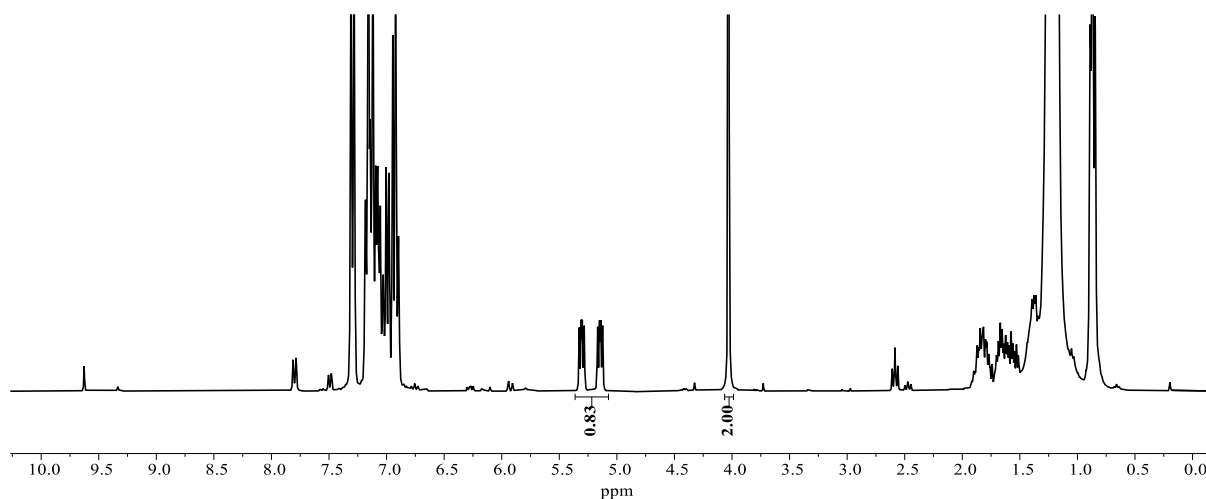
**Figure 5.6.41** Crude  $^{19}\text{F}\{^1\text{H}\}$ -NMR Spectrum ( $\text{CDCl}_3$ , 300 MHz) of the reaction mixture with  $\text{PhCF}_3$  (62  $\mu\text{L}$ , 0.50 mmol) as internal standard (-62.7 ppm). The signals of the resolved (side) product(s) and internal standard are integrated.

## 5.6.4 Solar Energy Enabled Fluorination

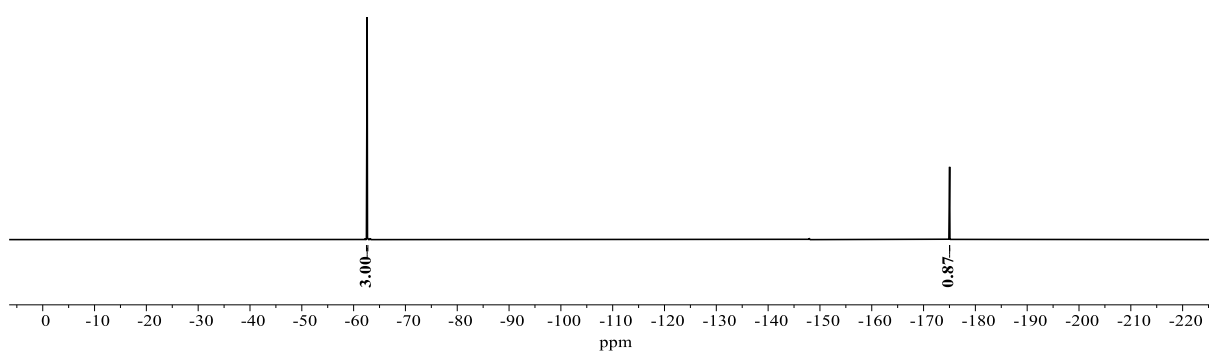


The general procedure G was followed using tridecylbenzene **63i** (131 mg, 0.50 mmol) on the 18<sup>th</sup> of March at the rooftop of the *Institute of Organic and Biomolecular Chemistry* in Göttingen from 12.50–5.20 p.m. The weather conditions were sunny and the temperature was  $10^\circ C$  in the shadow.

**Benzyl Fluoride C–H Shift:**  $^1H$ -NMR (300 MHz,  $C_6D_6$ )  $\delta = 5.23$  (ddd,  $J = 47.8, 8.2, 5.4$  Hz). Calibrated  $^1H$ -NMR yield from benzylic proton: 83%. **Benzylic Fluoride Shift:**  $^{19}F\{^1H\}$ -NMR (282 MHz,  $C_6D_6$ )  $\delta = -175.0$ . Calibrated  $^{19}F\{^1H\}$ -NMR yield from benzylic fluoride: 87%. **HR-MS** (EI)  $m/z$  calcd for  $C_{19}H_{31}F [M]^+$ : 278.2404, found: 278.2403.



**Figure 5.6.42** Crude  $^1H$ -NMR Spectrum (300 MHz,  $C_6D_6$ ) of the reaction mixture with  $CH_2Br_2$  (36  $\mu L$ , 0.50 mmol) as internal standard (4.03 ppm). The signals of the benzylic proton and internal standard are integrated.



**Figure 5.6.43**  $^{19}\text{F}$ -NMR Spectrum (282 MHz,  $\text{C}_6\text{D}_6$ ) of the reaction mixture with  $\text{PhCF}_3$  (62  $\mu\text{L}$ , 0.50 mmol) as internal standard (-62.6 ppm). The signals of the benzylic fluoride and internal standard are integrated.

## 6 REFERENCES

- [1] K. C. Nicolaou, *Angew. Chem. Int. Ed.* **2013**, *52*, 131–146.
- [2] The Nobel Prize Home Page: <https://www.nobelprize.org/prizes/lists/all-nobel-prizes-in-chemistry/> (accessed on April 28, 2022).
- [3] a) P. T. Anastas, M. M. Kirchhoff, *Acc. Chem. Res.* **2002**, *35*, 686–694; b) B. Trost, *Science* **1991**, *254*, 1471–1477.
- [4] a) J. B. Zimmerman, P. T. Anastas, H. C. Erythropel, W. Leitner, *Science* **2020**, *367*, 397–400; b) C. Jimenez-Gonzalez, C. S. Ponder, Q. B. Broxterman, J. B. Manley, *Org. Process Res. Dev.* **2011**, *15*, 912–917; c) P. T. Anastas, N. Eghbali, *Chem. Soc. Rev.* **2010**, *39*, 301–312; d) D. J. C. Constable, A. D. Curzons, V. L. Cunningham, *Green Chem.* **2002**, *4*, 521–527; e) P. T. Anastas, J. Warner, *Green Chemistry: Theory and Practice*, Oxford University Press, New York, **1998**.
- [5] a) A. de Meijere, S. Bräse, M. Oestreich, *Metal-Catalyzed Cross-Coupling Reactions and More*, Wiley-VCH, Weinheim, **2013**; b) L. Ackermann, *Modern Arylation Methods*, Wiley-VCH, Weinheim, **2009**; c) K. C. Nicolaou, P. G. Bulger, D. Sarlah, *Angew. Chem. Int. Ed.* **2005**, *44*, 4442–4489.
- [6] F. Ullmann, J. Bielecki, *Ber. Dtsch. Chem. Ges.* **1901**, *34*, 2174–2185.
- [7] I. Goldberg, *Ber. Dtsch. Chem. Ges.* **1906**, *39*, 1691–1692.
- [8] a) N. Miyaura, A. Suzuki, *J. Chem. Soc., Chem. Commun.* **1979**, 866–867; b) N. Miyaura, K. Yamada, A. Suzuki, *Tetrahedron Lett.* **1979**, *20*, 3437–3440; c) A. O. King, N. Okukado, E.-i. Negishi, *J. Chem. Soc., Chem. Commun.* **1977**, 683–684; d) E. Negishi, A. O. King, N. Okukado, *J. Org. Chem.* **1977**, *42*, 1821–1823; e) H. A. Dieck, R. F. Heck, *J. Org. Chem.* **1975**, *40*, 1083–1090; f) H. A. Dieck, R. F. Heck, *J. Am. Chem. Soc.* **1974**, *96*, 1133–1136; g) R. F. Heck, J. P. Nolley, *J. Org. Chem.* **1972**, *37*, 2320–2322; h) T. Mizoroki, K. Mori, A. Ozaki, *Bull. Chem. Soc. Jpn.* **1971**, *44*, 581–581.
- [9] a) C. C. C. Johansson Seechurn, M. O. Kitching, T. J. Colacot, V. Snieckus, *Angew. Chem. Int. Ed.* **2012**, *51*, 5062–5085; b) The Nobel Prize Home Page: <https://www.nobelprize.org/prizes/chemistry/2010/summary/> (accessed on February 1, 2022).
- [10] K. Sonogashira, Y. Tohda, N. Hagihara, *Tetrahedron Lett.* **1975**, *16*, 4467–4470.
- [11] a) A. S. Guram, S. L. Buchwald, *J. Am. Chem. Soc.* **1994**, *116*, 7901–7902; b) F. Paul, J. Patt, J. F. Hartwig, *J. Am. Chem. Soc.* **1994**, *116*, 5969–5970.
- [12] a) N. Y. S. Lam, K. Wu, J. Q. Yu, *Angew. Chem. Int. Ed.* **2021**, *60*, 15767–15790; b) T. Dalton, T. Faber, F. Glorius, *ACS Cent. Sci.* **2021**, *7*, 245–261; c) S. Rej, Y. Ano, N. Chatani, *Chem. Rev.* **2020**, *120*, 1788–1887; d) P. Gandeepan, T. Müller, D. Zell, G. Cera, S. Warratz, L. Ackermann, *Chem. Rev.* **2019**, *119*, 2192–2452; e) C. Sambriago, D. Schonbauer, R. Blicke, T. Dao-Huy, G. Pototschnig, P. Schaaf, T. Wiesinger, M. F. Zia, J. Wencel-Delord, T. Besset, B. U. W. Maes, M. Schnurch, *Chem. Soc. Rev.* **2018**, *47*, 6603–6743; f) M. M. Lorion, K. Maindan, A. R. Kapdi, L. Ackermann, *Chem. Soc. Rev.* **2017**, *46*, 7399–7420; g) T. Gensch, M. N. Hopkinson, F. Glorius, J. Wencel-Delord, *Chem. Soc. Rev.* **2016**, *45*, 2900–2936; h) L. Ackermann, *Acc. Chem. Res.* **2014**, *47*, 281–295; i) J. Wencel-Delord, F. Glorius, *Nat. Chem.* **2013**, *5*, 369–375; j) T. W. Lyons, M. S. Sanford, *Chem. Rev.* **2010**, *110*, 1147–1169; k) R. G. Bergman, *Nature* **2007**, *446*, 391–393.



- [13] a) Y. Yang, J. Lan, J. You, *Chem. Rev.* **2017**, *117*, 8787–8863; b) S. A. Girard, T. Knauber, C.-J. Li, *Angew. Chem. Int. Ed.* **2014**, *53*, 74–100; c) S. I. Kozhushkov, L. Ackermann, *Chem. Sci.* **2013**, *4*, 886–896; d) C. S. Yeung, V. M. Dong, *Chem. Rev.* **2011**, *111*, 1215–1292; e) S. H. Cho, J. Y. Kim, J. Kwak, S. Chang, *Chem. Soc. Rev.* **2011**, *40*, 5068–5083.
- [14] T. H. Meyer, L. H. Finger, P. Gandeepan, L. Ackermann, *Trends Chem.* **2019**, *1*, 63–76.
- [15] a) S. R. Neufeldt, M. S. Sanford, *Acc. Chem. Res.* **2012**, *45*, 936–946; b) L. Ackermann, in *Directed Metallation* (Ed.: N. Chatani), Springer, Berlin, Heidelberg, **2007**, pp. 35–60.
- [16] F. G. Bordwell, *Acc. Chem. Res.* **1988**, *21*, 456–463.
- [17] E. M. Beck, M. J. Gaunt, in *C-H Activation* (Eds.: J.-Q. Yu, Z. Shi), Springer, Berlin, Heidelberg, **2010**, pp. 85–121.
- [18] a) K. Shen, Y. Fu, J.-N. Li, L. Liu, Q.-X. Guo, *Tetrahedron* **2007**, *63*, 1568–1576; b) I. V. Seregin, V. Gevorgyan, *Chem. Soc. Rev.* **2007**, *36*, 1173–1193.
- [19] a) T. P. Pabst, P. J. Chirik, *Organometallics* **2021**, *40*, 813–831; b) I. A. I. Mkhaliid, J. H. Barnard, T. B. Marder, J. M. Murphy, J. F. Hartwig, *Chem. Rev.* **2010**, *110*, 890–931.
- [20] S. De Sarkar, W. Liu, S. I. Kozhushkov, L. Ackermann, *Adv. Synth. Catal.* **2014**, *356*, 1461–1479.
- [21] P. Gandeepan, L. Ackermann, *Chem* **2018**, *4*, 199–222.
- [22] a) S. Rej, N. Chatani, *Angew. Chem. Int. Ed.* **2019**, *58*, 8304–8329; b) W. Ma, P. Gandeepan, J. Li, L. Ackermann, *Org. Chem. Front.* **2017**, *4*, 1435–1467.
- [23] a) K. Korvorapun, R. C. Samanta, T. Rogge, L. Ackermann, *Synthesis* **2021**, *53*, 2911–2946; b) G. Meng, N. Y. S. Lam, E. L. Lucas, T. G. Saint-Denis, P. Verma, N. Chekshin, J.-Q. Yu, *J. Am. Chem. Soc.* **2020**, *142*, 10571–10591; c) J. Li, S. De Sarkar, L. Ackermann, in *C–H Bond Activation and Catalytic Functionalization I* (Eds.: P. H. Dixneuf, H. Doucet), Springer International Publishing, Cham, **2016**, pp. 217–257.
- [24] H. Yi, G. Zhang, H. Wang, Z. Huang, J. Wang, A. K. Singh, A. Lei, *Chem. Rev.* **2017**, *117*, 9016–9085.
- [25] a) K. M. Altus, J. A. Love, *Commun. Chem.* **2021**, *4*, 173; b) L. Ackermann, *Chem. Rev.* **2011**, *111*, 1315–1345; c) D. H. Ess, W. A. Goddard, R. A. Periana, *Organometallics* **2010**, *29*, 6459–6472; d) D. Balcells, E. Clot, O. Eisenstein, *Chem. Rev.* **2010**, *110*, 749–823; e) M. Albrecht, *Chem. Rev.* **2010**, *110*, 576–623; f) J. A. Labinger, J. E. Bercaw, *Nature* **2002**, *417*, 507–514.
- [26] V. I. Sokolov, L. L. Troitskaya, O. A. Reutov, *J. Organomet. Chem.* **1979**, *182*, 537–546.
- [27] a) D. L. Davies, S. A. Macgregor, C. L. McMullin, *Chem. Rev.* **2017**, *117*, 8649–8709; b) B. Biswas, M. Sugimoto, S. Sakaki, *Organometallics* **2000**, *19*, 3895–3908.
- [28] M. Lafrance, K. Fagnou, *J. Am. Chem. Soc.* **2006**, *128*, 16496–16497.
- [29] S. I. Gorelsky, D. Lapointe, K. Fagnou, *J. Am. Chem. Soc.* **2008**, *130*, 10848–10849.

- [30] a) Y. Boutadla, D. L. Davies, S. A. Macgregor, A. I. Poblador-Bahamonde, *Dalton Trans.* **2009**, 5887–5893; b) D. L. Davies, S. M. A. Donald, S. A. Macgregor, *J. Am. Chem. Soc.* **2005**, *127*, 13754–13755.
- [31] D. García-Cuadrado, A. A. C. Braga, F. Maseras, A. M. Echavarren, *J. Am. Chem. Soc.* **2006**, *128*, 1066–1067.
- [32] a) T. Rogge, J. C. A. Oliveira, R. Kuniyil, L. Hu, L. Ackermann, *ACS Catal.* **2020**, *10*, 10551–10558; b) E. Tan, O. Quinonero, M. Elena de Orbe, A. M. Echavarren, *ACS Catal.* **2018**, *8*, 2166–2172; c) D. Zell, M. Bursch, V. Müller, S. Grimme, L. Ackermann, *Angew. Chem. Int. Ed.* **2017**, *56*, 10378–10382; d) H. Wang, M. Moselage, M. J. González, L. Ackermann, *ACS Catal.* **2016**, *6*, 2705–2709; e) R. Mei, J. Loup, L. Ackermann, *ACS Catal.* **2016**, *6*, 793–797; f) W. Ma, R. Mei, G. Tenti, L. Ackermann, *Chem. Eur. J.* **2014**, *20*, 15248–15251.
- [33] a) O. Baudoin, *Angew. Chem. Int. Ed.* **2020**, *59*, 17798–17809; b) D. J. Abrams, P. A. Provencher, E. J. Sorensen, *Chem. Soc. Rev.* **2018**, *47*, 8925–8967; c) L. McMurray, F. O'Hara, M. J. Gaunt, *Chem. Soc. Rev.* **2011**, *40*, 1885–1898.
- [34] a) B. Liu, A. M. Romine, C. Z. Rubel, K. M. Engle, B.-F. Shi, *Chem. Rev.* **2021**, *121*, 14957–15074; b) J. He, M. Wasa, K. S. L. Chan, Q. Shao, J. Q. Yu, *Chem. Rev.* **2017**, *117*, 8754–8786; c) R. Jazzar, J. Hitce, A. Renaudat, J. Sofack-Kreutzer, O. Baudoin, *Chem. Eur. J.* **2010**, *16*, 2654–2672.
- [35] a) T. Yoshino, S. Matsunaga, *ACS Catal.* **2021**, *11*, 6455–6466; b) O. Vyhivskyi, A. Kudashev, T. Miyakoshi, O. Baudoin, *Chem. Eur. J.* **2021**, *27*, 1231–1257; c) J. Loup, U. Dhawa, F. Pesciaioli, J. Wencel-Delord, L. Ackermann, *Angew. Chem. Int. Ed.* **2019**, *58*, 12803–12818; d) T. G. Saint-Denis, R.-Y. Zhu, G. Chen, Q.-F. Wu, J.-Q. Yu, *Science* **2018**, *359*, eaao4798; e) C. G. Newton, S.-G. Wang, C. C. Oliveira, N. Cramer, *Chem. Rev.* **2017**, *117*, 8908–8976.
- [36] a) Q. Sun, H. Zhang, Q. Wang, T. Qiao, G. He, G. Chen, *Angew. Chem. Int. Ed.* **2021**, *60*, 19620–19625; b) W. Lv, Y. Chen, S. Wen, D. Ba, G. Cheng, *J. Am. Chem. Soc.* **2020**, *142*, 14864–14870; c) J. Wu, A. Kopp, L. Ackermann, *Angew. Chem. Int. Ed.*, *n/a*, e202114993.
- [37] a) H.-R. Tong, B. Li, G. Li, G. He, G. Chen, *CCS Chem.* **2021**, *3*, 1797–1820; b) J. Wu, N. Kaplaneris, S. Ni, F. Kaltenhäuser, L. Ackermann, *Chem. Sci.* **2020**, *11*, 6521–6526; c) W. Wang, M. M. Lorion, J. Shah, A. R. Kapdi, L. Ackermann, *Angew. Chem. Int. Ed.* **2018**, *57*, 14700–14717; d) A. F. M. Noisier, M. A. Brimble, *Chem. Rev.* **2014**, *114*, 8775–8806.
- [38] a) L. Guillemard, N. Kaplaneris, L. Ackermann, M. J. Johansson, *Nat. Rev. Chem.* **2021**, *5*, 522–545; b) T. Cernak, K. D. Dykstra, S. Tyagarajan, P. Vachal, S. W. Krska, *Chem. Soc. Rev.* **2016**, *45*, 546–576; c) J. Yamaguchi, A. D. Yamaguchi, K. Itami, *Angew. Chem. Int. Ed.* **2012**, *51*, 8960–9009.
- [39] S. D. Friis, M. J. Johansson, L. Ackermann, *Nat. Chem.* **2020**, *12*, 511–519.
- [40] L. A. Oro, C. Claver, *Iridium Complexes in Organic Synthesis*, Wiley-VCH, Weinheim, **2009**.
- [41] a) L. Vaska, R. E. Rhodes, *J. Am. Chem. Soc.* **1965**, *87*, 4970–4971; b) L. Vaska, J. W. DiLuzio, *J. Am. Chem. Soc.* **1961**, *83*, 2784–2785.
- [42] R. H. Crabtree, in *Iridium Catalysis* (Ed.: P. G. Andersson), Springer, Berlin, Heidelberg, **2011**, pp. 1–10.
- [43] J. A. Osborn, R. R. Schrock, *J. Am. Chem. Soc.* **1971**, *93*, 3089–3091.

- [44] a) R. Crabtree, *Acc. Chem. Res.* **1979**, *12*, 331–337; b) R. H. Crabtree, H. Felkin, G. E. Morris, *J. Organomet. Chem.* **1977**, *141*, 205–215.
- [45] a) H.-U. Blaser, in *Iridium Complexes in Organic Synthesis*, Wiley-VCH, Weinheim, **2008**, pp. 1–14; b) S. J. Roseblade, A. Pfaltz, *C. R. Chim.* **2007**, *10*, 178–187.
- [46] a) P. M. Maitlis, *Coord. Chem. Rev.* **1982**, *43*, 377–384; b) J. W. Kang, K. Moseley, P. M. Maitlis, *J. Am. Chem. Soc.* **1969**, *91*, 5970–5977; c) J. W. Kang, P. M. Maitlis, *J. Am. Chem. Soc.* **1968**, *90*, 3259–3261.
- [47] J. Chatt, J. M. Davidson, *J. Chem. Soc.* **1965**, 843–855.
- [48] a) A. E. Shilov, G. B. Shul'pin, *Chem. Rev.* **1997**, *97*, 2879–2932; b) A. E. Shilov, *Pure Appl. Chem.* **1978**, *50*, 725–733.
- [49] R. H. Crabtree, *J. Chem. Soc., Dalton Trans.* **2001**, 2437–2450.
- [50] A. H. Janowicz, R. G. Bergman, *J. Am. Chem. Soc.* **1982**, *104*, 352–354.
- [51] J. K. Hoyano, W. A. G. Graham, *J. Am. Chem. Soc.* **1982**, *104*, 3723–3725.
- [52] Y.-F. Han, G.-X. Jin, *Chem. Soc. Rev.* **2014**, *43*, 2799–2823.
- [53] J. M. Kisenyi, G. J. Sunley, J. A. Cabeza, A. J. Smith, H. Adams, N. J. Salt, P. M. Maitlis, *J. Chem. Soc., Dalton Trans.* **1987**, 2459–2466.
- [54] S. Murahashi, *J. Am. Chem. Soc.* **1955**, *77*, 6403–6404.
- [55] Y. Fujiwara, I. Moritani, S. Danno, R. Asano, S. Teranishi, *J. Am. Chem. Soc.* **1969**, *91*, 7166–7169.
- [56] L. N. Lewis, J. F. Smith, *J. Am. Chem. Soc.* **1986**, *108*, 2728–2735.
- [57] Y.-G. Lim, Y. H. Kim, J.-B. Kang, *J. Chem. Soc., Chem. Commun.* **1994**, 2267–2268.
- [58] C. Yuan, B. Liu, *Org. Chem. Front.* **2018**, *5*, 106–131.
- [59] a) J.-Y. Cho, C. N. Iverson, M. R. Smith, *J. Am. Chem. Soc.* **2000**, *122*, 12868–12869; b) C. N. Iverson, M. R. Smith, *J. Am. Chem. Soc.* **1999**, *121*, 7696–7697.
- [60] a) J. S. Wright, P. J. H. Scott, P. G. Steel, *Angew. Chem. Int. Ed.* **2021**, *60*, 2796–2821; b) T. Ishiyama, J. Takagi, K. Ishida, N. Miyaura, N. R. Anastasi, J. F. Hartwig, *J. Am. Chem. Soc.* **2002**, *124*, 390–391; c) J.-Y. Cho, M. K. Tse, D. Holmes, R. E. Maleczka, M. R. Smith, *Science* **2002**, *295*, 305–308.
- [61] T. Matsumoto, D. J. Taube, R. A. Periana, H. Taube, H. Yoshida, *J. Am. Chem. Soc.* **2000**, *122*, 7414–7415.
- [62] K.-i. Fujita, M. Nonogawa, R. Yamaguchi, *Chem. Commun.* **2004**, 1926–1927.
- [63] T. Yasukawa, T. Satoh, M. Miura, M. Nomura, *J. Am. Chem. Soc.* **2002**, *124*, 12680–12681.
- [64] K. Ueura, T. Satoh, M. Miura, *J. Org. Chem.* **2007**, *72*, 5362–5367.
- [65] X. Li, W. Ouyang, J. Nie, S. Ji, Q. Chen, Y. Huo, *ChemCatChem* **2020**, *12*, 2358–2384.
- [66] S. Yamane, T. Hinoue, Y. Usuki, M. Itazaki, H. Nakazawa, Y. Hayashi, S. Kawauchi, M. Miura, T. Satoh, *Chem. Eur. J.* **2018**, *24*, 7852–7855.
- [67] Ł. Woźniak, J.-F. Tan, Q.-H. Nguyen, A. Madron du Vigné, V. Smal, Y.-X. Cao, N. Cramer, *Chem. Rev.* **2020**, *120*, 10516–10543.

- [68] L. Capaldo, D. Ravelli, M. Fagnoni, *Chem. Rev.* **2021**.
- [69] S. Pan, T. Wakaki, N. Ryu, T. Shibata, *Chem. Asian. J.* **2014**, *9*, 1257–1260.
- [70] J. Kim, S.-W. Park, M.-H. Baik, S. Chang, *J. Am. Chem. Soc.* **2015**, *137*, 13448–13451.
- [71] L. Ackermann, L. Wang, R. Wolfram, A. V. Lygin, *Org. Lett.* **2012**, *14*, 728–731.
- [72] K. Elumalai, W. K. Leong, *Tetrahedron Lett.* **2018**, *59*, 113–116.
- [73] X. Yang, R. Sun, C. Zhang, X. Zheng, M. Yuan, H. Fu, R. Li, H. Chen, *Org. Lett.* **2019**, *21*, 1002–1006.
- [74] S. M. Khake, K. Yamazaki, Y. Ano, N. Chatani, *ACS Catal.* **2021**, *11*, 5463–5471.
- [75] a) J. A. Osborn, F. H. Jardine, J. F. Young, G. Wilkinson, *J. Chem. Soc. A* **1966**, 1711–1732; b) J. F. Young, J. A. Osborn, F. H. Jardine, G. Wilkinson, *Chem. Commun. (London)* **1965**, 131–132.
- [76] a) A. P. Evans, *Modern Rhodium-Catalyzed Organic Reactions*, Wiley-VCH, Weinheim, **2005**; b) D. Forster, in *Adv. Organomet. Chem.*, Vol. 17 (Eds.: F. G. A. Stone, R. West), Academic Press, **1979**, pp. 255–267.
- [77] a) G. Song, F. Wang, X. Li, *Chem. Soc. Rev.* **2012**, *41*, 3651–3678; b) T. Satoh, M. Miura, *Chem. Eur. J.* **2010**, *16*, 11212–11222.
- [78] a) D. A. Colby, A. S. Tsai, R. G. Bergman, J. A. Ellman, *Acc. Chem. Res.* **2012**, *45*, 814–825; b) D. A. Colby, R. G. Bergman, J. A. Ellman, *Chem. Rev.* **2010**, *110*, 624–655.
- [79] a) T. Matsumoto, R. A. Periana, D. J. Taube, H. Yoshida, *J. Catal.* **2002**, *206*, 272–280; b) M. Takaya, Y. Hajime, *Chem. Lett.* **2000**, *29*, 1064–1065.
- [80] K. Ueura, T. Satoh, M. Miura, *Org. Lett.* **2007**, *9*, 1407–1409.
- [81] a) A. Bechtoldt, M. E. Baumert, L. Vaccaro, L. Ackermann, *Green Chem.* **2018**, *20*, 398–402; b) A. Bechtoldt, C. Tirler, K. Raghuvanshi, S. Warratz, C. Kornhaaß, L. Ackermann, *Angew. Chem. Int. Ed.* **2016**, *55*, 264–267; c) S. Warratz, C. Kornhaaß, A. Cajaraville, B. Niepötter, D. Stalke, L. Ackermann, *Angew. Chem. Int. Ed.* **2015**, *54*, 5513–5517; d) L. Ackermann, J. Pospech, K. Graczyk, K. Rauch, *Org. Lett.* **2012**, *14*, 930–933; e) L. Ackermann, J. Pospech, *Org. Lett.* **2011**, *13*, 4153–4155.
- [82] D. R. Stuart, M. Bertrand-Laperle, K. M. N. Burgess, K. Fagnou, *J. Am. Chem. Soc.* **2008**, *130*, 16474–16475.
- [83] N. Guimond, K. Fagnou, *J. Am. Chem. Soc.* **2009**, *131*, 12050–12051.
- [84] L. Li, W. W. Brennessel, W. D. Jones, *J. Am. Chem. Soc.* **2008**, *130*, 12414–12419.
- [85] S. Mochida, M. Shimizu, K. Hirano, T. Satoh, M. Miura, *Chem. Asian. J.* **2010**, *5*, 847–851.
- [86] a) T. K. Hyster, T. Rovis, *J. Am. Chem. Soc.* **2010**, *132*, 10565–10569; b) M. Satoshi, U. Nobuyoshi, H. Koji, S. Tetsuya, M. Masahiro, *Chem. Lett.* **2010**, *39*, 744–746.
- [87] N. Umeda, K. Hirano, T. Satoh, N. Shibata, H. Sato, M. Miura, *J. Org. Chem.* **2011**, *76*, 13–24.
- [88] a) J. C. Leung, M. J. Krische, *Chem. Sci.* **2012**, *3*, 2202–2209; b) M. C. Willis, *Chem. Rev.* **2010**, *110*, 725–748.
- [89] K. Sakai, J. Ide, O. Oda, N. Nakamura, *Tetrahedron Lett.* **1972**, *13*, 1287–1290.

- [90] C. F. Lochow, R. G. Miller, *J. Am. Chem. Soc.* **1976**, *98*, 1281–1283.
- [91] M. Shimizu, H. Tsurugi, T. Satoh, M. Miura, *Chem. Asian J.* **2008**, *3*, 881–886.
- [92] Z. Shi, N. Schröder, F. Glorius, *Angew. Chem. Int. Ed.* **2012**, *51*, 8092–8096.
- [93] H. Zeng, C.-J. Li, *Angew. Chem. Int. Ed.* **2014**, *53*, 13862–13865.
- [94] R. Kuppusamy, P. Gandeepan, C.-H. Cheng, *Org. Lett.* **2015**, *17*, 3846–3849.
- [95] a) B. Liu, L. Yang, P. Li, F. Wang, X. Li, *Org. Chem. Front.* **2021**, *8*, 1085–1101; b) M. Maraswami, T.-P. Loh, *Synthesis* **2019**, *51*, 1049–1062; c) X. Shang, Z.-Q. Liu, *Chem. Soc. Rev.* **2013**, *42*, 3253–3260.
- [96] a) D. A. Colby, R. G. Bergman, J. A. Ellman, *J. Am. Chem. Soc.* **2008**, *130*, 3645–3651; b) D. A. Colby, R. G. Bergman, J. A. Ellman, *J. Am. Chem. Soc.* **2006**, *128*, 5604–5605; c) Y.-G. Lim, J.-B. Kang, B. Tak Koo, *Tetrahedron Lett.* **1999**, *40*, 7691–7694; d) Y.-G. Lim, J.-B. Kang, Y. Hae Kim, *J. Chem. Soc., Perkin Trans. 1* **1998**, 699–708; e) Y.-G. Lim, J.-B. Kang, Y. H. Kim, *Chem. Commun.* **1996**, 585–586.
- [97] S. Mochida, K. Hirano, T. Satoh, M. Miura, *J. Org. Chem.* **2009**, *74*, 6295–6298.
- [98] a) M. P. Huestis, L. Chan, D. R. Stuart, K. Fagnou, *Angew. Chem. Int. Ed.* **2011**, *50*, 1338–1341; b) D. R. Stuart, P. Alsabeh, M. Kuhn, K. Fagnou, *J. Am. Chem. Soc.* **2010**, *132*, 18326–18339.
- [99] a) B. Li, N. Wang, Y. Liang, S. Xu, B. Wang, *Org. Lett.* **2013**, *15*, 136–139; b) L. Wang, L. Ackermann, *Org. Lett.* **2013**, *15*, 176–179.
- [100] T. Brückl, R. D. Baxter, Y. Ishihara, P. S. Baran, *Acc. Chem. Res.* **2012**, *45*, 826–839.
- [101] a) M. P. Doyle, R. Duffy, M. Ratnikov, L. Zhou, *Chem. Rev.* **2010**, *110*, 704–724; b) H. M. L. Davies, J. R. Manning, *Nature* **2008**, *451*, 417–424.
- [102] a) S. Sarkar, K. P. S. Cheung, V. Gevorgyan, *Chem. Sci.* **2020**, *11*, 12974–12993; b) J. C. K. Chu, T. Rovis, *Angew. Chem. Int. Ed.* **2018**, *57*, 62–101; c) J. F. Hartwig, M. A. Larsen, *ACS Cent. Sci.* **2016**, *2*, 281–292.
- [103] a) J. D. Lasso, D. J. Castillo-Pazos, C.-J. Li, *Chem. Soc. Rev.* **2021**, *50*, 10955–10982; b) J. Robertson, J. Pillai, R. K. Lush, *Chem. Soc. Rev.* **2001**, *30*, 94–103.
- [104] a) H. Cao, X. Tang, H. Tang, Y. Yuan, J. Wu, *Chem Catalysis* **2021**, *1*, 523–598; b) L. Capaldo, D. Ravelli, *Eur. J. Org. Chem.* **2017**, *2017*, 2056–2071.
- [105] a) L. Ackermann, *Electrochemistry in Organic Synthesis*, Thieme, Stuttgart, **2021**; b) F. Wang, S. S. Stahl, *Acc. Chem. Res.* **2020**, *53*, 561–574; c) Y. Yuan, A. Lei, *Acc. Chem. Res.* **2019**, *52*, 3309–3324; d) H. Wang, X. Gao, Z. Lv, T. Abdelilah, A. Lei, *Chem. Rev.* **2019**, *119*, 6769–6787; e) D. Pletcher, *Electrochem. Commun.* **2018**, *88*, 1–4; f) M. Yan, Y. Kawamata, P. S. Baran, *Chem. Rev.* **2017**, *117*, 13230–13319; g) O. Hammerich, B. Speiser, *Organic Electrochemistry: Revised and Expanded*, CRC Press, Boca Raton, **2015**.
- [106] a) R. Lin, A. P. Amrute, J. Pérez-Ramírez, *Chem. Rev.* **2017**, *117*, 4182–4247; b) L. Wang, J. Xiao, *Topics in Current Chemistry* **2016**, *374*, 17.
- [107] a) S. J. Blanksby, G. B. Ellison, *Acc. Chem. Res.* **2003**, *36*, 255–263; b) a. D F McMillen, D. M. Golden, *Annu. Rev. Phys. Chem.* **1982**, *33*, 493–532.
- [108] X.-S. Xue, P. Ji, B. Zhou, J.-P. Cheng, *Chem. Rev.* **2017**, *117*, 8622–8648.

- [109] a) L. Hunter, *Beilstein J Org Chem* **2010**, *6*, 38; b) D. O'Hagan, *Chem. Soc. Rev.* **2008**, *37*, 308–319.
- [110] a) J. Wang, M. Sánchez-Roselló, J. L. Aceña, C. del Pozo, A. E. Sorochinsky, S. Fustero, V. A. Soloshonok, H. Liu, *Chem. Rev.* **2014**, *114*, 2432–2506; b) S. Purser, P. R. Moore, S. Swallow, V. Gouverneur, *Chem. Soc. Rev.* **2008**, *37*, 320–330; c) W. K. Hagmann, *J. Med. Chem.* **2008**, *51*, 4359–4369; d) K. Müller, C. Faeh, F. Diederich, *Science* **2007**, *317*, 1881–1886; e) K. L. Kirk, *J. Fluorine Chem.* **2006**, *127*, 1013–1029.
- [111] T. Fujiwara, D. O'Hagan, *J. Fluorine Chem.* **2014**, *167*, 16–29.
- [112] a) R. Berger, G. Resnati, P. Metrangolo, E. Weber, J. Hulliger, *Chem. Soc. Rev.* **2011**, *40*, 3496–3508; b) T. Hiyama, H. Yamamoto, *Organofluorine Compounds*, Springer, Berlin, Heidelberg, **2000**.
- [113] a) G. Tarantino, C. Hammond, *Green Chem.* **2020**, *22*, 5195–5209; b) R. Szpera, D. F. J. Moseley, L. B. Smith, A. J. Sterling, V. Gouverneur, *Angew. Chem. Int. Ed.* **2019**, *58*, 14824–14848; c) A. Koperniku, H. Liu, P. B. Hurley, *Eur. J. Org. Chem.* **2016**, *2016*, 871–886; d) P. A. Champagne, J. Desroches, J. D. Hamel, M. Vandamme, J. F. Paquin, *Chem. Rev.* **2015**, *115*, 9073–9174.
- [114] W.-L. Hu, X.-G. Hu, L. Hunter, *Synthesis* **2017**, *49*, 4917–4930.
- [115] J.-j. Ma, W.-b. Yi, G.-p. Lu, C. Cai, *Org. Biomol. Chem.* **2015**, *13*, 2890–2894.
- [116] Y. Amaoka, M. Nagatomo, M. Inoue, *Org. Lett.* **2013**, *15*, 2160–2163.
- [117] S. Bloom, M. McCann, T. Lectka, *Org. Lett.* **2014**, *16*, 6338–6341.
- [118] J.-B. Xia, C. Zhu, C. Chen, *J. Am. Chem. Soc.* **2013**, *135*, 17494–17500.
- [119] a) M. B. Nodwell, A. Bagai, S. D. Halperin, R. E. Martin, H. Knust, R. Britton, *Chem. Commun.* **2015**, *51*, 11783–11786; b) D. Cantillo, O. de Frutos, J. A. Rincon, C. Mateos, C. O. Kappe, *J. Org. Chem.* **2014**, *79*, 8486–8490.
- [120] a) A. Vasilopoulos, D. L. Golden, J. A. Buss, S. S. Stahl, *Org. Lett.* **2020**, *22*, 5753–5757; b) C. R. Pitts, S. Bloom, R. Woltornist, D. J. Auvenshine, L. R. Ryzhkov, M. A. Siegler, T. Lectka, *J. Am. Chem. Soc.* **2014**, *136*, 9780–9791; c) S. Bloom, C. R. Pitts, D. C. Miller, N. Haselton, M. G. Holl, E. Urheim, T. Lectka, *Angew. Chem. Int. Ed.* **2012**, *51*, 10580–10583.
- [121] S. Bloom, C. R. Pitts, R. Woltornist, A. Griswold, M. G. Holl, T. Lectka, *Org. Lett.* **2013**, *15*, 1722–1724.
- [122] W. Liu, J. T. Groves, *Angew. Chem. Int. Ed.* **2013**, *52*, 6024–6027.
- [123] X. Huang, W. Liu, H. Ren, R. Neelamegam, J. M. Hooker, J. T. Groves, *J. Am. Chem. Soc.* **2014**, *136*, 6842–6845.
- [124] W. Liu, X. Huang, M.-J. Cheng, R. J. Nielsen, W. A. Goddard, J. T. Groves, *Science* **2012**, *337*, 1322–1325.
- [125] I. N.-M. Leibler, M. A. Tekle-Smith, A. G. Doyle, *Nat. Commun.* **2021**, *12*, 6950.
- [126] a) Z. Wang, Y. Sun, L.-Y. Shen, W.-C. Yang, F. Meng, P. Li, *Org. Chem. Front.* **2022**, *9*, 853–873; b) B. Zhao, T. Rogge, L. Ackermann, Z. Shi, *Chem. Soc. Rev.* **2021**, *50*, 8903–8953; c) J.-D. Hamel, J.-F. Paquin, *Chem. Commun.* **2018**, *54*, 10224–10239; d) Q. Shen, Y.-G. Huang, C. Liu, J.-C. Xiao, Q.-Y. Chen, Y. Guo, *J. Fluorine Chem.* **2015**, *179*, 14–22; e) H. Amii, K. Uneyama, *Chem. Rev.* **2009**, *109*, 2119–2183.

- [127] M. M. Toteva, J. P. Richard, *J. Am. Chem. Soc.* **2002**, *124*, 9798–9805.
- [128] a) C. Houle, P. R. Savoie, C. Davies, D. Jardel, P. A. Champagne, B. Bibal, J.-F. Paquin, *Chem. Eur. J.* **2020**, *26*, 10620–10625; b) P. A. Champagne, J. Pomarole, M.-È. Thérien, Y. Benhassine, S. Beaulieu, C. Y. Legault, J.-F. Paquin, *Org. Lett.* **2013**, *15*, 2210–2213.
- [129] J. Zhu, M. Pérez, D. W. Stephan, *Angew. Chem. Int. Ed.* **2016**, *55*, 8448–8451.
- [130] a) V. Pozhydaiev, M. Power, V. Gandon, J. Moran, D. Lebœuf, *Chem. Commun.* **2020**, *56*, 11548–11564; b) J. Wencel-Delord, F. Colobert, *Org. Chem. Front.* **2016**, *3*, 394–400; c) P. A. Champagne, Y. Benhassine, J. Desroches, J.-F. Paquin, *Angew. Chem. Int. Ed.* **2014**, *53*, 13835–13839; d) J.-P. Bégué, D. Bonnet-Delpon, B. Crousse, *Synlett* **2004**, 18–29.
- [131] A. R. A. Spencer, R. Grainger, A. Panigrahi, T. J. Lepper, K. Bentkowska, I. Larrosa, *Chem. Commun.* **2020**, *56*, 14479–14482.
- [132] M. Faraday, *Annalen der Physik* **1834**, *109*, 433–451.
- [133] a) H. Kolbe, *Liebigs Ann. Chem.* **1849**, *69*, 257–294; b) H. Kolbe, *Liebigs Ann. Chem.* **1848**, *64*, 339–341.
- [134] a) S. Mohle, M. Zirbes, E. Rodrigo, T. Gieshoff, A. Wiebe, S. R. Waldvogel, *Angew. Chem. Int. Ed.* **2018**, *57*, 6018–6041; b) R. Francke, R. D. Little, *Chem. Soc. Rev.* **2014**, *43*, 2492–2521; c) J.-i. Yoshida, K. Kataoka, R. Horcajada, A. Nagaki, *Chem. Rev.* **2008**, *108*, 2265–2299; d) J. B. Sperry, D. L. Wright, *Chem. Soc. Rev.* **2006**, *35*, 605–621; e) R. D. Little, K. D. Moeller, *Electrochem. Soc. Interface* **2002**, *11*, 36–42.
- [135] A. Wiebe, T. Gieshoff, S. Möhle, E. Rodrigo, M. Zirbes, S. R. Waldvogel, *Angew. Chem. Int. Ed.* **2018**, *57*, 5594–5619.
- [136] D. S. P. Cardoso, B. Šljukić, D. M. F. Santos, C. A. C. Sequeira, *Org. Process Res. Dev.* **2017**, *21*, 1213–1226.
- [137] M. M. Baizer, *J. Electrochem. Soc.* **1964**, *111*, 215.
- [138] J. H. Simons, *J. Electrochem. Soc.* **1949**, *95*, 47.
- [139] a) Y. Jiang, K. Xu, C. Zeng, *Chem. Rev.* **2018**, *118*, 4485–4540; b) B. R. Rosen, E. W. Werner, A. G. O'Brien, P. S. Baran, *J. Am. Chem. Soc.* **2014**, *136*, 5571–5574; c) R. Scheffold, S. Abrecht, R. Orlinski, H.-R. Ruf, P. Stamouli, O. Tinembart, L. Walder, C. Weymuth, *Pure Appl. Chem.* **1987**, *59*, 363–372.
- [140] a) M. Oliva, G. A. Coppola, E. V. Van der Eycken, U. K. Sharma, *Adv. Synth. Catal.* **2021**, *363*, 1810–1834; b) M. D. Kärkäs, *Chem. Soc. Rev.* **2018**, *47*, 5786–5865.
- [141] M. Rafiee, F. Wang, D. P. Hruszkewycz, S. S. Stahl, *J Am Chem Soc* **2018**, *140*, 22–25.
- [142] H. Wang, K. Liang, W. Xiong, S. Samanta, W. Li, A. Lei, *Sci. Adv.* **2020**, *6*, eaaz0590.
- [143] a) R. Hayashi, A. Shimizu, Y. Song, Y. Ashikari, T. Nokami, J.-i. Yoshida, *Chem. Eur. J.* **2017**, *23*, 61–64; b) R. Hayashi, A. Shimizu, J.-i. Yoshida, *J. Am. Chem. Soc.* **2016**, *138*, 8400–8403; c) T. Morofuji, A. Shimizu, J.-i. Yoshida, *J. Am. Chem. Soc.* **2014**, *136*, 4496–4499.
- [144] Z.-W. Hou, D.-J. Liu, P. Xiong, X.-L. Lai, J. Song, H.-C. Xu, *Angew. Chem. Int. Ed.* **2021**, *60*, 2943–2947.

- [145] a) M. Berger, J. D. Herszman, Y. Kurimoto, G. H. M. de Kruijff, A. Schull, S. Ruf, S. R. Waldvogel, *Chem Sci* **2020**, *11*, 6053–6057; b) J. Xiang, M. Shang, Y. Kawamata, H. Lundberg, S. H. Reisberg, M. Chen, P. Mykhailiuk, G. Beutner, M. R. Collins, A. Davies, M. Del Bel, G. M. Gallego, J. E. Spangler, J. Starr, S. Yang, D. G. Blackmond, P. S. Baran, *Nature* **2019**, *573*, 398–402.
- [146] a) T. Fuchigami, S. Inagi, *Acc. Chem. Res.* **2020**, *53*, 322–334; b) T. Fuchigami, S. Inagi, *Chem. Commun.* **2011**, *47*, 10211–10223; c) K. M. Dawood, *Tetrahedron* **2004**, *60*, 1435–1451.
- [147] a) J. H. Simons, H. T. Francis, J. A. Hogg, *J. Electrochem. Soc.* **1949**, *95*, 53; b) J. H. Simons, W. J. Harland, *J. Electrochem. Soc.* **1949**, *95*, 55; c) J. H. Simons, W. H. Pearlson, T. J. Brice, W. A. Wilson, R. D. Dresdner, *J. Electrochem. Soc.* **1949**, *95*, 59; d) J. H. Simons, R. D. Dresdner, *J. Electrochem. Soc.* **1949**, *95*, 64.
- [148] a) S. Mattsson, G. Senges, S. Riedel, B. Paulus, *Chem. Eur. J.* **2020**, *26*, 10781–10786; b) P. Sartori, N. Ignat'ev, *J. Fluorine Chem.* **1998**, *87*, 157–162; c) P. Sartori, N. Ignat'ev, S. Datsenko, *J. Fluorine Chem.* **1995**, *75*, 157–161; d) A. Dimitrov, S. Rüdiger, N. V. Ignatyev, S. Datsenko, *J. Fluorine Chem.* **1990**, *50*, 197–205.
- [149] Y. Hou, S. Higashiya, T. Fuchigami, *Electrochim. Acta* **2000**, *45*, 3005–3010.
- [150] V. Dinoiu, T. Fukuhara, K. Miura, N. Yoneda, *J. Fluorine Chem.* **2003**, *121*, 227–231.
- [151] a) K. Momota, K. Mukai, K. Kato, M. Morita, *Electrochim. Acta* **1998**, *43*, 2503–2514; b) S. M. Lee, J. M. Roseman, C. Blair Zartman, E. P. Morrison, S. J. Harrison, C. A. Stankiewicz, W. J. Middleton, *J. Fluorine Chem.* **1996**, *77*, 65–70.
- [152] a) T. Tajima, H. Kurihara, A. Nakajima, T. Fuchigami, *J. Electroanal. Chem.* **2005**, *580*, 155–160; b) T. Tajima, H. Ishii, T. Fuchigami, *Electrochem. Commun.* **2002**, *4*, 589–592.
- [153] T. Sawamura, K. Takahashi, S. Inagi, T. Fuchigami, *Angew. Chem. Int. Ed.* **2012**, *51*, 4413–4416.
- [154] N. Shida, H. Takenaka, A. Gotou, T. Isogai, A. Yamauchi, Y. Kishikawa, Y. Nagata, I. Tomita, T. Fuchigami, S. Inagi, *J. Org. Chem.* **2021**, *86*, 16128–16133.
- [155] P. Peng, X. Yan, K. Zhang, Z. Liu, L. Zeng, Y. Chen, H. Zhang, A. Lei, *Nat Commun* **2021**, *12*, 3075.
- [156] N. Sauermann, T. H. Meyer, Y. Qiu, L. Ackermann, *ACS Catal.* **2018**, *8*, 7086–7103.
- [157] P. Alfonso-Suárez, A. V. Kolliopoulos, J. P. Smith, C. E. Banks, A. M. Jones, *Tetrahedron Lett.* **2015**, *56*, 6863–6867.
- [158] a) A. M. Jones, C. E. Banks, *Beilstein Journal of Organic Chemistry* **2014**, *10*, 3056–3072; b) T. Shono, H. Hamaguchi, Y. Matsumura, *J. Am. Chem. Soc.* **1975**, *97*, 4264–4268.
- [159] X. Tan, L. Massignan, X. Hou, J. Frey, J. C. A. Oliveira, M. N. Hussain, L. Ackermann, *Angew. Chem. Int. Ed.* **2021**, *60*, 13264–13270.
- [160] a) C. A. Malapit, M. B. Prater, J. R. Cabrera-Pardo, M. Li, T. D. Pham, T. P. McFadden, S. Blank, S. D. Minter, *Chem. Rev.* **2022**, *122*, 3180–3218; b) L. F. T. Novaes, J. Liu, Y. Shen, L. Lu, J. M. Meinhardt, S. Lin, *Chem. Soc. Rev.* **2021**, *50*, 7941–8002; c) C. Ma, P. Fang, D. Liu, K.-J. Jiao, P.-S. Gao, H. Qiu, T.-S. Mei, *Chem. Sci.* **2021**, *12*, 12866–12873; d) A. Dey, T. B. Gunnoe, V. R. Stamenkovic, *ACS Catal.* **2020**, *10*, 13156–13158; e) P. Gandeepan, L. H. Finger, T. H. Meyer, L.



- Ackermann, *Chem. Soc. Rev.* **2020**, *49*, 4254–4272; f) L. Ackermann, *Acc. Chem. Res.* **2020**, *53*, 84–104; g) N. Sauermann, T. H. Meyer, L. Ackermann, *Chem. Eur. J.* **2018**, *24*, 16209–16217; h) C. Ma, P. Fang, T.-S. Mei, *ACS Catal.* **2018**, *8*, 7179–7189.
- [161] C. Amatore, C. Cammoun, A. Jutand, *Adv. Synth. Catal.* **2007**, *349*, 292–296.
- [162] F. Kakiuchi, T. Kochi, H. Mutsutani, N. Kobayashi, S. Urano, M. Sato, S. Nishiyama, T. Tanabe, *J. Am. Chem. Soc.* **2009**, *131*, 11310–11311.
- [163] H. Aiso, T. Kochi, H. Mutsutani, T. Tanabe, S. Nishiyama, F. Kakiuchi, *J. Org. Chem.* **2012**, *77*, 7718–7724.
- [164] Q.-L. Yang, Y.-Q. Li, C. Ma, P. Fang, X.-J. Zhang, T.-S. Mei, *J. Am. Chem. Soc.* **2017**, *139*, 3293–3298.
- [165] Y.-Q. Li, Q.-L. Yang, P. Fang, T.-S. Mei, D. Zhang, *Org. Lett.* **2017**, *19*, 2905–2908.
- [166] A. Shrestha, M. Lee, A. L. Dunn, M. S. Sanford, *Org. Lett.* **2018**, *20*, 204–207.
- [167] Q.-L. Yang, C.-Z. Li, L.-W. Zhang, Y.-Y. Li, X. Tong, X.-Y. Wu, T.-S. Mei, *Organometallics* **2019**, *38*, 1208–1212.
- [168] C. Ma, C.-Q. Zhao, Y.-Q. Li, L.-P. Zhang, X.-T. Xu, K. Zhang, T.-S. Mei, *Chem. Commun.* **2017**, *53*, 12189–12192.
- [169] a) W. Wei, A. Scheremetjew, L. Ackermann, *Chem. Sci.* **2022**, *13*, 2783–2788; b) J. Frey, X. Hou, L. Ackermann, *Chem. Sci.* **2022**, *13*, 2729–2734; c) U. Dhawa, T. Wdowik, X. Hou, B. Yuan, J. C. A. Oliveira, L. Ackermann, *Chem. Sci.* **2021**, *12*, 14182–14188; d) U. Dhawa, C. Tian, T. Wdowik, J. C. A. Oliveira, J. Hao, L. Ackermann, *Angew. Chem. Int. Ed.* **2020**, *59*, 13451–13457.
- [170] a) S. Sunny, R. Karvembu, *Adv. Synth. Catal.* **2021**, *363*, 4309–4331; b) S. Prakash, R. Kuppusamy, C.-H. Cheng, *ChemCatChem* **2018**, *10*, 683–705; c) T. Yoshino, S. Matsunaga, **2017**, pp. 197–247; d) M. Moselage, J. Li, L. Ackermann, *ACS Catal.* **2016**, *6*, 498–525; e) K. Gao, N. Yoshikai, *Acc. Chem. Res.* **2014**, *47*, 1208–1219.
- [171] N. Sauermann, T. H. Meyer, C. Tian, L. Ackermann, *J. Am. Chem. Soc.* **2017**, *139*, 18452–18455.
- [172] C. Tian, L. Massignan, T. H. Meyer, L. Ackermann, *Angew. Chem. Int. Ed.* **2018**, *57*, 2383–2387.
- [173] S. Tang, D. Wang, Y. Liu, L. Zeng, A. Lei, *Nat. Commun.* **2018**, *9*, 798.
- [174] a) S. C. Sau, R. Mei, J. Struwe, L. Ackermann, *ChemSusChem* **2019**, *12*, 3023–3027; b) L. Zeng, H. Li, S. Tang, X. Gao, Y. Deng, G. Zhang, C.-W. Pao, J.-L. Chen, J.-F. Lee, A. Lei, *ACS Catal.* **2018**, *8*, 5448–5453.
- [175] R. Mei, N. Sauermann, J. C. A. Oliveira, L. Ackermann, *J. Am. Chem. Soc.* **2018**, *140*, 7913–7921.
- [176] U. Dhawa, C. Tian, W. Li, L. Ackermann, *ACS Catal.* **2020**, *10*, 6457–6462.
- [177] T. H. Meyer, J. C. A. Oliveira, S. C. Sau, N. W. J. Ang, L. Ackermann, *ACS Catal.* **2018**, *8*, 9140–9147.
- [178] C. Tian, T. H. Meyer, M. Stangier, U. Dhawa, K. Rauch, L. H. Finger, L. Ackermann, *Nat. Protoc.* **2020**, *15*, 1760–1774.
- [179] T. H. Meyer, J. C. A. Oliveira, D. Ghorai, L. Ackermann, *Angew. Chem. Int. Ed.* **2020**, *59*, 10955–10960.

- [180] S.-K. Zhang, R. C. Samanta, N. Sauermann, L. Ackermann, *Chem. Eur. J.* **2018**, *24*, 19166–19170.
- [181] S.-K. Zhang, J. Struwe, L. Hu, L. Ackermann, *Angew. Chem. Int. Ed.* **2020**, *59*, 3178–3183.
- [182] Q. L. Yang, X. Y. Wang, J. Y. Lu, L. P. Zhang, P. Fang, T. S. Mei, *J Am Chem Soc* **2018**, *140*, 11487–11494.
- [183] C. Tian, U. Dhawa, A. Scheremetjew, L. Ackermann, *ACS Catal.* **2019**, *9*, 7690–7696.
- [184] C. Zhu, M. Stangier, J. C. A. Oliveira, L. Massignan, L. Ackermann, *Chem. Eur. J.* **2019**, *25*, 16382–16389.
- [185] L. Massignan, C. Zhu, X. Hou, J. C. A. Oliveira, A. Salamé, L. Ackermann, *ACS Catal.* **2021**, *11*, 11639–11649.
- [186] F. Zhang, D. R. Spring, *Chem. Soc. Rev.* **2014**, *43*, 6906–6919.
- [187] H. Weissman, X. Song, D. Milstein, *J. Am. Chem. Soc.* **2001**, *123*, 337–338.
- [188] a) G. Duarah, P. P. Kaishap, T. Begum, S. Gogoi, *Adv. Synth. Catal.* **2019**, *361*, 654–672; b) P. B. Arockiam, C. Bruneau, P. H. Dixneuf, *Chem. Rev.* **2012**, *112*, 5879–5918.
- [189] a) F. Xu, Y.-J. Li, C. Huang, H.-C. Xu, *ACS Catal.* **2018**, *8*, 3820–3824; b) Y. Qiu, C. Tian, L. Massignan, T. Rogge, L. Ackermann, *Angew. Chem. Int. Ed.* **2018**, *57*, 5818–5822.
- [190] a) X. Tan, X. Hou, T. Rogge, L. Ackermann, *Angew. Chem. Int. Ed.* **2021**, *60*, 4619–4624; b) L. Yang, R. Steinbock, A. Scheremetjew, R. Kuniyil, L. H. Finger, A. M. Messinis, L. Ackermann, *Angew. Chem. Int. Ed.* **2020**, *59*, 11130–11135; c) Z.-Q. Wang, C. Hou, Y.-F. Zhong, Y.-X. Lu, Z.-Y. Mo, Y.-M. Pan, H.-T. Tang, *Org. Lett.* **2019**, *21*, 9841–9845; d) R. Mei, J. Koeller, L. Ackermann, *Chem. Commun.* **2018**, *54*, 12879–12882.
- [191] X. Hou, N. Kaplaneris, B. Yuan, J. Frey, T. Ohyama, A. M. Messinis, L. Ackermann, *Chem Sci* **2022**, *13*, 3461–3467.
- [192] Y. Wang, H. Simon, X. Chen, Z. Lin, S. Chen, L. Ackermann, *Angew. Chem. Int. Ed.* **2022**, e202201595.
- [193] a) Y. Qiu, C. Zhu, M. Stangier, J. Struwe, L. Ackermann, *CCS Chem.* **2021**, *3*, 1529–1552; b) Y. Qiu, W.-J. Kong, J. Struwe, N. Sauermann, T. Rogge, A. Scheremetjew, L. Ackermann, *Angew. Chem. Int. Ed.* **2018**, *57*, 5828–5832.
- [194] Y. Zhang, J. Struwe, L. Ackermann, *Angew. Chem. Int. Ed.* **2020**, *59*, 15076–15080.
- [195] I. Choi, A. M. Messinis, X. Hou, L. Ackermann, *Angew. Chem. Int. Ed.* **2021**, *60*, 27005–27012.
- [196] Y. Qiu, A. Scheremetjew, L. Ackermann, *J. Am. Chem. Soc.* **2019**, *141*, 2731–2738.
- [197] W.-J. Kong, L. H. Finger, J. C. A. Oliveira, L. Ackermann, *Angew. Chem. Int. Ed.* **2019**, *58*, 6342–6346.
- [198] W.-J. Kong, Z. Shen, L. H. Finger, L. Ackermann, *Angew. Chem. Int. Ed.* **2020**, *59*, 5551–5556.
- [199] Z.-J. Wu, F. Su, W. Lin, J. Song, T.-B. Wen, H.-J. Zhang, H.-C. Xu, *Angew. Chem. Int. Ed.* **2019**, *58*, 16770–16774.

- [200] Y. Wang, J. C. A. Oliveira, Z. Lin, L. Ackermann, *Angew. Chem. Int. Ed.* **2021**, *60*, 6419–6424.
- [201] Y.-K. Xing, X.-R. Chen, Q.-L. Yang, S.-Q. Zhang, H.-M. Guo, X. Hong, T.-S. Mei, *Nat. Commun.* **2021**, *12*, 930.
- [202] Q.-L. Yang, Y.-K. Xing, X.-Y. Wang, H.-X. Ma, X.-J. Weng, X. Yang, H.-M. Guo, T.-S. Mei, *J. Am. Chem. Soc.* **2019**, *141*, 18970–18976.
- [203] a) R. Karmakar, P. Pahari, D. Mal, *Chem. Rev.* **2014**, *114*, 6213–6284; b) J. J. Beck, S.-C. Chou, *J. Nat. Prod.* **2007**, *70*, 891–900.
- [204] W. K. Anderson, T. L. Boehm, G. M. Makara, R. T. Swann, *J. Med. Chem.* **1996**, *39*, 46–55.
- [205] S. Messaoudi, J.-D. Brion, M. Alami, *Eur. J. Org. Chem.* **2010**, *2010*, 6495–6516.
- [206] M. Gulias, J. L. Mascarenas, *Angew. Chem. Int. Ed.* **2016**, *55*, 11000–11019.
- [207] a) J. L. Röckl, M. Dörr, S. R. Waldvogel, *ChemElectroChem* **2020**, *7*, 3686–3694; b) I. Colomer, A. E. R. Chamberlain, M. B. Haughey, T. J. Donohoe, *Nat. Rev. Chem.* **2017**, *1*, 88; c) A. Berkessel, J. A. Adrio, D. Hüttenhain, J. M. Neudörfl, *J. Am. Chem. Soc.* **2006**, *128*, 8421–8426.
- [208] D. M. Heard, A. J. J. Lennox, *Angew. Chem. Int. Ed.* **2020**, *59*, 18866–18884.
- [209] Y. Qiu, M. Stangier, T. H. Meyer, J. C. A. Oliveira, L. Ackermann, *Angew. Chem. Int. Ed.* **2018**, *57*, 14179–14183.
- [210] D. Lapointe, K. Fagnou, *Chem. Lett.* **2010**, *39*, 1118–1126.
- [211] T. H. Meyer, *Dissertation 2021*, Georg-August-Universität Göttingen.
- [212] M. Quan, D. Sanchez, M. F. Wasylkiw, D. K. Smith, *J. Am. Chem. Soc.* **2007**, *129*, 12847–12856.
- [213] F. Zhen, P. Hapiot, *Electrochemical Science Advances* **2022**, *n/a*, e2100148.
- [214] a) H. Yousofian-Varzaneh, H. R. Zare, M. Namazian, *J. Electrochem. Soc.* **2015**, *162*, G63–G68; b) P. A. Staley, C. M. Newell, D. P. Pullman, D. K. Smith, *Anal. Chem.* **2014**, *86*, 10917–10924.
- [215] a) C. He, W. G. Whitehurst, M. J. Gaunt, *Chem* **2019**, *5*, 1031–1058; b) M. A. Larsen, J. F. Hartwig, *J. Am. Chem. Soc.* **2014**, *136*, 4287–4299.
- [216] Z. Shen, P. K. Dornan, H. A. Khan, T. K. Woo, V. M. Dong, *J. Am. Chem. Soc.* **2009**, *131*, 1077–1091.
- [217] a) A. Gaspar, M. J. Matos, J. Garrido, E. Uriarte, F. Borges, *Chem. Rev.* **2014**, *114*, 4960–4992; b) R. S. Keri, S. Budagumpi, R. K. Pai, R. G. Balakrishna, *Eur. J. Med. Chem.* **2014**, *78*, 340–374.
- [218] L. Zocchi, S. C. Wu, J. Wu, K. L. Hayama, C. A. Benavente, *Oncotarget* **2018**, *9*, 23505–23518.
- [219] S. Baruah, P. P. Kaishap, S. Gogoi, *Chem. Commun.* **2016**, *52*, 13004–13007.
- [220] M. Stangier, A. M. Messinis, J. C. A. Oliveira, H. Yu, L. Ackermann, *Nat. Commun.* **2021**, *12*, 4736.
- [221] a) A. Henninot, J. C. Collins, J. M. Nuss, *J. Med. Chem.* **2018**, *61*, 1382–1414; b) M. A. T. Blaskovich, *J. Med. Chem.* **2016**, *59*, 10807–10836.
- [222] J. Ohata, S. C. Martin, Z. T. Ball, *Angew. Chem. Int. Ed.* **2019**, *58*, 6176–6199.

- [223] a) A. G. Neo, C. López, V. Romero, B. Antelo, J. Delamano, A. Pérez, D. Fernández, J. F. Almeida, L. Castedo, G. Tojo, *J. Org. Chem.* **2010**, *75*, 6764–6770; b) F. B. Mallory, C. S. Wood, J. T. Gordon, *J. Am. Chem. Soc.* **1964**, *86*, 3094–3102.
- [224] Y. Kang, T. Wang, Y. Liang, Y. Zhang, R. Wang, Z. Zhang, *RSC Adv.* **2017**, *7*, 44333–44339.
- [225] W.-J. Kong, L. H. Finger, A. M. Messinis, R. Kuniyil, J. C. A. Oliveira, L. Ackermann, *J. Am. Chem. Soc.* **2019**, *141*, 17198–17206.
- [226] T. Naveen, *Tetrahedron* **2021**, *84*, 132025.
- [227] a) T. Fuchigami, S. Inagi, in *Organic Electrochemistry: Revised and Expanded*, 5 ed. (Eds.: O. Hammerich, B. Speiser), CRC Press, Boca Raton, **2015**, pp. 807–828; b) T. Fuchigami, S. Inagi, in *Fundamentals and Applications of Organic Electrochemistry* (Eds.: T. Fuchigami, M. Atobe, S. Inagi), **2014**, pp. 83–128.
- [228] a) J. Ammer, H. Mayr, *J. Phys. Org. Chem.* **2013**, *26*, 59–63; b) S. Minegishi, S. Kobayashi, H. Mayr, *J. Am. Chem. Soc.* **2004**, *126*, 5174–5181; c) T. W. Bentley, P. v. R. Schleyer, *J. Am. Chem. Soc.* **1976**, *98*, 7658–7666.
- [229] A. Scheremetjew, *Dissertation* **2022**, Georg-August-Universität Göttingen.
- [230] M. Aoyama, T. Fukuhara, S. Hara, *J. Org. Chem.* **2008**, *73*, 4186–4189.
- [231] S. Zhang, L. Li, H. Wang, Q. Li, W. Liu, K. Xu, C. Zeng, *Org. Lett.* **2018**, *20*, 252–255.
- [232] B. W. Lund, F. Piu, N. K. Gauthier, A. Eeg, E. Currier, V. Sherbukhin, M. R. Brann, U. Hacksell, R. Olsson, *J. Med. Chem.* **2005**, *48*, 7517–7519.
- [233] Y.-J. Kang, J.-H. Oh, H. Seok, Y.-Y. Jo, D.-W. Kim, U. Garagiola, J.-Y. Choi, S.-G. Kim, *Appl. Sci.* **2020**, *10*, 1737.
- [234] E. Baciocchi, F. D'Acunzo, C. Galli, O. Lanzalunga, *J. Chem. Soc., Perkin Trans. 2* **1996**, 133–140.
- [235] a) S. Tang, R. Guillot, L. Grimaud, M. R. Vitale, G. Vincent, *Org. Lett.* **2022**, *24*, 2125–2130; b) T. Shen, T. H. Lambert, *J Am Chem Soc* **2021**, *143*, 8597–8602.
- [236] a) E. Baciocchi, M. Bietti, O. Lanzalunga, *Acc. Chem. Res.* **2000**, *33*, 243–251; b) M. Schmittel, A. Burghart, *Angew. Chem. Int. Ed.* **1997**, *36*, 2550–2589.
- [237] a) P. R. D. Murray, J. H. Cox, N. D. Chiappini, C. B. Roos, E. A. McLoughlin, B. G. Hejna, S. T. Nguyen, H. H. Ripberger, J. M. Ganley, E. Tsui, N. Y. Shin, B. Koronkiewicz, G. Qiu, R. R. Knowles, *Chem. Rev.* **2022**, *122*, 2017–2291; b) C. M. Morton, Q. Zhu, H. Ripberger, L. Troian-Gautier, Z. S. D. Toa, R. R. Knowles, E. J. Alexanian, *J. Am. Chem. Soc.* **2019**, *141*, 13253–13260; c) W. D. Morris, J. M. Mayer, *J. Am. Chem. Soc.* **2017**, *139*, 10312–10319; d) E. C. Gentry, R. R. Knowles, *Acc. Chem. Res.* **2016**, *49*, 1546–1556; e) H. G. Yayla, R. R. Knowles, *Synlett* **2014**, *25*, 2819–2826.
- [238] M. Stangier, A. M. Messinis, J. C. A. Oliveira, H. Yu, L. Ackermann, *Nat. Commun.* **2021**, *12*, 4736.
- [239] M. J. Mio, L. C. Kopel, J. B. Braun, T. L. Gadzikwa, K. L. Hull, R. G. Brisbois, C. J. Markworth, P. A. Grieco, *Org. Lett.* **2002**, *4*, 3199–3202.
- [240] B. G. Van den Hoven, B. E. Ali, H. Alper, *J. Org. Chem.* **2000**, *65*, 4131–4137.

- [241] D. Strübing, H. Neumann, S. Klaus, S. Hübner, M. Beller, *Tetrahedron* **2005**, *61*, 11333–11344.
- [242] B. M. Pierce, B. F. Simpson, K. H. Ferguson, R. E. Whittaker, *Org. Biomol. Chem.* **2018**, *16*, 6659–6662.
- [243] K. Hirano, A. T. Biju, I. Piel, F. Glorius, *J. Am. Chem. Soc.* **2009**, *131*, 14190–14191.
- [244] B. C. Raju, A. K. Tiwari, J. A. Kumar, A. Z. Ali, S. B. Agawane, G. Saidachary, K. Madhusudana, *Bioorganic & Medicinal Chemistry* **2010**, *18*, 358–365.
- [245] B. Djukic, P. K. Poddutoori, P. A. Dube, T. Seda, H. A. Jenkins, M. T. Lemaire, *Inorganic Chemistry* **2009**, *48*, 6109–6116.
- [246] N. U. S. Hofsløkken, Lars, *Acta Chem. Scand.* **1999**, *53*, 258–262.
- [247] D. J. Moon, M. Al-Amin, R. S. Lewis, K. M. Arnold, G. P. A. Yap, J. Sims-Mourtada, W. J. Chain, *Eur. J. Org. Chem.* **2018**, *2018*, 3348–3351.
- [248] a) K. A. Kalesh, L. P. Tan, K. Lu, L. Gao, J. Wang, S. Q. Yao, *Chem. Commun.* **2010**, *46*, 589–591; b) K. Shen, L. Qi, M. Ravula, *Synthesis* **2009**, *2009*, 3765–3768.
- [249] Bruker, *SAINT+ Integration Engine and Data Reduction Software*, v8.38A, Bruker AXS Inc., Madison, Wisconsin, USA, **2015**.
- [250] Bruker, *SADABS Bruker AXS Area Detector Scaling and Absorption Correction*, 2016/2, Bruker AXS Inc., Madison, Wisconsin, USA, **2016**.
- [251] G. Sheldrick, *Acta Crystallogr. A* **2015**, *71*, 3–8.
- [252] G. Sheldrick, *Acta Crystallogr. C* **2015**, *71*, 3–8.
- [253] O. V. Dolomanov, L. J. Bourhis, R. J. Gildea, J. A. K. Howard, H. Puschmann, *J. Appl. Crystallogr.* **2009**, *42*, 339–341.
- [254] F. Zhu, Z. Wang, Y. Li, X.-F. Wu, *Chem. Eur. J.* **2017**, *23*, 3276–3279.
- [255] R. Bam, W. A. Chalifoux, *J. Org. Chem.* **2018**, *83*, 9929–9938.
- [256] M. Yoshida, K. Saito, Y. Fujino, T. Doi, *Chem. Commun.* **2012**, *48*, 11796–11798.
- [257] H. Wang, F. Xie, Z. Qi, X. Li, *Org. Lett.* **2015**, *17*, 920–923.
- [258] M. Yoshida, Y. Fujino, T. Doi, *Org. Lett.* **2011**, *13*, 4526–4529.
- [259] J. Sheng, H.-Q. Ni, H.-R. Zhang, K.-F. Zhang, Y.-N. Wang, X.-S. Wang, *Angew. Chem. Int. Ed.* **2018**, *57*, 7634–7639.
- [260] W. Deng, W. Feng, Y. Li, H. Bao, *Org. Lett.* **2018**, *20*, 4245–4249.
- [261] O. A. Wong, Y. Shi, *J. Org. Chem.* **2009**, *74*, 8377–8380.
- [262] S. Zhao, Y. Guo, Z. Su, W. Cao, C. Wu, Q.-Y. Chen, *Org. Lett.* **2020**, *22*, 8634–8637.

## **7 APPENDIX**

## ACKNOWLEDGMENT

Zuallererst möchte ich mich sehr herzlich bei meinem Doktorvater Prof. Dr. Lutz Ackermann bedanken, für die Möglichkeit meine Promotion in seinem Team unter exzellenten Bedingungen, in wissenschaftlicher, aber auch persönlicher Hinsicht, anzufertigen. Die Mischung aus wertvollen Ratschlägen, akademischem Input, und des entgegen gebrachten Vertrauens, eigene Ideen zu verfolgen und zu realisieren, haben mir ein ideales Umfeld für eine erfolgreiche Promotion gegeben.

Bei Prof. Dr. Koszinowski möchte ich mich für die Übernahme des Zweitgutachtens und die hilfreichen Besprechungen bedanken. Ebenso möchte ich den Mitgliedern der Prüfungskommission Prof. Dr. Stalke, Jun.-Prof. Walker, Dr. Janßen-Müller und Dr. John für deren Mitwirken danken.

Einen besonderen Dank möchte ich an die analytischen Abteilungen des IOBCs, für die Messung meiner Proben und wertvollen Hilfen bei Problemen, richten. Besonders hervorzuheben ist dabei Dr. John, der mir half, knifflige Fragestellungen hinsichtlich komplexerer NMR Analytik zu beantworten. Vielen Dank an dieser Stelle auch an Dr. Golz für das Messen und die Lösung der Kristallstrukturen.

Bei Bianca und Gabi möchte ich mich für die Unterstützung bei bürokratischen Anliegen bedanken. Stefan danke ich sehr für die Freundschaft, die Hilfe bei allen möglichen Problemen und die Betreuung der Geräte, welche sehr bedeutsam für die reibungslose wissenschaftliche Arbeit sind. Außerdem möchte ich mich bei Karsten für die Bereitstellung von Katalysatoren, trockener Lösungsmittel und anderer Geräte bedanken.

Des Weiteren möchte ich den Werkstätten der Universität Göttingen der chemischen Institute danken, für die kreative und zuverlässige Umsetzung von Ideen und Aufträgen hinsichtlich neuer Set-Ups, Reparaturen oder anderer technischer Lösungen. Hervorzuheben sind an dieser Stelle vor allem Van Thao Nguyen (Mechanik), Annika von Roden-Wendhausen (Glastechnik) und Stephan Dullnig sowie Dominik Oberdiek (beide Elektronik).

I would like to thank Matthew, Johanna, Nikos, Suman, Hendrik, Alexej, Philipp, Lin, Simon, Jun, and Tsuyoshi for their helpful proofreading. Additionally, I would like to thank my co-workers Youai, João, Antonis, Alexej and Tjark among many others for the fruitful and inspiring collaboration during the work on different projects. I really appreciated to work

in neighborhood to Nikos, who was always helpful and my first colleague to discuss scientific questions.

I particularly thank my lab mates during my PhD namely, Julia, Wen, Johanna, Agnese, Jongwoo, Hui and Melanie for the fun atmosphere and chats about all different topics. Of course, I would like to thank all the other group members who made working in the Ackermann group and the free time activities so enjoyable. Special moments during the group trip to Cuxhaven, BBQs, soccer sessions, PhD parties and many more will keep you in my memories. Especially I would like to thank João, Julia, Lina, Stefan, Nikos and Lin as well as the former group members Tjark, Leonardo, Ramesh, Benz, Jongwoo, Thomas, Cuiju for the great times and your friendships! Your accompany made the time in Göttingen extremely valuable.

Außerdem möchte ich meinen Bachelorstudenten Jan Fleischer und Linus Groß für deren motivierte Mitarbeit an den verschiedenen Projekten danken.

Abschließend möchte ich meinen größten Dank meiner Familie, besonders meinen Eltern und meinem Stiefvater, aussprechen, die mir mein Studium überhaupt ermöglicht, mich immer bestmöglich unterstützt und starken Rückhalt geboten haben. Jacqueline danke ich für Ihre grenzenlose Liebe, bedingungslose Unterstützung, auch wenn uns meine Laufbahn zeitweise geographisch getrennt hat, Kraft, auch in stressigen Zeiten, und vielem mehr. All das war so wichtig, um diesen schönen, aber auch anstrengenden Lebensabschnitt zu meistern.

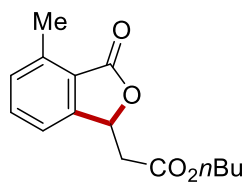
Maximilian Stangier

Mai 2022

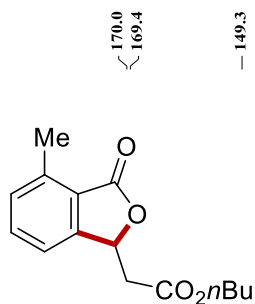
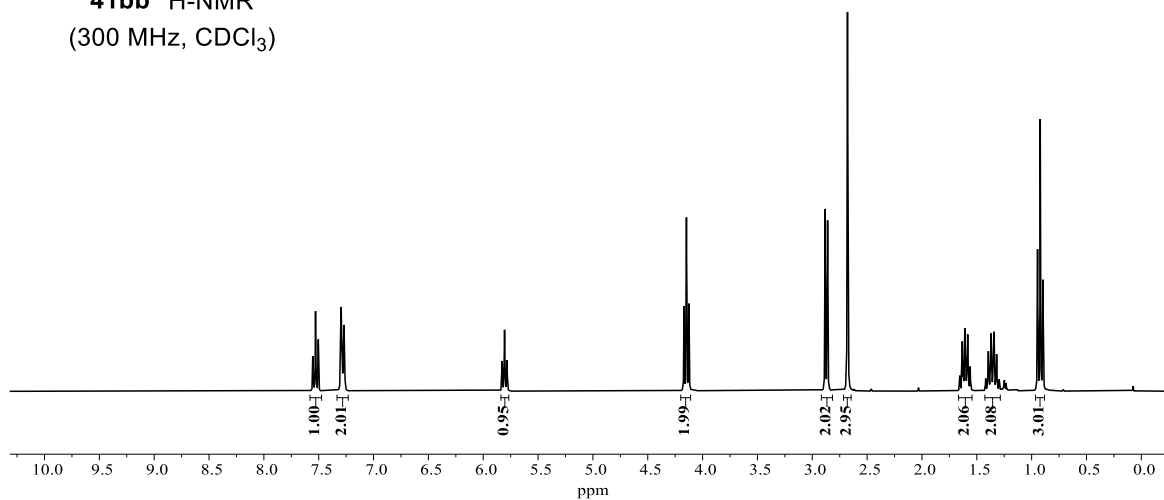




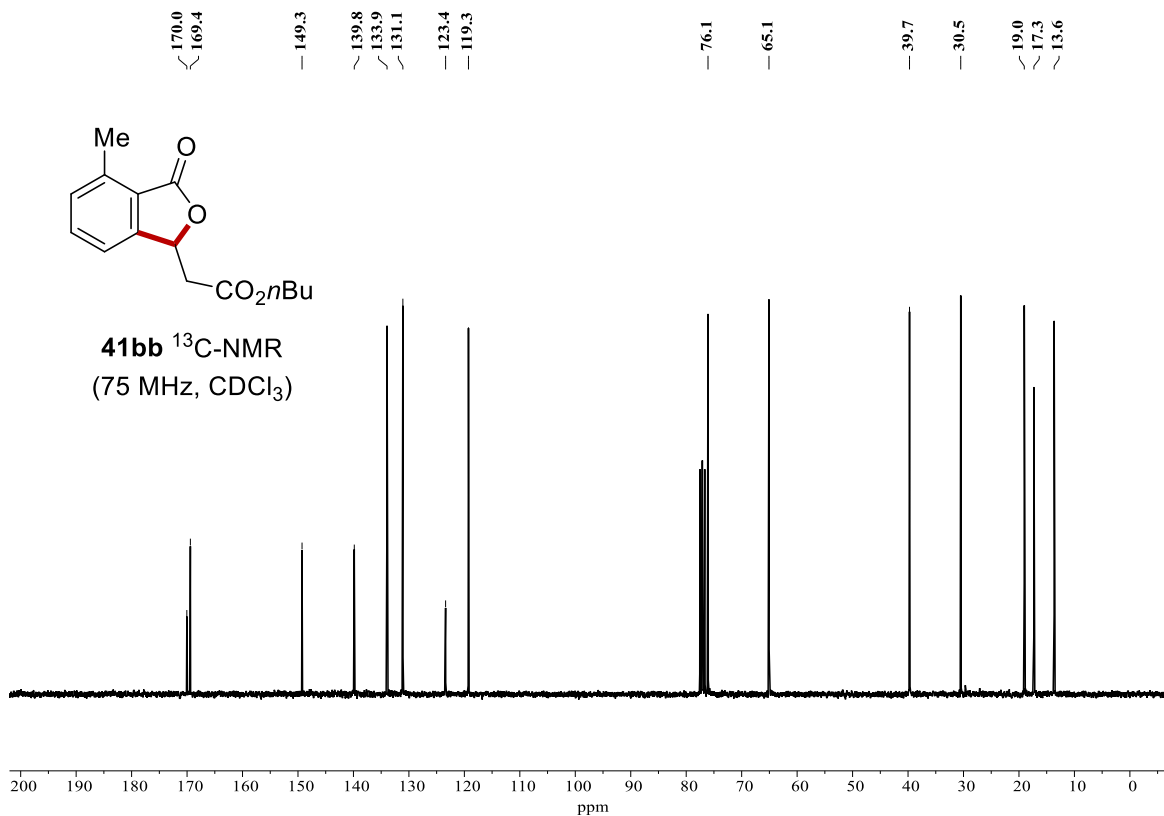
## 7.1 NMR Spectra

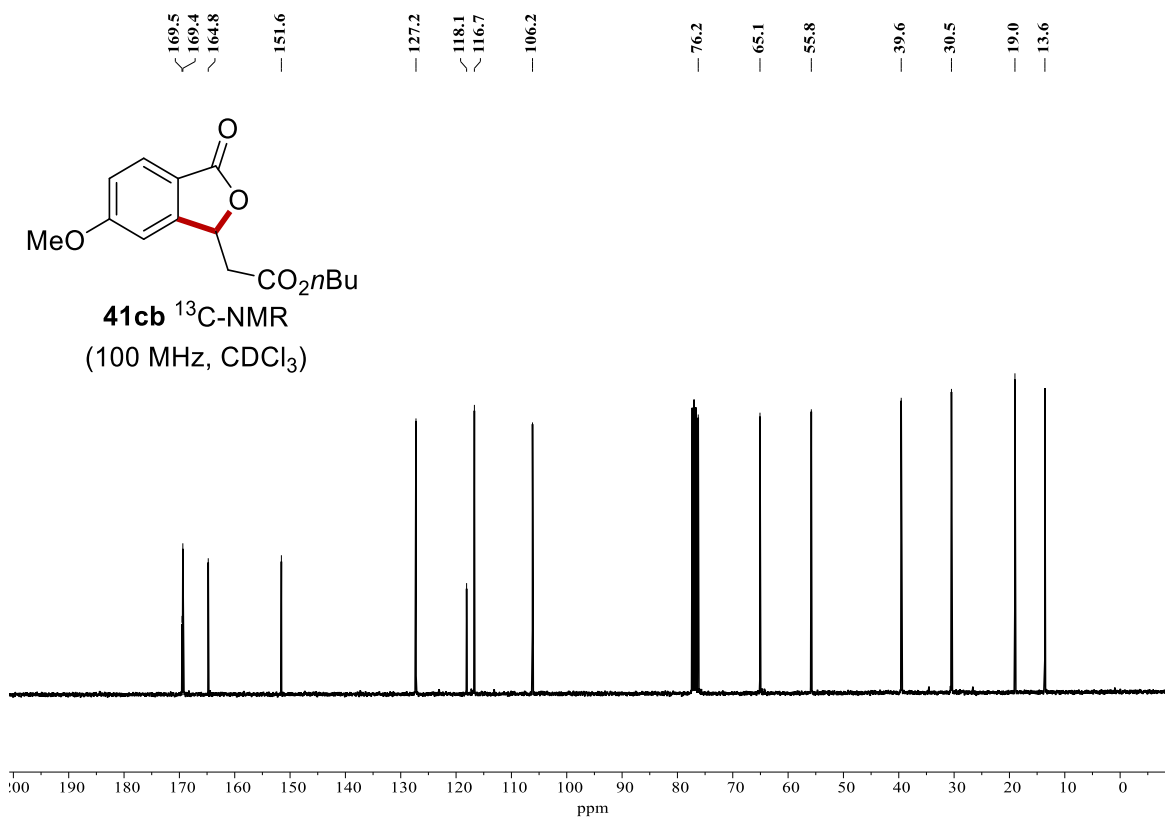
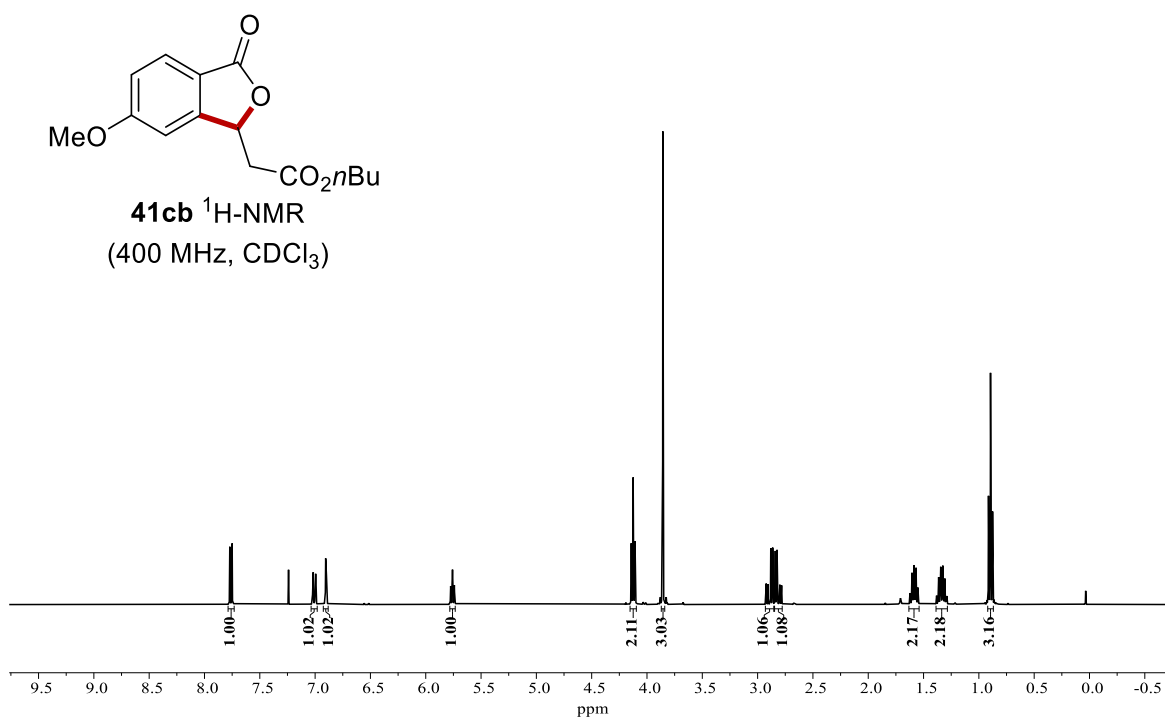


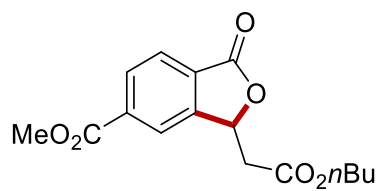
**41bb**  $^1\text{H-NMR}$   
(300 MHz,  $\text{CDCl}_3$ )



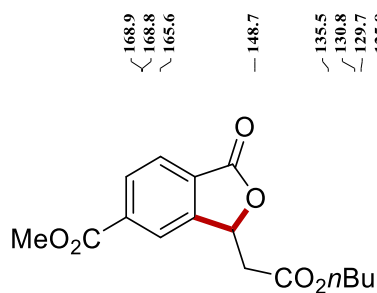
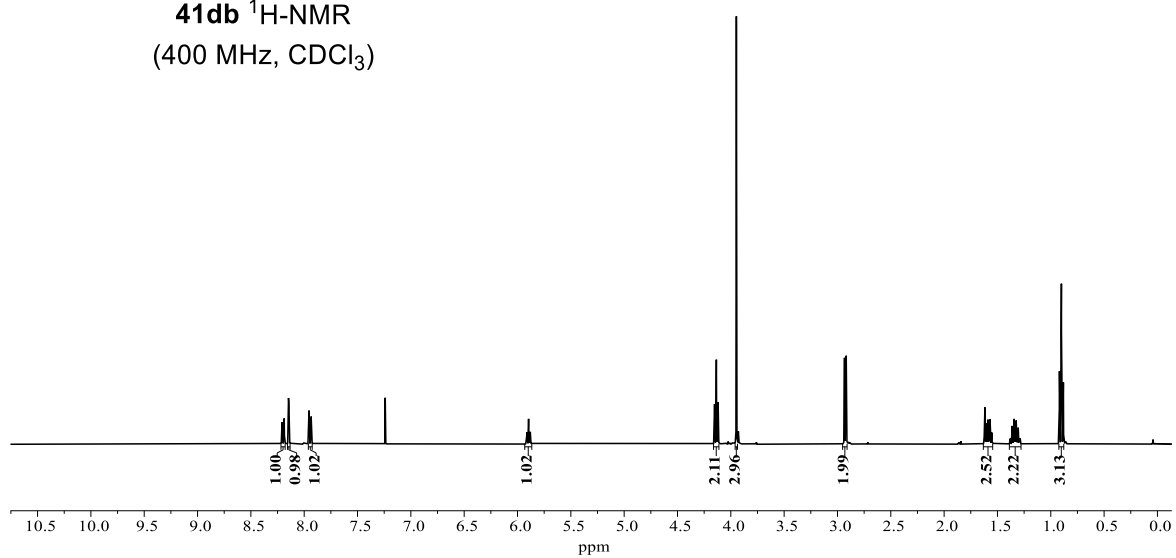
**41bb**  $^{13}\text{C-NMR}$   
(75 MHz,  $\text{CDCl}_3$ )



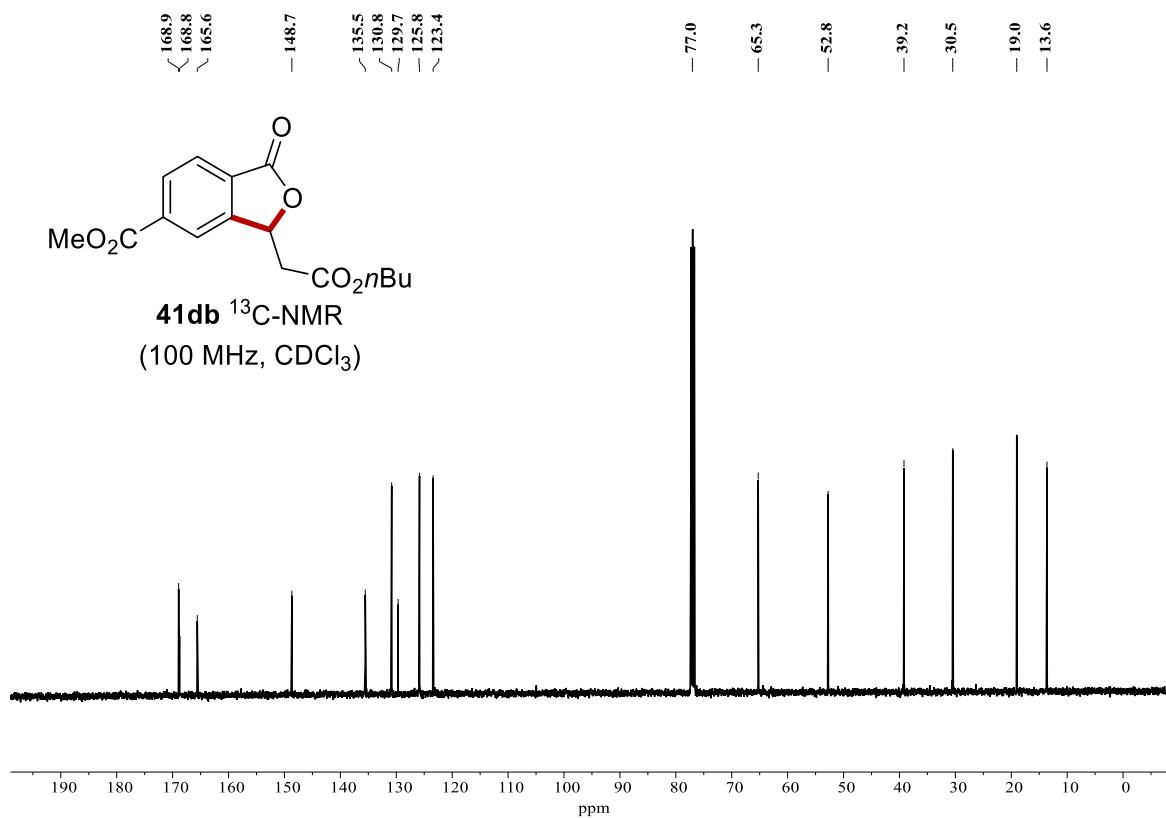


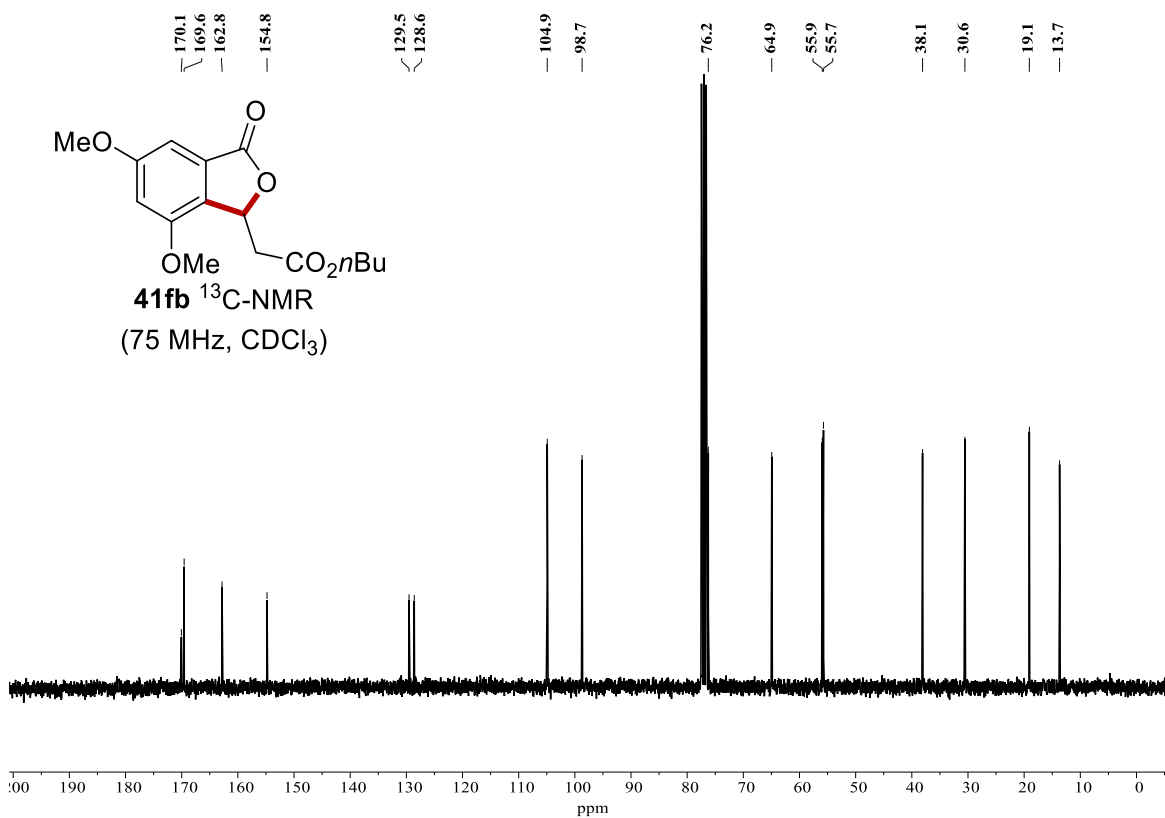
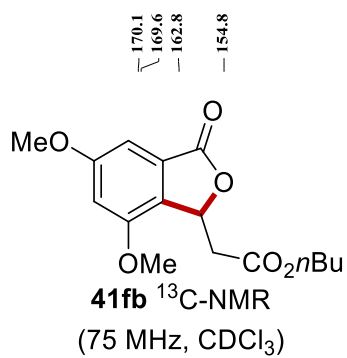
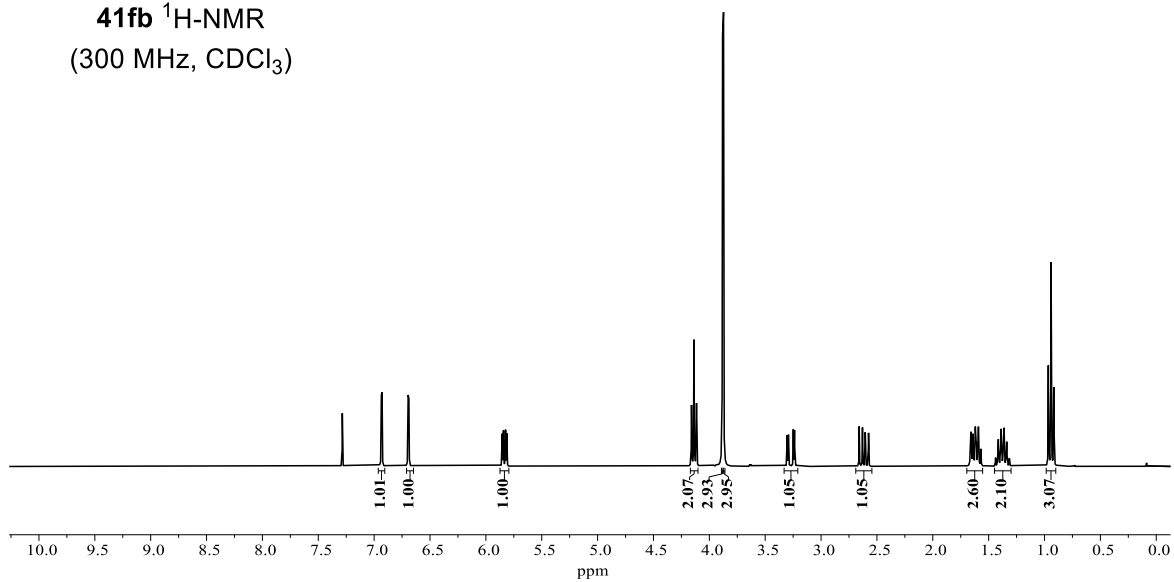
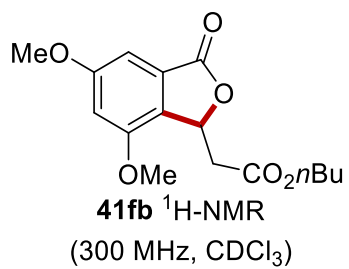


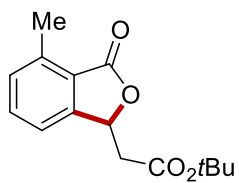
**41db** <sup>1</sup>H-NMR  
(400 MHz, CDCl<sub>3</sub>)



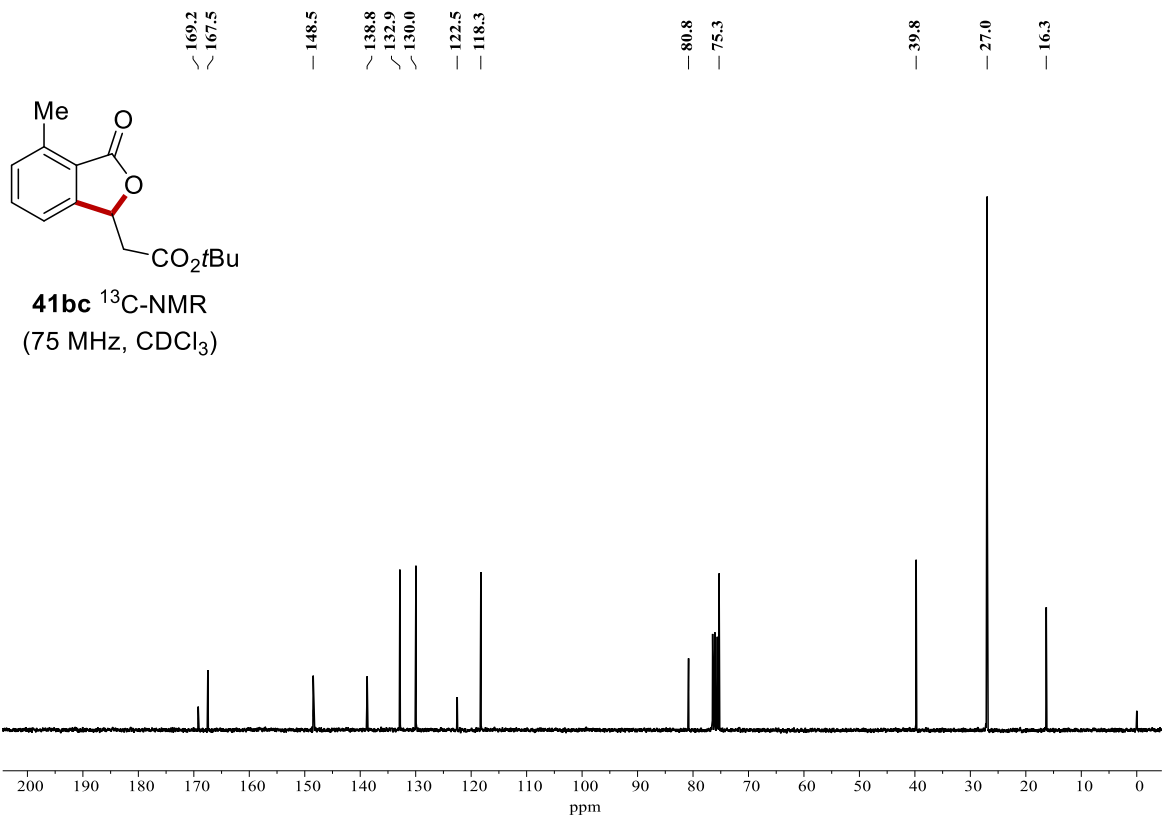
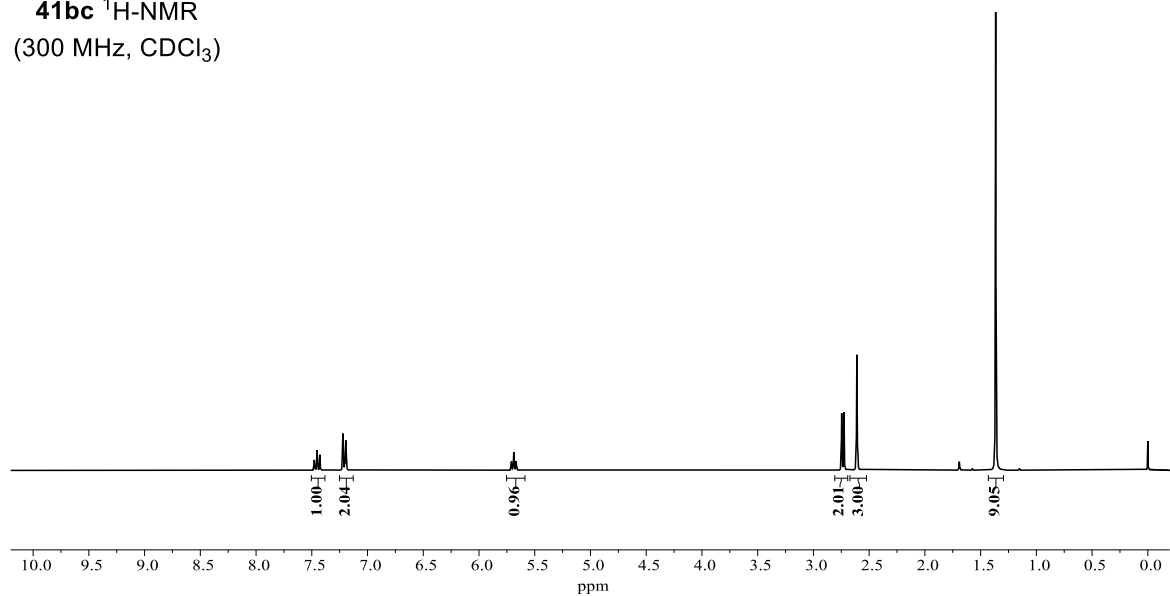
**41db** <sup>13</sup>C-NMR  
(100 MHz, CDCl<sub>3</sub>)

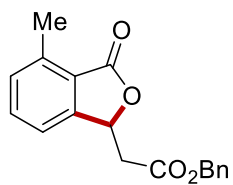




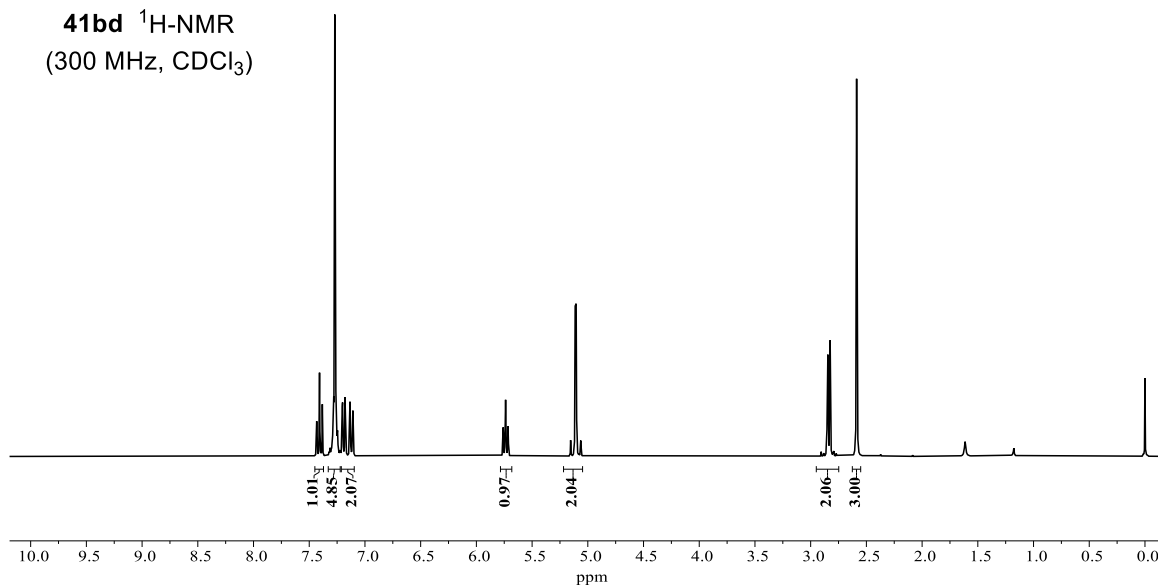


**41bc** <sup>1</sup>H-NMR  
(300 MHz, CDCl<sub>3</sub>)

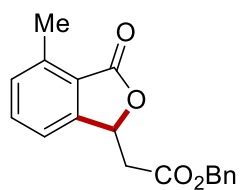




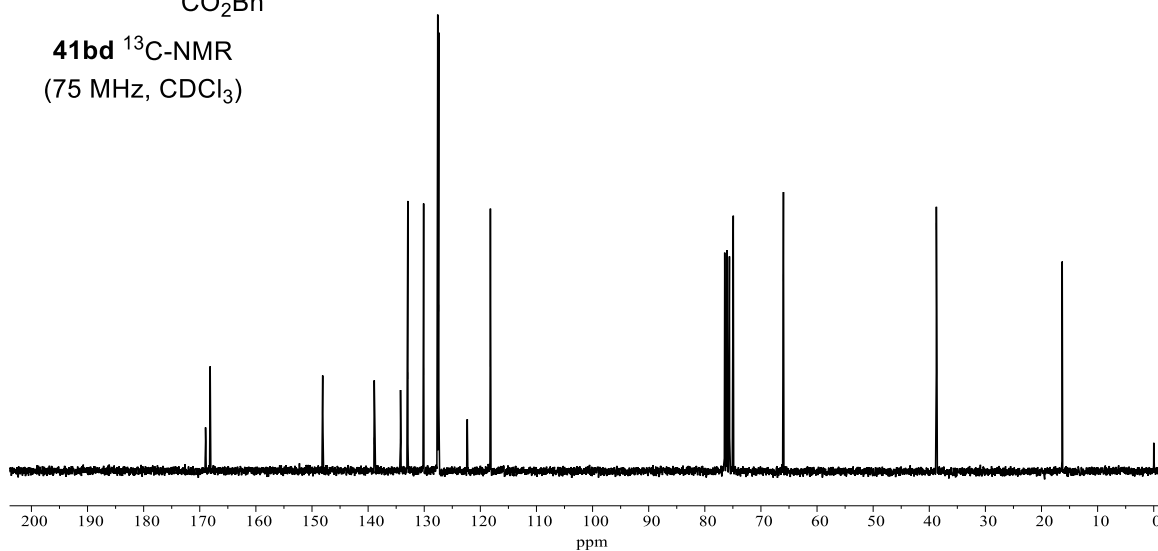
**41bd**  $^1\text{H-NMR}$   
(300 MHz,  $\text{CDCl}_3$ )

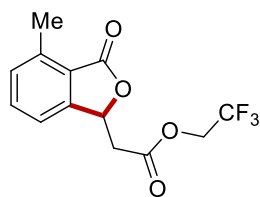


169.0  
168.2  
148.1  
138.9  
134.2  
132.9  
130.1  
127.6  
127.5  
127.4  
122.3  
118.2  
74.9  
66.0  
38.7  
16.3

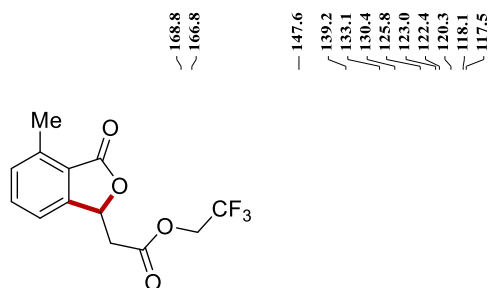
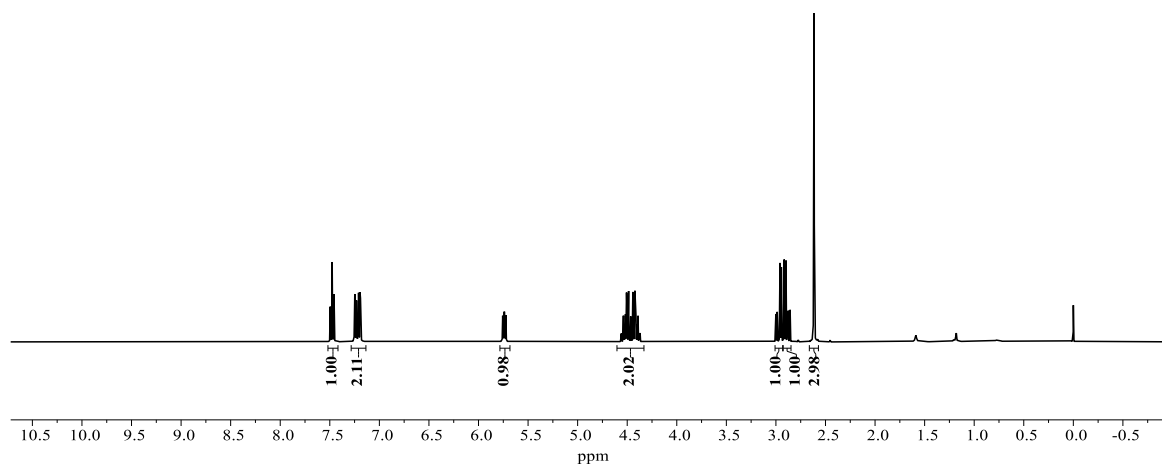


**41bd**  $^{13}\text{C-NMR}$   
(75 MHz,  $\text{CDCl}_3$ )

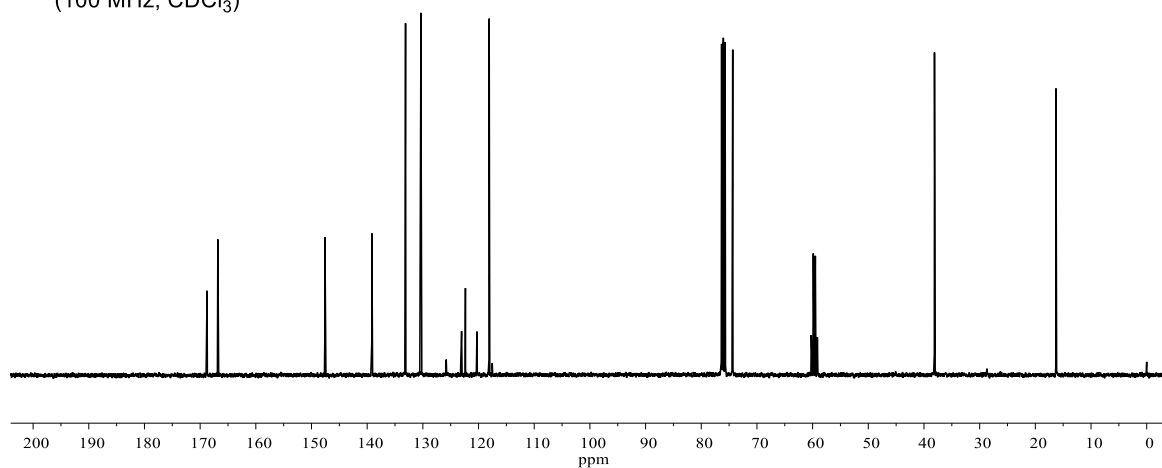




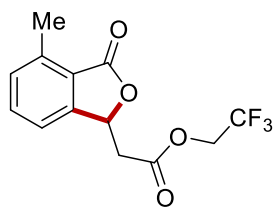
**41be**  $^1\text{H-NMR}$   
(400 MHz,  $\text{CDCl}_3$ )



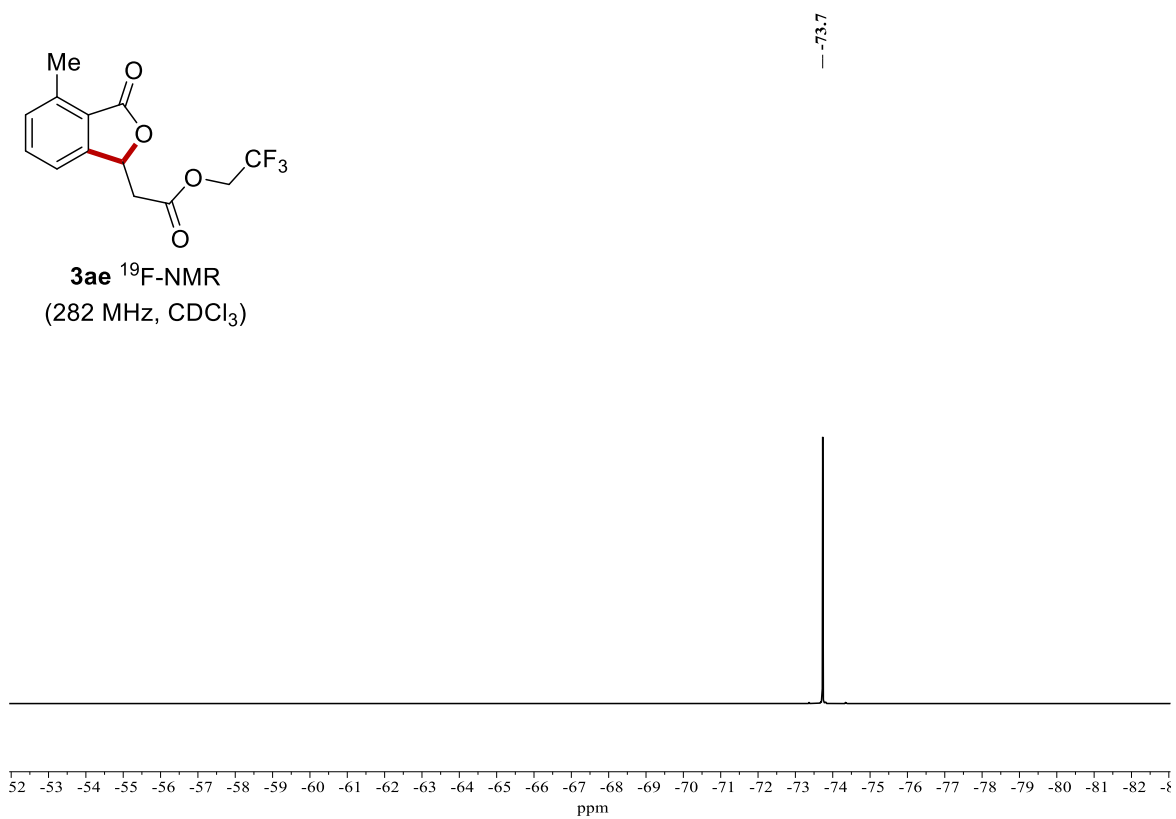
**41be**  $^{13}\text{C-NMR}$   
(100 MHz,  $\text{CDCl}_3$ )

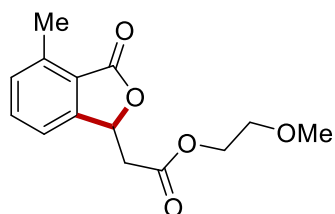




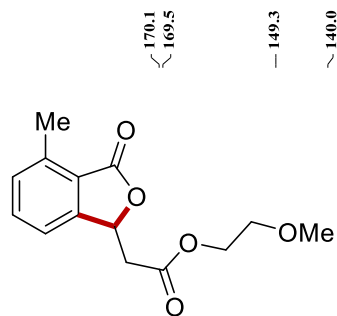
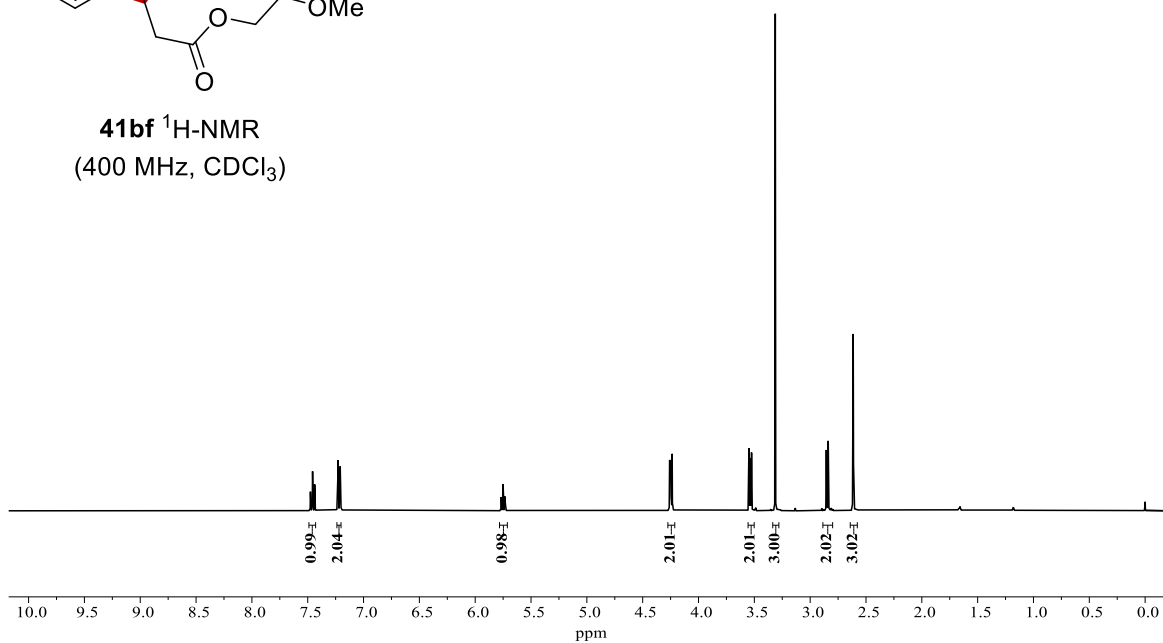


**3ae** <sup>19</sup>F-NMR  
(282 MHz, CDCl<sub>3</sub>)

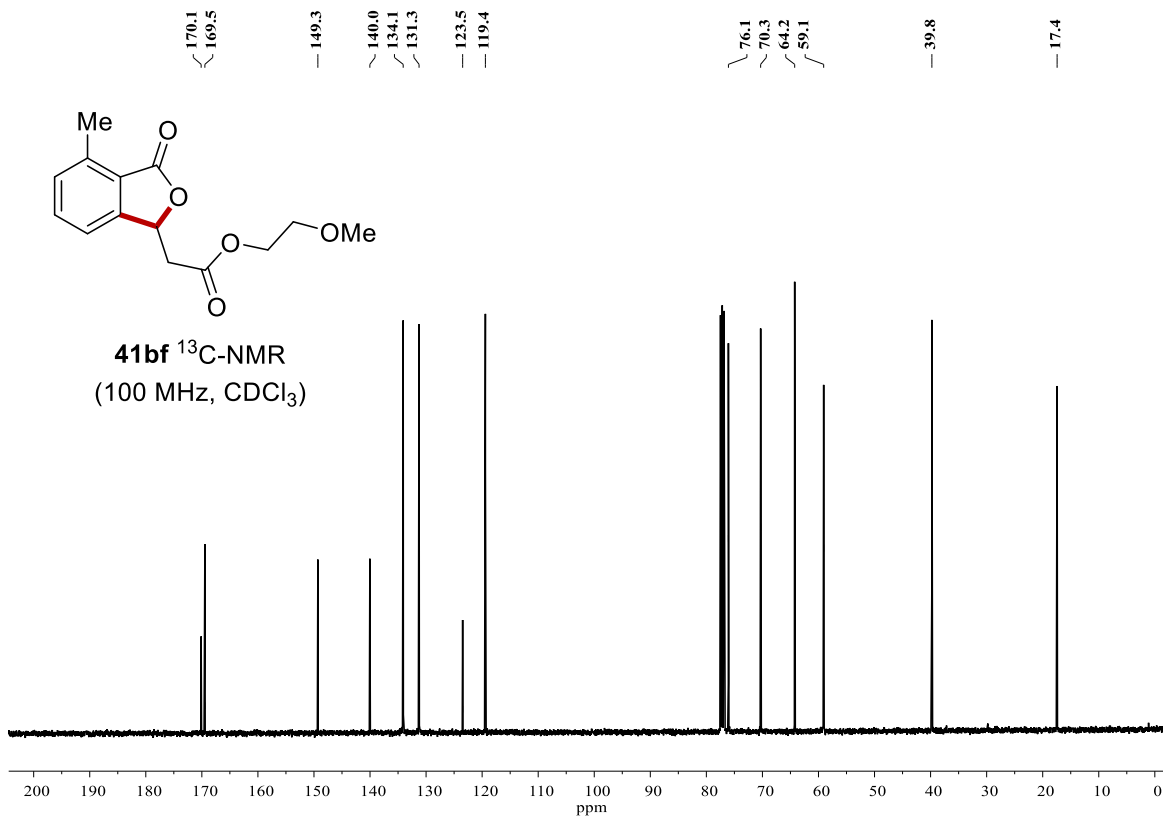


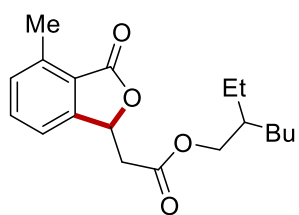


**41bf**  $^1\text{H-NMR}$   
(400 MHz,  $\text{CDCl}_3$ )

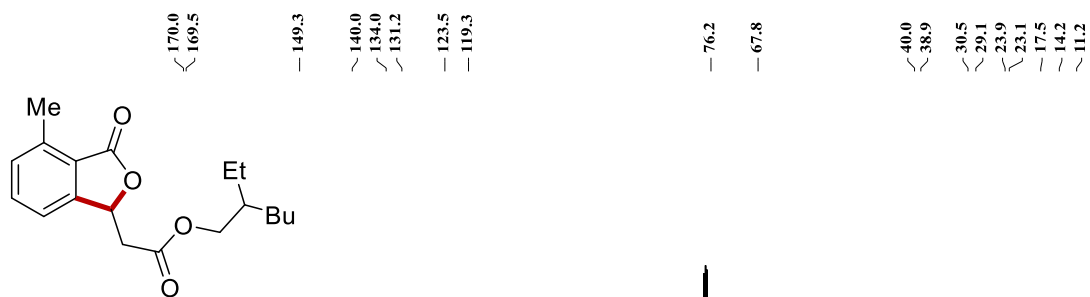
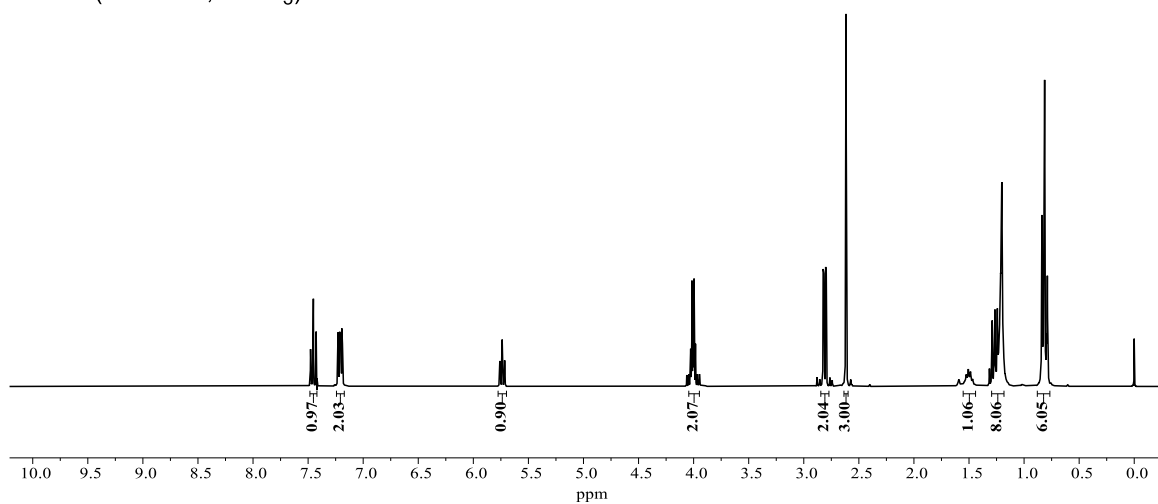


**41bf**  $^{13}\text{C-NMR}$   
(100 MHz,  $\text{CDCl}_3$ )

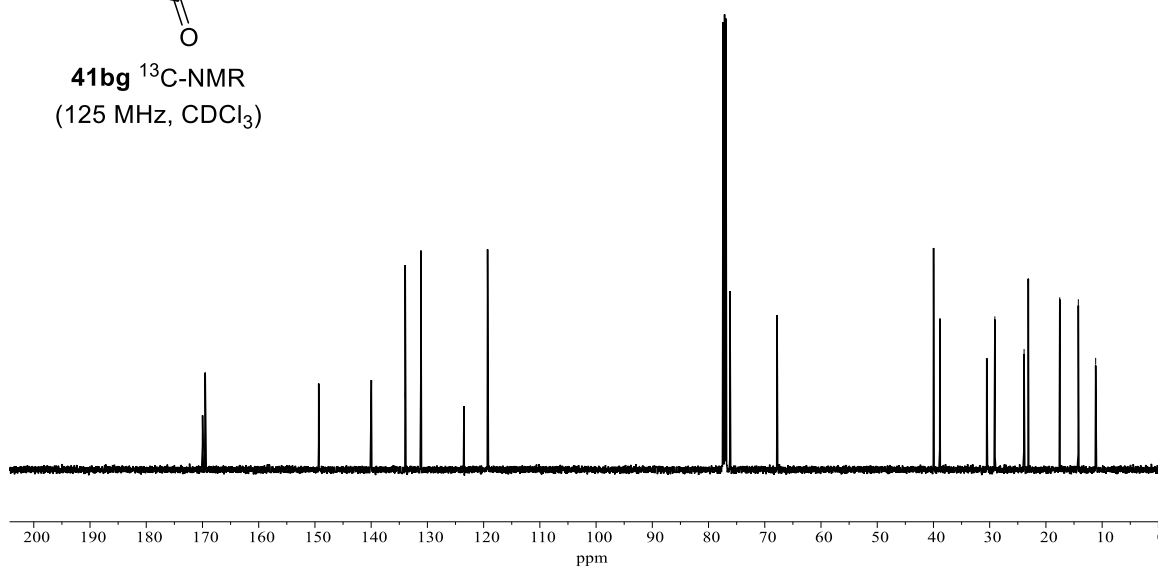


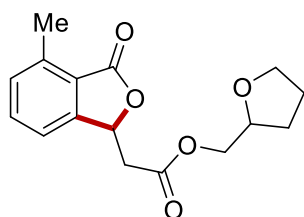


**41bg**  $^1\text{H-NMR}$   
(400 MHz,  $\text{CDCl}_3$ )

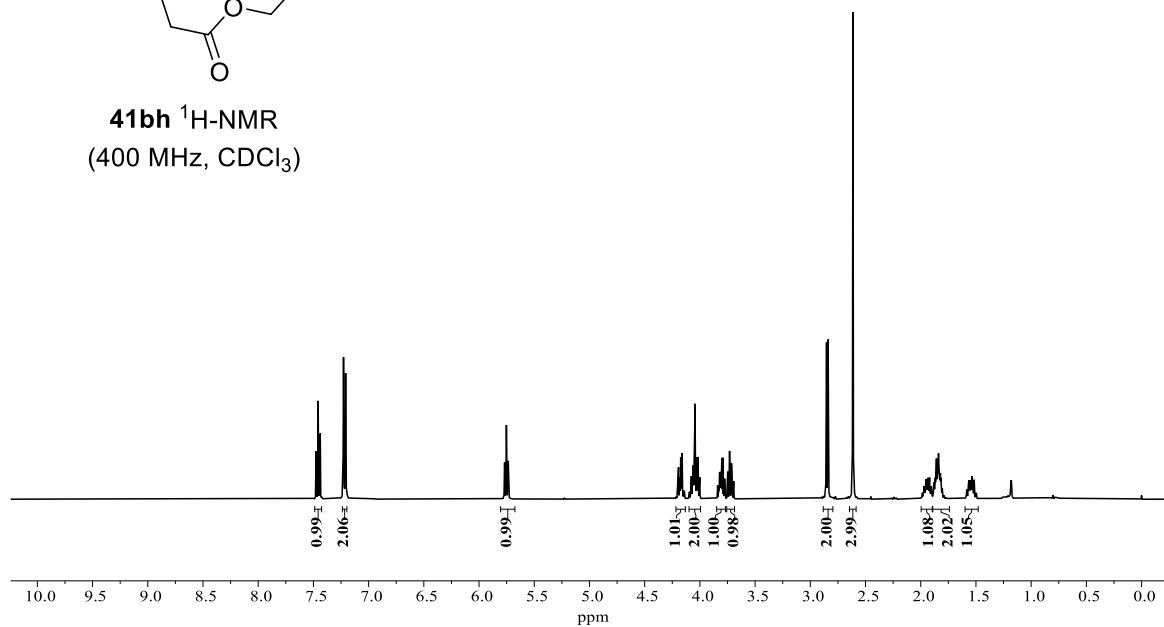


**41bg**  $^{13}\text{C-NMR}$   
(125 MHz,  $\text{CDCl}_3$ )

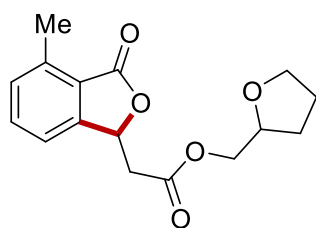




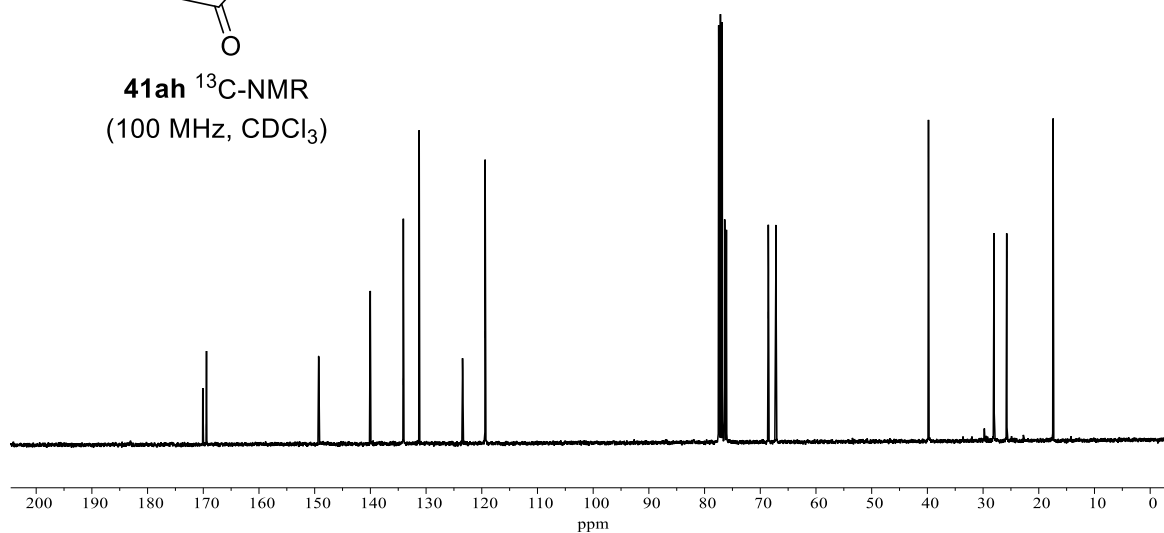
**41bh**  $^1\text{H-NMR}$   
(400 MHz,  $\text{CDCl}_3$ )

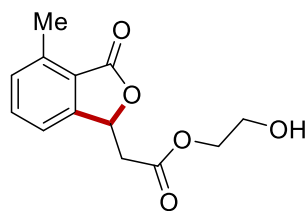


170.1  
169.4  
149.3  
140.0  
134.1  
131.2  
123.5  
119.4  
76.4  
76.1  
68.6  
67.2  
39.8  
28.0  
25.8  
17.4

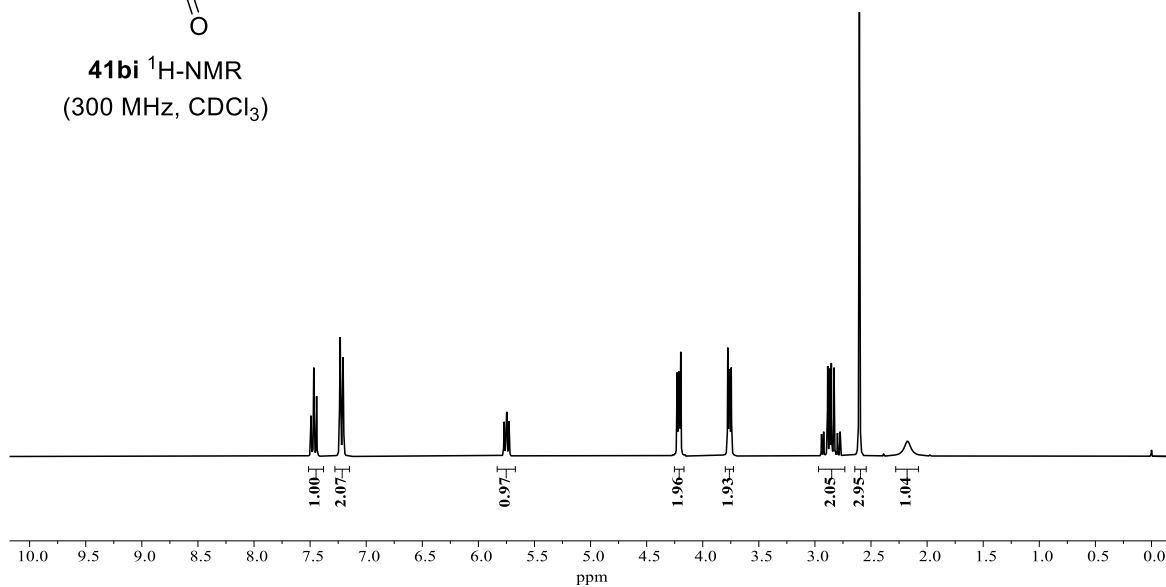


**41ah**  $^{13}\text{C-NMR}$   
(100 MHz,  $\text{CDCl}_3$ )

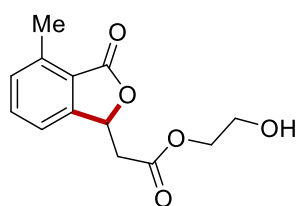




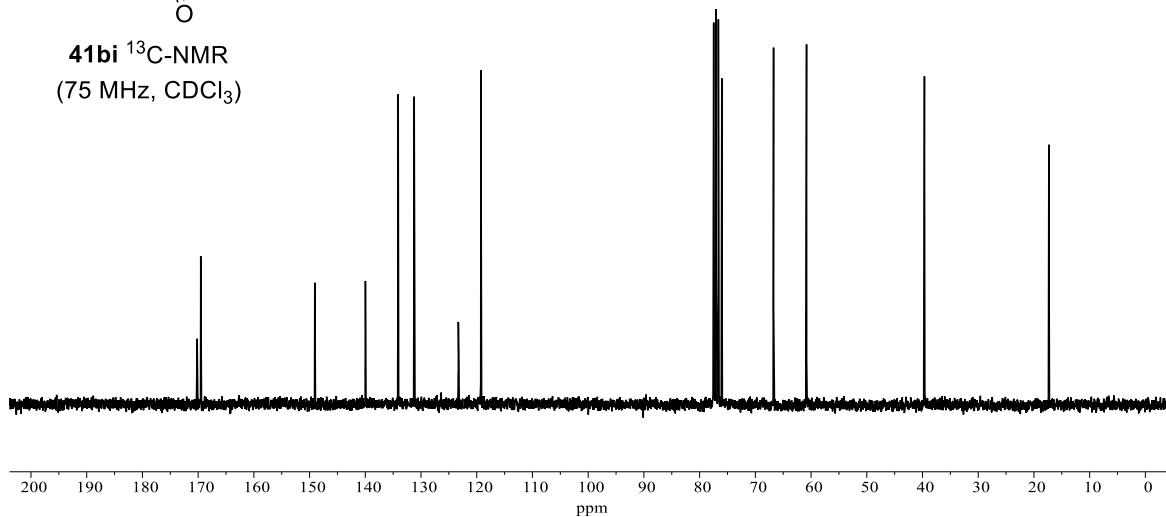
**41bi**  $^1\text{H-NMR}$   
(300 MHz,  $\text{CDCl}_3$ )

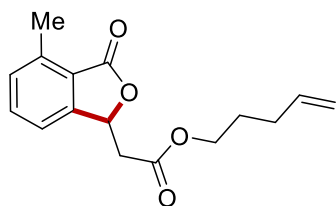


170.2  
169.6  
149.1  
140.0  
134.1  
131.2  
123.3  
119.3  
76.0  
66.7  
60.8  
39.7  
17.3

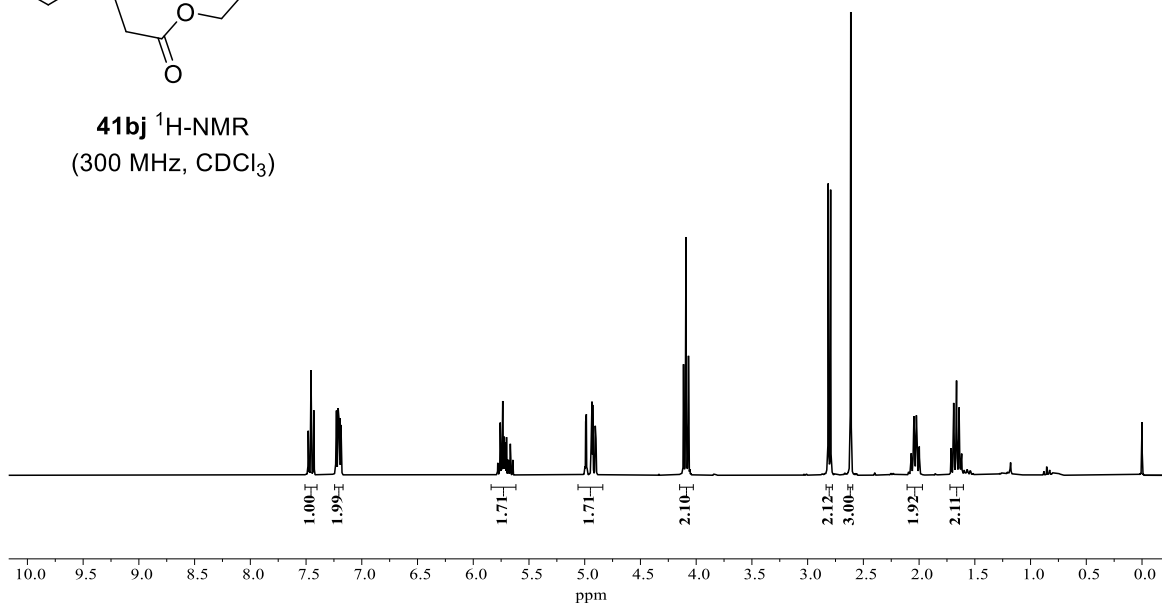


**41bi**  $^{13}\text{C-NMR}$   
(75 MHz,  $\text{CDCl}_3$ )

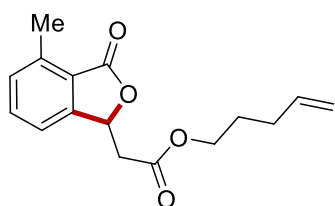




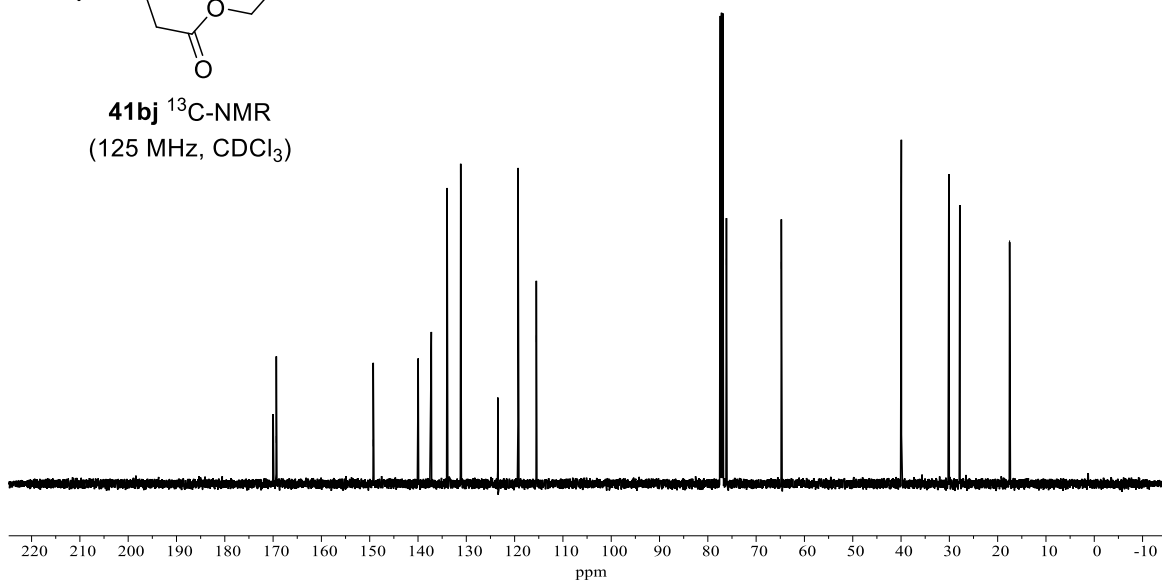
**41bj**  $^1\text{H-NMR}$   
(300 MHz,  $\text{CDCl}_3$ )

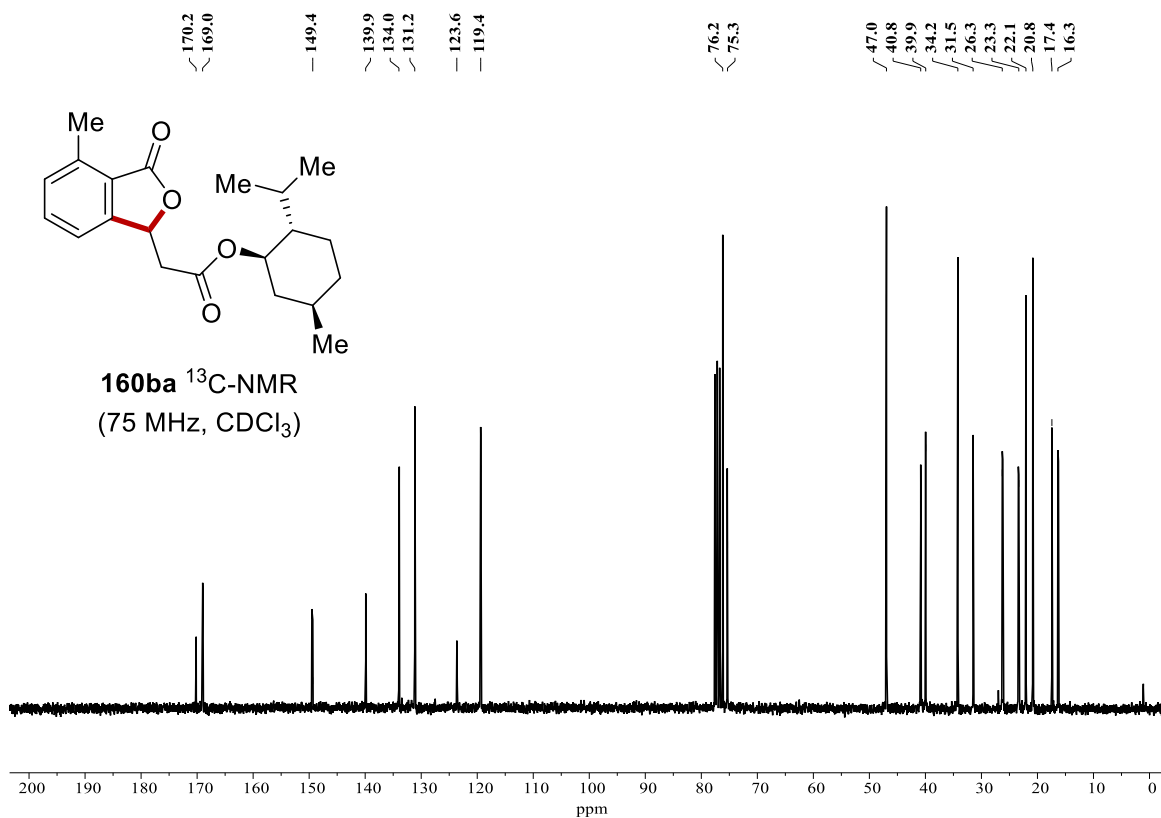
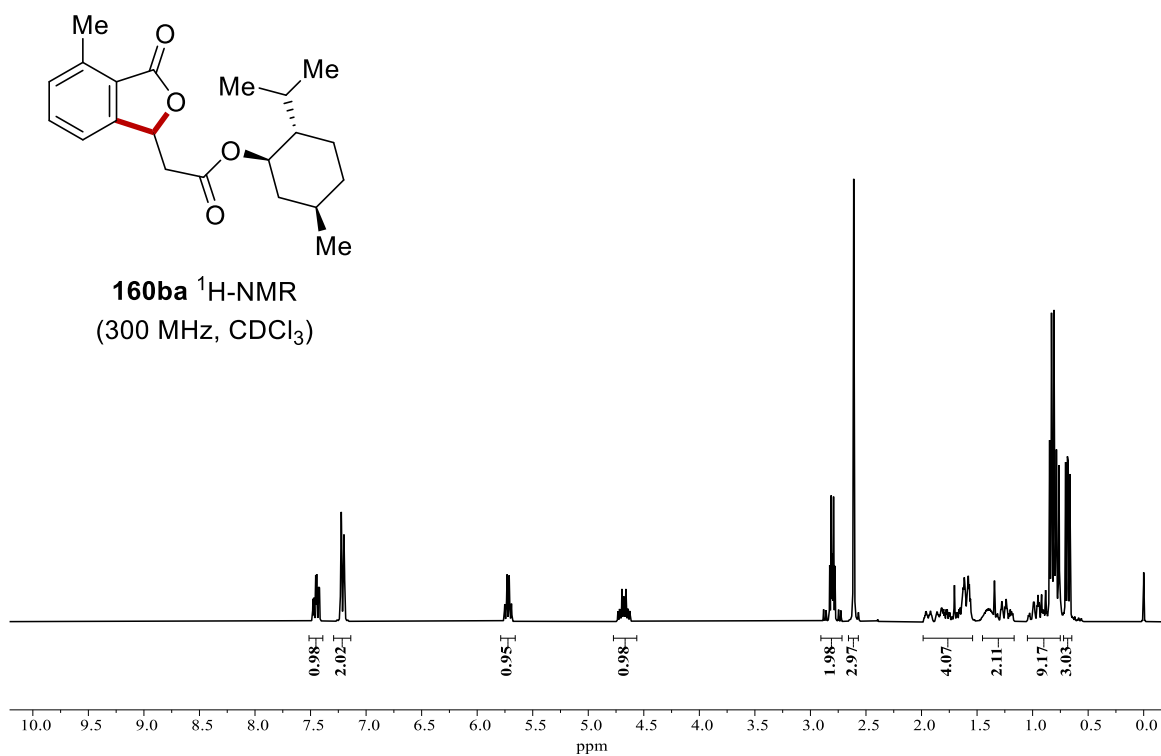


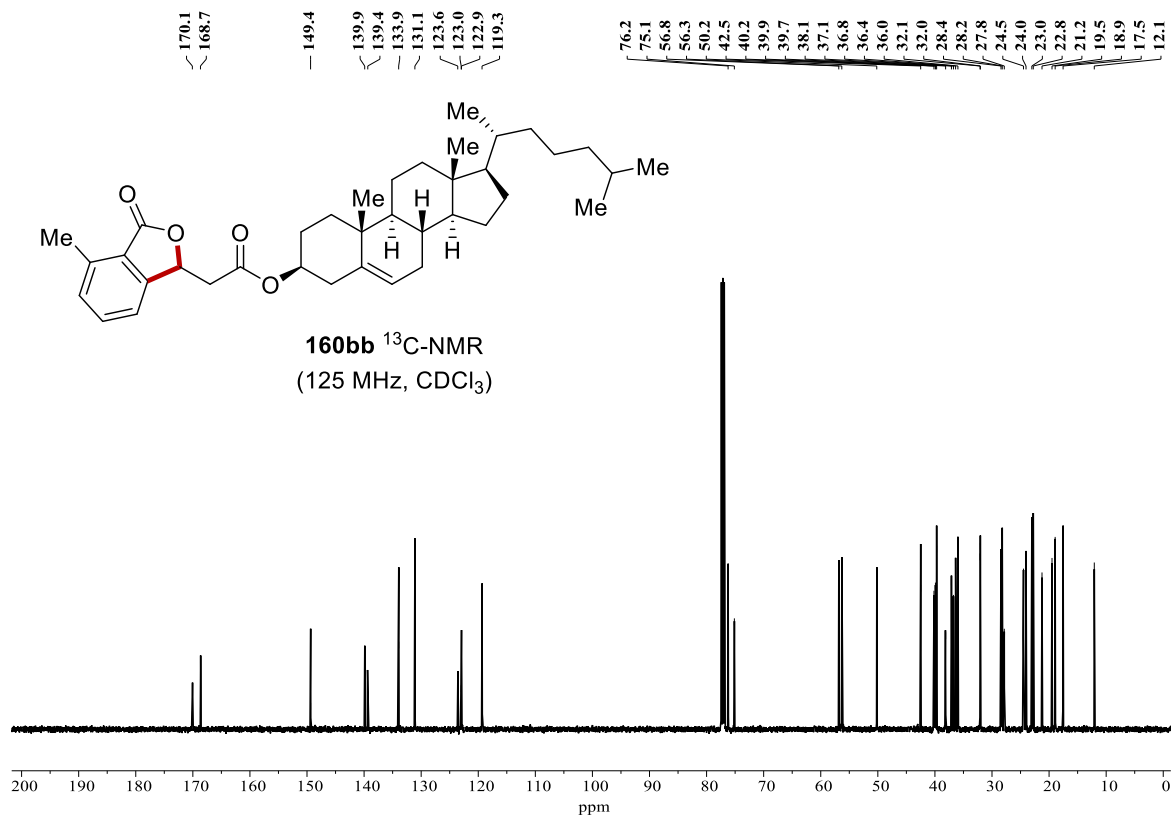
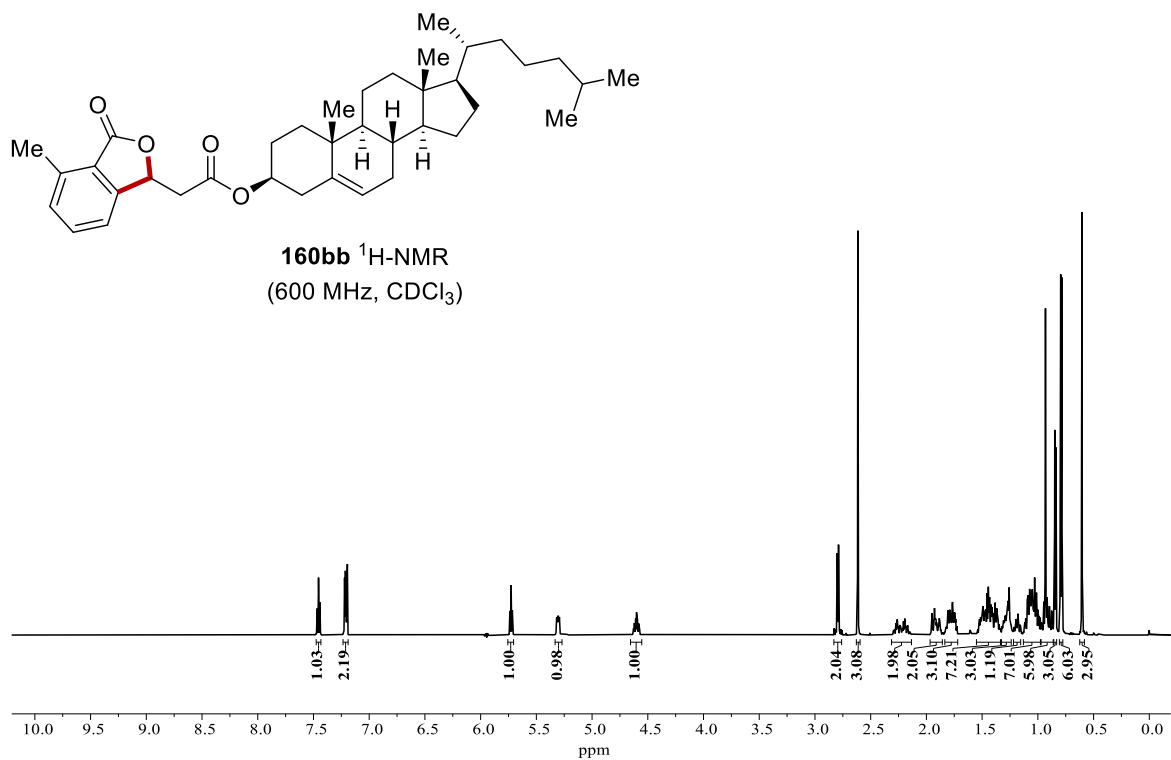
170.0  
169.3  
149.3  
140.0  
137.3  
134.0  
131.2  
123.5  
119.3  
115.5  
76.2  
64.8  
39.9  
30.1  
27.9  
17.5



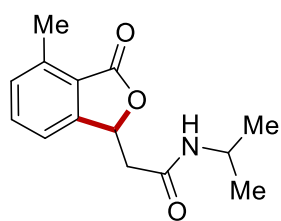
**41bj**  $^{13}\text{C-NMR}$   
(125 MHz,  $\text{CDCl}_3$ )



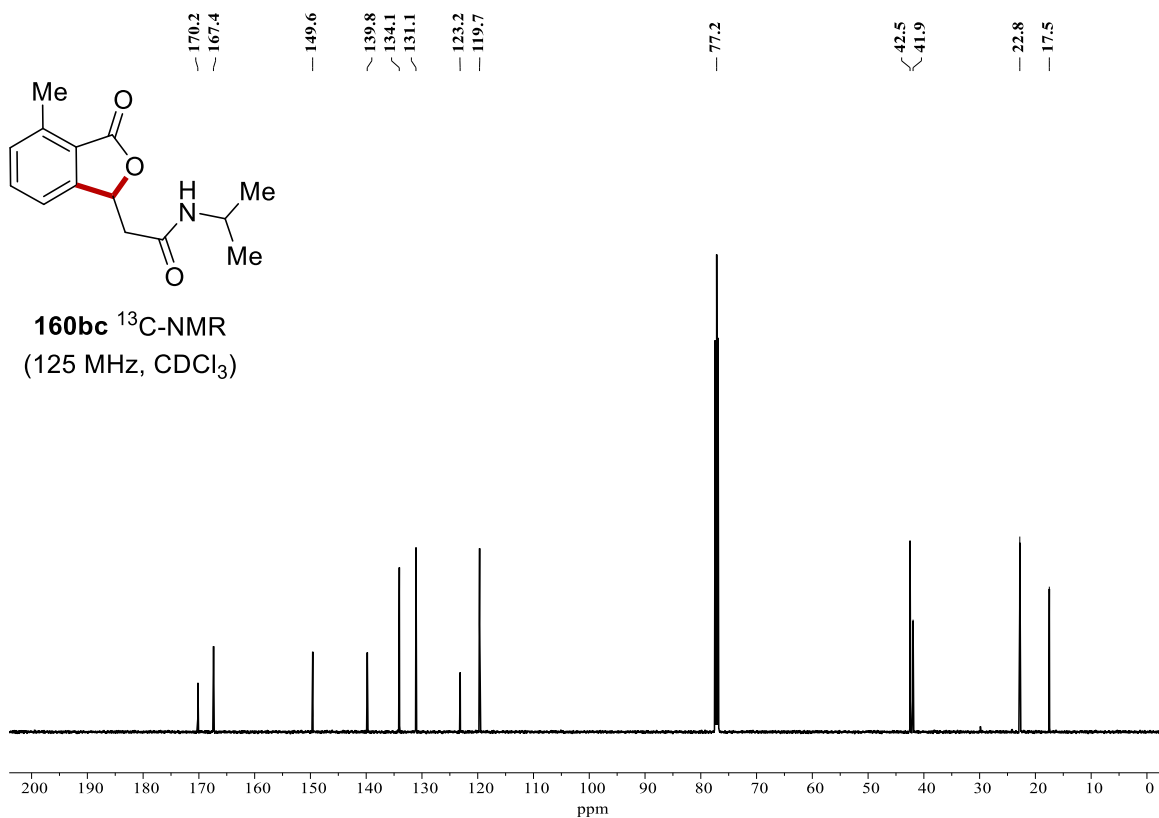
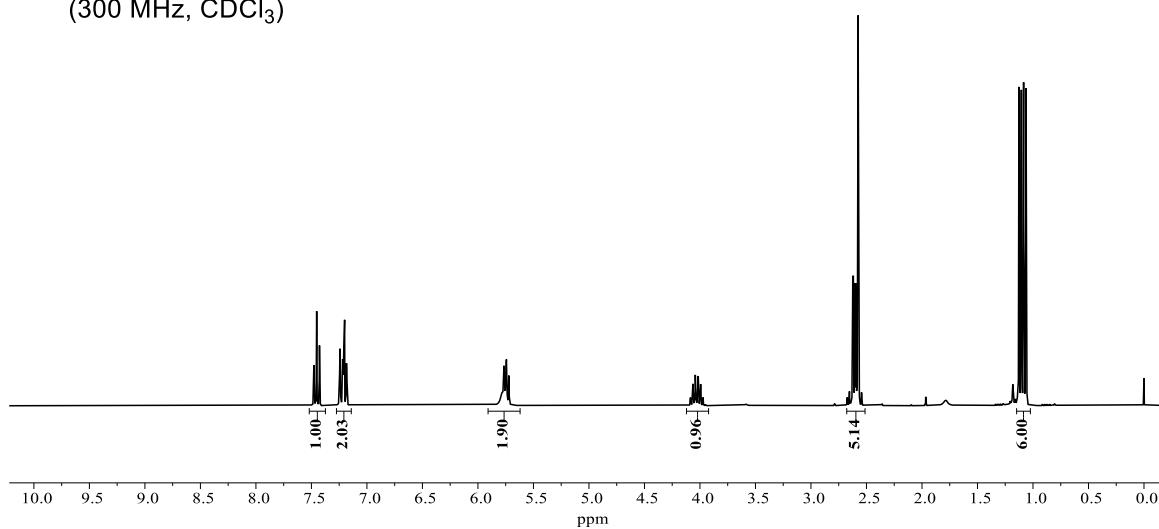


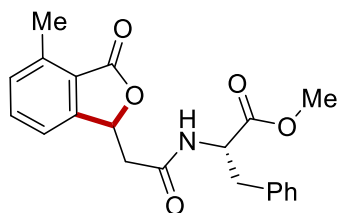




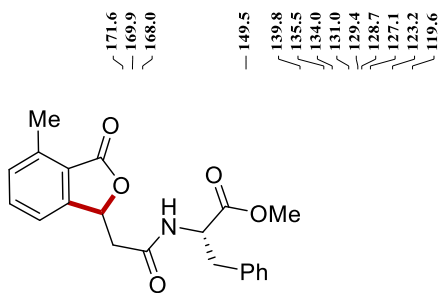
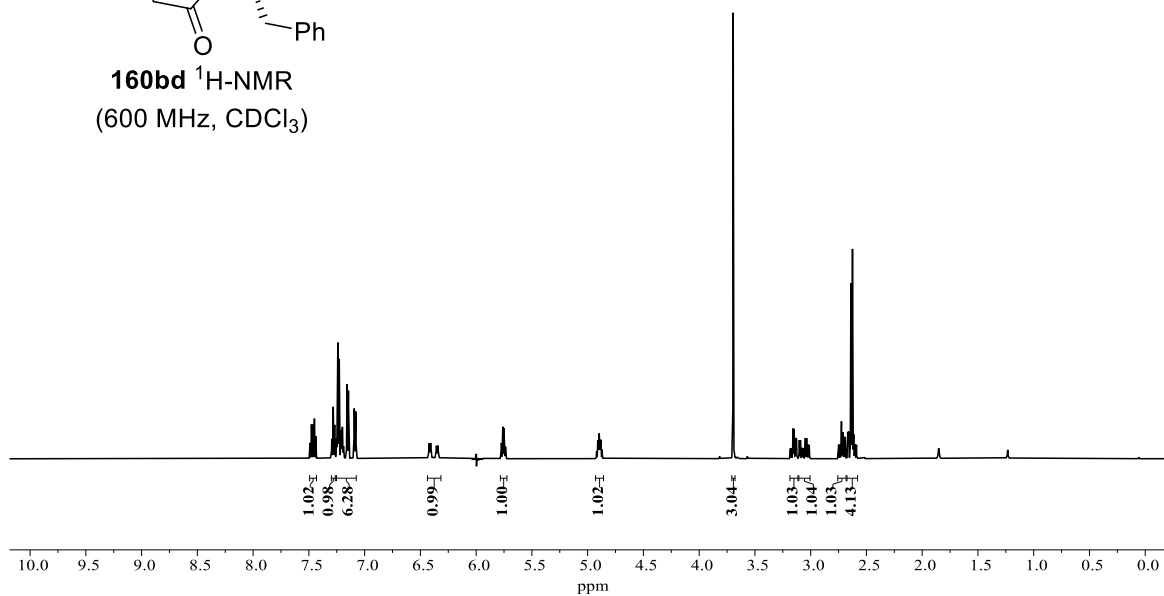


**160bc**  $^1\text{H-NMR}$   
(300 MHz,  $\text{CDCl}_3$ )

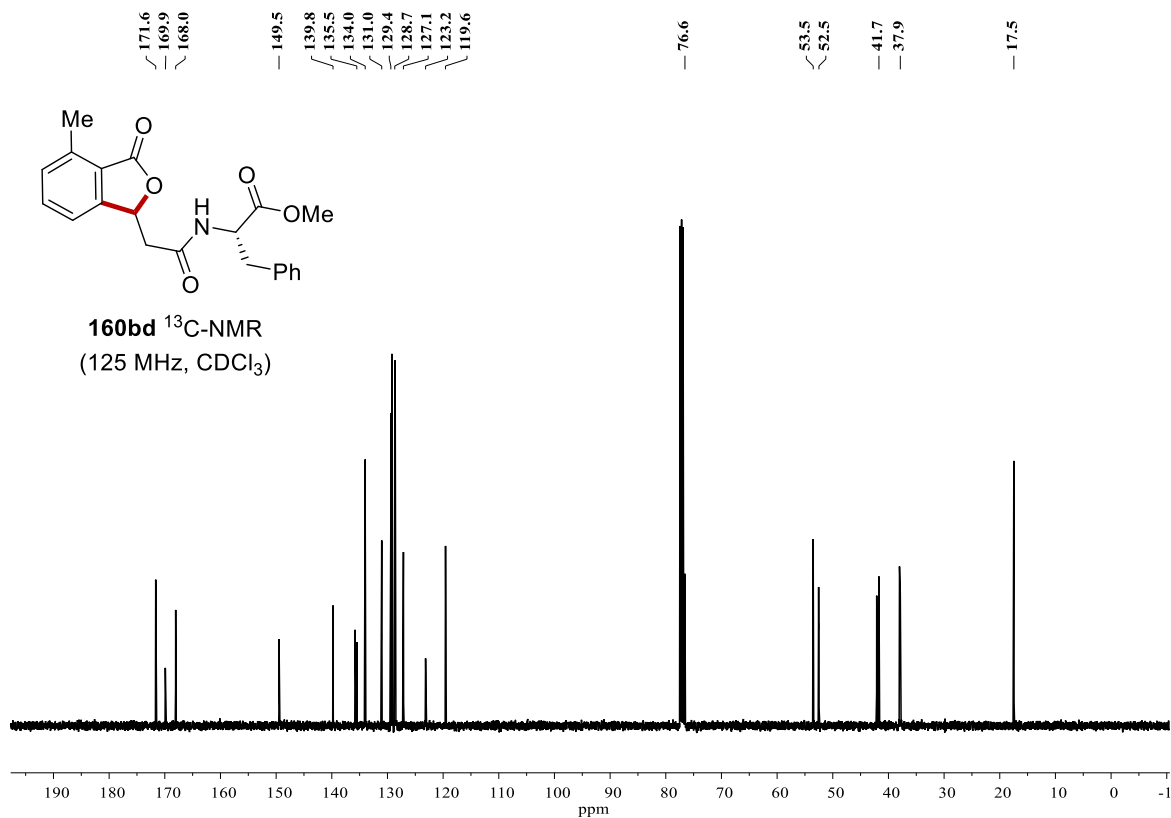


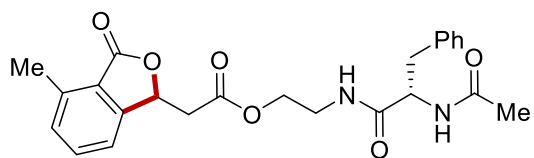


**160bd**  $^1\text{H-NMR}$   
(600 MHz,  $\text{CDCl}_3$ )

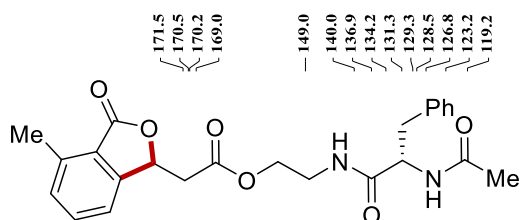
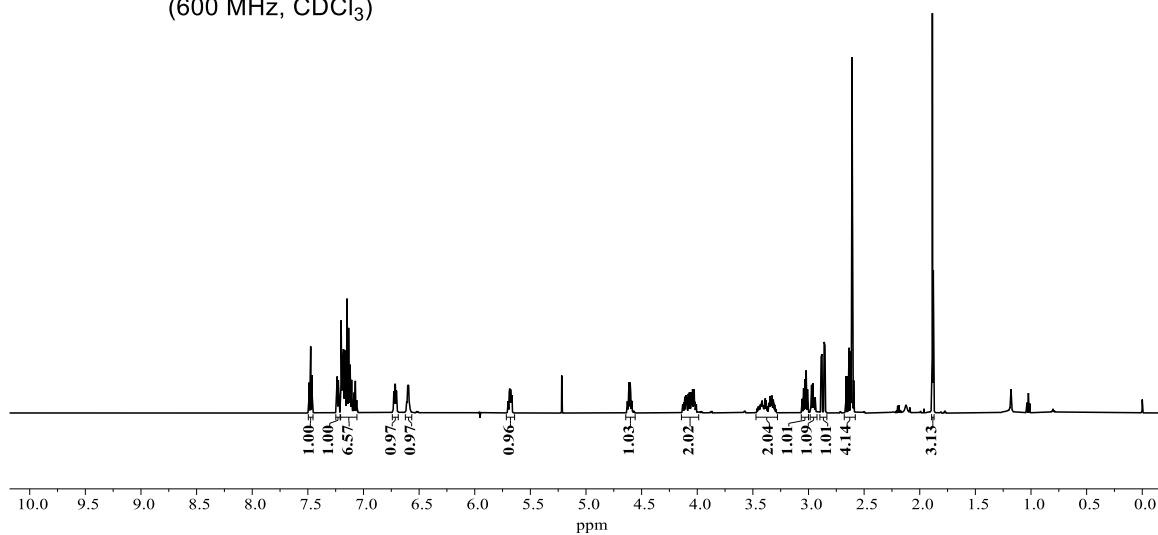


**160bd**  $^{13}\text{C-NMR}$   
(125 MHz,  $\text{CDCl}_3$ )

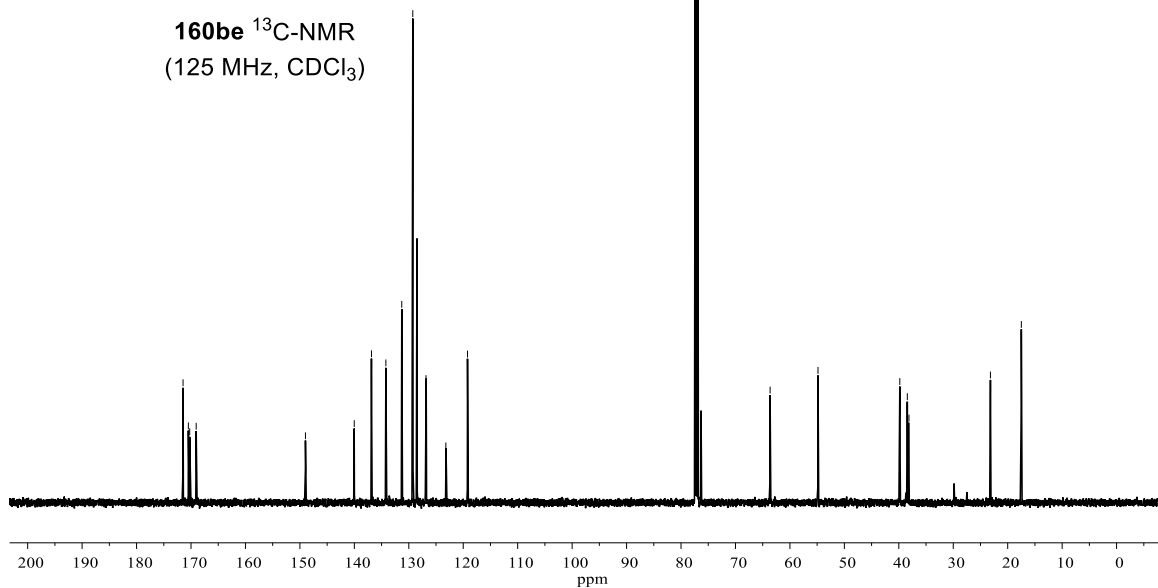


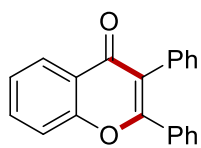


**160be**  $^1\text{H-NMR}$   
(600 MHz,  $\text{CDCl}_3$ )

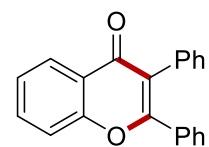
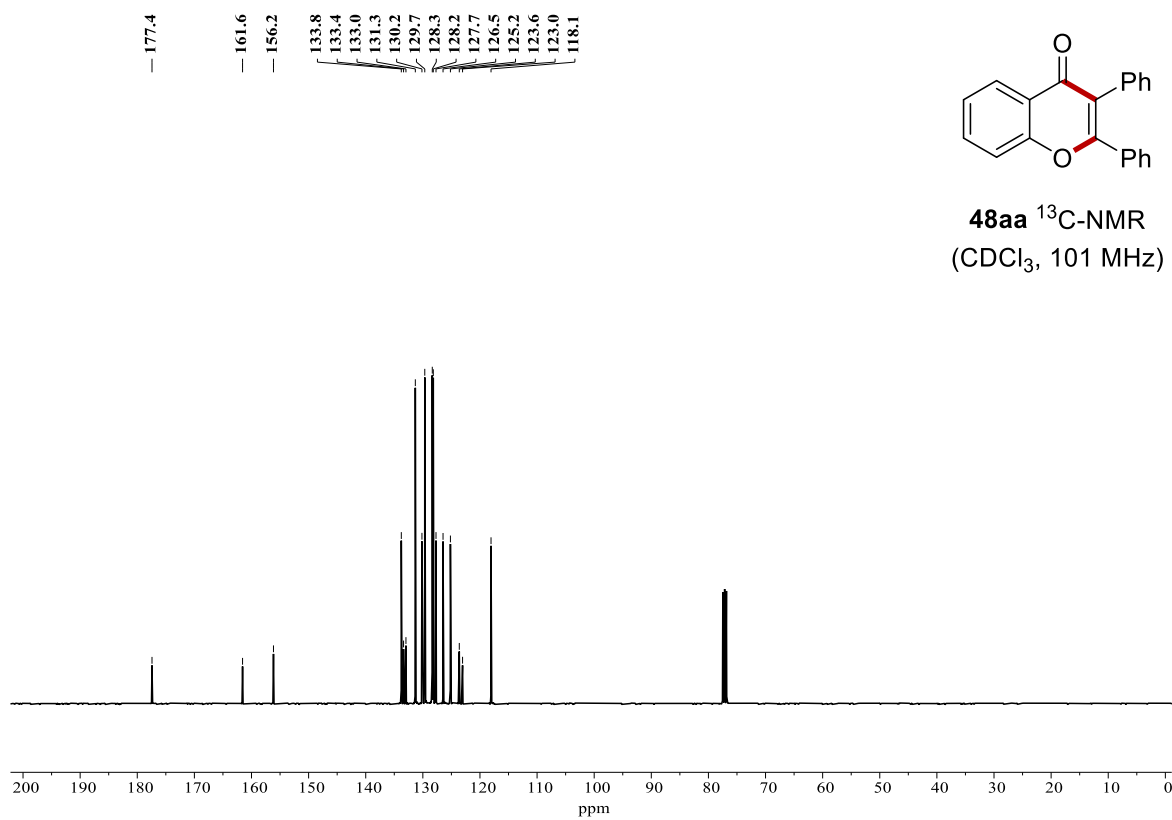
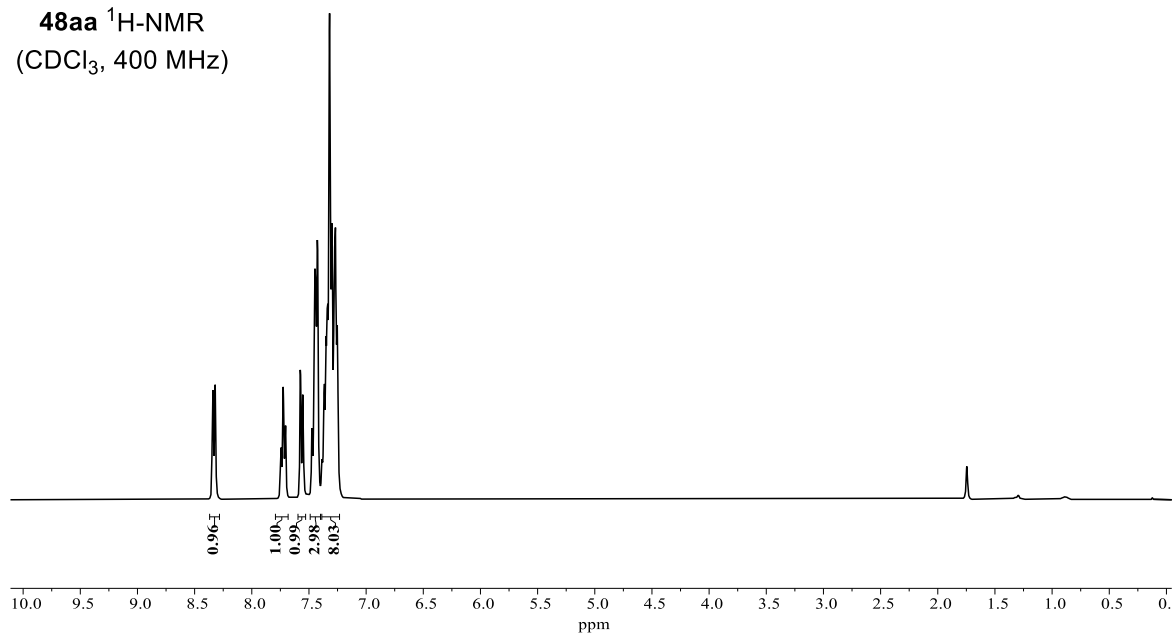


**160be**  $^{13}\text{C-NMR}$   
(125 MHz,  $\text{CDCl}_3$ )

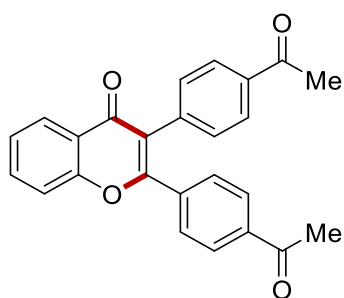




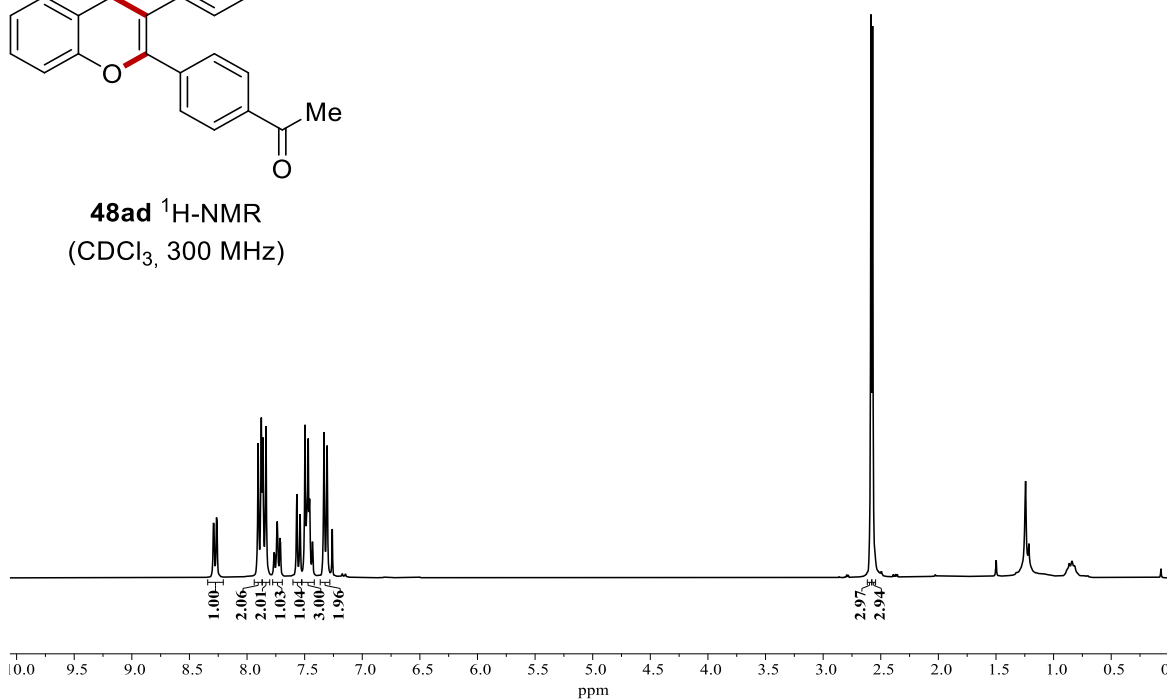
**48aa**  $^1\text{H-NMR}$   
( $\text{CDCl}_3$ , 400 MHz)



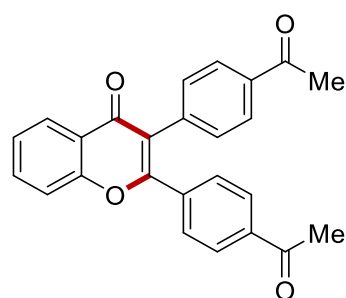
**48aa**  $^{13}\text{C-NMR}$   
( $\text{CDCl}_3$ , 101 MHz)



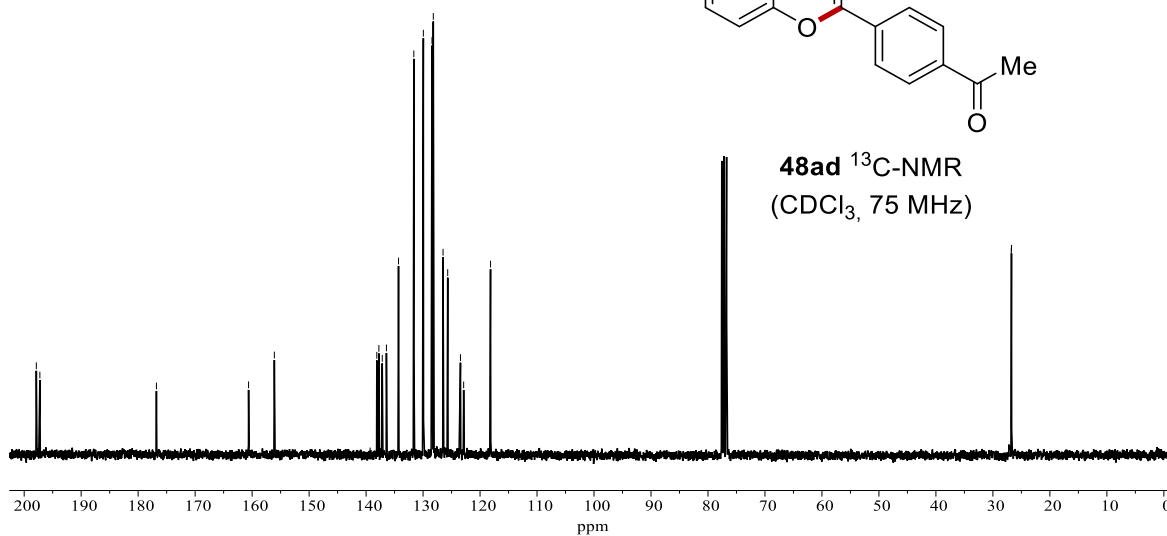
**48ad**  $^1\text{H-NMR}$   
( $\text{CDCl}_3$ , 300 MHz)

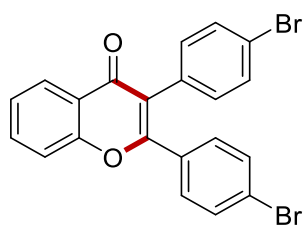


197.9  
197.2  
176.8  
160.6  
156.1  
139.3  
138.1  
137.8  
137.2  
136.4  
134.3  
131.6  
129.9  
128.4  
128.2  
126.5  
125.7  
123.4  
122.9  
118.2  
26.8  
26.7

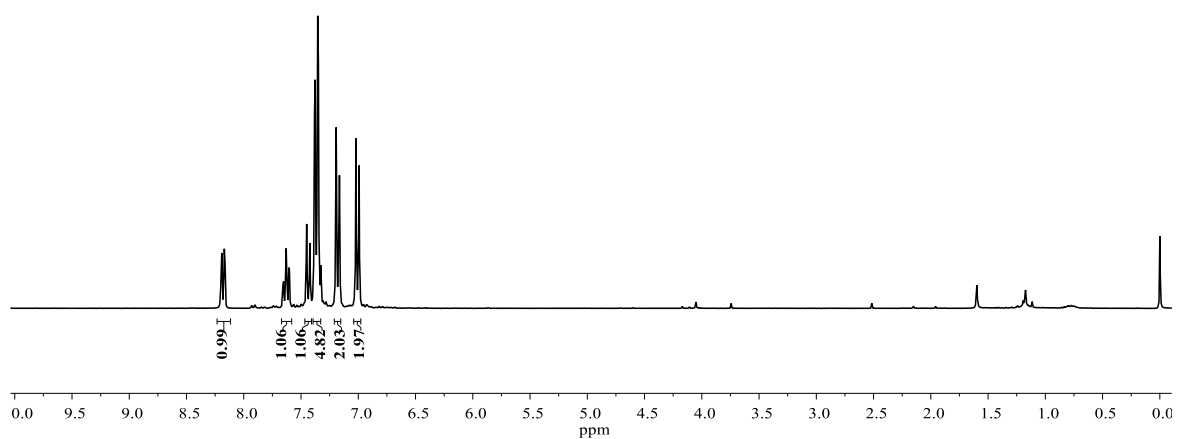


**48ad**  $^{13}\text{C-NMR}$   
( $\text{CDCl}_3$ , 75 MHz)

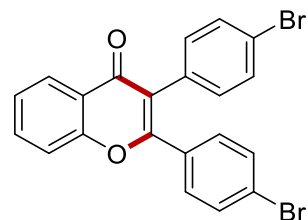




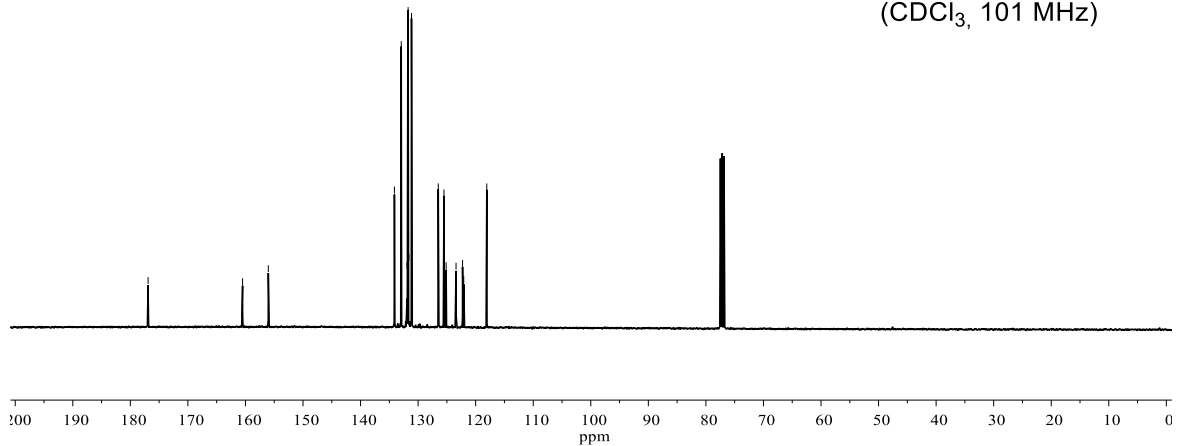
**48ae**  $^1\text{H-NMR}$   
( $\text{CDCl}_3$ , 400 MHz)

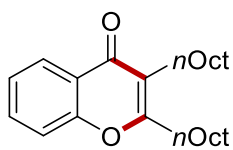


$^13\text{C-NMR}$  chemical shifts (ppm):  
 176.9, 160.5, 156.0, 134.1, 132.9, 131.9, 131.8, 131.7, 131.6, 131.2, 126.5, 125.5, 125.1, 123.4, 122.3, 122.1, 118.1

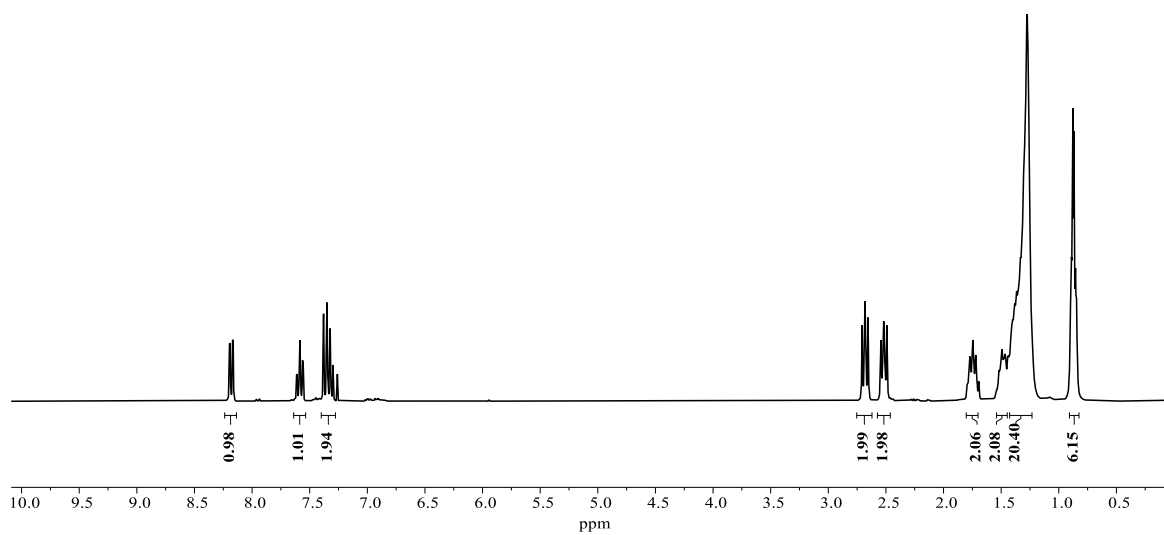


**48ae**  $^{13}\text{C-NMR}$   
( $\text{CDCl}_3$ , 101 MHz)





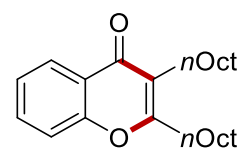
**48af**  $^1\text{H-NMR}$   
( $\text{CDCl}_3$ , 400 MHz)



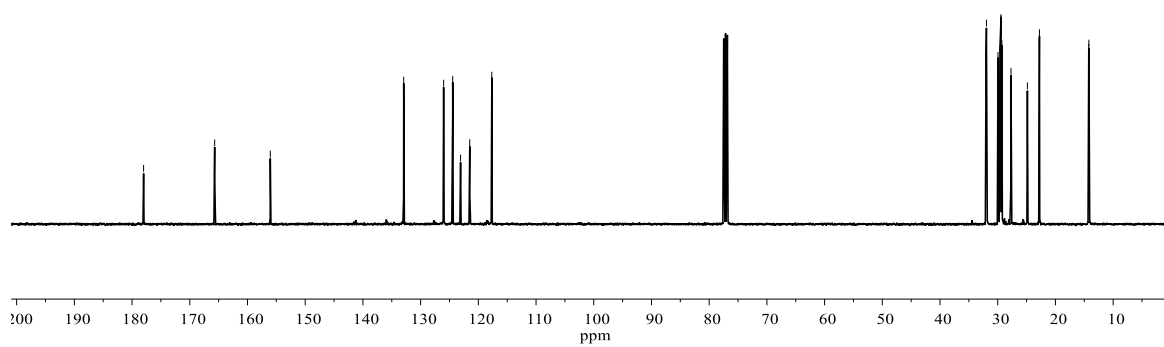
— 178.0  
— 165.7  
— 156.0

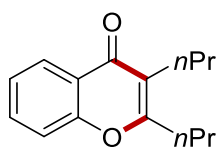
— 132.9  
— 126.0  
— 124.4  
— 123.1  
— 121.5  
— 117.7

32.0  
32.0  
32.0  
30.0  
29.6  
29.5  
29.5  
29.5  
29.4  
29.3  
27.7  
24.9  
22.8  
22.8  
14.2  
14.2

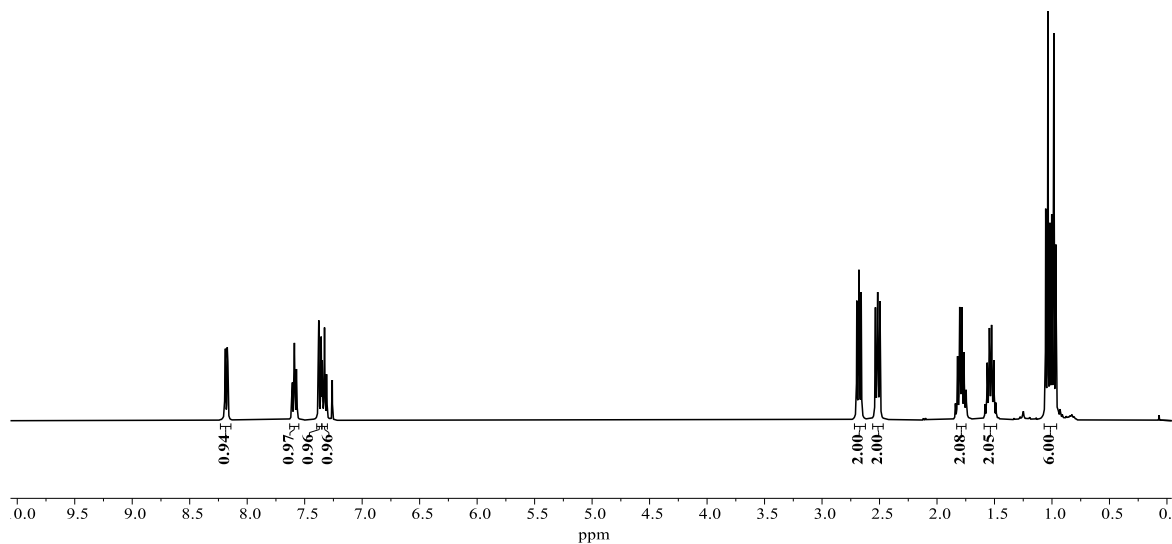


**48af**  $^{13}\text{C-NMR}$   
( $\text{CDCl}_3$ , 101 MHz)

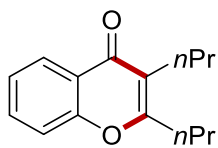




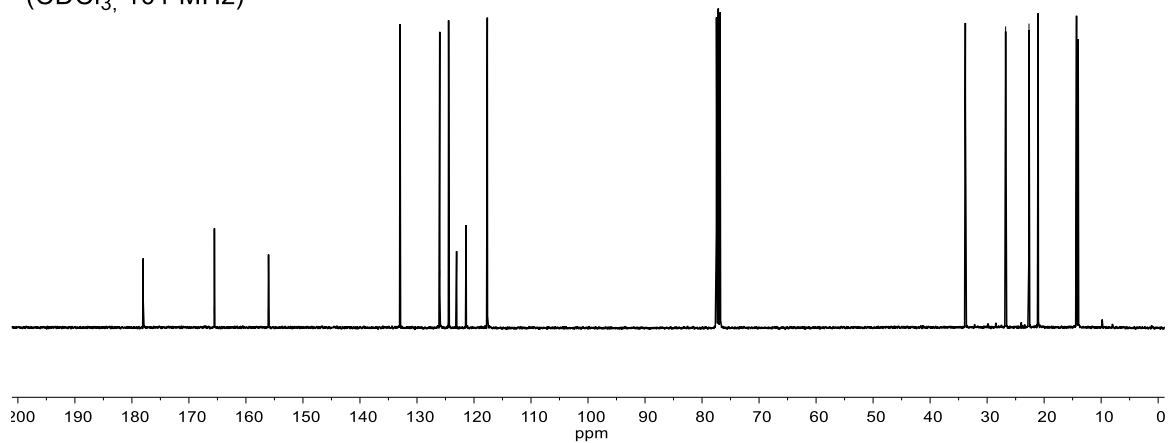
**48ag**  $^1\text{H-NMR}$   
( $\text{CDCl}_3$ , 400 MHz)



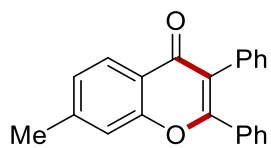
178.0, 165.5, 156.1, 133.0, 126.0, 124.5, 123.1, 121.4, 117.7, 33.8, 26.8, 22.7, 21.1, 14.3, 14.0



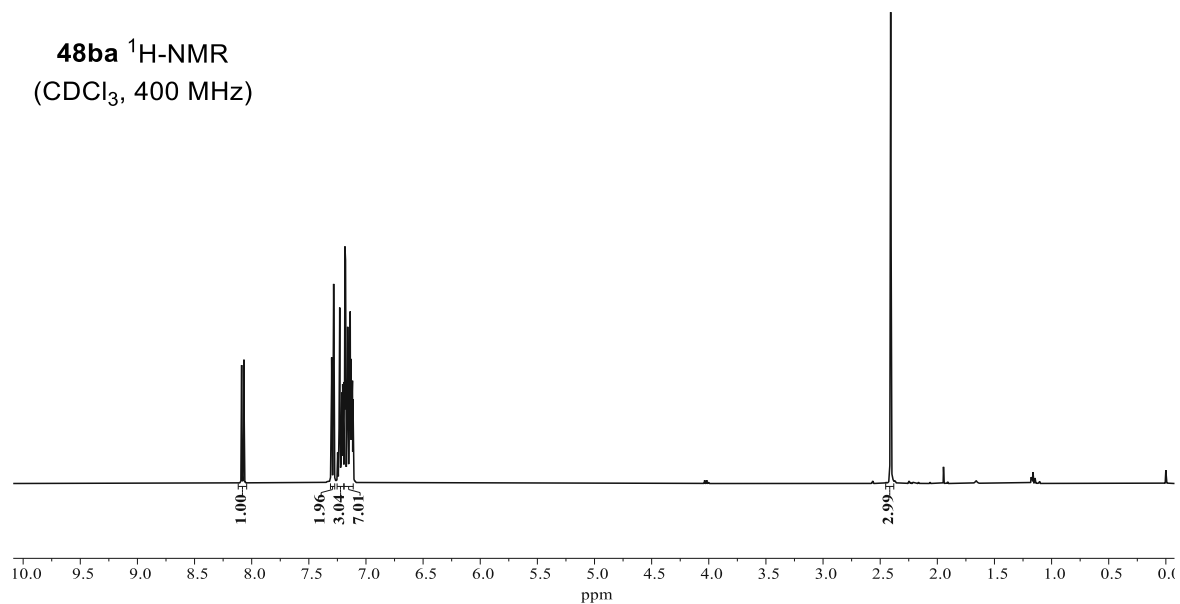
**48ag**  $^{13}\text{C-NMR}$   
( $\text{CDCl}_3$ , 101 MHz)



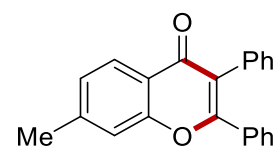




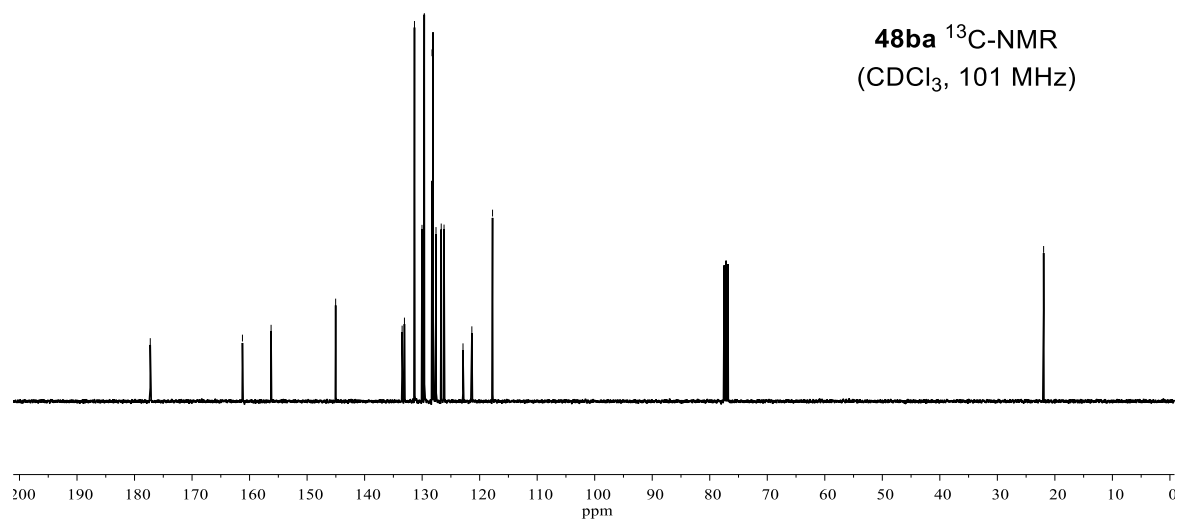
**48ba**  $^1\text{H-NMR}$   
( $\text{CDCl}_3$ , 400 MHz)

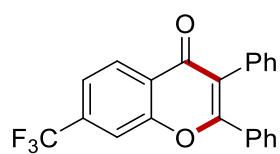


— 177.3 — 161.2 — 156.3 — 145.0 — 133.5 — 133.1 — 131.3 — 130.0 — 129.6 — 128.3 — 128.1 — 127.6 — 126.7 — 126.2 — 122.9 — 121.4 — 117.8 — 22.0

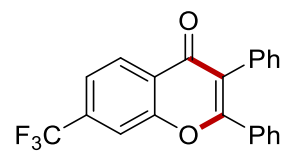
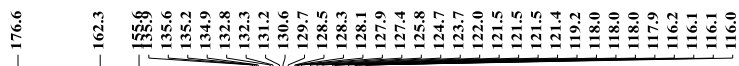
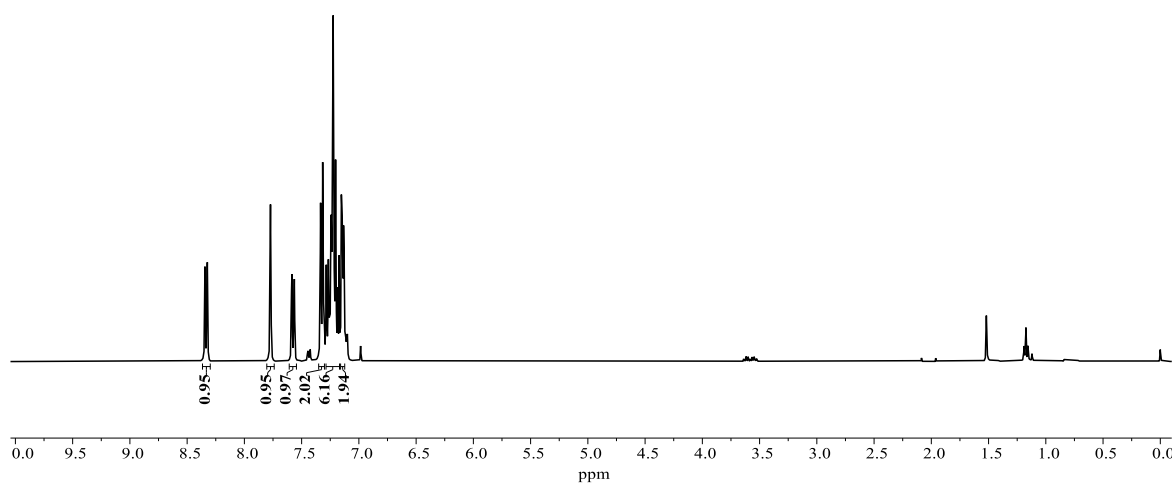


**48ba**  $^{13}\text{C-NMR}$   
( $\text{CDCl}_3$ , 101 MHz)

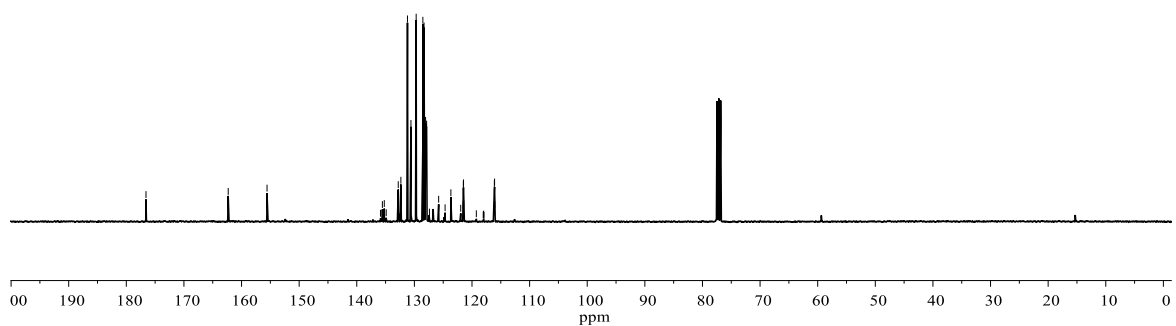


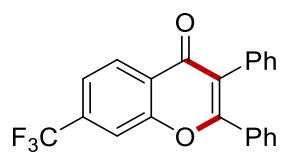


**48ca**  $^1\text{H-NMR}$   
( $\text{CDCl}_3$ , 400 MHz)

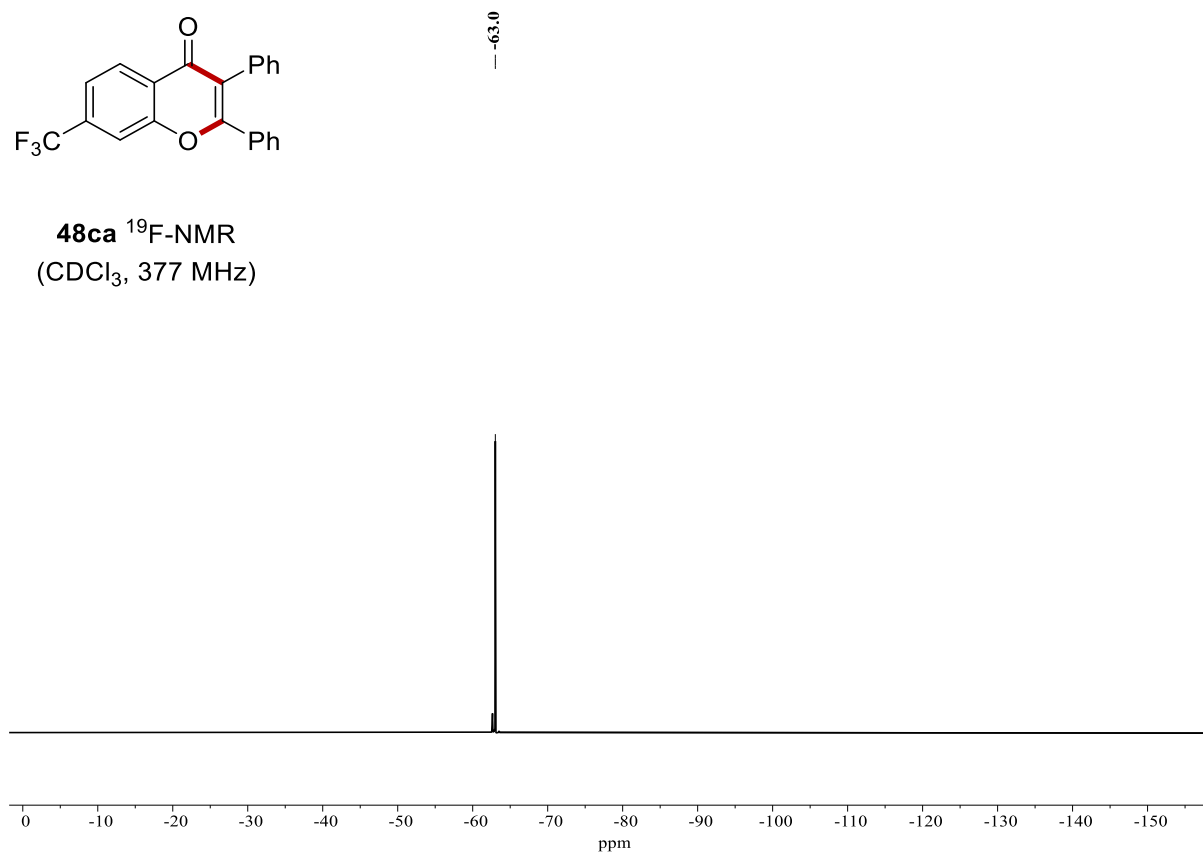


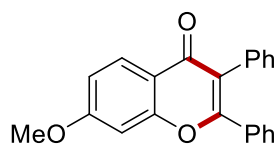
**48ca**  $^{13}\text{C-NMR}$   
( $\text{CDCl}_3$ , 101 MHz)



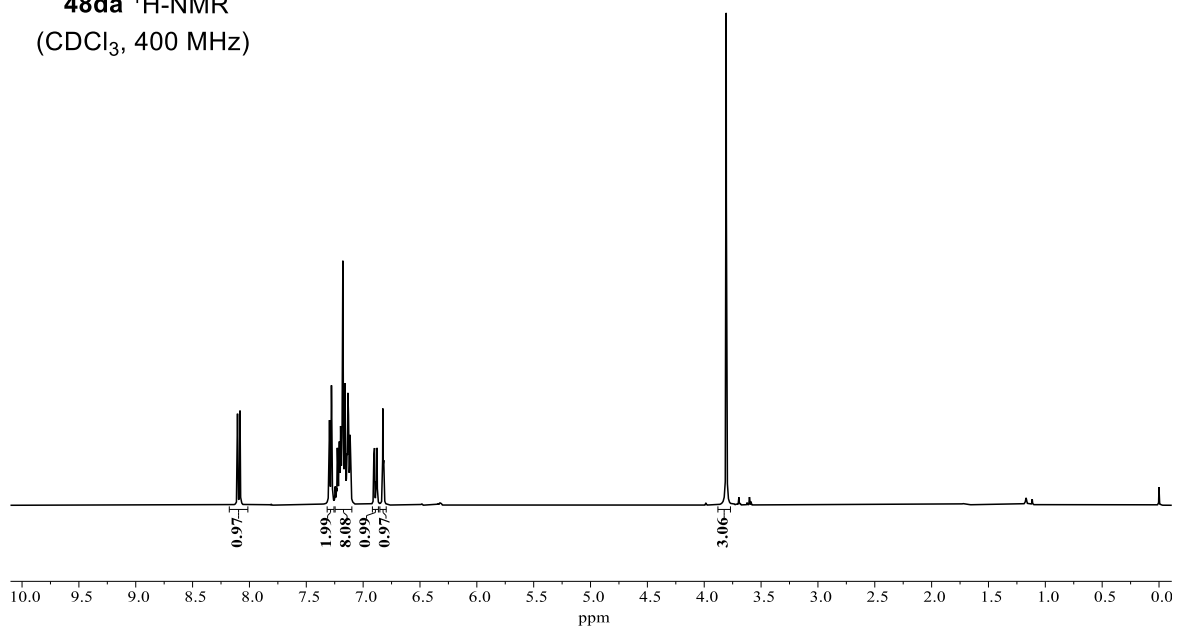


**48ca** <sup>19</sup>F-NMR  
(CDCl<sub>3</sub>, 377 MHz)

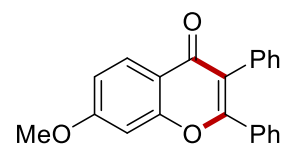




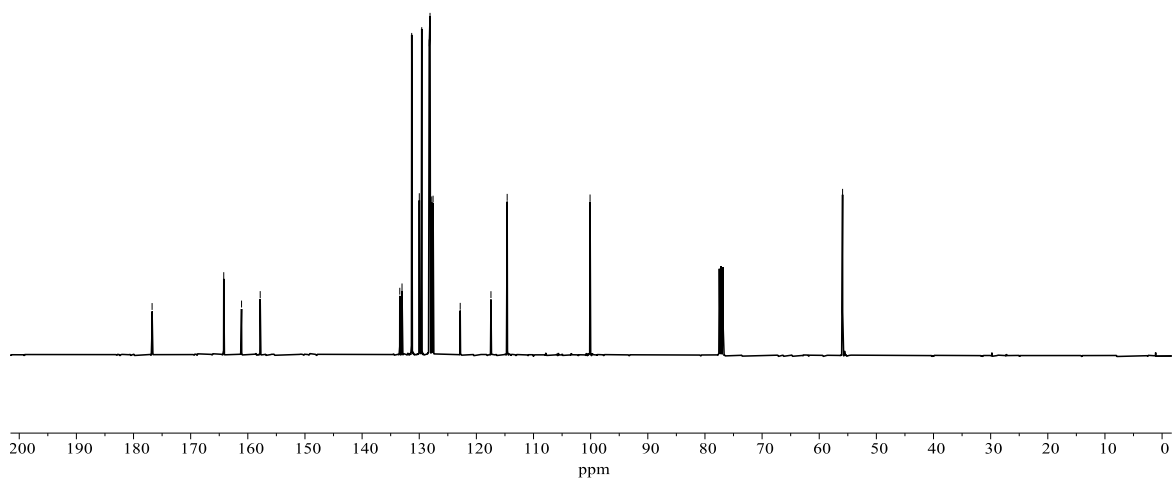
**48da**  $^1\text{H-NMR}$   
( $\text{CDCl}_3$ , 400 MHz)

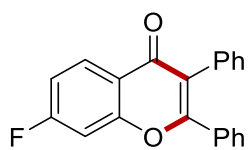


176.8  
164.2  
161.1  
157.8  
133.4  
133.0  
131.3  
130.0  
129.6  
128.3  
128.1  
127.8  
127.6  
122.8  
117.5  
114.6  
100.1  
55.9

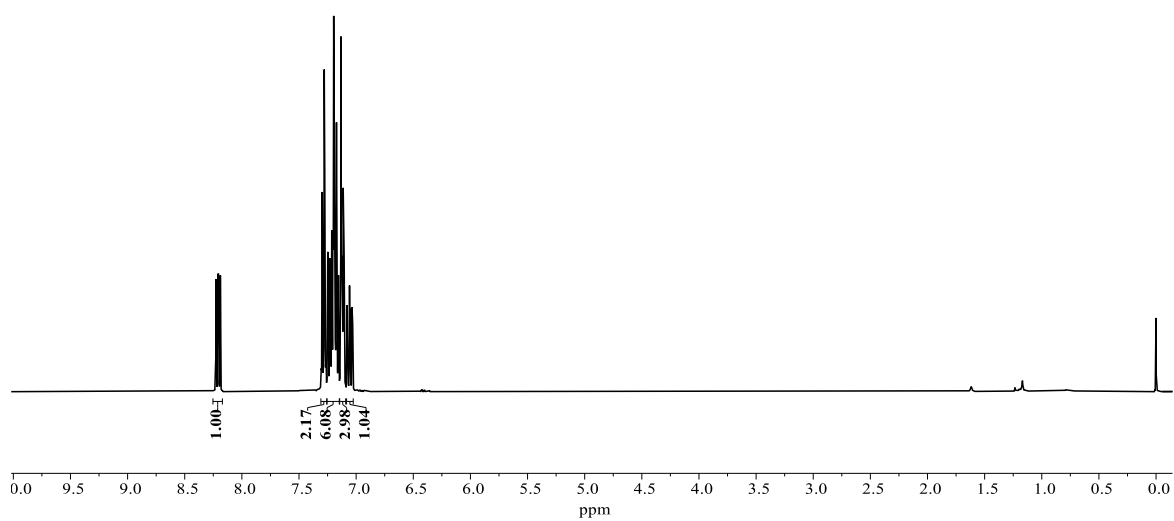


**48da**  $^{13}\text{C-NMR}$   
( $\text{CDCl}_3$ , 101 MHz)

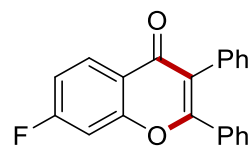




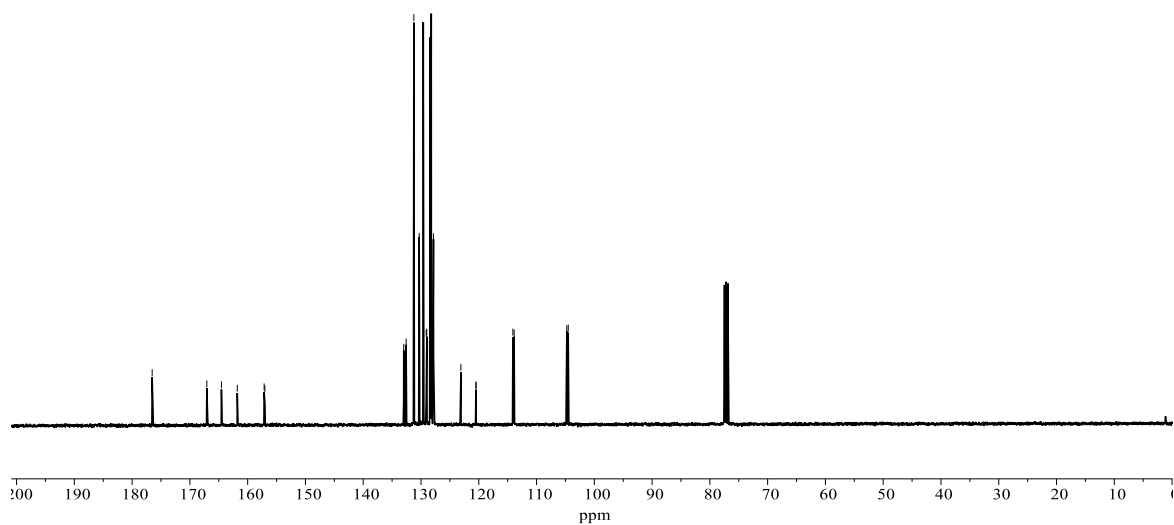
**48ea**  $^1\text{H-NMR}$   
( $\text{CDCl}_3$ , 400 MHz)

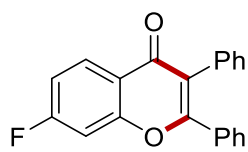


176.5  
167.1  
164.5  
161.8  
157.2  
157.0  
133.0  
132.6  
131.2  
130.3  
129.6  
129.1  
129.0  
128.4  
128.2  
127.8  
123.1  
120.5  
120.5  
114.1  
113.9  
104.8  
104.5

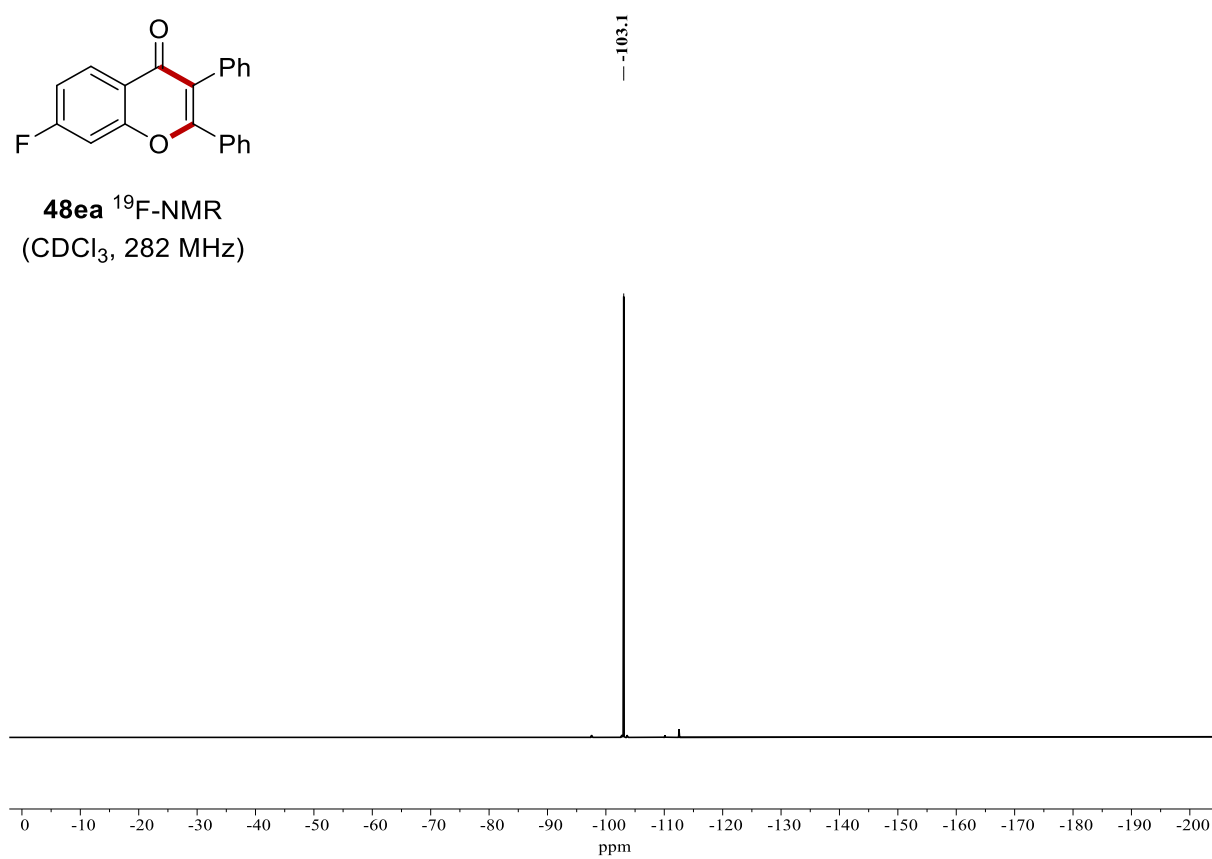


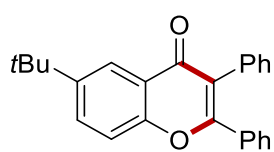
**48ea**  $^{13}\text{C-NMR}$   
( $\text{CDCl}_3$ , 101 MHz)



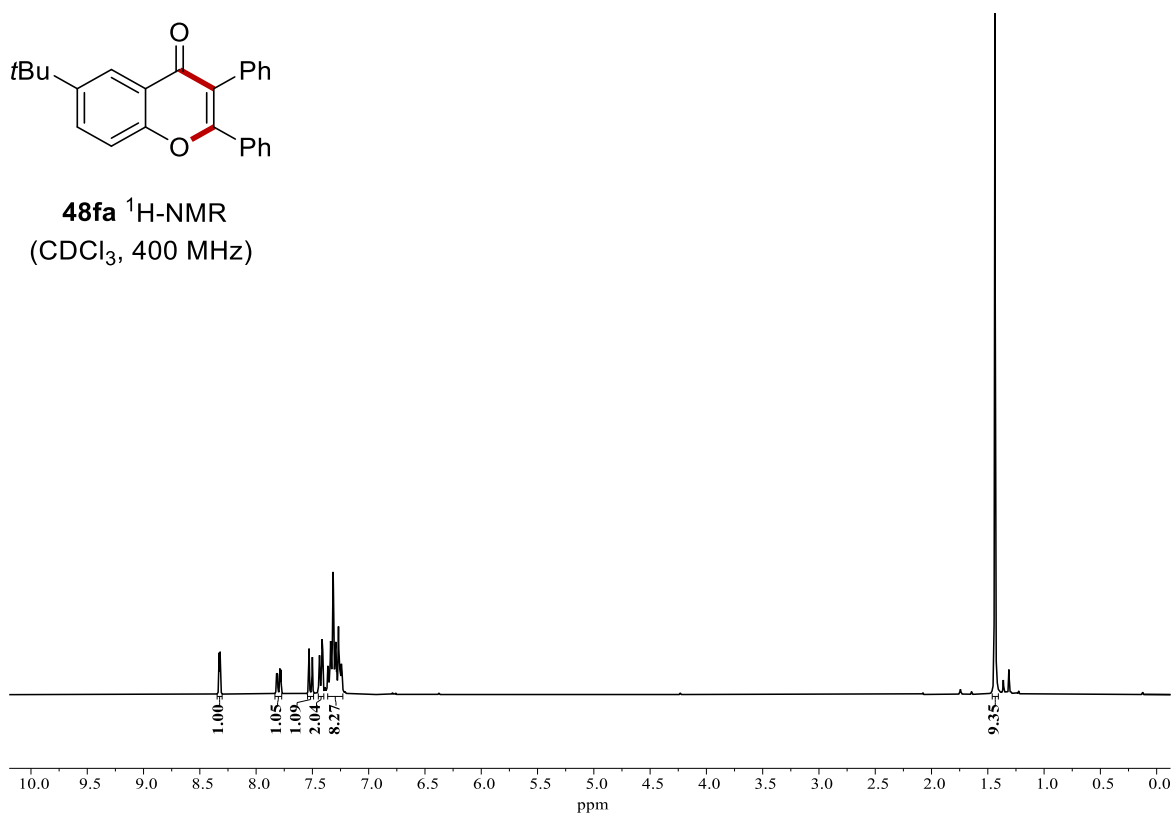


**48ea**  $^{19}\text{F}$ -NMR  
( $\text{CDCl}_3$ , 282 MHz)

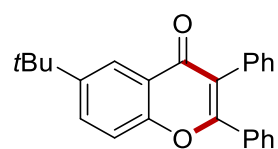




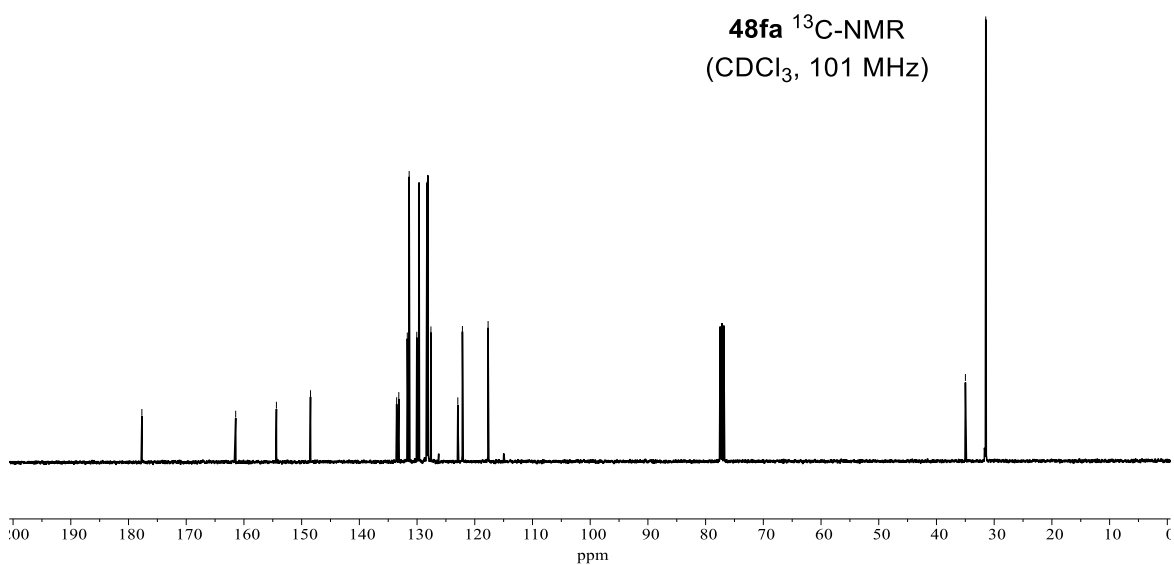
**48fa**  $^1\text{H-NMR}$   
( $\text{CDCl}_3$ , 400 MHz)

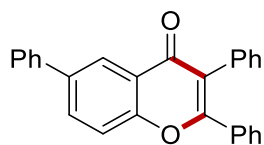


— 177.7  
— 161.4  
— 154.4  
— 148.5  
— 133.2  
— 133.5  
— 131.7  
— 131.4  
— 130.1  
— 129.6  
— 128.3  
— 128.1  
— 127.6  
— 122.9  
— 122.1  
— 117.7

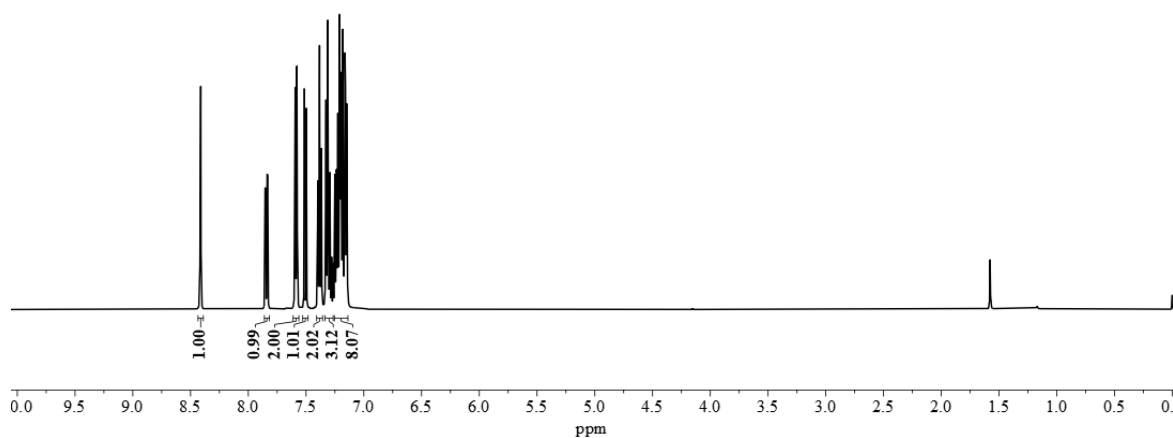


**48fa**  $^{13}\text{C-NMR}$   
( $\text{CDCl}_3$ , 101 MHz)

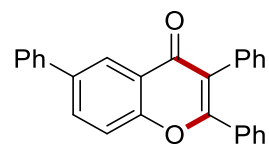




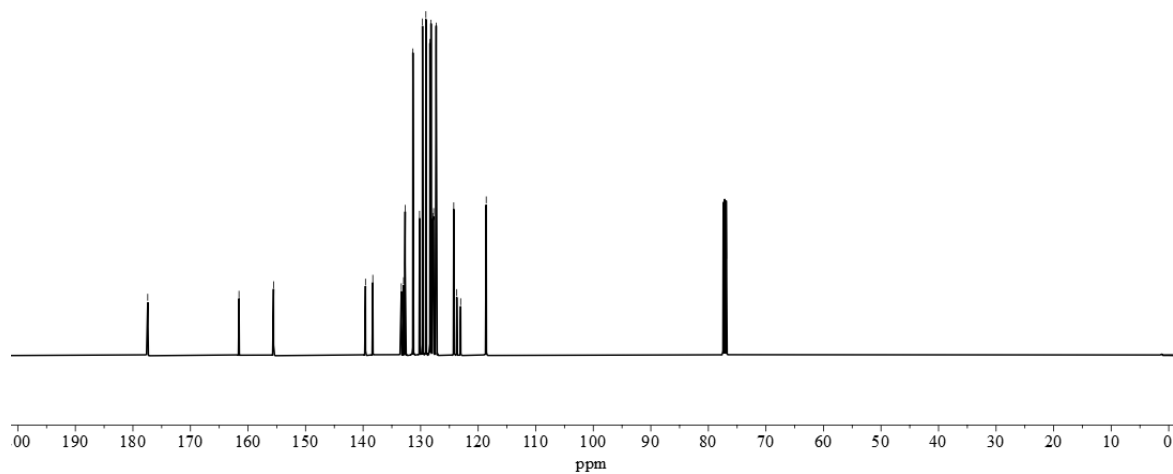
**48ga**  $^1\text{H-NMR}$   
( $\text{CDCl}_3$ , 500 MHz)



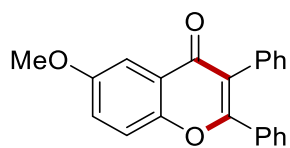
$^13\text{C-NMR}$  chemical shifts (ppm):  
 -177.4, -161.6, -155.6, -138.3, -133.4, -133.0, -132.7, -131.3, -130.2, -129.7, -129.1, -128.4, -128.2, -127.9, -127.7, -127.3, -124.2, -123.7, -123.0, -118.6



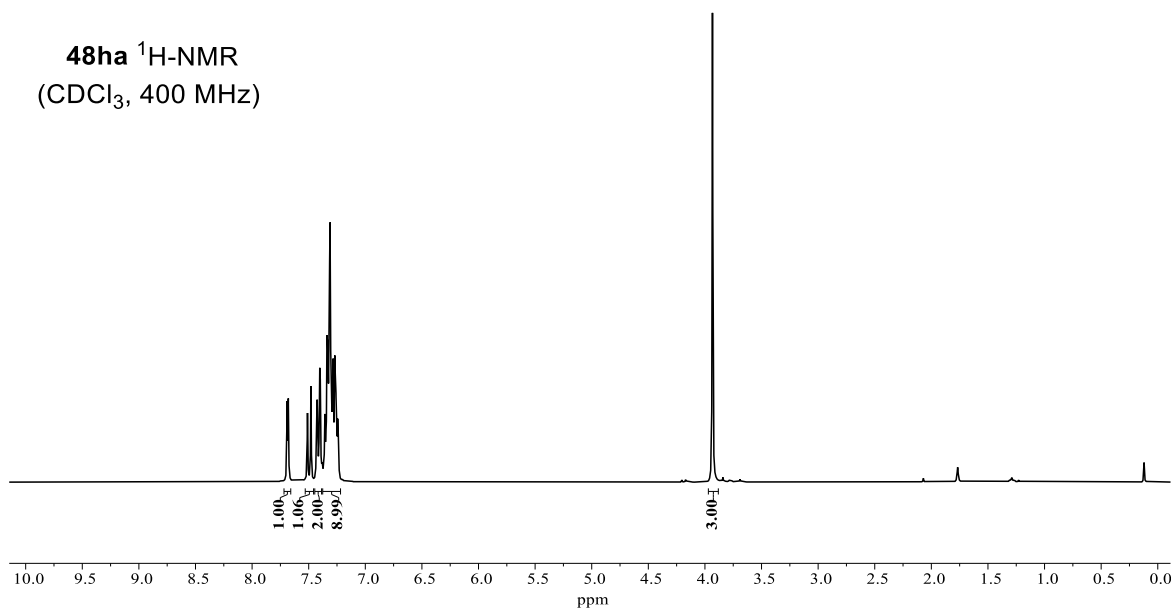
**48ga**  $^{13}\text{C-NMR}$   
( $\text{CDCl}_3$ , 126 MHz)





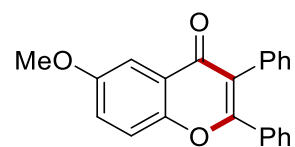


**48ha**  $^1\text{H-NMR}$   
( $\text{CDCl}_3$ , 400 MHz)

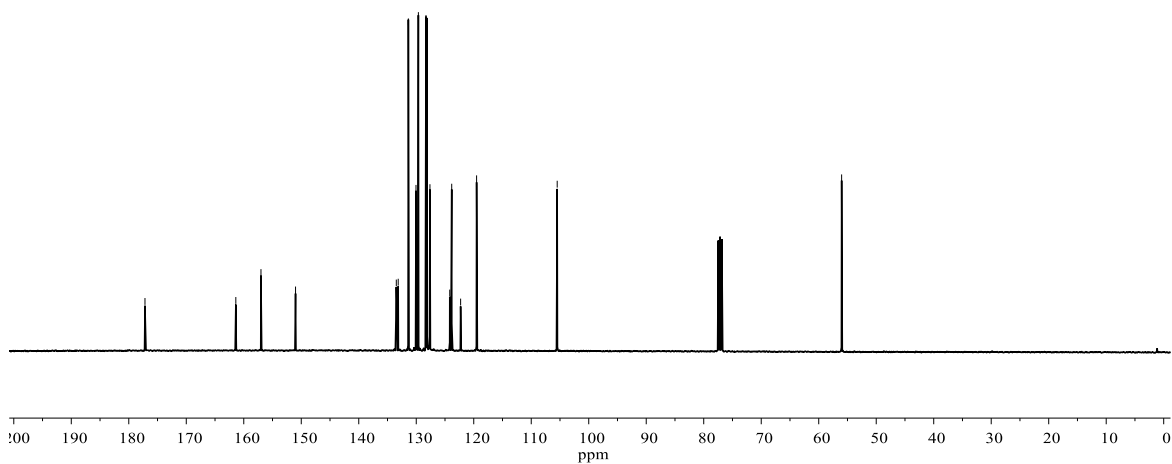


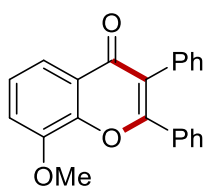
177.2  
161.4  
157.0  
151.0  
133.5  
133.1  
131.4  
130.0  
129.6  
128.3  
128.1  
127.6  
124.2  
123.8  
122.3  
119.5  
105.5

56.0

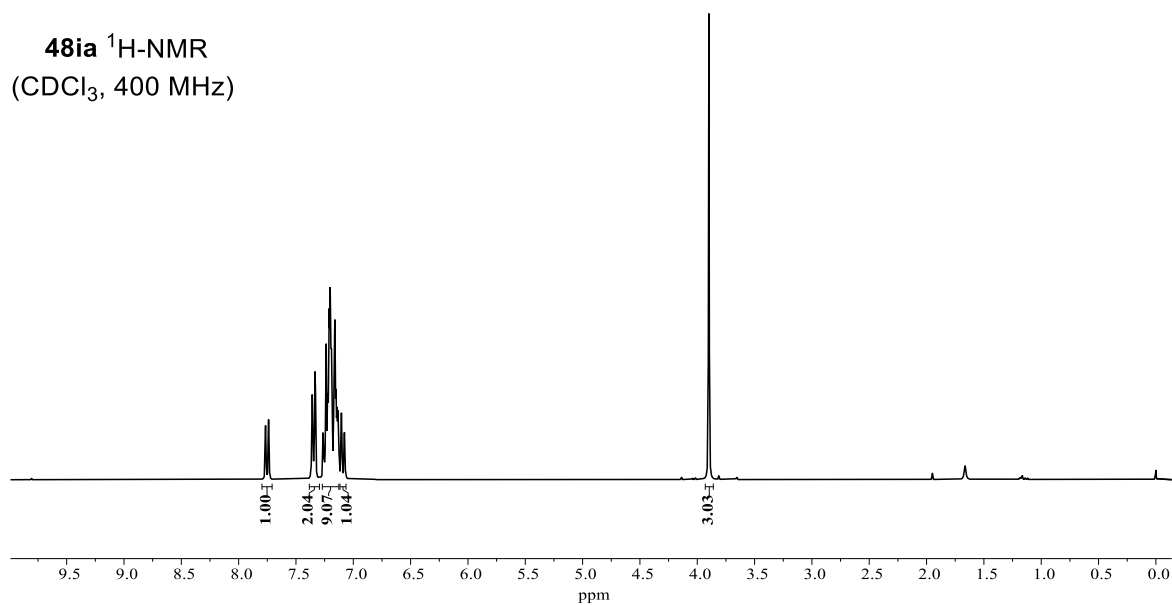


**48ha**  $^{13}\text{C-NMR}$   
( $\text{CDCl}_3$ , 101 MHz)

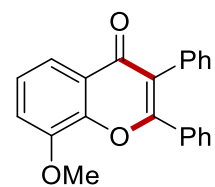




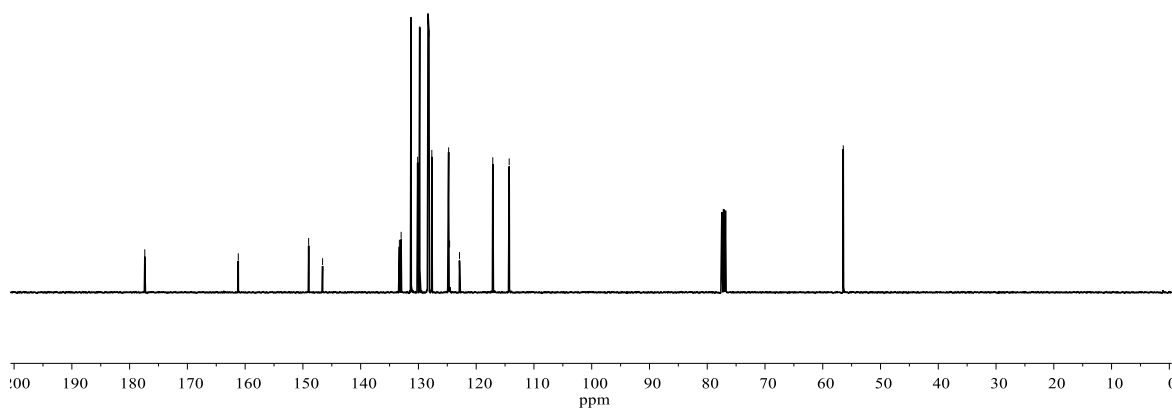
**48ia**  $^1\text{H-NMR}$   
( $\text{CDCl}_3$ , 400 MHz)

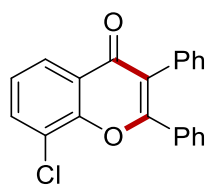


177.4  
161.2  
149.0  
146.6  
133.3  
133.0  
131.3  
130.1  
129.8  
128.3  
128.2  
127.7  
124.8  
124.6  
122.9  
117.1  
114.3  
56.4

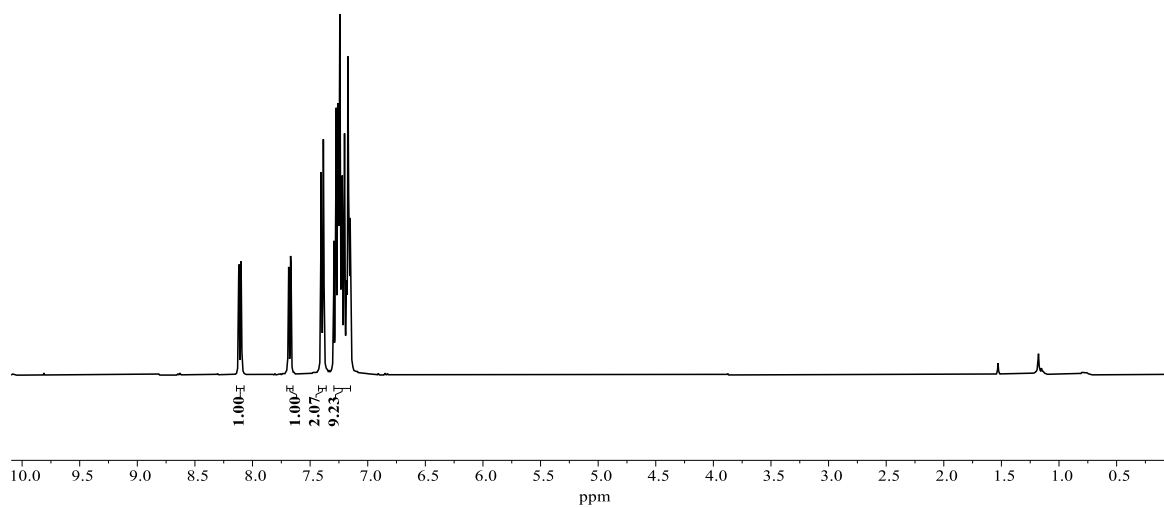


**48ia**  $^{13}\text{C-NMR}$   
( $\text{CDCl}_3$ , 101 MHz)

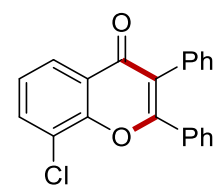




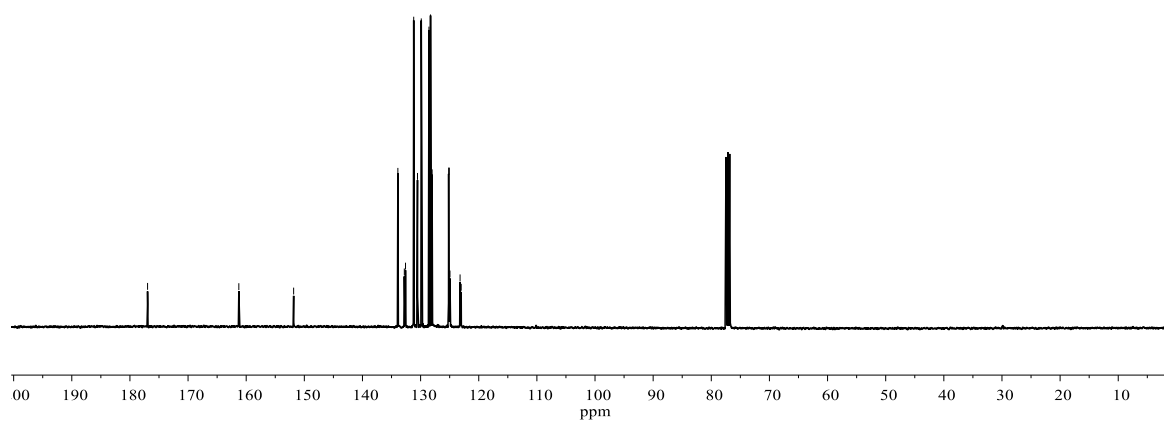
**48ja**  $^1\text{H-NMR}$   
( $\text{CDCl}_3$ , 400 MHz)

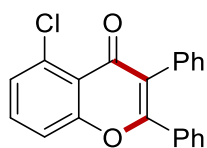


177.0  
161.3  
151.8  
133.9  
132.8  
132.6  
131.2  
130.5  
129.9  
128.6  
128.3  
128.0  
125.2  
125.1  
125.0  
123.2  
123.0

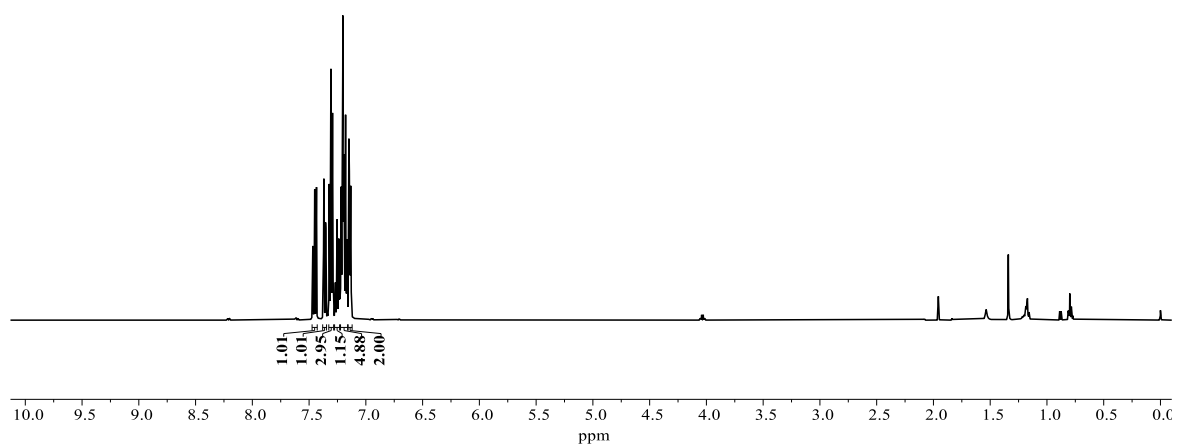


**48ja**  $^{13}\text{C-NMR}$   
( $\text{CDCl}_3$ , 101 MHz)

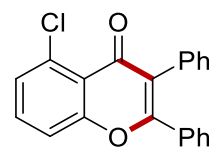




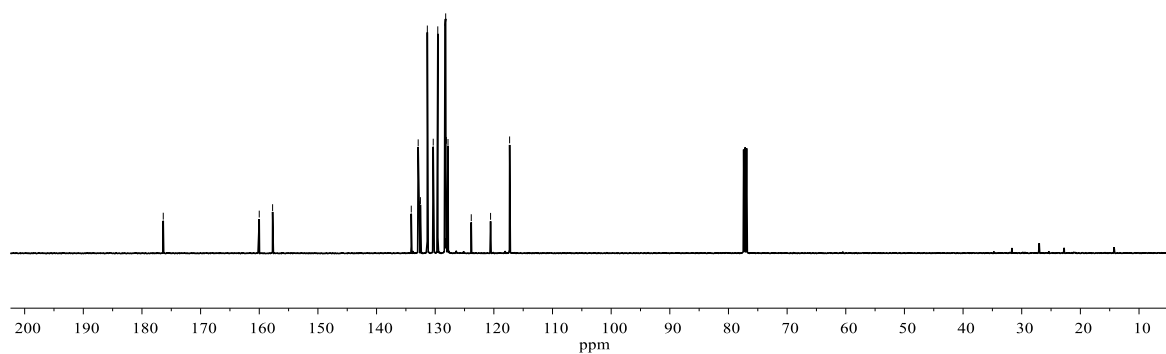
**48ka**  $^1\text{H-NMR}$   
( $\text{CDCl}_3$ , 500 MHz)

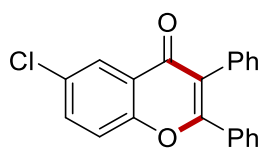


176.4  
160.0  
157.7  
134.1  
132.9  
132.7  
132.5  
131.3  
130.3  
129.6  
128.3  
128.2  
128.1  
127.8  
123.9  
120.6  
117.3

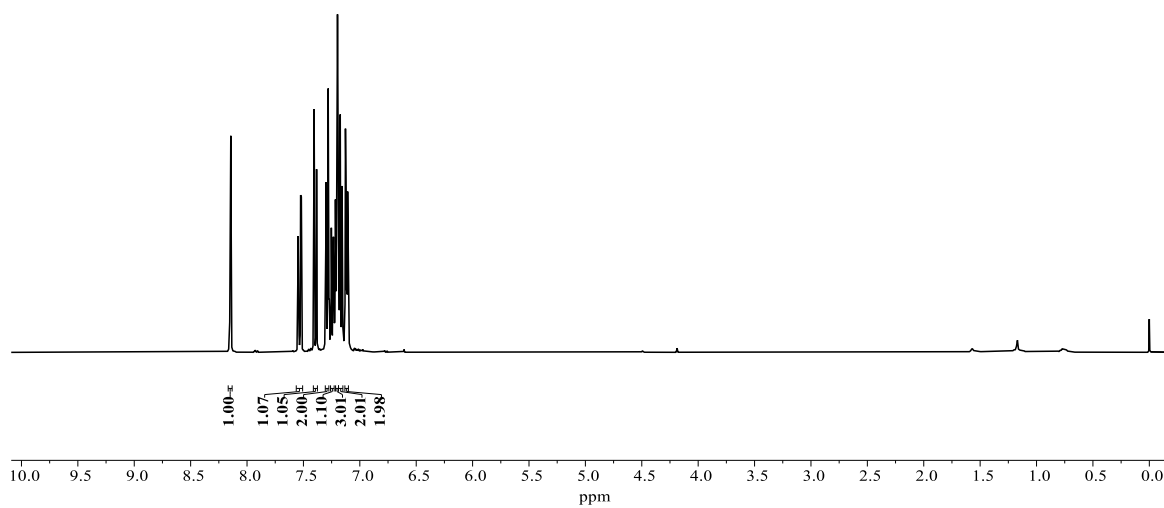


**48ka**  $^{13}\text{C-NMR}$   
( $\text{CDCl}_3$ , 126 MHz)

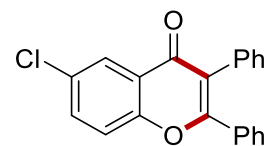




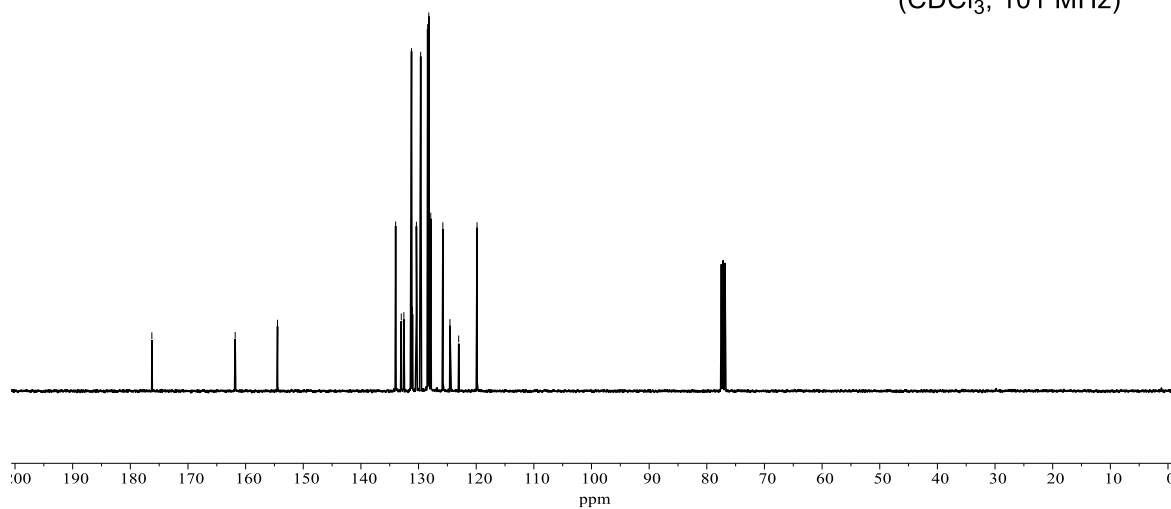
**481a**  $^1\text{H-NMR}$   
( $\text{CDCl}_3$ , 400 MHz)

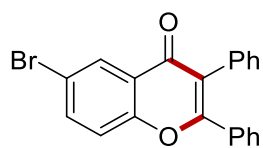


176.3  
161.8  
154.5  
134.0  
133.0  
132.5  
131.2  
131.1  
130.4  
129.6  
128.4  
128.2  
127.9  
125.8  
124.6  
123.0  
119.9

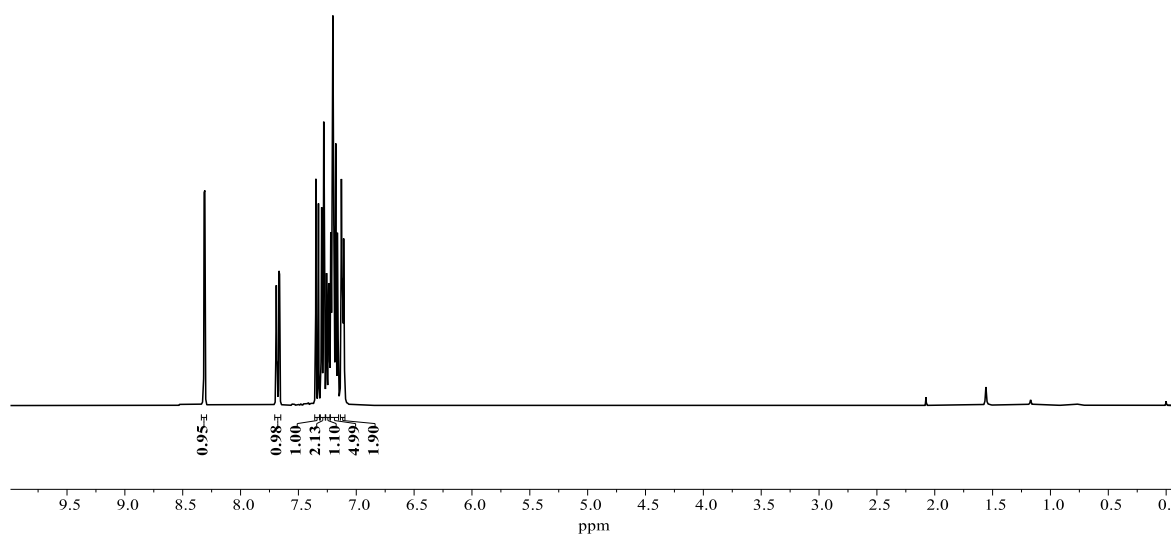


**481a**  $^{13}\text{C-NMR}$   
( $\text{CDCl}_3$ , 101 MHz)

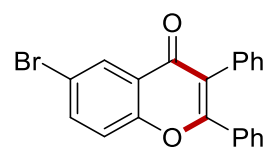




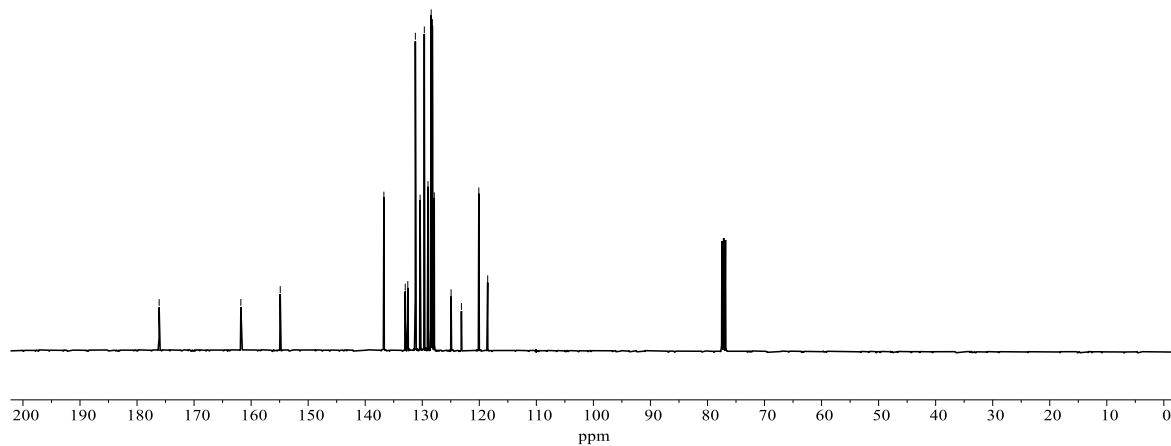
**48ma**  $^1\text{H-NMR}$   
( $\text{CDCl}_3$ , 400 MHz)

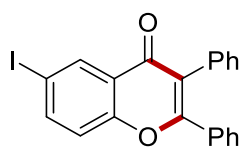


176.1  
161.8  
154.9  
136.7  
133.0  
132.5  
131.2  
130.4  
129.6  
129.0  
128.4  
128.2  
127.9  
124.9  
123.1  
120.1  
118.5

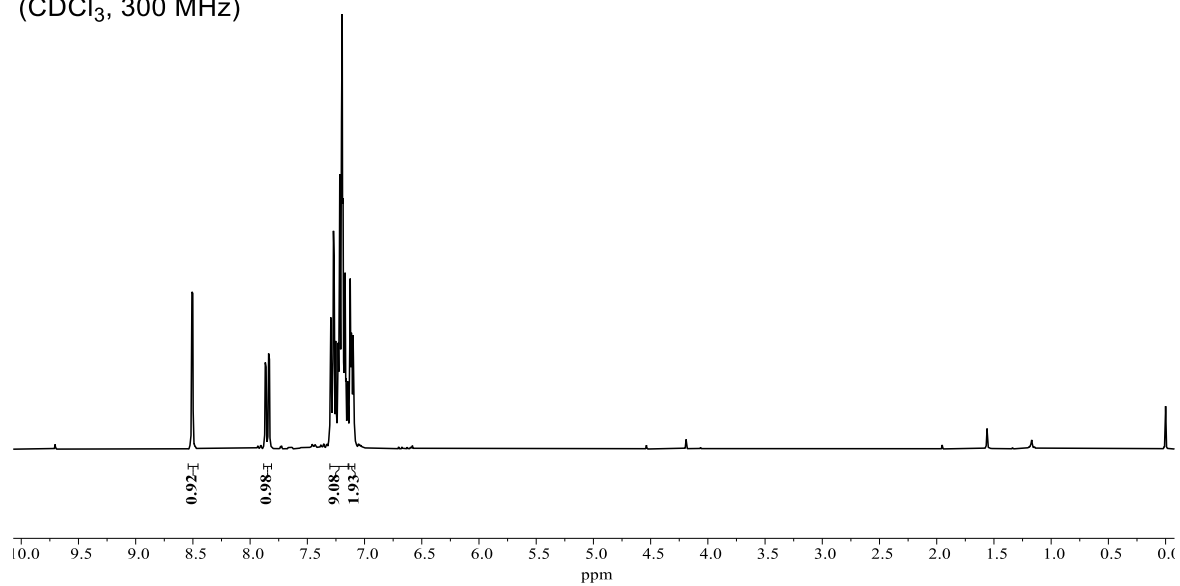


**48ma**  $^{13}\text{C-NMR}$   
( $\text{CDCl}_3$ , 101 MHz)

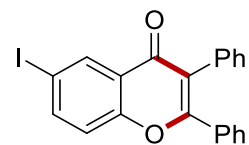




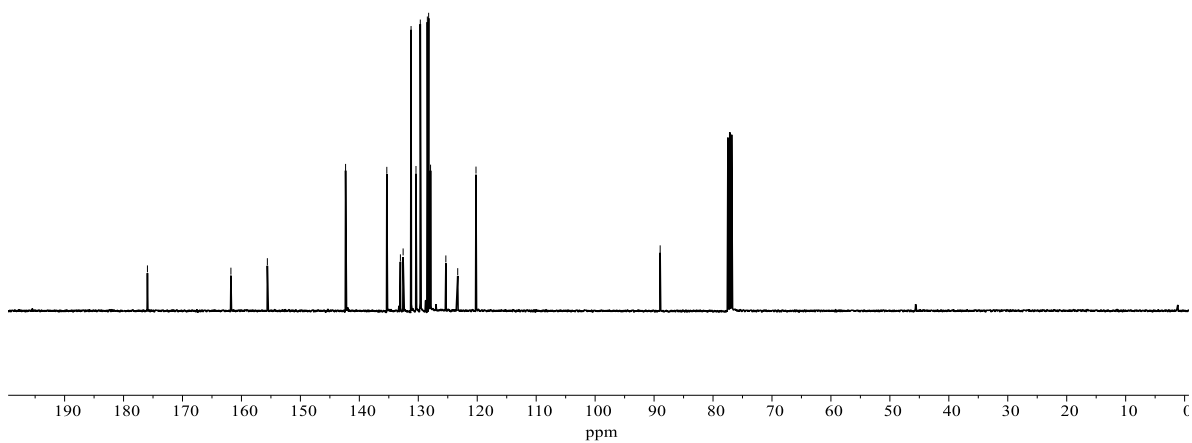
**48na**  $^1\text{H-NMR}$   
( $\text{CDCl}_3$ , 300 MHz)

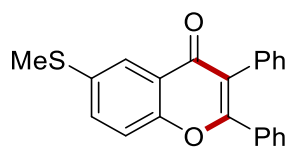


175.9  
161.8  
155.6  
142.3  
135.3  
133.0  
132.6  
131.2  
130.4  
129.7  
128.5  
128.2  
127.9  
125.3  
123.3  
120.2  
89.0

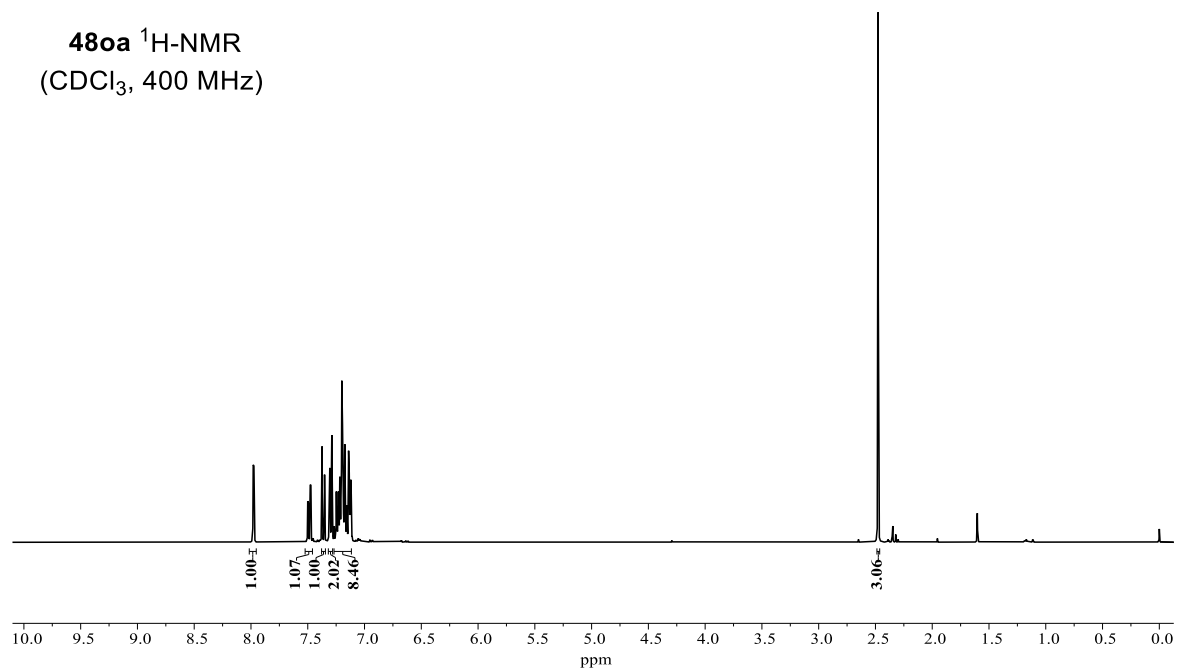


**48na**  $^{13}\text{C-NMR}$   
( $\text{CDCl}_3$ , 101 MHz)



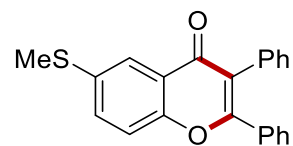


**480a**  $^1\text{H-NMR}$   
( $\text{CDCl}_3$ , 400 MHz)

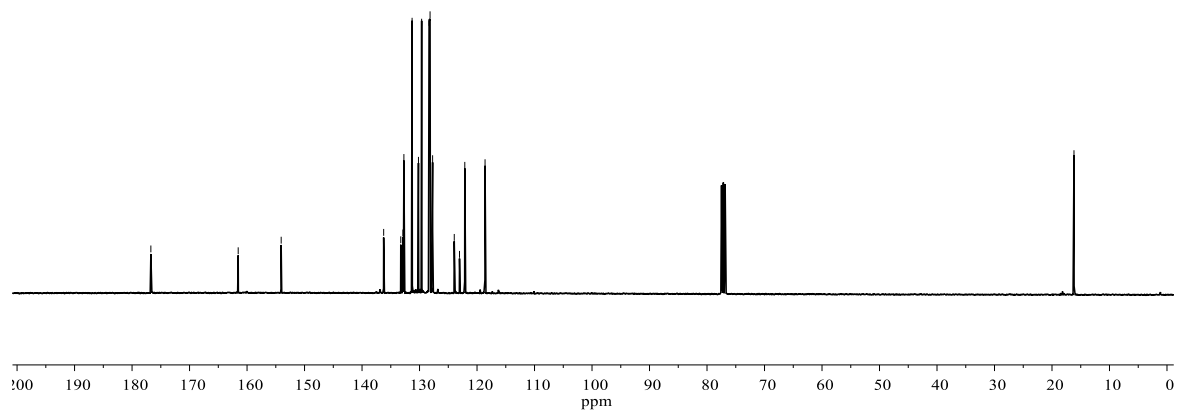


176.7  
161.5  
154.1  
136.2  
133.3  
132.9  
132.7  
131.3  
130.2  
129.6  
128.3  
128.2  
127.7  
124.0  
123.0  
122.1  
118.6

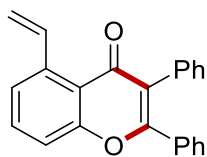
16.2



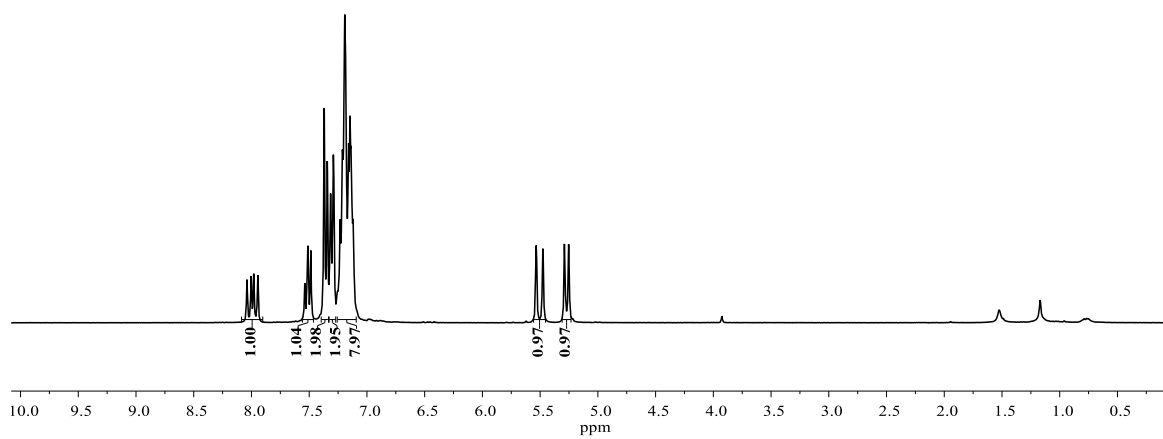
**480a**  $^{13}\text{C-NMR}$   
( $\text{CDCl}_3$ , 101 MHz)



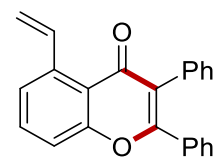




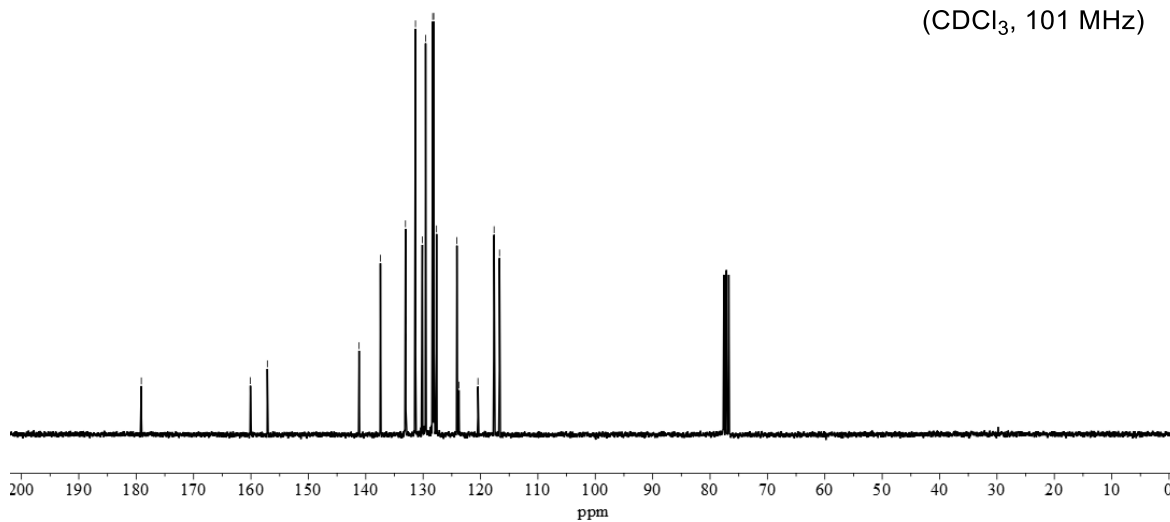
**48pa**  $^1\text{H-NMR}$   
( $\text{CDCl}_3$ , 400 MHz)

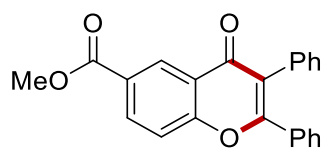


179.1  
160.1  
157.1  
141.2  
137.4  
133.1  
133.0  
133.0  
131.3  
130.1  
129.6  
128.3  
128.1  
127.7  
124.1  
123.8  
120.4  
117.6  
116.7

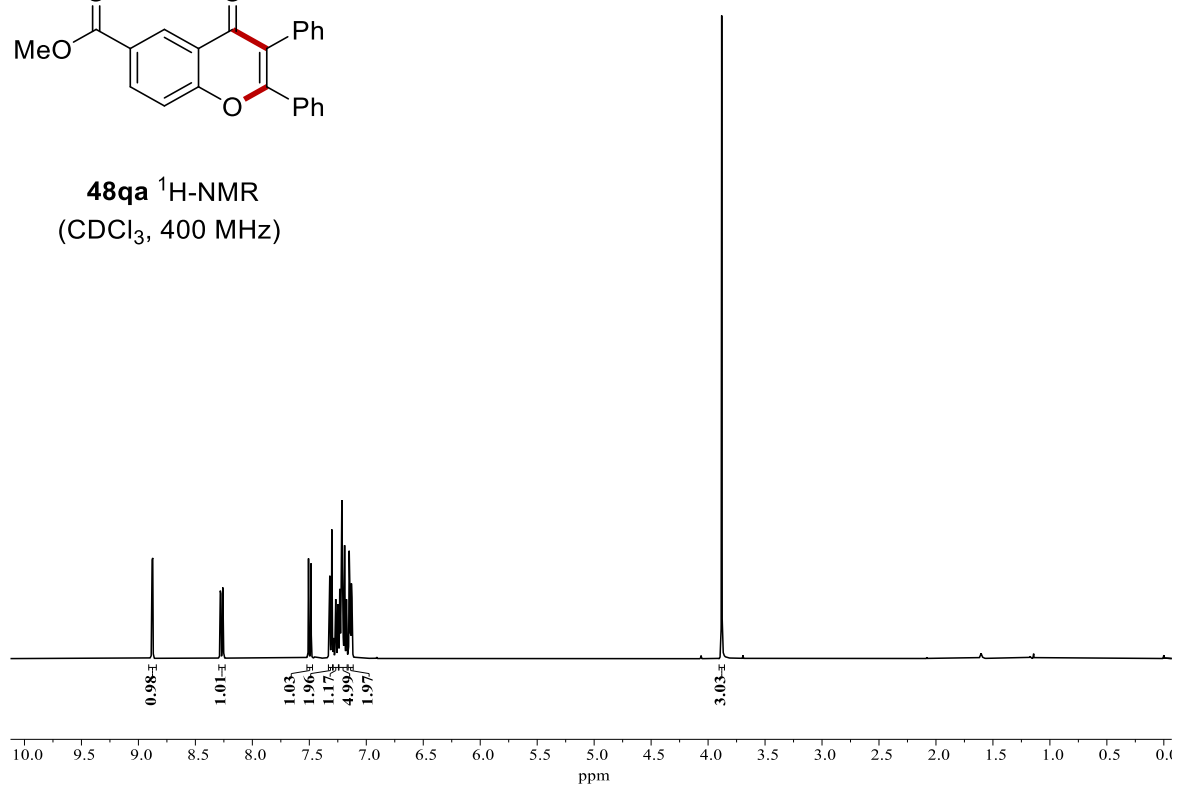


**48pa**  $^{13}\text{C-NMR}$   
( $\text{CDCl}_3$ , 101 MHz)

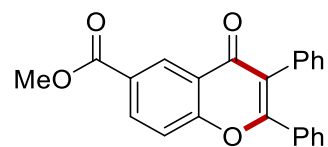




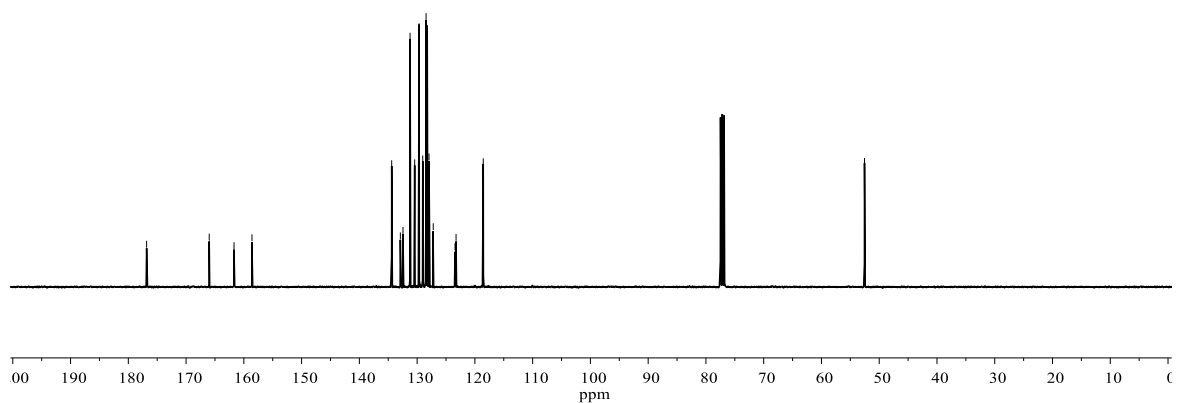
**48qa**  $^1\text{H-NMR}$   
( $\text{CDCl}_3$ , 400 MHz)

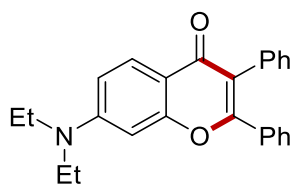


176.8  
166.0  
161.7  
158.6  
134.4  
132.9  
132.4  
131.2  
130.4  
129.7  
129.0  
128.4  
128.2  
127.9  
127.2  
123.4  
123.3  
118.6

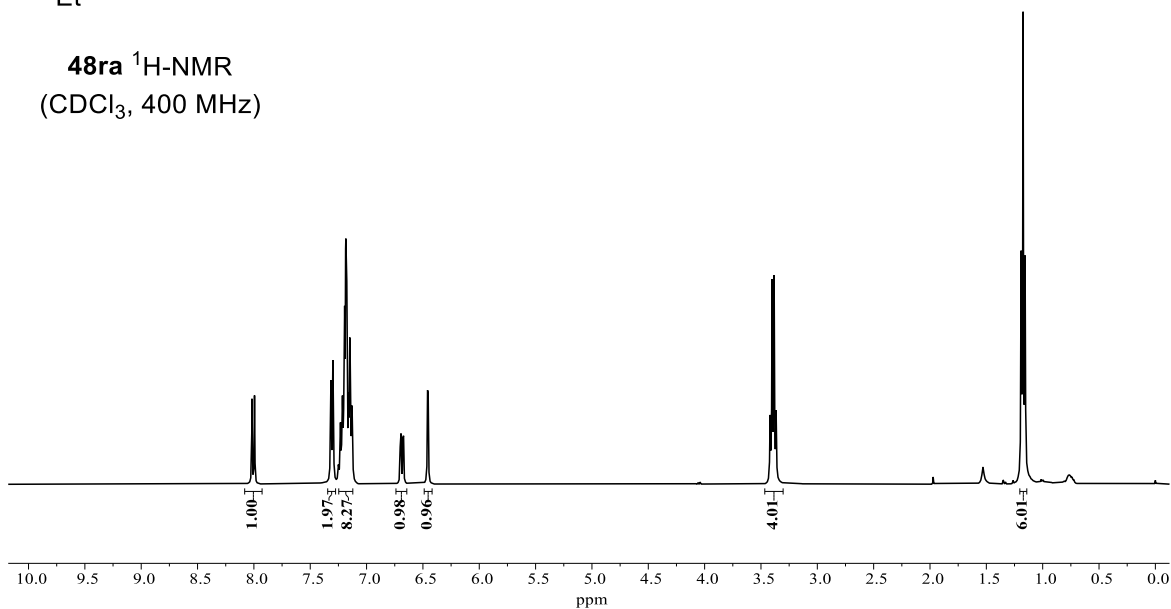


**48qa**  $^{13}\text{C-NMR}$   
( $\text{CDCl}_3$ , 101 MHz)

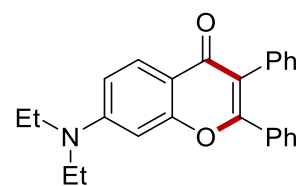




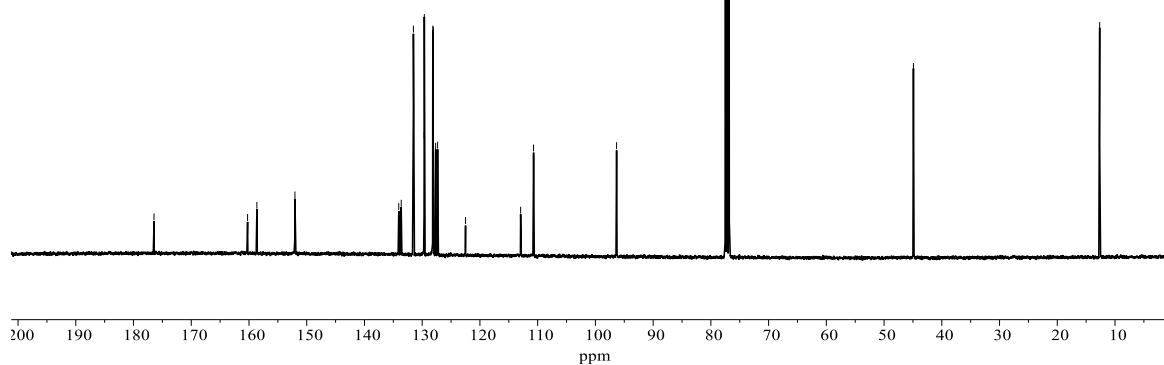
**48ra**  $^1\text{H-NMR}$   
( $\text{CDCl}_3$ , 400 MHz)

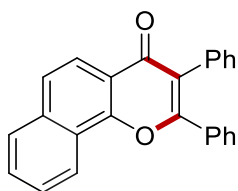


176.5  
160.2  
158.6  
152.0  
134.1  
133.6  
131.5  
129.7  
129.6  
128.2  
128.1  
127.7  
122.5  
112.9  
110.7  
96.3  
44.9  
12.7

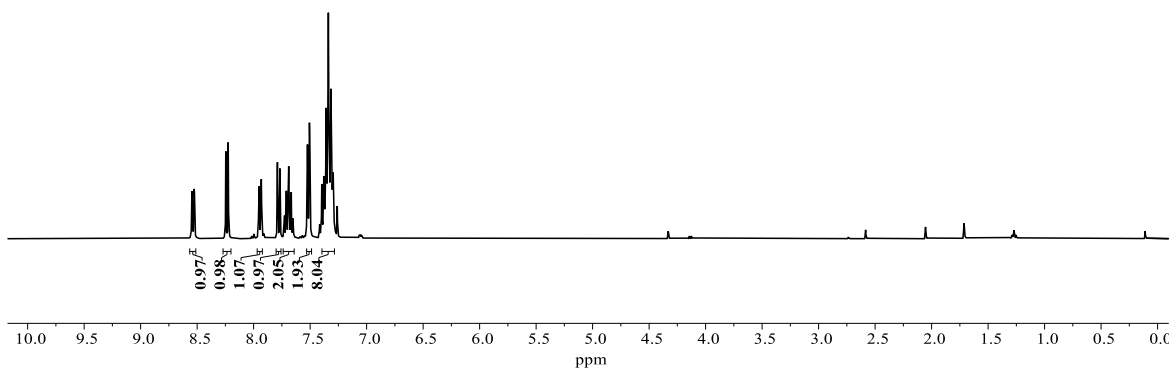


**48ra**  $^{13}\text{C-NMR}$   
( $\text{CDCl}_3$ , 101 MHz)

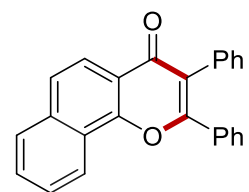




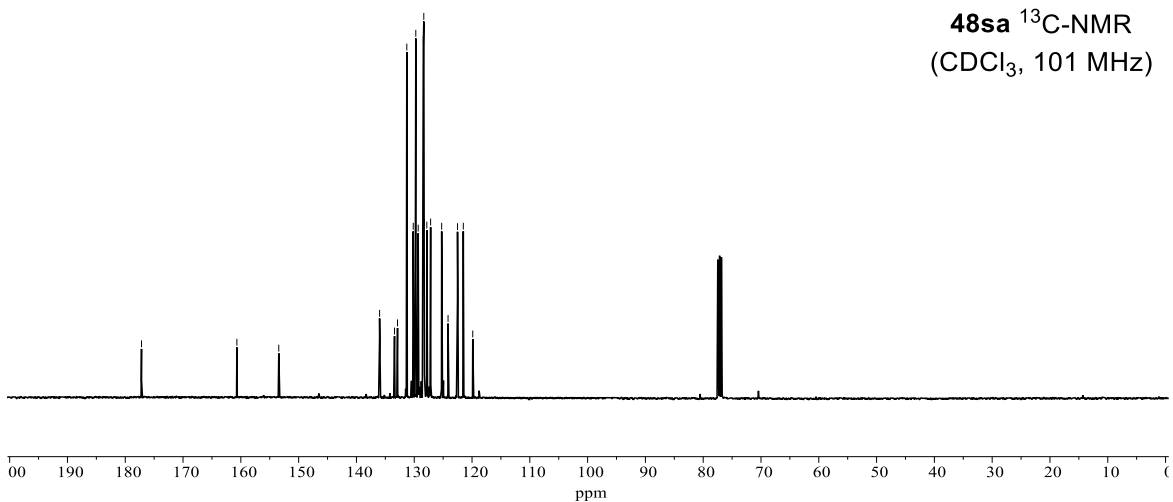
**48sa**  $^1\text{H-NMR}$   
( $\text{CDCl}_3$ , 400 MHz)

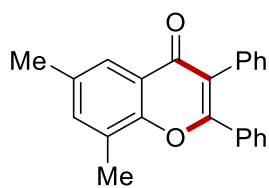


177.2  
160.7  
153.4  
136.0  
133.4  
132.9  
131.3  
130.2  
129.7  
129.3  
128.4  
128.3  
128.3  
127.8  
127.2  
125.3  
124.1  
122.5  
121.5  
119.9

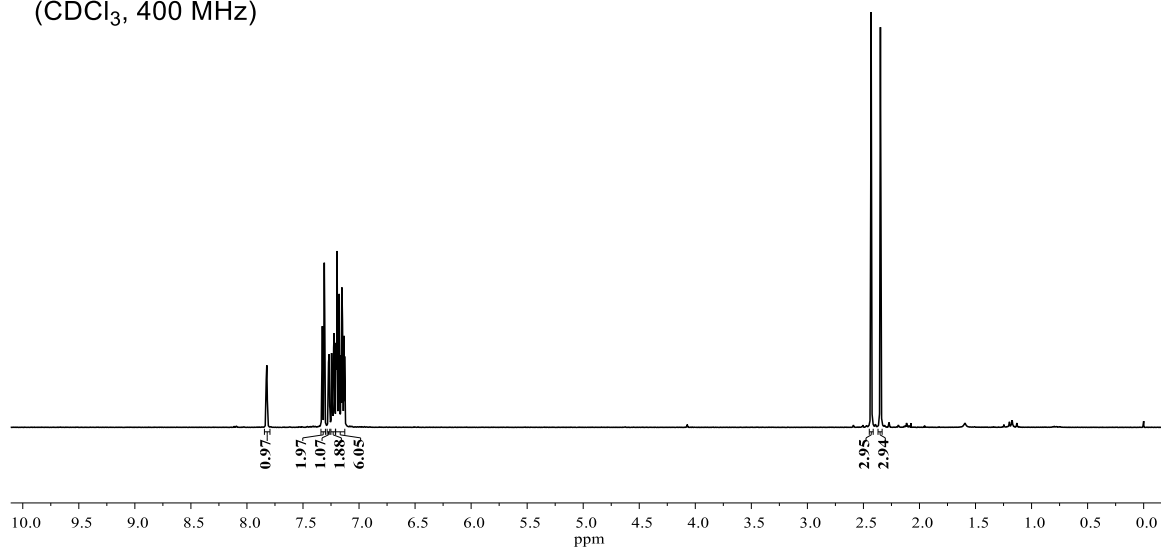


**48sa**  $^{13}\text{C-NMR}$   
( $\text{CDCl}_3$ , 101 MHz)



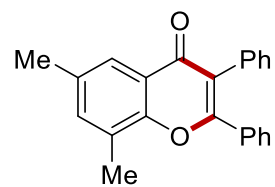


**48ta**  $^1\text{H-NMR}$   
( $\text{CDCl}_3$ , 400 MHz)

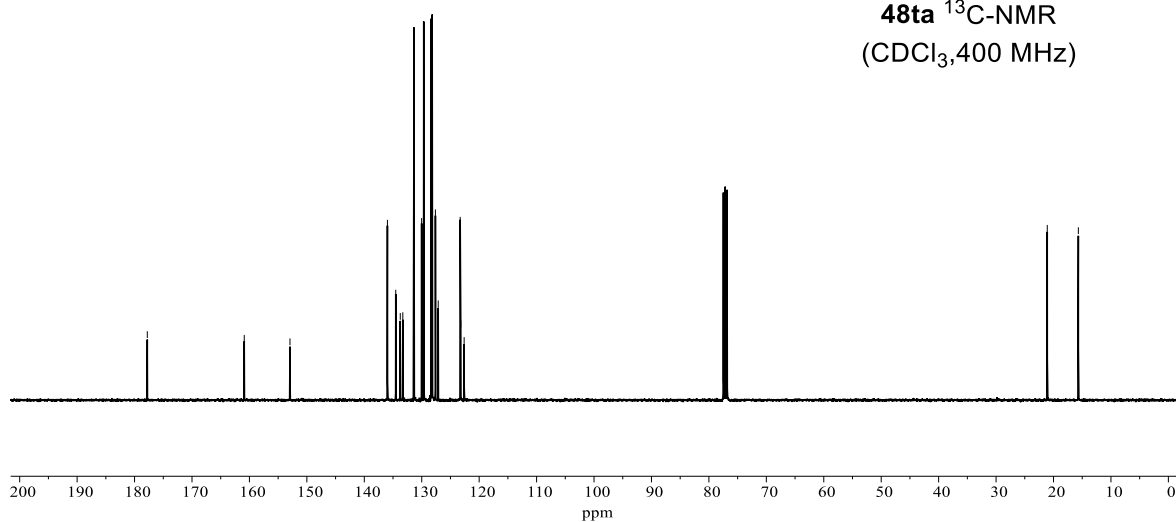


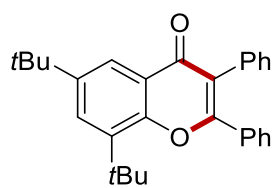
— 177.8  
— 160.9  
— 152.9  
— 136.0  
— 134.5  
— 133.7  
— 133.3  
— 131.4  
— 130.0  
— 129.7  
— 128.3  
— 128.2  
— 127.6  
— 127.1  
— 123.3  
— 123.2  
— 122.6

— 21.1  
— 15.7

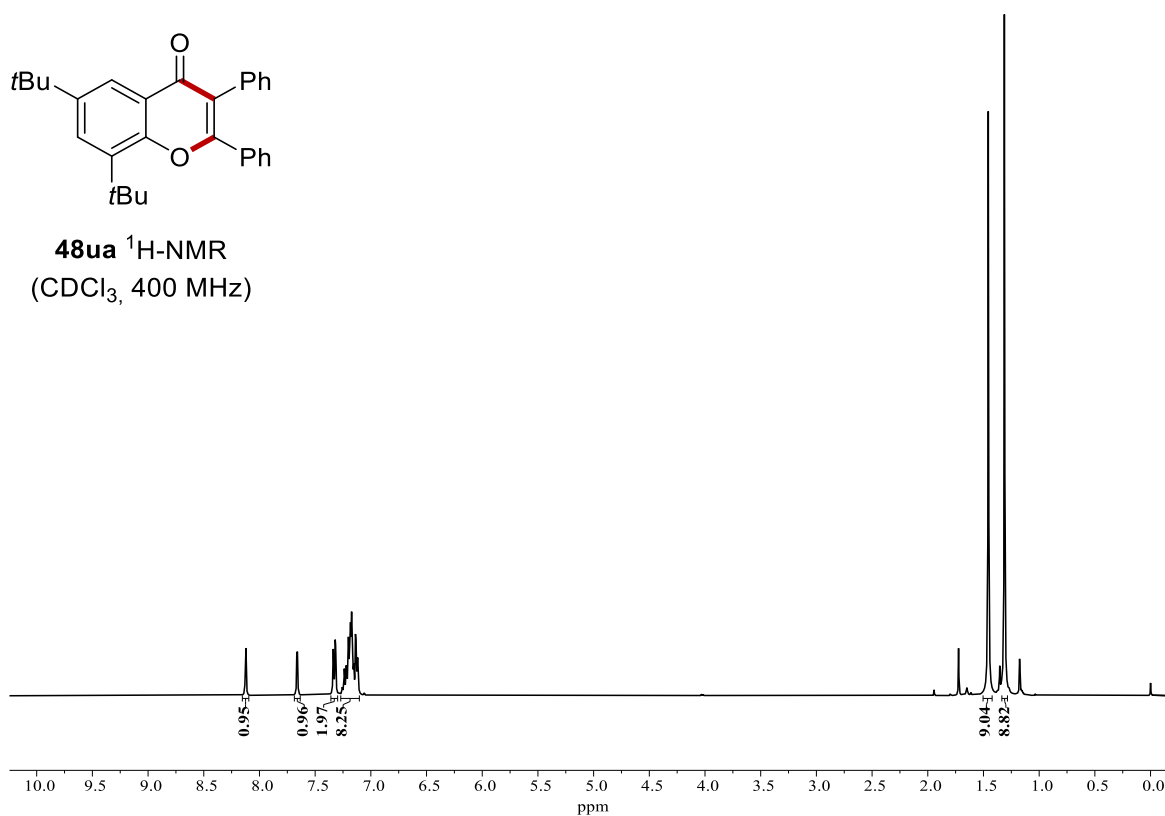


**48ta**  $^{13}\text{C-NMR}$   
( $\text{CDCl}_3$ , 400 MHz)



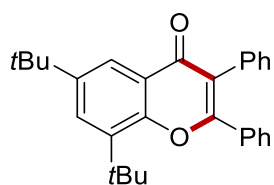


**48ua**  $^1\text{H-NMR}$   
( $\text{CDCl}_3$ , 400 MHz)

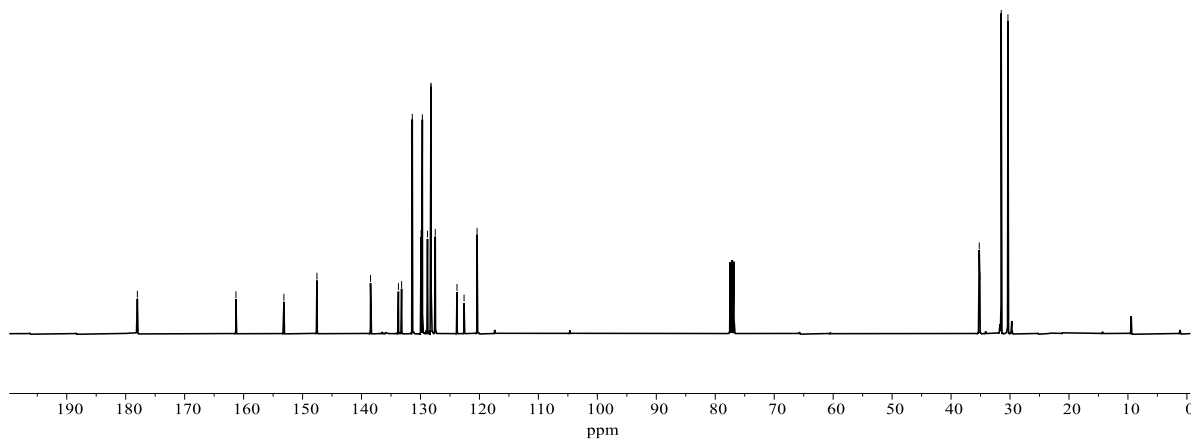


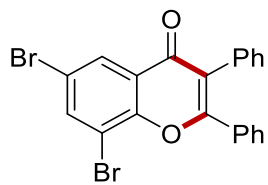
— 178.0  
— 161.3  
— 153.2  
— 147.6  
— 138.5  
— 133.7  
— 133.2  
— 131.4  
— 129.9  
— 129.7  
— 128.8  
— 128.2  
— 128.2  
— 127.5  
— 123.8  
— 122.6  
— 120.4

— 35.2  
— 35.1  
— 31.5  
— 30.4

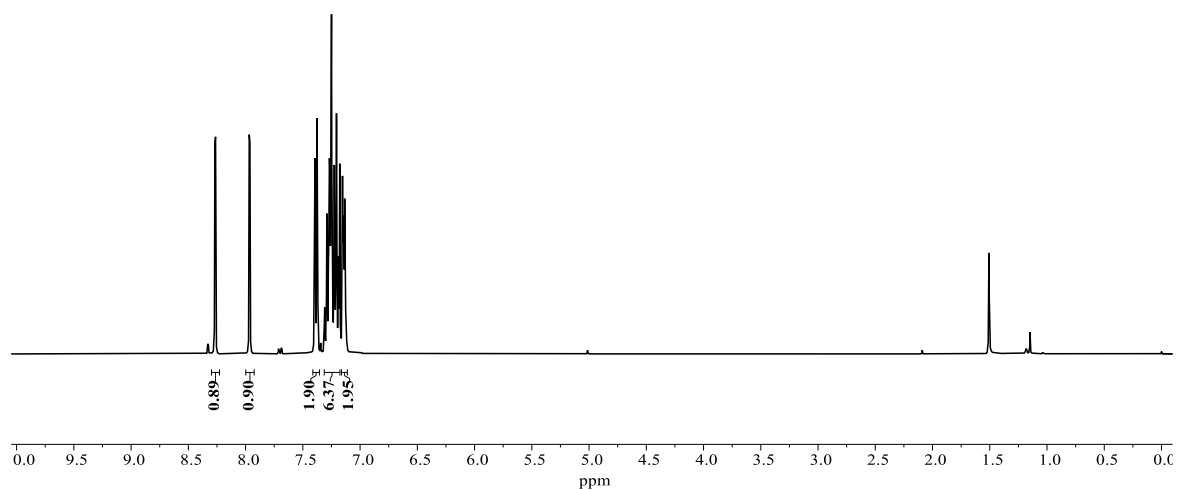


**48ua**  $^{13}\text{C-NMR}$   
( $\text{CDCl}_3$ , 101 MHz)

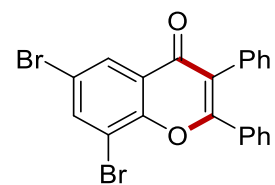




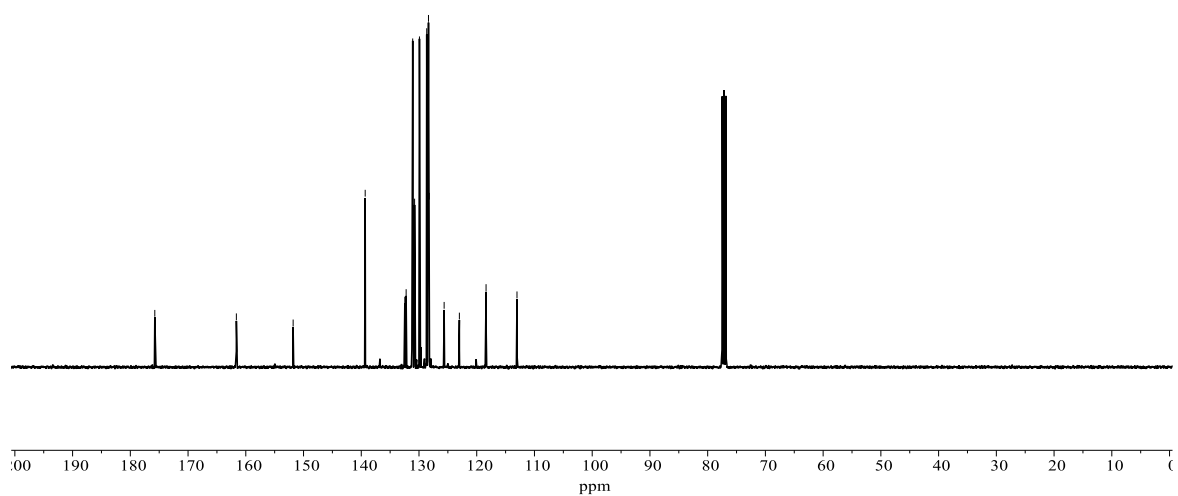
**48va**  $^1\text{H-NMR}$   
( $\text{CDCl}_3$ , 400 MHz)

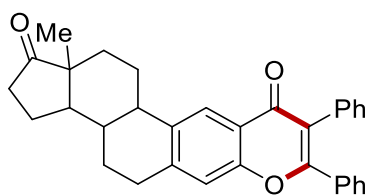


— 175.8  
— 161.6  
— 151.8  
— 139.3  
— 132.5  
— 132.2  
— 131.1  
— 130.8  
— 129.9  
— 128.7  
— 128.4  
— 128.4  
— 128.2  
— 125.6  
— 123.0  
— 118.4  
— 113.0

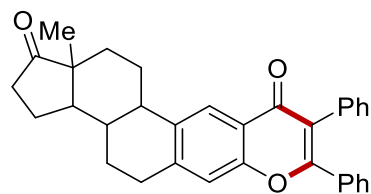
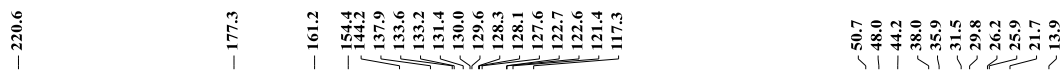
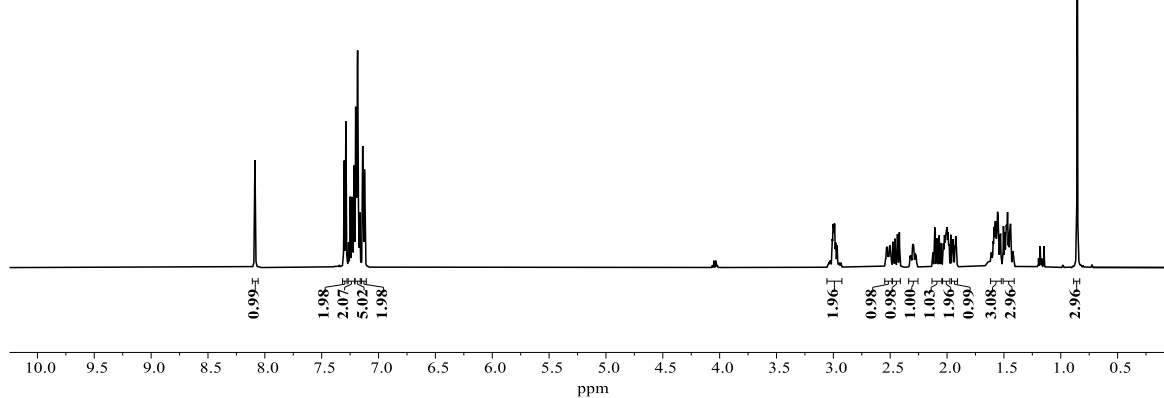


**48va**  $^{13}\text{C-NMR}$   
( $\text{CDCl}_3$ , 101 MHz)

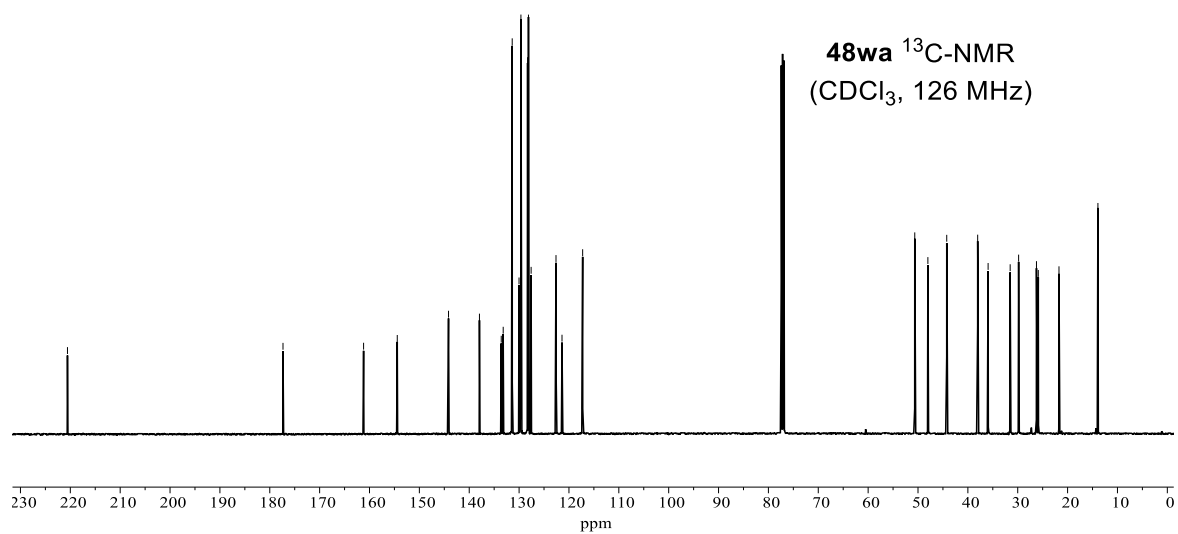




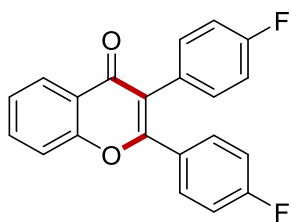
**48wa**  $^1\text{H-NMR}$   
( $\text{CDCl}_3$ , 500 MHz)



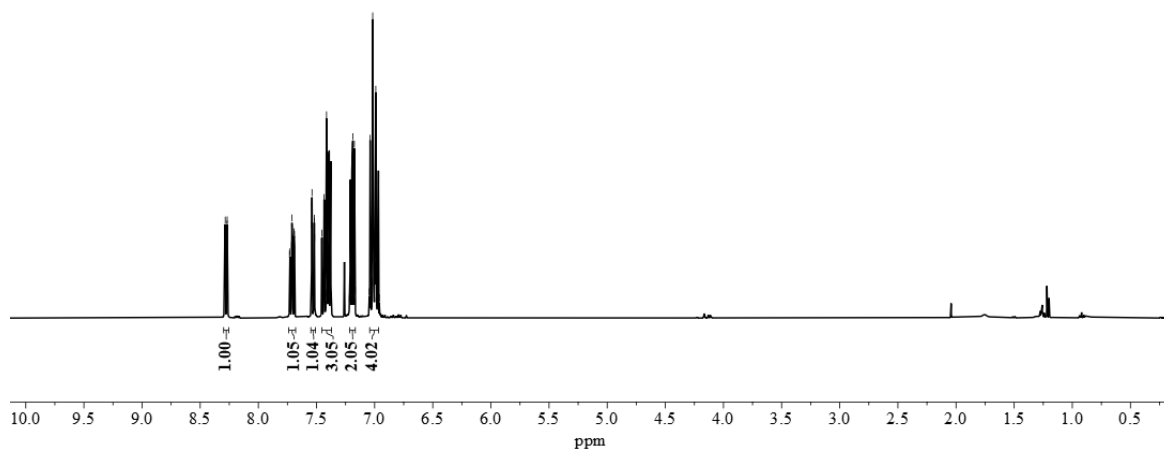
**48wa**  $^{13}\text{C-NMR}$   
( $\text{CDCl}_3$ , 126 MHz)



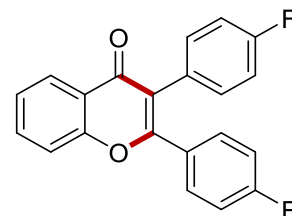




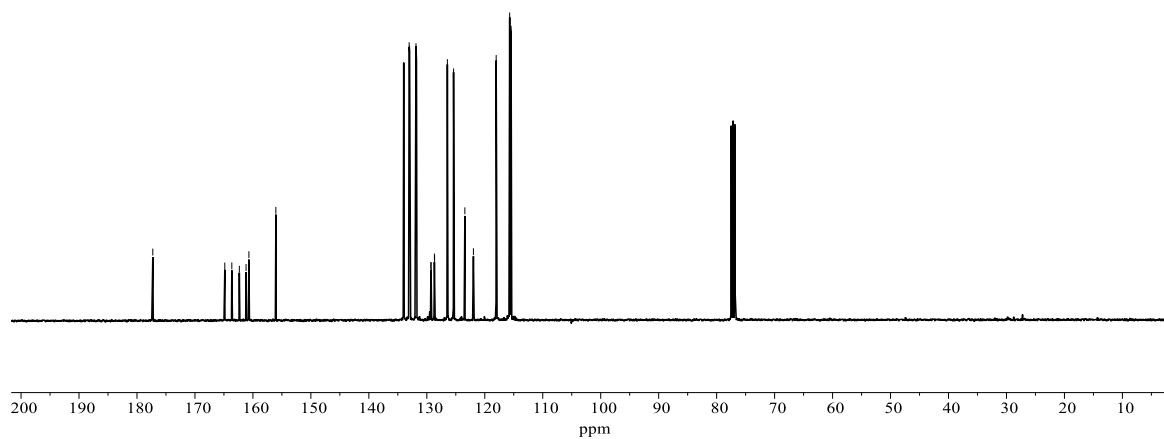
**48ac**  $^1\text{H-NMR}$   
( $\text{CDCl}_3$ , 400 MHz)

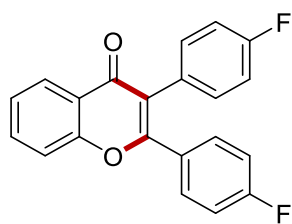


$^{13}\text{C-NMR}$  chemical shifts (ppm): 177.3, 164.9, 163.6, 162.3, 161.2, 160.7, 156.0, 134.0, 133.0, 133.0, 131.9, 131.8, 129.3, 129.3, 128.7, 128.7, 126.5, 125.4, 123.4, 122.0, 118.0, 115.7, 115.5, 115.5.

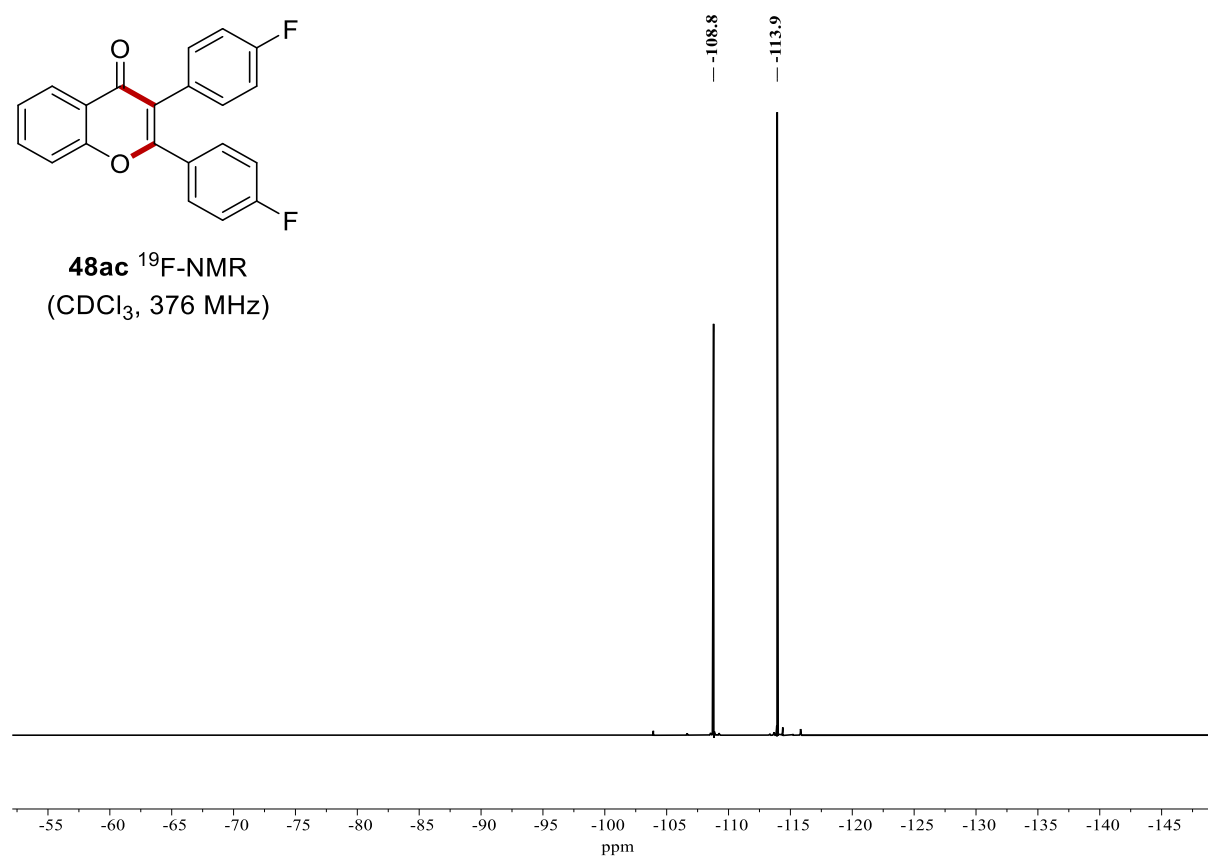


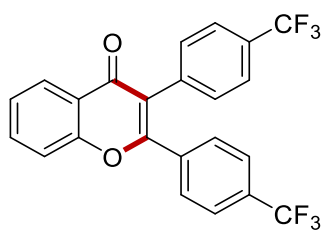
**48ac**  $^{13}\text{C-NMR}$   
( $\text{CDCl}_3$ , 101 MHz)



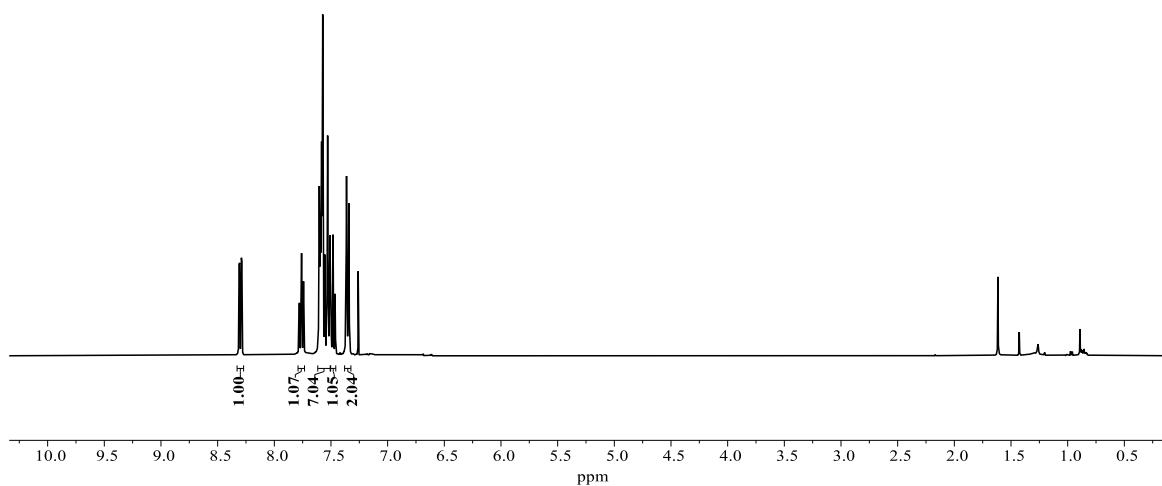


**48ac**  $^{19}\text{F}$ -NMR  
( $\text{CDCl}_3$ , 376 MHz)

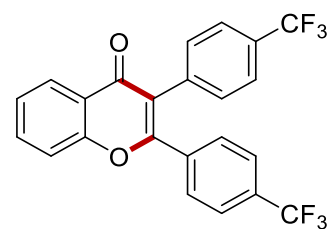




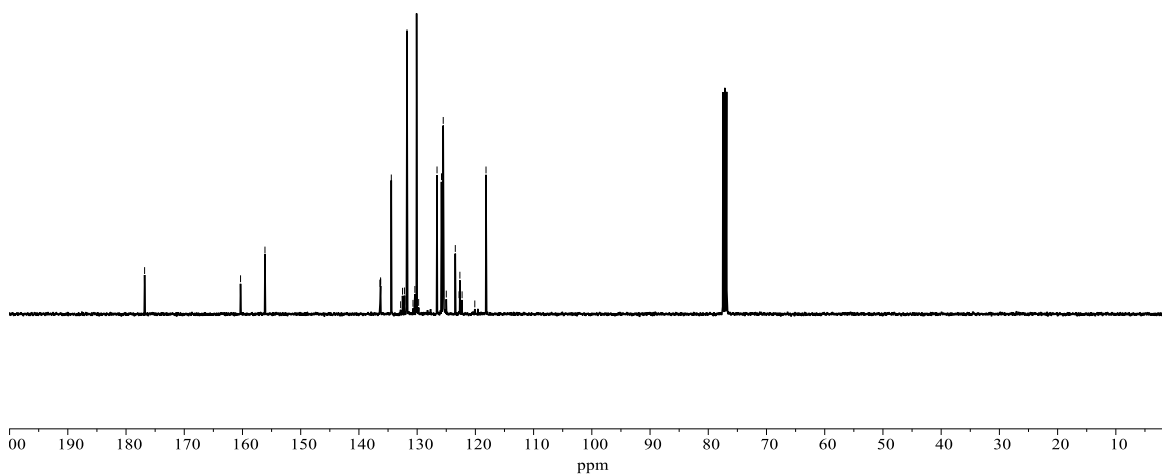
**48ah**  $^1\text{H-NMR}$   
( $\text{CDCl}_3$ , 400 MHz)

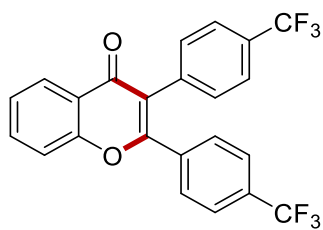


176.8  
160.3  
156.1  
136.4  
136.4  
136.3  
136.3  
134.4  
132.8  
132.5  
132.2  
131.9  
131.7  
130.7  
130.4  
130.1  
129.7  
126.6  
125.8  
125.5  
125.0  
123.4  
122.8  
122.7  
122.3  
120.1  
118.2

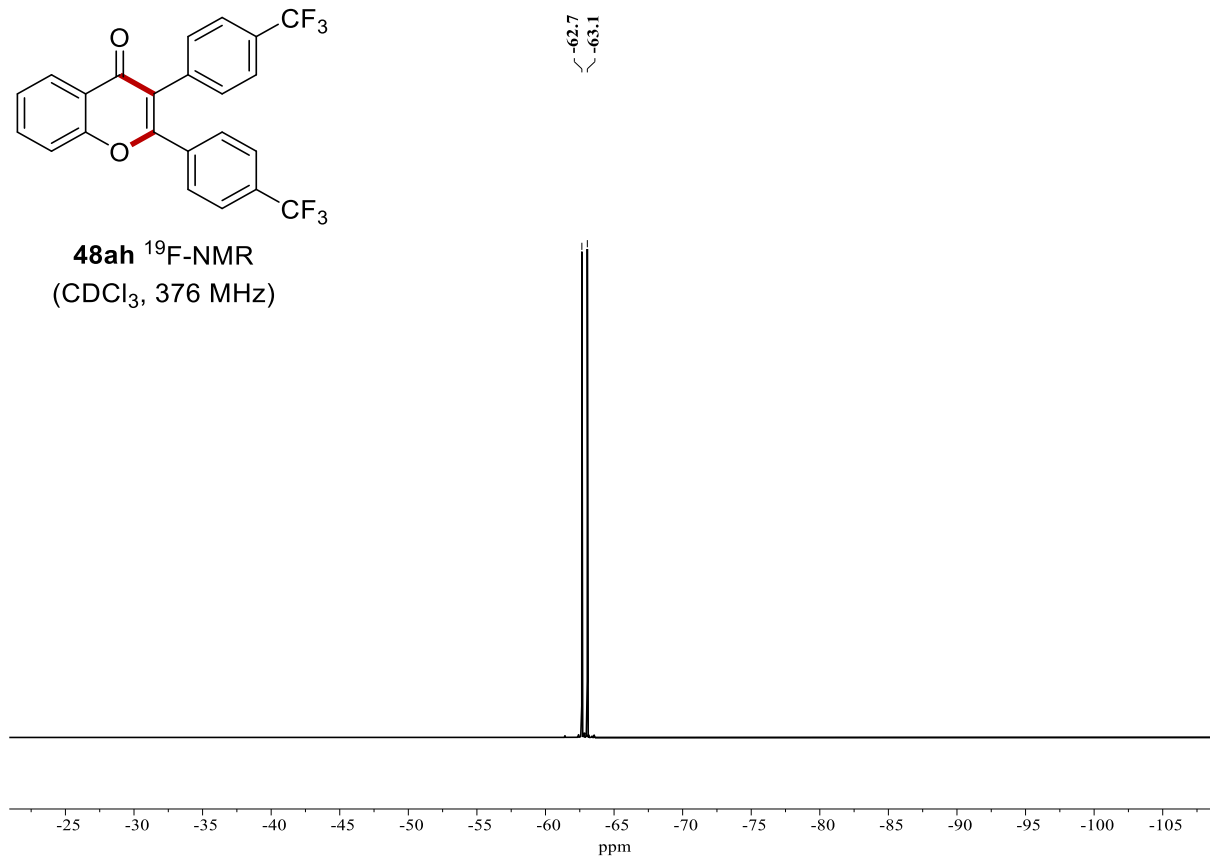


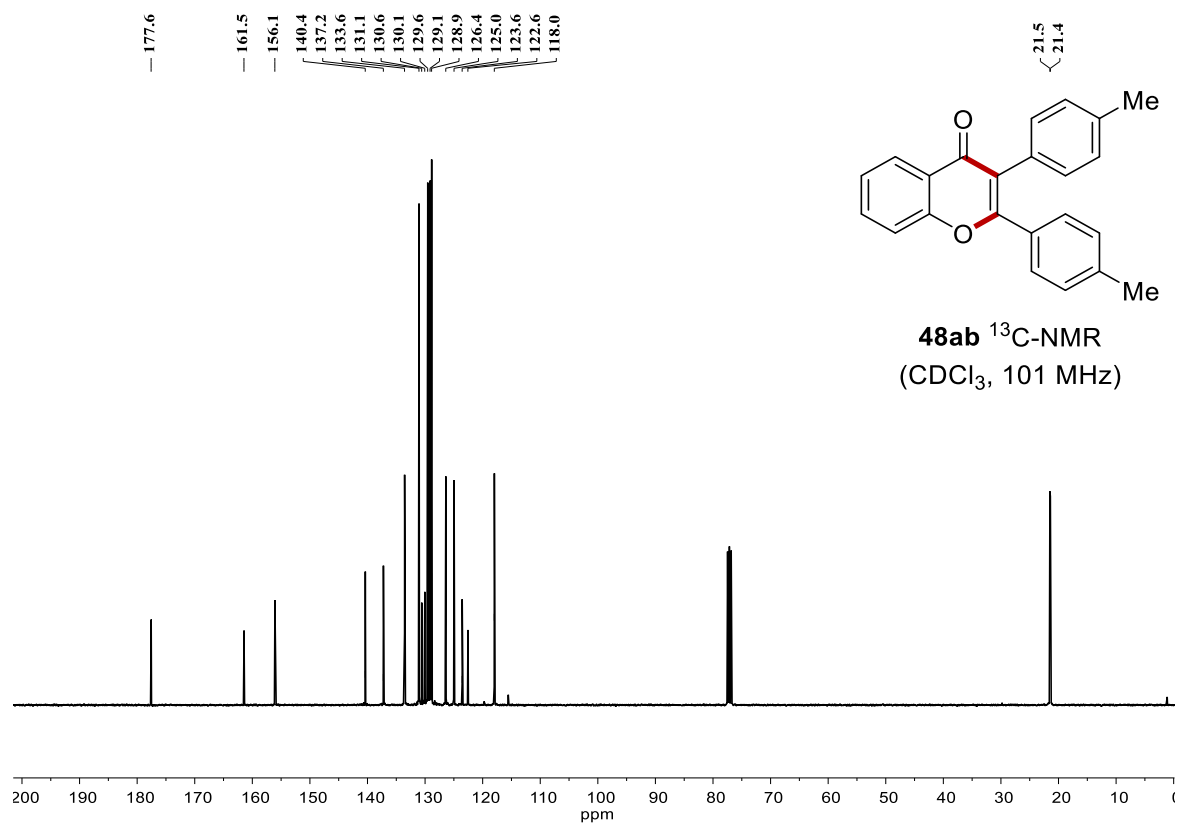
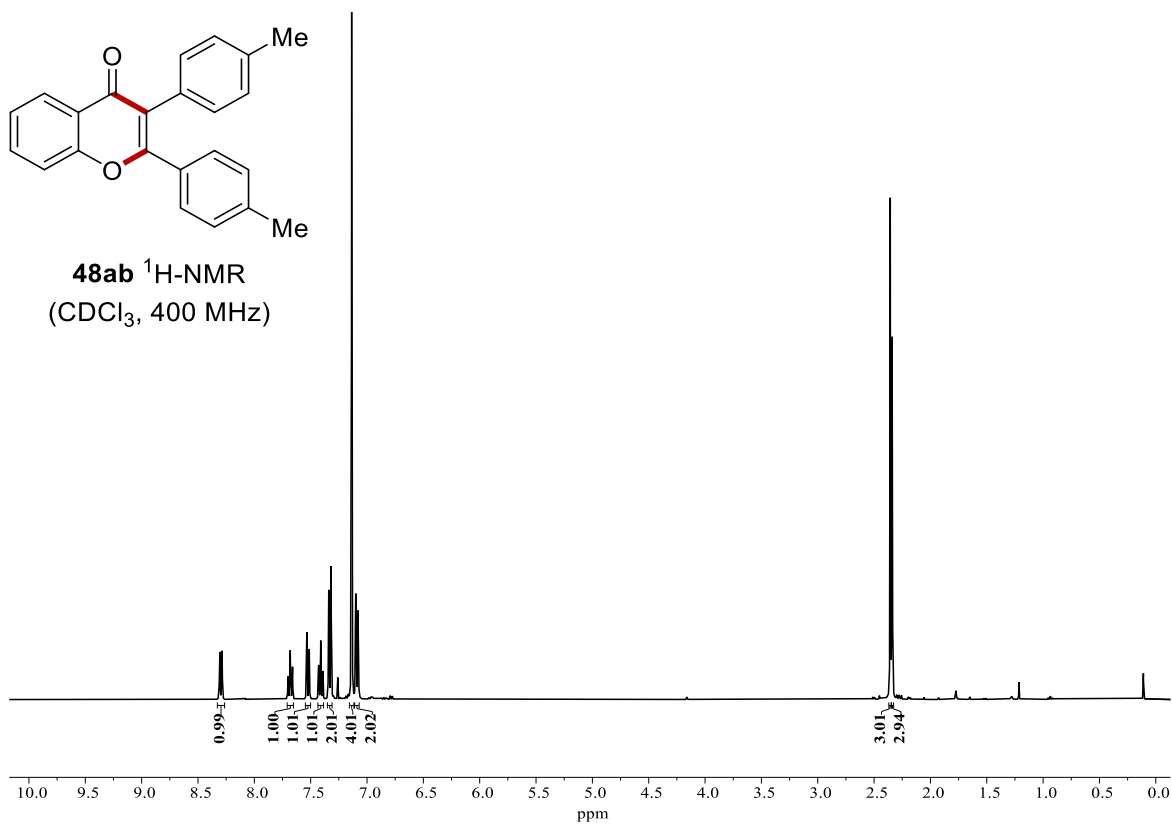
**48ah**  $^{13}\text{C-NMR}$   
( $\text{CDCl}_3$ , 101 MHz)

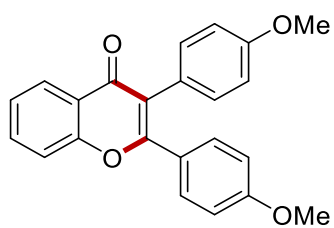




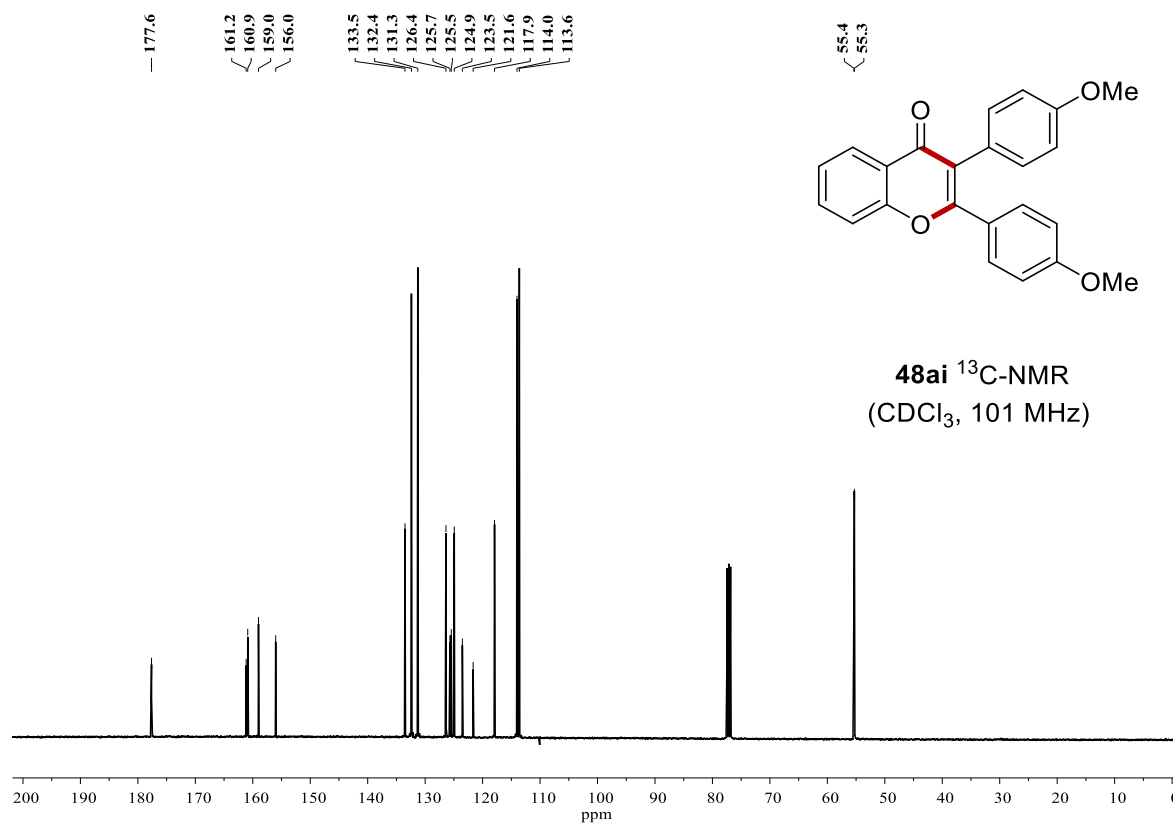
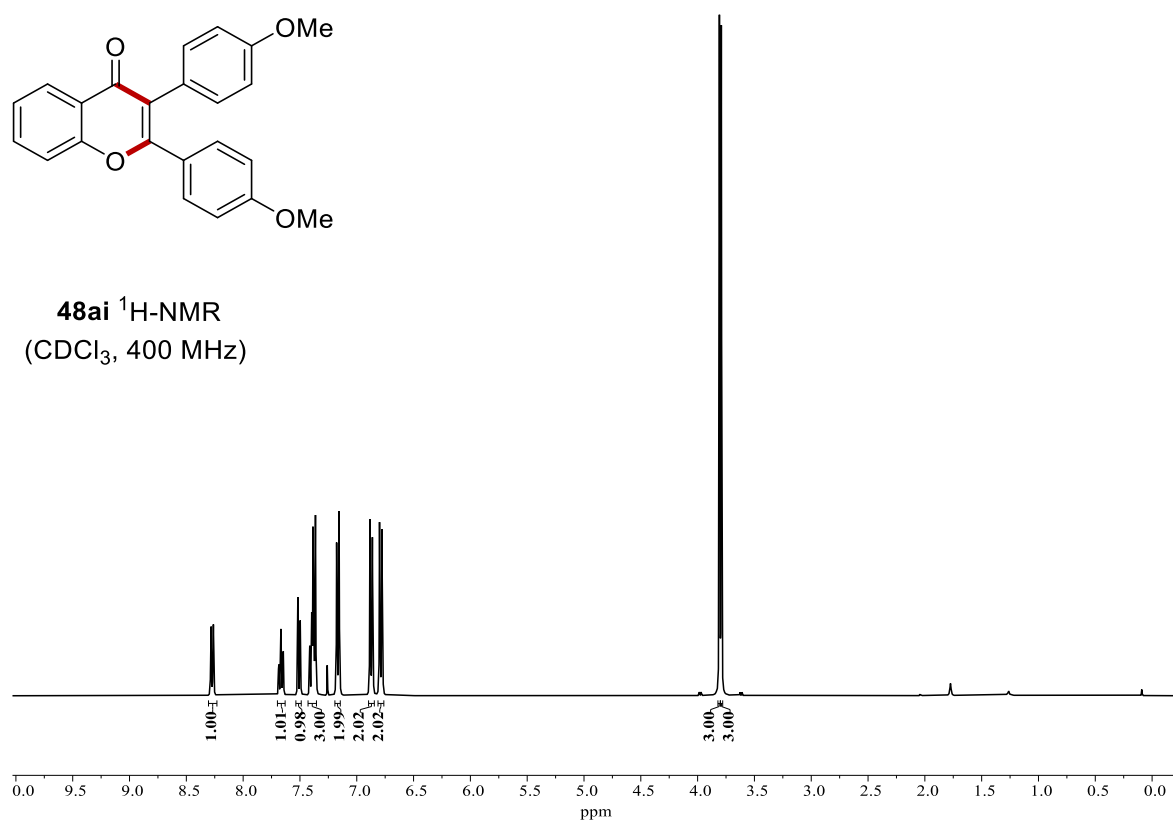
**48ah** <sup>19</sup>F-NMR  
(CDCl<sub>3</sub>, 376 MHz)

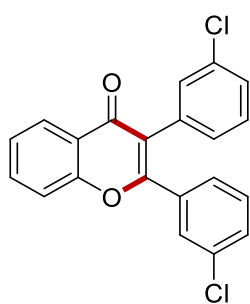




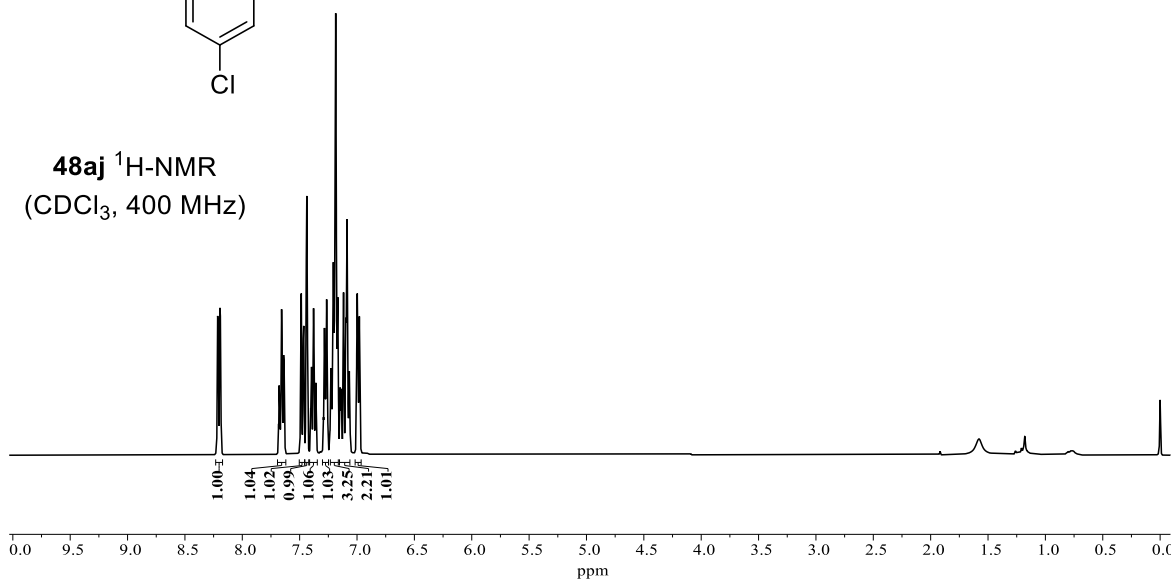


**48ai**  $^1\text{H-NMR}$   
( $\text{CDCl}_3$ , 400 MHz)

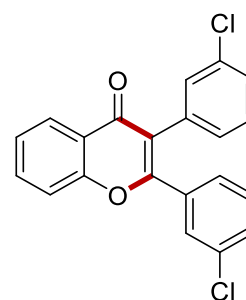




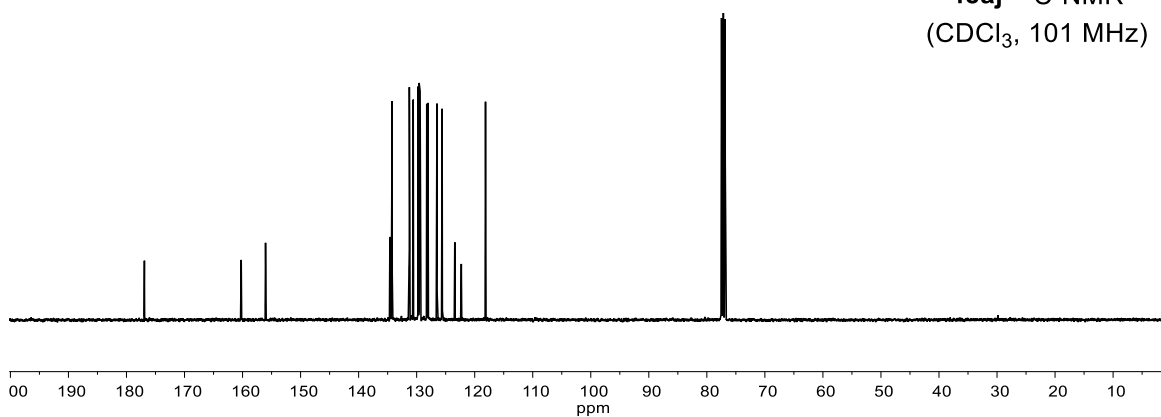
**48aj**  $^1\text{H-NMR}$   
( $\text{CDCl}_3$ , 400 MHz)

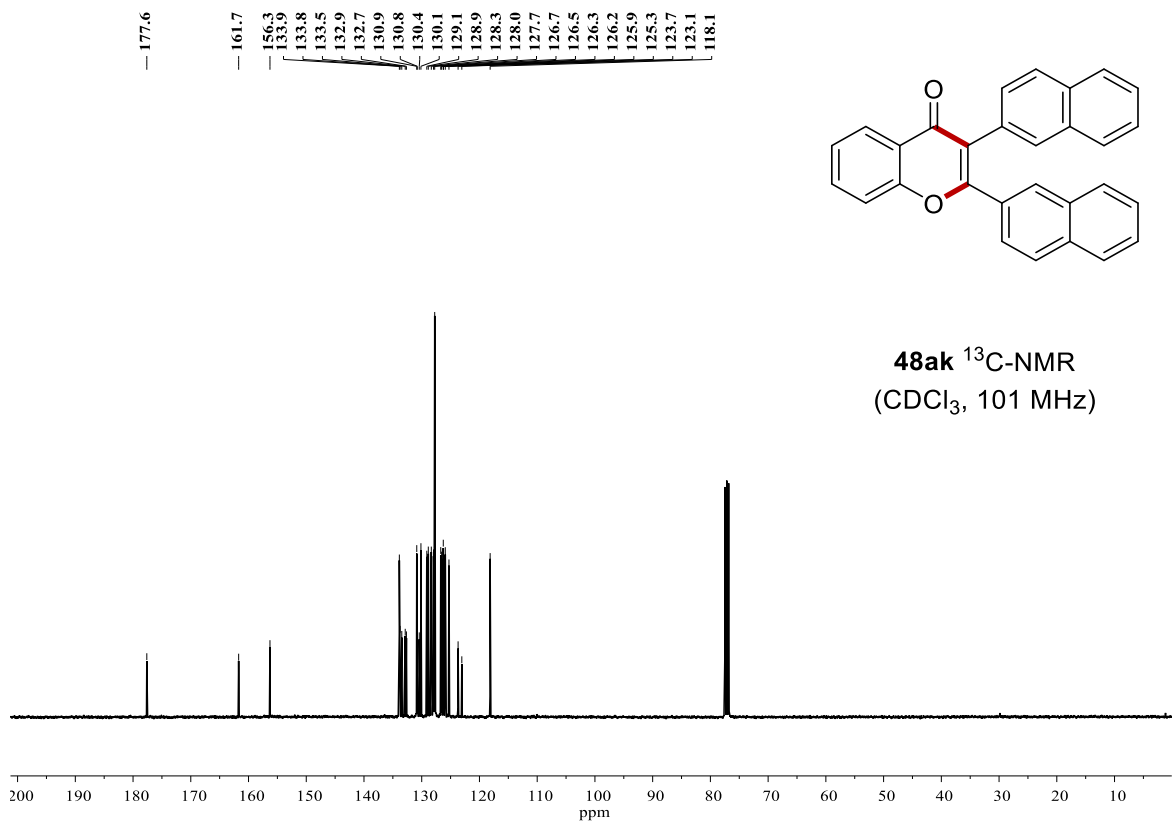
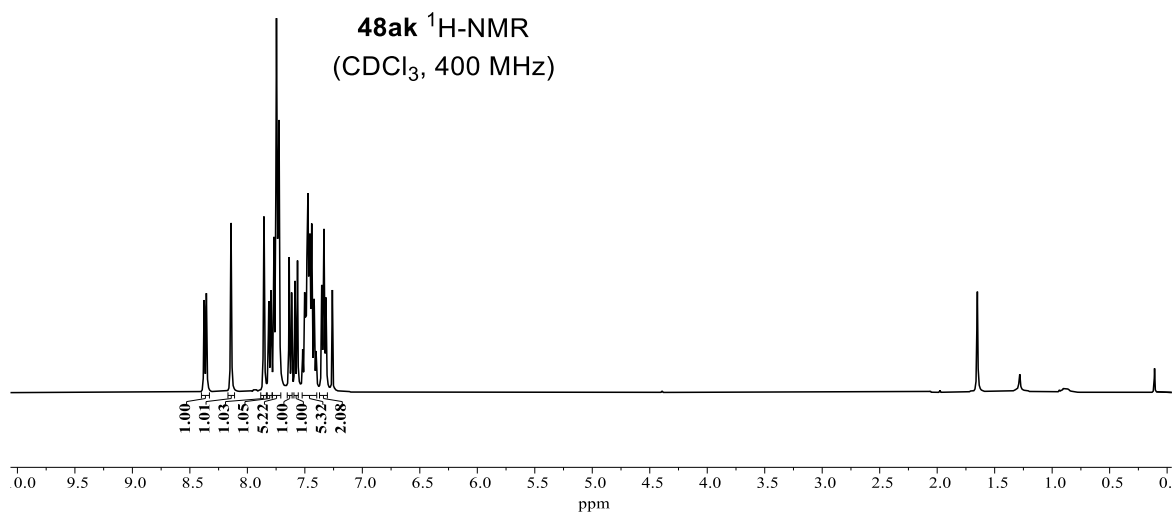
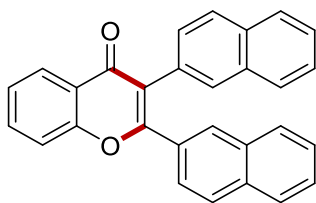


176.9  
160.2  
156.1  
134.6  
134.5  
134.4  
134.2  
131.3  
130.6  
129.8  
129.6  
129.5  
129.4  
128.3  
126.5  
125.6  
123.4  
122.3  
118.1

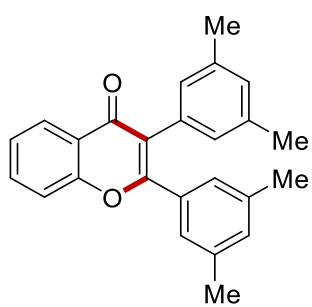


**48aj**  $^{13}\text{C-NMR}$   
( $\text{CDCl}_3$ , 101 MHz)

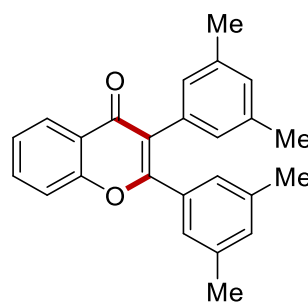
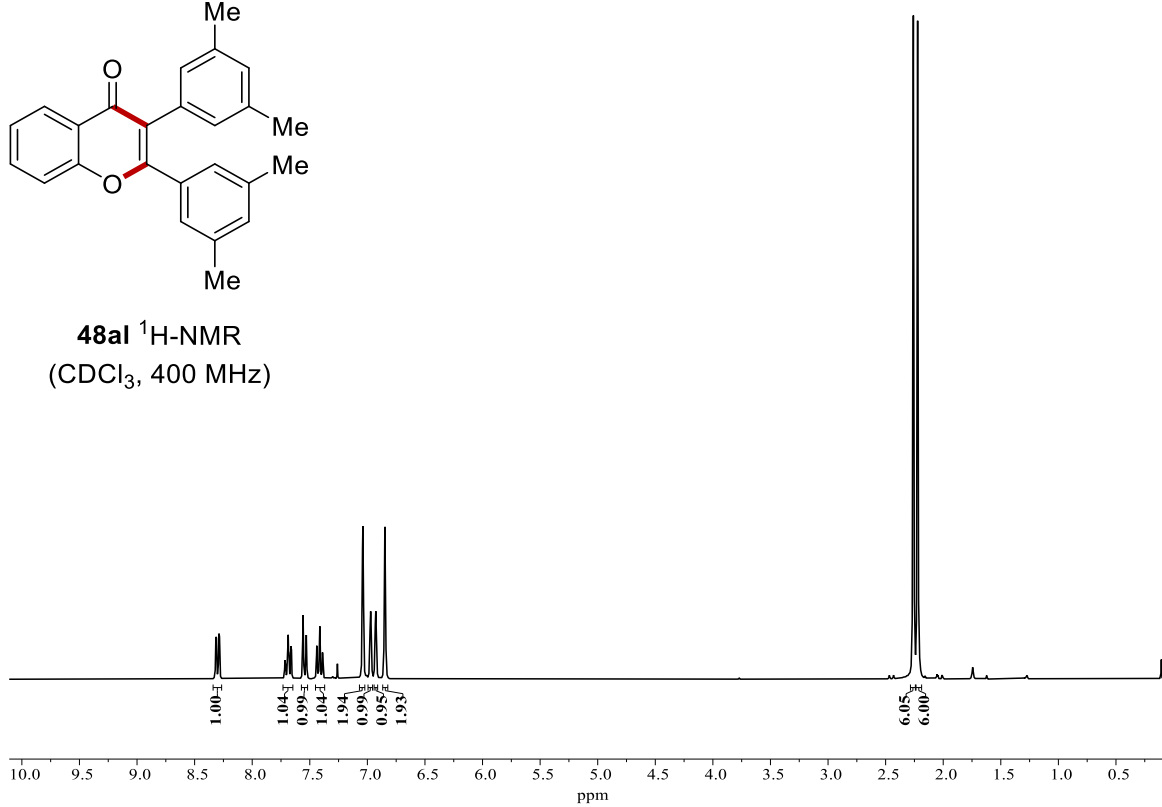




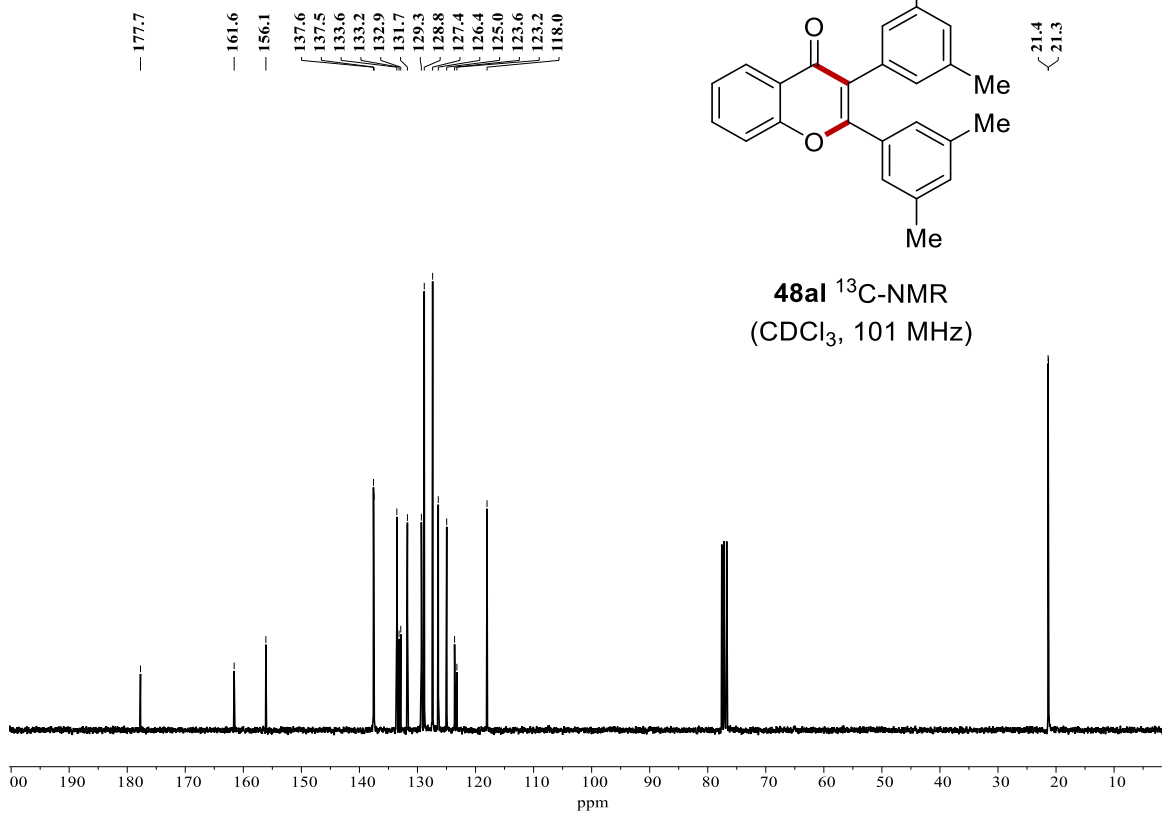


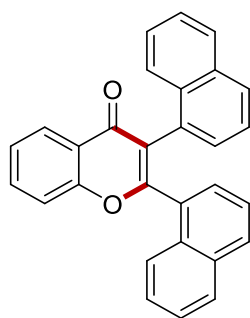


**48a1**  $^1\text{H-NMR}$   
( $\text{CDCl}_3$ , 400 MHz)

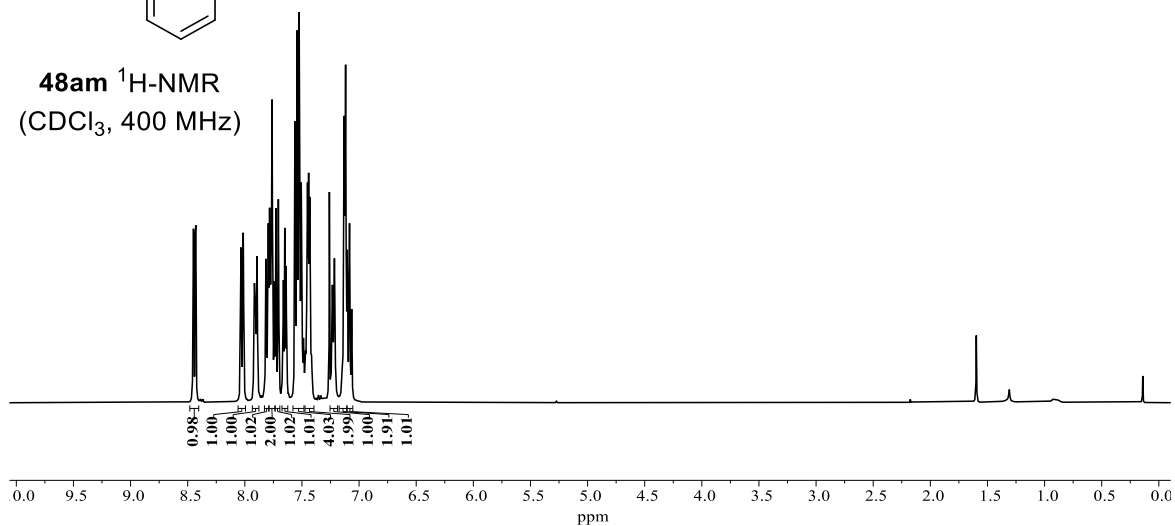


**48a1**  $^{13}\text{C-NMR}$   
( $\text{CDCl}_3$ , 101 MHz)

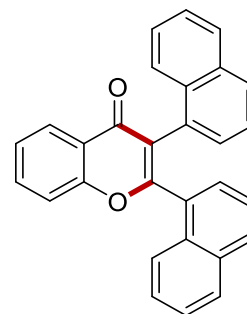




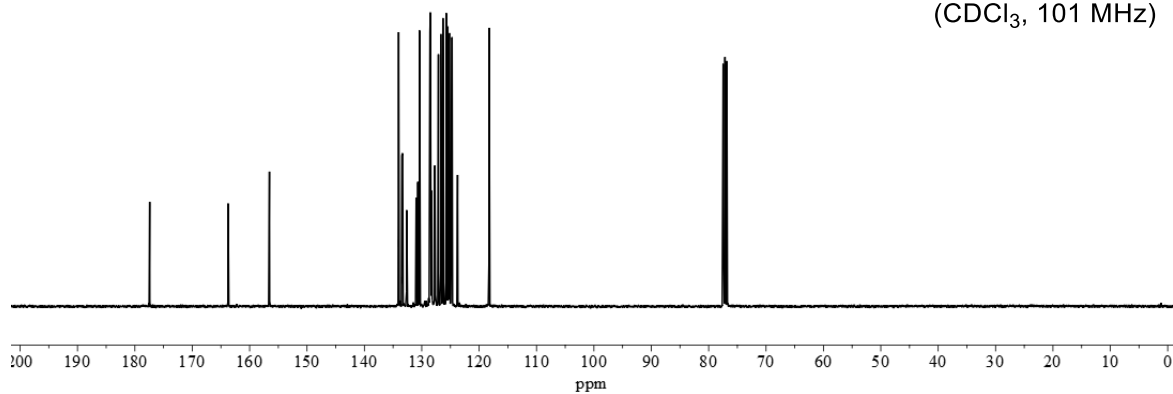
**48am**  $^1\text{H-NMR}$   
( $\text{CDCl}_3$ , 400 MHz)

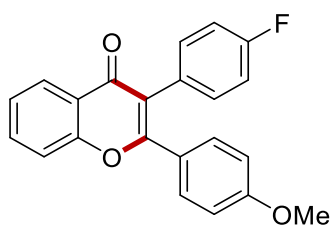


-177.4  
 -163.8  
 -156.6  
 -134.0  
 -133.5  
 -133.3  
 -132.6  
 -131.0  
 -131.0  
 -130.7  
 -130.4  
 -128.6  
 -128.5  
 -128.5  
 -128.3  
 -127.7  
 -127.1  
 -126.7  
 -126.3  
 -126.3  
 -125.7  
 -125.7  
 -125.5  
 -125.3  
 -125.2  
 -124.9  
 -124.7  
 -123.8  
 -118.3

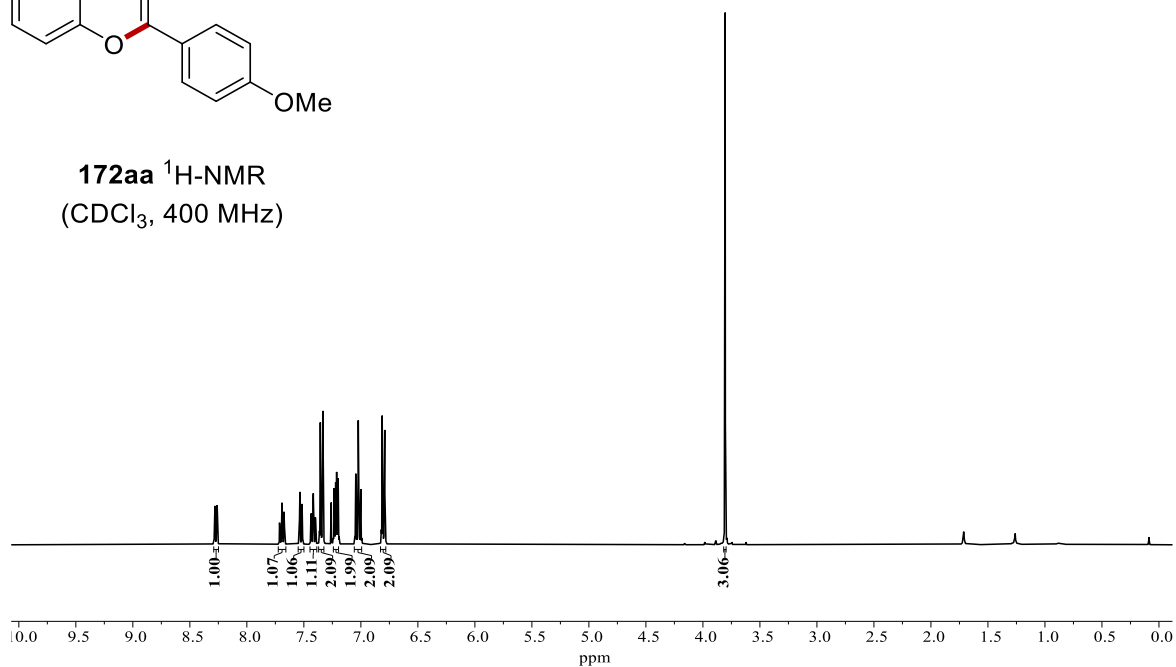


**48am**  $^{13}\text{C-NMR}$   
( $\text{CDCl}_3$ , 101 MHz)



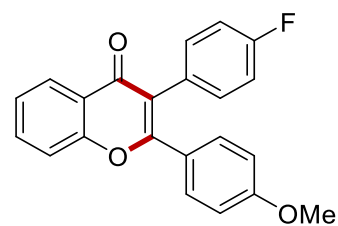


**172aa**  $^1\text{H-NMR}$   
( $\text{CDCl}_3$ , 400 MHz)

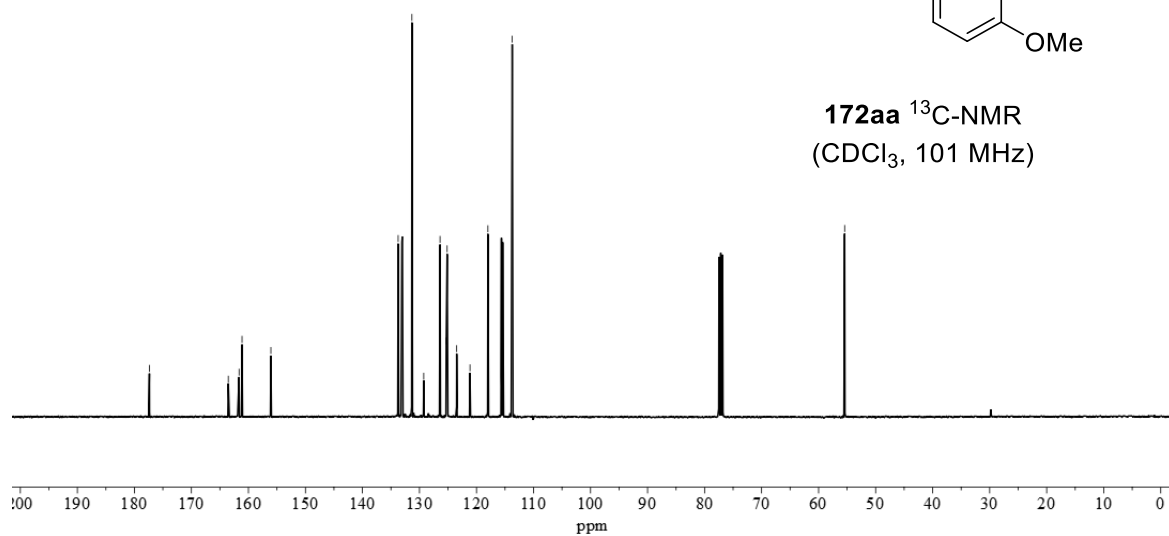


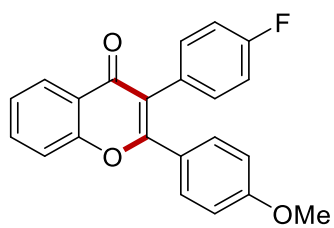
177.4  
163.5  
161.6  
161.1  
156.1  
133.7  
133.1  
131.3  
129.2  
126.4  
125.3  
125.2  
123.5  
121.1  
118.0  
113.7

55.4

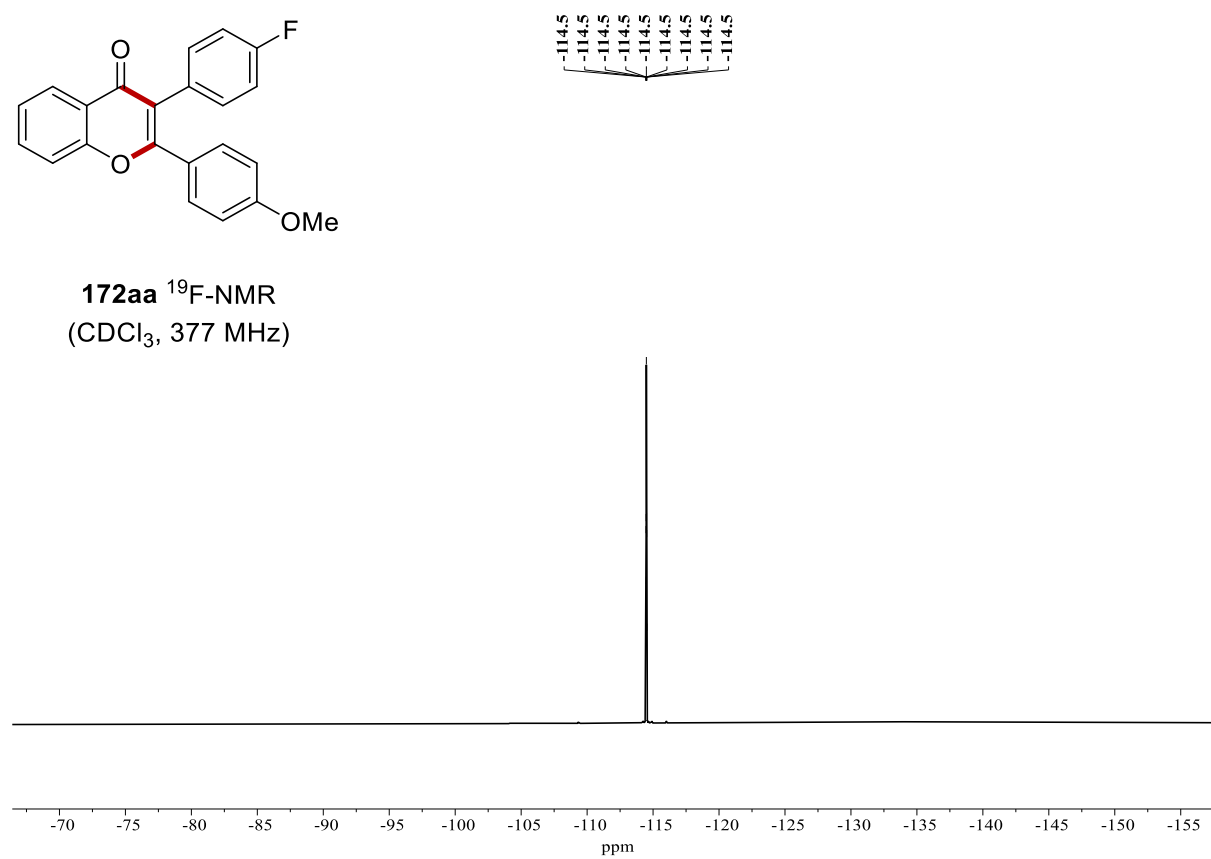


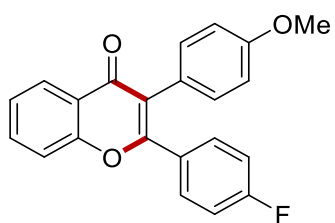
**172aa**  $^{13}\text{C-NMR}$   
( $\text{CDCl}_3$ , 101 MHz)



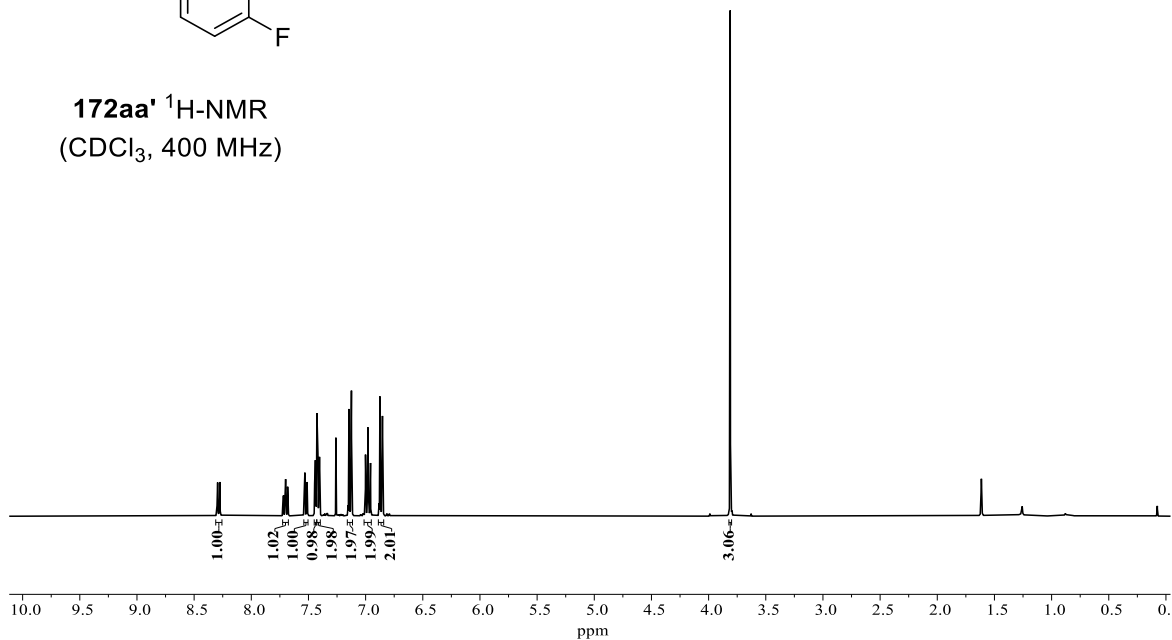


**172aa**  $^{19}\text{F}$ -NMR  
( $\text{CDCl}_3$ , 377 MHz)



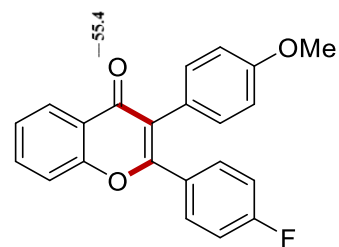


**172aa'**  $^1\text{H-NMR}$   
( $\text{CDCl}_3$ , 400 MHz)

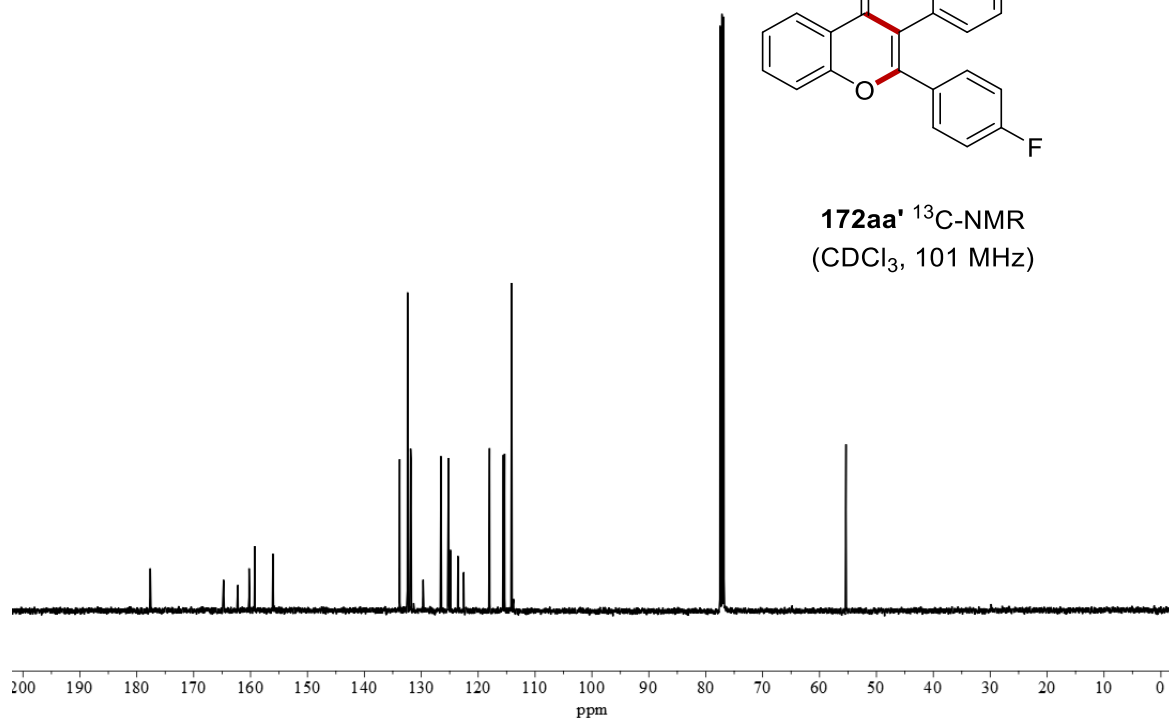


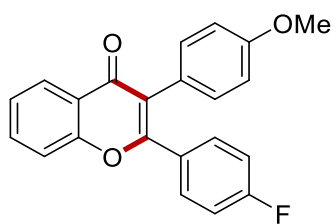
Chemical shift values (ppm) for  $^{13}\text{C-NMR}$  spectrum:

- 177.6
- 164.8
- 162.3
- 160.3
- 159.3
- 156.1
- 133.8
- 132.4
- 131.9
- 131.8
- 129.7
- 129.7
- 126.6
- 125.2
- 124.9
- 123.6
- 122.6
- 118.0
- 115.6
- 115.4
- 114.1

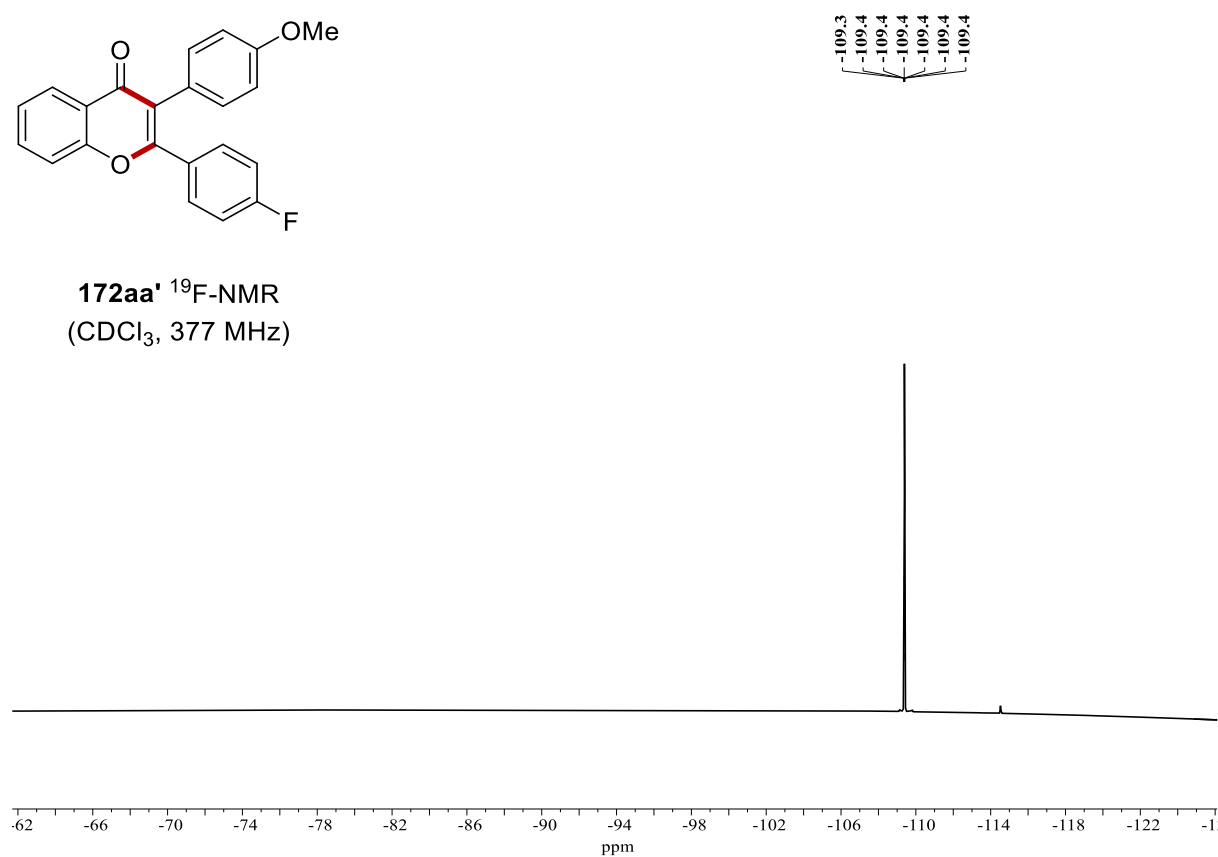


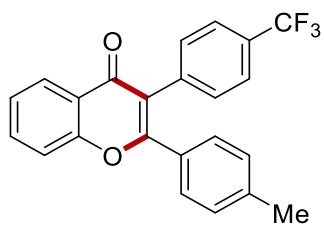
**172aa'**  $^{13}\text{C-NMR}$   
( $\text{CDCl}_3$ , 101 MHz)



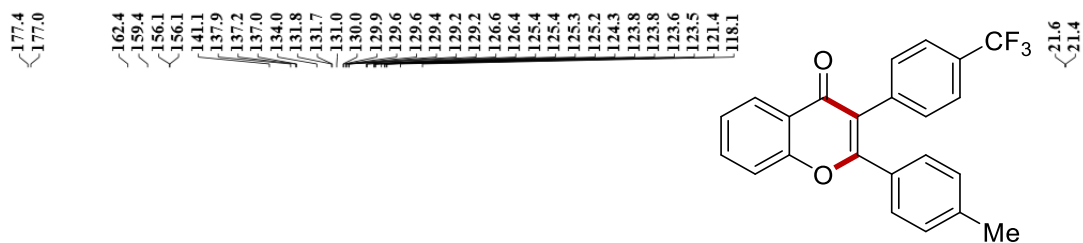
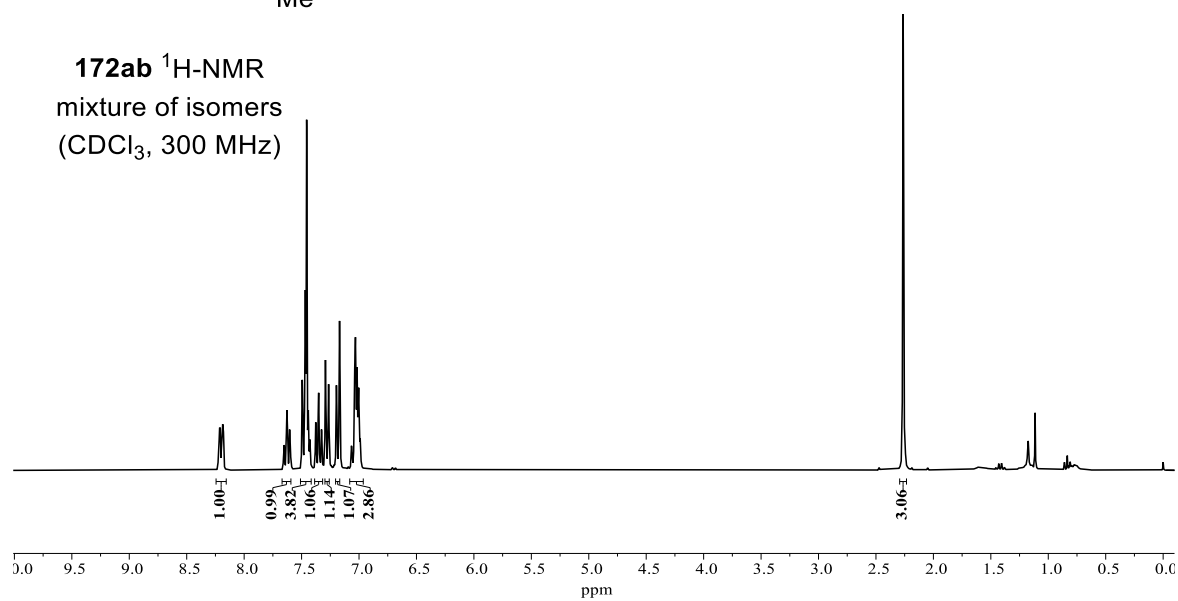


**172aa'**  $^{19}\text{F}$ -NMR  
( $\text{CDCl}_3$ , 377 MHz)

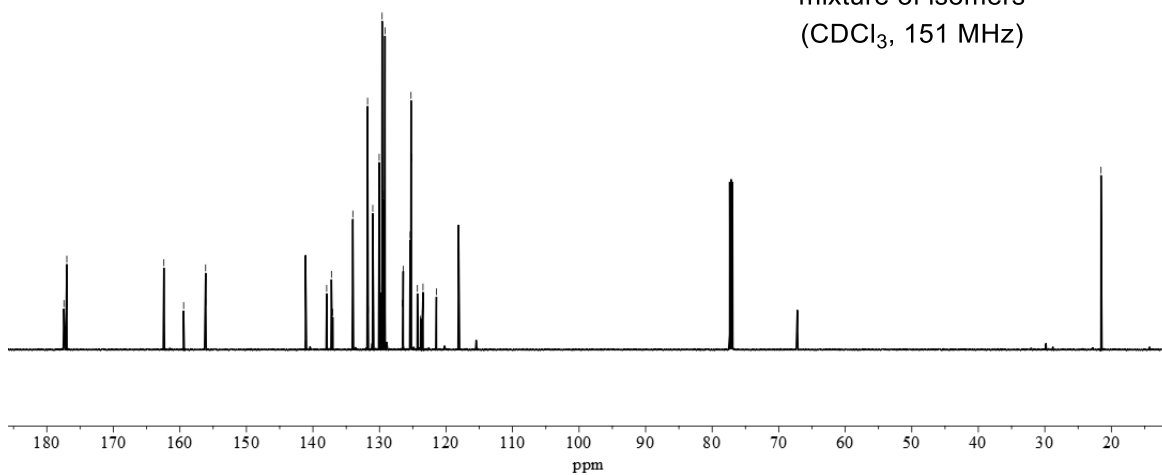


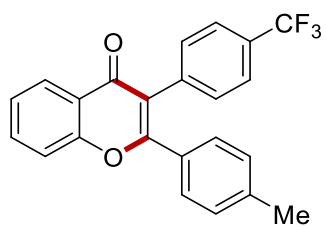


**172ab**  $^1\text{H-NMR}$   
mixture of isomers  
( $\text{CDCl}_3$ , 300 MHz)

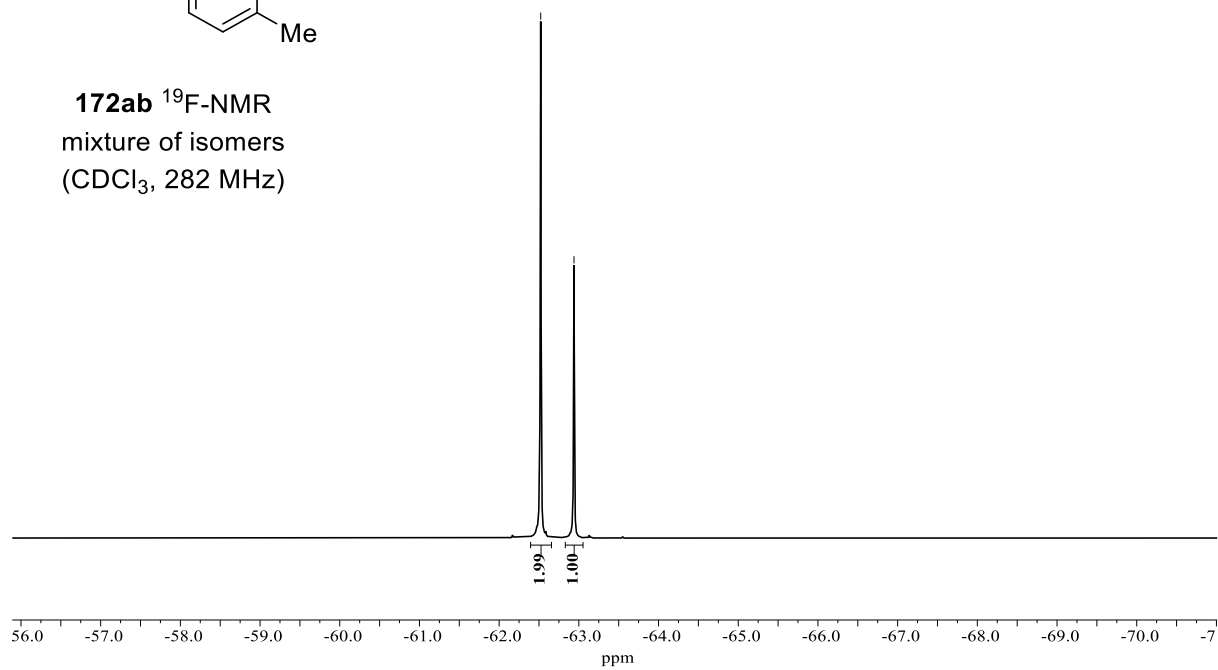


**172ab**  $^{13}\text{C-NMR}$   
mixture of isomers  
( $\text{CDCl}_3$ , 151 MHz)

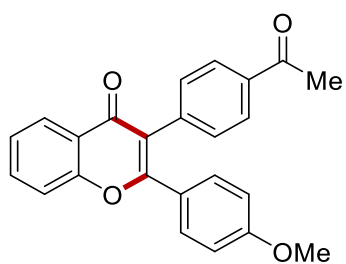




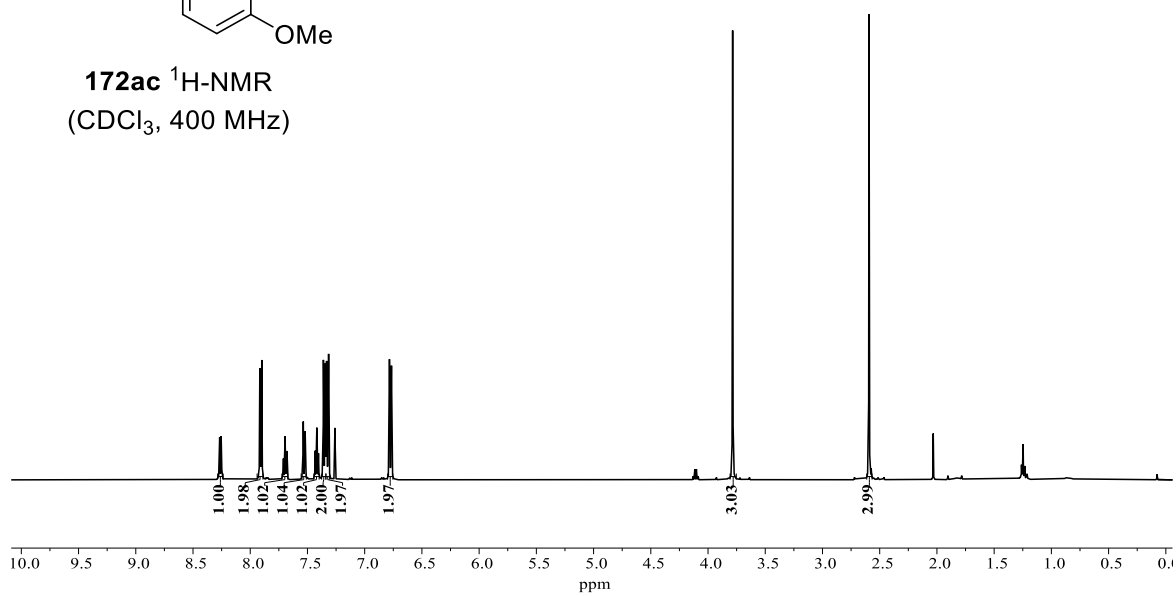
**172ab**  $^{19}\text{F}$ -NMR  
mixture of isomers  
( $\text{CDCl}_3$ , 282 MHz)





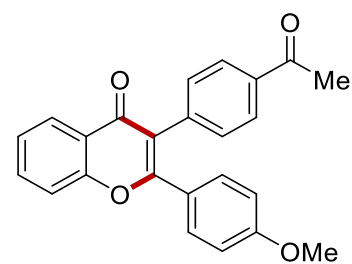


**172ac**  $^1\text{H-NMR}$   
( $\text{CDCl}_3$ , 400 MHz)

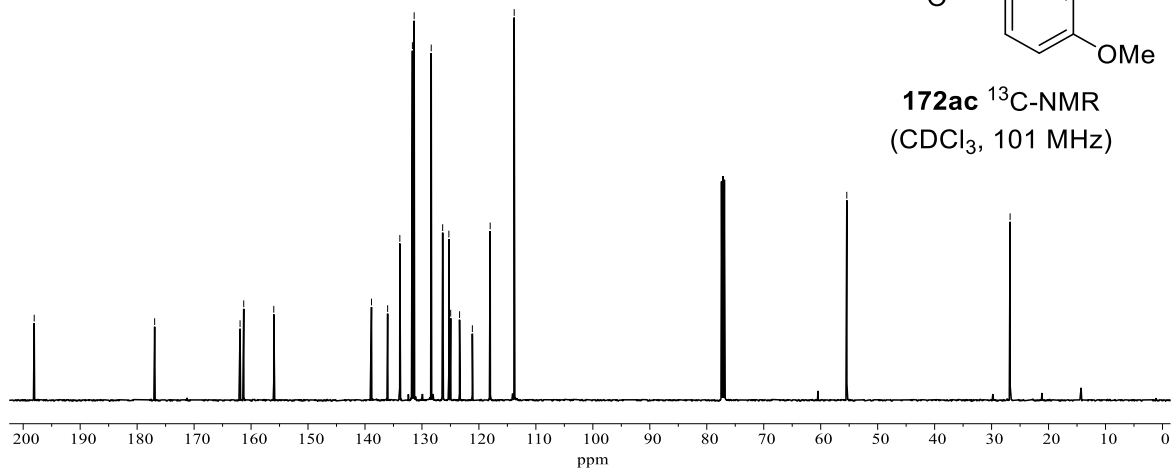


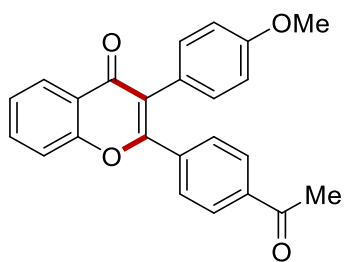
198.1  
176.9  
161.9  
161.3  
156.0  
138.9  
136.0  
133.9  
131.7  
131.4  
128.4  
126.4  
125.3  
125.0  
123.4  
121.1  
118.0  
113.8

55.4  
26.8

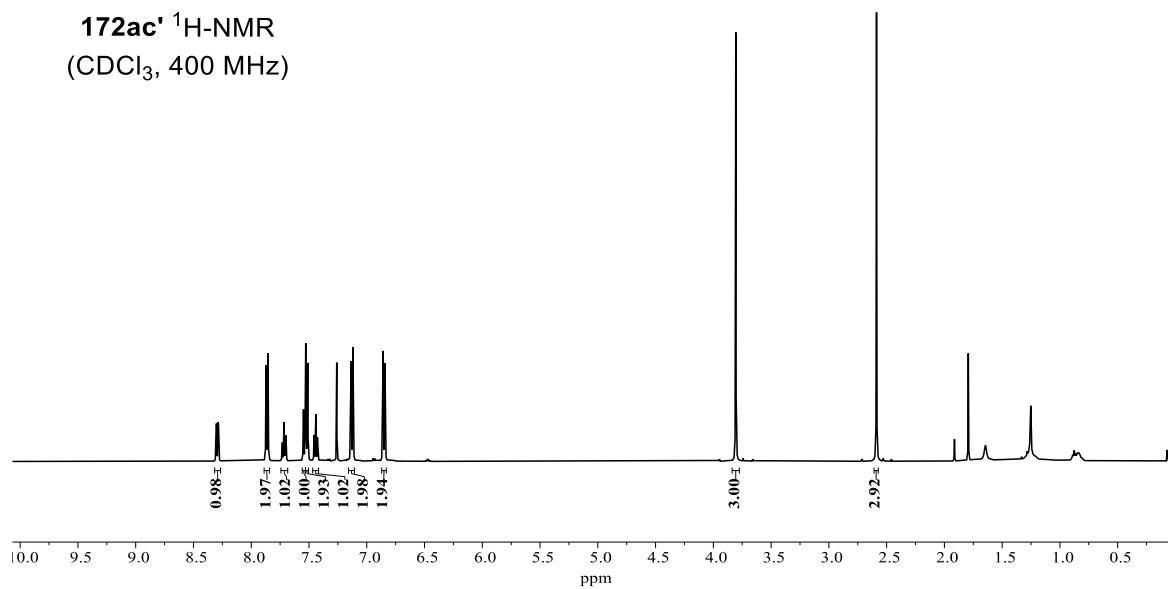


**172ac**  $^{13}\text{C-NMR}$   
( $\text{CDCl}_3$ , 101 MHz)

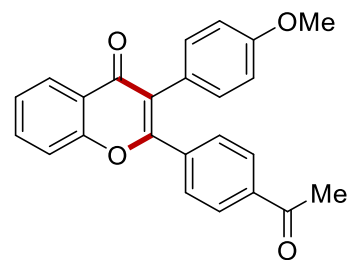




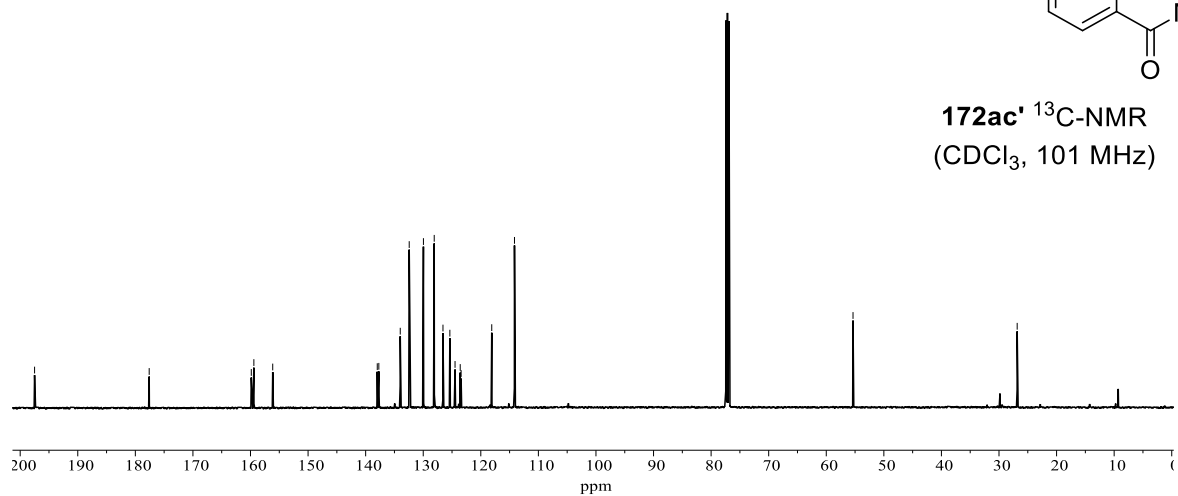
**172ac'**  $^1\text{H-NMR}$   
( $\text{CDCl}_3$ , 400 MHz)

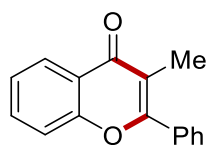


$^13\text{C-NMR}$  chemical shifts (ppm):  
 197.5, 177.6, 159.9, 159.4, 156.1, 138.0, 137.7, 134.0, 132.4, 130.0, 128.1, 126.6, 125.4, 124.5, 123.6, 123.4, 118.1, 114.1, 55.4, 26.8

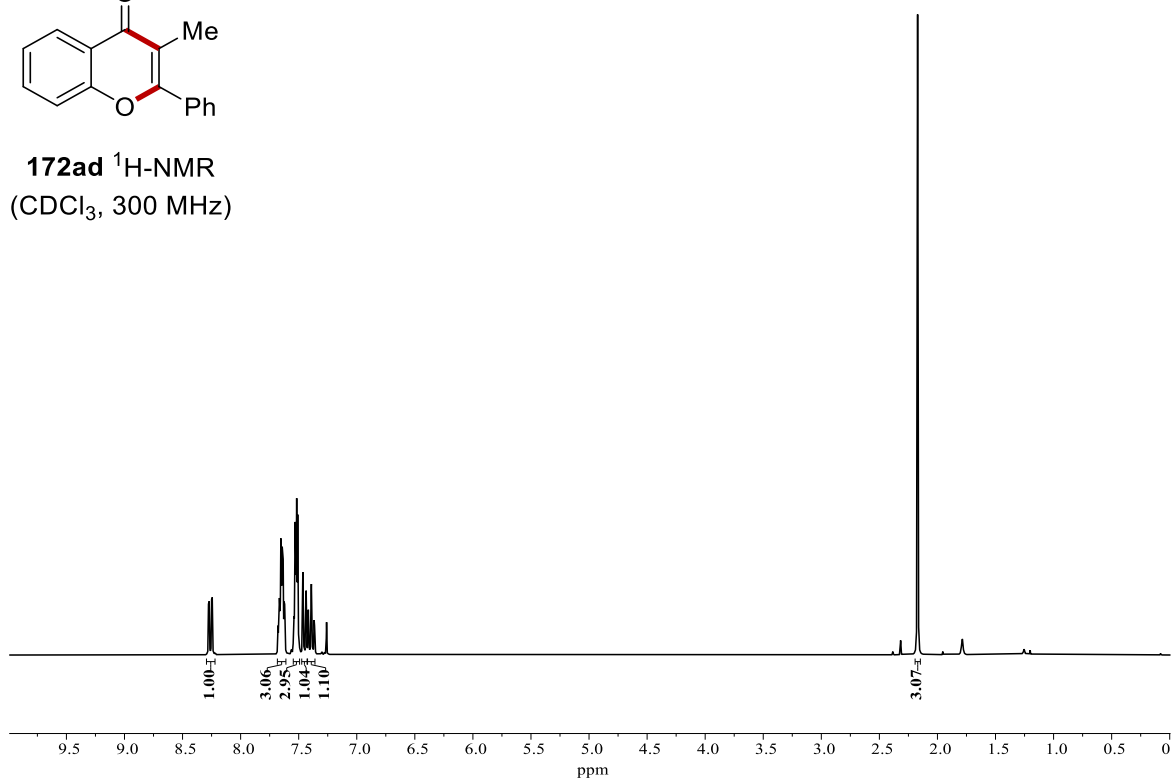


**172ac'**  $^{13}\text{C-NMR}$   
( $\text{CDCl}_3$ , 101 MHz)

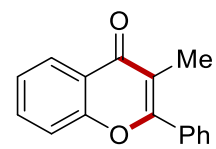




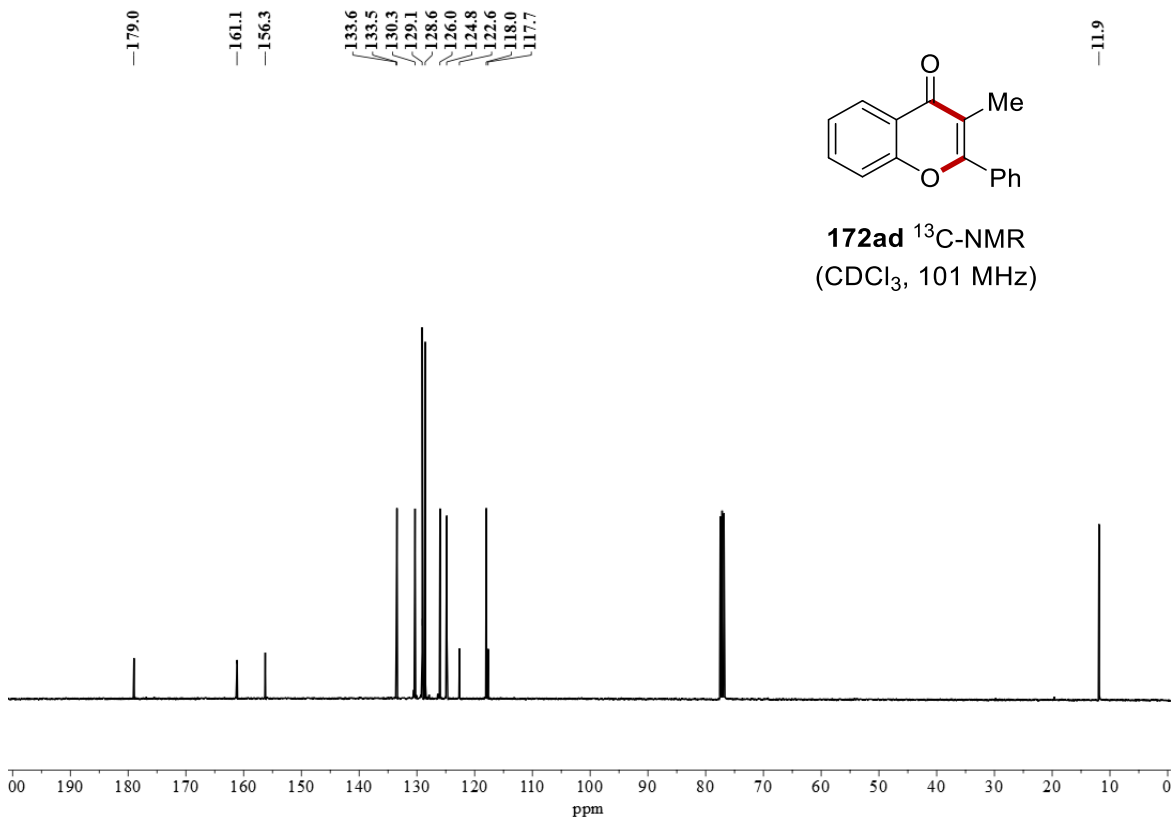
**172ad**  $^1\text{H-NMR}$   
( $\text{CDCl}_3$ , 300 MHz)

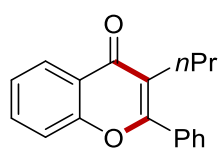


179.0  
161.1  
156.3  
133.6  
133.5  
130.3  
129.1  
128.6  
126.0  
124.8  
122.6  
118.0  
117.7

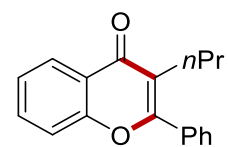
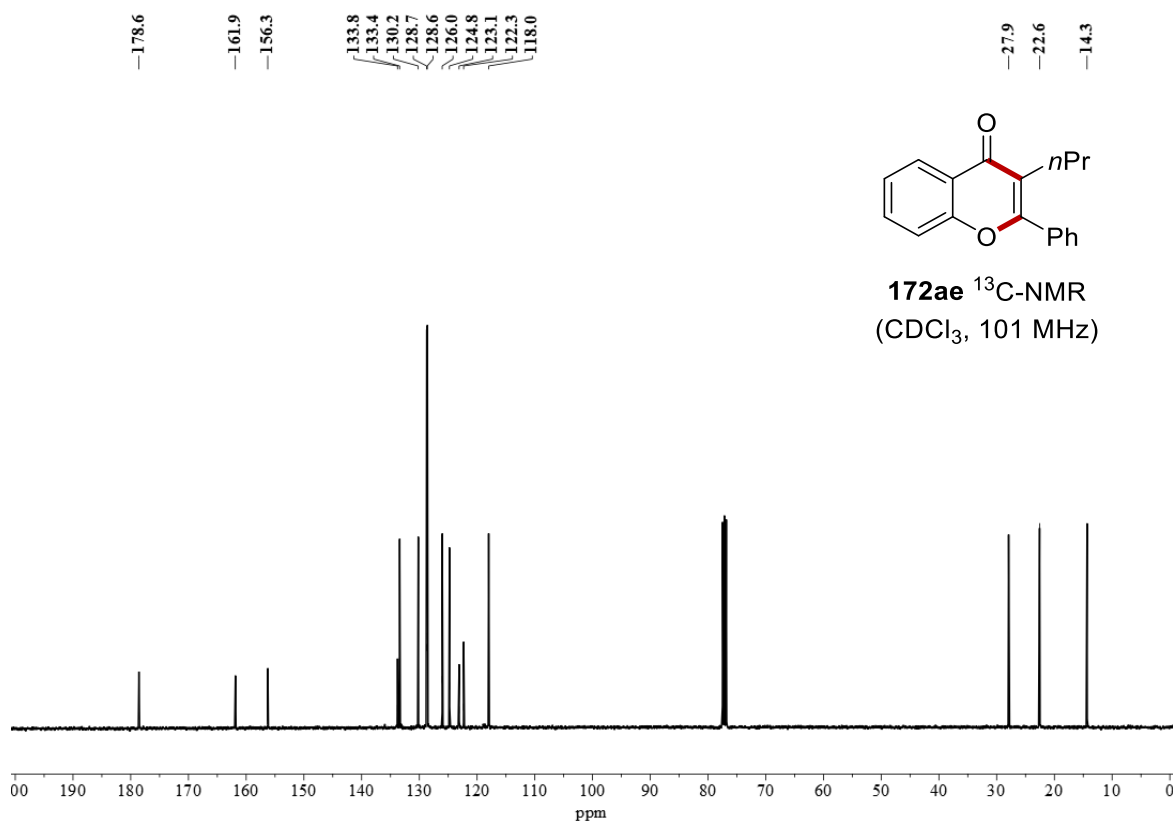
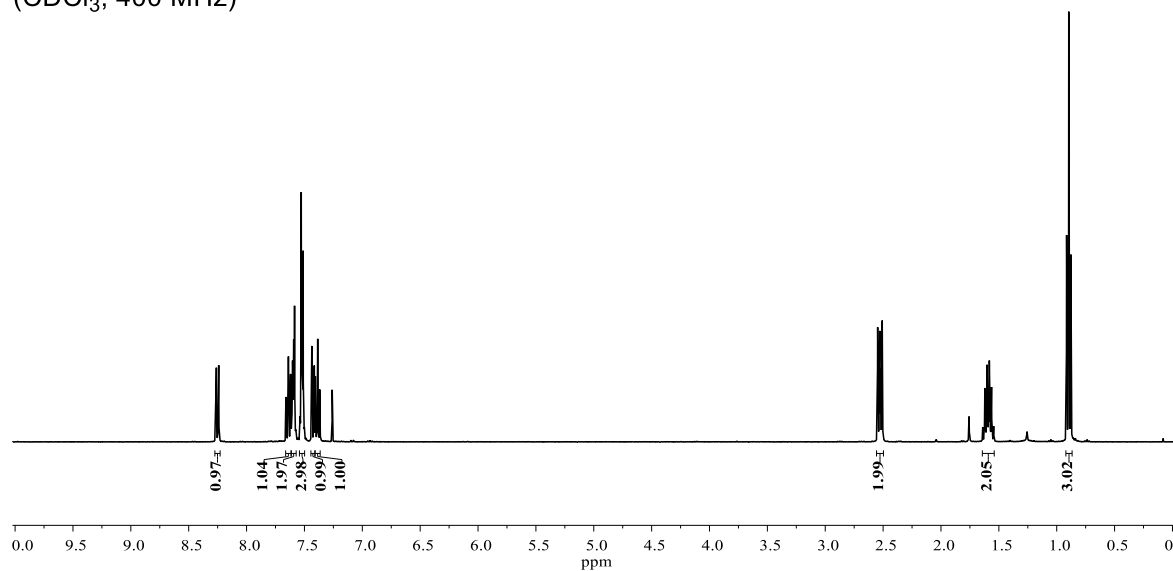


**172ad**  $^{13}\text{C-NMR}$   
( $\text{CDCl}_3$ , 101 MHz)

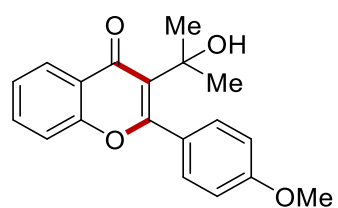




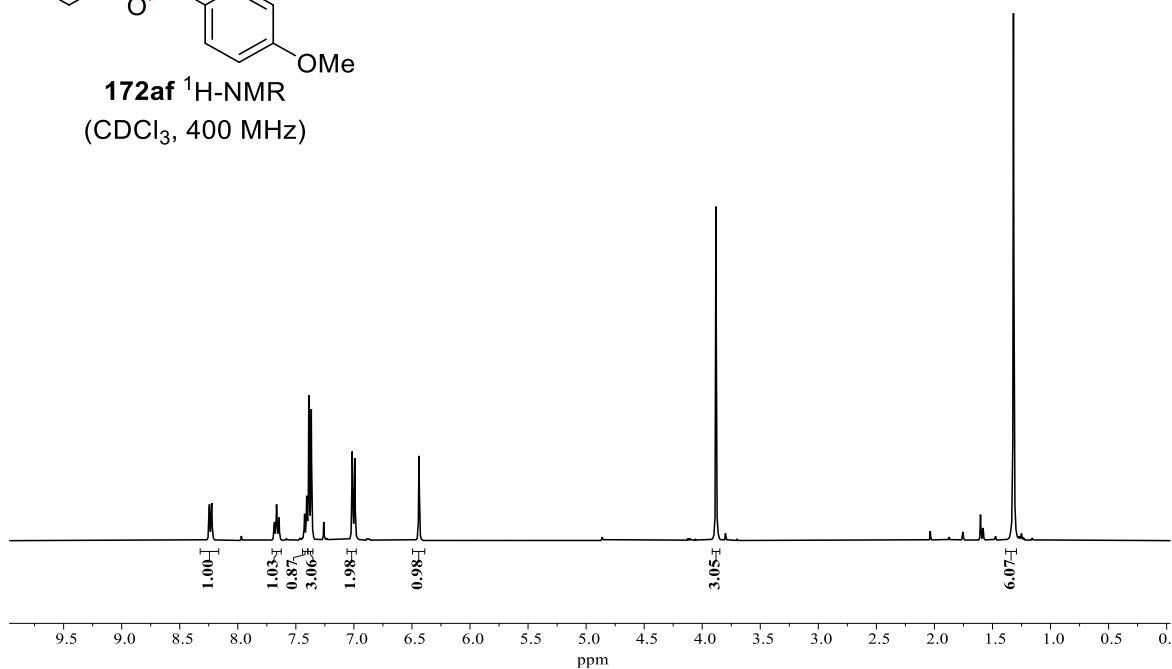
**172ae**  $^1\text{H-NMR}$   
( $\text{CDCl}_3$ , 400 MHz)



**172ae**  $^{13}\text{C-NMR}$   
( $\text{CDCl}_3$ , 101 MHz)



**172af**  $^1\text{H-NMR}$   
( $\text{CDCl}_3$ , 400 MHz)

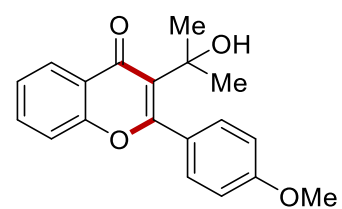


181.3  
162.4  
161.1  
155.5  
134.2  
130.2  
127.8  
127.5  
126.1  
125.2  
123.1  
117.8  
113.9

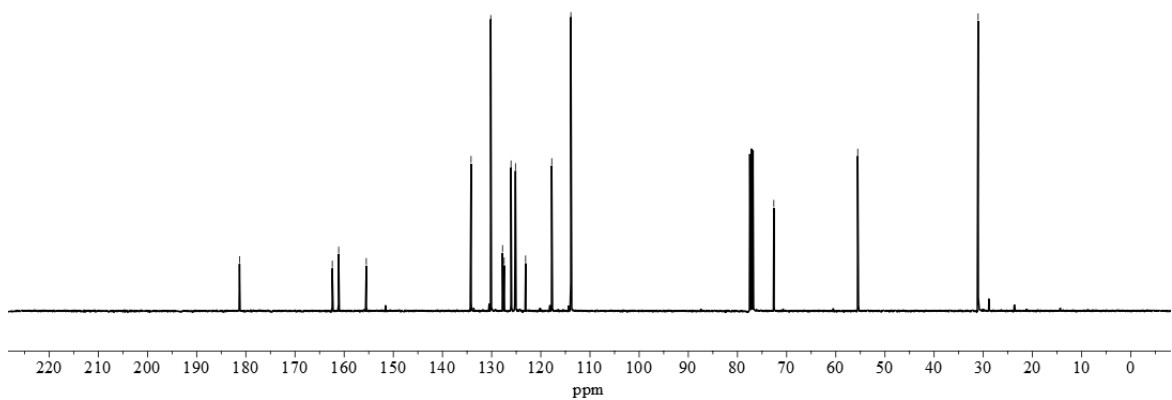
72.6

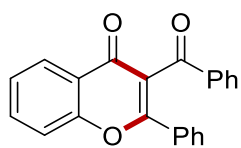
55.5

31.1

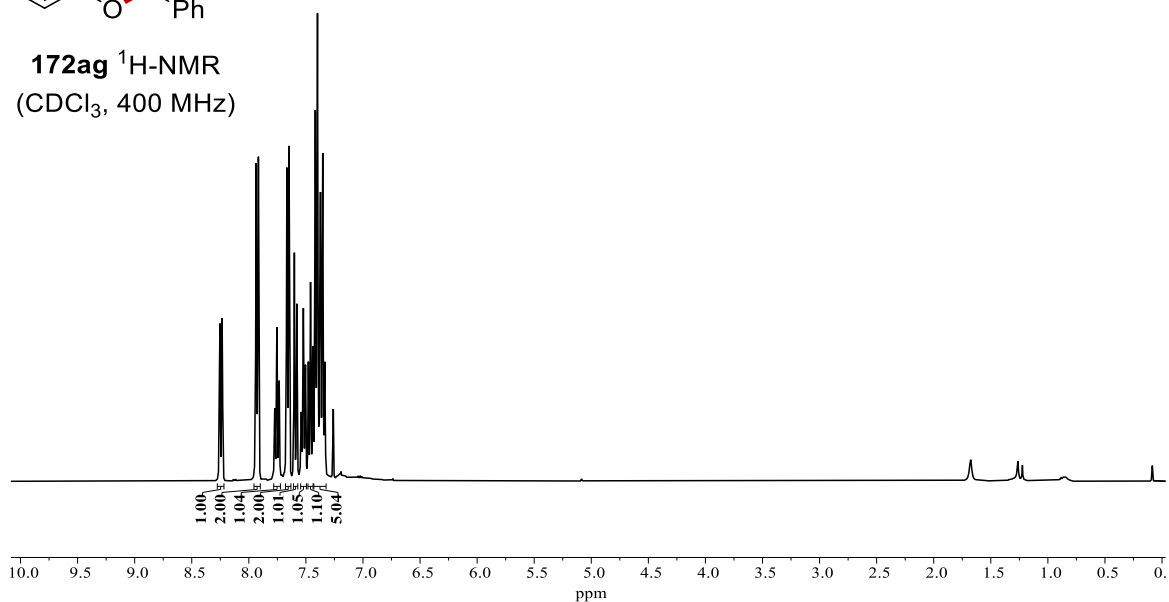


**172af**  $^{13}\text{C-NMR}$   
( $\text{CDCl}_3$ , 101 MHz)

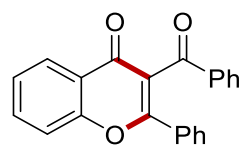




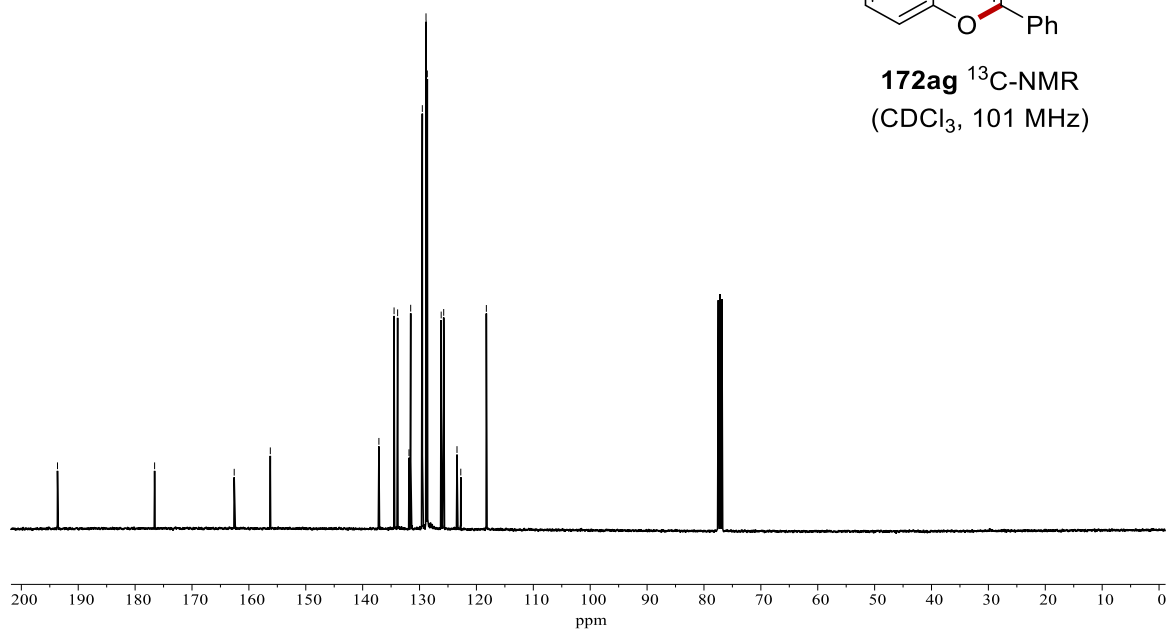
**172ag**  $^1\text{H-NMR}$   
( $\text{CDCl}_3$ , 400 MHz)

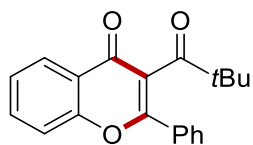


— 193.6  
— 176.6  
— 162.6  
— 156.2  
137.1  
134.5  
133.9  
131.9  
131.6  
129.5  
128.9  
128.8  
128.6  
126.2  
125.8  
123.4  
122.7  
118.3

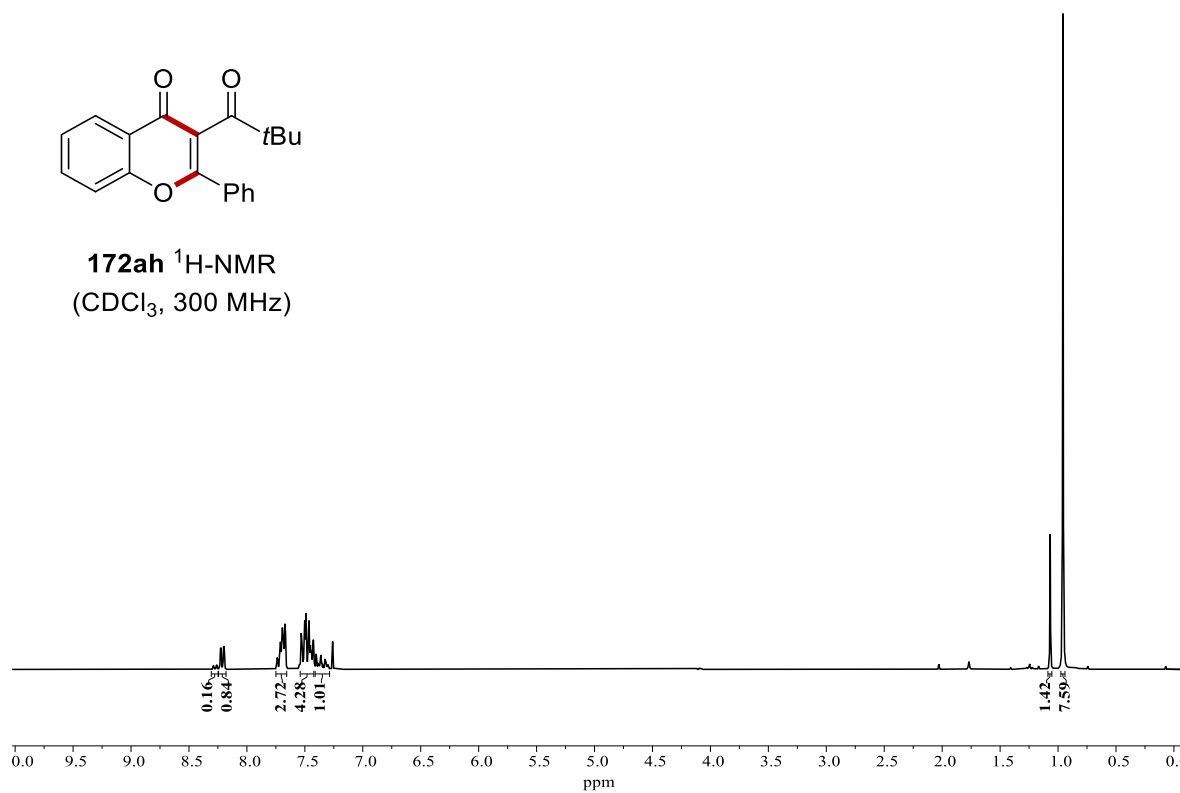


**172ag**  $^{13}\text{C-NMR}$   
( $\text{CDCl}_3$ , 101 MHz)





**172ah**  $^1\text{H-NMR}$   
( $\text{CDCl}_3$ , 300 MHz)



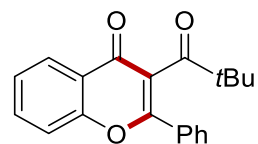
— 210.5  
— 204.3

— 176.6  
— 176.6

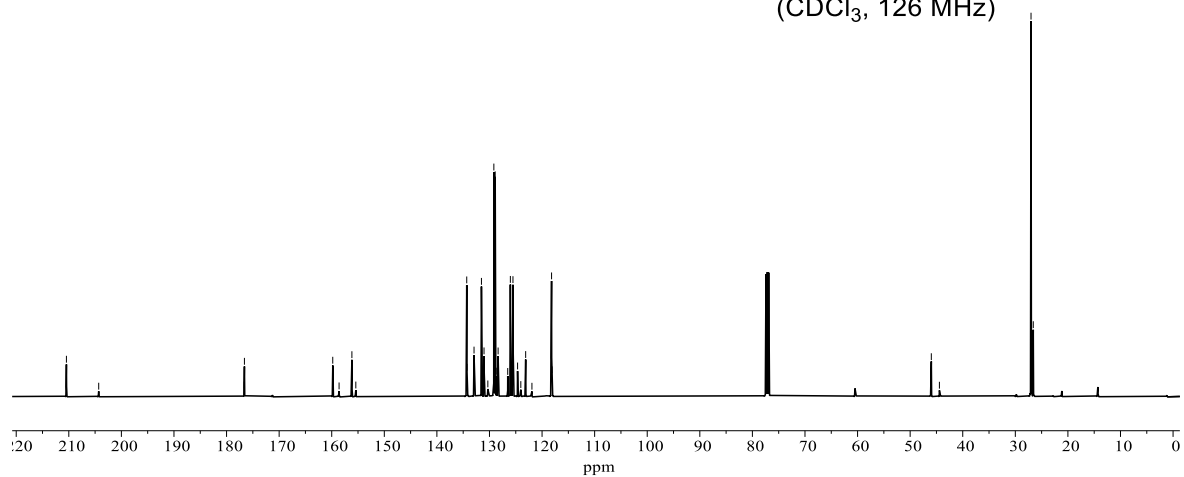
— 159.8  
— 158.6  
— 156.2  
— 155.4  
— 134.3  
— 134.3  
— 132.9  
— 131.5  
— 131.0  
— 130.3  
— 129.2  
— 128.9  
— 128.6  
— 128.4  
— 126.5  
— 126.0  
— 125.8  
— 125.5  
— 124.7  
— 124.0  
— 123.1  
— 121.9  
— 118.2  
— 118.1

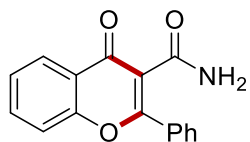
— 46.0  
— 44.4

— 27.0  
— 26.6

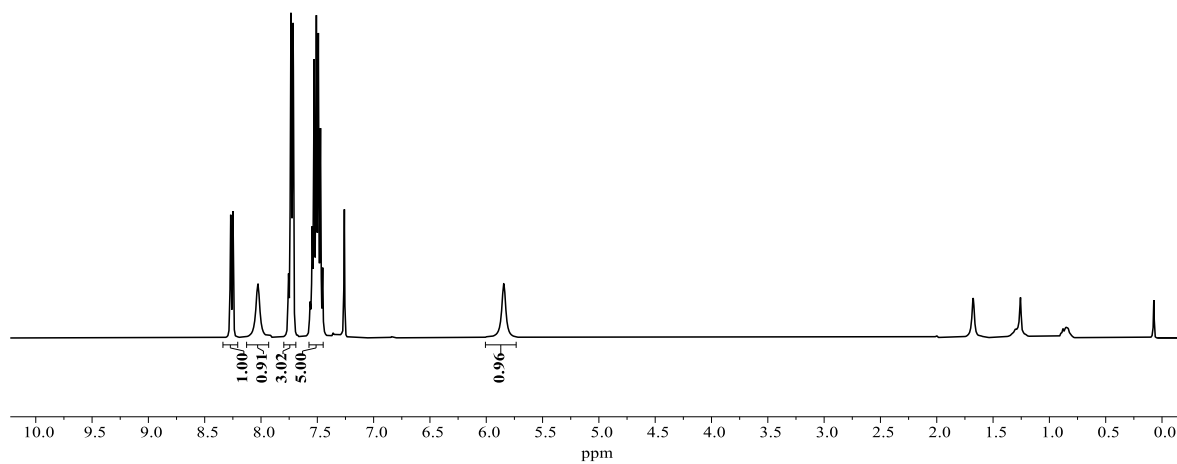


**172ah**  $^{13}\text{C-NMR}$   
( $\text{CDCl}_3$ , 126 MHz)

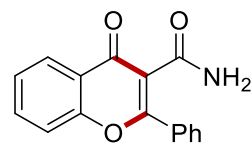




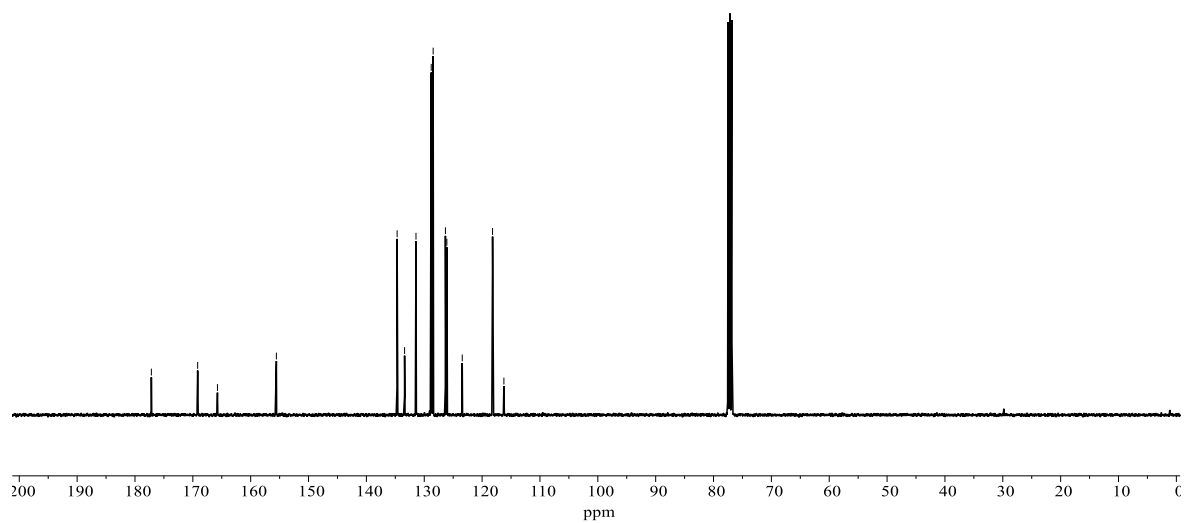
**172ai**  $^1\text{H-NMR}$   
( $\text{CDCl}_3$ , 400 MHz)



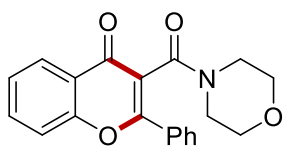
— 177.2  
 — 169.2  
 — 165.7  
 — 155.6  
 — 134.7  
 — 133.4  
 — 131.4  
 — 128.8  
 — 128.5  
 — 126.3  
 — 126.1  
 — 123.4  
 — 118.2  
 — 116.2



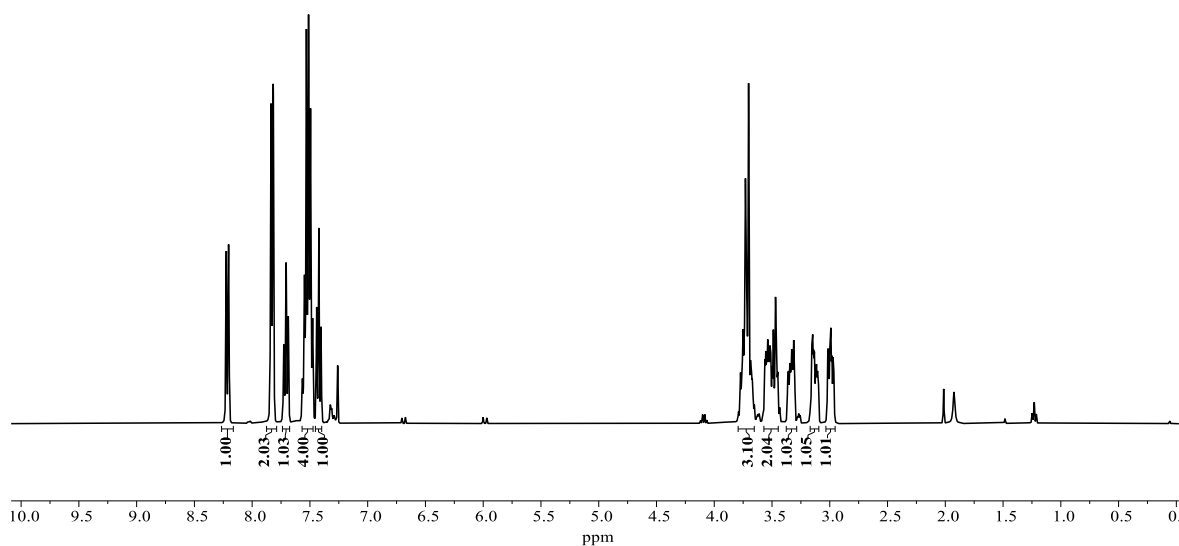
**172ai**  $^{13}\text{C-NMR}$   
( $\text{CDCl}_3$ , 101 MHz)





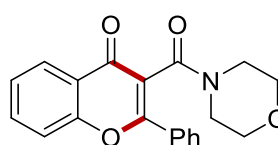


**172aj**  $^1\text{H-NMR}$   
( $\text{CDCl}_3$ , 400 MHz)

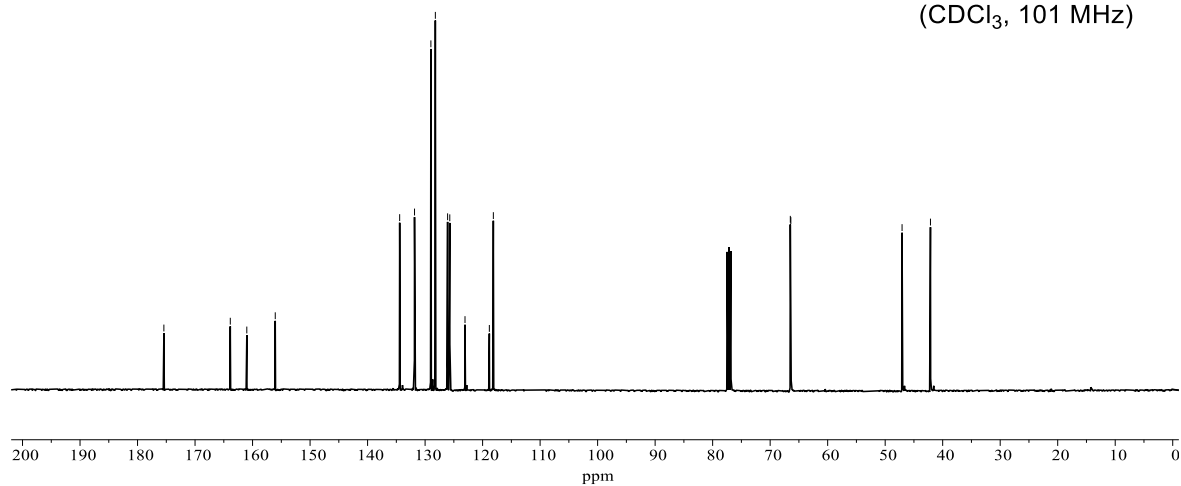


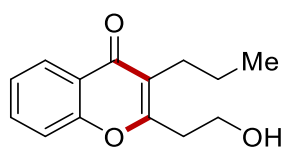
175.4  
163.9  
161.0  
156.1  
134.4  
131.8  
131.8  
129.0  
128.2  
126.1  
125.7  
123.1  
118.8  
118.1

66.5  
66.4

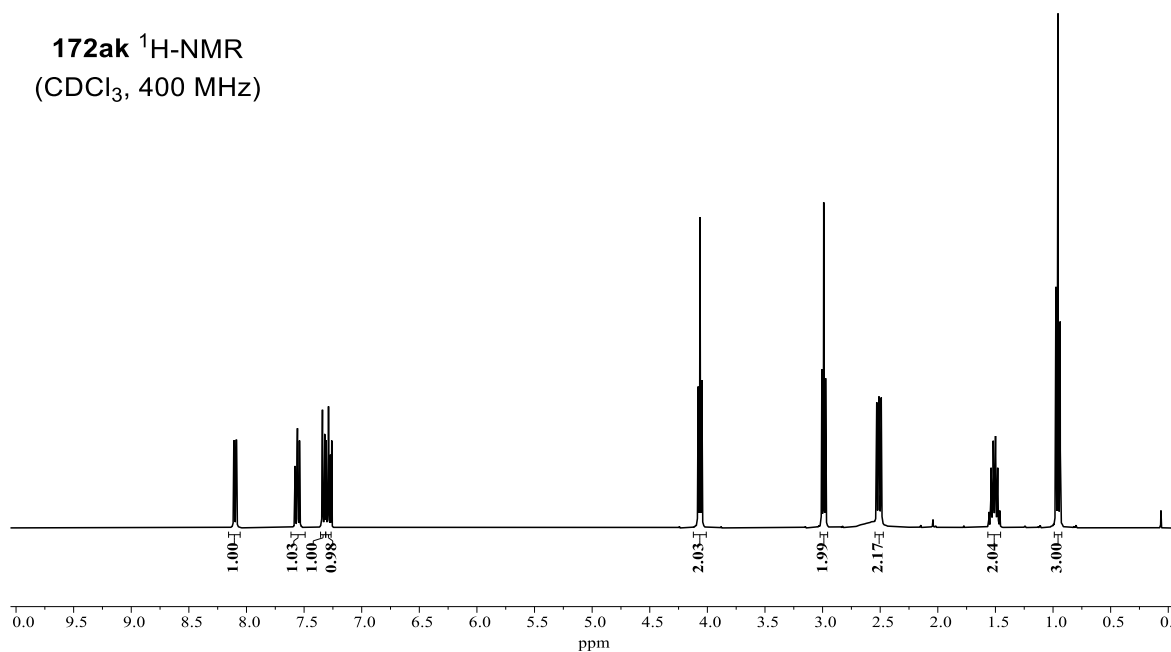


**172aj**  $^{13}\text{C-NMR}$   
( $\text{CDCl}_3$ , 101 MHz)

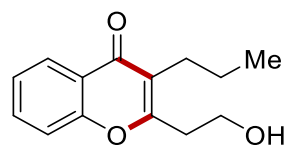




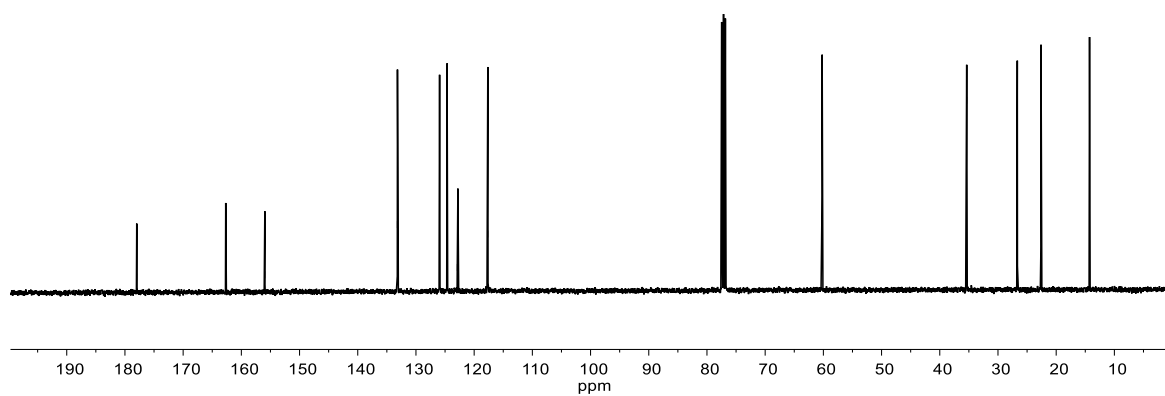
**172ak**  $^1\text{H-NMR}$   
( $\text{CDCl}_3$ , 400 MHz)

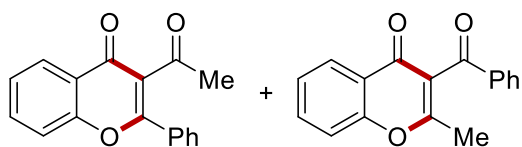


$^13\text{C-NMR}$  chemical shifts (ppm):  
 - 178.0, - 162.7, - 156.0, - 133.2, - 126.0, - 124.7, - 122.9, - 122.8, - 117.7, - 60.2, - 35.4, - 26.7, - 22.6, - 14.3

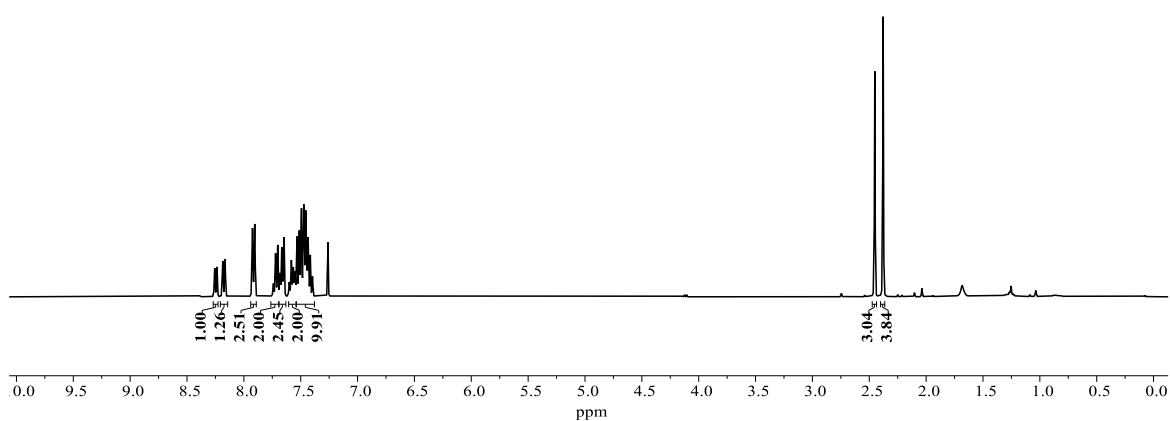


**172ak**  $^{13}\text{C-NMR}$   
( $\text{CDCl}_3$ , 101 MHz)

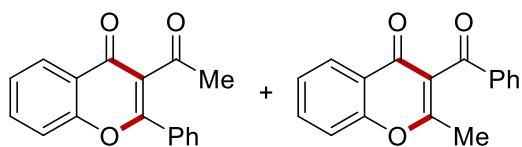




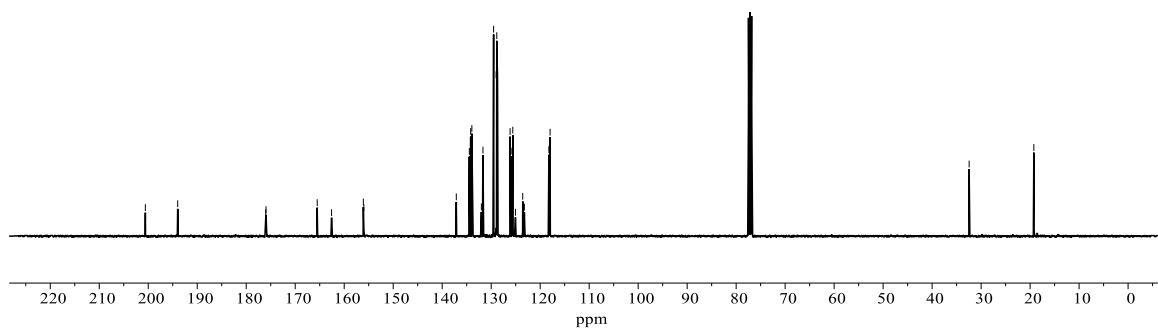
172al/172al'  $^1\text{H-NMR}$   
( $\text{CDCl}_3$ , 400 MHz)

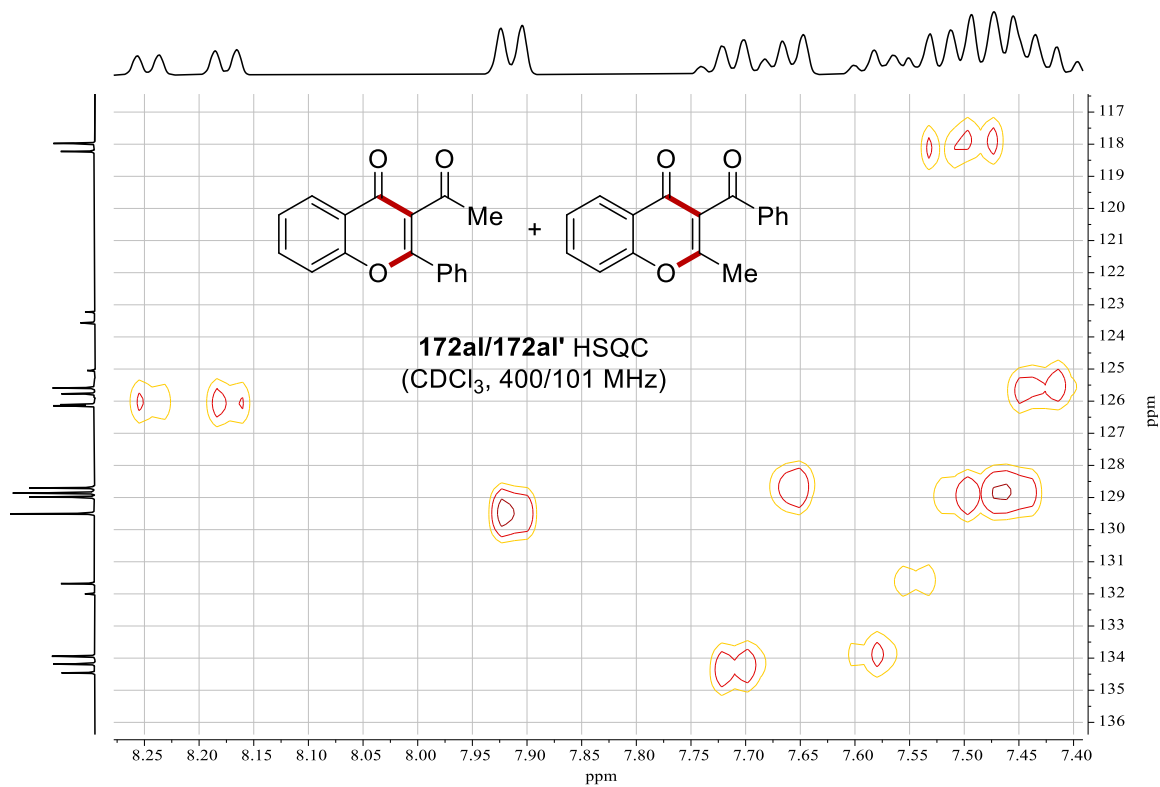
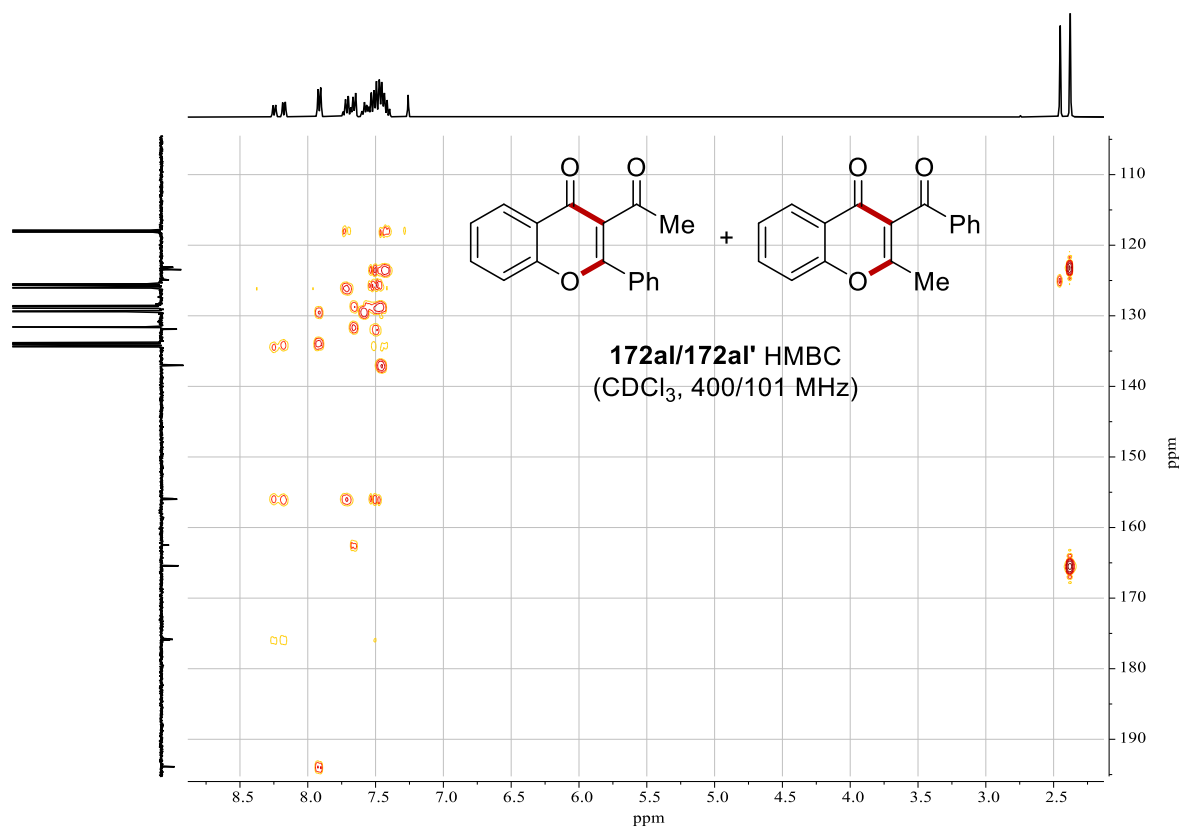


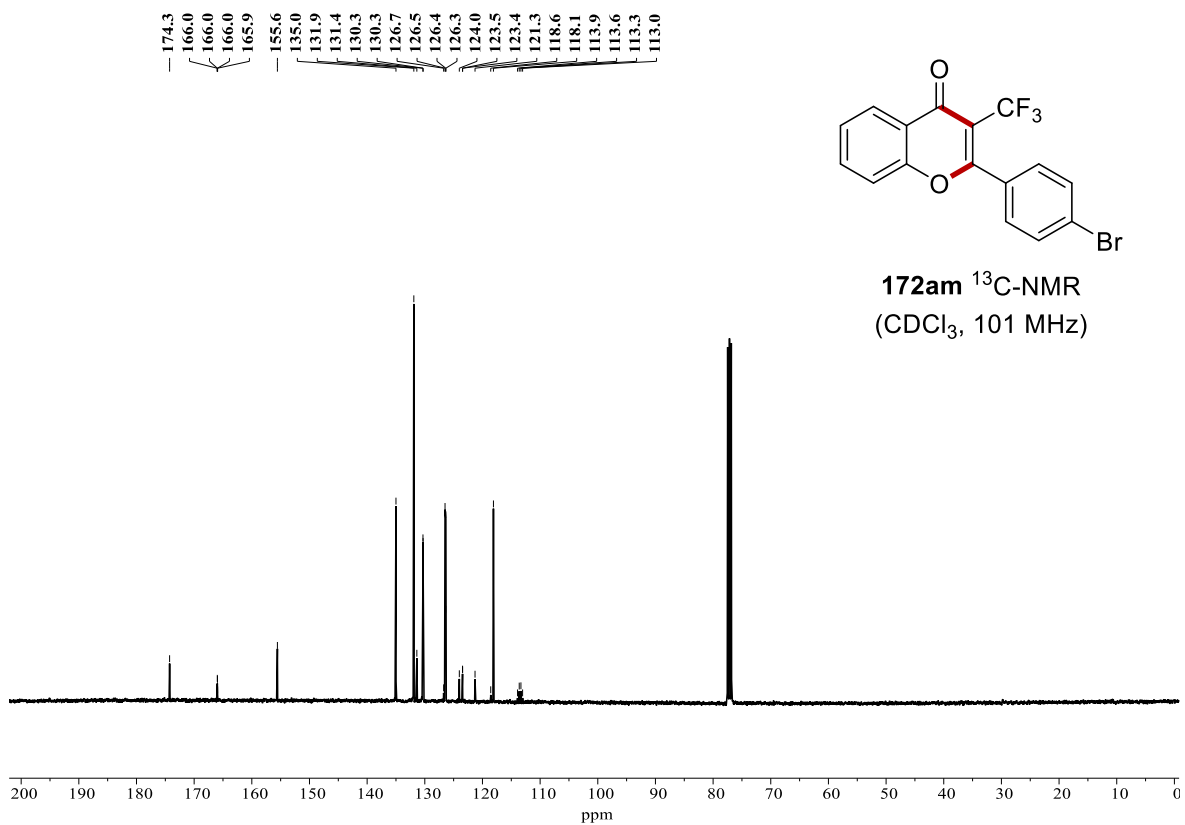
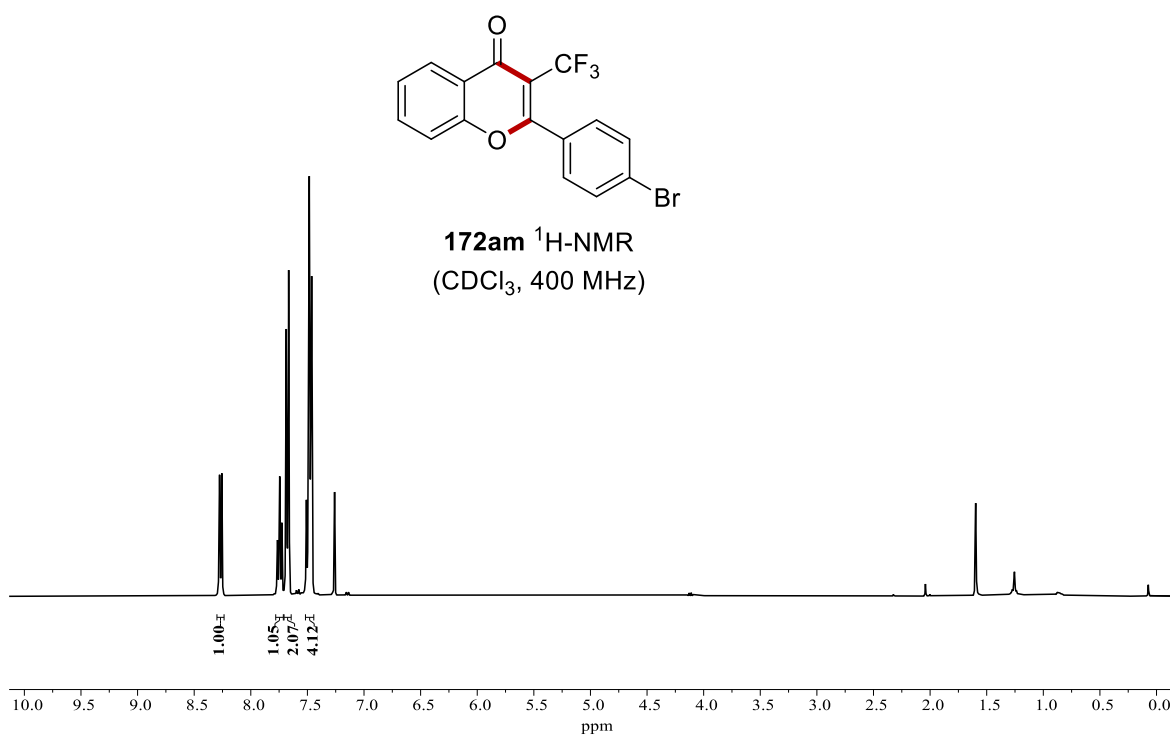
200.6  
194.0  
176.0  
176.0  
165.5  
162.6  
156.1  
156.0  
137.1  
134.5  
134.2  
133.9  
132.0  
131.7  
129.5  
129.0  
128.9  
128.7  
126.1  
126.1  
125.8  
125.6  
125.0  
123.6  
123.6  
123.2  
118.2  
118.0  
32.4  
19.2

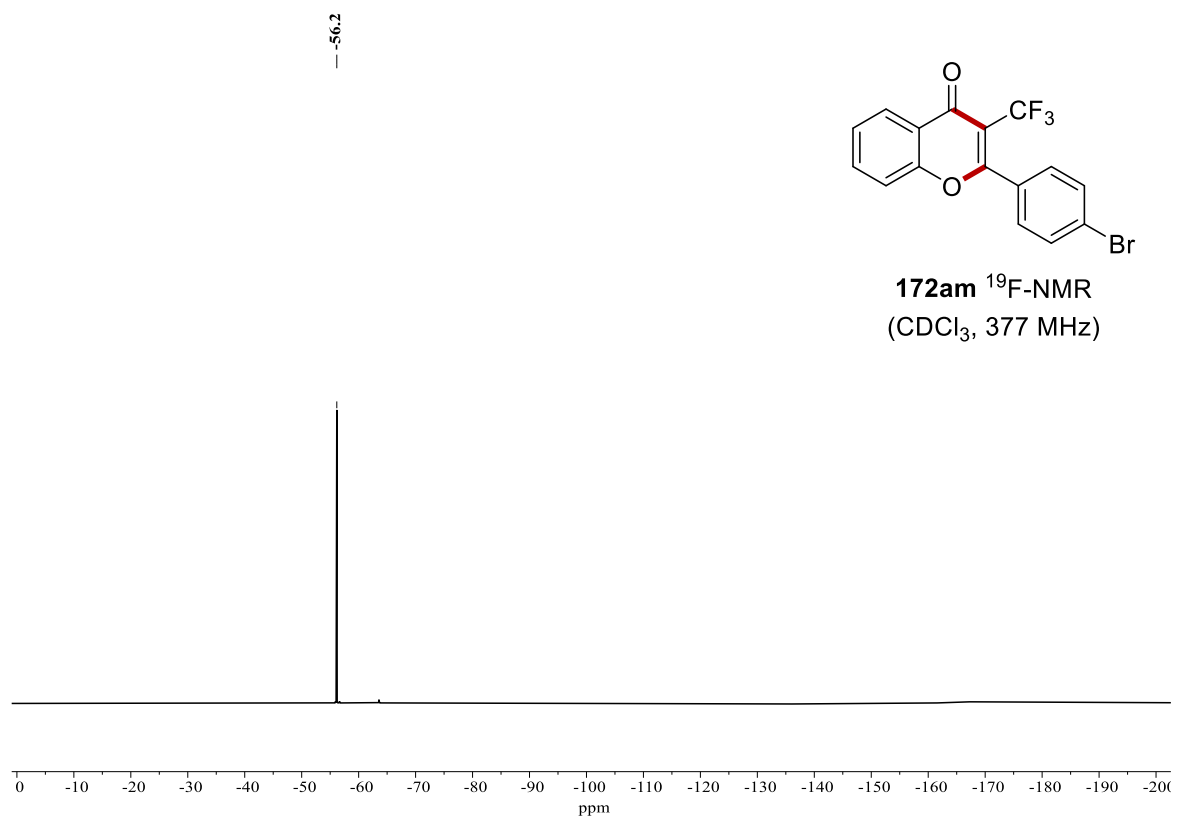


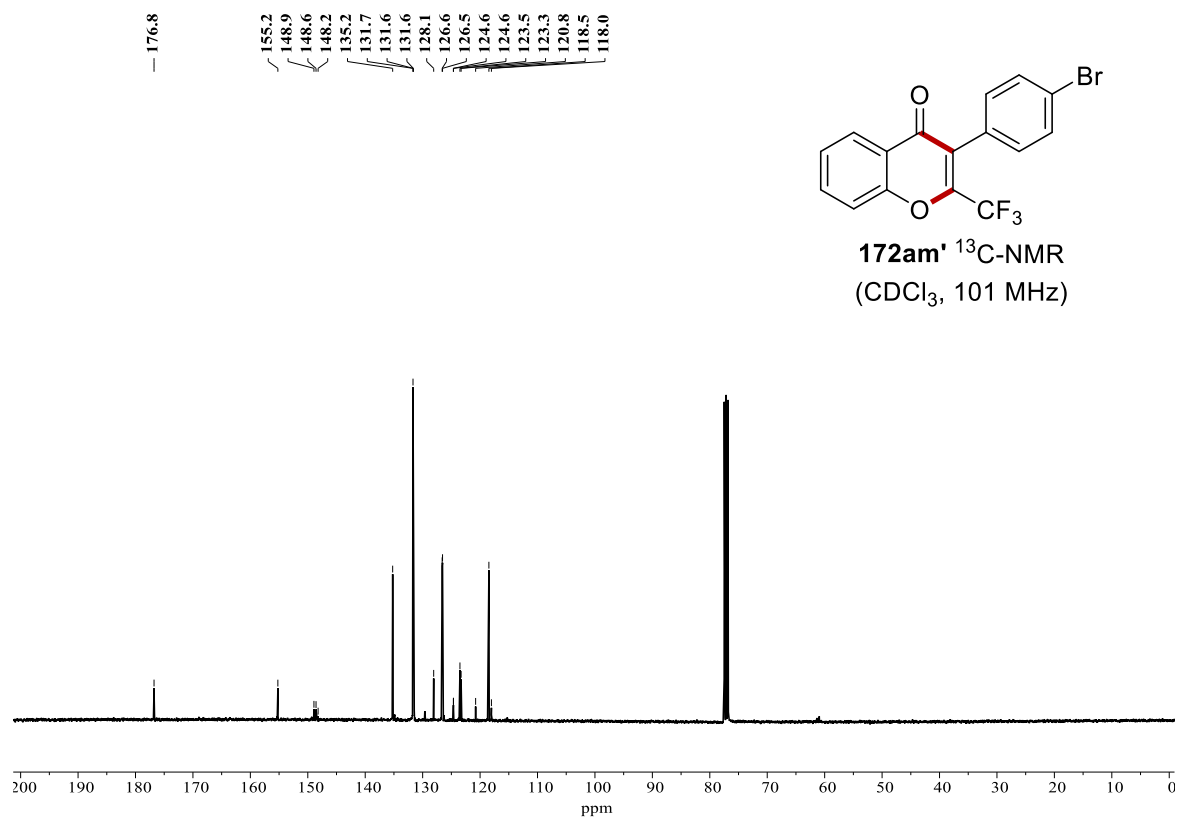
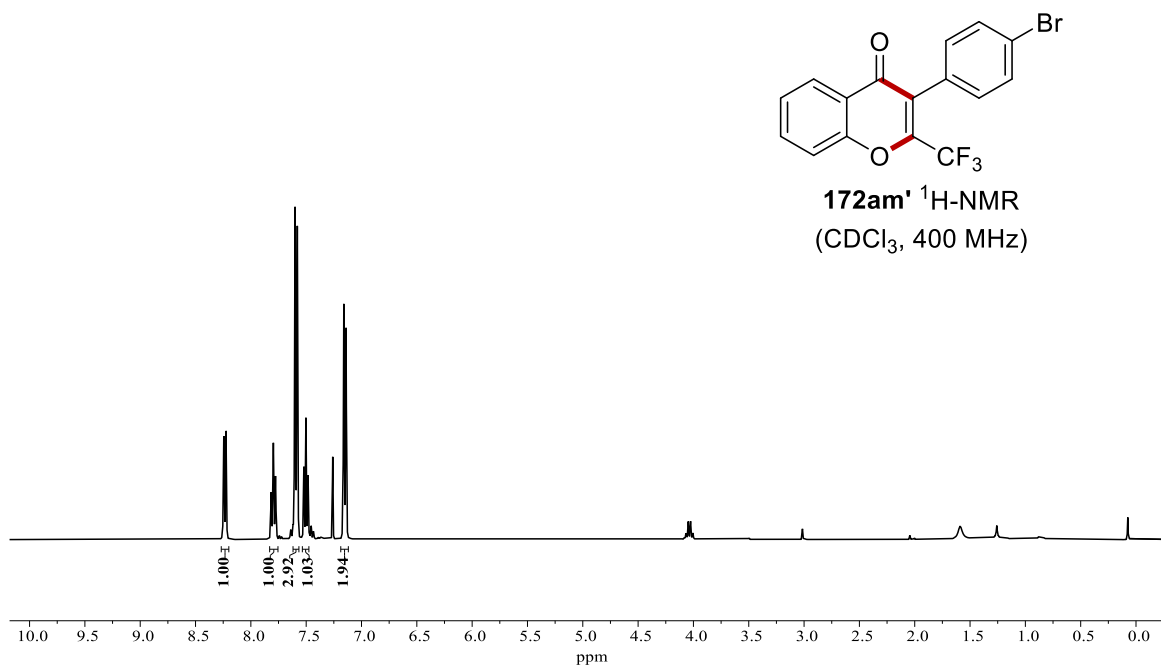
172al/172al'  $^{13}\text{C-NMR}$   
( $\text{CDCl}_3$ , 101 MHz)

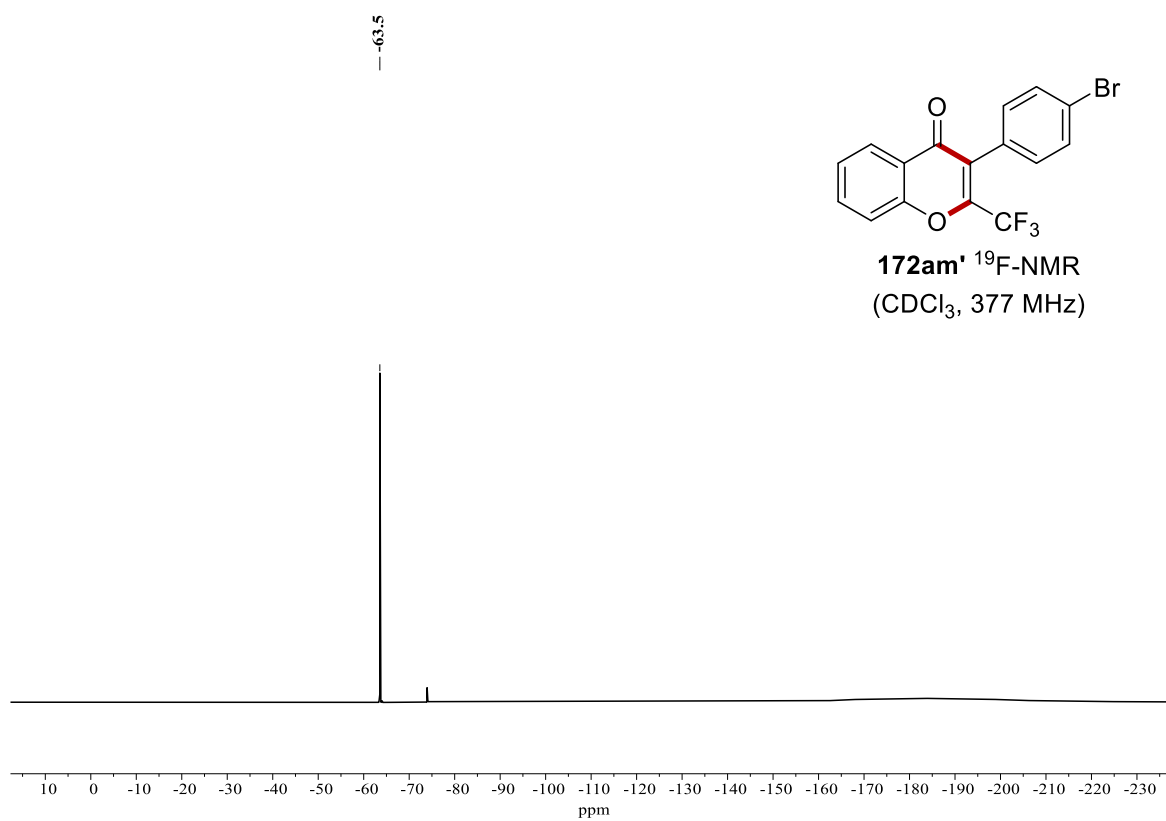




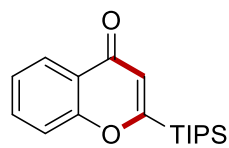




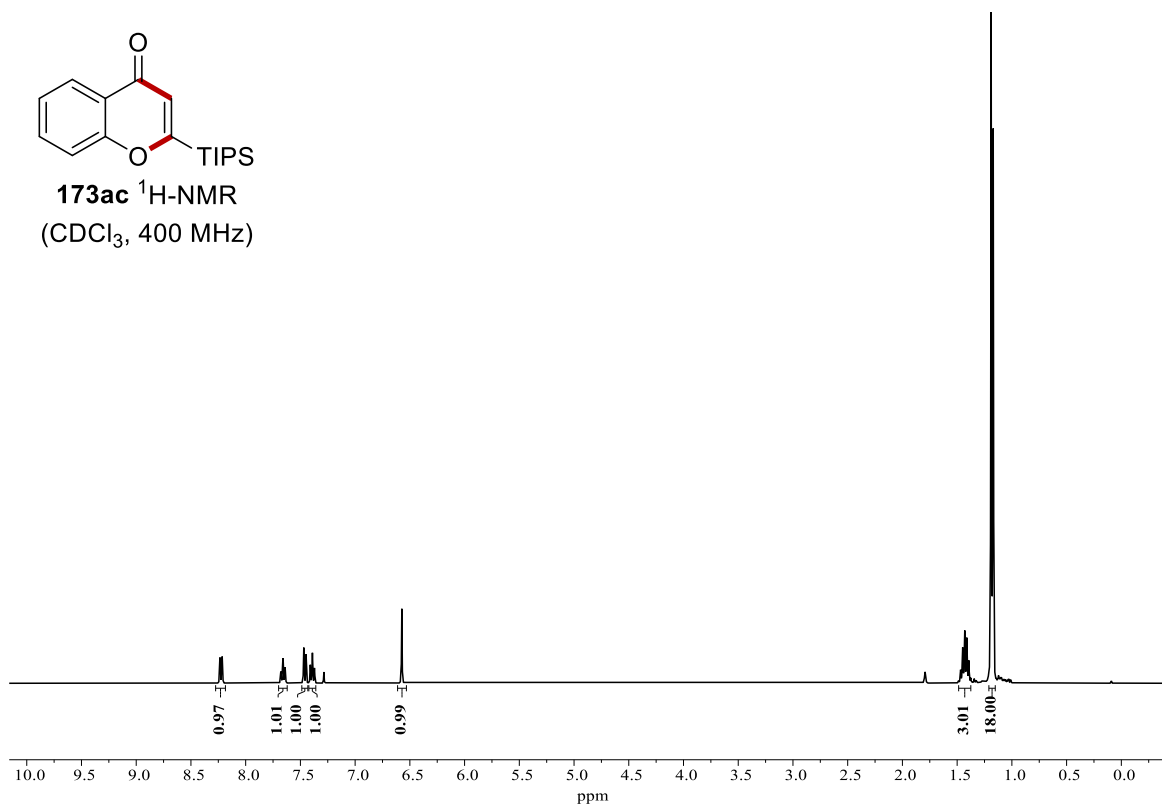






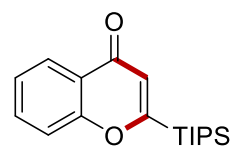


**173ac**  $^1\text{H-NMR}$   
( $\text{CDCl}_3$ , 400 MHz)

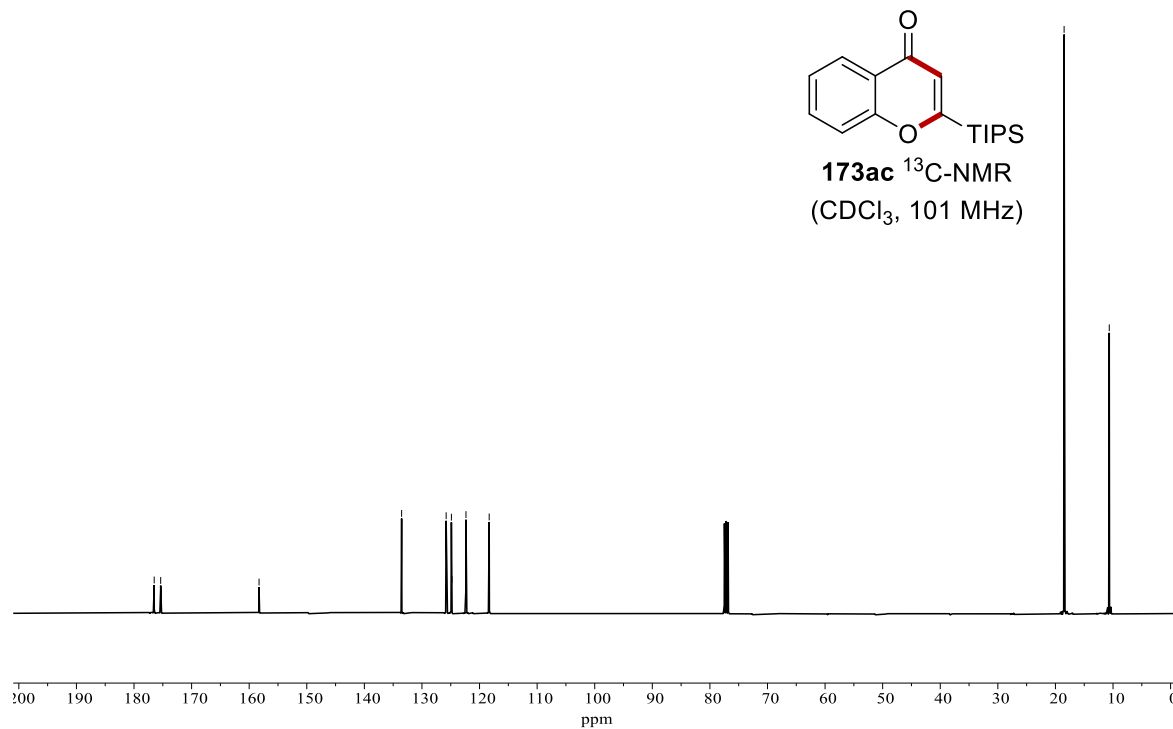


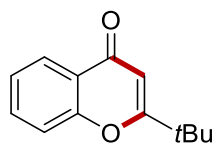
176.5  
175.4  
158.3  
133.5  
125.8  
124.9  
124.8  
122.4  
118.3

18.5  
10.7

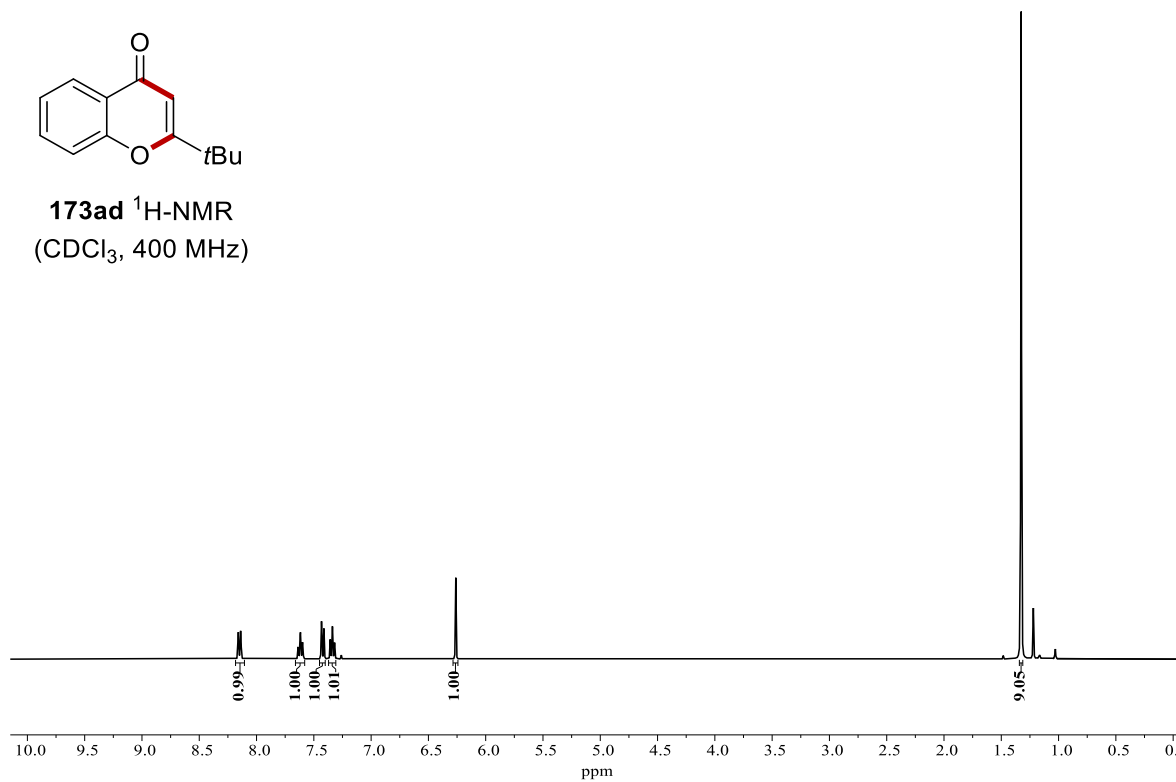


**173ac**  $^{13}\text{C-NMR}$   
( $\text{CDCl}_3$ , 101 MHz)

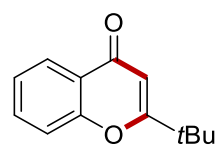




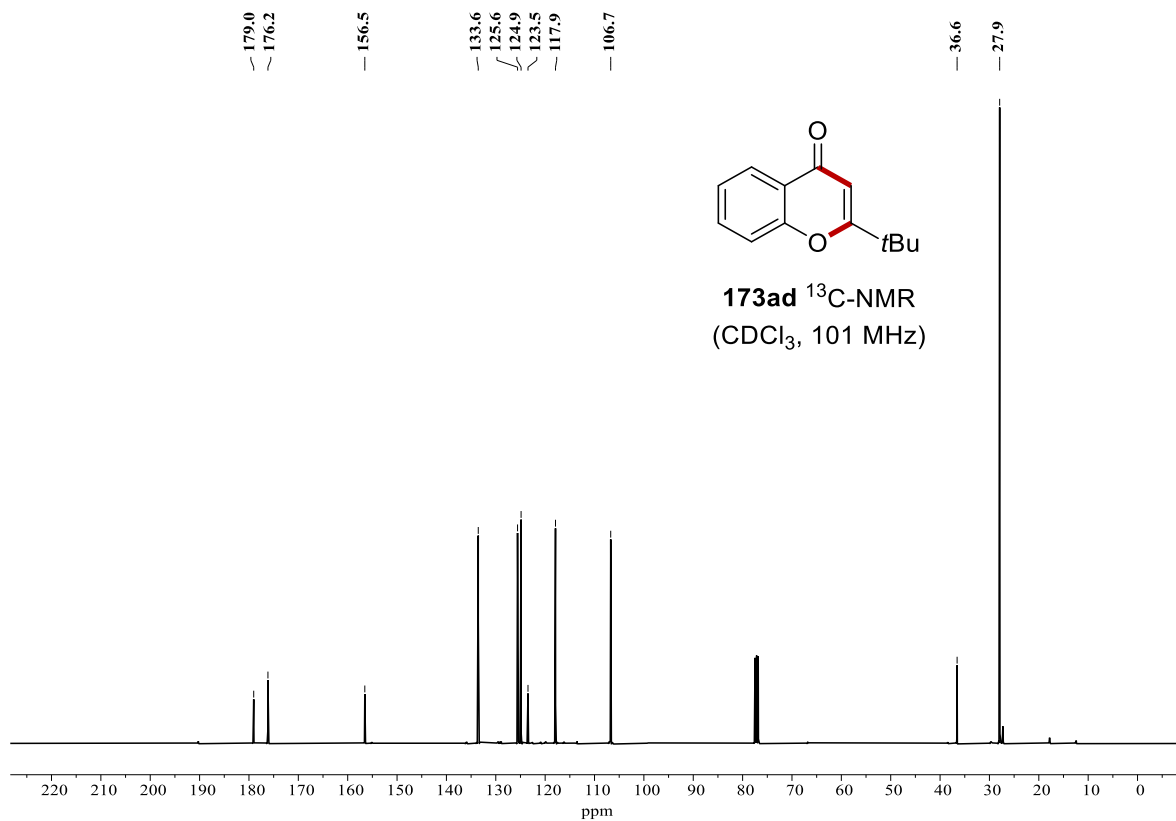
**173ad**  $^1\text{H-NMR}$   
( $\text{CDCl}_3$ , 400 MHz)

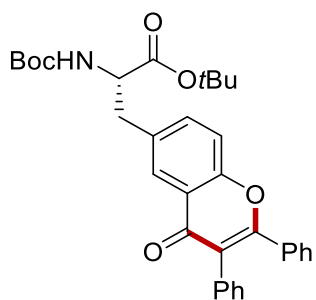


179.0  
176.2  
156.5  
133.6  
125.6  
124.9  
123.5  
117.9  
106.7

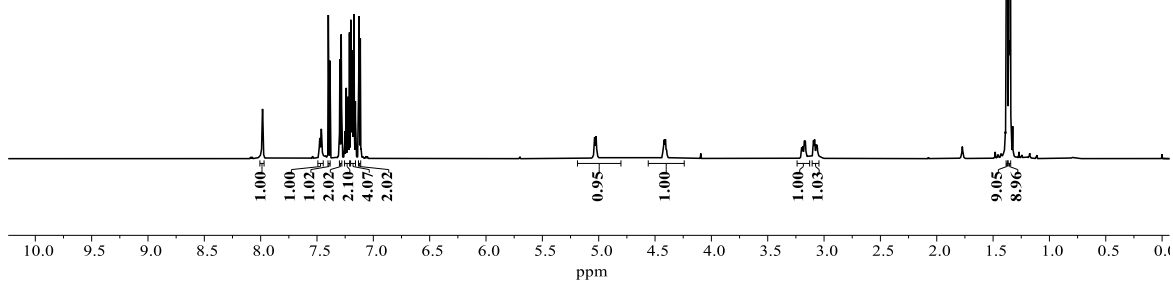


**173ad**  $^{13}\text{C-NMR}$   
( $\text{CDCl}_3$ , 101 MHz)

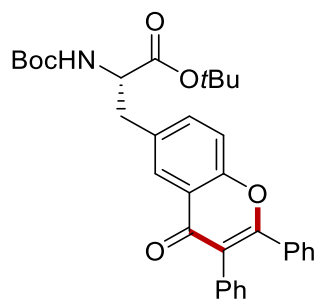




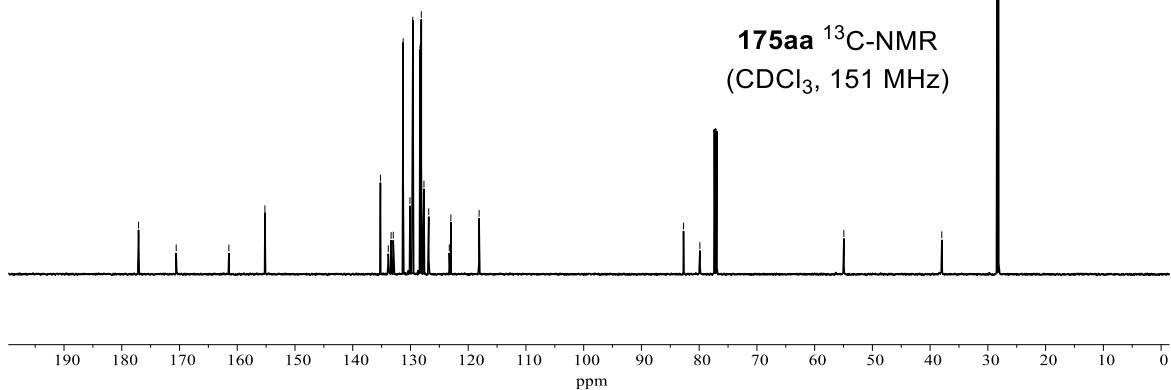
**175aa**  $^1\text{H-NMR}$   
( $\text{CDCl}_3$ , 600 MHz)

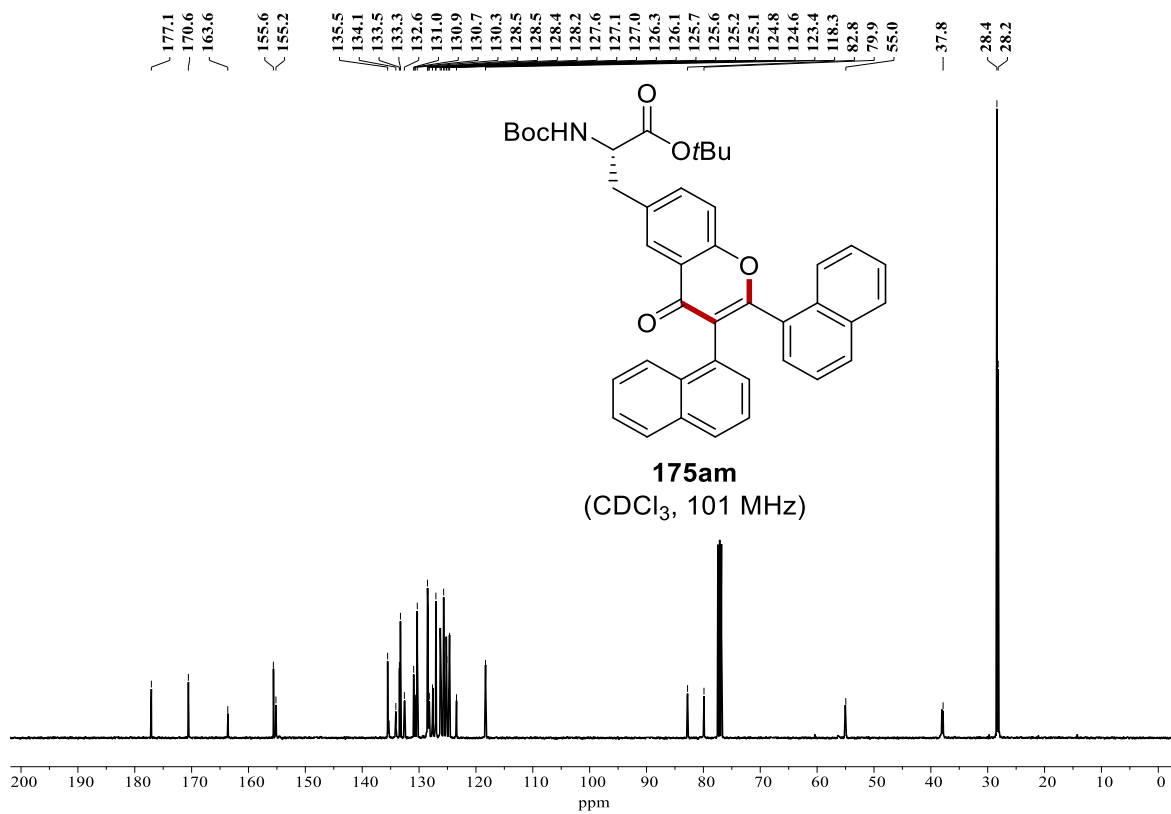
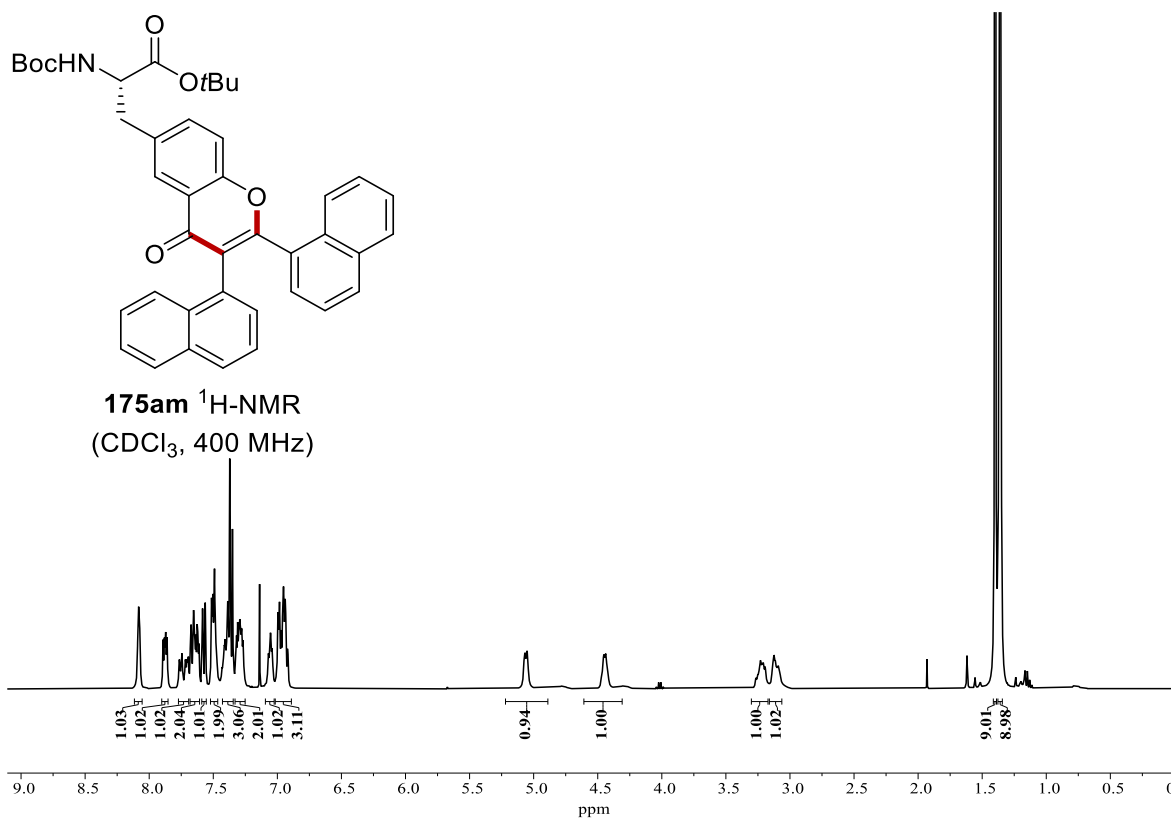


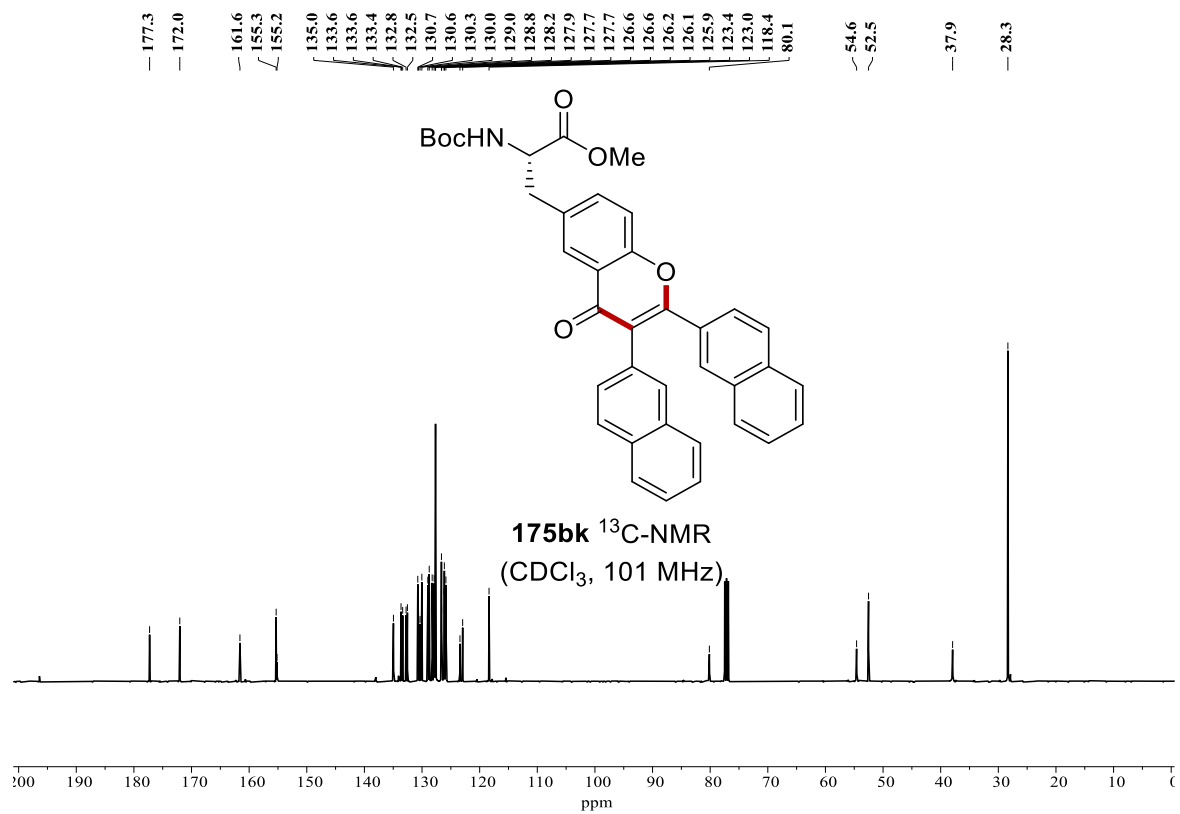
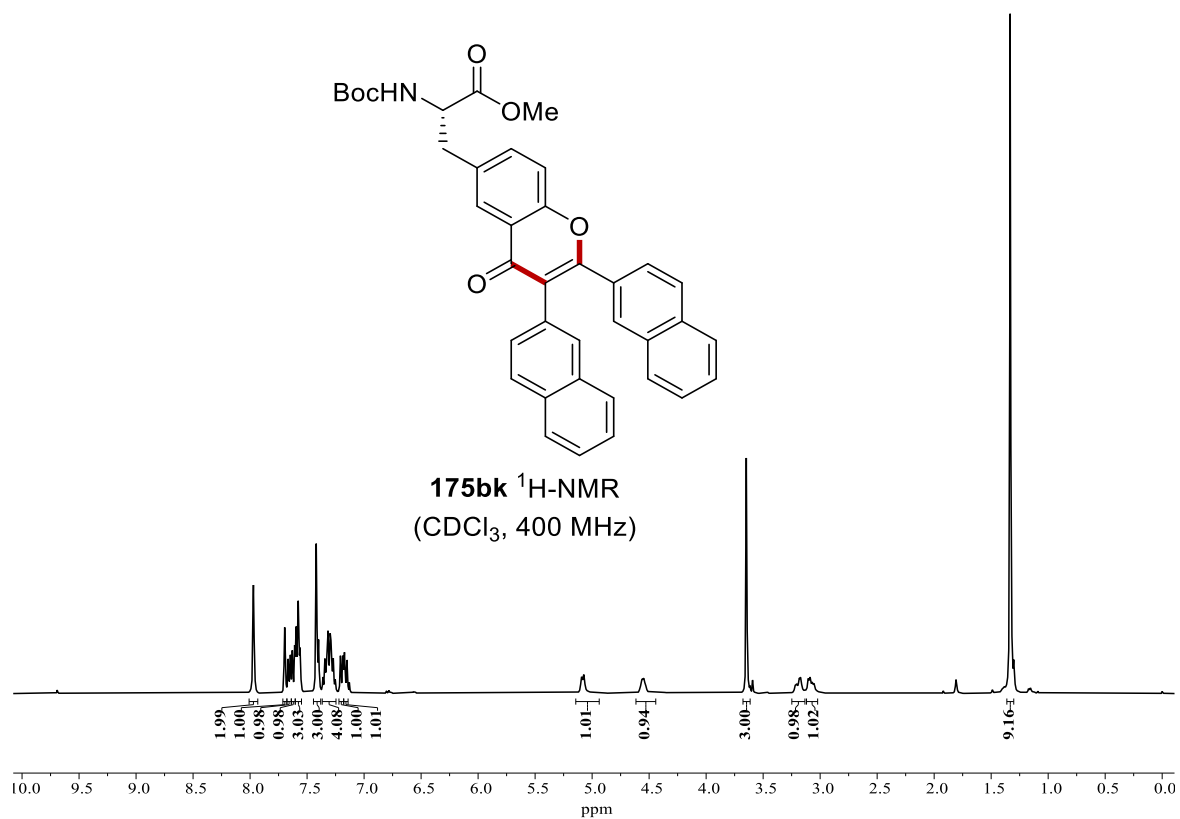
177.1  
170.6  
161.5  
155.2  
155.2  
135.2  
133.8  
133.4  
133.0  
131.3  
130.1  
129.6  
128.3  
128.1  
127.7  
126.8  
123.3  
123.0  
118.1  
82.7  
79.9  
54.9  
38.0  
28.4  
28.1

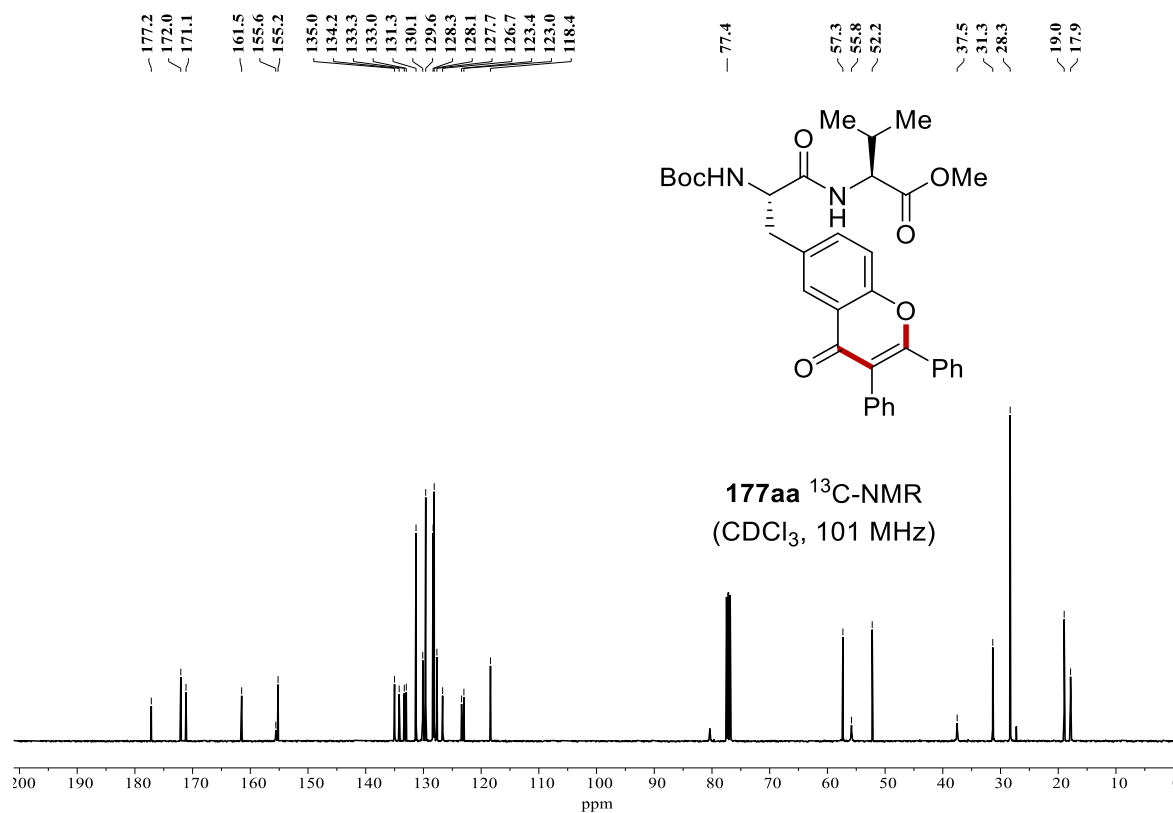
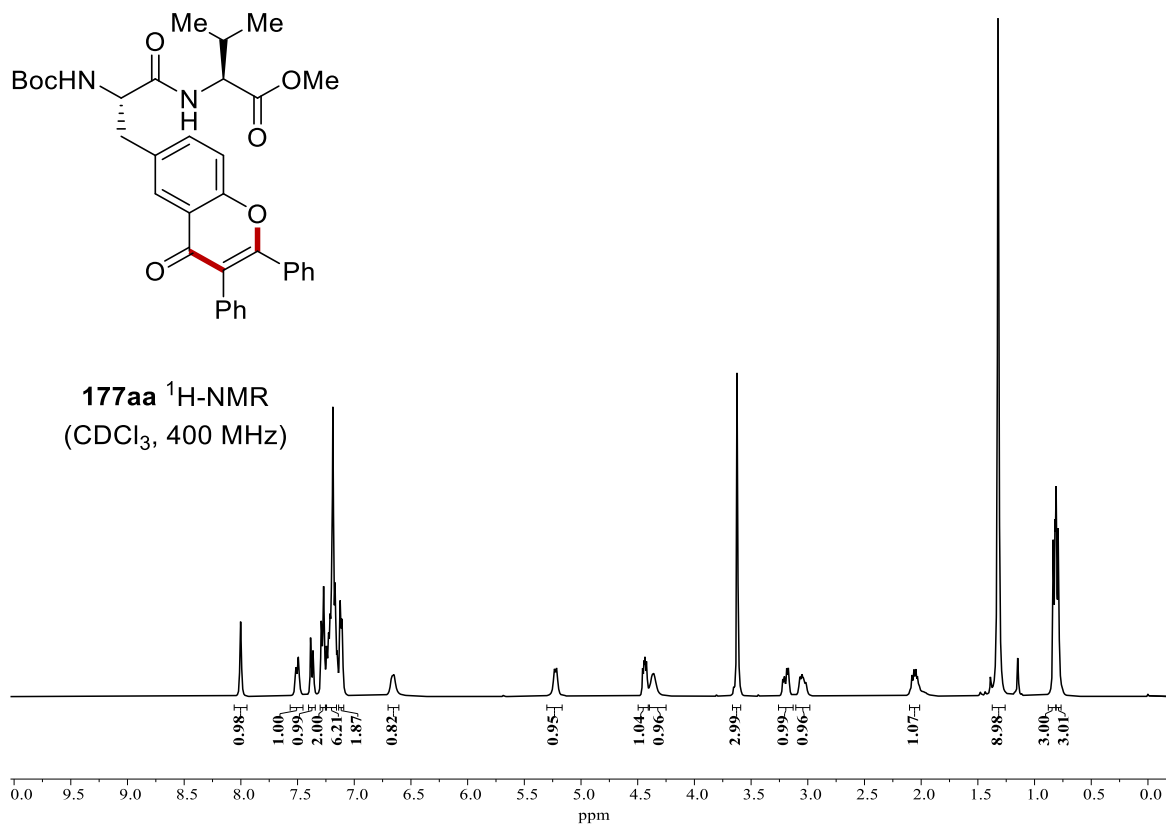


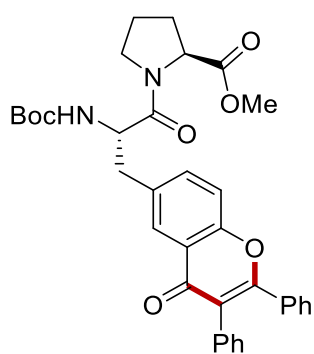
**175aa**  $^{13}\text{C-NMR}$   
( $\text{CDCl}_3$ , 151 MHz)



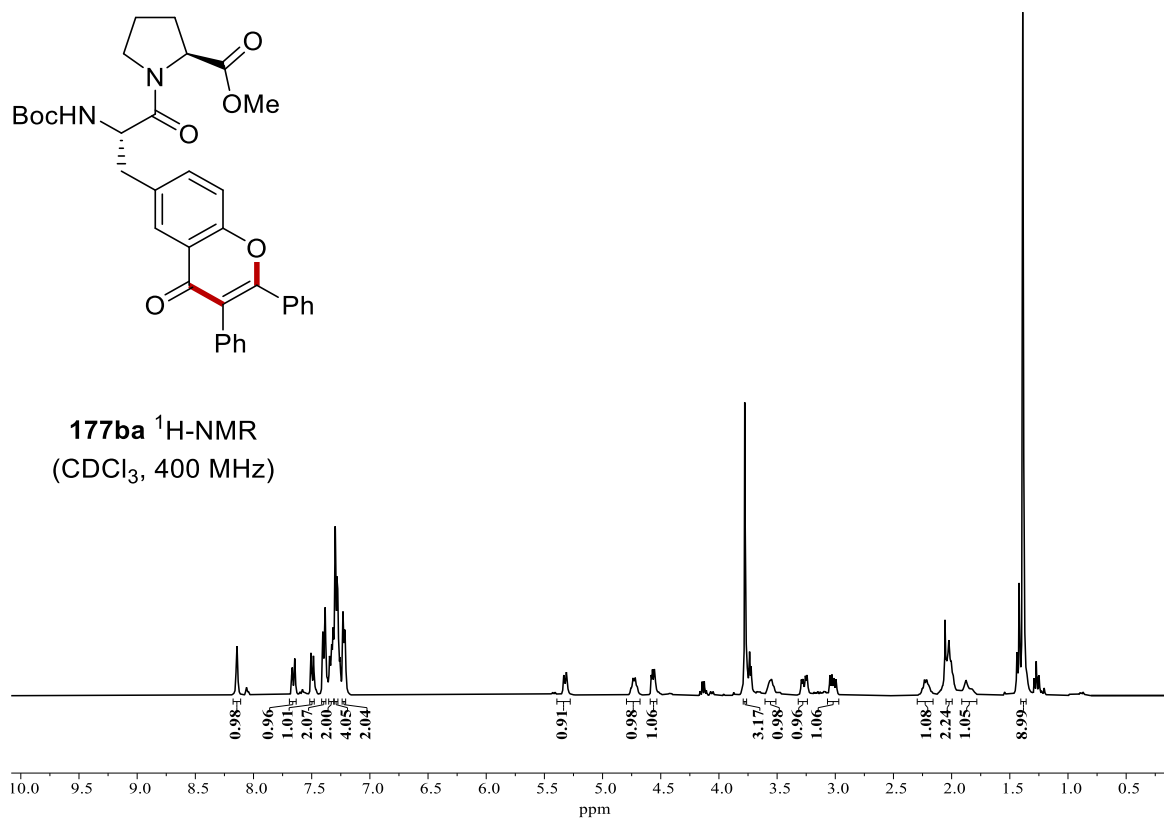








**177ba** <sup>1</sup>H-NMR  
(CDCl<sub>3</sub>, 400 MHz)



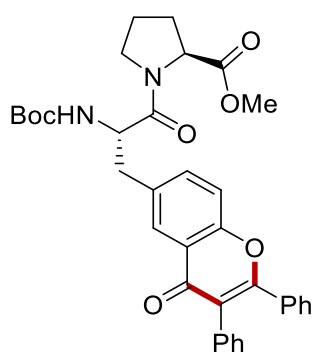
177.2  
172.4  
170.3  
161.3  
155.2  
155.2  
135.5  
133.7  
133.4  
133.0  
131.7  
131.2  
131.2  
130.0  
129.6  
128.3  
128.2  
128.1  
128.1  
127.6  
126.8  
123.3  
122.9  
118.0

79.8

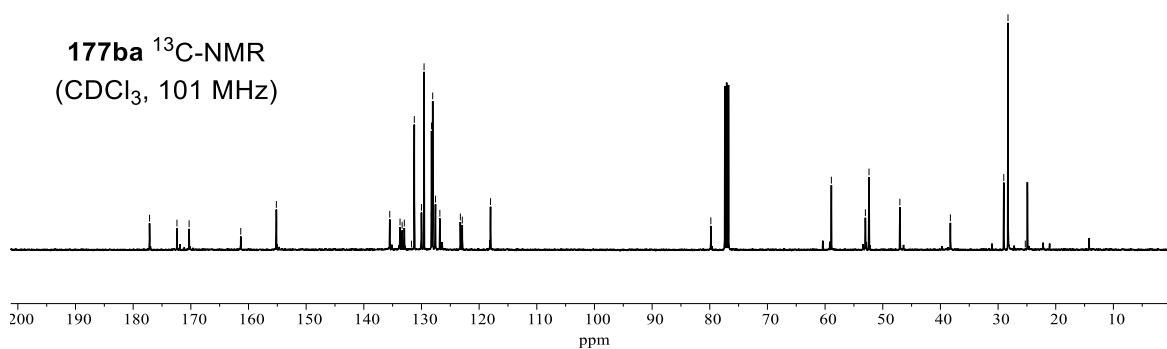
58.9  
53.0  
52.4  
47.0

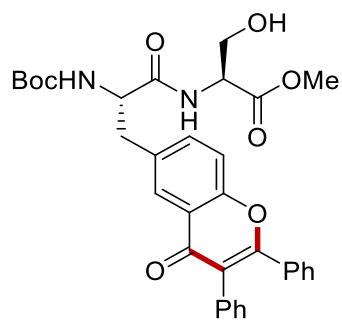
38.3

29.0  
28.3  
25.3

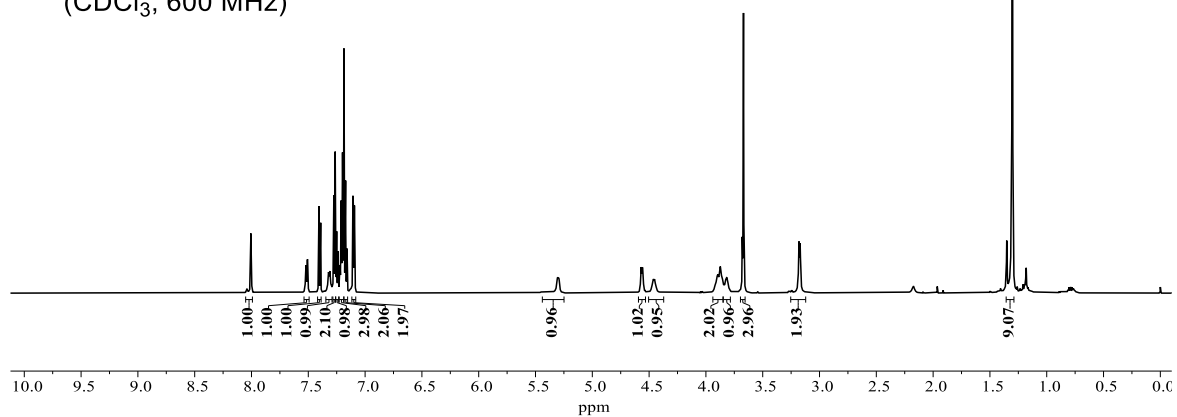


**177ba** <sup>13</sup>C-NMR  
(CDCl<sub>3</sub>, 101 MHz)



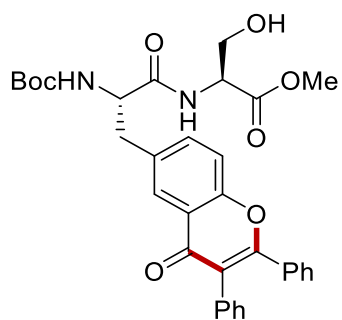


**177ca**  $^1\text{H-NMR}$   
( $\text{CDCl}_3$ , 600 MHz)

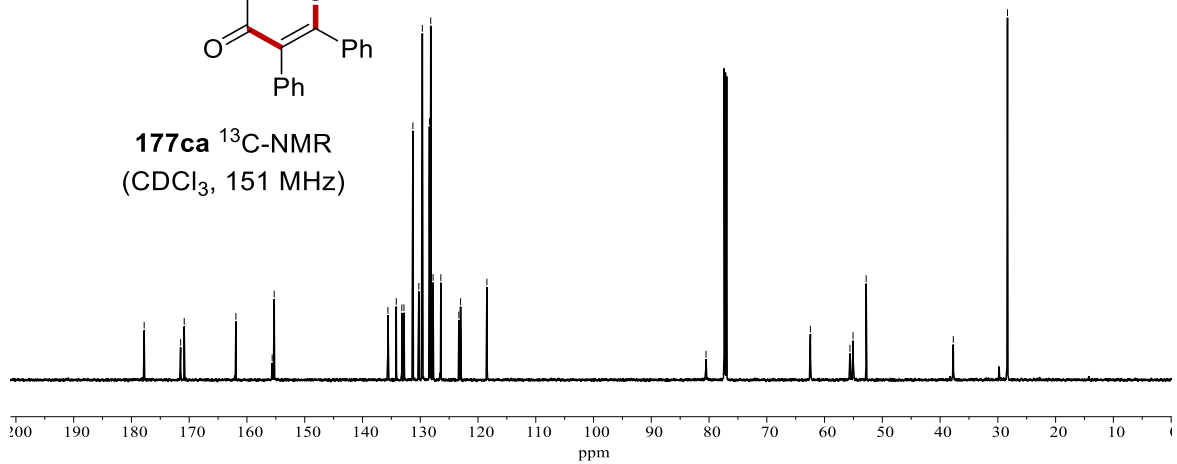


177.8  
171.5  
170.9  
161.9  
155.6  
155.3  
135.6  
134.1  
133.2  
132.8  
131.3  
130.2  
129.6  
128.4  
128.2  
127.8  
126.4  
123.3  
123.0  
118.5

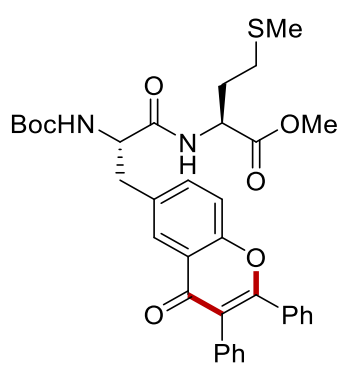
80.5  
62.5  
55.6  
55.1  
52.8  
37.7  
28.3



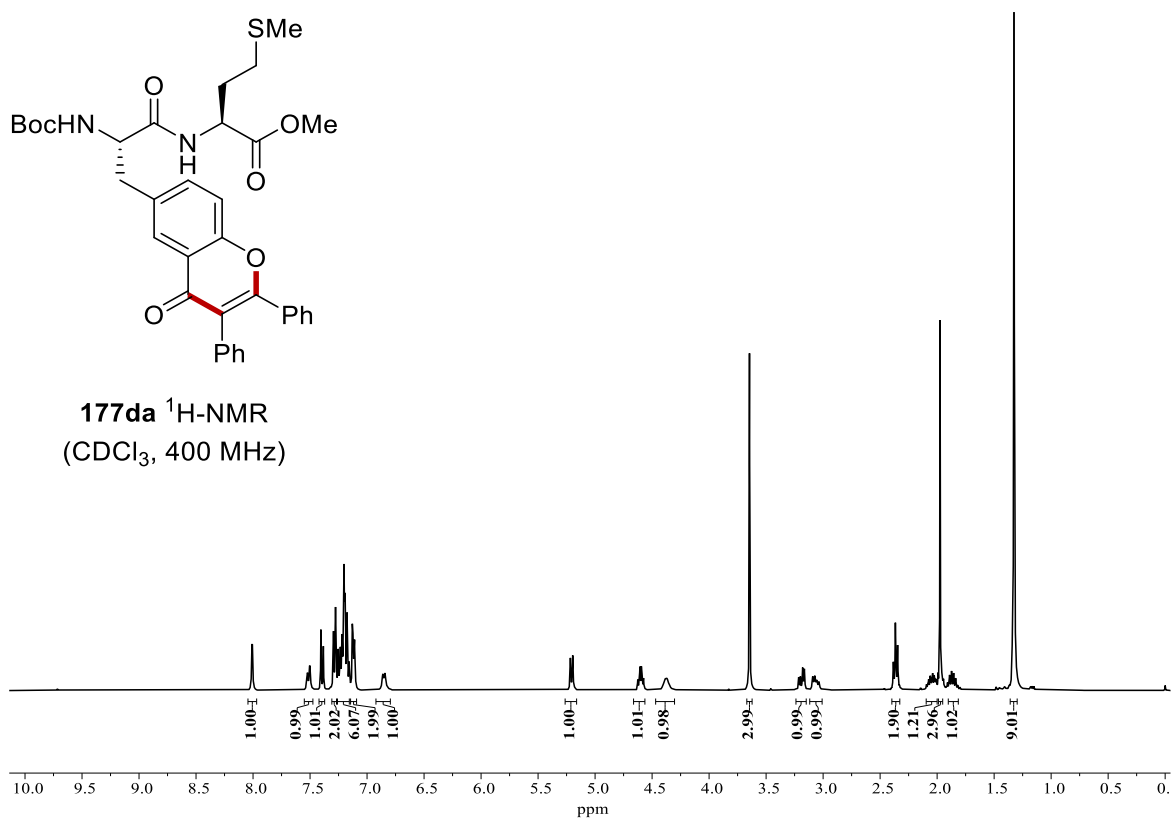
**177ca**  $^{13}\text{C-NMR}$   
( $\text{CDCl}_3$ , 151 MHz)







**177da**  $^1\text{H-NMR}$   
( $\text{CDCl}_3$ , 400 MHz)



177.2  
172.0  
171.1  
161.6  
155.5  
155.2  
135.1  
134.1  
133.3  
133.0  
131.3  
130.2  
129.6  
128.4  
128.2  
127.7  
126.7  
123.4  
123.0  
118.4

80.5

55.7

52.6

51.7

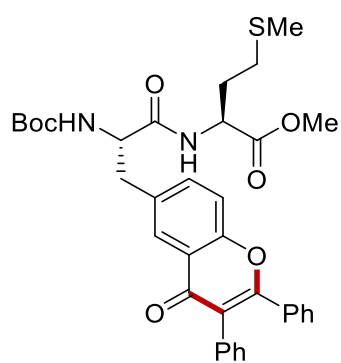
37.7

31.6

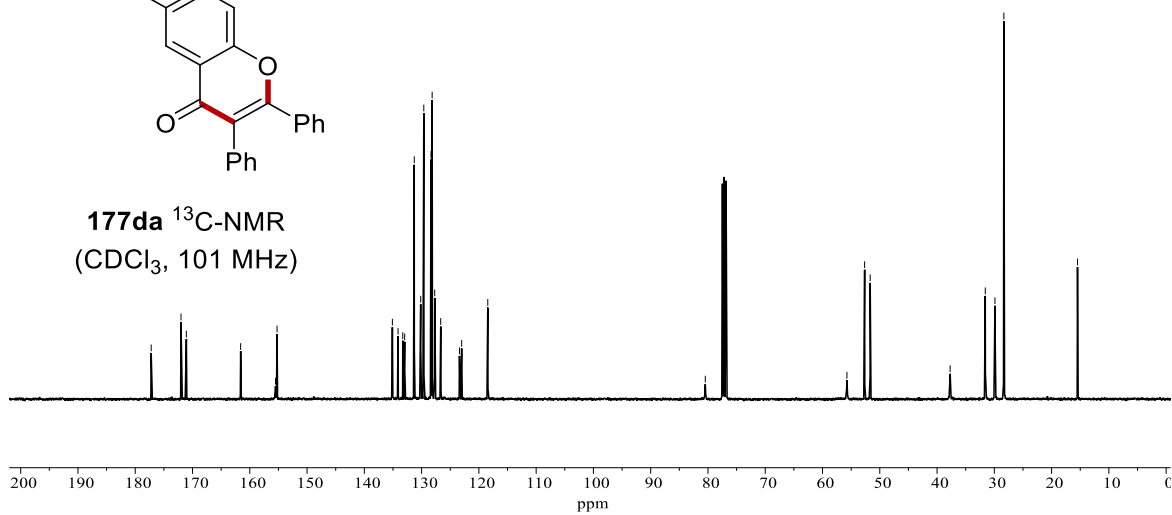
29.9

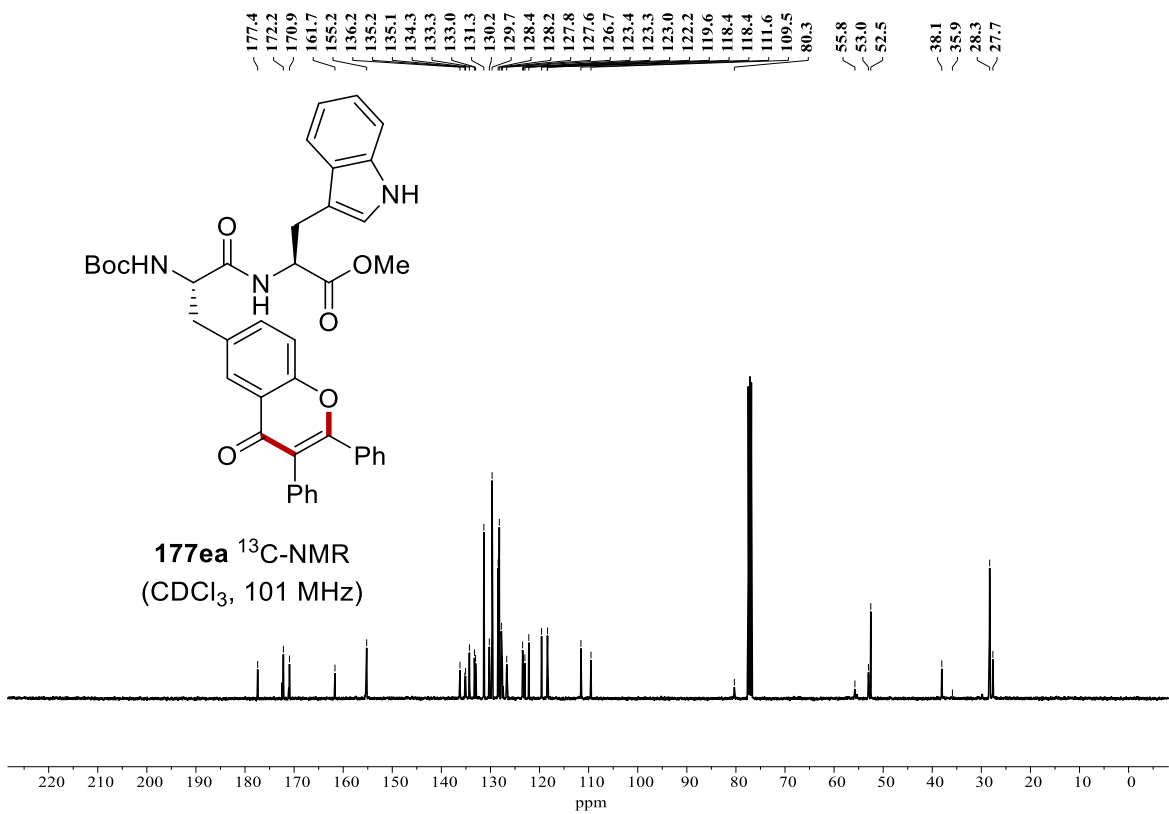
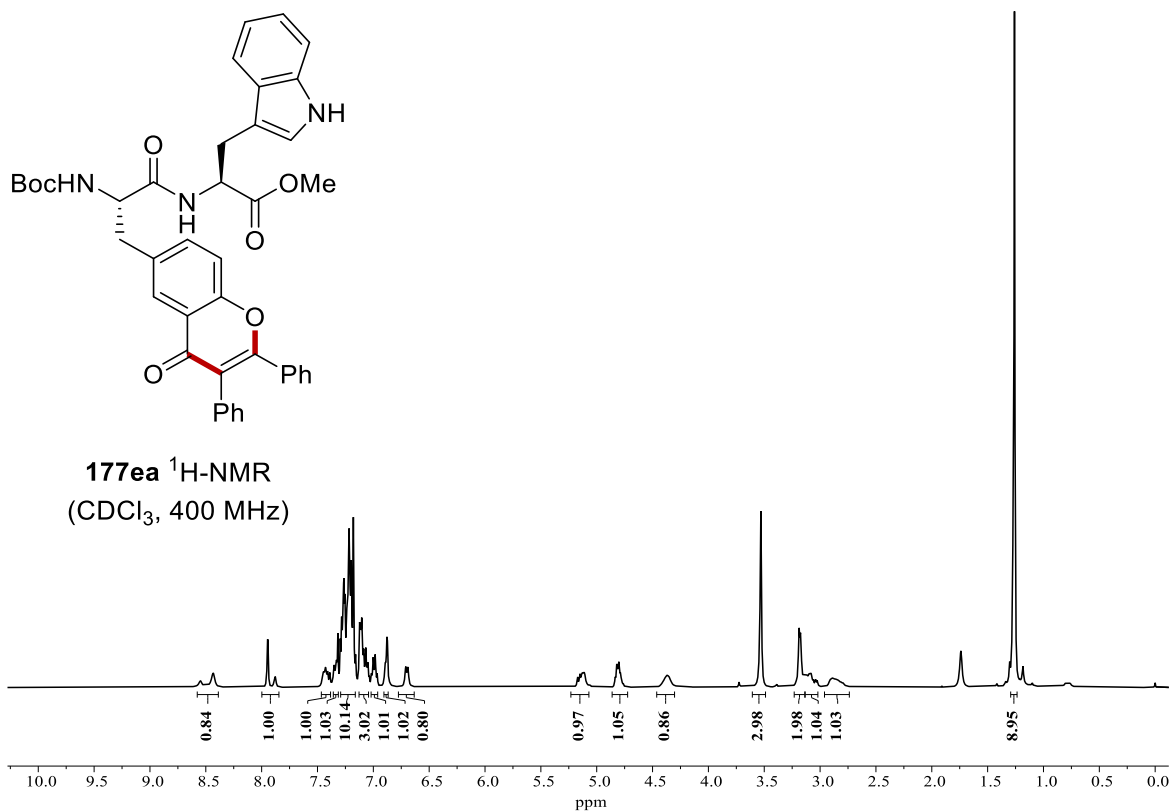
28.3

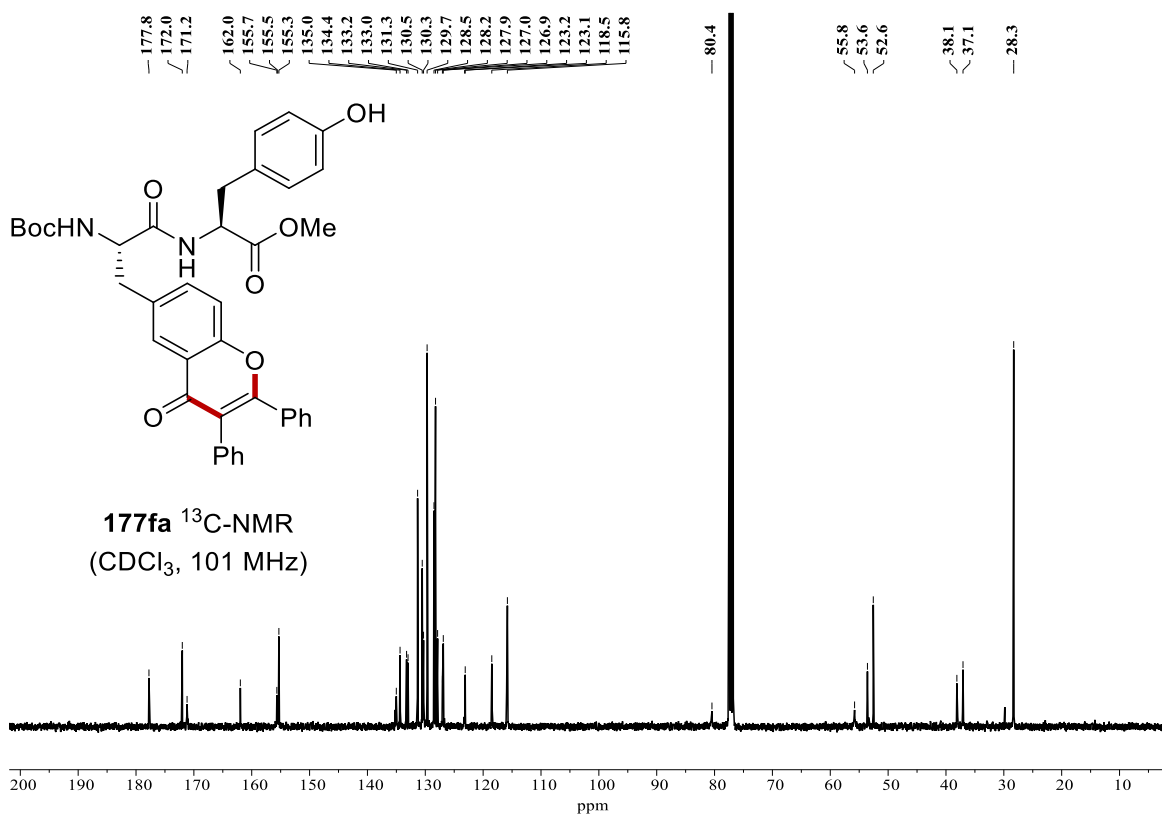
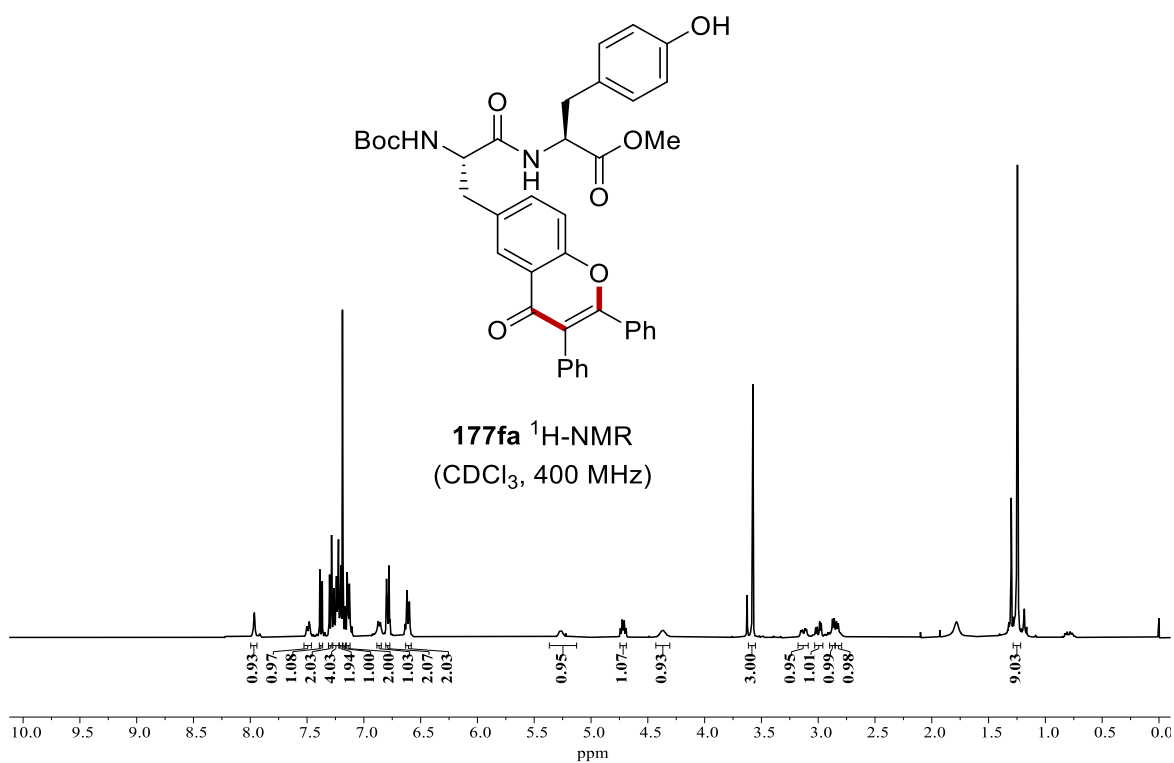
15.5

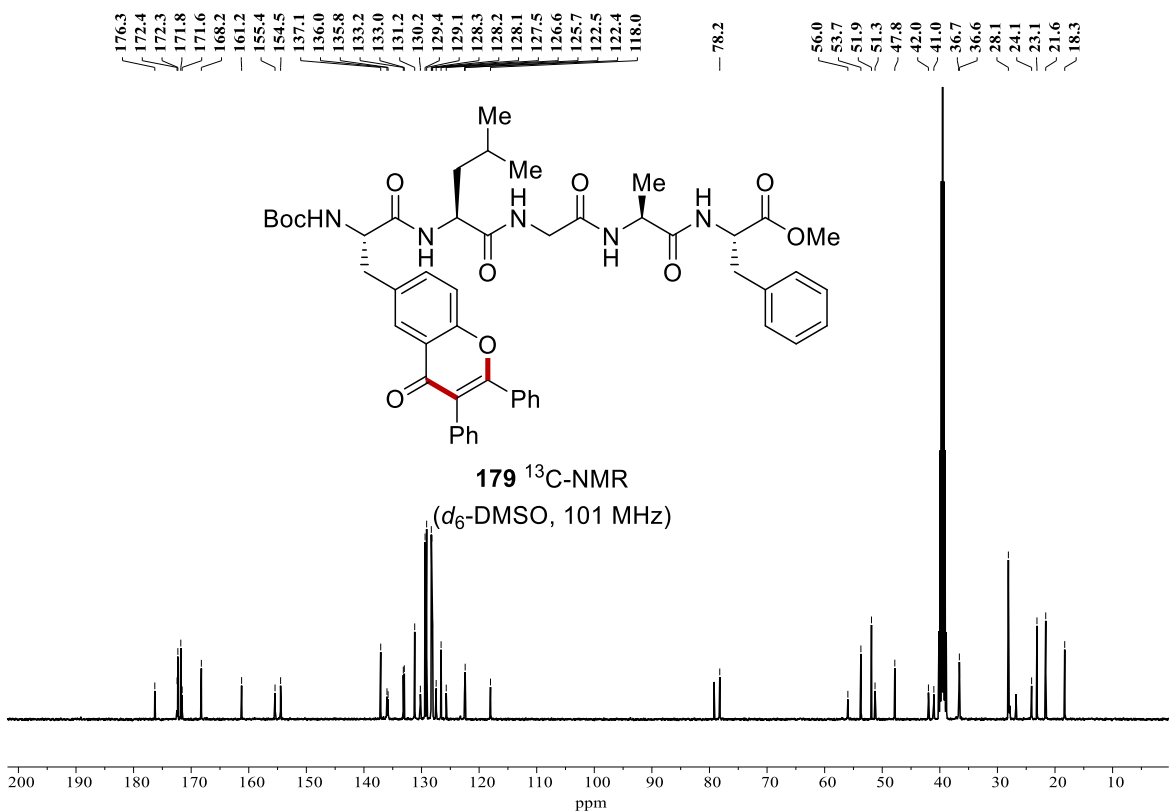
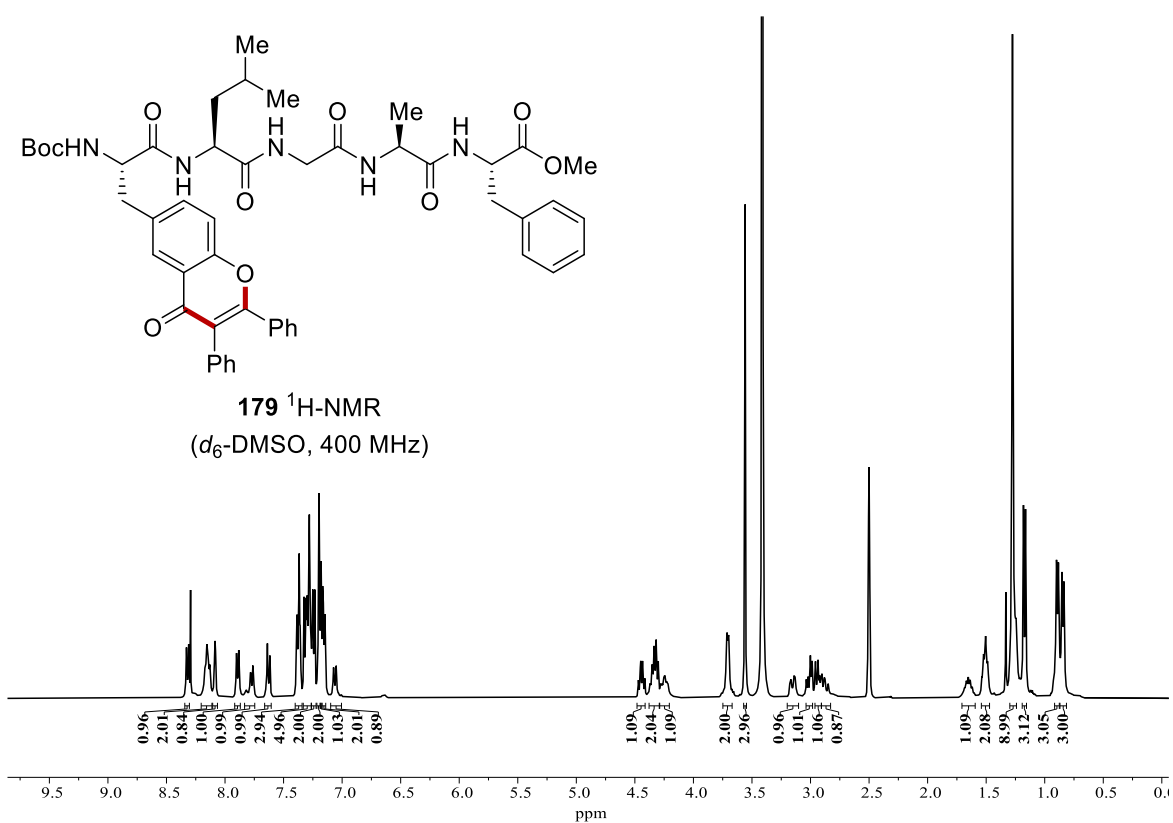


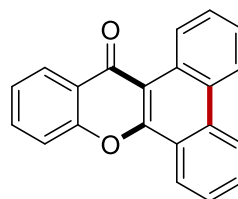
**177da**  $^{13}\text{C-NMR}$   
( $\text{CDCl}_3$ , 101 MHz)



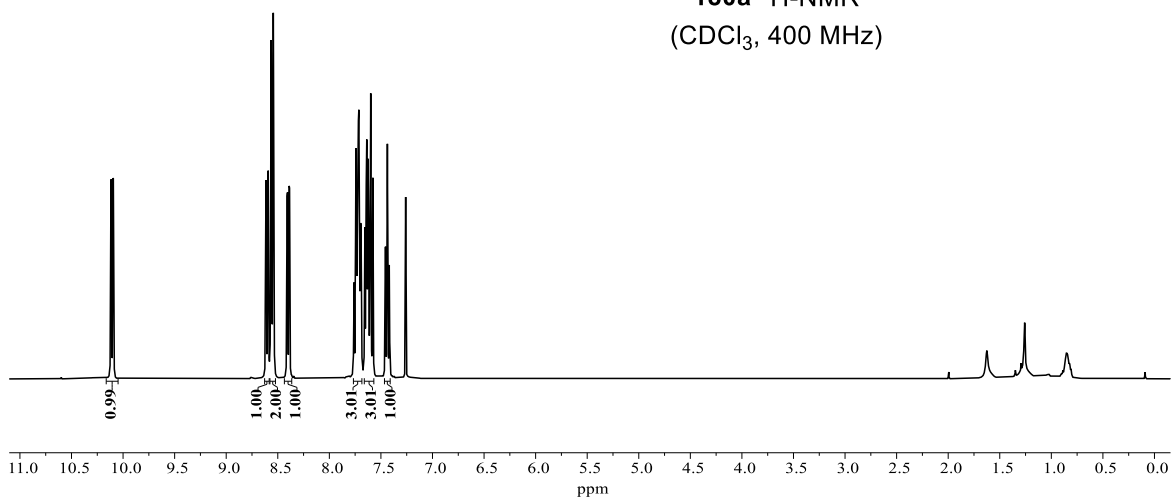




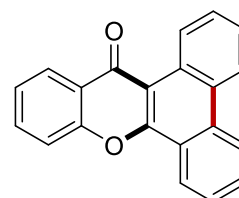




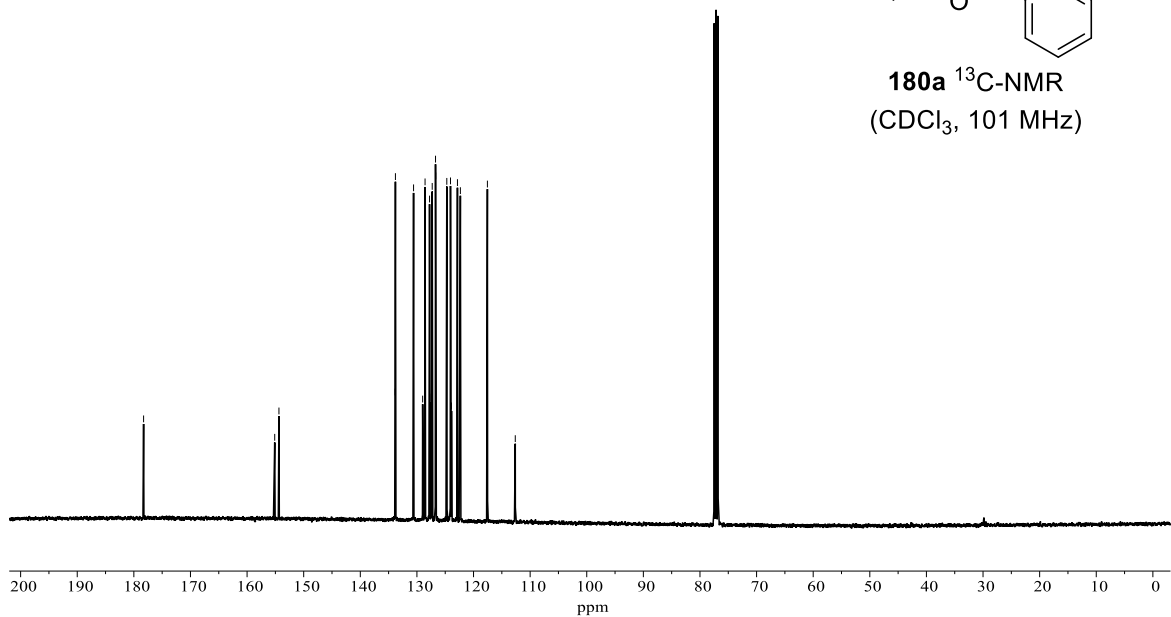
**180a**  $^1\text{H-NMR}$   
( $\text{CDCl}_3$ , 400 MHz)

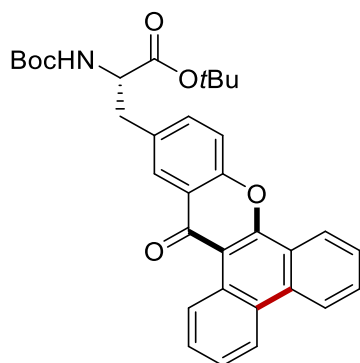


178.3  
155.1  
154.4  
133.8  
133.8  
130.6  
129.0  
128.6  
127.8  
127.5  
127.3  
126.7  
126.7  
124.7  
124.1  
124.0  
123.9  
122.8  
122.3  
117.5  
112.6

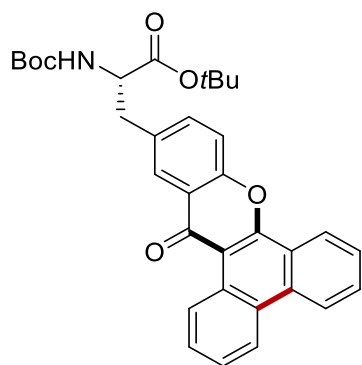
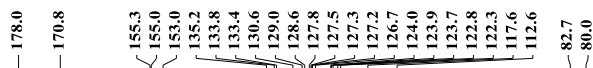
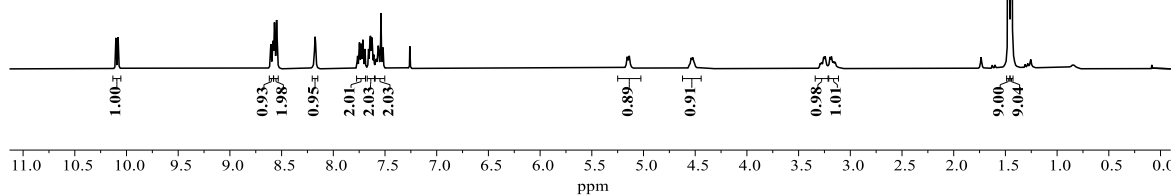


**180a**  $^{13}\text{C-NMR}$   
( $\text{CDCl}_3$ , 101 MHz)

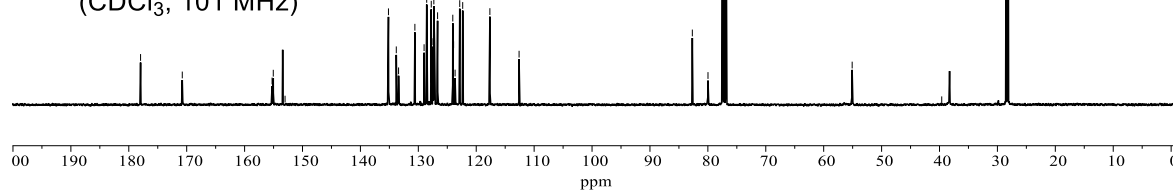


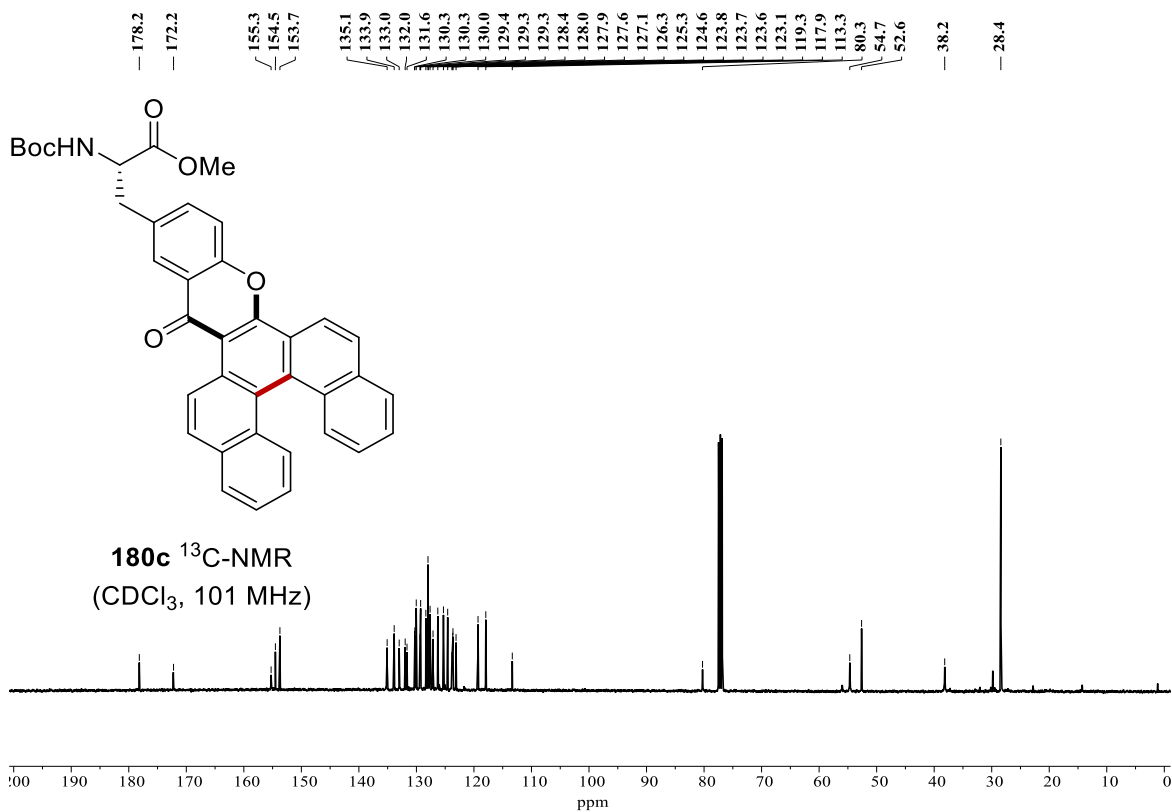
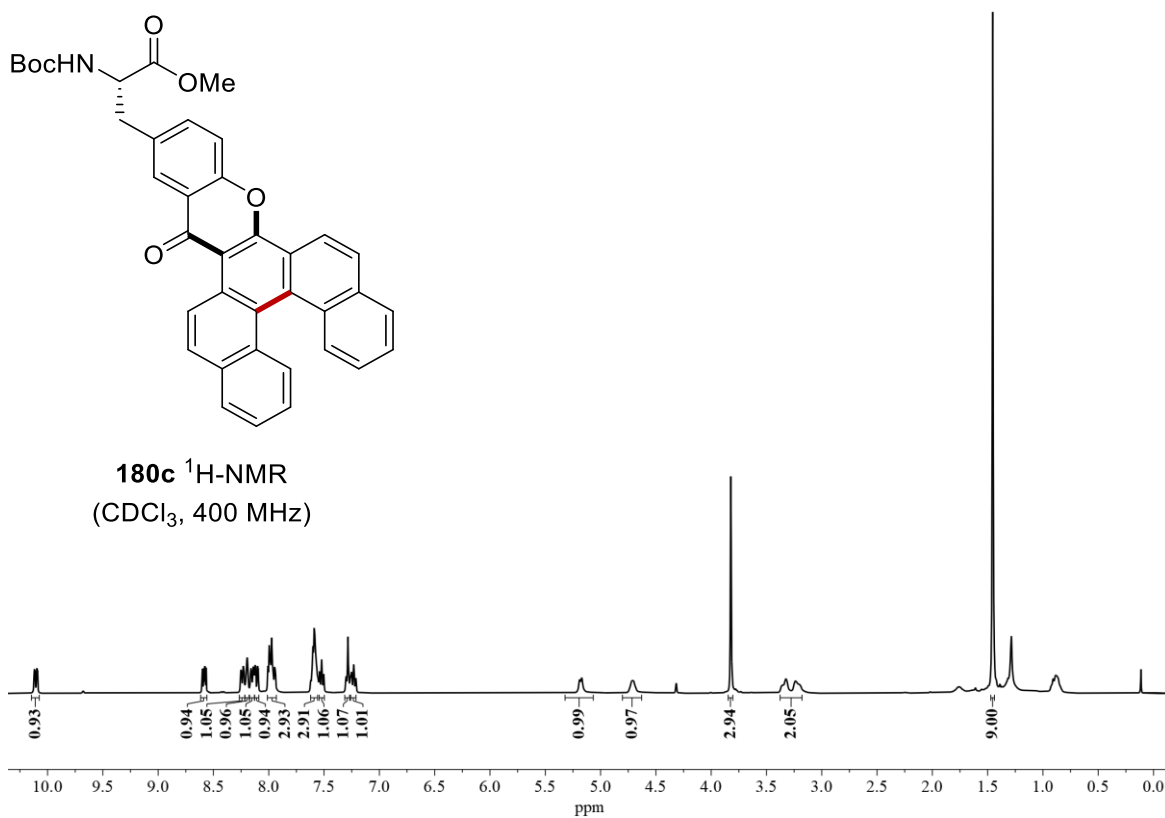


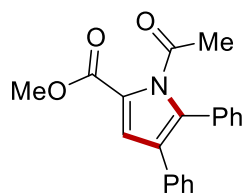
**180b**  $^1\text{H-NMR}$   
( $\text{CDCl}_3$ , 400 MHz)



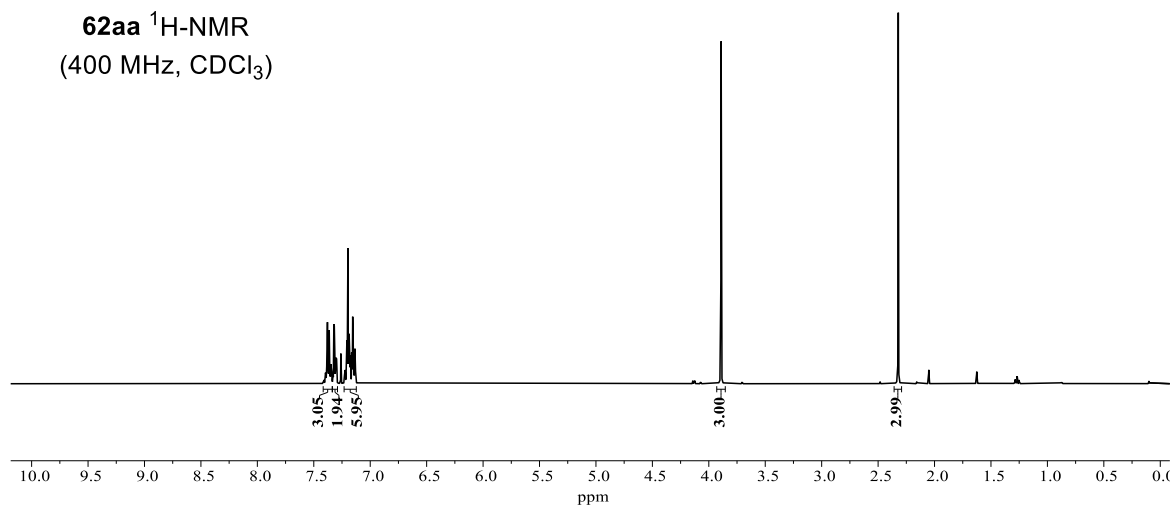
**180b**  $^{13}\text{C-NMR}$   
( $\text{CDCl}_3$ , 101 MHz)



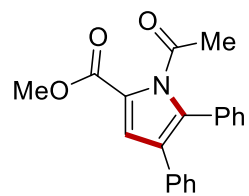




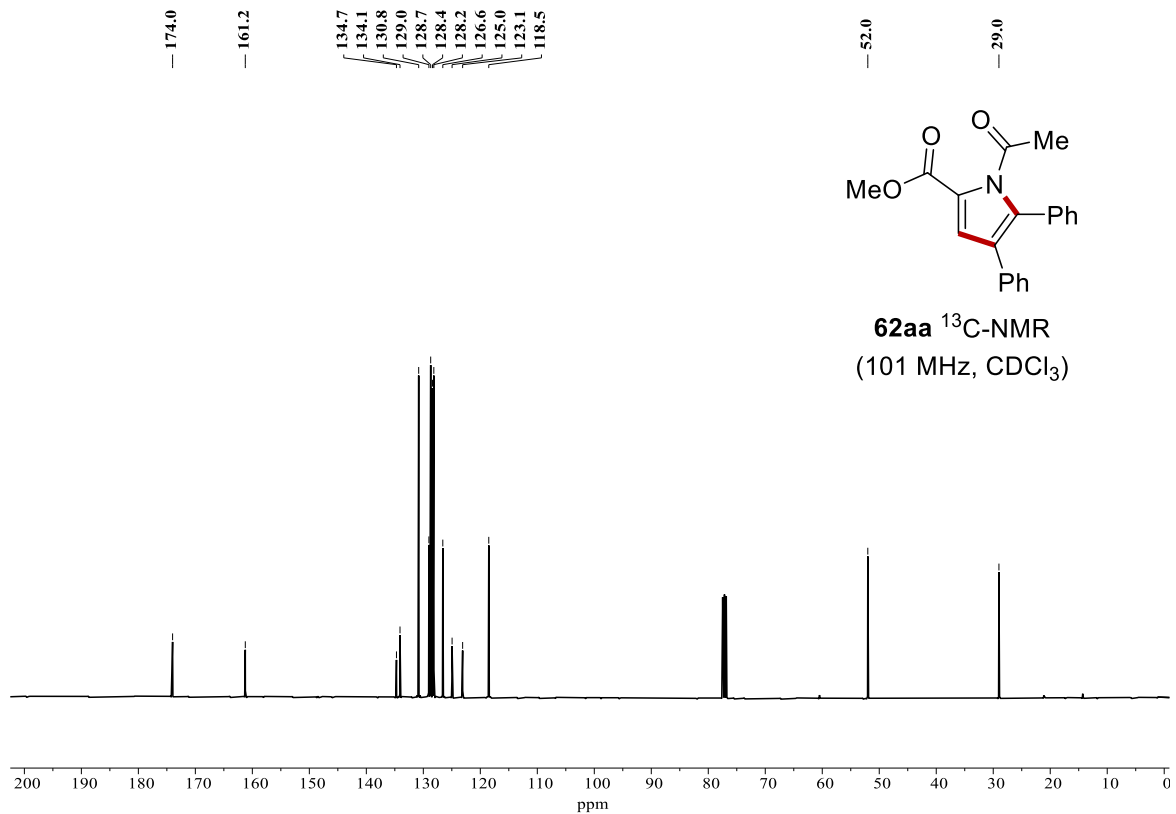
**62aa**  $^1\text{H-NMR}$   
(400 MHz,  $\text{CDCl}_3$ )



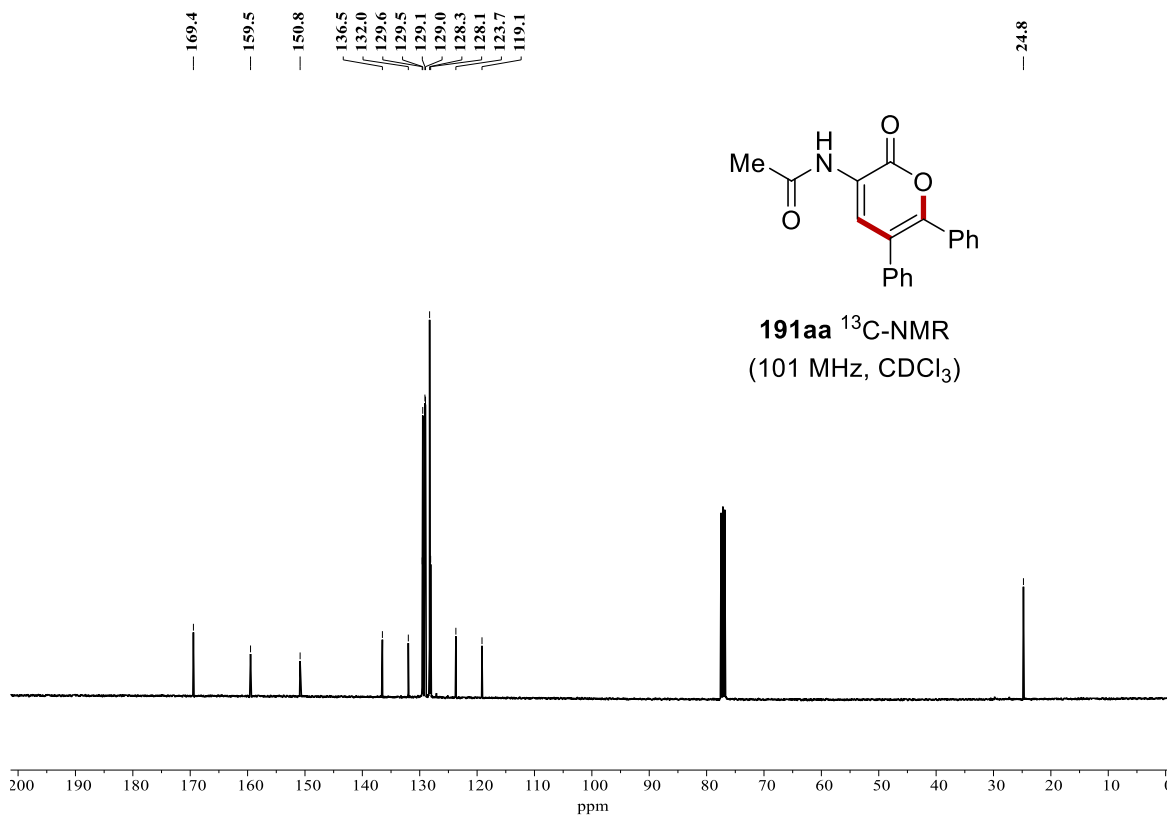
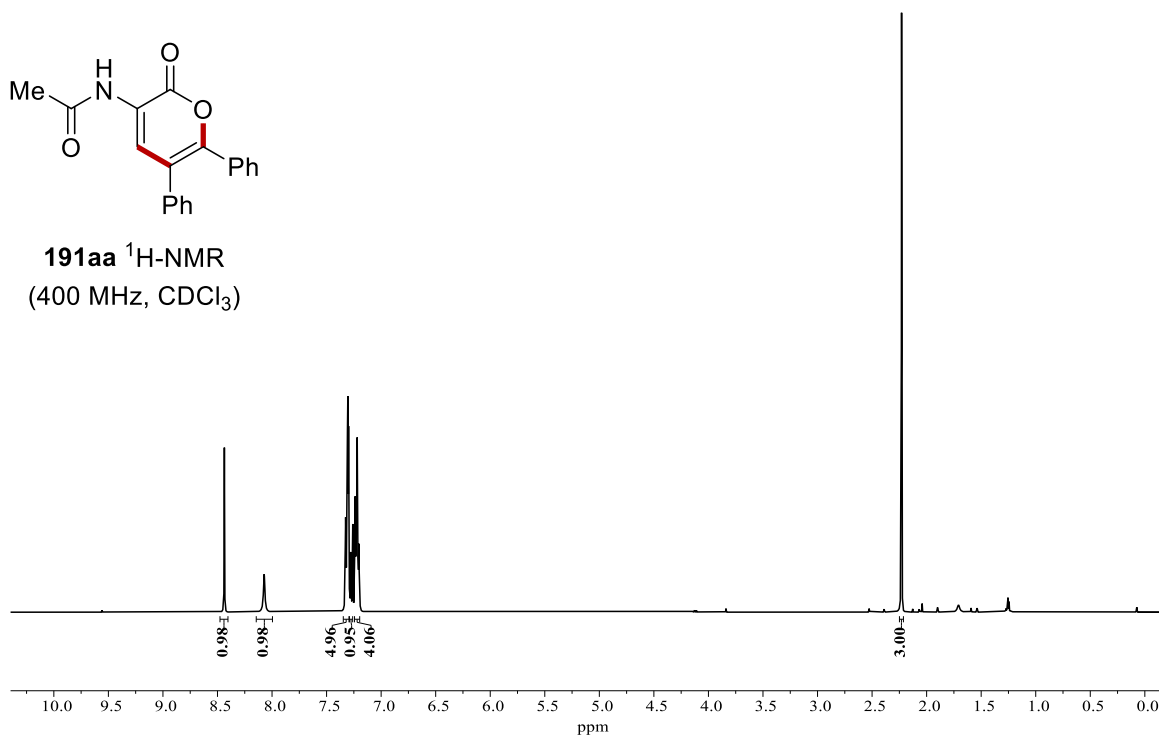
— 174.0 — 161.2 —  
 134.7 134.1 130.8 129.0 128.7 128.4 128.2 126.6 125.0 123.1 118.5

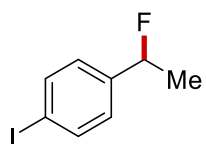


**62aa**  $^{13}\text{C-NMR}$   
(101 MHz,  $\text{CDCl}_3$ )

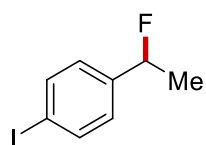
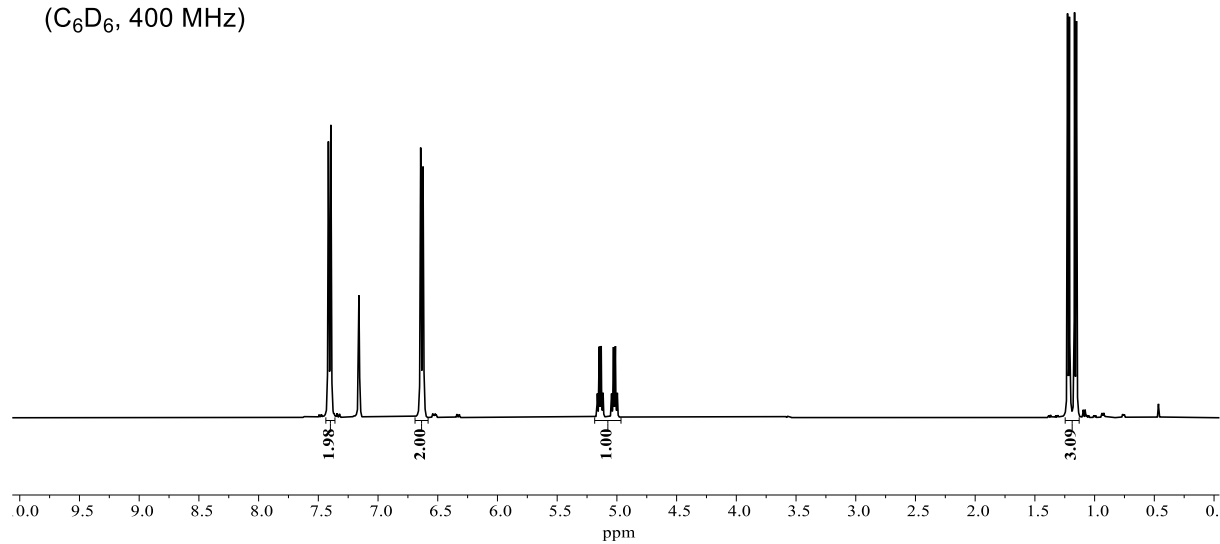




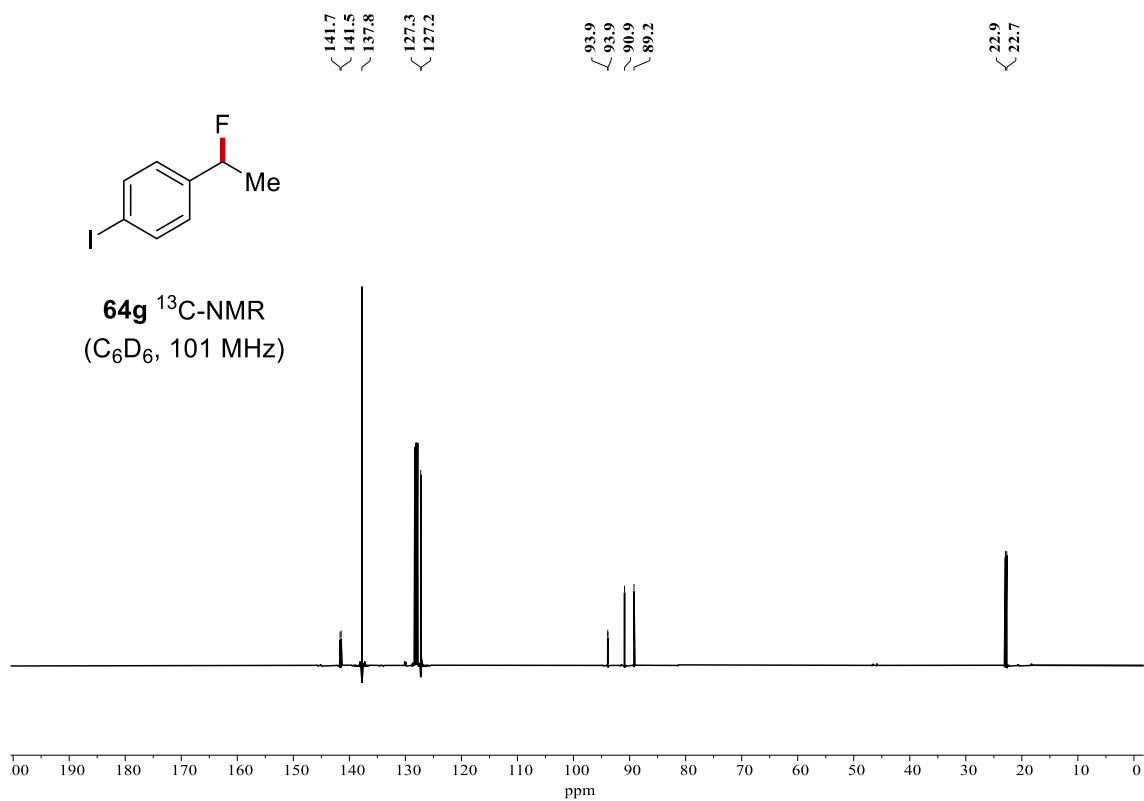


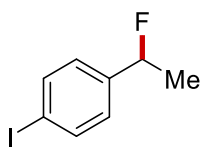


**64g**  $^1\text{H-NMR}$   
( $\text{C}_6\text{D}_6$ , 400 MHz)

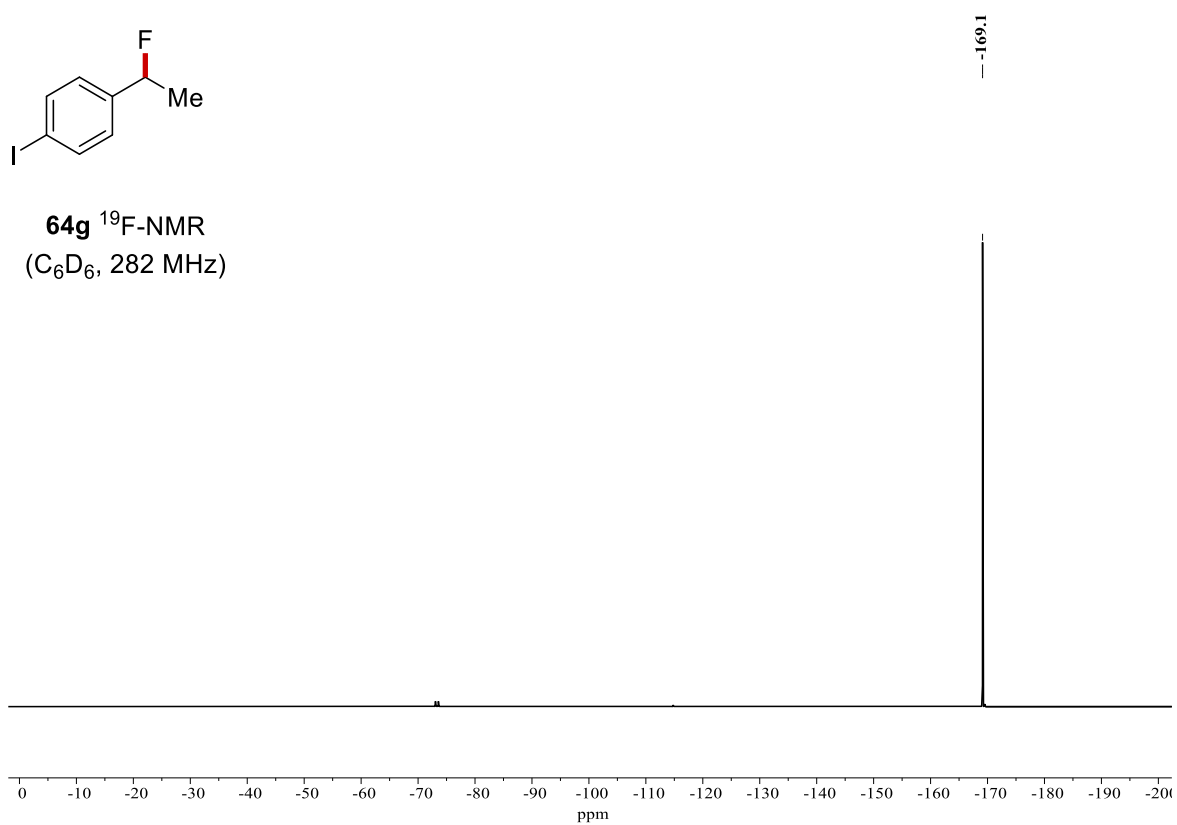


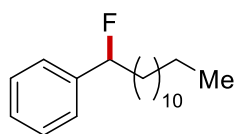
**64g**  $^{13}\text{C-NMR}$   
( $\text{C}_6\text{D}_6$ , 101 MHz)



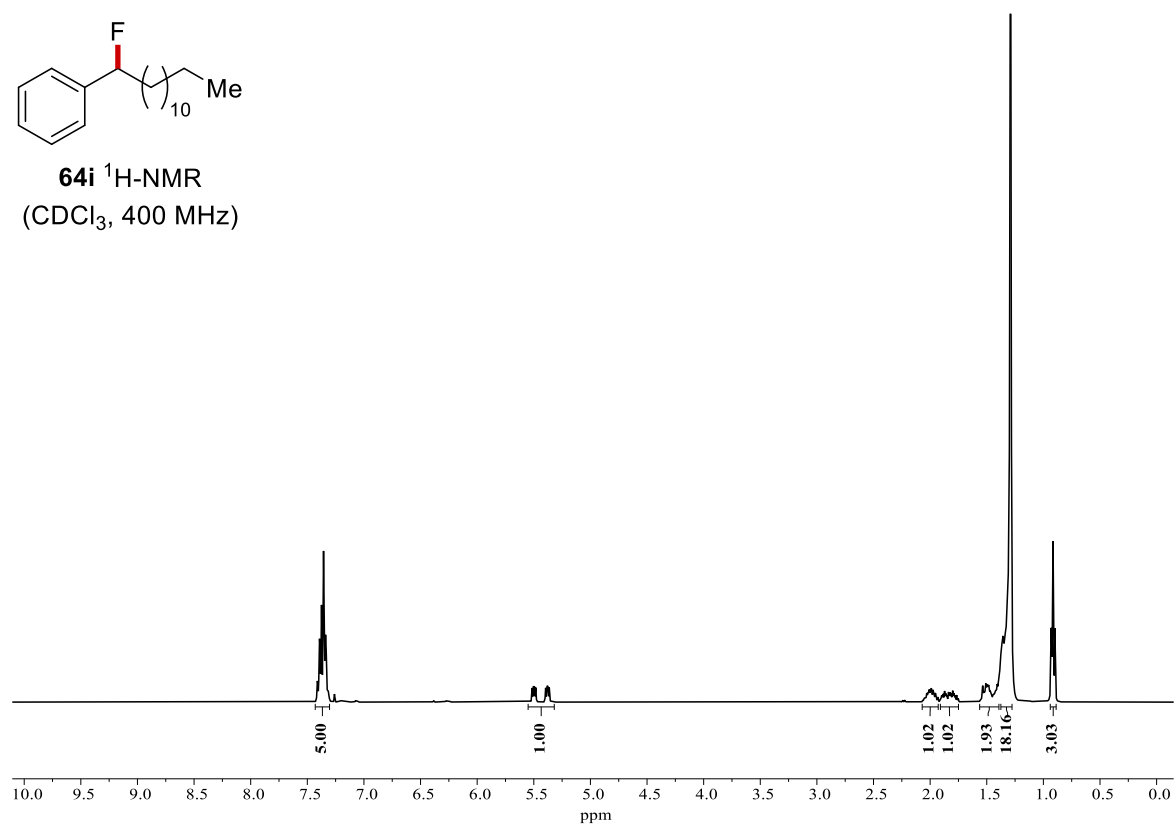


**64g**  $^{19}\text{F}$ -NMR  
( $\text{C}_6\text{D}_6$ , 282 MHz)





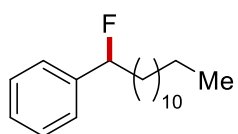
**64i**  $^1\text{H-NMR}$   
( $\text{CDCl}_3$ , 400 MHz)



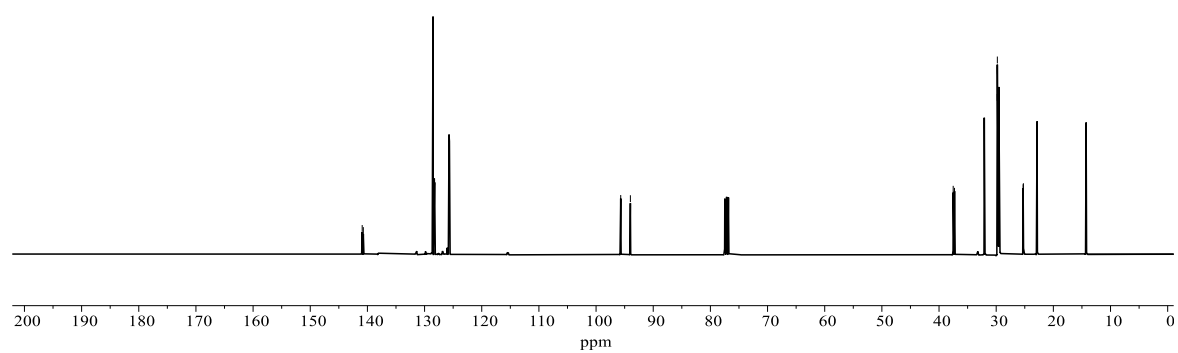
140.9  
140.7  
128.5  
128.3  
128.2  
125.7

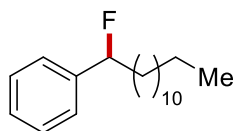
95.7  
94.0

37.5  
37.3  
32.1  
29.8  
29.8  
29.7  
29.6  
29.5  
29.5  
25.3  
25.2  
22.9  
14.3

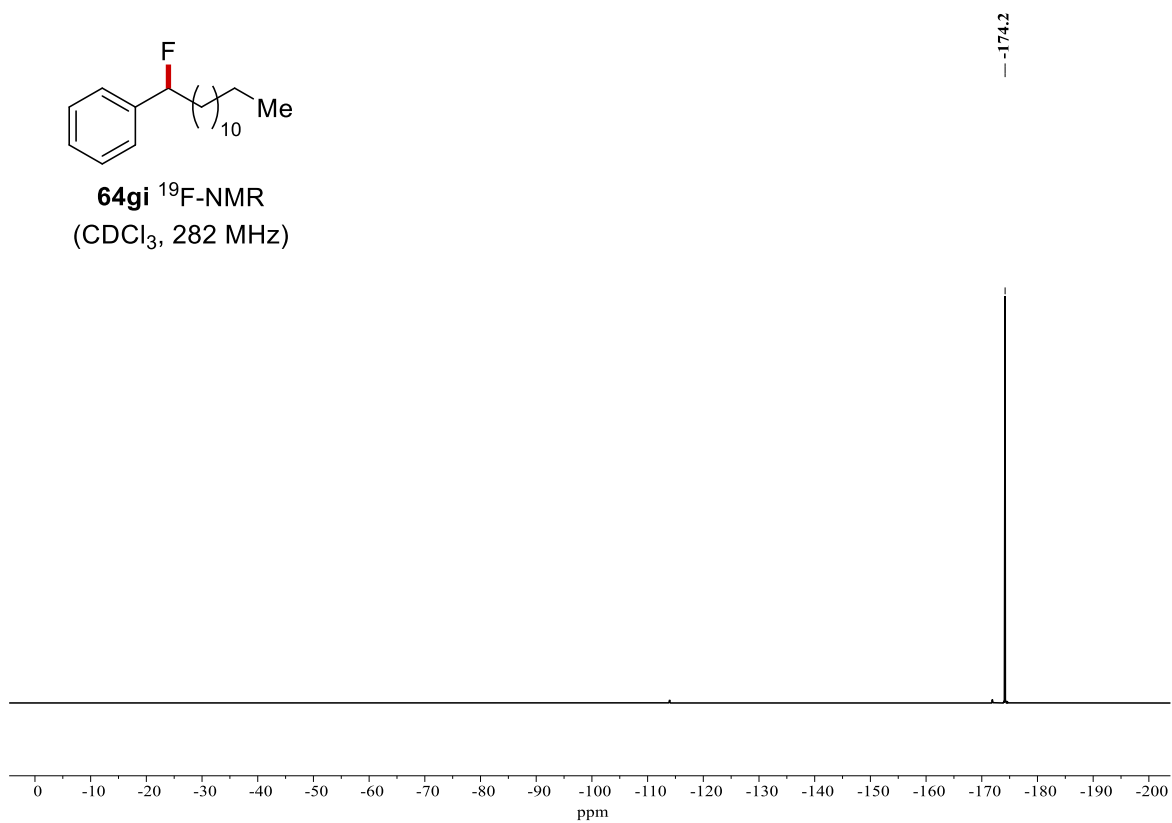


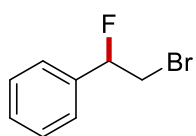
**64i**  $^{13}\text{C-NMR}$   
( $\text{CDCl}_3$ , 101 MHz)



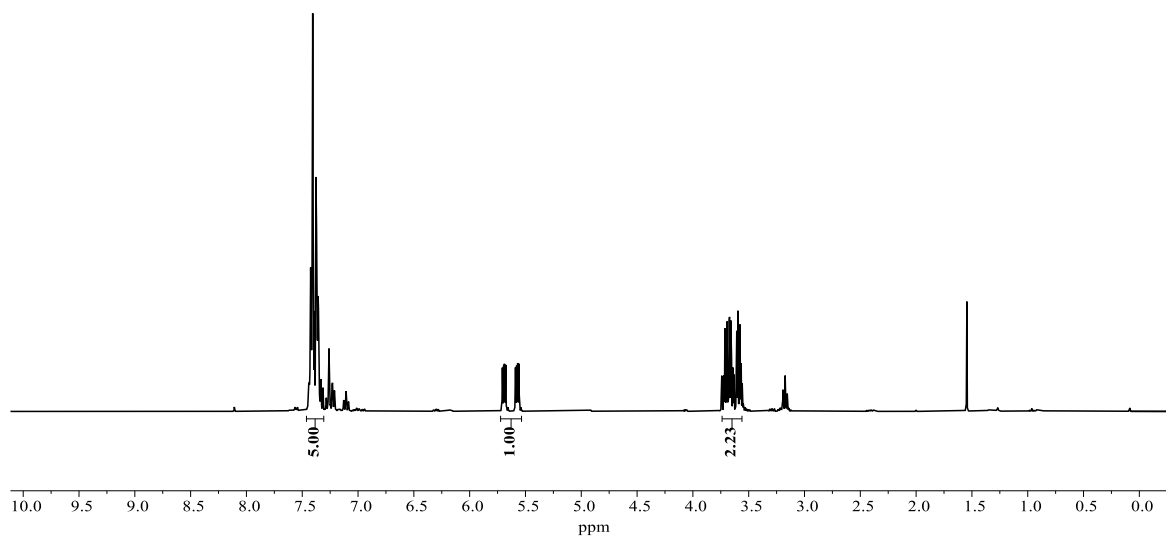


**64gi**  $^{19}\text{F}$ -NMR  
( $\text{CDCl}_3$ , 282 MHz)

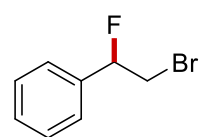




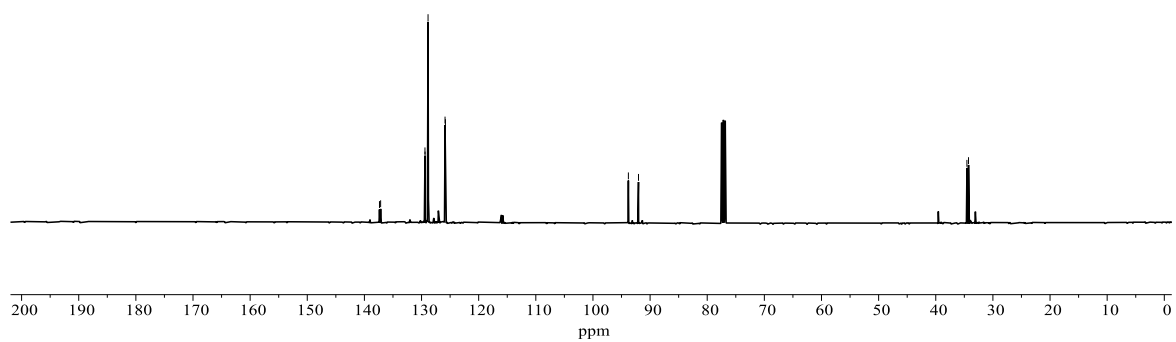
**64I**  $^1\text{H-NMR}$   
( $\text{CDCl}_3$ , 400 MHz)

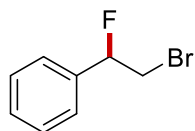


$\left\{ \begin{array}{l} 137.4 \\ 137.2 \\ 129.4 \\ 129.4 \\ 128.9 \\ 125.9 \\ 125.8 \end{array} \right.$ 
 $\left\{ \begin{array}{l} 93.8 \\ 92.0 \end{array} \right.$ 
 $\left\{ \begin{array}{l} 34.5 \\ 34.3 \end{array} \right.$

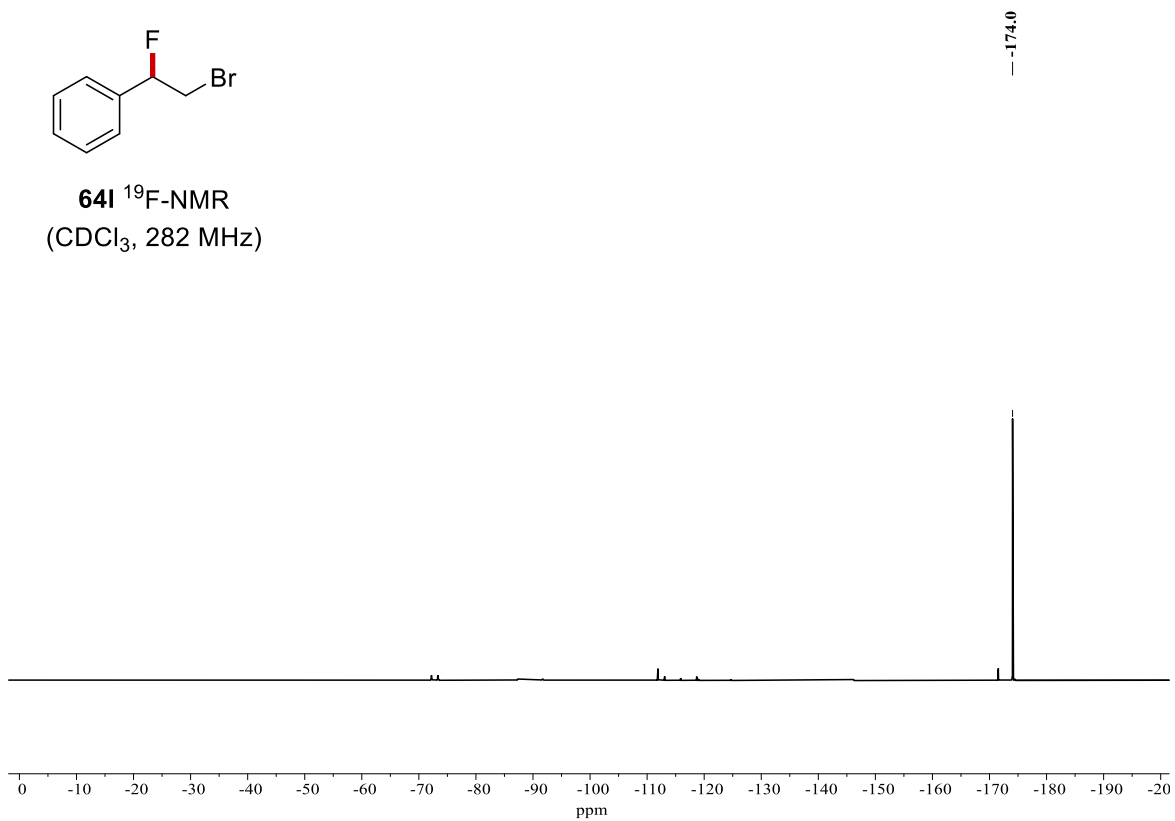


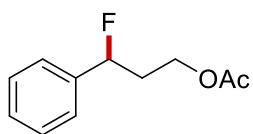
**64I**  $^{13}\text{C-NMR}$   
( $\text{CDCl}_3$ , 101 MHz)



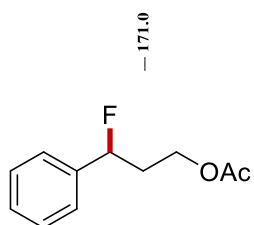
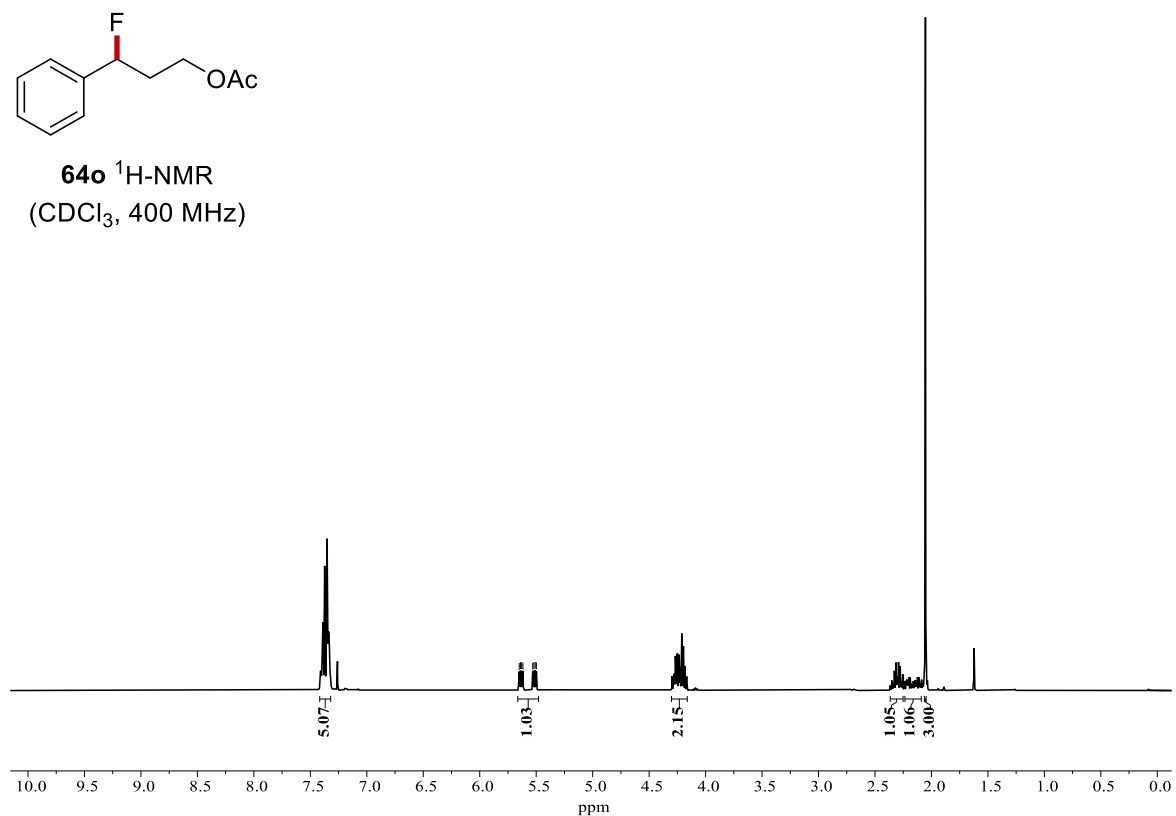


**64I** <sup>19</sup>F-NMR  
(CDCl<sub>3</sub>, 282 MHz)

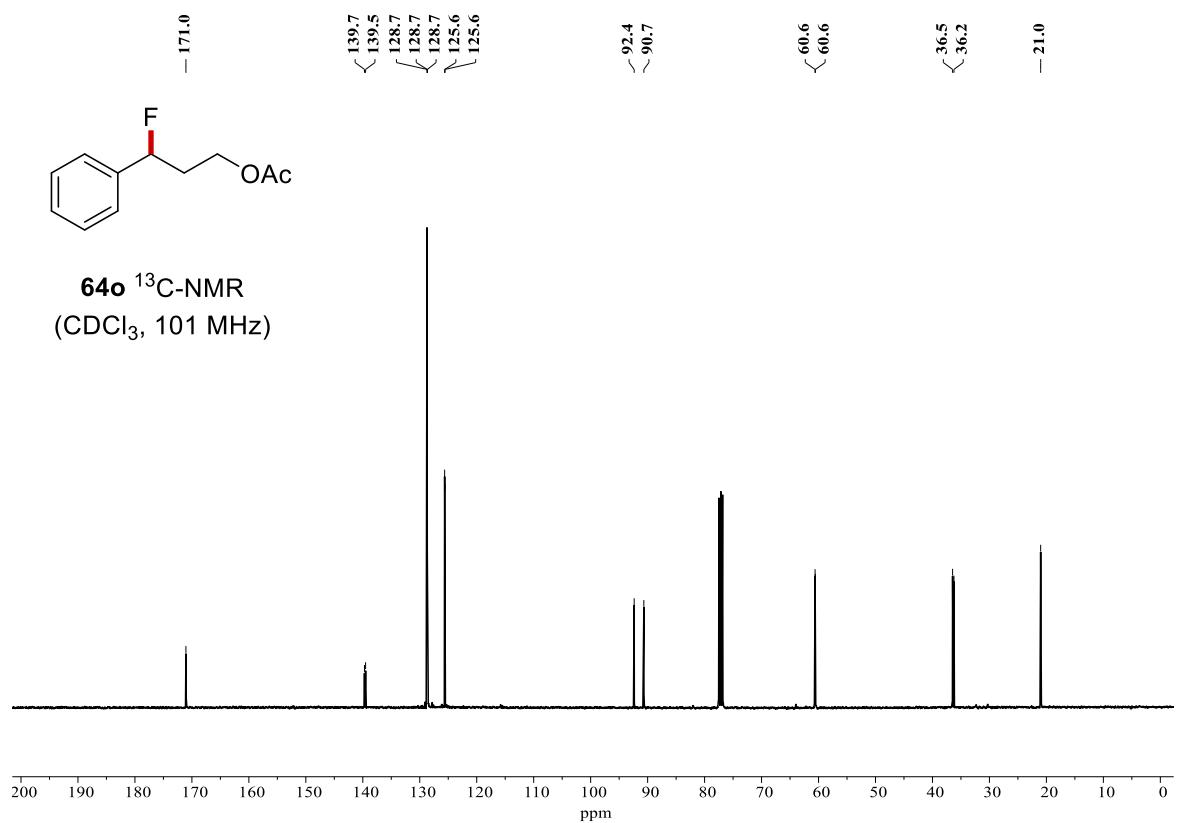




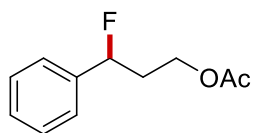
**64o**  $^1\text{H-NMR}$   
( $\text{CDCl}_3$ , 400 MHz)



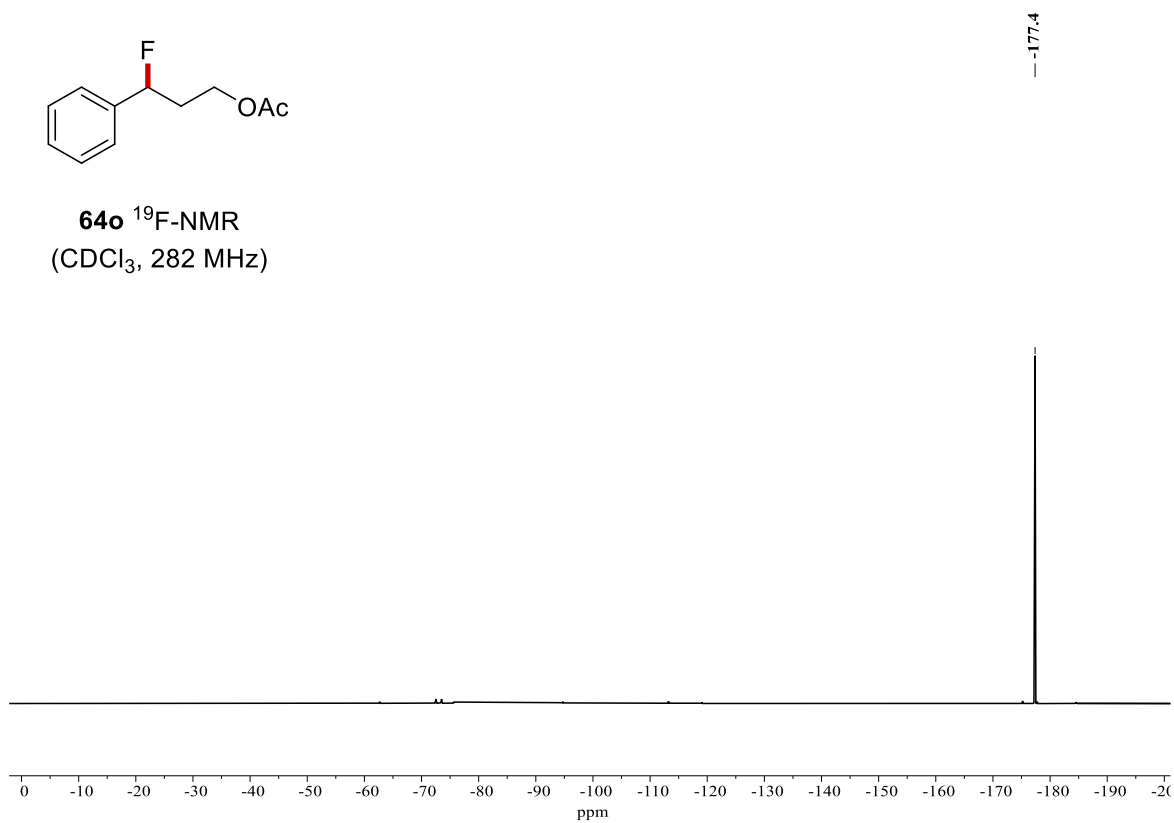
**64o**  $^{13}\text{C-NMR}$   
( $\text{CDCl}_3$ , 101 MHz)

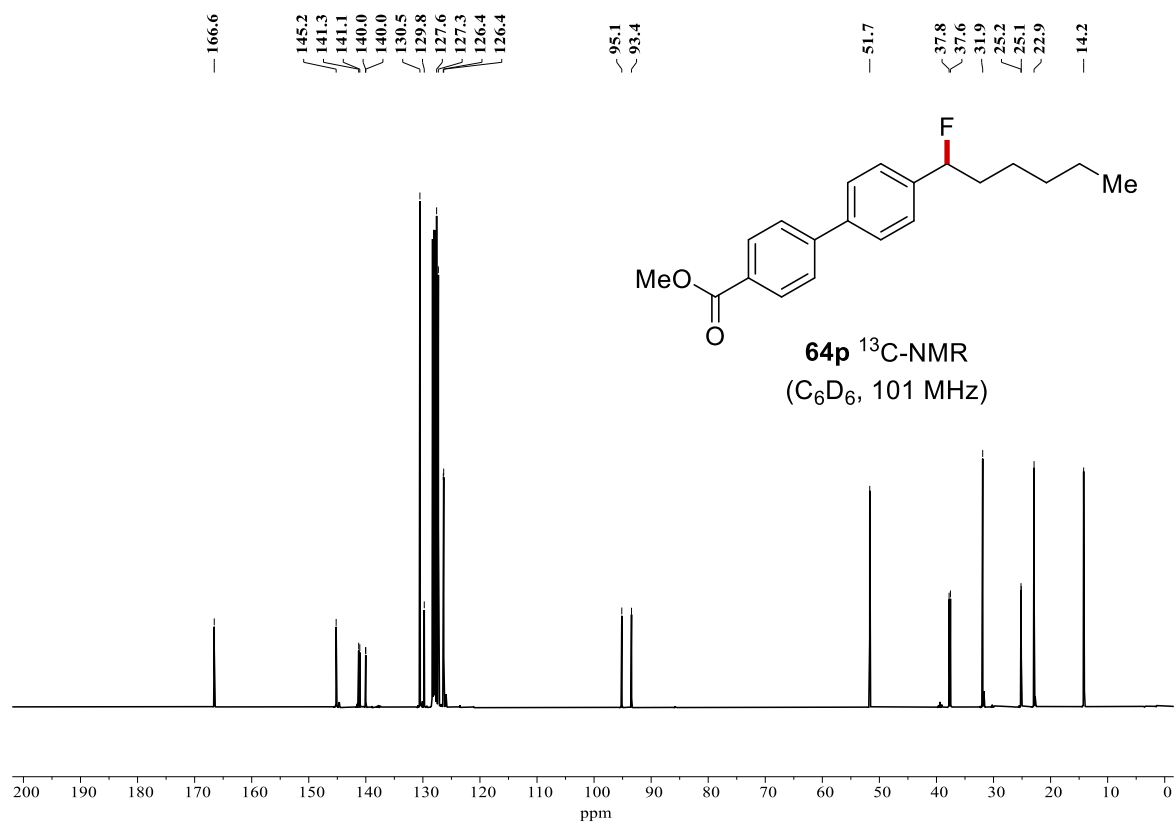
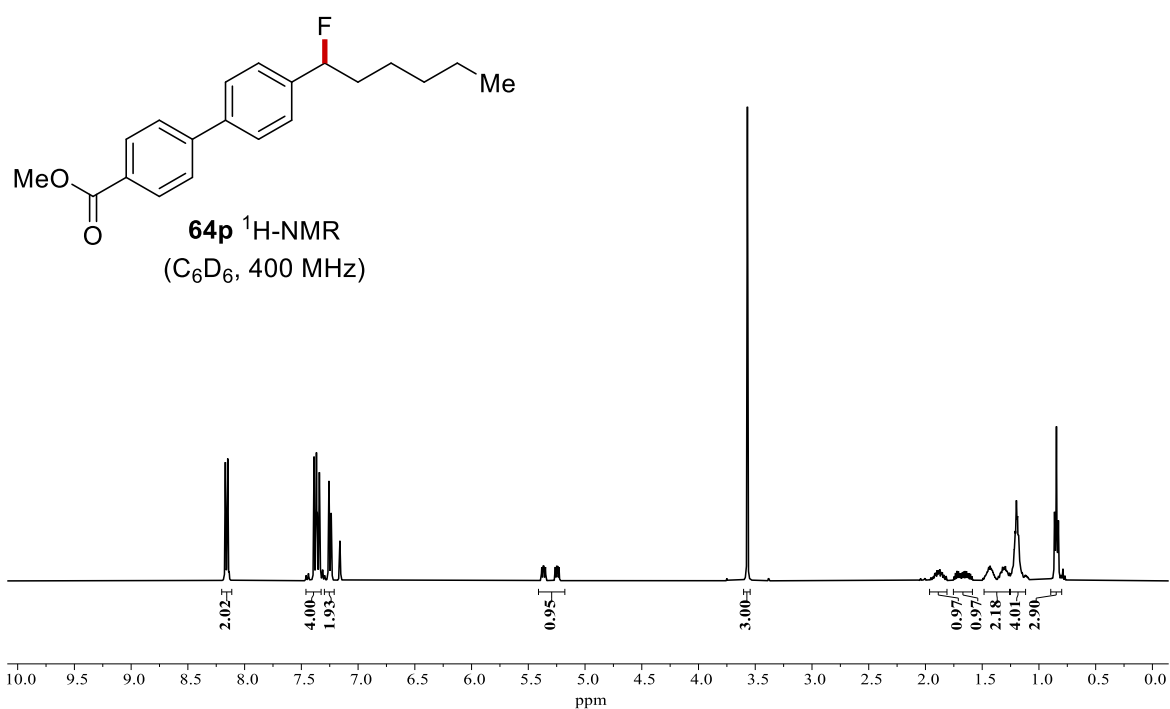


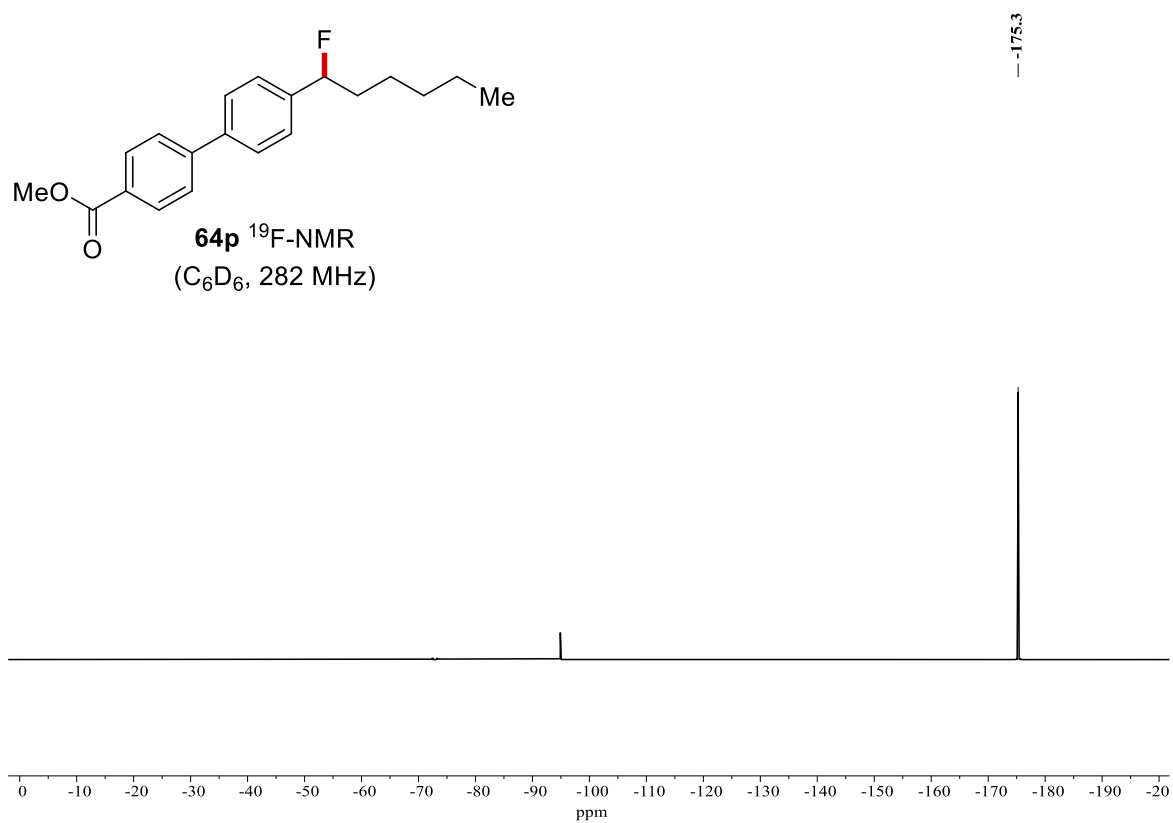


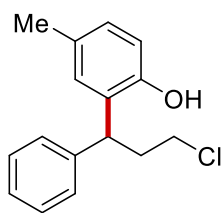


**64o**  $^{19}\text{F}$ -NMR  
( $\text{CDCl}_3$ , 282 MHz)

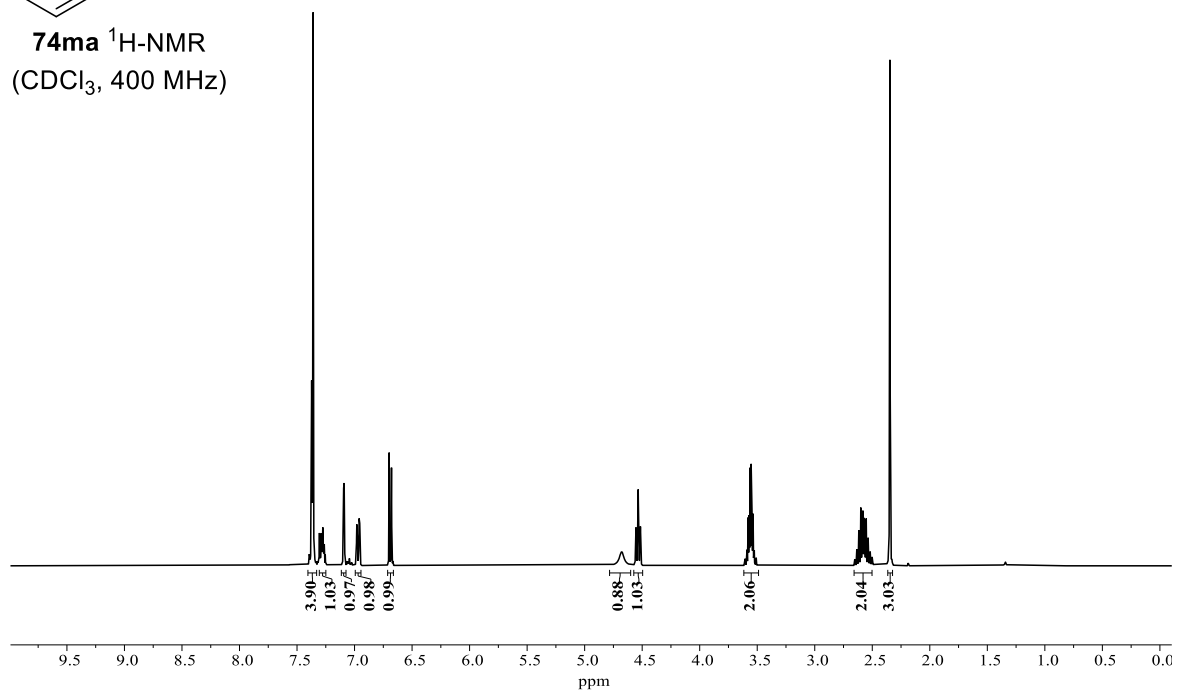




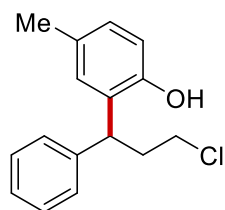




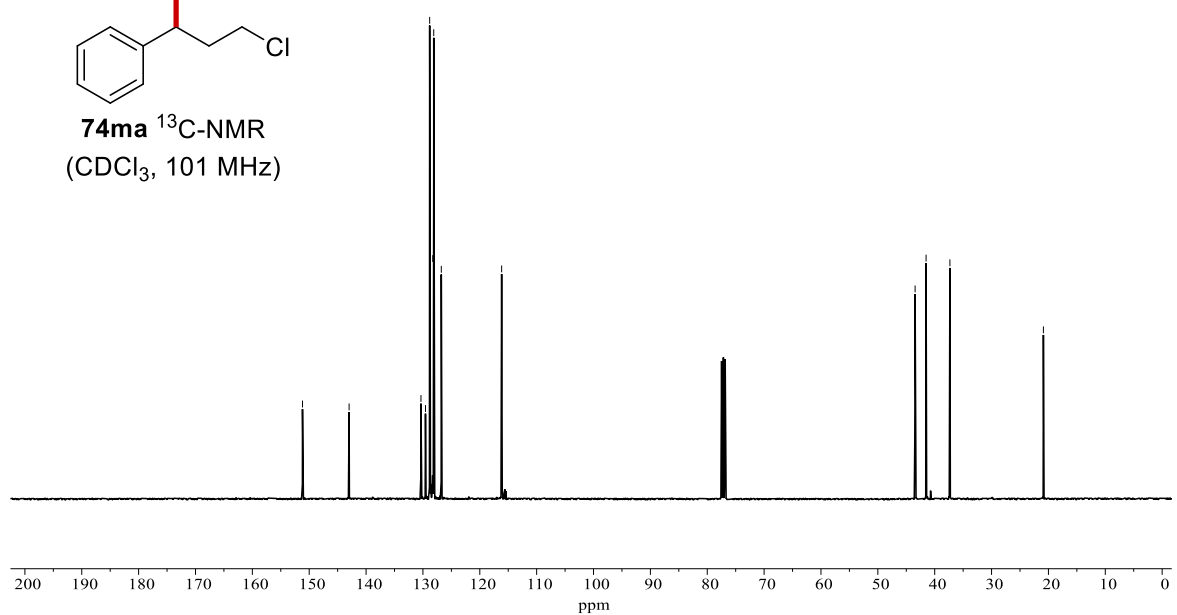
**74ma**  $^1\text{H-NMR}$   
( $\text{CDCl}_3$ , 400 MHz)

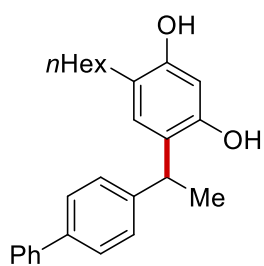


151.2  
143.0  
130.3  
129.5  
128.8  
128.7  
128.3  
128.1  
126.8  
116.2  
43.4  
41.5  
37.3  
20.9

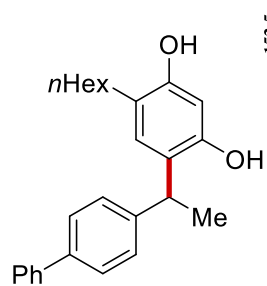
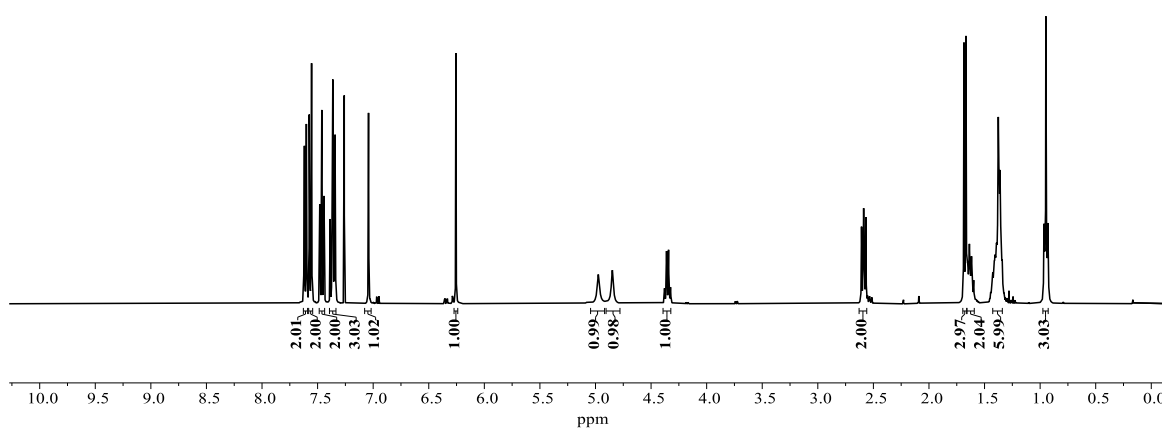


**74ma**  $^{13}\text{C-NMR}$   
( $\text{CDCl}_3$ , 101 MHz)





**74bb**  $^1\text{H-NMR}$   
( $\text{CDCl}_3$ , 400 MHz)



**74bb**  $^{13}\text{C-NMR}$   
( $\text{CDCl}_3$ , 101 MHz)

